HEAT AND MASS TRANSFER IN CONFINED SPACES.

A thesis

submitted in fulfilment

of the requirements for the Degree

of

Doctor of Philosophy

in Chemical and Process Engineering

in the

University of Canterbury

by

H. K. Wee

University of Canterbury

1986

ACKNOWLEDGEMENTS

My sincere thanks to the many persons who had given me help and advice during the course of this research project. In particular, I acknowledge the efforts of the following persons and organizations; without whom the conclusion of this work would not be possible :-

Professor R.B. Keey who had initiated this project and arranged for the financial support. As a supervisor, his willingness to discuss any problems at short notice and his advice in time of doubt is most valuable.

The Building Research Association of New Zealand for its financial support, both in the form of a Research Fellowship and support for the purchase of equipment.

The technicians of this Department, especially Mr.D.P.Brown for constructing the "Guarded Box" and Mr.W.M.Earl for making the electronic equipment. Messrs N.W.Foot and R.G.Gordan for modifying and repairing the equipment at frequent requests, Mr.T.R.Berry for taking and printing the photographs and Mr.I.H.Torrens for purchaing the many needed items.

Fellow postgraduates for their helpful discussion and many useful suggestions. Pat Janssen and Huub Bakker for their help in using the computing and graphic equipment. Miss L.K. Anderson and Mr.C.W. Tan for their help in typing part of this thesis.

My parents and all members of my family who are many miles away but never failed to show their moral support and encouragement. Finally, my wife Ching Wang, who has always helped me when things got tough and who never complained about my absence from home during all those times when experiments and writing-up of the thesis needed to be done.

Dedicated to my parents and my wife

CONTENTS

ABSTRACT

A novel experimental technique had been used to investigate the simultaneous transfer of heat and moisture in a simulated building cavity by natural convection. This technique employed two porous plastic plates as the two cavity walls and this arrangement allowed the imposition of a simultaneous moisture gradient on top of a temperature gradient and vice-versa. Both aiding and opposing-flow conditions were investigated for the vertical and horizontal cavity configuration . The aspect-ratio of the experimental cavity used was 7.0 and the fluid investigated was air.

The experimental results were correlated in the form of Nusselt and/or Sherwood number versus an appropriately defined Rayleigh number which depended on the type of gradient causing the flow. The Nusselt and Sherwood numbers were found to agree well with the theoretical values of this work obtained from numerical calculation using a finite-difference technique. The temperature, concentration, stream-function and velocity fields from the numerical calculation also augmented the experimental results.

As no previous results on the rate of moisture-transfer and its interaction with the rate of heat-transfer in an actual building cavity were available, the results of this work addresses this gap in the literature. Under the conditions investigated, which corresponded to the actual temperature and moisture gradients in a typical building cavity in New Zealand, the simultaneous temperature gradient had increased significantly the rate of moisture transfer while the presence of the simultaneous moisture gradient had not increased significantly the rate of heat transfer.

CHAPTER 1

INTRODUCTION.

1.1 BACKGROUND OF PROBLEM.

1.1.1. Heat Transfer and Building Cavity.

The fact that air has a very low conductivity, small density, and is transparent to radiation has been realised and utilised in the field of insulation for a long time. It is not an uncommon practice to construct dwellings with timber-framed walls which result in a gap of about 100mm in the middle between the inner lining and the other cladding. This gap has insulating features when poorly ventilated. Such a gap in the wall will be termed a "confined space" or a "cavity", a term which will also be applied to the space between the ceiling and the roof. Heating engineers are concerned with the rate of heat transfer across each cavity which in turn determines the rate of heat leak from a building [6,7,8,9].

Three modes of heat transfer occur in the cavity :- namely, conduction, convection and radiation. Radiation is electromagnetic in nature and is present as long as two viewing surfaces differ in temperature. If a transparent and hence non-absorbing gas like dry air is present in the cavity, radiation can be said to take place independently of the other two modes of heat transfer and does not depend significantly on the shape and size of the air space. The magnitude of radiant transfer is not negligible, but can be found independently once the nature of the surface of the boundaries and their temperatures have been specified. The other two modes of heat transfer, conduction and convection, are more closely related.Whether conduction or convection will be the dominant mode of heat flow in the cavity will depend on: (i) the geometrical arrangement of the cavity (aspect ratio); (ii) the fluid property (Prandtl number) and (iii) the temperature difference across the cavity (characterised by the

Grashof number)[3],[12]. Generally for a given Prandtl number, convection will be the dominant mode if the Grashof number is large, i.e. the temperature difference across the plates is large and/or the aspect ratio (ratio of plate dimension to the cavity thickness - see section 1.2) is small. Convective heat transfer is typically much greater than conductive heat transfer.

Double glazing of windows is another example where cavity insulation has been utilised in building. Cavity insulation, however, is not restricted to building insulation alone, but finds application in many industrial areas, such as insulation in solar-energy collectors and nuclear-fuel containers. Large temperature difference across the cavity walls (greater than 200°C) are encountered in furnace-wall design and cryogenic installations [Ref 11]. Radiant transfer is normally more pronounced in the high-temperature installations.

1.1.2 Moisture Transfer and Cavity.

Condensation of moisture and the growth of mildew has always been a problem associated with dwellings [13,14,15] with some authors claiming that this is especially so for buildings with thermal insulation.[15, 16]. As water evaporates in the living space of houses, some water vapour penetrates the walls and ceilings and may condense on cold surfaces. When insulation is added into the wall or ceiling cavities, certain surfaces remain cooler than in the uninsulated case resulting in the risk of increased condensation [16,17]. If a significant amount of condensation takes place on wooden structural elements,then the wood may rot and serious damage to the house may ensue.[16, 18]. The moisture that accumulates within the insulation (air or fibrous material) of wood-frame walls may also increase heat transmission, although no conclusive data on this aspect have been reported [17, 19]. If this is true, then the effectiveness of thermal insulation is reduced. Trethowen[19] has reported the work of Powell and Robinson [69] which showed that the thermal resistance of concrete and brick can fall to as little as 30 percent of their normal dry value when moisture is present.

However, more proof is needed before any definitive conclusion can be drawn concerning the effect of moisture on the thermal conductivity of building materials.

Quantiitative prediction of moisture movement through building walls and ceilings is thus important; especially in a cavity where condensation is most likely to occur. If the mechanism and the conditions for the onset of moisture transfer across a cavity are known, a more effective way of controlling the moisture content in the cavity may be possible. At the moment it is only known that ventilation is necessary for moisture-control purposes, but it is often uncontrolled with gross excesses of ventilation at some times and insufficient ventilation at other times. Since excess ventilation leads to excess heat loss and insufficient ventilation leads to moisture condensation, the correct rate of ventilation is obviously needed.

1.2 DEFINITION AND DIMENSIONS OF "CONFINED SPACES".

A "confined space" or a "cavity" in this work will have one of the following definitions:-

1.2.1. Vertical cavity.

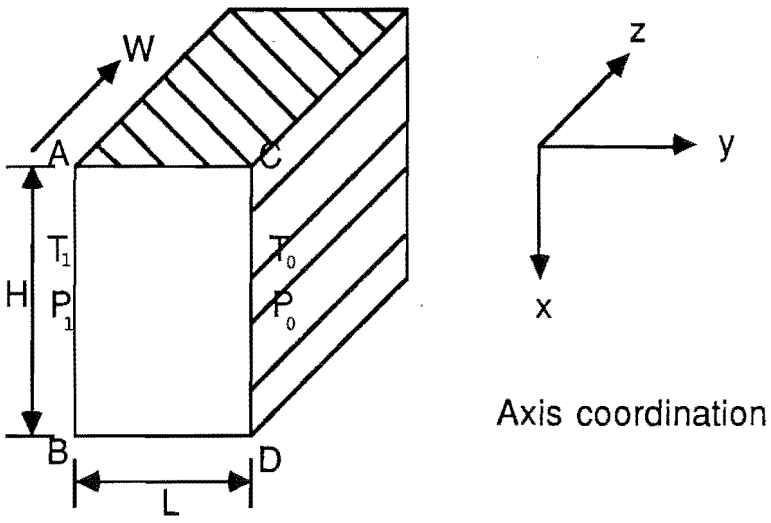

Fig. 1.1 Vertical Cavity.

Nomenclature:

(i) H = height of cavity
(ii) L = width (thickness) of cavity
(iii) W = length of cavity
(iv) T = temperature
(v) P = vapour pressure
(vi) $\Delta T = (T_1 - T_0)$ can be positive or negative
(vii) $\Delta P = (P_1 - P_0)$ can be positive or negative
(viii) A = aspect ratio = H/L.

Assumptions:

(i) The width W in the y direction is sufficiently large to make the flow and temperature fields everywhere two-dimensional in the cavity.

(ii) Flow and temperature fields near the end faces (y = 0 and y = d) are neglected.

Definition:

A cavity is defined as "vertical" when the two opposite vertical walls (with edges AD and BC) are at different but uniform temperatures and humidities. The two horizontal walls (with edges AB and DC) are assumed to present total resistance to heat and moisture flow ie. $\partial T/\partial z=0$ and $\partial P/\partial z=0$ at z=0 and z=H or no resistance to heat and moisture flow i.e. $T = T_1(x/L)\Delta T$ and $P = P_1-(x/L)\Delta P$ at z=0 and z=H or a combination of these four conditions. Also, A = H/L is not less than 1, with h = 1 chosen as the lower limit.

1.2.2 Horizontal Cavity.

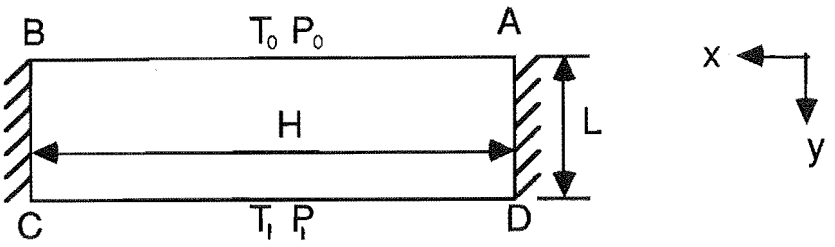

Fig. 1.2 Horizontal Cavity.

Nomenclature:

(i) H = height (thickness) of cavity
(ii) L = width of cavity
(iii) A = aspect ratio = L/H or H/L
The rest of the symbols is the same as 1.2.1.

Assumptions:

As for the vertical cavity in 1.2.1.

Definition:

A cavity is defined as "horizontal" when the two opposite horizontal faces (with edges DA and CB) are at different but uniform temperatures and humidities. The two vertical faces are assumed to share any combination of the following conditions:- (i) or (ii) and (iii) or (iv):-

(i) offer total resistance to heat flow
(ii) offer total resistance to moisture flow
(iii) offer no resistance to heat flow
(iv) offer no resistance to moisture flow.
We have H/L not very much less than and larger than 1.

1.2.3. Inclined Cavity.

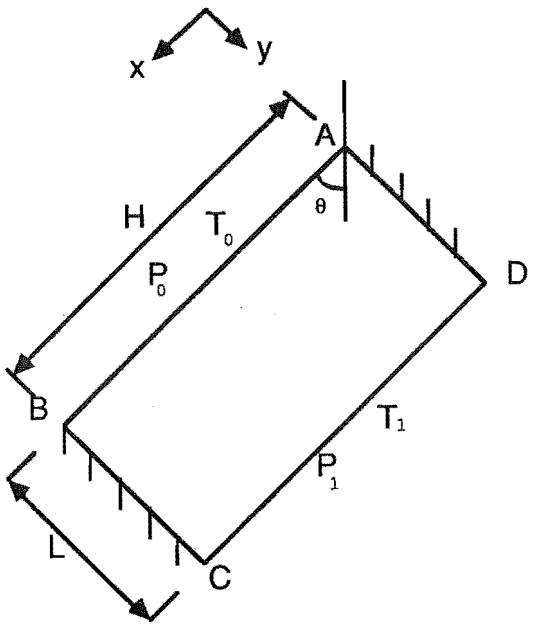

Fig. 1.3 Inclined Cavity.

Nomenclature:

As for the vertical cavity in 1.2.1 but with the following modifications:-

(i) X is in the direction of DC i.e. at inclination cos θ to the horizontal;

(ii) y is in the direction of DA i.e. at inclination sin θ to the horizontal;

(iii) The angle of inclination θ is measured from the vertical. If θ = 0 degrees, AD is vertical. If θ = 90 degrees, AD is horizontal. θ is greater than 0 and less than 90 degrees when AD is as shown in the figure.

Assumptions:

As for the vertical cavity in 1.2.1.

Definition:

As for the vertical cavity in 1.2.1, but the cavity is inclined at angle θ to the vertical. For θ between 0 and 90 degrees, the plate with temperature T_1 and vapour pressure P_1 is facing downwards; and for θ between 0 and - 90 degrees , the plate with temperature T_1 and vapour pressure P_1 is facing upwards. Note that for θ = 0 degrees, the cavity is a vertical cavity (1.2.1) and for θ = + 90 degrees, it corresponds to a horizontal cavity.

1.3 OBJECTIVE OF RESEARCH.

The aim of the research is thus the investigation of combined heat and moisture transfer across a typical building cavity with the hope that the results will be useful to the design of buildings. Indeed, as recently pointed out by Alandari et al [151], the accuracy of existing heat transfer models for use in building design was limited by the uncertainties of the data used in the models. It is thus hoped that the data obtained in this research will be of use to the building designers with the following designed objectives:-

(i) comfortable living spaces;
(ii) minimum heat losses from living spaces;
(iii) minimum unwarranted moisture condensaiton.

CHAPTER 2

LITERATURE SURVEY

2.1 FLOW PATTERNS IN CAVITIES.

The presence of a temperature or moisture difference across a cavity as a result of opposing faces at different temperature or/and humidity level will induce flow in a cavity. The temperature /concentration gradient between the walls and the neighbouring fluid causes the density of the fluid to change. This density difference gives rise to buoyancy effects which cause fluid motion. This onset of motion as a result of density variations in a gravitational force field is termed "natural" or "free" convection.

The cases described in the following sections are mainly restricted to analytical solutions or experimental results of air-flow patterns associated with heat-transfer conditions in cavities of aspect ratio greater than 1.0 only. Very little information on air-flow patterns associated with mass transfer or simultaneous heat and mass transfer in a cavity has been encountered in the literature except in the field of thermohaline convection. Some flow patterns for air were given for flow from a single vertical or inclined plate with simultaneous heat and mass transfer but it is felt that the flow patterns in a cavity would be substantially different. Neverthless, some of the results for motion about such a single plate will be given, as an indication of likely flows in cavities.

A review of the subject can be found from many articles in the literature[6,27,67].

2.1.1 Flow Paterns in Vertical cavity.

The flow in the cavity is specified by three dimensionless parameters:-

(i) Prandtl number $Pr = \upsilon/\alpha$

(ii) aspect ratio $A = H/L$

(iii) Rayleigh number $Ra = (g\beta\Delta T\ L^3/\upsilon\alpha) \equiv Gr.Pr$

where υ = kinematic viscosity.

α = thermal diffusivity

H = height of cavity

L = width (thickness) of cavity

β = coefficient of thermal expansion

g = gravitational constant

and ΔT = temperature difference across the cavity.

The Prandtl number characterises the property of the fluid i.e. it indicates the relative size of the boundary-layer thicknesses for momentum and for heat transfer. The aspect ratio characterises the geometrical arrangement of the cavity and the Rayleigh number characterises the temperature-difference across the cavity.

In general, fluid motion exists for any finte Rayleigh number.However, provided the Rayleigh number is sufficiently small the motion is relatively simple, consisting of one large cell which fills the whole slot, the flow rising at the hot wall, falling down the cold wall and turning at the opposite ends of the slot (Fig.2.1). Fig.2.2 indicates the velocity at mid-height across the cavity.

This flow was first described by Batchelor [1]. Hollands et al [21] have called this the "base flow". The stability of this base flow was investigated by numerous investigators [21, 22, 23, 24] who came to the conclusion that the instability appears to be brought on by the hydrodynamic breakdown of the base flow due to the increasing significance of the inertial effects. Vest and Arpaci [22] found that the critical condition is dependent only on the Grashof number and independent of the Prandtl number and gave a critical value of Gr = 7880. All other studies eg.[23,24] have found slight but significant dependence of the critical Grashof

number on Prandtl number. For Pr = 0.71, Vest and Arpaci [22] and Hart [24] obtain a critical Grashof number of about 8000, while Unny [23] and Hollands and Konicek [21], however, have obtained critical Grashof number of about 11,000.

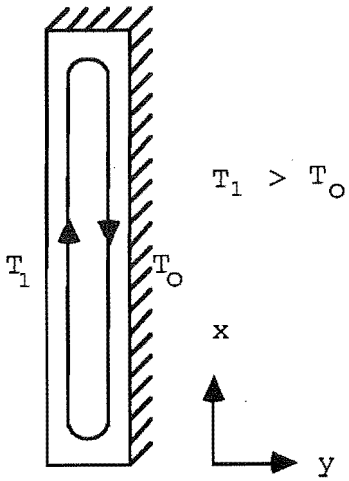

Fig.2.1 The Base Flow

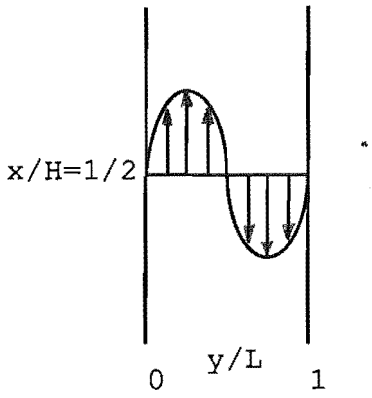

Fig 2.2 Dimensionless velocity at cavity mid-height.

All the previous studies [1, 21, 22, 23, 24] only investigated the critical condition from which the stable laminar base flow became unstable but did not give the flow details. The first phenomonological study of the flow structure in a vertical cavity was carried out by Elder [5]. His experimental conditions were (i) Aspect ratio, A, in the range of 1 to 60, (ii) Prandtl number equal to =1000 and (iii) Rayleigh number range, less than 10^8. He made use of aluminium powder suspended in the fluid to measure the fluid velocity either by timing the passage of a single particle between fixed marks in the eyepiece of a travelling microscope, or from lapsed-time photographs, in which the streak-length is proportional to the velocity.

For Rayleigh numbers, Ra less than 1000 and for the aspect ratio greater or equal to 20, the flow is vertical throughout the slot except for regions near the ends (Fig.3.3). SEE ERRATA

For Ra greater than 10^3 and less than 10^5, the flow tends to boundary layer flow for increasing values of Ra, and similar to that near an isolated, heated vertical plate, except that the

vertical growth of the wall layers is inhibited in the central part of the slot by the presence of the other layer. The core did not rotate as a solid body with constant vorticity as predicted by Batchelor [1], but only with cross-flow into and out of the boundary layer.

Near Ra = 3 x10^5, the interior region of the flow generates a steady secondary flow. A regular cellular pattern becomes superimposed on the basic flow to produce a "cats-eye" pattern of streams. Near Ra = 10^6 when the secondary cell amplitude is large, a further steady cellular motion (tertiary flow) is generated in the weak shear regions between each secondary cells. Fig2.3illustrates all these features. The figures below the flow structures corresponds to the dimensionless velocity profile at mid-height of the cavity, by Elder [5].

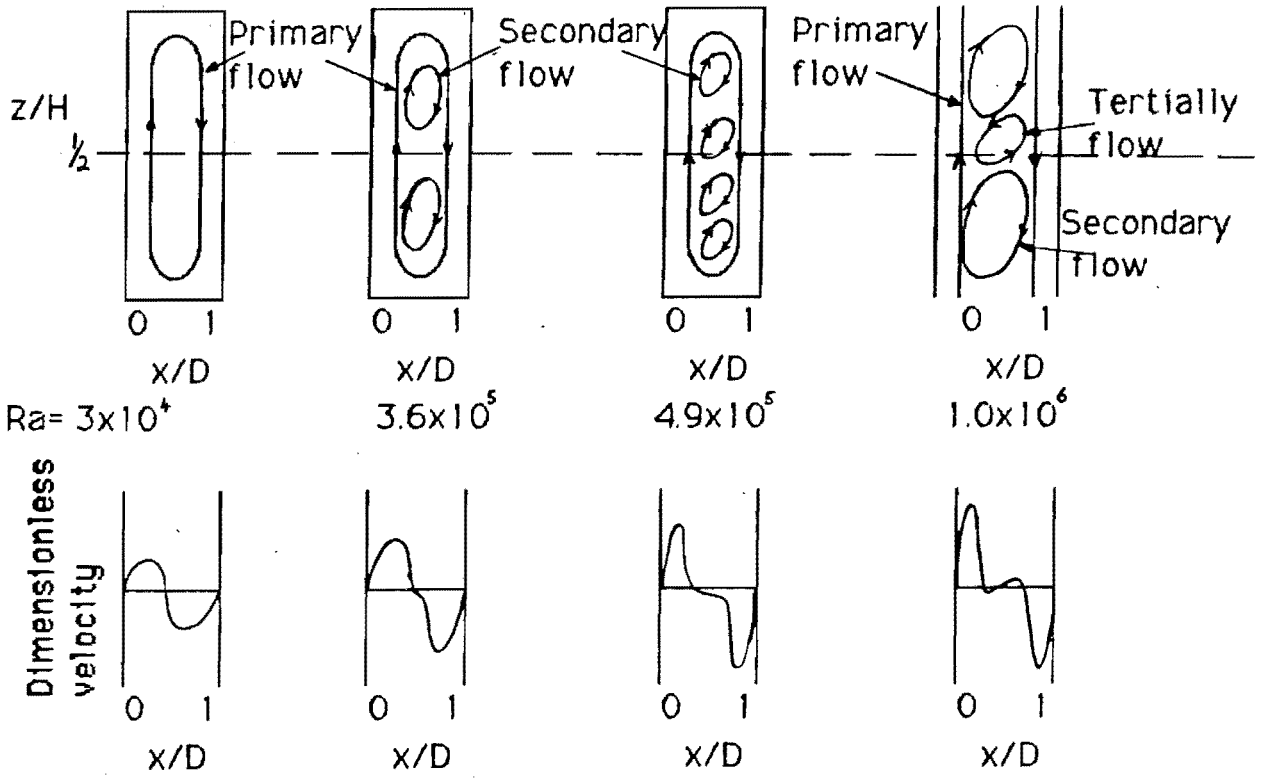

Fig. 2.3 Flow profiles and corresponding velocity profile at mid-height of cavity i.e. z/H= 1/2 for a cavity with A = 20, Pr=1000 and d = 4 cm.

It must be emphasized again that the above flow structure was observed by Elder in a cavity with a large aspect ratio "A" greater or equal to 20 and Pr=1000. For a nearly square cavity, different form of secondary and tertially flows were induced as seen in figure 2.4.

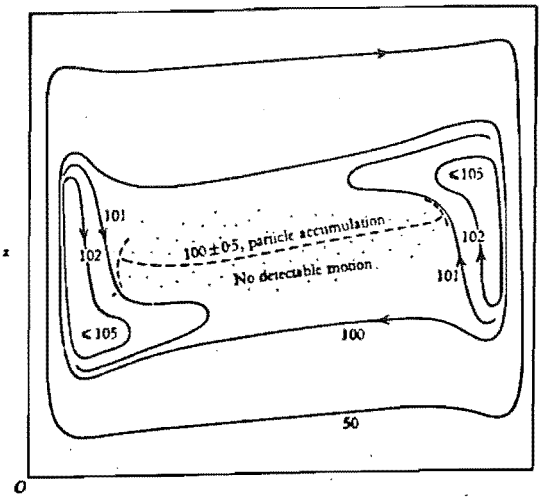

Fig. 2.4 Laminar streamline in a nearly square cavity at Ra= 9.6×10^6.

This flow structure was confirmed by the numerical calculation of Quon[26] using a laminar flow model and later by Markatos[108] using a turbulence model.

Thus it can be seen that the reverse tertiary flows generated for a cavity of large aspect ratio (A > 20) were situated between the secondary cells and lay in a line near the middle of the cavity. For a small aspect ratio (say A=1), the reverse flows generated were at both side of the cavity near to the vertical boundary.

Gill [4] has studied the two-dimensional convective motion analytically for the boundary layer (high Rayleigh number) case. He used air as the fluid for which Pr = 0.71. He made use of the boundary-layer approximation to the set of governing equations for mass, momentum and energy transfer. He then assumed that a stratified fluid cone existed far away from both vertical walls. Boundary-layer solutions were then obtained near the two vertical walls. Matching the boundary-layer solution with the core solution led to a consistent picture for the free-convection pattern in the cavity, but because of the boundary layer approximation adopted, his solution cannot satisfy all the boundary conditions physically

present along the top and bottom horizontal walls. The desired conditions are walls impermeable to mass flow and a cavity that is adiabatic. Gill was able to choose the conditiion of impermeabnility only to obtain solutions which he claimed compared favourably with Elder's experiments [5]. The discrepancy that he noted was accounted for by the variation of air properties with temperature in his opinion. The general behaviour of the cavity was well demonstrated in regard to the entrainment of fluid by the boundary layer in the lower half of the slot and ejection by the boundary layer in the upper half on the warmer wall.

Quon [28] argued that the condition of impermeability as chosen by Gill did not always represent the flow condition. He attempted to improve on Gill's solutions by matching them with a numerical solution for the stream-function and vertical velocity profile in the cavity and obtained improved agreement with experimental values.

Bejan [30] claimed that as Gill's solution was a discontinuous approximation of the real velocity profile, the solution could be improved in principle. He made use of the "net-upward flow of energy" in the cavity and set it equal to zero near the top and bottom horizontal walls. In this, the boundary conditions of impermeability and adiabatic top and bottom walls are simultaneously satisfied. His results agreed well with available experimental and numerical data.

The effect of a variety of horizontal, dynamic boundary conditions was studied by Quon [26], using seven finite-difference compulations for $Ra=10^6$ ie.boundary-layer flow. His results indicated that the various horizontal boundary conditions virtually made no difference to the main boundary-layer flow. The scaled velocity fields in the vertical boundary layers were independent of Rayleigh number and to a large extent Prandtl number when the two vertical boundary layers were distinct (the last result was also deduced by Gill [4]).

Morrison and Tran [31] have measured the fluid velocity profile at $Ra = 5 \times 10^4$ and $A = 5$ using the technique of laser-doppler anemometry. The three-dimensional flow structure was determined and it was found that the end-wall conduction affect the whole flow structure. Unless the end (side) walls were

insulated properly, the two-dimensional flow approximation would break down and three-dimensional flow would set in. They also concluded that the horizontal boundaries(top and bottom) exert little influence on the vertical flow pattern, as the velocity profiles in the central section of the cavity were observed to be independent of those boundaries.

Another excellent article on the visualization of flow in a narrow vertical cavity is that by Seki et al [29]. Several kinds of fluid were used to test the effects of Prandtl number over the range from 4 to 12,500. The effect of cavity width was also investigated by varying the aspect ratio A from 6 to 30. This supplemented the experiment of Elder [5], reported earlier, as he only investigated the effect of Rayleigh number Ra. Polystyrene spheres 0.2 mm in diameter were first introduced as a more effective form of tracer particles than the traditionally-used aluminium powder. The flow patterns obtained agreed with Elder's result i.e. consisted of primary, secondary and tertiary flows, depending on the value of Ra. The results also indicated that flow pattern depended considerably on Pr and cavity width L. The flow pattern in the fluid layer is easily shifted from laminar flow to transitional flow, which is partially turbulent, by decreasing the Prandtl number and increasing the cavity width L for a given Ra.

de Vahl Davis and Mallison [65] studied the secondary and tertiary motions numerically for aspect ratios A up to 20 and Rayleigh numbers up to 3×10^6; Pr was equal to 1000. The numerical model was successful in generating the complex secondary and tertiary motion observed by Elder [5].

Lee et al [103] also presented numerical solution of multicelllar natural convection in long cavities of aspect ratio from 5 to 20 and Pr ranged from 0 to 1000. For air as the fluid in the cavities, it was observed that the transition from a unicellular to multicellular flow was depended not only on the Grashof number, as observed by Elder[5], but also on the aspect ratio. For Gr=15000, multicellular flow was observed only in cavities with A greater than 12.5. In another paper [104], the same authors and Drummond demonstrated that it was possible to switch from unicellular to multicellular and back to unicellular flow

merely by changing the aspect ratio of the cavity. The fluid used was air and the range of aspect ratio tested from 10 to 20, with Gr based on cavity height of 6.4×10^7. It was therefore apparent that a combination of Gr, Pr and A would determine the type of flow structure in a cavity, but a broad generalisation of flow is often difficult.

Mallison and de Vahl Davis[111,132] studied three-dimensional natural convection in a rectangular box [132] and a cube [111] using finite-difference methods. Ra ranged from 10^4 to 10^6, with Pr= 0.7, 1.0 and 100. Flow structures were described in terms of particle tracks, while the condition of the end wall was shown to influence the flow structure. The flow structure basically consisted of spirals at each end of the box and symmetrical with respect to the central vertical plane. But the flow's fine structure was rather complex. A full description can be found in the work cited.

2.1.2. Flow Patterns in Horizontal Cavity.

SEE PAGE 17

2.1.2.1 Horizontal Cavity Heated From Above. This corresponds to a stable condition. As long as the temperature of the top plate is greater than the temperature of the bottom plate, and both plates are maintained at constant temperature, no convection exists for a fluid whose density decreases with an increase in temperature [36]. The air between the plates is stratified with a positive temperature gradient extending upwards.

Luikov et al [25]have considered the stimulation of natural convective flow by heating from above and obtained the result that the temperature of the top plate should either be non-uniform or variable with time. The flow was observed experimentally and theoretical predictions were validated. [Chapter 7, Ref 36].

The suppression of free convection for a downward-facing heated plate only occurs in a confined cavity and does not happen for an isolated plate in a body of fluid. In such cases, the "hydrostatic pressure gradient in the direction normal to the plate is first induced, and then its horizontal gradient acts as the direct motive force of convection" [124]. The convective air is

SEE PAGE 17

being able to escape from the bottom of the plate via the unconfined edges and thus convection is being maintained. [120, 121, 123,124]

2.1.2.2 Horizontal Cavity Heated From Below. Distinction has to be drawn between a "horizontal layer" and a "horizontal enclosure" [67,118]. A fluid layer is an enclosure whose horizontal length and width dimensions have been made so big with respect to its gap thickness that the vertical side walls have ceased to effect significantly the natural convection in the cavity. The same distinction also applied to an Inclined Cavity described in 2.1.3.

2.1.2.2.1 Horizontal Fluid layer. Natural convection of an infinite horizontal layers of fluid heated from below was first observed by Bernad [36] in 1901 and hence often termed the "Bernad Problem". Other early investigators were Lord Rayleigh [39] and Jeffreys [40],[41]. From their work it was concluded that the sole parameter determining stability was the Rayleigh number which is a measure of buoyancy compared to viscous and conduction effects. No fluid motion was observed until the critical Rayleigh number, $Ra_{critical}$, was reached. $Ra_{critical}$ was found to have a value of around 1708 although higher values around 1800 [9] and 2300 [63] have also been reported. The flow field has a structure made up of fairly circular roll cells, inside which the flow moves upward and near the rim of which it moves downward [36].[This is different from the original hexagonal cells observed by Bernad which was actually due to surface-tension effects rather than gravity [67]).The flow is laminar, but with increasing Rayleigh number Ra, it becomes more complicated as it undergoes transition to turbulence. Even in the laminar connection regime the flow is not steady with position or time, and it is sometimes hard to distinguish between "rolls" and "cells" when observing the pattern of the flow.

One of the most successful investigations of the onset of turbulence was by Malkus [42, 43]. He first experimentally determined the transition from laminar to turbulent flow using an apparatus which approximated to two infinitely-horizontal

conducting surfaces. He found six discrete transitions in the heat-transfer curve between Ra = 1700 and Ra = 10^6. He explained the discrete transitions in terms of a progressive transition from laminar to turbulent flow. In a subsequent paper[43], he attempted to predict the various transitions using a statistical analysis. He assumed that the heat transport between the plates was a maximum and the temperature gradient would be no where positive. The temperature distribution is represented by a truncated series of Fourier modes, the highest wave number (smallest eddy size) being assumed to be the mode which is marginally stable for the given mean temperature profile. The smallest eddy size is then thought of as a parameter representing the stability restriction on the fluid motion. The spectrum of connecting motions was then determined in terms of this minimum eddy size. His mathematical manipulation was elaborate and difficult to understand. The agreement of his theory and experimntal results for the occurance of the various transitions in heat flow was within 10 percent..

2.1.2.3 Horizontal Enclosures Every fluid-filled horizontal enclosure is characterised by a critical Rayleigh number $Ra_{critical}$, which depends upon the enclosure's various geometric and thermal properties. $Ra_{critical}$ has been successfully calculated for the many principal cross-sectional shapes and their values can be readily obtained from the many correlations given [27,67].

Ozoe and Churchill [45] have reported on the effect of several boundary conditions on the orientation of roll-cells in a rectangular channel heated from below. The prefered mode in a channel heated from below and cooled on the top was found to consist of a series of two-dimensional roll-cells with the axis horizontal and perpendicular to the long dimension of the channel (Fig 2.5). Complete numerical solutions were developed for this mode of motion in the same paper.

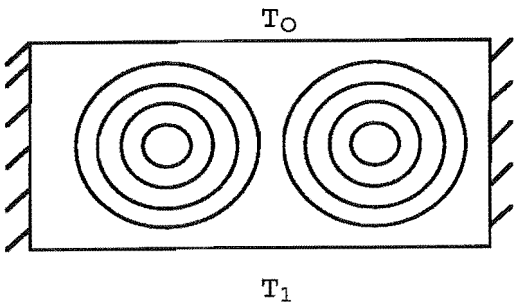

FIG.2.5 Roll-cells in a rectangular channel

$T_1 > T_O$

Oertel[106] used the technique of differential interferometry to study natural convection in a horizontal fluid layer heated from below. He presented flow fields in the form of interferograms for Ra from 1900-6300.

Linthorst et al [105] used smoke-injection and laser-anemometry techniques to study the convective flow in cavities of aspect ratio of 0.25 to 7.0. The cavities were orientated between 0 and 90 degrees to the horizontal. For the case of the horizontal cavity, the number of stable roll-cells was dependent on the aspect ratio of the cavity and the side walls have a great influence on the number of rolls.

The three dimensional flow pattern has also been studied by some investigators [110,116,117]. Streak-lines of particle paths in the laminar region are generally double helices and are confined to one or the other half of a roll-cell. More complicated fluid motions are also described in these papers (as Ra is increased). For the cubical enclosure, Churchill et al [63] have obtained the critical Rayleigh number to be 3500 by extrapolation to Nu = 1, which agreed with the computed value of 3446 by Cotton [51] and the experimental value of 3700 by Heitz and Westwater [52].

Features of the flow with a heated protuberance placed at the bottom of the cavity have been studied by Klyushniknov [47] and Petrazhitskiii [48] The vertical face of the heater projection ensured that at any Rayleigh number greater than zero, there is a weak fluid motion; and at Ra approximately equal to 7100, circulation currents commenced. At Ra approximately equal to 71000, warm currents ascend along the vertical surfaces of the protruding section, curve along its upper horizontal surface continue to the upper cold surface of the cavity, and finally descend along the side wall of the space, see Fig.2.6.

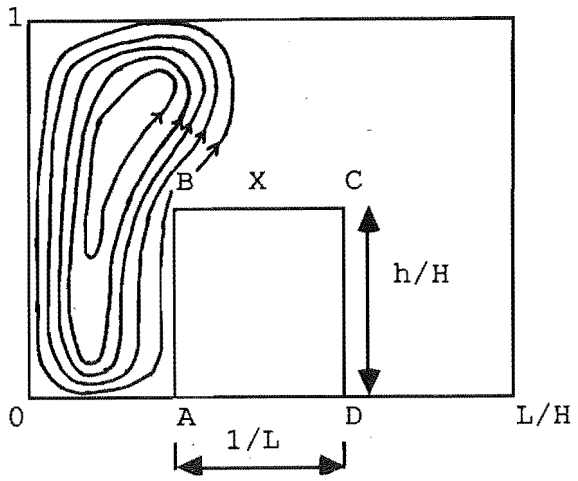

Fig 2.6. Streamlines in flow region. (L/H = 1; h/H = 0.5; 1/L =1/3; Ra= 4 x 10^5 . ABCD is the heater projection) X is the stagnation zone, ie. no flow. Flow in one side is illustrated only.

With increasing Rayleigh number, this pattern either developed further resulting in the displacment of the vortex centre upwards or a disintegration of this pattern and the development of a new one. The new pattern had a main vortex, whirling in the direction opposite to that of the vortex in the first pattern and occupied the originally-stagnant zone X above the heated protuberance. Kaviany[109] studied the effect of a semi-cylindrically-shaped protuberance located at the bottom of a square cavity with differentially heated vertical walls. The maximum value of Ra was 10^4 for Pr=0.71. Only one cell was observed to form in the cavity (the same as that observed in the absence of the protuberance) except at the lower corner next to the cold vertical surface and in the area near the intersection of the protuberance and the bottom surface where the flow was reduced. Thus, the type of protuberance present in the cavity would have had a great effect on the resultant flow pattern.

2.1.3 Inclined Cavity.

Hollands and Konicek [21] have studied the natural convection of an air layer in an inclined cavity of large aspect ratio (A=41). Their apparatus consisted of two parallel copper plates and was placed in a vacuum vessel whose pressure can be varied. The flow structure was found to resemble that in a vertical cavity for angle of inclination of greater than 75 degrees to thehorizontal. For

angle of inclinations less than 75 degrees, the flow structures resembled that in a horizontal cavity. Critical Rayleigh numbers $Ra_{critical}$ for various inclinations governing the stability of inclined air layers was investigated . The $Ra_{critical}$, which is the Rayleigh number when convection significantly increases the rate of heat transfer, increased from 1900 for an inclination (to the horizontal) of 15 degrees to about 8000 for vertical (90 degrees) inclination for an air layer with Pr = 0.71. The result was in agreement with the predictions of Unny [23] and Hart [24].

Ozoe, Sayama and Churchill [50] have experimentally investigated the flow in an inclined cavity of moderate aspect ratio (ie.an inclined enclosure) . Their apparatus consisted of copper plates at the top and bottom and adiabatic side plates in the form of a long channel of square cross-section. Their bottom plate was hinged to a large desk so that the inclination of the channel could be changed. The bottom plate was kept at a higher uniform temperature than the top plate. The flow observed consisted of two-dimensional roll-cells with their axes perpendicular to channel when it was placed in the horizontal orientation. When the channel was rotated through 90 degrees, so that one vertical side was heated and the other cooled, a long two-dimensional roll-cell appeared. When the degree of inclination was decreased step by step from 90 degrees, the long two-dimensional cell kept its shape down to about 10 degrees of inclination to the horizontal. Between 10 degrees and zero inclination (to the horizontal), complex flow patterns appeared which suggested the possibility of multiple, stationary modes. When the channel was kept almost horizontal, with say less than 1 degree of inclination, a series of side-by-side, two-dimensional roll-cells eventually were established. Thus a long two-dimensional roll-cell was the prefered mode in a long square channel with an inclination greater than 10 degrees. Below 10 degrees side-by-side rolls or even more complex behaviour mostly took place. The above flow patterns were necessarily restricted to Ra less than 8000 and applicable only for laminar natural convection.

SEE ERRATA

Subsequently Ozoe et al [133,134] reported that the angle of inclination for the transition in the mode of circulation depends

strongly on the aspect ratio. This is then supplemented later by the publication of the fine structure of the transition of flow from zero up to a 7-degree inclination to the horizontal using a flow visualization technique [116]. Corresponding numerical results were presented in a companion paper [117]. Symons[107] studied flow pattern in a rectangular slot(aspect ratio very much less than 1.0) which can be orientated at various angles to the horizontal. The aspect ratio used varied from 6 to 12. From the horizontal cavity position up to an angle of inclination of 15 degree to the horizontal, the convective flow comprises counter-rotating cells as found in other studies. This form of flow pattern would transform to the unicellular pattern of a vertical cavity at an angle of inclination of 24 degrees for the longitutinal slot, and at 78 degrees for the transverse slot, respectively.

2.2 HEAT TRANSFER IN CAVITIES.

2.2.1. Vertical Cavity.

2.2.1.1. Temperature Field Regimes. As for the flow, the heat transfer across a vertical cavity is governed by three dimensionless parameters:

(i) Prandtl number Pr;

(ii) aspect ratio A and

(iii) Rayleigh Number Ra = Gr.Pr.

(for definition, see 2.1.1.)

For a given fluid over a limited temperature range (constant Prantdl number), the temperature field resulted from heat transfer can be classified into three regimes. These regimes are called conduction, transition and boundary-layer regimes, depending on the aspect ratio and Grashof number. [1, 3, 12, 53]. The criteria given by various authors differ but, all generally agree with the limits given by figure 2.7.

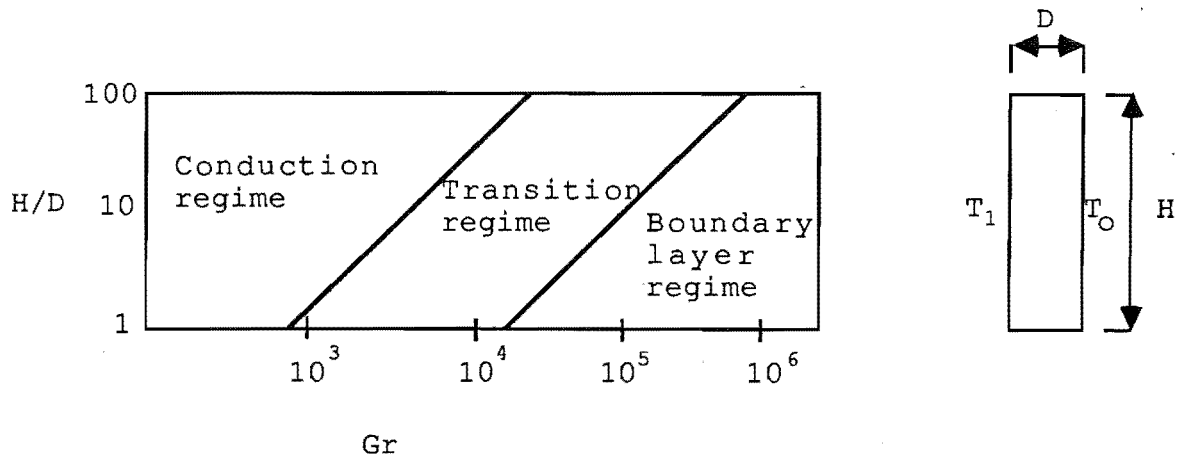

Fig.2.7 Various temperature field regimes.

H/D - aspect ratio; height /thickness of air gap
Gr - Grashof number based on gap thickness.

The conduction regime is characterised by a constant temperature gradient across the cavity [3,53] and the main heat-transfer mode across the cavity is by conduction. A weak base flow described in 2.1.1. exists, but only assists the heat transfer near the end regions. (Fig.2.8).

The boundary-layer regime is characterised by large temperature gradients near the wall and a nearly isothermal core with a positive temperature gradient(Fig.8). The heat transfer is mainly by convection, but conduction is also present. Flow is still vertical primarily, and is well-developed,although a horizontal strong inflow and an outflow also exist. Both laminar and turbulent flow regimes are possible, depending upon the values of the aspect ratio and Grashof number based on air-gap thickness.

The transition regime is found between these two regimes mentioned above. Here the temperature profile is curved everywhere and heat transfer is by free convection and conduction. It is the extreme case of the boundary-layer regime where the two boundary layers touch each other (Fig 2.8). Much stronger flows in than the conduction regime occur but still a single cell exists mainly in the laminar-flow regime.

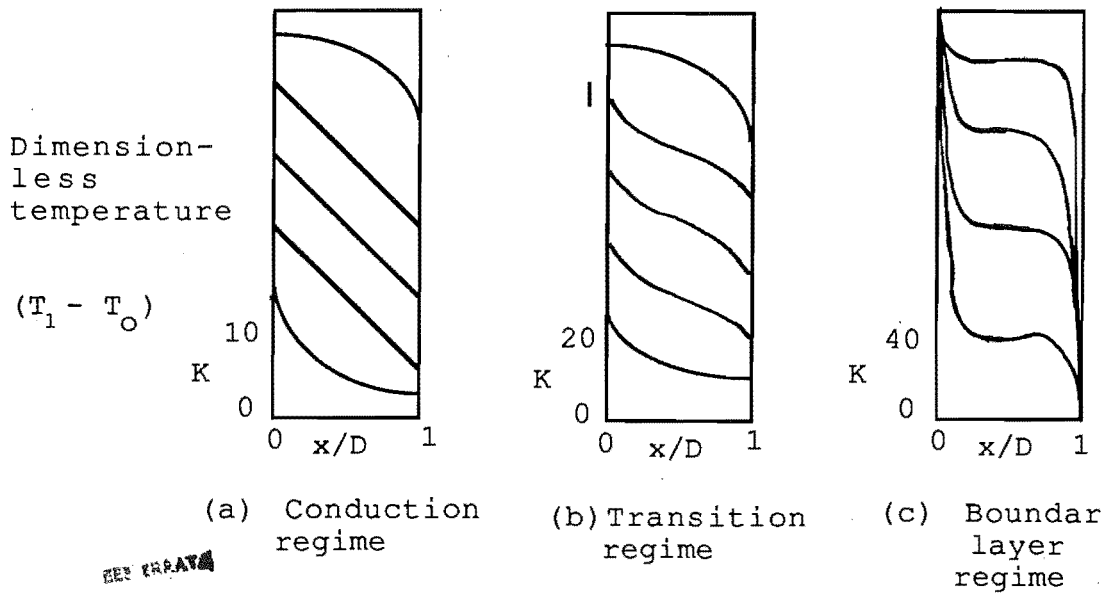

Fig.2.8 Temperature field in a vertical cavity. (scale indicated are for lowest line. Other scales are shifted vertically.)

The fact that one can manupilate the aspect ratio of the cavity to cut down on the rate of heat transfer was demonstrated in a paper by Probert [125].

2.2.1.2. Heat-Transfer Rate. As the heat-transfer rate is related directly to temperature field via the temperature gradient,

the governing parameters are again Ra (or Gr), Pr, and aspect ratio A. The heat-transfer coefficient is often expressed in the dimensionless form of the Nusselt number Nu, where:

$$Nu_L = h\ L/k = f(Ra, Pr, A)$$

where Nu_L = Nu based on thickness of gap L

h = heat-transfer coefficient

k = thermal conductivity

L = width or thickness of gap

and A = aspect ratio.=H/L

In the conduction regime,

$$q_c = k\ A_q\ (T_1 - T_2)/L \text{ for the cavity.}$$

$$= h\ A_q\ (T_1 - T_2)$$

where q_c = heat-transfer across the cavity

A_q = cross-sectional area of heat-transfer.

It follows that h.L= k and Nu_L= 1.

If the data are for one fluid only and the temperature range of the data is suffiently small, then Pr may be considered as constant and thus:-

$$Nu_L = f'(Ra, A)$$

Further, since Ra = Gr x Pr,

$$Nu_L = f''(Gr, A).$$

First elaborate experiments to determine the Nusselt number were performed by Mull and Reihner [54] with air for the boundary-layer regime case when convective heat transfer is important. Jakob [49] simplified and generalized Mull and Reihner's vast amount of data and presented the expressions:

$$Nu_L = 0.180\ (Gr_L)^{1/4}\ A^{-1/9} \text{ for } Gr_L = 2 \times 10^4 \text{ to } 2 \times 10^5 \ldots (A)$$

$$Nu_L = 0.065\ (Gr_L)^{1/3}\ A^{-1/9} \text{ for } Gr_L = 2 \times 10^5 \text{ to } 1 \times 10^7 \ldots (B)$$

Both equations (A) and (B) are valid for cavities with aspect ratios from 3 to 42. Eq.(A) corresponds to the laminar

free-convection case, while Eq.(B) corresponds to the turbulent-free convection case.

Since then, the form $Nu = C_v(Gr)^n(A)^m$, has been adopted widely by the investigators in latter years although the values of C_v, n and m are often different.

Batchelor [1] studied the same problem analytically for three special cases:- (i) small Ra ($Ra \approx 1000$) with A approximately equal to one; (ii) any Ra with large A and (iii) large Ra with any A. He was able to obtain the solution for case (i) and rough approximations for cases (ii) and (iii). He came to the conclusion that the flow and heat transfer depend on Ra and A (aspect ratio) for fixed Pr. For his cases (i) and (ii), he deduced a linear temperature gradient in the central portion of the cavity and heat transfer was by conduction only. For his case (iii), he proposed a boundary layer along the outer surfaces, and a vortex core of uniform temperature, which is supported by the work of Poot's [55].

Eckert and Carlson [3] have studied the temperature field in a air-filled cavity using a Zehnder-Mach interferomter. The aspect ratio A ranged from 2.1 to 46.7, while Ra ranged from 200 to 2×10^5. Ra was changed by varying the temperature difference and physical dimensions of the cavity. The various heat-transfer regimes described in 2.2.1.1 were observed. Nusselt number expressions of the form Nu = f(Gr, A) similar to those of Jakob [49] were proposed for the various regimes. However, in the boundary-layer regime the core of the cavity was not found to be isothermal as predicted by Batchelor [1], but instead the temperature was uniform along horizontal lines only and increased in the vertical direction. Their findings were supported by Wilkes [55], who had solved the transient and steady-state problem for natural correction in rectangular cavities by a finite-difference method.

Experiments which further supported the stratified-core behaviour were performed by Elder [5]. His experimental conditions were similar to those studied by Wilkes [55] with aspect ratios ranging from 1 to 60, Pr = 1000 and Ra 10^8 .

To improve Batchelor's solution for large Rayleigh numbers, Gill [4] analysed the configuration studied experimentally by Elder [5]. By an order of magnitude argument, Gill was the first to

show analytically that there can only be horizontal motions for the core and the temperature can be a function of vertical co-ordinate only as found by Eckert [3] and Wilkes [55].

A numerical study similar to that of Wilkes [55] was made by de Val Davis [32] for steady flows in which Ra ranged from 10^5 to 10^6. Again horizontal isotherms in the core were indicated, with the slope of these isotherms tending to become negative for increasing Ra, ie heat could be transported back from outside the boundary layer on the cold wall to the region outside the boundary layer on the hot wall, although the overall heat transfer was from the hot wall to the cold wall by convection. The reverse flow of heat was related to the secondary flow generated, as observed by Elder[5] and described in Section 2.1.1.

Elder's [5] experiment was supplemented by Nobuhiro [29] when the effect of cavity width and Pr was investigated. Three working fluids: water (Pr = 7.1), transformer oil (Pr = 480) and glycerine (Pr = 12500), were used. Aspect ratio ranged from 6 to 30 and the experiment was conducted in the laminar to transition flow regime. As expected, the mode of laminar, convective heat transfer was shifted to transition heat transfer at smaller Rayleigh numbers as A was decreased. The secondary and tertiary flows observed did not contribute much to the heat transfer between the two vertical walls during the laminar-flow region. However, this contribution was increased during the transition flow region.

Yin et al [12] has extended the study of free-connective heat transfer to a cavity with large absolute dimensions. The height of the cavity equaled to 1 meter, with aspect ratio ranging from 4.9 to 78.7. Grashof numbers ranged from 1.5×10^5 to 7.0×10^6 and air was the fluid used. Similar to other test rigs of smaller dimensions, the various temperature field regimes described in Section 2.2.1.1 were observed. The dimensionless temperature ratio = $(T-T_o)/(T_1-T_o)$ (where T, T_o and T_1 were temperature of fluid, cold wall and hot wall respectively for a given height) was found to be independent of the temperature difference between the plates for temperature difference from 20 to 80 degrees C. Also, for A=H/D less than 10 and large Ra, a temperature inversion similar to that predicted by de Val Davis [32] was observed. Nu_L

was found to depend on Gr_L and only to a small extent on the aspect ratio A. (Pr is constant)

Said and Trupp[7] have studied laminar free convection numerically in a vertical cavity with an adiabatic top and bottom with mixed boundary conditions, i.e. the cold wall was maintained at constant temperature while the hot wall was subjected to a uniform heat flux. Air was the fluid used(Pr=0.7), the aspect ratio A ranged from 0.5 to 15 and Ra ranged from 690 to 1.3×10^6. For A greater than 2, Nu is known to increase as A decreases. Since $Nu_L = 1$ as A tends to zero, Nu_L must peak at some value of A between 0 and 2.0 and in this range its dependence on the intermediate cavity dimension L reverses. It was found that the average Nu_L peaked at an aspect ratio of about 1.5 i.e. at this aspect ratio, the change from the transition regime to the boundary-layer regime was occuring for minimum possible value of Ra. Similar results were presented by the same authors for cavity with uniform boundary conditions [127].

Recently Elsherbiny et al [115] proposed a correlation applicable over the range for Ra from 10^2 to 2×10^7 and aspect ratio from 5 to 110 as:-

$$Nu_1 = 0.0605\ (Ra)^{1/3}$$

$$Nu_2 = (1+(0.104\ Ra^{0.293}/(1+(6310/Ra)^{1.36}))^3)^{1/3}$$

$$Nu_3 = 0.242\ (Ra/A)^{0.272}$$

$$Nu = (Nu1, Nu2, Nu3)_{max}$$

which is a form quite different from that proposed by Jakob mentioned earlier. Agreement with other eperimental data was good for aspect ratios between 5 and 20, but the agreement became poorer at aspect ratios between 40 and 110 when compared with the results of Yin et al [12] and Randall et al[131].

For moderate to small aspect ratio , Said and Trupp[127] had presented a correlation of the form $Nu = C\ (Ra)^m$. Values of C and m were given for each aspect ratio from 0.5 to 5.0 in steps of 0.5.

2.2.2 Horizontal Cavity.

2.2.2.1 Horizontal cavity heated from the top. The heat transfer is by conduction for cases where the top plate is kept at a higher uniform temperature than the bottom plate and with isothermal or adiabatic side walls. The steady-state heat flow "q" is calculated from:

$$q = -k A_q (\Delta T)/L$$

where k = thermal conductivity;

A_q = heat-transfer area;

ΔT = temperature difference between the plates;

and L = air layer thickness.

The temperature profile is linear across the cavity and Nu is equal to 1.

2.2.2.2 Heating from below - Horizontal cavity.

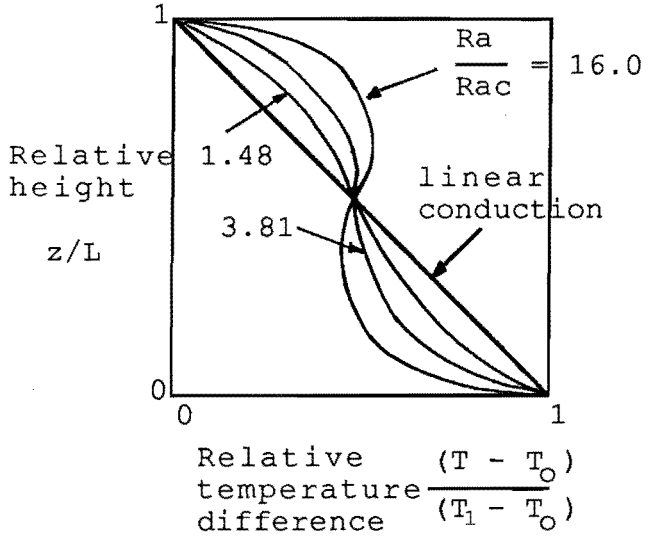

Fig.2.9 Dimensionless temperature profile across a horizontal cavity for various Ra

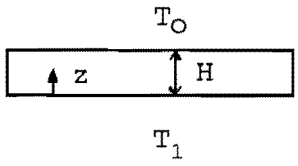

As mentioned in section 2.1.2.2; there is no flow for Ra less than $Ra_{critical}$; and hence heat flow between the plates is by conduction. The temperature gradient is linear and Nu =1. For Ra greater than $Ra_{critical}$, convective flows set up and the heat transfer is by both

conduction and convection. At high values of Ra, convection is the main form of heat transfer. A typical temperature profile of a horizontal fluid layer for various values of Ra is given in Fig.2.9 [36,57].

Thus the fluid-temperature profile at high Rayleigh numbers shows a boundary-layer-type structure, with an essentially isothermal inner region and high temperature gradients near the surface. Thermals, which are localised bursts of warm fluid breaking away from the regions near lower(hotter) surface and a key heat transfer mechanism of turbulent thermal convection, was observed in water but not in air.[37].

In the turbulent convection regime, it was proposed by Malkus in a theoretical study [43] that the temperature defect ΔT_z followed an inverse distance(z) law, where z is the vertical coordinate and ΔT_z is the difference of temperature between any point at Z with mid-plane temperature T_f, T_f being the average of the face temperatures T_1 and T_2. Herring [44,46] has similarly found the temperature defect to follow the inverse-distance law by a numerical analysis.

Chu and Goldstein [9] have investigated this behaviour over the range of Ra from $6x10^5$ to $6x10^6$ and $9x10^6$ to $2x10^8$ experimentally using a Mach-Zehnder interferometer and find that although the temperature defect followed the inverse-disrance behaviour, the experimental values were some what higher than theoretical values, ie.the variation of ΔT_z with distance were similar, but absolute values of ΔT_z were different. The discrepancy seemed to be smaller at higher Ra values.

Some other authors, eg.Kraichaan [60] who use a mixing length approach, find that the temperature defects ΔT_z varies as z^{-1} near the wall and as $z^{-1/3}$ away from the wall.

For heat transfer, Malkus [43] has found that Nu was proportional to $Ra^{1/3}$ for the free-convection turbulent regime. Howard [61], in a similar analysis following Malkus, has obtained Nu to be proportional to $Ra^{3/8}$ for large Ra, while Fromm [62] found

Nu was proportional to $Ra^{0.296}$ .All the above theoretical analysis seem to suggest Nu is independent of aspect ratio for the horizontal case at large Ra for a horizontal fluid layer.

O'Toole and Silveston [58] have presented a summary of the results for heat-transfer experiments up to 1961. Based on the experimental data of five studies, they have proposed the following correlations for free-convection heat transfer:-

Regime	Ra Range	Equation
Initial	1700 - 3500	$Nu= 0.00238\ (Ra)^{0.816}$
Laminar	3500 - 10^5	$Nu= 0.229\ (Ra)^{0.252}$
Turbulent	10^5 - 10^8	$Nu= 0.104\ (Ra)^{0.305}(Pr)^{0.084}$

Both Nu and Ra are calculated in terms of the gap dimension.

The above results were claimed to be applicable for a horizontal fluid layer as well as a completely enclosed region of aspect ratio (length/thickness)greater or equal to 2. It appeared that the effect of Pr is only felt on the turbulent regime and the aspect ratio does not influence significantly on the heat transfer.

From the above results it appears that the Rayleigh number is the single most important parameter in determining heat transfer between confining parallel horizontal plates, as predicted by the theoretical studies.

Goldstein and Chu [9] have studied heat transfer with turbulent thermal convection of a horizontal fluid layer and obtained the correlation $Nu = 0.123(Ra)^{0.294}$ for Ra ranging from 6.88×10^5 to 1.23×10^8 which agrees well with O'Toole's [58] results as quoted above.

These experimental results tend to suggest that Nu is proportional to $Ra^{0.3}$ for Ra greater than 10^6; although Jakob [63] in one of the earliest publication had obtained Nu proportional to $Ra^{1/3}$ using the experimental data of Mull and Reihner [54].

Hollands et.al.[64], in an experiment covering Ra from sub-critical values to 4×10^6, obtained results which, when combined with the data of Goldstein and Chu [9] previously mentioned, yield Nu proportional to $Ra^{1/3}$ as Ra tends to infinity. It thus appears that, depending on the range of Ra values chosen, a best-fit

correlation found by, say, a least-squares technique can give no certain dependence of Nu on Ra.

Another form of correlation given in the literature is of the form,

$$Nu = 1 + C(1-Ra_c/Ra) + D((Ra/B)^{1/3}-1)$$

as presented by Hollands et al [21,59,64]. Ra_c is the cricital Rayleigh number for the onset of convection, normally taken as equal to 1708 for a horizontal fluid layer. Goldstein and Chu [9] have attempted to fit their experimental data to an equation of this form, but find that the fit was poorer than a correlation of the form $Nu=C(Ra)^m$, as given by O'Toole and others [58].

More recently Hollands [118] modified the correlations given in [64] for air and water and presented an altered form of the correlations which fits all reliable available experimental data relevant to horizontal layers, regardless of the Prandtl numbers. A correlation for horizontal enclosures was also given which requires the calculation of the appropriate critical Rayleigh number. Methods of calculating $Ra_{critical}$ can be found in references [27] and [67].

Prediction of the overall Nusselt numbers based on a theoretical calculation for a rectangular enclosure of arbitrary dimensions, heated from below, was presented by Ozoe et al [135]. It is however restricted to Ra less than 2×10^4 but is applicable to all aspect ratios greater than unity.

Other forms of Nu-vs.-Ra correlations for conditions such as a heated projection was placed at the bottom of the cavity or variable top wall temperature con be found in references [47] and [48].

2.2.3. Inclined Cavity.

Comparatively less work has been done on the inclined-cavity case. Ozoe and Churchill [50] have experimentally and numerically computed values for Nusselt numbers for natural-convection heat transfer in an inclined square channel. The range of computation was limited to Ra up to 8000,ie. the laminar convection region.

The maximum rate of heat transfer is found to occur at an angle of inclination of about 50 degrees to the horizontal and minimum rate of heat transfer occurs at about 10 degrees of inclination. Thus the orientation of a cavity to the horizontal has an effect on the rate of heat transfer.

Churchill [67] gave correlations of Nu as a function of the modified Rayleigh number and the angle of inclination θ to the horizontal for an inclined channel:

$$Nu = f(Ra \cos\theta, \theta)$$

for range of θ from 0 to 180 degrees. The Nusselt number for an inclined cavity of large aspect ratio decreases almost continuously as θ is increased from 0 to 180 degrees. But for a cavity of moderate aspect ratio, the behaviour of Nu is known to decrease to a minimum value, then increasing to a maximum and thereafter decreasing to unity for heating from above (θ =180 degrees). Some uncertainties still exist for Nu values for an inclined cavity of moderate aspect ratio.

Elsherbiny et al [115] have measured the heat transfer for an inclined air layer and presented a Nu= f(Ra) correlation for θ =60 degrees. A procedure to interpolate Nu values between 60 and 90 degrees was given. A correlation for a cavity of large aspect ratio and for θ from 0 to 60 degrees was given by Hollands et al [136].

2.3.1 Prediction of moisture condensation in cavities.

Very little work on moisture transfer in a building cavity has been found, although the adverse effects of excessive moisture condensation on building structure has long been realised. Traditionally the method used to predict the occurance of moisture condensation in building cavities had assumed that the moisture diffusion from the living space through the wall or ceiling components to be the only source of moisture. Steady-state heat and vapour-diffusion processess were also assumed. One common example of such method is the "dew point-profile" method, as outlined in the ASHRAE Handbook [66]. The success of the method depends on the choice of "design values" used in the calculation, eg.that of indoor/outdoor temperature and vapour pressure values which would normally be obtained from experimental measurements or from previous knowledge. The result of the calculation is illustrated below for a case which would indicate a high risk of condensation on the cladding board and part of the cavity space:-

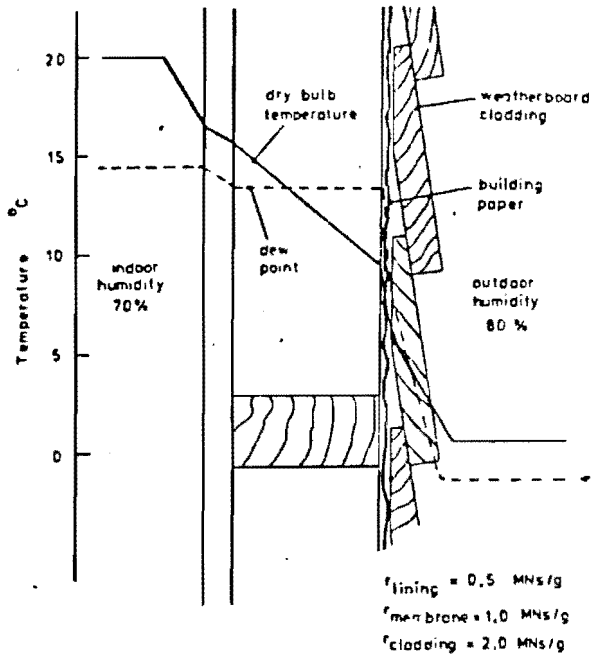

Fig.2.10 Dew point profile for traditional timber wall without cavity ventilation. In this case it indicates a serious risk of condensation on the building paper and cladding. (Figure from Trethowen[13]).

This method of predicting cavity moisture condensation has

been critically examined by Trethowen [13] who concluded that it did not produce a satisfactory result for New Zealand conditions if extreme winter conditions were to be used as design values. This procedure would involve the assumption of unexceptionally high vapour-pressure design values and did not consider the possible moisture-adsorption property of the timber structure. The use of mean winter conditions, however, has produced satisfactory results due to the long response time of the timber-frame structure to moisture changes in the air.

In a subsequent paper, Trethowin [68] proposed the Keiper method for predicting moisture condensation in buildings. This method, although in a crude sense, includes the source of moisture production not only from the occupants' living activity, but also from the moisture present as a result of wet construction materials, evaporation from the ground as well as moisture from air infiltration. Since the "dew point-profile" method only assumes moisture production from the living activity of occupants only; the Keiper method respresents a more realistic approach to the problem of condensation prediction. One important conclusion from Trethowen's [68] paper was that air infiltration had a large effect on the moisture accumulation on the cavity. The same conclusion was obtained by Dutt in two separate studies [16,20] for houses in the United States. In his approach, Dutt proposed that moisture transfer between the living space and the cavity was by diffusion through wall and by convection. An integral approach was adopted and perfect gas behaviour was assumed. Based on experimental values of air-infiltration rates and water-permeability values for the various construction materials of the wall from the ASRHAE Handbook [66], he was able to show that moisture transfer by bulk air-flow was by far the more important mechanism than diffusion.

However, in a different laboratory study carried out at about the same time as Dutt's, Douglas et al [17] found that moisture transfer due to diffusion was at least as important as that due to air infiltration for a test wall with a cavity. Thus it appeared that whether air infiltration or moisture diffusion was the important mechanism in moisture transfer would depend on the type and the constructional details of the cavity concerned. Nonetheless, it was clear that moisture transfer by air infiltration was an important mechanism and this observation

points to the inadequacy of the traditional analysis which assumes moisture transfer is by diffusion through walls only.

Cunningham [137,138,139] has presented an analytical model whereby moisture concentration in a building cavity containing hygroscopic materials and with air infiltration can be predicted. The aim was to form an improvement over the Keiper method mentioned earlier, whereby the moisture transport process into the cavity was more clearly defined and the hygroscopicity of the cavity materials was recognised. Various types of building-cavity conditions were considered which include condensing [138] and non-condensing cavities [137] and cavities which contain evaporating surfaces [139]. Comparison with field data has indicated that the model is adequate to predict the long-term behaviour of the cavity's moisture content in all but the tightest building cavities.

2.3.2 Mass Transfer in Confined Spaces.

Work done on mass transfer in a confined space without simultaneous heat transfer is restricted to the field of electrolysis [70,71]. The importance of such studies concern the design and operation of electrochemical reactors working under natural convection and is not connected directly with this project.

2.4 SIMULTANEOUS HEAT AND MASS TRANSFER FROM A SINGLE PLATE.

The effect of simultaneous heat and mass transfer from the surface of an isolated plate in an ambient fluid has received considerable attention in the literature. As the temperature and flow profile for the case of a single plate would be expected to differ considerably from that in a cavity, only those aspects of the results which concern the influence of mass transfer on heat transfer will be reported herein.

Somers[72] has carried out one of the earliest studies on combined thermal and mass diffusion-driven flow that would arise adjacent to a wetted, isothermal vertical surface in a un-saturated atmosphere. The condition of very small concentration of diffusion species was used and an integral-method analysis was carried out

for uniform surface temperature and diffusion-species concentration. The result obtained was a transport relation with the result that a combined driving force might be written in which the mass diffusion contribution was modified by the square root of the Lewis number,

i.e $Nu=f(Gr_T+ Gr_C(Pr/Sc)^{1/2})$

and $Sh=f((Le)^{1/2}, Nu)$

where Nu = Nusselt number.
Sh = Sherwood number.
Le = Lewis number =Sc/Pr
Gr_T = Thermal Grashof number.
Gr_c = Concentration Grashof number.

Following Somers[72], Mathers[73] and Wilcox[74] also carried out integral analysis of the same problem. Both obtained transport relations which were similar to that of Somers'. However their results for Nusselt number were good only for Prandtl number less than 1 while for Sherwood number the results were good for Prandtl number greater than 1000.

Adams and McFaddin [76] performed an experimental study on heat and mass transfer of p-dichlorobenzene sublimating from a heated vertical surface into air by means of a Mach-Zehnder interferometer. The two buoyancy effects were opposing and their data were 10 to 15 percent lower than the the values predicted by Somers[72] and Wilcox[74]. Their results, however, correlated well with Somers'[72] results when the factor Le was omited in calculating the net buoyancy force. The same result was obtained by Den Bouter et al [77] when the experimental data disagreed with theoretical heat and mass-transfer rates correlated in terms of a combined buoyancy effects, calculated with the Le term included, when the two buoyancy effects were opposing. Agreement between experimental and theoretical values were good, however, for the two effects aiding each other.

An excellent review of the work up to 1971 was given by Gebhart and Pera [78]. They concluded that the integral method of

solution follows from somewhat arbitrary assumptions and formulations concerning the boundary-layer profiles of velocity, temperature and concentration, and were at variance with experimental results and more exact analytical solutions . They were not known to provide a reliable guide for processes with widely different Prandtl and Schmidt numbers nor with a large difference in aiding and opposing driving forces. In this paper, a similarity analysis was carried out whereby the velocities, temperature and mass concentrations were written in terms of a single similarity variable in place of the coordinates x and y. A boundary layer approximation was used and the governing partial differential equations were transformed into ordinary differential equations by the use of the similarity parameter. A laminar flow regime was considered and all diffusion-species concentration levels were assumed small so that the interfacial velocity could be neglected. The calculations were restricted to air and water with Prandtl number of 0.7 and 7.0 respectively. In air, the diffusing species of most common interest have Schmidt numbers in the range from 0.1 to 10. These species include carbon dioxide, water, oxygen and similar gases. Non-dimensionalisation of the governing boundary-layer equations resulted in the following governing parameters:-

1. Prandtl number. $Pr= \upsilon/\alpha$
2. Schmidt number. $Sc=\upsilon/D$
3. The buoyancy ratio parameter N

where $N = Gr_C/Gr_T = \beta_C(C_w-C^*)/b(Tw-T_\infty)$

subscripts w and ∞ denotes the surface and far-stream condition respectively.

Thus the quantity N measures the relative importance of chemical and thermal diffusion in causing the density difference which drives the flow. It was noted that N is zero for no diffusion of material, infinite for no thermal diffusion, positive for both effects combining to drive the flow and negative for the effects opposing each others. For opposing driving forces, the value of N has a limiting negative value to assume flow in the

positive x direction where the similarity solutions applied. For Pr=Sc this limiting value is N=-1. For Pr not equal to Sc, the condition on N is not always this stringent. The similarity analysis mentioned here will not work for the case of transport within a cavity because the boundary-layer type approximation could not be applied, and this led to a breakdown of the similarity theory. (pg.37 ref.36). Nonetheless, the results of Gebhart and Pera [78] are the most comprehensive to date and they would serve to illustrate the possible interaction between heat and mass transfer and the resulting effects on the natural convective velocity, temperature and concentration profiles. Their resulrs were summarised in Tables 2.1, 2.2 and 2.3

Table 2.1 Effect on Velocity (at constant Prandtl number)

		Fluid Properties	
		Pr =Sc	Pr ≠ Sc
Effect of Increasing N for :	N positive and Sc constant	Increase in velocity and the magnitude of the velocity is greater than the corresponding pure thermally-induced flow.	As for Pr = Sc
	N negative and Sc constant	Decrease in velocity and the magnitude is less than the corresponding pure thermally induced flow.	As for Pr = Sc
Effect of Increasing Sc for :	N positive and constant	———	Decrease in the magnitude of the velocity and vice versa.
	N negative and constant	———	Increase in the magnitude of the velocity and vice versa.

Table 2.2 Effect on Temperature Profile (at constant Prandtl number)

		Fluid Properties	
		Pr = Sc	Pr ≠ Sc
Effect of Increasing N for:	N positive and Sc constant	N has no effect on the temperature boundary ie. it is identical to that induced by thermal diffusion only.	The thermal boundary layer decreases as N is increased and its thickness is thinner than the corresponding layer induced by pure thermal diffusion only.
	N negative and Sc constant	As above.	The thermal boundary layer is thicker than the corresponding thermal layer induced by pure thermal diffusion only.
Effect of Increasing Sc for :	N positive and constant		The thermal boundary layer thickness increases.
	N negative and constant		The thermal boundary layer thickness decreases.

Table 2.3 Effect on Concentration Profile (at constant Prandtl number)

		Fluid Properties	
		Pr = Sc	Pr ≠ Sc
Effect of Increasing N for :	N positive and Sc constant	N has no effect on the concentration boundary ie. it is identical to that if mass diffusion is present only.	The concentration boundary layer thickness decreases and is thinner than the corresponding boundary layer thickness induced by mass diffusion only.
	N negative and Sc constant	As above.	The boundary thickens and is thicker than the corresponding boundary layer induced by mass diffusion only.
Effect of Increasing Sc for :	N positive and constant	———	The concentration boundary layer thickness decreases.
	N negative and constant	———	The concentration boundary layer thickness decreases.

2.4.1 Effect on Heat Transfer Parameter Nu (Nusselt number).

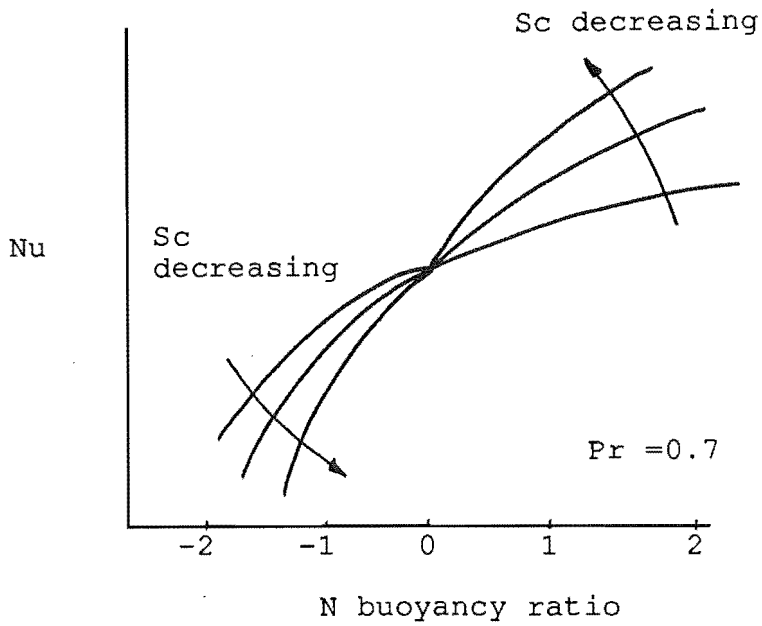

Around N=0, Nu is not strongly influenced by Sc. For N <0, Nu falls off rapidly with N while for N >0 , Nu increases with N. Expression for Nusselt number in terms of "N" and Schmidt number is much more complicated than that obtained by Somers[72] and other earlier studies.[73,74,76]

2.4.2 Effect on Mass Transfer Parameter Sh (Sherwood number).

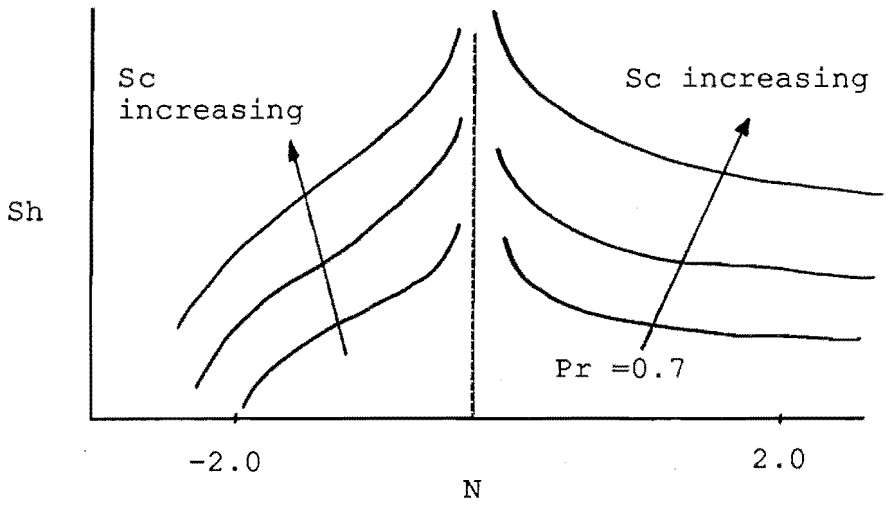

Around N=0, Sh is very large. This is because the flow is induced entirely by thermal buoyancy and produces a very effective

mass-diffusion effect at very low concentrations. For N <0, Sh falls off rapidly with N while for N >0, Sh decreases toward the values which would pertain for flows driven primarily by mass diffusion-caused buoyancy. A much more complicated expression for the Sherwood number in terms of "N" and Schmidt number compared with those of earlier studies [72,73,74] is obtained.

The general trend of the results was supported later by the work of Pera and Gebhart[79] for flow adjacent to a horizontal plate; of Callahan[80], Boura and Gebhart[81] and Soundalgeka[82] for the steady-state flow adjacent to vertical plate. Both the fluid and diffusing species properties, characterised by the Prandtl and Schmidt number respectively, together with imposed relative buoyancy driving-force parameter for the flow, N, control the rate of heat and mass transfer from the plate, but the phenomena so far described are by no means the only effects observed. The complicated interaction between heat and mass transfer can give rise to other peculiar behaviour, for instance:-

(i) For cases when the Schmidt number is less than the Prandtl number, ie. Sc<Pr and the two buoyancy effects are opposing, ie,N<0, the velocity may become negative relative to the main direction of flow at the outer region of the flow, while for Sc>Pr and N<0, the velocity may become negative in the inner region of the flow. [78,79].

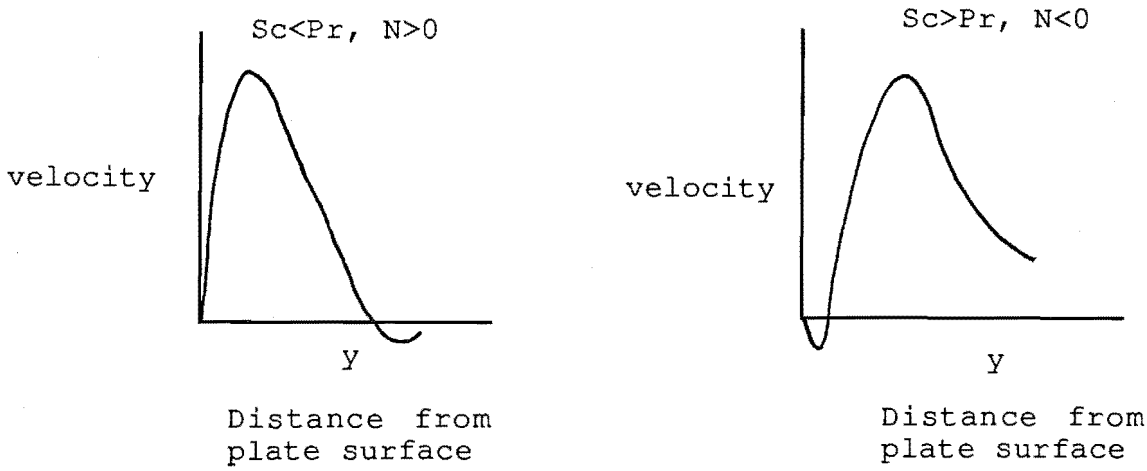

The reason postulated to account for the above behaviour is that, when Sc<Pr, the concentration boundary layer is observed to

be thicker than the thermal boundary layer and hence the opposing effect of mass transfer may dominate in the outer flow region and cause the flow to be in the opposite direction. For Sc>Pr, the smaller concentration boundary layer near to the surface creates a strong driving force which causes a flow opposite in direction to the main flow in the main boundary layer.

(ii) Also with the Prandtl number fixed, the effect of the parameter N on the Nussest number is noted to become less pronounced with increasing Schmidt number. As Sc increases, the difference between the Nusselt number at N=2.0 and N=0.0 becomes smaller [80].However just the opposite effect is observed in the case of the Sherwood number. As Schmidt number increases, the concentration boundary-layer decreases. Although the conservation equations are coupled, the thermal boundary layer thickness is not highly sensitive to the increase in the Schmidt number for a fixed value of the Prandtl number. Thus, as the Schmidt number increases, the concentration boundary-layer thickness becomes smaller than the thermal boundary layer thickness. Consequently, the bouyancy effects due to mass transfer are diminished in the thermal boundary layer, and hence the influence of the parameter N, which measures the relative importance of the concentration and thermal driving force, diminishes with increasing Schmidt number. On the other hand, as the Schmidt number increases, the buoyancy effects due to thermal convection become less important in comparison to those due to mass transfer in the thinner concentration boundary layer. Hence, as the Schmidt number also increaes, the influence of N on Sherwood number also increases.

Recently Nilson [83] in a numerical study concluded that the above self-similar structure proposed by Gebhart and Pera[78] existed only within two distinct and disconnected domains. The two regimes were defined as (1) outer-dominated subdomain; and (2) inner-dominated subdomain. To illustrate this point let us assume a situation whereby Le>1, Pr>1 ie.$\delta_c < \delta_T < \delta_v$ where δ is the boundary-layer thickness and subscripts c, T, and v stand for concentration, thermal and velocity respectively.
Nilson presents a graph of the following form to classify the various domains :-

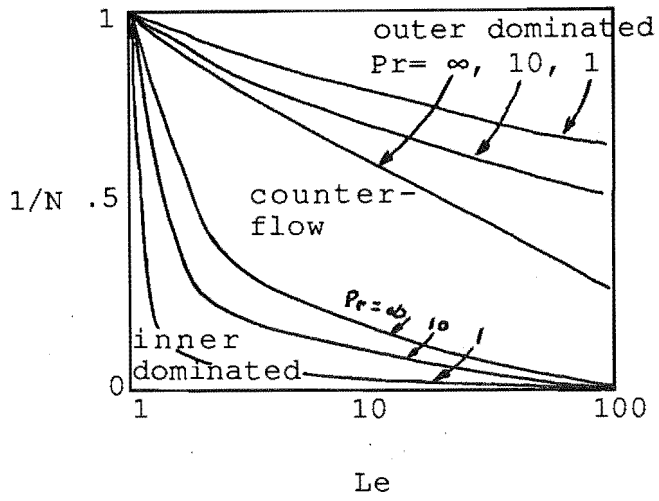

Limits of incipient counterflow for various Prandtl numbers

The outer-dominated flows occur when 1/N is sufficiently large ie. thermal(outer) driving force is much greater than the concentration(inner) driving force and thus it is the more diffusive(outermost) of the buoyancy mechanisms which controls the primary direction of the flow. The inner-dominated flows occur when 1/N is sufficiently small ie. thermal(outer) driving force is much less than concentration(inner) driving force and thus it is the less diffusive(innermost) of the buoyancy mechanism which controls the primary direction of the flow.

In both the above domains, unidirectional flows described by the similarity principle exist. Between the inner-dominated and outer-dominated domains, there lies a still-unexplored domain of non-similar flows in which flow reversal either in the inner or outer boundary layer can occur; which is a peculiarity described earlier (case (1)) but did not being investigated further by Gebhart and Pera [78,79].

ERRATA

So far only the steady-state behaviour has been mentioned. Since the time to reach steady state is not generally expected to be greater than a few minutes [82], transient behaviour will be omitted here. These transient phenomena are relating to the build up of concentration, temperature and velocity boundary layer with time and the influence of Prandtl and Schmidt numbers on the time required to reach steady state. The studies by Callahan [80] and Soundalgekar [82] have investigated such transient behaviour.

2.5 HEAT AND MASS TRANSFER IN CONFINED SPACES.

2.5.1 Double - Diffusive Convection.

Another area of interest in the study of simultaneous heat and mass transfer is the field of double-diffusive convection. When the diffusing quantities are heat and salt, the process is called thermohaline convection. In such studies a concentration gradient is generated by the presence of a suitable salt (eg. sodium chloride) and a temperature gradient is then imposed on the density-stratified solution. The resulting flow patterns are then studied. The main aim of these studies are mainly concerned with the onset of convective fluid motion and the associated instability phenomena. With the introduction of two potential differences ΔT and ΔC between the boundaries and two different molecular diffusivities α and D, four nondimensional parameters are required to specify the system. These are :-

(i) Thermal Rayleigh number Ra_T

(ii) Prandtl number Pr

(iii) The ratio $D/\alpha = 1/Le$; and

(iv) The density ratio $R= \beta_C \Delta C/\beta \Delta T$

A frequently used combination is the salinity Rayleigh number $Rs= \beta_C \Delta C/\beta \Delta T \; Ra_T$. In all practical purposes the two diffusive processes can be assumed to be non-interactive as pointed out by Hurle and Jakeman [91].An excellent review on this subject has been given by Turner[99].

As the Le number for a salt solution is typically 300 times larger than the Lewis number for a air-water vapour mixture, the flow structures and the stability criteria for a thermohaline convective process is not expected to be directly relevant to this work. The mathematical principle and the set of the non-dimensional parameters ,however, is expected to be similar to the case of combined heat and moisture transfer by natural convection. The practical application in the study of double-

diffusive convection will aid in the understanding of layered structures both in salinity and temperature as well as the vertical transport of heat and salt which exist in some parts of the ocean and in salt-water lakes. This is evident from the large amount of work that hadbeen done on thermohaline convection using sodium chloride as the stabilising salt. Such layered structures has also been utilized in a solar pond as an engineering application for space heating [108].

2.5.2 Flow Through Vertical Cylinder

Craig and Liedenfrost [140] studied the laminar free convection flow through a vertical cylinder induced by thermal and concentration buoyancy forces by numerical method. The flow geometry for an opened-ended vertical tube is expected to be considerably different from that in a completely enclosed cavity, but again the interaction of heat and mass transfer would be of interest. They concluded that the local Nusselt and Sherwood numbers increase as the second buoyancy force assists the flow. Similarly, they decrease when the second buoyancy force opposes the flow, which is the trend reported earlier for flows adjacent to a single plate.

2.6 DISCUSSION.

In section 1.1, the significance of heat and moisture transfer in building cavities was discusssed in relation to the design of buildings with minimum heat loss and unwarranted moisture ondensation. A survey of existing literature revealed the fact that, while heat transfer in confined spaces had received wide attention (section 2.1 and 2.2), work on combined heat and moisture transfer in confined spaces was very limited (section 2.5) and I am not aware of any work that has been carried out to determine the simultaneous transfer heat and moisture by natural convection across a building cavity. This sentiment were shared by Craig and Liedenfrost [140] and Hassan and Mujumdar [119] when they carried

out their studies on the subject but for different conditions. Mass-transfer studies in confined spaces without simultaneous heat transfer are mainly concerned with the design of electrochmical reactor and are not a direct concern of this project.

Therefore, by using existing results from studies on heat transfer on confined spaces; the type of flow situation, the temperature field and the rate of heat transfer across the gap of the cavity can be fairly accurately predicted if the boundary conditions are known. The type of cavities covered in the survey ranged from a vertical cavity , to inclined cavity and right down to a horizontal cavity.(as defined in 1.2). They were all rectangular in shape to reflect the resemblence to a typical building cavity. For cavities of other shapes, such as a cylindrical cavity , there have been also considerable studies carried out [141 -145] and the results can be easily obtained from the available literature. Other studies which concern the effect of inclusion of baffles on the heat transfer in the cavity are also available [125,146,147,148].

The studies carried out to predict the risk of moisture condensation in the cavity (2.3.1) were intended purely for practical design purposes and do not give both the flow and the temperature field as well as explicit moisture transfer path in the cavity. Moreover the area and scale of the transfer processes under study by these authors [13 to 20, 137 to 139, 151] are quite different from that envisaged in this project. Those studies were concerned with the heat loss from the living space as a whole and the possibility of moisture condensation and/or its long-term behaviour in the cavity. The main objective of this project is to investigate the simultaneous heat and moisture transfer across a building cavity only. The boundary conditions for those studies were the indoor and outdoor temperature and vapour-pressure values; plus other relevant information such as hygroscopicity of the cavity material, the air infiltration rate etc, while the boundary conditions relevant to this project are the building structural surfaces that enclose the cavity. Thus, although the idea of performing this research programme originated from a need of better insulation of buildings, as well as minimisation of unwarranted condensation, it is not the prime aim of this project

to consider the net heat and moisture transfer from the building as a whole, nor is the aim to consider the strategy to manipulate the various heat and moisture-transfer processes to achieve optimum living conditions. Therefore, heat and moisture losses from building as a result of direct ventilation through cracks of the building to the environmint; or heat loss by solid conduction through the floor; or heat gain as a result of sun radiation as well as heat and moisture gain from other casual activities such as cooking or lighting will not be considered. The presence of insulation in the cavity wall will also be neglected. The effect of insulation in a building cavity on the rate of heat transfer has been studied extensively in references [10,89,90] concerned with the effect of conductive and radiative heat transfer in fibrous insulation material, while other references [84,85,86] were concerned with the convective and radiative heat transfer in a porous medium. Therefore, only a cavity filled with air will be considered in this preliminary investigation of the heat and moisture transfer phenomena.

As stated in section 1.1, radiative heat transfer will not be investigated. Its magnitude is not negligible; for instance, in the work of Lufwendo[10], radiative heat transfer accounted for 2 to 15 percent of the total heat transfer across the gap of the cavity when air was the fluid. This proportion of radiation transfer is of course a function of the surface properties and the thermal condition of the cavity bounding materials, as well as its geometrical arrangement with respect to the fluid, which itself can be either a radiation-absorbing or non-absorbing gas. However, as stated in the literature [1,11,87,88], when the fluid is air, it can be considered essentially as transparent to radiation and the radiation heat transfer can be calculated from known laws of thermal radiation and is independent of the conductive and concective heat transfer which are occuring at the same time. Thus, when evaluating experimental results, only the magnitude of the thermal radiation across the cavity will be calculated for use in the energy balances; and it will not form part of the differential equations which are postulated to characterise the dynamic behaviour of the cavity. Full interaction of thermal radiation with natural convection in an environment of a totally-

absorbing gas such as carbon dioxide can be found in the literature [87,150].

It is therefore proposed that the project will study the process of heat and moisture transfer across an air-filled cavity of known boundary conditions. The dimensions and configuration of the cavity will be that similar to the cavity found in the wall and ceiling of a typical building. Uniform boundary conditions can be adopted in this preliminary study and different constant boundary conditions in the study can approximate the actual mean condition of the wall components which constitute the boundaries of the cavity over a fairly long period. This assumption will be reasonable if the response-time constant of the wall components is large compared with the time constant involved for the heat and moisture-transfer processes. In the case of moisture content in building structures, Trethowen[13] pointed out that the response time for drying out of the structure can be as long as several months when responding to the changes in the surrounding air humidity. The experimental apparatus will be expected to be large in the third dimension to induce two-diminsional flows except near the ends. A theoretical model based on constant boundary conditions will be sought.A two-dimensional analysis will be carried out to reduce the difficulty of obtaining a theoretical solution. A theoretical model will help to gain better insight into the dynamic behaviour of the cavity as no hydrodynamic measurements was to be made. It will also allow the interpolation of results to other parametric values without the need to carried out experiments.

Finally, an analogy is proposed for heat and mass transfer in a cavity based on the observed governing parameter in the case of :-

(1) Heat transfer from a single plate;
(2) Heat transfer in a cavity;
(3) Heat and mass transfer from a single plate;
(4) Thermohaline Convection.

The governing parameters expected to be important in the heat and moisture transfer in a cavity are:-

(1) The Prandtl number Pr.

(2) The Schmidt number Sc.

(3) The buoyancy ratio N.

(4) The aspect ratio A.

CHAPTER 3

THEORY AND NUMERICAL MODELLING.

3.1 INTRODUCTION

Natural convection is the transfer of heat and/or mass by flow of fluid due to the interaction between the field of gravity and temperature and/or concentration induced density variation in the fluid. The equations governing the natural convection of fluid can be derived from a study of a control volume of the fluid and by applying the conservation principles of mass, momentum, energy and/or concentration (e.g. Bird, Steward and Lightfoot [152], Rouche [153]). The differential equations which forms the theoretical basis of the numerical model used in this research will be given in Section 3.3, with the appropriate boundary conditions given in Section 3.4 as applied to either a vertical or a horizontal cavity. The method of non-dimensionalisation and the choice of scaling factors for the model will be discussed in Section 3.5. Section 3.6 gives a brief overview of the various numerical techniques currently in use and Section 3.7 concentrates on the methods which will be used in this work. Finally in Section 3.8, an example of the finite-difference approximation as applied to the differential equation is presented.

3.2 STATEMENT OF PROBLEM

Fluid is confined in a rectangular cavity of dimensions L, H and W (Figures 1.1 to 1.3, Chapter 1). Natural convection occurs because the walls of the cavity are not uniform in temperature and/or concentration. The equations governing the conservation of mass, momentum and energy or concentration are given in the next section subjected to the following conditions :-

(1) Viscous dissipation can be neglected.

(2) No internal heat/mass source or sink is present.

(3) The fluid is Newtonian.

(4) Compressibility effects are negligible.

(5) The fluid is essentially incompressible, i.e. it satisfies the Boussinesq [154] approximations that the variation of density with temperature and concentration is negligible except in the buoyancy term of the equation of motion. This assumption is reasonable if the variation in temperature and concentration is small compared with their absolute values, and the pressure differences arising from inertia and gravitational forces are negligible in comparison to absolute pressure.

(6) All other thermodynamic and transport properties of the fluid are constant.

(7) The dimension W of the enclosure (Figure 1.1) is much greater than the other dimension H and L, i.e. a two dimensional analysis will be sufficient.

(8) The cavity will have either one of its geometrical arrangement with respect to gravity as outlined in Section 1.2.

The above assumptions have been commonly employed for natural convective heat-transfer case alone(eg.reference [156]). With the simultaneous transfer of heat and moisture, the following additional condition is added (similar to Gehbart's formulation [155] for flow a djacent to a single plate):

(9) The buoyancy-generating capability of heat and moisture are identical in kind, except in the absolute magnitude of the buoyancy generated which will be characterised by the respective gradients present, i.e. if B_T is the buoyancy force calculated in terms of temperature gradient:

$$B_T = g \rho \beta (T - T_o)$$

where B_T is the coefficient of expansion with temperature, the total buoyancy for B calculated in terms of temperature and species concentration gradients can be written as:

$$B = B_T + B_c = g\,\rho\beta\,(T - T_o) + g\,\rho\beta_c\,(C - C_o)$$

where B_c is the buoyancy force due to concentration difference and β_c is the coefficient of expansion with concentration.

Therefore the variation in bulk fluid density which causes the motion is a linear combination of the quantities which cause the change, i.e. ΔT and ΔC. The dependency of the density variation (i.e. buoyancy forces) on these quantities is assumed to be linear, which requires the differences in temperature and concentration to be small, an assumption made earlier. It also follows from the last assumption that both the Soret and Dufor diffusion effects are negligible in a convective circumstance.

3.3 GOVERNING DIFFERENTIAL EQUATIONS

A convection process is governed by the basic conservation principles of mass, momentum, energy and species concentration. The governing equations are obtained from these basic principles by applying them to a control volume, which is a region defined in space across whose surfaces mass, momentum, energy and species concentration can occur and within which the amount contained of these physical quantities may vary. The governing equations are defined in many tests (e.g. BSL [152] and Roache [153]). Thus only the two-dimensional form of the equations, subject to the conditions mentioned in 2.1, will be presented here, as it is these equations which form the basis of the theoretical calculations [156,158]. A diagram of the coordinate system is presented in Fig. 3.1.

We have:
The equation of Continuity:

$$\frac{\partial u}{\partial x} + \frac{\partial v}{\partial y} = 0 \qquad (3.1)$$

The equation of Motion:

$$\frac{\partial u}{\partial t} + u\frac{\partial u}{\partial x} + v\frac{\partial u}{\partial y} = -\left(\frac{\partial P}{\rho\,\partial x}\right) + \upsilon\nabla^2 u - \beta g(T - T_o)\cos\theta$$

$$- \beta_c g(C - C_o)\cos\theta \qquad (3.2)$$

$$\frac{\partial v}{\partial t} + u\frac{\partial v}{\partial x} + v\frac{\partial v}{\partial y} = -\left(\frac{\partial P}{\rho\,\partial y}\right) + \upsilon\nabla^2 v - \beta g(T - T_o)\sin\theta$$

$$- \beta_c g(C - C_o)\sin\theta \qquad (3.3)$$

The equation of energy:

$$\frac{\partial T}{\partial t} + u\frac{\partial T}{\partial x} + v\frac{\partial T}{\partial y} = \alpha\nabla^2 T \qquad (3.4)$$

The equation of species concentration:

$$\frac{\partial C}{\partial t} + u\frac{\partial C}{\partial x} + v\frac{\partial C}{\partial y} = D\nabla^2 C \qquad (3.5)$$

Here ∇^2 is the two dimensional del operator :

$$i\frac{\partial^2}{\partial x^2} + j\frac{\partial^2}{\partial y^2} \qquad (3.6)$$

The rest of the symbols can be found from the Nomenclature. Equations 3.1 to 3.5 have 5 unknown in u, v, P, T and C.

If Eq.3.2 is differentiated with respect to y and Eq.3.3 is differentiated with respect to x and we subtract Eq.3.2 from Eq.3.3, we obtain :

$$\frac{\partial}{\partial t}\left(\frac{\partial v}{\partial x} - \frac{\partial u}{\partial y}\right) + u\left\{\frac{\partial}{\partial x}\left(\frac{\partial v}{\partial x} - \frac{\partial u}{\partial y}\right)\right\} + v\left\{\frac{\partial}{\partial y}\left(\frac{\partial v}{\partial x} - \frac{\partial u}{\partial y}\right)\right\}$$

$$= \upsilon\left(\frac{\partial}{\partial x}\nabla^2 v - \frac{\partial}{\partial y}\nabla^2 u\right) - \beta\, g\left[\frac{\partial T}{\partial x}\sin\theta - \frac{\partial T}{\partial y}\cos\theta\right]$$

$$- \beta_c\, g\left[\frac{\partial C}{\partial x}\sin\theta - \frac{\partial C}{\partial y}\cos\theta\right] \qquad (3.7)$$

We introduce a vorticity function defined as:

$$\zeta = \frac{\partial v}{\partial x} - \frac{\partial u}{\partial y} \qquad (3.8)$$

where the vorticity is the measure of the local spin of a portion of fluid.

Note also that:

$$\frac{\partial}{\partial x}(\nabla^2 v) - \frac{\partial}{\partial y}(\nabla^2 u) = \nabla^2 \zeta \qquad (3.9)$$

SEE ERRATA

Substituting Eq.3.7 and Eq.3.8 into Eq.3.6 we obtain the vorticity transport equation:

$$\frac{\partial \zeta}{\partial t} + u\frac{\partial \zeta}{\partial x} + v\frac{\partial \zeta}{\partial y} = \upsilon \nabla^2 \zeta - \beta\, g\left[\frac{\partial T}{\partial x}\sin\theta - \frac{\partial T}{\partial y}\cos\theta\right]$$

$$- \beta_c\, g\left[\frac{\partial C}{\partial x}\sin\theta - \frac{\partial C}{\partial y}\cos\theta\right] \qquad (3.9)$$

We now define a stream function φ by:

$$u = \frac{\partial \varphi}{\partial y} \quad \text{and} \quad v = -\frac{\partial \varphi}{\partial x} \tag{3.10}$$

$$\text{and} \quad \zeta = -\nabla^2 \varphi \tag{3.11}$$

Lines of constant φ constitute streamlines.

Equations 3.4, 3.5, 3.9 and 3.11 therefore constitute the set of governing equations for the determination of T, C, ζ , and φ . Note that by the introduction of the vorticity and the stream-function, the unknown variables need to be solved are reduced from five to four. These equations will be solved with the appropriate boundary conditions to yield either transient or steady-state temperature field, concentration field, streamlines and velocity components as a result of convection.

3.4 INITIAL AND BOUNDARY CONDITION

3.4.1 Initial Conditions

The fluid will be assumed to be at complete equilibrium at time "t" less than 0. At time zero, the fluid is suddenly subjected to a temperature and/or concentration difference across its boundaries, be it vertical or horizontal, but not both. The set of governing equations are then solved for advancing time domain for either the transient solutions or the steady state solutions, whichever the case may be. As only steady state experiments are performed in this work, the corresponding steady state solutions from numerical calculations will be of upmost interest. As it will be explained in Section 3.6 and 3.7, modifications can be applied to the set of governing equations such that the rate of convergence to steady state solution can be speeded up considerably, but in

the expanse of the true transient behaviour of the system being lost. In such cases the initial conditions do not form part of either the physical or mathematical description of the problem. The initial conditions are only needed to start the numerical calculation. We can thus use either the state of a completely stagnant fluid calculation or the steady state solution of some convective state as the initial condition.

3.4.2 Boundary Conditions

As mentioned in section 3.2, fluid convection commences because there is a temperature and/or concentration difference across the fluid in the cavity. We are only concerned with the case where the two opposite walls (either vertical or horizontal) are at different potential and the other two walls are:

(i) adiabatic;
(ii) impermeable to species diffusion and bulk flow;
(iii) non-slip, i.e u = v = 0 at the wall;
(iv) stationary.

Therefore the thermal boundary conditions are:

$$T = T_o \quad \text{at} \quad y = 0 \qquad (3.12a)$$

SEE ERRATA

$$T = T_1 \quad \text{at} \quad y = L \qquad (3.12a)$$

$$\frac{\partial T}{\partial x} = 0 \quad \text{at} \quad x = 0 \qquad (3.12c)$$

$$\frac{\partial T}{\partial x} = 0 \quad \text{at} \quad x = H \qquad (3.12d)$$

The concentration boundary conditions are:

$$C = C_o \quad \text{at} \quad y = 0 \qquad (3.13a)$$

SEE ERRATA

$$C = C_1 \quad \text{at} \quad y = L \qquad (3.13a)$$

$$\frac{\partial C}{\partial x} = 0 \quad \text{at } x = 0 \tag{3.13c}$$

$$\frac{\partial C}{\partial x} = 0 \quad \text{at } x = H \tag{3.13d}$$

The hydrodynamic boundary conditions are:

$$u = v = 0 \tag{3.14a}$$

$$\varphi = \text{constant} = 0 \text{ set arbitrarily} \tag{3.14b}$$

and

$$\frac{\partial \varphi}{\partial n} = 0 \tag{3.14c}$$

where n is the coordinate direction normal to the wall.

3.5 METHOD OF NON-DIMENSIONALISATION AND NON DIMENSIONAL EQUATIONS

There are obvious advantages in the introduction of proper scaling parameters and convert the foregoing dimensional equations into their corresponding dimensionless forms. The advantages are:

(i) The reduction of independent variables by the use of dimensionless group . This not only increases the generality of a solution for a given set of parameters, but also made the presentation of results easier.

(ii) Scaled dependent variables will be ensured to fall within the allowable numerical range of the computing equipment.

We first introduced a non-dimensional form for temperatures and concentration where:

$$T' = \frac{T - T_o}{T_1 - T_o} \tag{3.15a}$$

$$C' = \frac{C - C_o}{C_1 - C_o} \tag{3.15b}$$

where ' indicates the non dimensional quantity.

Equation 3.15 ensures T' and C' is between 0 and 1.0 and can provide an indication of a programming error or a lack of convergence in the numerical solution. It also ensures T' and C', and to some extent their derivatives, to be of the order of unity, thereby reducing the risks of the problems of numerical instability and removing the need to specify T_1 and T_o.

Substitution of equation 3.15 into equations 3.4, 3.5 and 3.9 leads to:

$$\frac{\partial T'}{\partial t} + u\frac{\partial T'}{\partial x} + v\frac{\partial T'}{\partial y} = \alpha \nabla^2 T' \qquad (3.16)$$

$$\frac{\partial C'}{\partial t} + u\frac{\partial C'}{\partial x} + v\frac{\partial C'}{\partial y} = D \nabla^2 C' \qquad (3.17)$$

$$\frac{\partial \zeta}{\partial t} + u\frac{\partial \zeta}{\partial x} + v\frac{\partial \zeta}{\partial y} = \upsilon \nabla^2 \zeta - \beta\, g\, \Delta T\left[\frac{\partial T'}{\partial x}\sin\theta - \frac{\partial T'}{\partial y}\cos\theta\right] - \beta_c\, g\, \Delta C\left[\frac{\partial C'}{\partial x}\sin\theta - \frac{\partial C'}{\partial y}\cos\theta\right] \qquad (3.18)$$

where $\Delta T = T_1 - T_o$ and $\Delta C = C_1 - C_o$

We then introduce the following reference quantities:

φ_s, L_s, and t_s for φ, x or y and t respectively,

where φ_s, L_s, and t_s are yet to be defined.

Therefore,

$$\varphi' = \frac{\varphi}{\varphi_s}, \quad X' = \frac{x}{L_s}, \quad Y' = \frac{y}{L_s} \quad \text{and} \quad t' = \frac{t}{t_s} \qquad (3.19)$$

It follows from Eq.3.10 and Eq. 3.19 that,

$$U' = u\left(\frac{L_s}{\varphi_s}\right) \qquad (3.20a)$$

$$V' = v\left(\frac{L_s}{\varphi_s}\right) \qquad (3.20b)$$

Thus φ_s/L_s is a reference velocity.

It also follows from Eqs. 3.11 and 3.20 that:

$$\zeta' = \zeta\left(\frac{L_s^2}{\varphi_s}\right) \qquad (3.21)$$

Thus L_s^2 / φ_s is a reference vorticity.

The use of Eqs. 3.19 to 3.21 in Eqs.3.16 to 3.18 yields:

$$\frac{\partial T'}{\partial t'} + \frac{\varphi_s t_s}{L_s^2}\left(U'\frac{\partial T'}{\partial X'} + V'\frac{\partial T'}{\partial Y'}\right) = \alpha\frac{t_s}{L_s^2}\nabla^2 T' \qquad (3.22)$$

SEE ERRAT.

$$\frac{\partial C'}{\partial t'} + \frac{\varphi_s t_s}{L_s^2}\left(U'\frac{\partial C'}{\partial X'} + V'\frac{\partial C'}{\partial Y'}\right) = D\frac{t_s}{L_s^2}\nabla^2 C' \qquad (3.22)$$

$$\frac{\partial \zeta'}{\partial t'} + \frac{\varphi_s t_s}{L_s^2}\left(U'\frac{\partial \zeta'}{\partial X'} + V'\frac{\partial \zeta'}{\partial Y'}\right) = \upsilon\frac{t_s}{L_s^2}\nabla^2 \zeta'$$

$$- \frac{\beta g \Delta T t_s L_s}{\varphi_s}\left[\frac{\partial T'}{\partial x}\sin\theta - \frac{\partial T'}{\partial y}\cos\theta\right] -$$

$$\frac{\beta_c\, g\, \Delta C\, t_s\, L_s}{\varphi_s}\left[\frac{\partial C'}{\partial x}\sin\theta - \frac{\partial C'}{\partial y}\cos\theta\right] \qquad (3.18)$$

SEE ERRATA

where ∇^2 now denotes the Laplacian with respect to X' and Y'. We will now consider the choice of values to be assigned to the scaling parameter φ_s, t_s and L_s.

In general, for sufficiently large velocity scales, enclosed flows cannot be expected to scale uniformly in space. Thus ideally, different scaling criteria would be used for different regions of the enclosure where the appropriate scaling criterion may be applied. For example, at high velocities we would expect boundary layers to form near the walls and viscous effects will be important in this thin region. The space scale parallel to the wall in the boundary-layer region is expected to be much smaller than the perpendicular space scale. Thus a suitable scaling parameter for the spare coordinates is the boundary layer thickness "δ" and force balances should be made between viscous, inertia and buoyant forces as these are all significant in the boundary layer. But this procedure will be wasteful for the flow outside the boundary layers, i.e. in the core flow where the flow is relatively slow and the horizontal and vertical space scale are compatible with each other. A suitable choice of the scaling parameter for this region is "L", the enclosure dimension, and the force balances to find φ_s can be made between inertial and buoyant forces. The "Order of Magnitude" analysis is used(BSL [152]) and possible sets of scaling parameters are given in de Vahl Davis [156] and Noble [88] for different flow regions and fluid type. If different sets of appropriate scaling parameters are used for different regions of the flow, different sets of differential equations will result and some matching technique is necessary where the two sets of equations "meet". Alternatively, one can use a single set of scaling parameters for the whole flow region with the most points in the boundary layer and less points in the core region. This procedure also leads to sets of differential equations. One can

also use a single set of scaling parameters on a uniform grid system imposed on the whole solution domain. This is very inefficient in terms of grid-point distribution, but it is the most straightforward method. Large numbers of grid points would be wasted in the core if the boundary layer structure is to be refined,or an inadequate boundary-layer structure will result if grid points in the core is kept to a minimum. Insufficient grid points in the boundary layer will also lead to erroneous results.

One way to overcome this problem of grid-point distribution for a single set of scaling parameters and uniform grid size distributions is by coordinates transformation technique (Chenoweth and Paolucci, [157]). The method basically make a change of the independent variables so that the domain is mapped into a new coordinate system where the variation of the solution are not so rapid. The mapping is chosen so that the solutions when regarded as a function of the new variables, has no boundary layers. The use of a coordinate transformation technique increases the mathematical complexity of the problem compared with a uniform grid calculation in the physical plane [157], but it also increases the accuracy of the numerical solution for the same number of grid-points used [27].

Thus depending on the criteria an investigator seeks, various forms of scaling the system of equations can be made. As the investigation of "new" and "more efficient" numerical techniques is not a primary aim of this research work, a simple straightforward case of a single set of scaling parameters and uniform grid size without coordinate transformations will be used for this preliminary investigation. Whenever needed, more grid points will be used to resolve the boundary-layer characteristics without the need to worry about the inefficient use of computing facilities. Some coordinate transformation technique will be tried if the situation allows.

One set of scaling parameters were chosen arbitrarily for this work. These use the cavity dimension L (the air-layer thickness) to be the characteristic length scale. A scaling stream function term φ_s is calculated from a force balance between inertia and viscous forces, i.e. that applicable for most parts of the cavity except in the thin boundary layer region. A slightly

modified form of this scaling procedure was recently used by a number of authors in a comparative exercise for the natural convection of air in a two dimensional square cavity [158]. An alternate form of the scaled equations, which is based on a balance between the viscous and buoyant forces (more suitable for use in the boundary layers [156]), will also be tried if the preceding scale equations are unable to produce a solution.

Thus we choose:

$$L_s = L \quad \text{and} \quad \varphi_s = \upsilon \tag{3.25a}$$

which implies:

$$U_s = V_s = \frac{\upsilon}{L} \tag{3.25b}$$

$$\zeta_s = \frac{\upsilon}{L^2} \tag{3.25c}$$

$$t_s = \frac{L_s}{U_s} = \frac{L^2}{\upsilon} \tag{3.25d}$$

If Eq.3.25 is substituted into Eqs.3.22 to 3.24 we obtain:

$$\frac{\partial T'}{\partial t'} + U' \frac{\partial T'}{\partial X'} + V' \frac{\partial T'}{\partial Y'} = Pr \, \nabla^2 T' \tag{3.26}$$

where $Pr = \alpha/\upsilon$ is the Prandtl number,

$$\frac{\partial C'}{\partial t'} + U' \frac{\partial T'}{\partial X'} + V' \frac{\partial T'}{\partial Y'} = Sc \, \nabla^2 C' \tag{3.27}$$

where $Sc = D/\upsilon$ is the Schmidt number,

$$\frac{\partial \zeta'}{\partial t'} + U'\frac{\partial \zeta'}{\partial X'} + V'\frac{\partial \zeta'}{\partial Y'} = \nabla^2 \zeta'$$

$$- Gr_T \left[\frac{\partial T'}{\partial X'} \sin\theta - \frac{\partial T'}{\partial Y'} \cos\theta\right]$$

$$- Gr_C \left[\frac{\partial C'}{\partial X'} \sin\theta - \frac{\partial C'}{\partial Y'} \cos\theta\right] \qquad (3.28)$$

where $Gr_T = \dfrac{\beta\, g\, \Delta T\, L^3}{\upsilon^2}$ thermal grashof number

and $Gr_C = \dfrac{\beta_c\, g\, \Delta C\, L^3}{\upsilon^2}$ concentration grashof number

The form of equations 3.10 and 3.11 are unchanged in dimensionless form:

$$U' = \frac{\partial \varphi'}{\partial Y'} \quad \text{and} \quad V' = \frac{-\partial \varphi'}{\partial X'} \qquad (3.29)$$

$$\zeta' = -\nabla^2 \varphi' \qquad (3.30)$$

Equations 3.26 to 3.30 now form the dimensionless form of the equations governing the system.

This equation formulation is a cross between pure natural convection due to temperature difference only [34,35,158] and heat and mass transfer from a single plate [78,79]. In the case of the heat transfer alone, the buoyancy term due to concentration gradient is absent and there is no conservation of species concentration. For heat and mass transfer from a single plate [78,79,82], the boundary-layer assumption was used and some terms in the above equations vanish. Craig and Leidenfrost [140] used the

same formulation recently (1984) to solve for the problem of free convective flow by thermal and concentration gradient through a vertical tube with entrance and exit. His boundary conditions were different from the ones considered here.

The reason why a solution of the problem listed above has not been presented in the literature before is perhaps the lack of suitable experimental data (where moisture flow is very small) to compare with the numerical solution.

3.6 GENERAL DESCRIPTION OF VARIOUS NUMERICAL SCHEMES USED

The methods of Wilkes and Churchill [34], Mallinson and de Vahl Davis [132] and Doss and Miller [160] form the basis of the numerical schemes tried in this work.

3.6.1 Method of Wilkes and Churchill [34].

The governing equations (3.26, 3.28, 3.30) were first solved by Wilkes and Churchill about twenty years ago. They employ the technique of Alternating Direction Implicit (ADI) scheme of Peachman-Rachford to solve the parabolic equations 3.26 and 3.28 and the method of Successive Over Relaxation (SOR) to solve the elliptic equation 3.30. It is rather slow compared with the later methods and does not produce a result in general for $Gr > 2 \times 10^5$. It is comparatively easy to implement and useful to gain an insight into the later methods.

3.6.2 Method of Mallinson and de Vahl Davis [132]

They employed a technique known as "False Transient" whereby a "false" time term is added to the elliptic equation (3.30) to transform into a parabolic one, thereby allowing a marching solution procedure (e.g. the ADI method) to be employed rather than using the slower point-by-point iteration method of successive over relaxation. False-transient factors are also added to the time term in equations 3.26 and 3.28 thereby effectively making each

equation of having its own effective time step.

$$\text{ie.} \quad \frac{\partial \varphi'}{a_\varphi \, \partial t'} = \nabla^2 \varphi' + \zeta' \quad \text{replaces Eq.3.30}$$

$$\text{and} \quad \frac{\partial T'}{a_T \, \partial t'} \quad \text{replaces} \quad \frac{\partial T'}{\partial t'} \quad \text{in Eq.3.26}$$

$$\text{and} \quad \frac{\partial \zeta'}{a_\zeta \, \partial t'} \quad \text{replaces} \quad \frac{\partial \zeta'}{\partial t'} \quad \text{in Eq.3.28}$$

$$\text{and} \quad \frac{\partial C'}{a_C \, \partial t'} \quad \text{replaces} \quad \frac{\partial C'}{\partial t'} \quad \text{in Eq.3.27}$$

Where a_φ, a_T, a_ζ and a_C are the false-transient factors employed in the false-transient method.

If a true steady state solution exists, the false time term should decay to zero at steady-state and the true solutions obtained. The advantage of this method is that the speed of convergence is much faster than the method of Wilkes, but the price to pay is a loss of the true transient solutions. Provision is provided to obtain a true transient solution, but it generally reverts back to the method of Wilkes, although more effective way of solving the elliptic equation Eq.3.32, e.g. by cyclic reduction [35] or a Galerkin method [159] can be employed.

3.6.3 Method of Doss and Miller [160]

Doss and Miller [160] proposed the method of "Dynamic Alternative Direction Implicit" (DADI) method. In this method, the stream-function equation is again converted into a parabolic form by the introduction of a false time term. But instead of using a fixed time step for each iteration as in the previous two methods mentioned, a procedure for automatic time step adjustment is

incorporated. The time step is so adjusted so that local truncation error is kept small and the rate of convergence of the solution is forced to lie within a region of fast convergence. Doss and Miller did not solve the full set of equations governing the natural convection of air and only single linear and non-linear Laplace equations were tested. Philips [112] recently used the DADI method and solved the problem of natural convection in a square cavity for Rayleigh Number up to 1×10^6.

Thus it can be concluded from the above work that the desired features to be used in the numerical schemes are:

(i) false time factor of Mallinson and de Vahl Davis [132];

(ii) automatic time step adjustment of Doss and Miller [160].

Note that the false transient factors used in de Vahl Davis method are constant for all time steps, i.e. the factor has to be chosen a priori and does not change later even if this factor is no longer effective. The method of Philips [112] adjusts one common time step in all equations although the false transient factor was used in one of his equations.

3.6.4 The Hybrid Method.

It is therefore proposed here to proceed one step further in this direction that we not only automatically update the step after each iteration as recommended by Doss and Miller and used by Philips, but we also update this time step separately for each governing equation, i.e. following the principles of Mallinson and de Vahl Davis, but with variable, effective time steps adjusted for each individual governing equations instead of fixed ones. This procedure will be called the "Hybrid method".

All three methods will be used to solve equations 3.26 to 3.30 for simultaneous heat and moisture transfer by natural convection in a cavity of aspect ratio = 7.0.

Although quite a number of studies [56] [114] [103] have investigated the natural convection of air in a tall cavity of aspect ratio 5 or greater, the greatest value of Gr (based on air gap thickness) reported is 6×10^5 by Probert and Dixon [114]. The value of Gr expected in this work would be of the order of 1.0×10^6.

Thus extending the numerical calculation to the range of GR = 1.0×10^6 and beyond would be another aim of the numerical investigation, as well as having a means for easy interpolation of heat and mass transfer results to other conditions not covered by the physical experiments.

3.7 MORE DETAILED DESCRIPTION OF THE NUMERICAL SOLUTIONS PROCEDURE

Using the numerical technique of false transient, the governing equations can be written as:

$$\frac{1}{a_T}\frac{\partial T}{\partial t} + U\frac{\partial T}{\partial X} + V\frac{\partial T}{\partial Y} = Pr\,\nabla^2 T \tag{3.31}$$

$$\frac{1}{a_C}\frac{\partial C}{\partial t} + U\frac{\partial C}{\partial X} + V\frac{\partial C}{\partial Y} = Sc\,\nabla^2 C \tag{3.32}$$

$$\frac{1}{a_\zeta}\frac{\partial \zeta}{\partial t} + U\frac{\partial \zeta}{\partial X} + V\frac{\partial \zeta}{\partial Y} = \nabla^2 \zeta$$

$$- Gr_T \left[\frac{\partial T'}{\partial X'}\sin\theta - \frac{\partial T'}{\partial Y'}\cos\theta\right]$$

$$- Gr_C \left[\frac{\partial C'}{\partial X'}\sin\theta - \frac{\partial C'}{\partial Y'}\cos\theta\right] \tag{3.33}$$

$$\frac{1}{a_\varphi}\frac{\partial \varphi}{\partial t} = \nabla^2 \varphi + \zeta \tag{3.34}$$

$$U' = \frac{\partial \varphi}{\partial Y} \quad \text{and} \quad V' = \frac{-\partial \varphi}{\partial X} \tag{3.35}$$

The variables are understood to be non-dimensional and the prime has been dropped.

These governing equations are to be solved on a rectangular mesh to be imposed on the solution region (Fig.3.1). There are M mesh points in the X direction and N in the Y direction. The mesh is uniform in each direction and the mesh spacings are therefore :

$$\Delta X = \frac{A}{(M-1)} \quad \text{and} \quad \Delta Y = \frac{1}{(N-1)} \tag{3.36}$$

where A is the aspect ratio of the cavity.

The differential equations are replaced by finite-difference approximations (FDA), using forward differences for the time derivatives and central differences for all space derivatives.

The FDAs are solved by the ADI procedure of Peaceman and Rachford [162], which leads to a tridiagonal system of equations allowing the use of the Thomas algorithm.

The essentials of the numerical schemes used are illustrated in Fig.3.2 and 3.3. The method of false transient is well documented elsewhere [132,156], and will not be elaborated here. Briefly, the method of DADI involved the calculation of a new field, not only from n to (n + 1) time level, but also from (n + 1) to (n + 2) time level using the step Δt. One then calculates a different field for (n + 2) time level from n level using a time step of $2\Delta t$. A test parameter TP is then computed which gives an estimate of the local truncation error. Using the criteria of Doss and Miller [160] one then adjusts Δt so that the ADI scheme in advancing all the fields lies in a region of fast convergence.

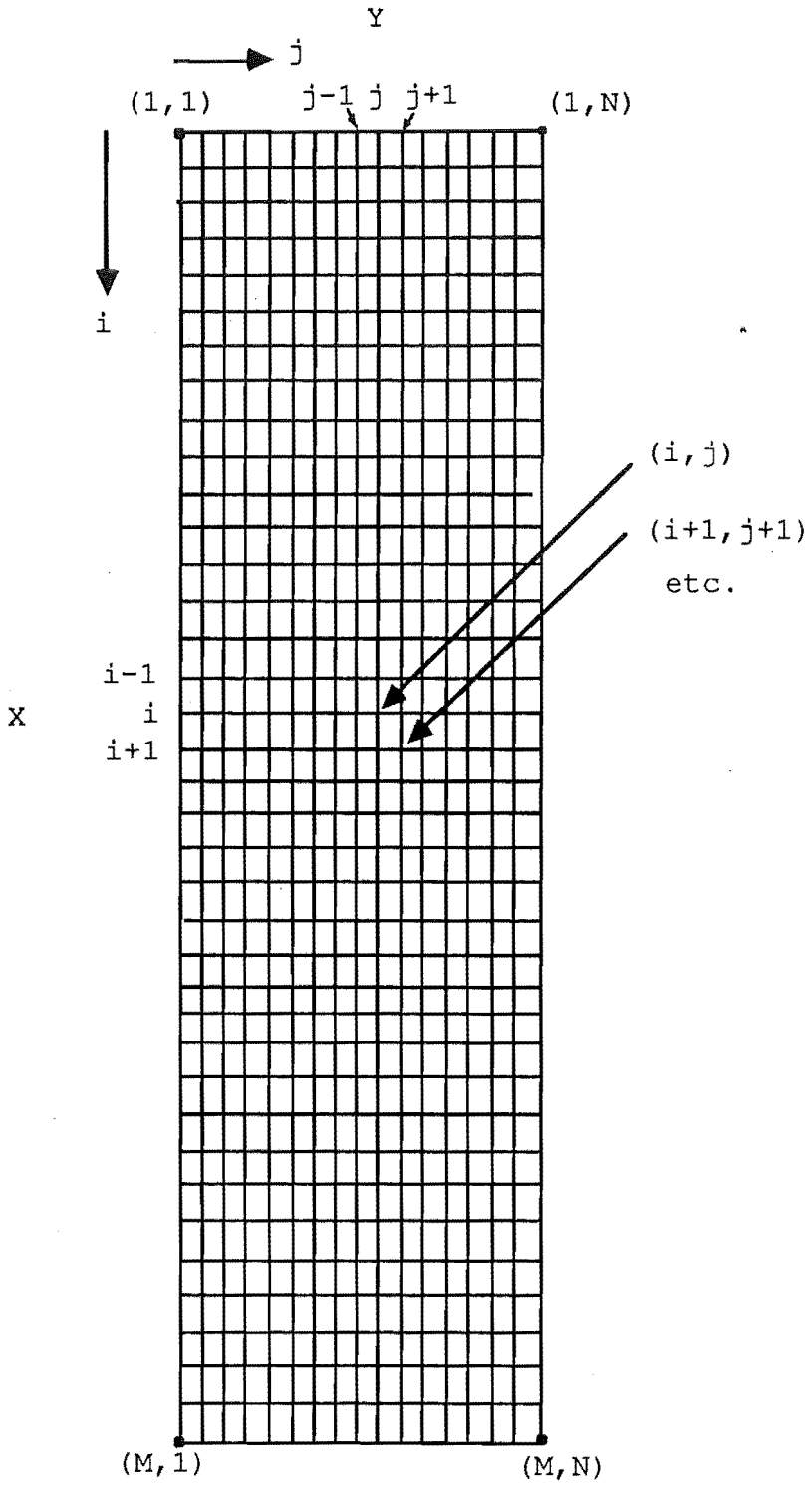

Fig 3.1 Grid-points arrangement for numerical method.

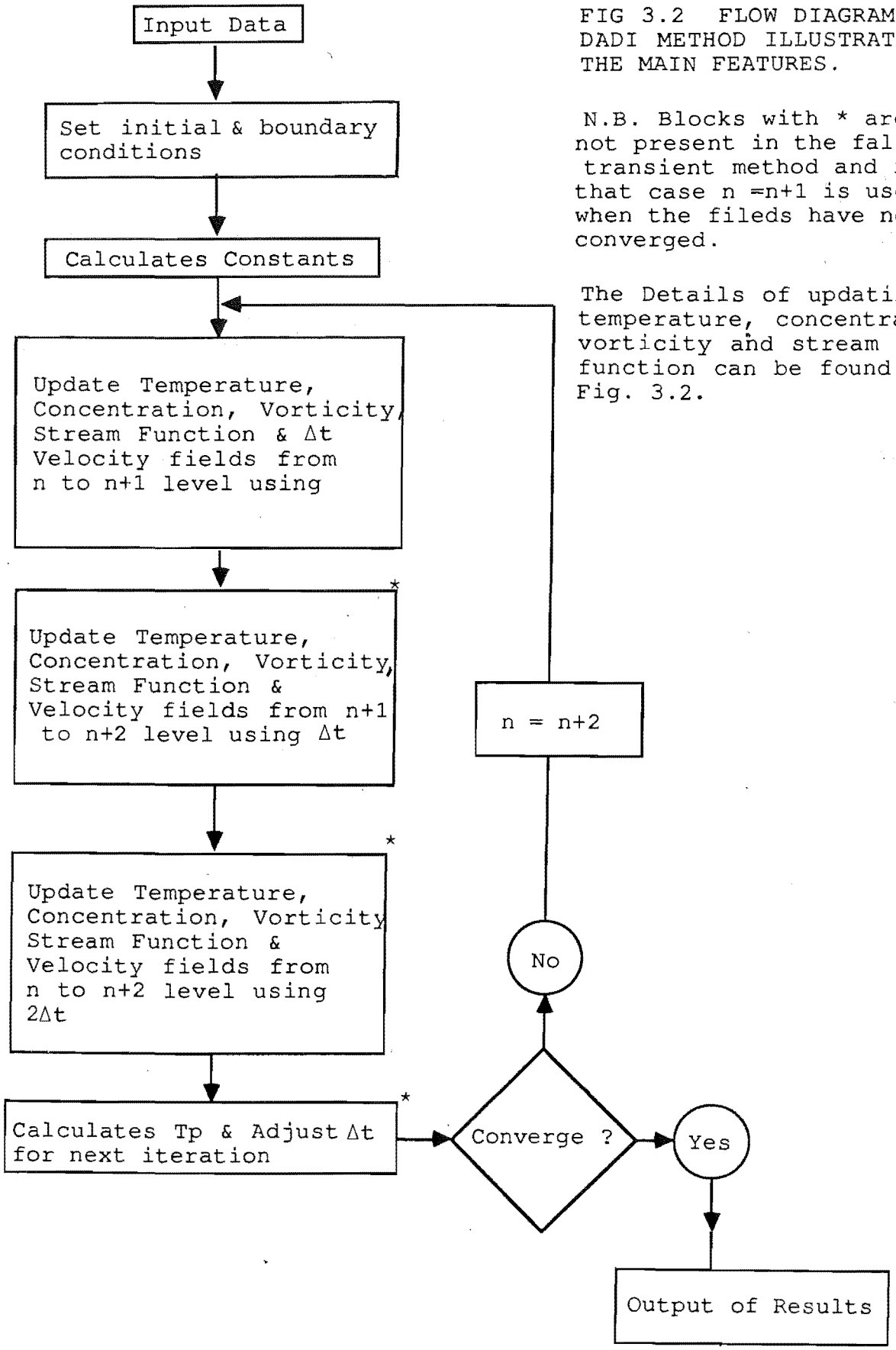

FIG 3.2 FLOW DIAGRAM OF DADI METHOD ILLUSTRATING THE MAIN FEATURES.

N.B. Blocks with * are not present in the false-transient method and in that case n =n+1 is used when the fileds have not converged.

The Details of updating temperature, concentration, vorticity and stream function can be found in Fig. 3.2.

FIG. 3.3 FLOW DIAGRAM TO ILLUSTRATE THE ADVANCEMENT OF FIELD VARIABLES FROM TIME LEVEL N TO N+1

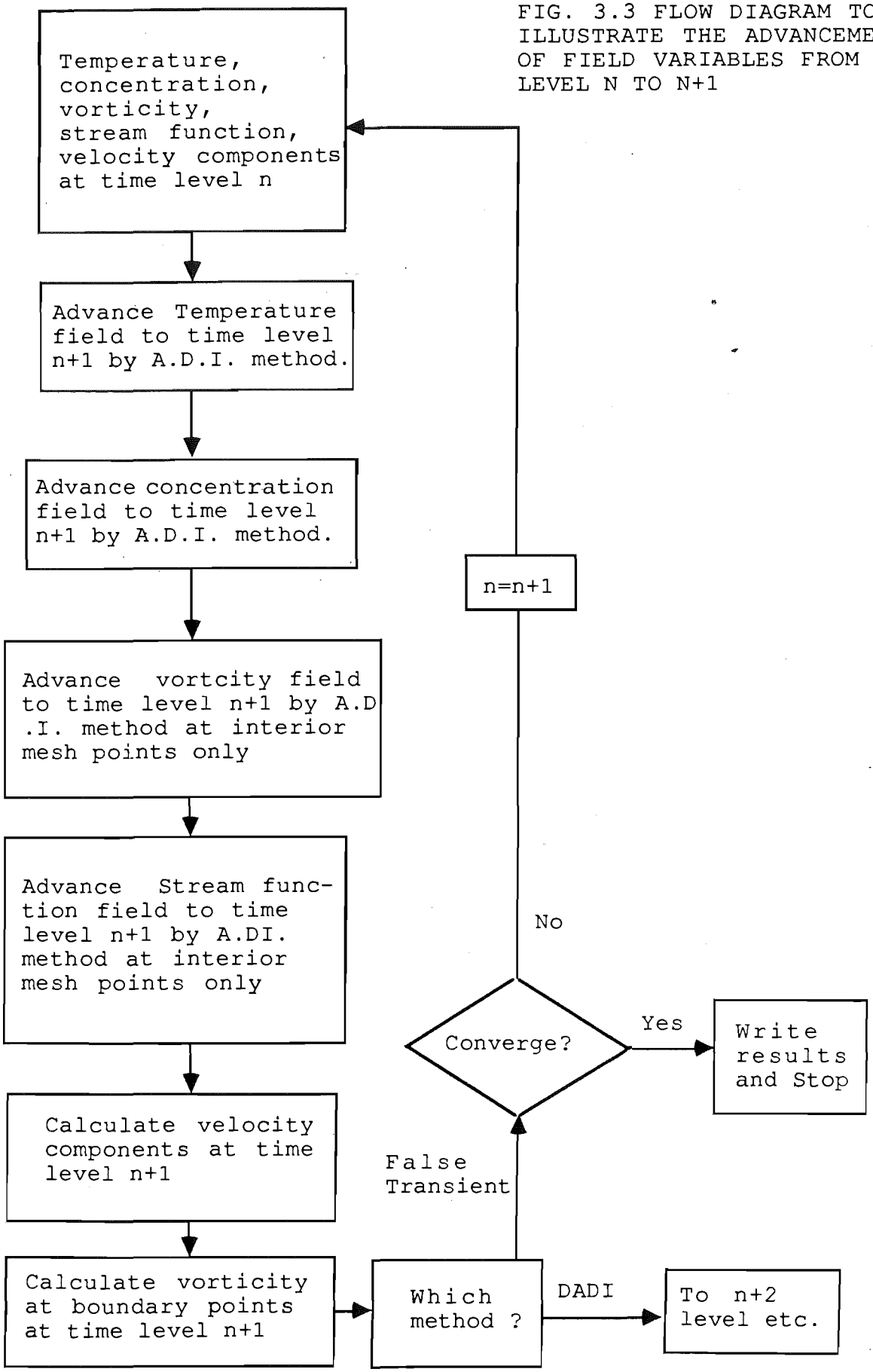

Note that DADI involves one and a half times more calculation for each step than the corresponding false transient method. However the advantages of having an automatic time step adjustment which decreases Δt when instabilities occur and attempts to keep Δt within a region of fast convergence seem to outweigh this extra computation.

The testing parameter TP is defined as follows [160]:

$$TP = \frac{|| Z^{n+2} - \overline{Z^{n+2}} ||_2}{|| Z^{n+2} - Z^n ||_2} \qquad (3.37)$$

where Z^{n+2} is the field variable at the (n+2) level calculated using Δt

$\overline{Z^{n+2}}$ is the field variable at the (n+2) level calculated using $2\Delta t$

Z^n is the field variable at the n level

The norm used is the root mean square or Euclidean norm defined as:

$$||Z||_2 = \left(\sum_{i=1}^{n} \sum_{k=1}^{n} | Z_{ik} |^2 \right)^{1/2} \qquad (3.38)$$

(for more information see Korn & Korn [130] p.13.2-1)

In his paper Philips [112] used the definition which is equivalent to the following:

$$TP = \frac{|| T^{n+2} - \overline{T^{n+2}} ||_2 + || \zeta^{n+2} - \overline{\zeta^{n+2}} ||_2 + || \varphi^{n+2} - \overline{\varphi^{n+2}} ||_2}{|| T^{n+2} - T^n ||_2 + || \zeta^{n+2} - \zeta^n ||_2 + || \varphi^{n+2} - \varphi^n ||_2}$$

..... (3.39)

The strategy for changing Δt was given a theoretical justification by Doss and Miller [160] with the aid of two simplifying

assumptions. This strategy is as follows:

(i) If TP is greater than 0.6, then we reject the present DADI step and start the step again with Δt reduced by a factor of 1/16.

(ii) If TP is less than or equal to 0.6 then we accept the present DADI step and change Δt according to the strategy : if TP falls in the intervals |0, 0.05|, |0.05, 0.1|, |0.1, 0.3|, |0.3, 0.4|, |0.4, 0.6|; we change Δt by the factors of 4, 2, 3, 1/2 , 1/4 respectively for the next DADI step.

But in this work we would attempt to define separate TPs for the Hybrid method so that each equations can be updated individually.

$$TTP = \frac{|| T^{n+2} - \overline{T^{n+2}} ||_2}{|| T^{n+2} - T^n ||_2} \qquad (3.40a)$$

$$STP = \frac{|| \varphi^{n+2} - \overline{\varphi^{n+2}} ||_2}{|| \varphi^{n+2} - \varphi^n ||_2} \qquad (3.40b)$$

$$VTP = \frac{|| \zeta^{n+2} - \overline{\zeta^{n+2}} ||_2}{|| \zeta^{n+2} - \zeta^n ||_2} \qquad (3.40c)$$

$$CTP = \frac{|| C^{n+2} - \overleftarrow{C^{n+2}} ||_2}{|| C^{n+2} - C^n ||_2} \qquad (3.40d)$$

The strategy for changing Δt, however, will be similar to that proposed by Doss and Miller [160].

3.8 FINITE DIFFERENCE APPROXIMATION

As an example the stream-function equations will be used to illustrate the transformation of the governing differential equations into the corresponding finite difference equations by the ADI method:

$$\frac{1}{a_\varphi}\frac{\partial \varphi}{\partial t} = \frac{\partial^2 \varphi}{\partial X^2} + \frac{\partial^2 \varphi}{\partial Y^2} + \zeta \quad \text{from (3.34)}$$

We define the stream function φ as follows:

$$\varphi_{i,j,n} \tag{3.41}$$

where $i,j \equiv$ grid-point at (i,j) (see Fig.3.1)

$n \equiv$ time level n

If only φ_n is written, it is understood that the default grid point values are i and j:

ie. $\varphi_{i+1,n} \equiv \varphi_{i+1,j,n}$ (3.41a)

and $\varphi_{j-1,n+1} \equiv \varphi_{i,j-1,n+1}$ (3.41a)

We also define an intermediate stream function quantity φ_k which is used in the ADI method, e.g. see Peaceman and Rachford [162].

In the ADI method, we do a double sweep of the solution region, the first sweep (arbitrarily set) is carried out over a time step of $\Delta t/2$ and is implicit in the X direction and explicit in the Y direction. The 2nd sweep is implicit in the Y direction and explicit in the X direction. This is done as follows :-

First half time step:

$$\frac{1}{a_\varphi}\left(\frac{\varphi_k - \varphi_n}{\Delta t/2}\right) = \frac{\varphi_{i+1,k} + \varphi_{i-1,k} - 2\varphi_k}{(\Delta X)^2} + \frac{\varphi_{j+1,n} + \varphi_{j-1,n} - 2\varphi_n}{(\Delta Y)^2} + \zeta_{n+1} \qquad (3.42)$$

Rearranging,

$$-\left(\frac{a_\varphi}{(\Delta X)^2}\right)\varphi_{i-1,k} + \left(\frac{2}{\Delta t} + \frac{2\,a_\varphi}{(\Delta X)^2}\right)\varphi_k - \left(\frac{a_\varphi}{(\Delta X)^2}\right)\varphi_{i+1,k}$$

$$= \frac{2}{\Delta t}\varphi_n + \frac{a_\varphi}{(\Delta Y)^2}\left(\varphi_{j+1,n} + \varphi_{j-1,n} - 2\varphi_n\right) + a_\varphi\,\zeta_{n+1} \qquad (3.43)$$

This completes the first half sweep of the method.

Second half time step:

$$\frac{1}{a_\varphi}\left(\frac{\varphi_{n+1} - \varphi_k}{\Delta t/2}\right) = \frac{\varphi_{i+1,k} + \varphi_{i-1,k} - 2\varphi_k}{(\Delta X)^2} + \frac{\varphi_{j+1,n+1} + \varphi_{j-1,n+1} - 2\varphi_{n+1}}{(\Delta Y)^2} + \zeta_{n+1} \qquad (3.44)$$

Rearranging,

$$-\left(\frac{a_\varphi}{(\Delta Y)^2}\right)\varphi_{i-1,n+1} + \left(\frac{2}{\Delta t} + \frac{2\,a_\varphi}{(\Delta Y)^2}\right)\varphi_{n+1} - \left(\frac{a_\varphi}{(\Delta Y)^2}\right)\varphi_{i+1,n+1}$$

$$= \frac{2}{\Delta t}\varphi_k + \frac{a_\varphi}{(\Delta X)^2}\left(\varphi_{j+1,k} + \varphi_{j-1,k} - 2\,\varphi_k\right) + a_\varphi\,\zeta_{n+1} \qquad (3.45)$$

This completes the full sweep of the method.

Equations 3.43 and 3.45 are tridiagonal systems of equations and can be solved with the appropriate boundary conditions which are set at zero for this problem (Eq.3.14) using the Thomas Algorithm.

The complete set of FDAs for Equations 3.31 to 3.35 are presented in Appendix 8 together with a full discussion on the special treatment required for the formulation of boundary values for temperature, concentration and vorticity where their values at the boundaries are not equal to zero.

CHAPTER 4

EXPERIMENTAL ARRANGEMENTS

An experimental rig was designed and built in the Department of Chemical and Process Engineering to measure small transfers of heat and moisture across a cavity. The basic design principle is similar to that given in ASTM C236 [163], with the exception that the moisture-transfer rate is also measured and an air "cavity" is incorporated.

4.1 PRINCIPAL DESIGN CONSIDERATIONS

The principal requirement of the experimental rig is the ability to impose a moisture gradient as well as a temperature gradient across the air cavity. The mechanism with which the heat and moisture gradient is set up preferably should be independent of each other (so that the individual effect of heat and moisture transfer can be separated). The traditionally-used technique in heat-transfer experiments, where copper or aluminium plates is used as the boundary surfaces of the cavity, is not suitable here because of its inability to provide a simultaneous moisture gradient in addition to the temperature gradient. The use of the free water surfaces at different temperatures as commonly employed in studies of solar ponds [164], [165] is not suitable because we do not generally expect to find the two boundary surfaces of a building cavity to be covered with water. Hence the rate of moisture transfer and the resultant moisture gradient in a solar pond situation is typically many (about 50 or more) times greater than the rate expected in a building cavity. Besides, it will be very difficult to maintain a free water surface in all but the horizontal situation when the water surface is facing upwards.

A new experimental method is therefore proposed in this work whereby inert porous plastic sheets are used to isolate the test "cavity" from chambers with controlled air conditions. As the two

controlled chambers at both sides of the cavity are at different temperatures and moisture levels and because the boundaries separating these controlled chambers from the test cavity are porous, the boundary conditions across the test cavity will approach that in each controlled chamber. Heat and moisture gradients are set up and convection will commence. If a steady supply of heat and moisture is being supplied continuously from the high-potential chamber and removed from the low-potential chamber, steady state transfer would be established.

The choice of the porous plastic plate (or any other type of similar porous membranes) is important. It has to be thin enough to reduce its resistance to heat and moisture transfer but at the same time thick enough to provide sufficient strength and rigidity to maintain a flat bounding surface for the cavity. It is unlikely that the resistance of such a porous plastic sheet will be negligible when compared with the resistance of air gap to heat and moisture transfer. Thus the resistance value will have to be accurately determined so that cavity boundary values can be decided. It is also important that the porous plate be non-hygroscopic so that no moisture adsorption will occur to interfere with the boundary conditions and rate of mass transfer. Based on these considerations, a selection is made on the choice of the porous plate in Section 4.3.2.

"Perspex" was chosen to be the constructional material of the guarded box because of its transparency. Although no flow visualisation work was to be performed in the present project, the possibility that this might be done in a later work was not to be discounted. The transparent nature of the apparatus is also useful in the initial commissioning stage of the guarded box especially in assessing the performance of the fan stirrers by smoke injection. The maximum operating temperature of 80 °C for Perspex is adequate to provide the necessary temperature gradient in the test cavity which is analogous to that found in an actual building cavity.

4.2 BASIC MEASUREMENT ZONES

The basic arrangements of the various measurement and guarding chambers which allows the heat and mass balance method to be employed for the determination of heat and moisture-transfer flux across the cavity, are as follows:

4.2.1 Guarded Box.

The guarded box consists of the following measurement and guarding chambers (with reference to figure 4.1):

(1) Controlled chamber A and B;
(2) Guard chambers C and D;
(3) Test Cavity E;
(4) "Passive" guard chamber F;
(5) Porous plastic sheet X;
(6) Compartments G, H and K which are optional, but are incorporated at this stage (their functions will be explained subsequently).

4.2.2 Geometric Arrangement

The test equipment, as shown in the figure 4.1, has the test cavity in a "vertical" position. It is also possible to arrange the test cavity in a horizontal position by tilting the apparatus by 90 degrees.

4.2.3 Basic Control Strategy.

4.2.3.1 Controlled chambers, A and B. Temperature and humidities are the variables controlled. The two controlled chambers are at different temperature and humidity levels so that the heat and moisture transfer can take place. One chamber (e.g.A in this case) acts as the heat and moisture source, while the opposite chamber (B) acts as the sink. The hygrothermal condition in the controlled chambers is made uniform by mixing the air with

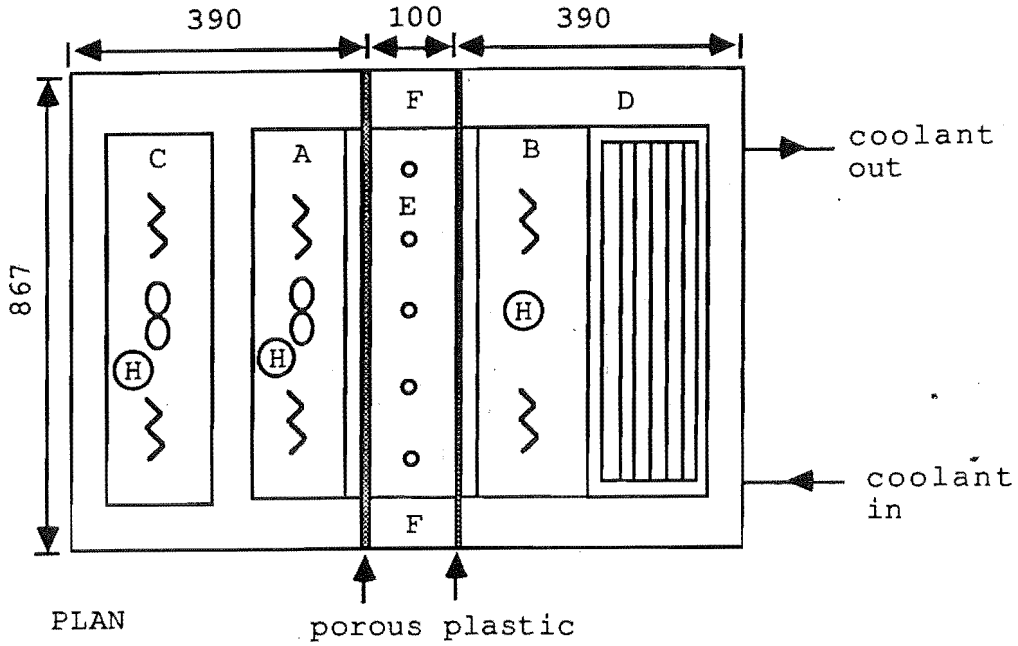

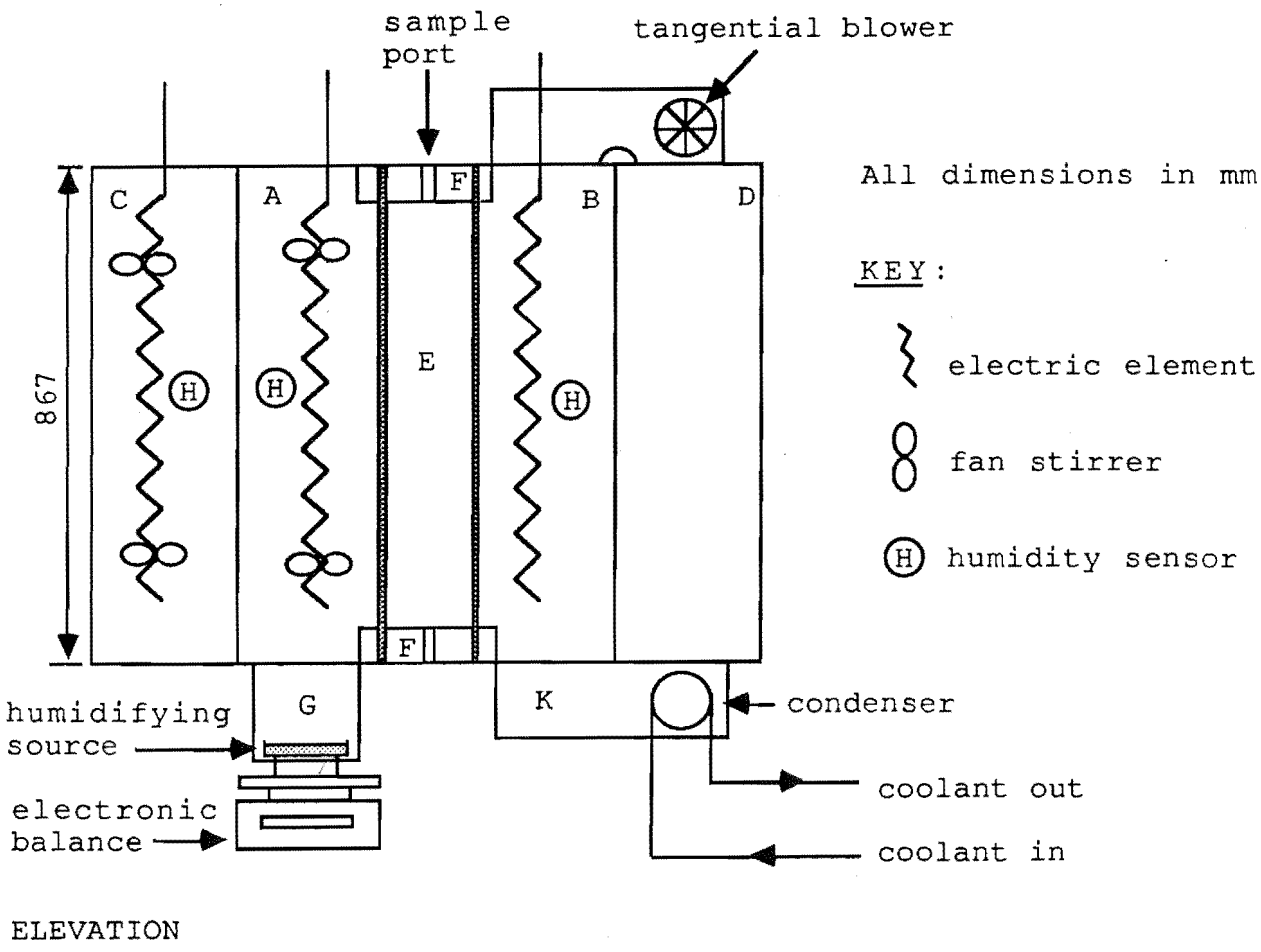

Fig. 4.1 Schematic Diagram of the Test Equipment.

an appropriately placed fan. Note that, in the present set up, the controlled chamber "B" is joined to guard chamber "D" by means of compartments "H" and "K". This point will be referred to later.

4.2.3.2 Guard chamber C,D. In the present arrangement, only chamber "C" is strictly regarded as a guard chamber. Temperature is the only variable controlled in this guard chamber, such that its value is equal to the air temperature in the controlled chamber "A" which it is guarding. This policy will eliminate any heat flow across the wall separating the two chambers. Moisture permeability through the Perspex wall separating the two chambers is assumed to be nil as water vapour permeability through perspex has a value 5.2×10^{-8} g cm cm^{-2} h^{-1} (1.4×10^{-13} g m^{-1} s^{-1} [184] compared with the value of 0.16 g cm cm^{-2} h^{-1} (4.4×10^{-7} g m^{-1} s^{-1}) (from experiment) for the porous plastic at ambient temperature. Hence no control on the humidity in the guard chamber is necessary. The space in the guard chamber "C" is again well-stirred by an appropriate fan.

4.2.3.3 Test cavity "E". This is the region through which the heat and moisture-transfer rates are measured. The space is not stirred and access into the test cavity is possible by means of the sample ports situated at the top and bottom of the cavity. When not in use, these sample ports are sealed by suitable Perspex cylinders blanked at one end to plug up the openings in the test cavity wall. This arrangement will minimise the disturbance to the air flow in the test cavity by the presence of the sample ports.

4.2.3.4 Passive guard chamber "F". The passive guard chamber "F" is a rectangular space surrounding the whole perimeter of the test cavity "E". The condition in the guard chamber is made to be as close as possible to the condition in the test cavity (as both passive guard chamber and the test cavity experience the same boundary conditions). The purpose of this arrangement is to eliminate any heat and moisture loss from the test cavity to the surroundings. The passive guard chamber is, of course, not stirred

4.3 DIMENSIONS OF EXPERIMENTAL RIG AND TECHNICAL SPECIFICATIONS OF TEST EQUIPMENT ITEMS.

4.3.1 Guarded Box.

As mentioned previously in Section 4.2,1, the guarded box consists of a "measurement zone" which is insulated from the surroundings by a "guarding zone". The constructional set up and detailed dimensions of the guard hot box are given in Figures 4.2 and 4.3. All the box's surfaces were made of 6 mm thick Perspex sheet, while the flanges were made of 12 mm thick sheet (see ICI Technical Note PX127[166] for more information on "Perspex" sheet). The sheets were cut to the required sizes in accordance with the procedure set up in ICI technical note PX127[166] using a "router". The appropriate edges were then cleaned with dichloromethane before they were glued together using the Perspex glue, "Tensol No.70". The glued edges were held in place by masking tape and all the air bubbles were expelled from the joints. (see ICI technical note PX128[167] for more details).

Six mm diameter stainless steel nuts and bolts were used to hold the flanges together as normal mild steel ones would rust due to the high level of water vapour encountered in the chambers during an experiment. Silicone Rubber (RTV) was used to seal any gaps that may have been present due to constructional constraints (see Figure 4.2). Silicone rubber is a good seal for Perspex as it is quite ductile, yet at the same time it is easily peeled off when the seal was no longer required.

The whole guarded box was then covered with 50 mm thick polystyrene insulating pads. Aluminium papers were glued onto both sides of the polystyrene pads to reduce radiative heat transfer (see Figure 4.8). The inclusion of insulating pads increased the accuracy of control by cutting down the influence of the ambient condition would have on the chambers; the most important of which is the visible light radiation which is trapped by the "green house" effect of the Perspex guarded box. At places where it was not feasible to have the rigid polystyrene pads instored, mineral wool (20 mm thick) were used as insulation which was again covered at both sides by aluminium paper. SEE ERRATA SEE ERRATA SEE ERRATA

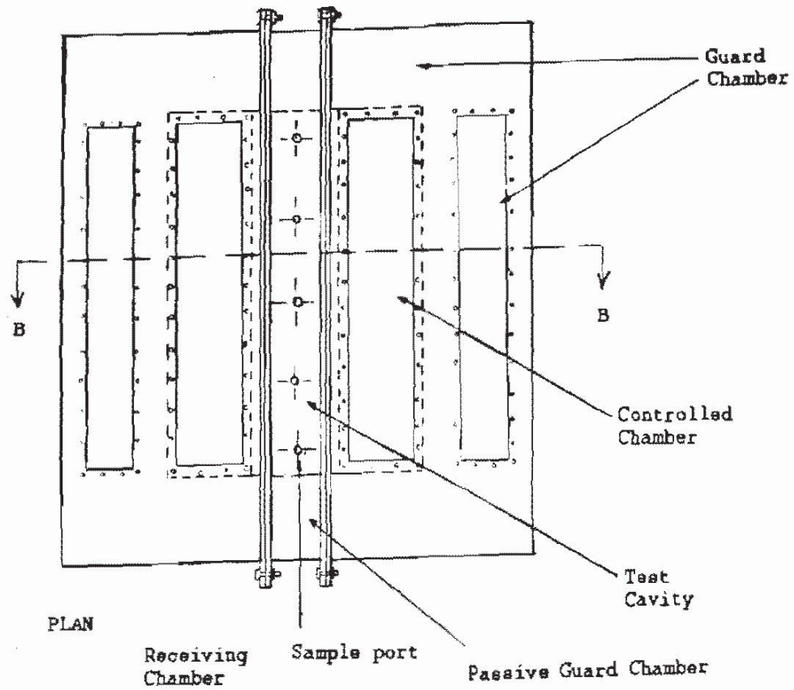

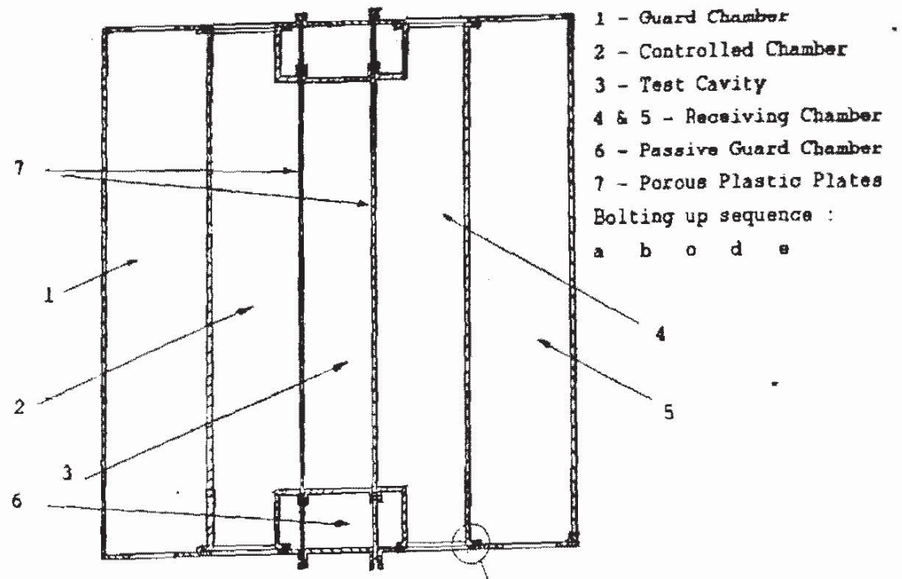

SECTION BB

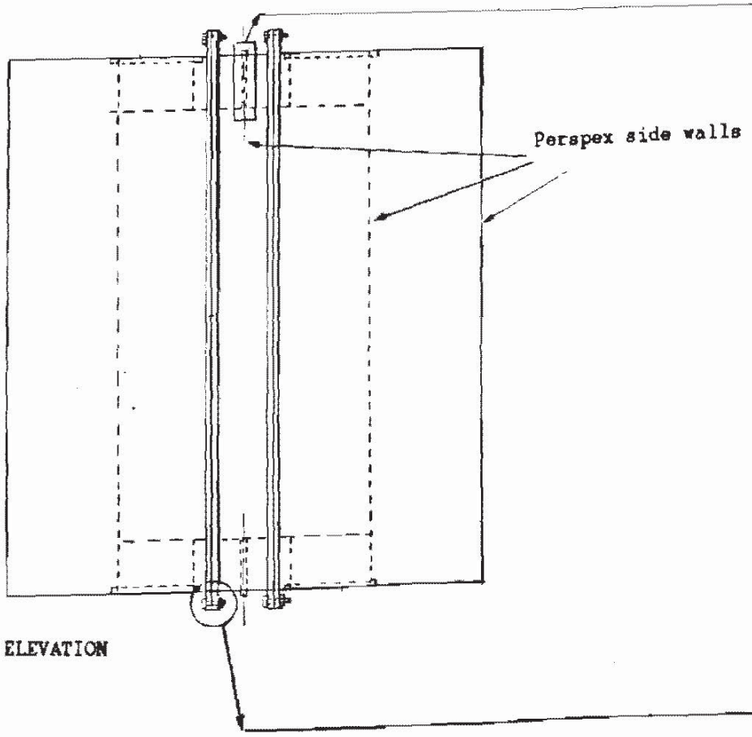

ELEVATION

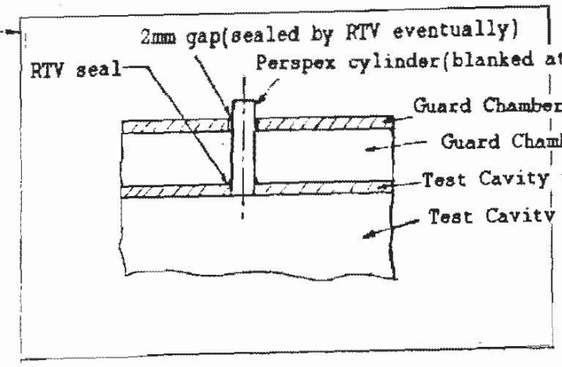

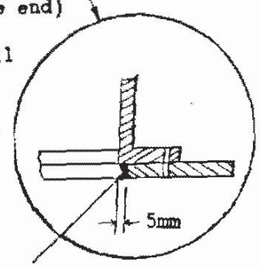

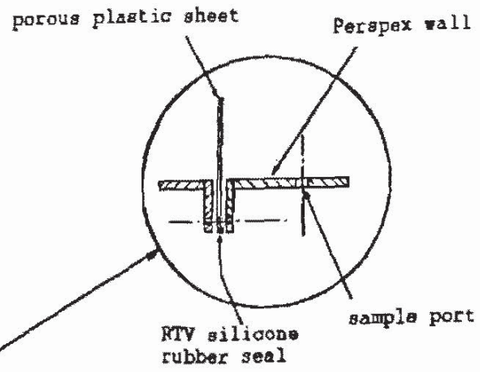

Fig. 4.2 Guarded Box Constructional Set-Up. For detailed dimensions, see Fig.4.3

Fig 4.3 Components of the Guarded Box.
Dimension in mm

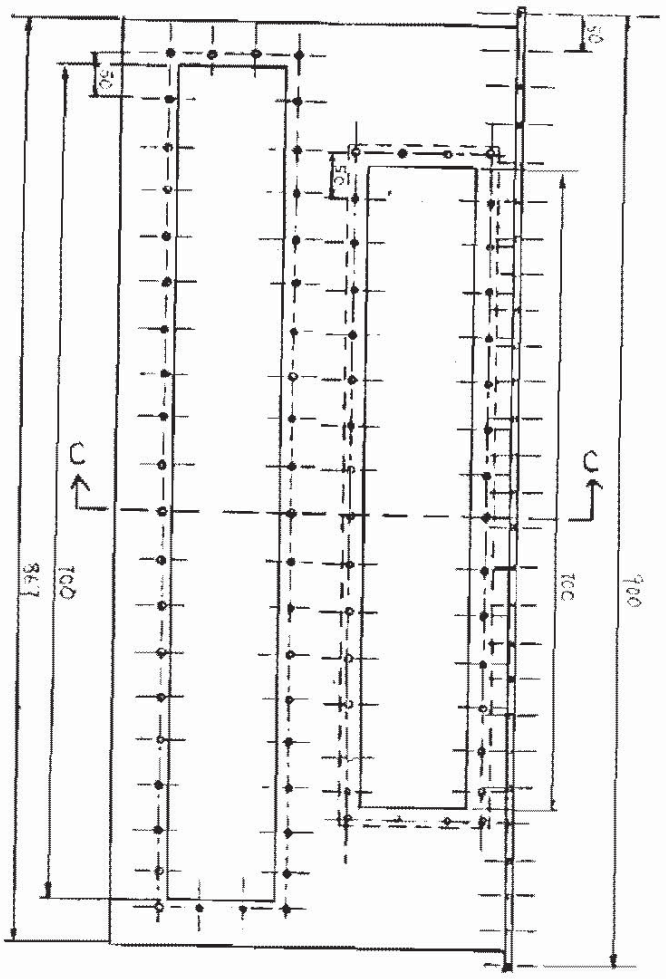

PLAN- CHAMBERS 1 & 5

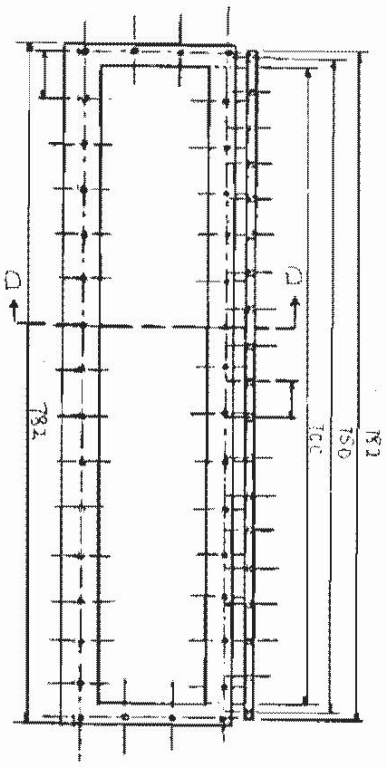

PLAN- CHAMBERS 2 & 4

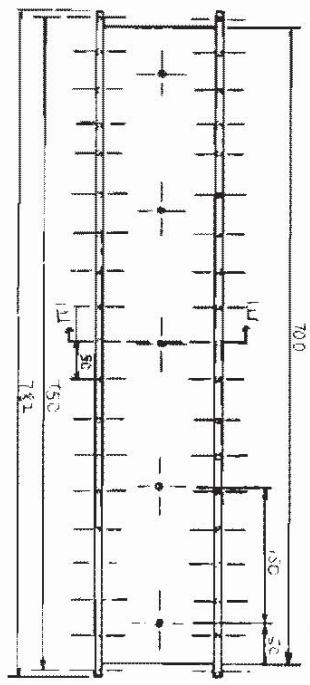

PLAN- CHAMBER 3

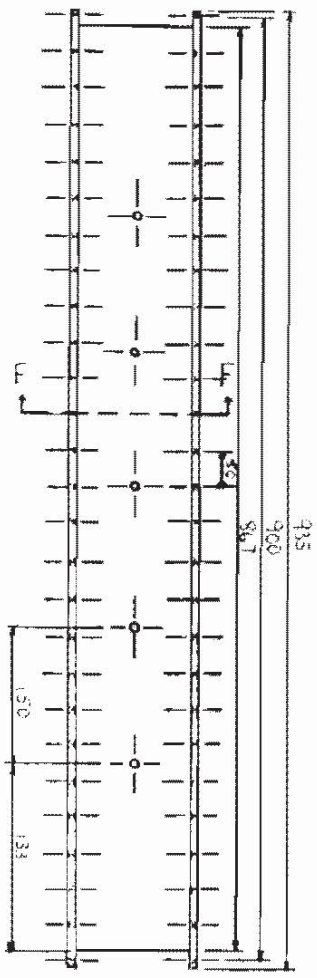

PLAN- CHAMBER 6

SECTION CC

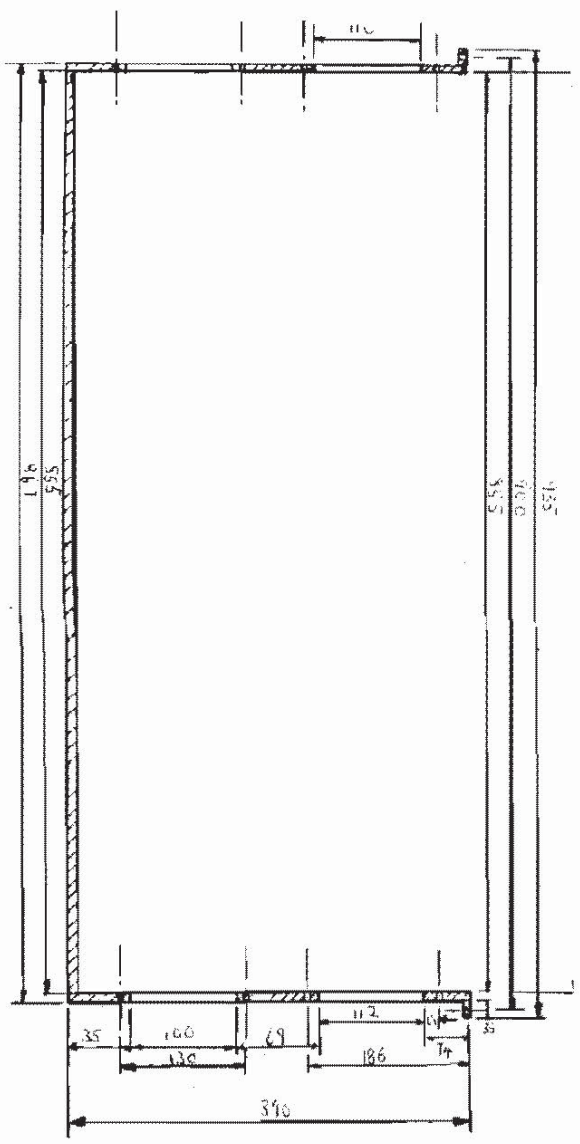

SECTION DD

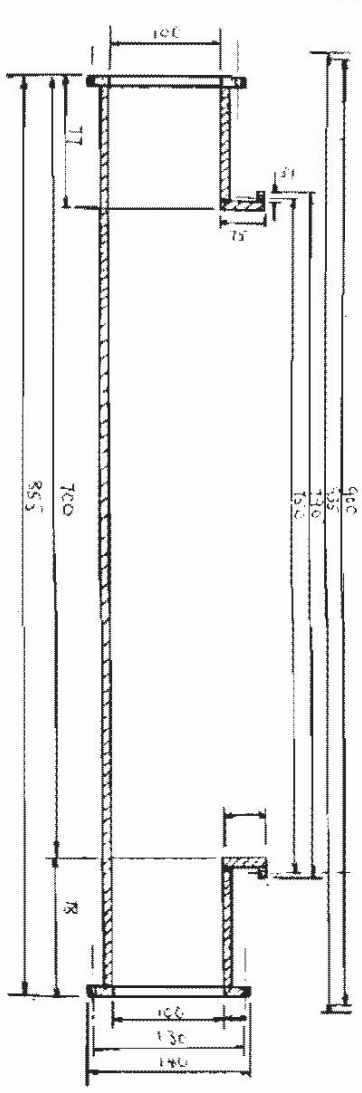

POROUS PLATE

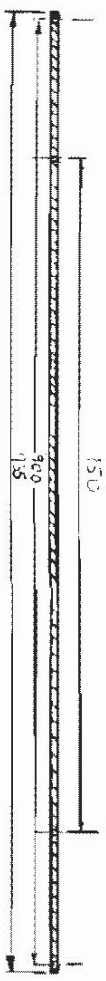

SECTION EE

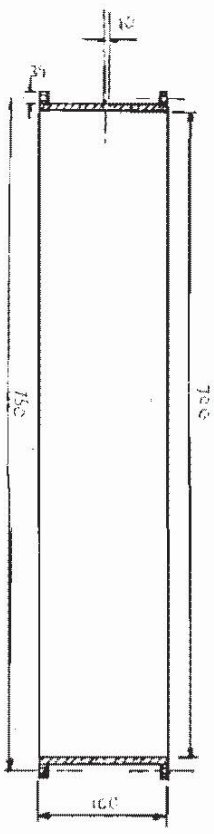

SECTION FF

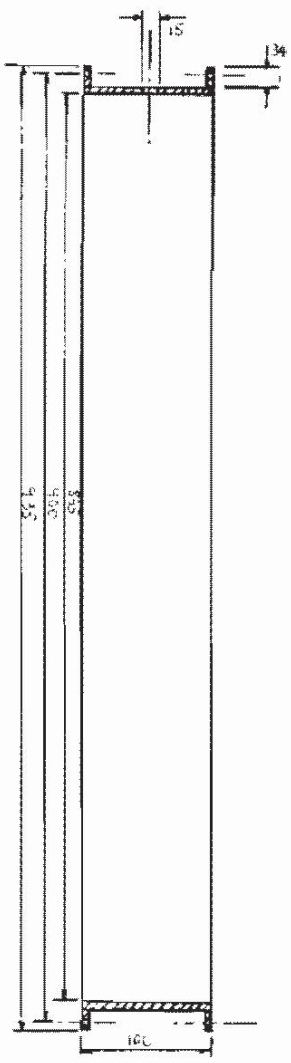

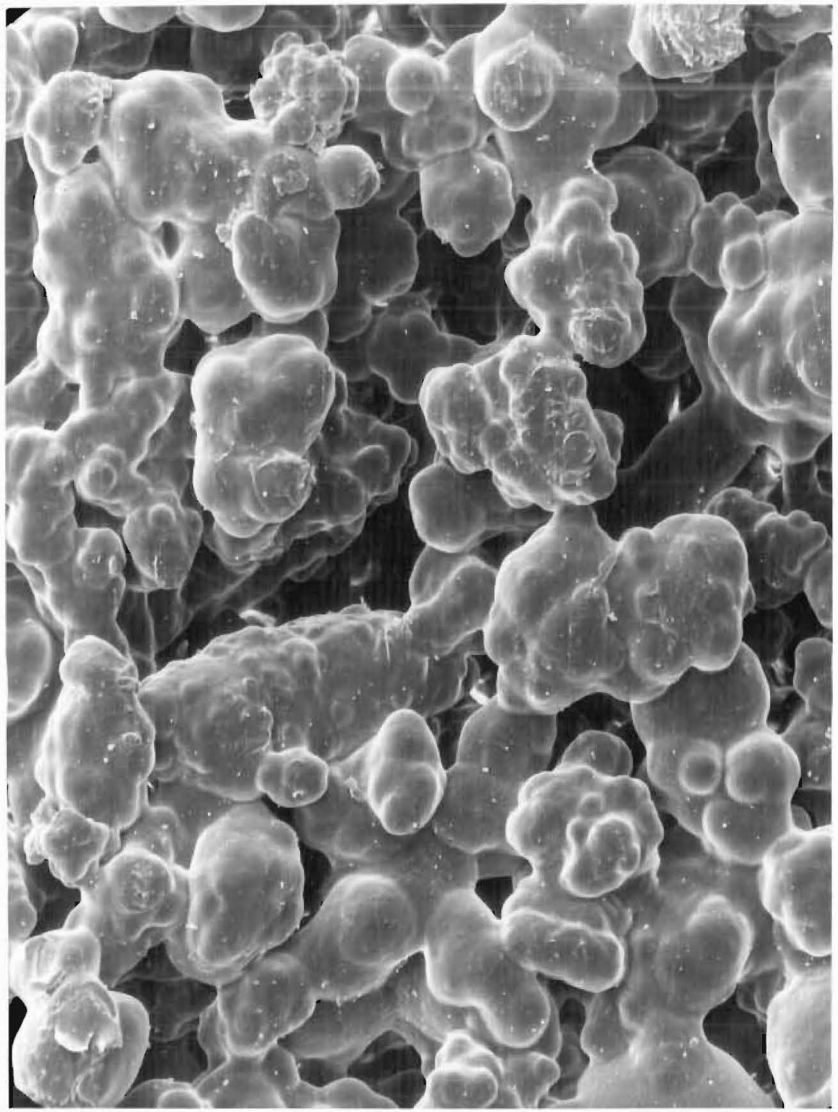

(a) Magnification x 180

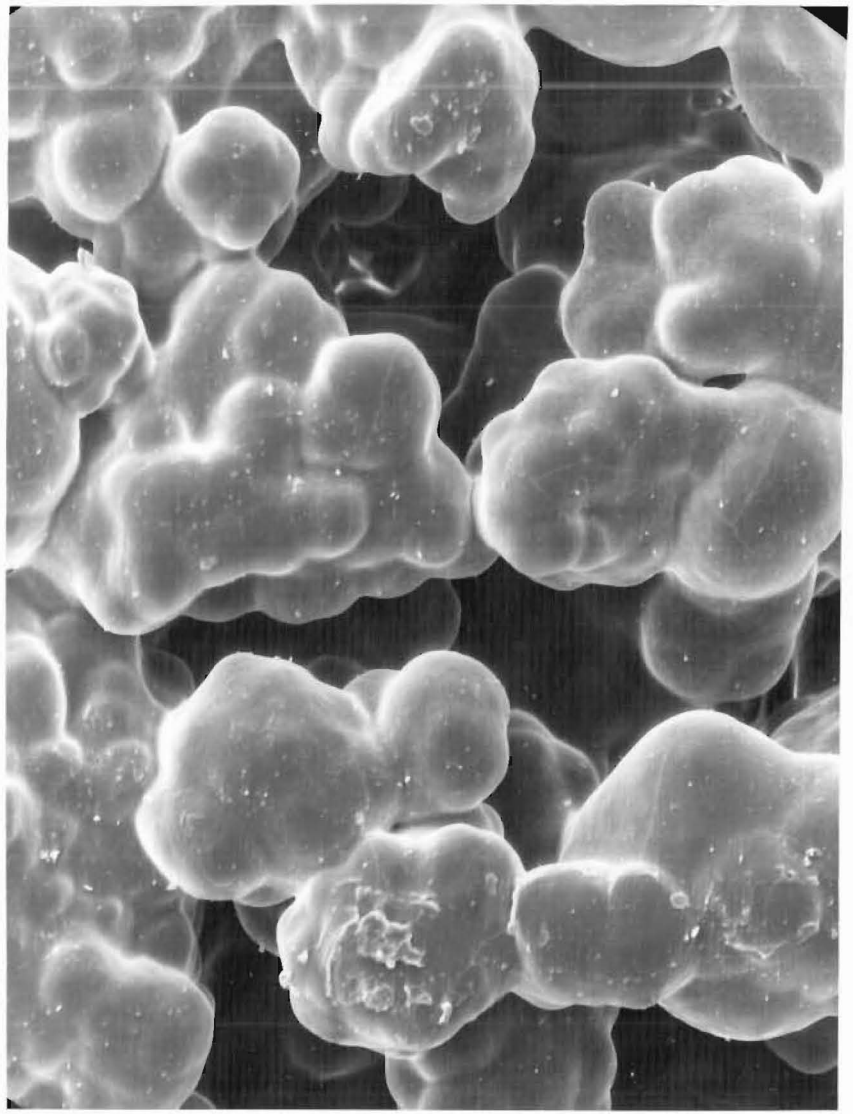

(b) Magnification x 400

Fig. 4.4: Microscopic Structures of Vyon Porous Plastic - Coarse Side.

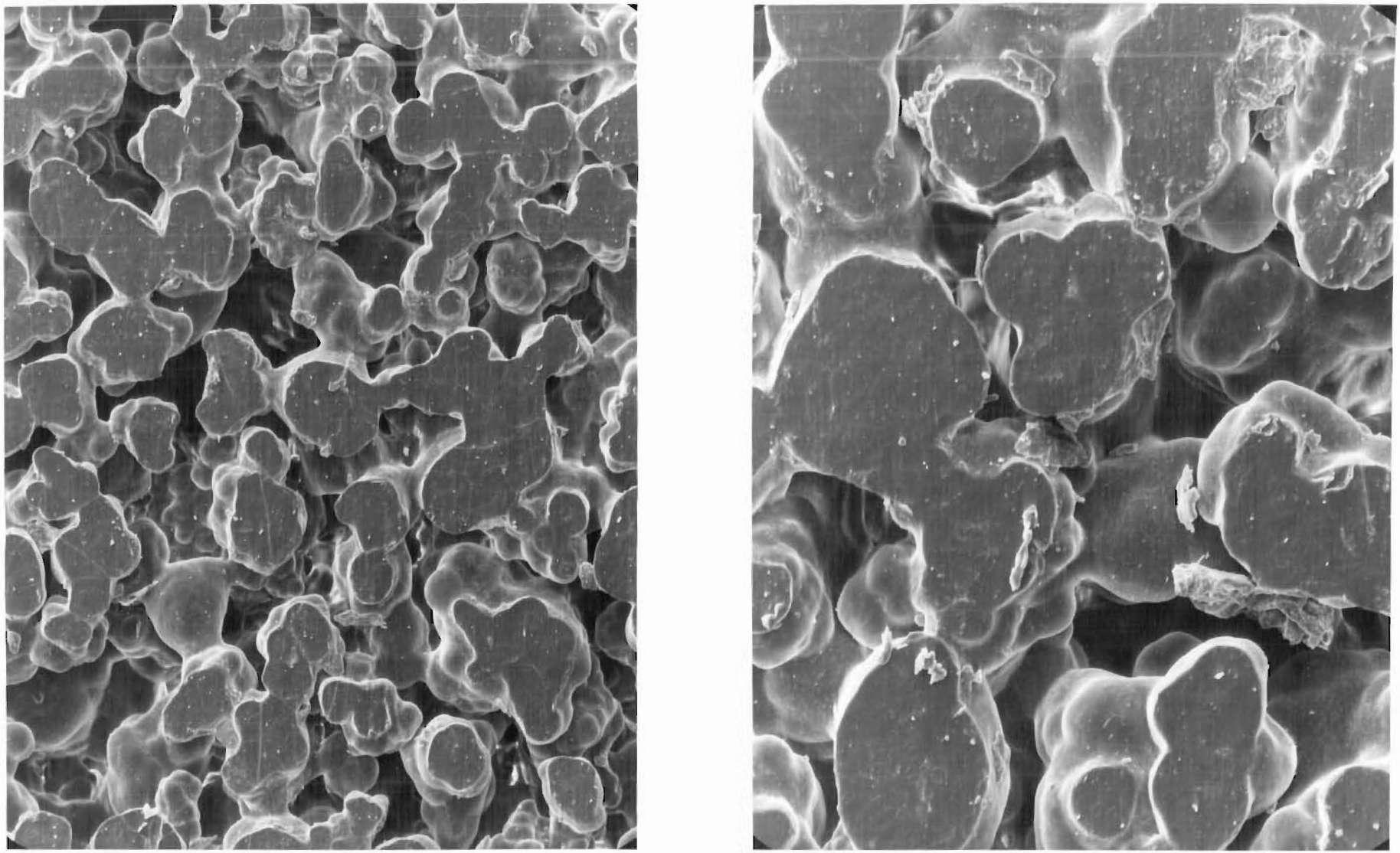

(a) Magnification x 180

(b) Magnification x 400

Fig. 4.5: Microscopic Structures of Vyon Porous Plastic - Smooth Side.

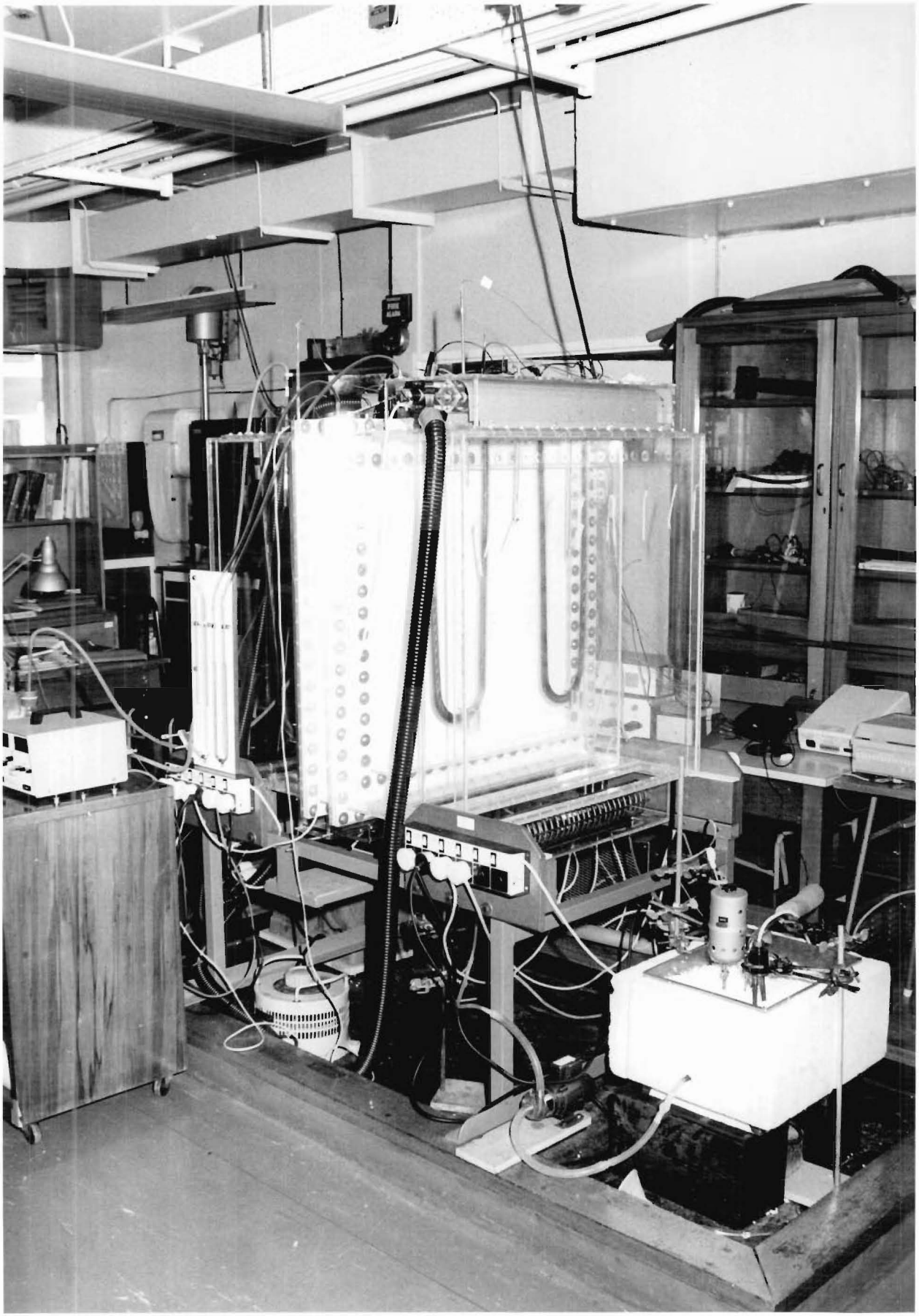

Fig. 4.6: The Guarded Box with the Condenser Circuit Located at the Bottom Right of the Picture.

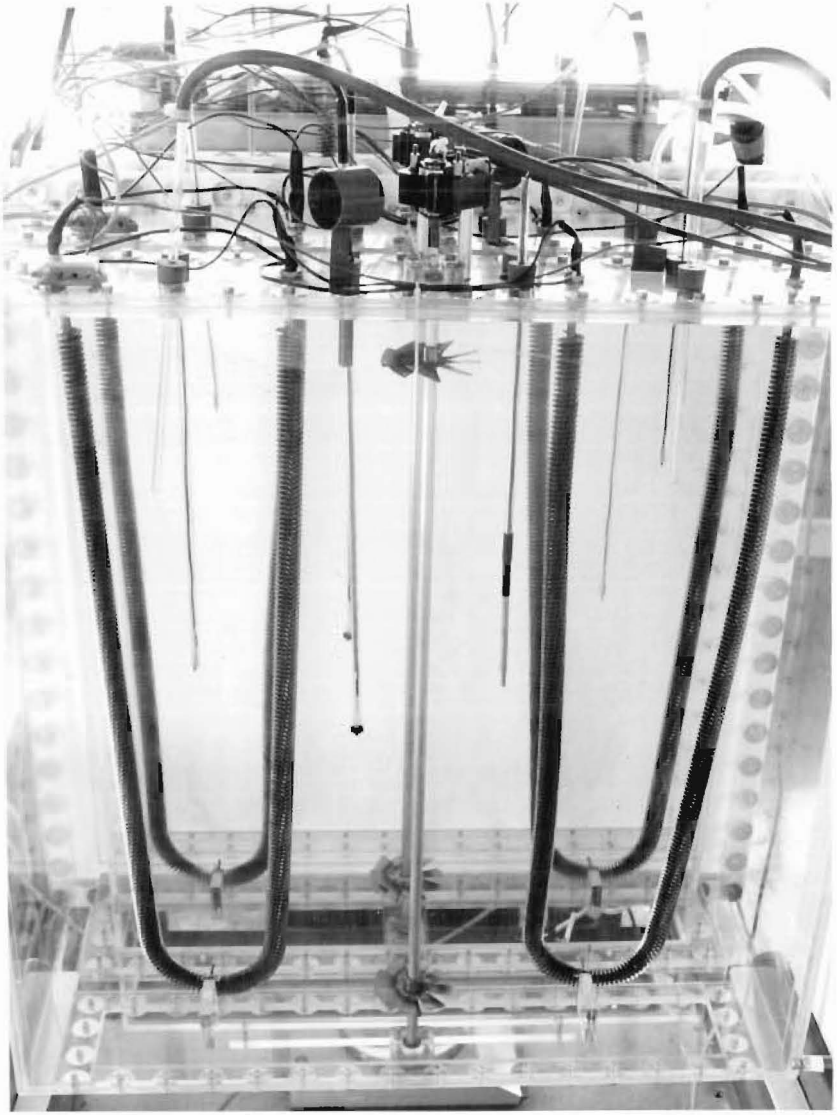

Fig. 4.7: The Finned Electric Resistance Heaters and the Fan Stirrers in the Controlled and Receiving Chambers. The Control and Measuring Sensors enter from the Top and the Electronic Balance is Located at the Bottom.

Fig. 4.8: The Insulated Guarded Box with the Temperature Controllers to the left on the Table and the Cooling Fan for the Fan Stirrers on the Ground.

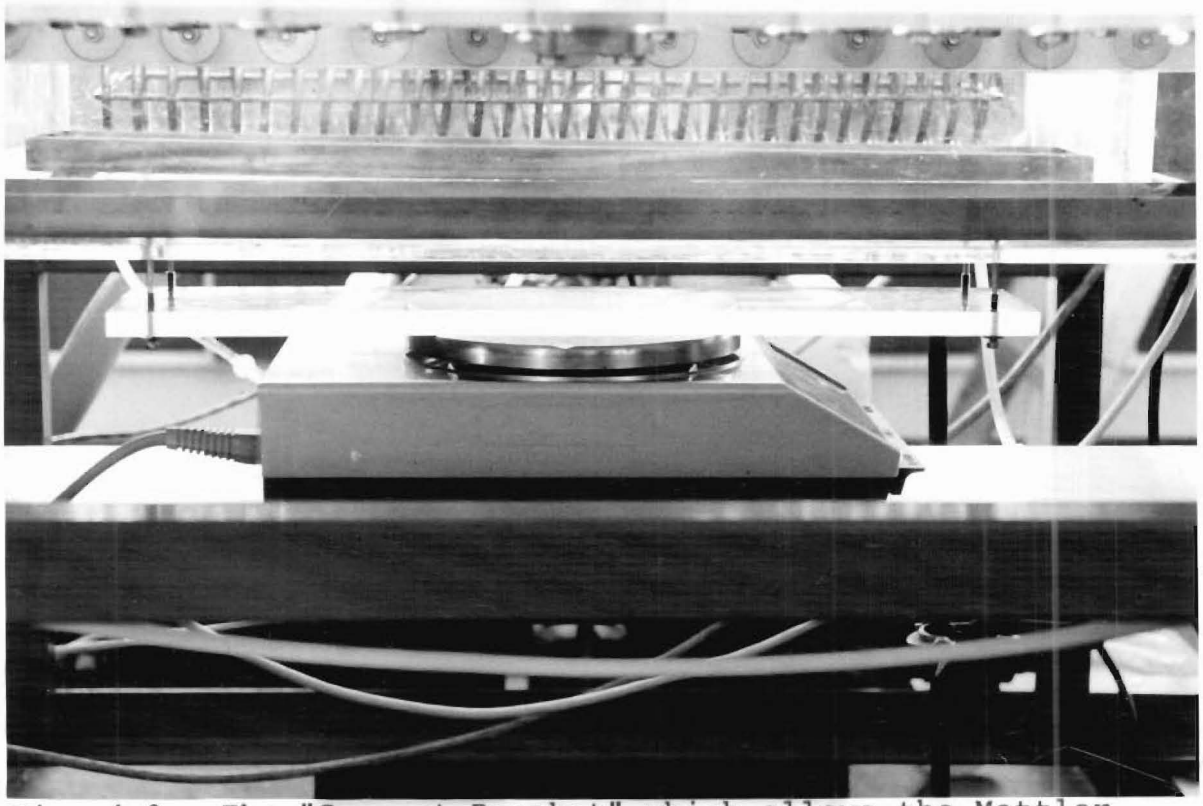

Fig. 4.9: The "Support Bracket" which allows the Mettler Electronic Balance to Measure the Weight Loss of the Evaporating Pan from the Outside of the Controlled Chamber.

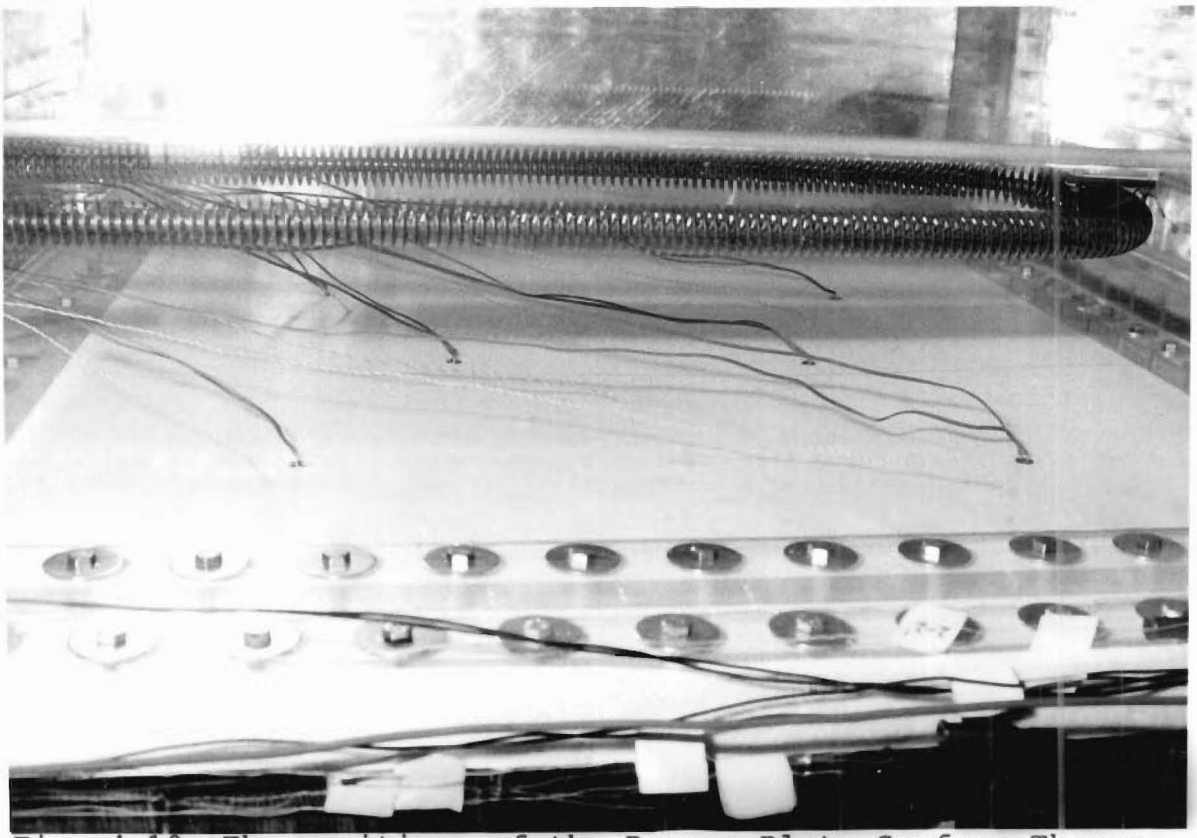

Fig. 4.10: The positions of the Porous Plate Surface Thermocouples in the Controlled and the Receiving Chambers (and for the "One Porous Plate" Case).

4.3.2 Inert Porous Plastic.

The inert porous plastic sheet used is made from high density polythene particles by a powder-sintering process with an average pore size of 200 μm. The thickness of the plate used was 4.75 mm and the material was found to be non-hygroscopic. It is manufactured by Porvair Limited of Norfolk, England under the trade name of "Vyon". Preliminary tests have indicated that the moisture transfer rate through the porous plastic sheet is slower than one would have expected from diffusional transfer, but surface adsorption effects are unlikely because of the size and the nature of the pores. A typical value for the mass-transfer coefficient K for the porous sheet is 0.95 g m^{-2} s^{-1} compared with K = 6.6 g m^{-2} s^{-1} for moisture diffusion through air under similar conditions (with vapour pressure difference of 450 Pa over a distance of 4.75 mm). Thus, the resistance for moisture diffusion through the plate is about 6.9 times as great as the resistance for moisture diffusion through air, and is comparable with diffusion resistance coefficients of porous plates reported by Krisher [173]. The rate of moisture diffusion through the porous plate also varies with the humidity potential applied across it. Each value of this diffusion rate will have to be found so that the transfer of moisture across the cavity can be measured. This is described in Section 5.1. Figures 4.4 to 4.7 illustrate the microscopic structure of the porous plastic taken with a "Joel JSM35" scanning electron microscope located in the Mechnical Engineering Department, University of Canterbury.

4.3.3 Auxiliary Equipment and Instrumentation.

Table 4.1 summarise all the equipment used to maintain the temperature and moisture gradient across the cavity in the guarded box; the subsequent measurement of the heat and moisture-transfer rates that results from it, and the eventual logging onto the computer of all these data. Some of the more important aspects of the equipment and instrumentation are elaborated in Section 4.4.

Table 4.1 Summary of Equipment and Items.

INSTRUMENT NO.	EQUIPMENT OR ITEMS	FUNCTION	COMMENTS
P111 to P116 1535 1536 1537 P125 P122 P123 P124	Finned Electric Resistance Heaters 125 W or 500 W rating Time proportional on-off temperature controller 10 K ohms Philips NTC thermistor Propeller stirrer powered by 50 W Betts Electric Motor with auto overload Tangential blower powered by 50 W Betts Electric motor with auto overload	Maintain the temperature levels in controlled, guard and receiving chambers to the desired values	See Section 4.4 for detailed description and results of preliminary testing
1148	Average power meter	Measure the power used by the resistance heaters in controlled chamber	See Section 4.4 for more details uncertainty ± 0.1%
315	Sorensen voltage stabilizer - output range 220 to 240 V	Supply a stabilized voltage to the electric resistance heaters	Langham Thomson AC voltage regulator, England, Uncertainty ± 0.3 V
P117 P118 P119	Honeywell Temperature Cut-off controller	To prevent the overheating of chambers when the controllers fail and the electric heaters are left to turn on continuously	Honeywell model T675A. Range from 75 to 125 degrees Celsius and temperature cut off is set at 80 degrees Celsius

Table 4.1 Contd.

P126	Thermocouple wires (6 with inter-changeable positions)	To measure bulk air temperature in all the chambers	24 SWG PVC covered. Also see Section 4.4 for details uncertainty ± 0.2 degrees Celsius
P127	Thermocouple wires (24 fixed on surface)	To measure porous plastic surface temperature	36 SWG PTFE covered. Also see Section 4.4 for details. uncertainty ± 0.2 degrees celsius
P120	Thermocouple Amplifier	To convert bulk air thermo-couples (P126) output from -40 µV/degrees Celsius into 10 mV/degrees Celsius with ice point compensation	Analog devices AD595 Monolithic Thermocouple amplifier with cold junction compensation. No ice point needed
P121	Thermocouple Switch	This selects the output of the thermo-couples (P126) to be displayed on the DC volt-meter (1260) or chart recorder (1596)	Single-pole switching only
1671	Thermocouple Amplifier	Converts the output of the surface differential thermocouple (P127) into a 0 to 10 V signal which is logged by the VAX computer	Low pass filter included and ice reference point is needed

Table 4.1 Contd.

1260	Data Precision DC Voltmeter	To read the output of Inst P121	Resolution is ± 0.5 mV which is equivalent to ± 0.05 degrees Celsius
1482	Hewlett-Packard 3468A Digital Multimeter	To read the output of surface thermocouples (P127)	Resolution is ± 0.001 mV which is equivalent to ± 0.025 degrees Celsius
1026	DC Power Supply	To power Thermocouple amplifier P120	DC 12 Volts
1596	2 Pen Chart Recorder	1. To record temperature, % power usage or any other desired quantities, 2. To check for steady state conditions	Graphtec Servo-recorder, SR6312 Tokyo Japan, Hot pen action inkless
P128	Condenser	To regulate the dry-bulb and dew-point temperature in the receiving chamber	6 mm O.D. copper tube of total length 9 mm wound into a coil
P129	Condenser coolant bath	To supply coolant of desired temperature to condenser	Total capacity of coolant in the insulated bath = 24 litres
147	Resistance Electric Element 1 kW rating	To control the cool bath temperature	See Section 4.4.4 for more details
1326 and 599	Norson "Liqua-cool" portable refrigeration units (400 W rating)		

Table 4.1 Contd.

1538	Time Proportional on/off temperature controller		
P125A	4.7 K ohms Philips NTC thermistor		
31	"Ranco" refrigerator controller 15 to -15 degrees Celsius range	Broad band control of the portable refrigerator - normally only used to prevent overcooling of the bath	
146	Stuart Turner 200 W centrifugal pump	For circulating coolant between the condenser and the bath	
682	Variable speed mixer	For mixing the contents of condenser coolant bath	
733	Variable power supply 0 - 240 V	To control the voltage to the circulating pump (146) so that rate of coolant flow can be regulated	See Section 4.4.4 for details
1110	AC Ammeter	Monitoring the current drawn by the circulating pump (146)	Range : 0 to 1 A
P30	Mercury in glass thermometer	Monitoring the coolant bath temperature	range -20 to +30 degrees Celsius uncertainty ± 0.05 degrees Celsius

Table 4.1 Contd.

1366	"Dew-All" Dew Point Sensor EG and G Model 911 Digital Humidity Analyser Massachusetts, USA	For measuring the dew-points in all the chambers	Uncertainty: Dew point = ± 0.3 degrees C Dry bulb = ±0.3 degrees Celsius rh = 0.5% nominal. See Section 4.4 for details
P131	Saturated salt solutions	To control the relative humidity in each chamber to the desired level	See Section 4.4 and Appendix 3 for details
1579	Mettler Electronic Balance Model PE3600 with RS232C output capability (using Mettler data output option 016)	To measure the rate of moisture transfer. The weight on the balance is logged inter-mittently onto the VAX computer to allow the rate of moisture transfer to be calculated	PE3600 Delta Range: Weighing range = 3600 g Delta range = 600 g Readability = 0.1 g In the delta range = 0.01 g
1568	Serial Parallel Interface (SPI)	To interface the Mettler balance average power meter, thermo-couple amplifier and Dew-All humidity sensor with the VAX computer	Accepts 0 to 10 V analog inputs RS232C to the VAX Accepts RS232C input from the VAX and outputs 0 to 10 V signal to the instrument's 5 channels

Table 4.1 Contd.

	Departmental VAX Computer	Data logger for the experiments and calculate all relevant information from the input raw data	Digital equipment corporation VAX 11/730 mini computer
1505	Computer Terminal	To communicate with the VAX computer	Digital Equipment Corporation VT05 terminal
752	Dew All Humidity Sensor Sample Circulating Pump	These constitute the Dew All humidity sensor sampling circuit which is trace heated all round to prevent un-wanted condensation of water vapour in the sampling system	240 V positive displacement piston pump Nominal flow rate = 1.20 lit/min
P132	Teflon sample tubes 6 mm I.D. tubes		Recommended by Dew-All humidity sensors manu-facturer - especially for low dew points
P133	6 mm O.D. glass tubes		For insertion into the various chambers
366	Casella Relative Humidity Recorder	Records R.H. of ambient Condition	Hair humidity measuring elements
P134 P135	Stainless steel pans: dimensions: length = 660 mm breadth = 90 mm depth = 20 mm	To contain the saturated salt solutions in the chambers for humidity control and for mass transfer measurement	Stainless steel pans have been coated with polyurethane to increase their chemical resistance

Table 4.1 Contd.

736	Variable power supply	Control and monitor the power supply to the Dew All sampling circuit trace heater	0 to 260 V
1108	AC Voltmeter		0 to 30 V
1107	DC Voltmeter		0 to 2.5 A
260	Lawson centrifugal blower	For forced convection cooling of the stirrer motors Inst. P122, P123 and P124	0.74 hp made in England
688	Variable power supply	To control the speed of the Lawson Centrifugal blower (Inst. 260)	0 to 240 V normally set at 100 V
1406	Hot wire anemometer "Davimeter" Air flow Developments Limited England	To measure air current circulation speeds in the chambers	Uncertainty ± 0.5 ms^{-1} instantaneous reading. Good at 25 degrees Celsius only
527	"Hydrophil" forced convection Psychrometer (Ultrahust, West Germany)	Cross checking the readings of Dew-All humidity sensor	Uncertainty ± 0.3 degrees Celsius. Less accurate than the Dew-All meter
	Hewlett Packard Quartz Thermometer Model 2801A	Calibrating the thermocouples	Uncertainty: better than ± 0.1 degree Celsius. This instrument is no longer available for use in the department as it the DSIR who owns it

4.4 DETAILED DESCRIPTION OF PRINCIPAL EQUIPMENT ITEMS

4.4.1 Electric Resistance Heaters (Inst. No. P111-P116) and Temperature Controllers (Inst. No. 1535-1537)

Six electrical resistance heating elements have been installed in the guarded box. Two heaters each were mounted into the guard, controlled and receiving chambers respectively (see Figure 4.7). The maximum power output for the two heating elements in each chamber is either 125 or 500 W depending on whether the two heaters are connected in series or in parallel. The temperature controller (see Figure 4.8) can vary the output from the heater from 0 to 100 percent of the maximum power available by means of a time proportional on/off control (e.g. if controller is on for 50 % of the time and if the nominal heater output is 500 W, then the average power output over that one second period is 250 W). The percentage of the power output can be logged continuously by the average power meter (Section 4.3.2.2). The nominal power output of the heater elements is measured precisely by measuring the resistances of the elements periodically at the operating temperature (using a precise ohmmeter (Inst. No. 1482)) and having a known, stabilised voltage supply to the elements (by Inst. No. 315). Thermistors, of 10 K ohm and having negative temperature coefficient (Inst. P125), are used as sensor elements for the time-proportional on/off controller.

4.4.2 Average Power Meter (Inst. No. 1148)

This instrument is simply a counter which displays the total number of cycles of the AC line which has been impressed across a resistance load (the heaters) as a percentage of the time period selected. The periods available are 10 seconds, 30 seconds, 1, 2, 4 or 8 minutes. The input into the counter must be an integral cycle of the power supply and the counter as such is not suitable for instruments which rely on phase control of the AC supply and therefore pass fractions of a cycle of the supply to the load. The counter is plugged in parallel with the AC supply to the load being measured. This inlet consumes negligible power and is

optically isolated from the electronics and earth. The output is displayed on the meter as a percentage of the time period selected when the known voltage was applied across the load. Both analog and digital output capabilities are available for continuous data logging onto the VAX computer via the Serial-Parallel interface (SPI) (Inst. No. 1568) or onto a chart recorder.

4.4.3 Fan Stirrers (Inst. No. 1535-1537)

Propeller stirrers have been installed in the guard and controlled chambers, while a tangential blower is used for the receiving chamber. Each of these stirrers is powered by a 50 W Betts motor which is located outside of the respective chambers (see Figure 4.9). These motors in turn have to be cooled by a separate blower (Inst. 260) (Figure 4.8) to prevent them from overheating.

4.4.4 Condenser (Inst. No. P128) and Constant Temperature Water-Bath (Inst. No. P129)

The condenser in the receiving chamber consists of a 6 mm O.D. copper coil of length 9 m through which coolant at a controlled condition is passed (Figure 4.6). The temperature of the coolant (60 % ethylene glycol and 40 % water) is regulated in an insulated bath by means of refrigerating (Inst. 1326 or 599) and heating (Inst. 147) units to within ± 0.1 °C. The heating unit is being controlled by a time proportional on/off controller (Inst. 1538) as described before while the refrigerator unit is set at such a rate that it is on all the time, so in effect the control action is done entirely to the heater only (a stirrer is provided in the bath to ensure uniform temperature throughout the bath). A pump (Inst. 146) circulates the coolant through the coil. The rate of circulation can be controlled by controlling the voltage input to the pump by the use of a variac. The coolant temperature used would correspond to the dew-point temperature of the air in the receiving chambers, and temperatures as low as -20 °C can be achieved in the coolant temperature. The connecting hoses from the controlled bath to the condenser are insulated to improve control

accuracy. A collecting tray arrangement underneath the condenser remove the condensate from the receiving chamber.

4.4.5 Thermocouples and Temperature Measurement

The combination of the items mentioned in Section 4.3.2.1 to 4.3.2.4 will allow the control of the temperature level in each chamber. The temperature is measured by copper constantine SEE ERRATA thermocouples. Both bulk air and surface temperatures are measured. Thermocouple wire of 24 swg is used to measure bulk air temperature in the chambers. The thermocouple junctions are mounted at the end of a glass tube which is inserted into the chambers via openings at the top (see Figure 4.7). The positions of the thermocouple junctions in the chamber can be varied by changing the length of the glass tube or by inserting it through other openings, but generally an average of four positions were used to determine the bulk air temperature. The output of the thermocouples was amplified by a monolithic thermocouple amplifier (Inst. P120) from about 0.040 mV/°C to about 10 mV/°C. This allows the recording of the bulk air temperature onto a chart recorder (Inst. No. 1596). The thermocouples were calibrated against a standard reference source (Appendix 6) before being used in the experiment. Plate surface temperatures were measured using 36 swg thermocouple wires using a differential mode of measurement. Surface temperature measurement is difficult and there are a variety of ways surface thermocouples can be attached (see Ref. 168, 169, 172). Other factors such as conduction effects along the thermocouple wires and radiative heat transfer interference can also lead to erroneous readings. A full treatment on this subject is beyond the scope of this work. Thus only the methods used are described here. The effectiveness of each method can be judged in the end by the final results obtained.

Surface thermocouple junctions would affect the surface characteristics of the material being measured no matter which methods are used. Good surface contact is the main consideration in this work. Thus the thermocouple junctions are soldered onto a brass ring of outer diameter 9.5 mm which is in turn heat pressed into the porous plastic sheet (Fig.4.11). This ensures good thermal contact between the plate surface and the brass ring which

is essentially isothermal. Two different variations of this principle was adopted. The first was to leave the thermocouple junctions exposed, while the second version was to insulate the thermocouple junction with silicone rubber and shining aluminium paper to eliminate completely surface radiation effect (but with added insulation effect introduced by the silicone rubber)

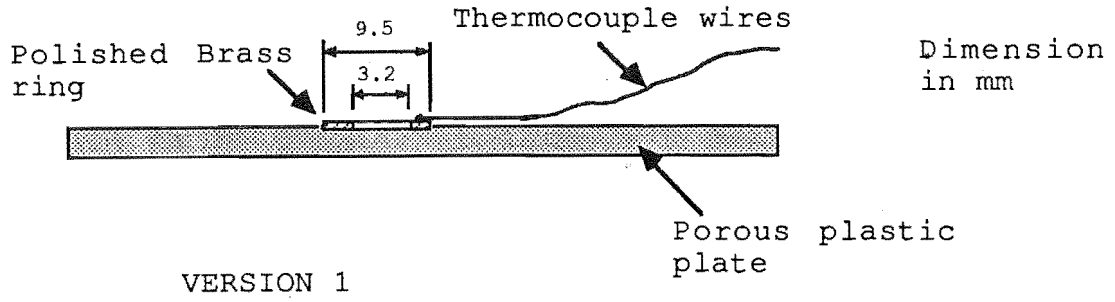

VERSION 1

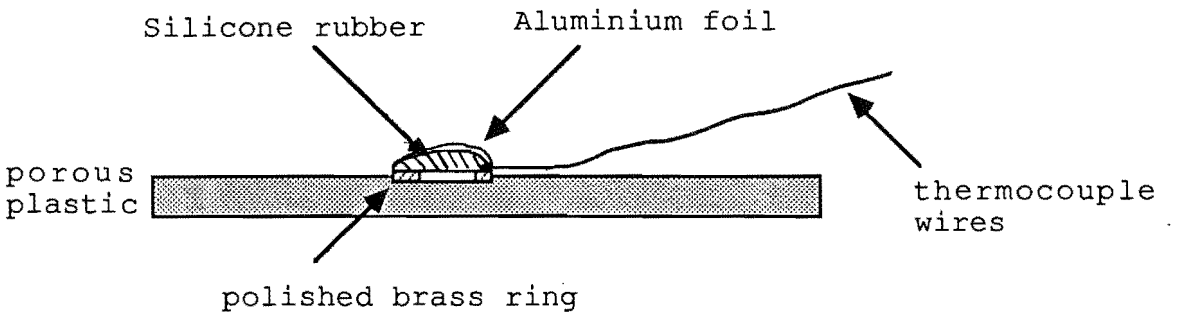

VERSION 2

Fig.4.11 Arrangements of Porous Plate Surface Thermocouple.

Tests later have indicated that Version 1 gives a better estimate of the surface temperature than Version 2 which consistently overestimate the surface temperature (from heat balance considerations). It was thought that the surface thermocouples in Version 2 actually measured the sub-surface temperature of the porous plate due to the insulating effect of the silicone rubber which completely surrounds the thermocouple. In Version 1, although exposed to thermal radiation effect, this effect is small because the thermal absorbance and emittance of a

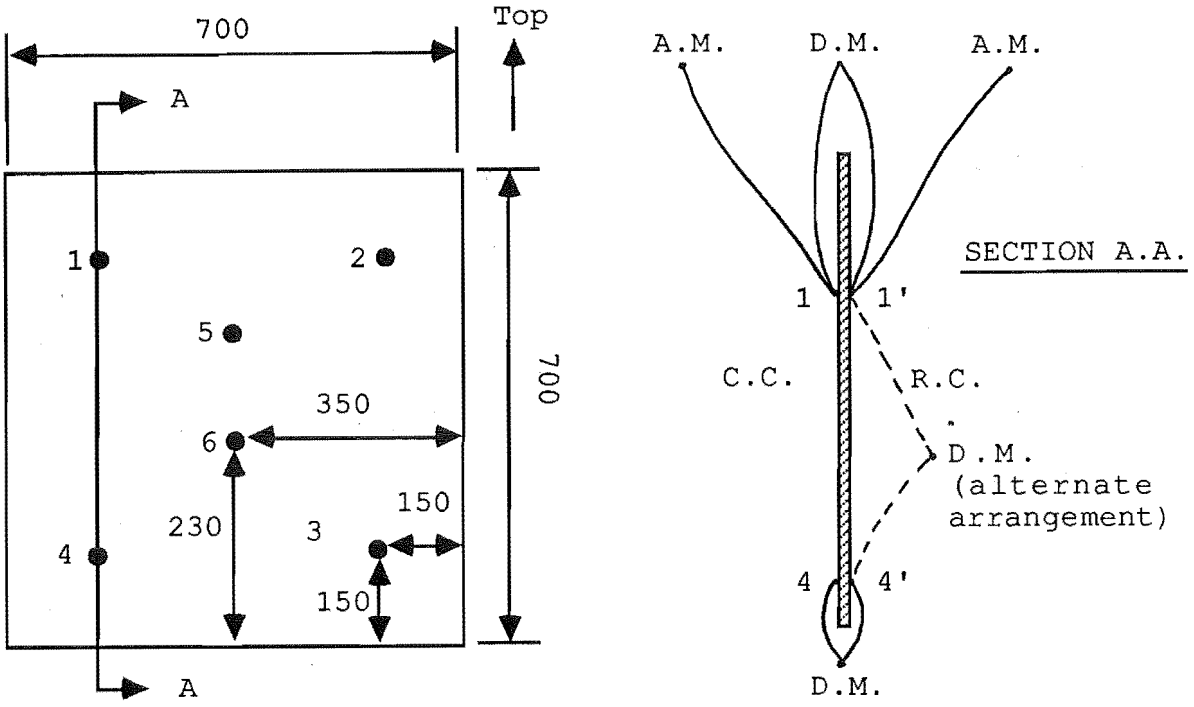

● Thermocouple positions on the porous plate in vertical mode viewed from Controlled Chamber. (Points are symmetrically placed)

Dimensions in mm

A.M. : Absolute measurement

D.M. : Differential measurement

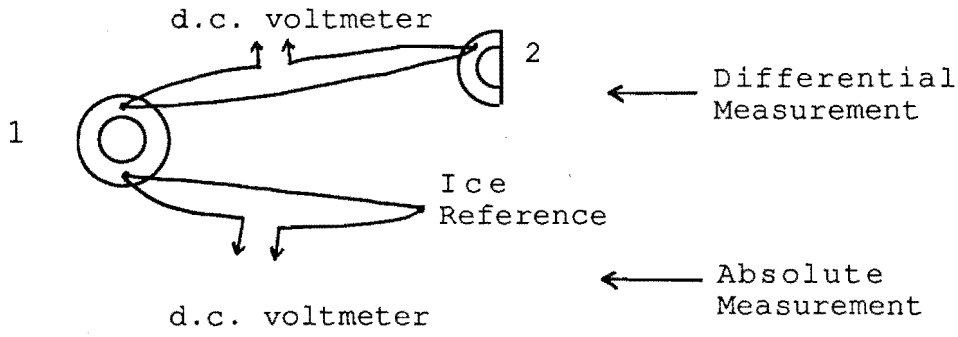

Each point 1-6 has two thermocouple junctions on an isothermal brass ring, thus allowing differential and absolute measurement across the plate or around the surface of the plate depending on the type of connection made. Measurement of thermocouples voltages is done in isolation with a HP multimeter to eliminate the generation of current loop between the thermocouples. The same procedure is carried out when logging selective thermocouple voltages onto the VAX computer.

Fig. 4.12 Arrangement of Surface Thermocouples on Porous Plate.

polished brass ring is only about 0.03 (e.g. Ref. 171). The emmitance and absorbance of solder is less clear as only a single value was found with e = 0.047 at T = 77 K [161]. Thus its reflects more closely the surface temperature of the porous plate surface. Of course, Version 1 is still not the perfect arrangement for the surface thermocouple as the emittance of the ring and solder are not identical to that of the porous plastic sheet. To just heat- fuse a single thermocouple junction directly onto the porous plastic plate is difficult because the strength of adhesion was found to be low and the risk of thermocouple junction falling off is high (it takes about a week to dismantle everything and to reinstore the thermocouple point). To hold the thermocouple junction onto the porous plate surface by a glue similar in emittance to the porous plastic would work, but this technique also introduces the additional insulating effect as occurred for Version 2 mentioned earlier. Thus Version 1 was the configuration chosen for this work.

Six pairs of differential thermocouples are used to determine the surface temperature variation of each of the porous plastic plates (see Figures 4.10 and 4.12). Two additional thermocouple junctions are used to determine the absolute temperature level. The reference junction used is ice-water mixture and the output in μV is measured by the precision HP multimeter (Inst. 1482). All the thermocouples are isolated from each other and no current loop is generated between them. When a certain thermocouple needs to be logged onto the VAX computer, they are done so in such a way that no current loop is generated between them.

4.3.6 Mass Transfer and Humidity Measurement.

The Mettler balance (Inst. 1579) used for mass-transfer rate measurements has a sliding "delta range" within which the accuracy of the balance is ± 0.01 g. This balance records the evaporating loss from the surface of a pan containing distilled water or saturated salt solution (see Figure 4.9). The balance weights readings are converted into a RS232C signal which is then accepted by the VAX computer via the serial parallel interface (SPI). The frequency of data transfer is being controlled by a program being

run on the VAX which utilises the VAX'S electronic clock. Normally a weight reading is transferred in every 4 minutes for a run which might last for 30 hours (steady state). The rate of mass transfer is found by the simple second-order central difference formula (Appendix 1). The rate encountered in the experiments ranged from 3 to 16 g h^{-1} under steady-state conditions. Hence the balance is sufficiently accurate for this purpose.

The Dew All humidity sensor gives the moisture-gradient across the cavity by measuring the dew points in each chamber. It also has a platinum resistance sensor to measure dry-bulb temperature. It outputs a 0-10 V signal and this is logged by the VAX computer via the SPI.

Thus to summarise, Figure 4.13 illustrates the operating characteristics of the equipment in the controlled chamber.

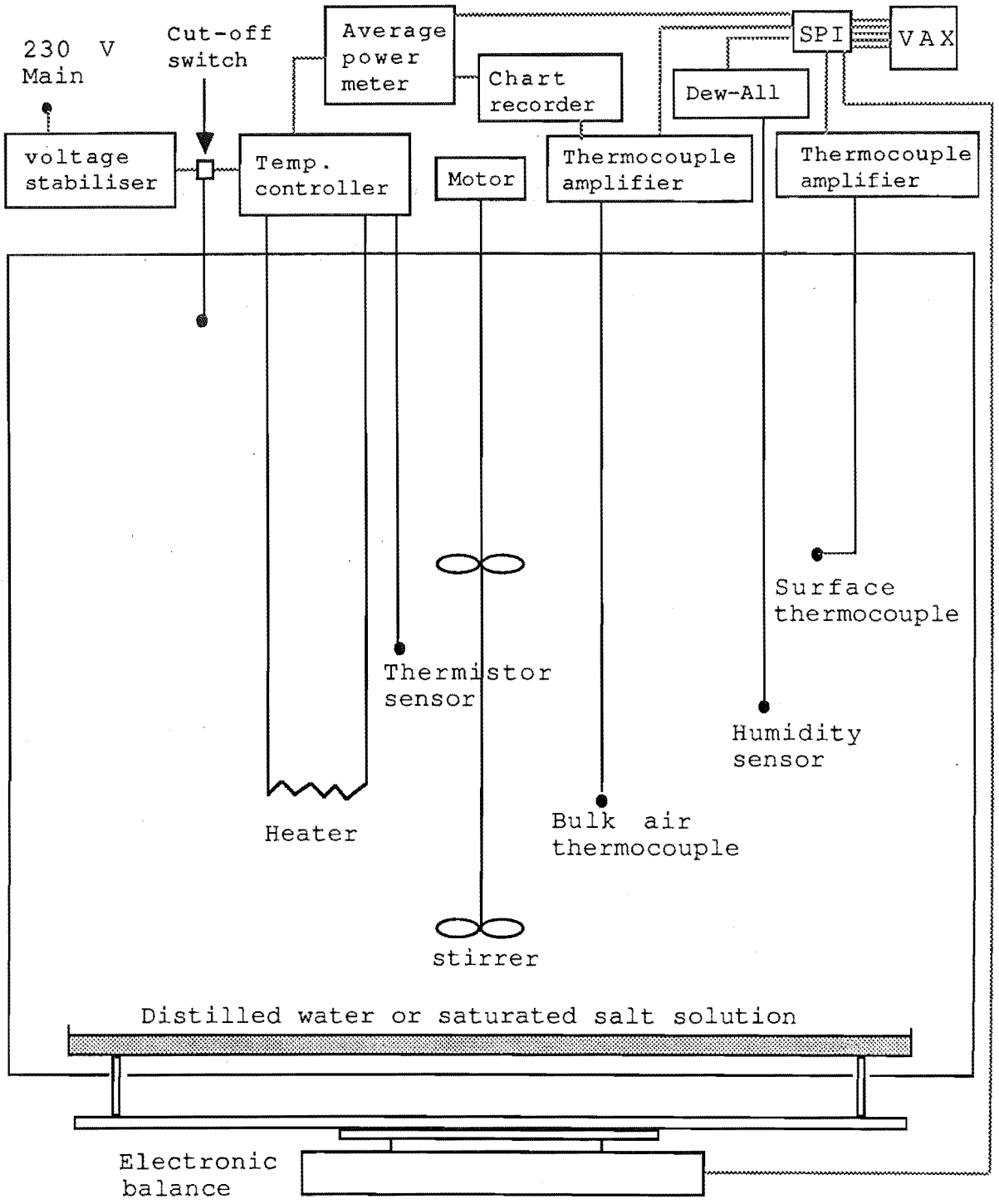

Fig. 4.13 Controlled Chamber Instrumentation.

4.4.7. Summary of Preliminary Tests.

Table 4.2

Function Tested	Equipment Used	Tests Results
Uniformity of Bulk Air temperature in Chambers by Fan stirrer. All chambers are heated simultaneously to the same temperature.	1. Temperature controller 2. Electric heaters 3. Fan Stirrers 4. Temperature sensors	Within ± 0.1°C of set point from point to point in the chamber if temperature excess over ambient is 15°C and within ±3°C if temperature excess is 40°C (Insulated chambers).
Heating Effect of fan stirrers.	1. Fan stirrers 2. Temperature sensors	The rise is about 0.7°C for the uninsulated hot box and about 5 to 7 °C for the insulated hot box (with 50 mm thick aluminium paper covered polystyrene pads.
Combined effect of condenser and heater in the Receiving chamber.	1. Fan stirrers 2. Electric heaters 3. Temperature controller 4. Temperature sensor 5. Fan stirrer	The largest variation in bulk air temperature is 0.8°C from point to point with bulk air temperature = 35°C and the condenser coolant temperature = 2°C.
Control of relative humidity.	1. Salt solution 2. Condenser 3. Equipment to control dry bulb temperature.	Relative humidity from 35 to 85% is easily achieved depending on the situation. Due to some openings in the Guarded box (eg. where the balance support goes through - see fig 4.7), rh greater than 85% is difficult to achieve. Changing the condenser condition not only affects the rh in the Receiving Chamber, but also has an effect in the rh in the controlled chamber. Hence total independent control of rh in the two chambers is not achieved. However sufficient flexibility still exists to allow a wide range of vapour pressure to be imposed across the cavity by manipulating a range of evaporative source in the Controlled Chamber and condenser conditions in the Receiving Chamber.

Calibration of Thermocouples	1. Thermocouple wires 2. Quartz Thermometer 3. "Dew-All" dry bulb probe.	Accuracy of calibrated thermocouple = ± 0.2°C (see Appendix 6 for details).
Calibration of Dew Point Sensor	1. Dew Point sensor 2. Selected saturated salt solution 3. Temperature controlled bath.	Accuracy of dew point sensor = ± 0.3°C (see Appendix 6 for details).
Hygroscopicity of porous plastic plate.	1. Porous plastic 2. Humidity chambers 3. Dessicator 4. Weighing balance.	The porous plastic from the dessicator into the humidifying chamber does not cause a weight change after 1 to 7 days. Conclude that porous plastic is non-hydrogroscopic.
Hygroscopicity of perspex sheet	1. Perspex strip 2. Humidifying 3. Dessicator 4. Weighing balance.	Perspex is found to be hygro-scopic. Only maximum likely adsorption/desorption rate is found.No attempt was made to determine this rate as a function of rh explicitly. A strategy is proposed to eliminate the error due to this effect on the moisture transfer - see Section 5.5.2 and Appendix 5.
Infra-red Transmittance of perspex sheet	1. Perspex strips 2. Perkin-Elmer Infrared spectro-photometer model 377 (Instr no. 349).	6 mm perspex sheet is found to be opaque to infra-red radiation emitted by the electric resistance heater over the wavelength range 2.5 to 25 micron (see Section 5.5.1 and Appendix 5 for details).

CHAPTER 5

EXPERIMENTAL PROCEDURE AND PRINCIPLES OF MEASUREMENT

5.1 ESTABLISHING STEADY-STATE CONDITION

5.1.1 Steady State Temperature Level

The fan stirrers in the chambers are first turned on. To maintain a steady-state temperature level higher than the ambient temperature, the heater controller is set to its maximum value during initial heating up. The temperature in the chambers is monitored by the four thermocouple junctions which measure the bulk air temperature and by the surface thermocouples on the porous plates. The power requirement of the heaters is also monitored by the average power meter. During the process of transient heating, the power requirement of the heaters is progressively becoming smaller as steady state is approached. This reduction in power consumption is accordingly adjusted by the heater controller during the heating up process as guided by the average power meter. Steady state is achieved when the thermocouple outputs and the heater power consumption, as shown on the chart recorder, are constant. The power setting on the temperature controllers at this stage is adjusted so that just enough power is supplied to the heaters to maintain the temperature. The transient heating up process normally takes from 2 to 5 hours depending on the final temperature level required and the controller setting. To achieve best control, it is always advisable to adjust the controller setting so that the maximum power output by the heaters is about 5 to 10 W above the required power during transient heating up and not more than 2 W above the required power level during steady-state heating. The well stirred, insulated chambers with their large time constants are adequately served by these simple on off controllers as bulk air temperature fluctuations of not more than ± 0.5 °C are encountered for even the most severe situation. The temperature variation on the porous plate surface is greater and can reach ±

1.0 °C for the worst case.

To maintain a temperature level lower than the ambient condition (in the Receiving chamber only); the heater is not turned on initially and only, the condenser is used to cool the air in the chamber. Coolant at temperature 15 to 20 °C lower than the ambient is circulated through the condenser. The temperature level in the chamber is again monitored by the four thermocouple positions and the thermocouples on the porous plate surface. When the desired set-point temperature is reached, the coolant capacity is eased back and the temperature controller is turned on. As the control action of the heater on the air is much faster than the cooling coil, it is the fine control element. The capacity of the heater and condenser is adjusted to their respective minima to minimise the overshoot and undershoot of the air temperature about its set point. Transient cooling time is typically from 3 to 6 hours depending on the final temperature required. Temperature fluctuations similar to that found in the Controlled Chamber are encountered.

SEE ERRATA

5.1.2 Steady State Moisture Level.

To humidify the controlled chamber, a pan of distilled water or saturated salt solution is placed in the controlled chamber. This pan rests on a support which in turn sits on the electronic balance. The evaporative loss from the pan is indicated by the readings on the electronic balance. The "Dew-All" humidity sensor is used to measure the dew point of the bulk air in the chamber. Steady state is achieved when the dew-point reading and the evaporative loss rate remain constant. Normally 8 to 10 hours are allowed for this process. A longer time than this is necessary if the Perspex chamber had not been previously exposed to the level of relative humidity required in the chamber. This " conditioning" period is normally 24 hours or more. The purpose is to reduce the moisture loss/gain due to adsorption/desorption by the Perspex.

This adsorption rate is only significant when averaged over the first 24 hours even for the most extreme case tested (with a relative humidity change of 100 percent which is not to be

SEE ERRATA

encountered in this work). A desorption rate of similar (but not equal) magnitude is found when the reverse test is carried out (see Section 5.5.2 and Appendix 5). The level of relative humidity encountered in the controlled chamber mostly ranged from 30 to 70 percent which is not too much a deviation from the room relative humidity of about 30 to 50 percent. Under such cases, the adsorption/desorption rate is tested to be normally under 0.1 g m^{-2} s^{-1} after 8 hours of "conditioning". In reality, the Perspex chamber would go on for weeks for a series of experiments with the change of relative humidity not more than a few percent when going from one condition to the next, thus making this adsorption/ desorption rate negligible.

The humidity level in the Receiving Chamber is controlled by either a pan of saturated salt solution or the condenser. Normally the condenser is used. The outlet water of the condenser is adjusted so that it corresponds to the dew point required in the Receiving Chamber. As no measurement on moisture transfer is made in the Receiving Chamber, the Perspex adsorption/desorption rate is not a factor here.

The humidity level in the Guard Chamber is also not controlled for the reason outlined in Section 4.2.

5.2 CORRECTION FOR HEAT LOSS TO SURROUNDINGS AND HEAT GAIN FROM FAN STIRRER ACTION IN CONTROLLED CHAMBER.

In order to use the power dissipation of the electric heater in the Controlled Chamber as a measure of heat transfer across the porous plastic sheet and the cavity, two additional heat generating mechanisms need to be identified and measured. These are:

(i) the portion of power dissipated by the heater which is lost to the surroundings;

(ii) the amount of heat generated by the shearing action of the fan stirrer.

The procedure to compensate for these two disturbances is as follows:

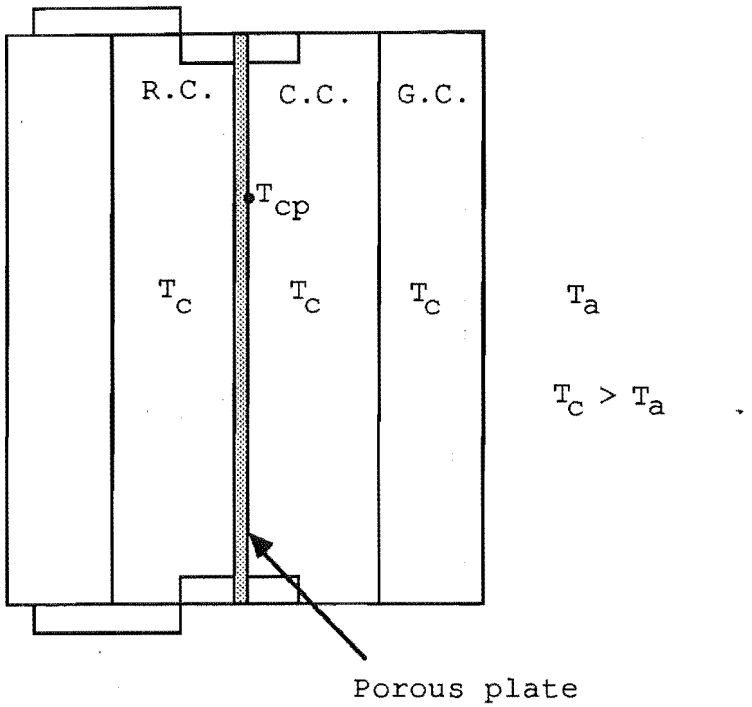

Fig.5.1 Heat Loss Measurement from the Controlled Chamber to the Surroundings.

The temperature in all three chambers is controlled to a certain level, say T_c, and the temperature of the ambient (T_a) is noted over a given period. The heater power readings are logged periodically onto the VAX computer while T_c is monitored on the chart recorder. As no temperature gradient exists between the various chambers, the power input into the Controlled Chamber should be equal to the heat leak from the Controlled Chamber to the surroundings.

$$\text{i.e.} \qquad q_1 = k_1 (T_c - T_a) \tag{5.1}$$

where: q_1 = heat loss from Controlled Chamber

and k_1 = lumped thermal conductance.

If T_c is maintained at such a level that:

$$q_1 = q_{h1} + q_s \tag{5.2}$$

where: q_{h1} = heat input from heater

and q_s = heat input from fan stirrer,

then q_s represents a constant portion of the value of q_1 and is independent of $(T_c - T_a)$.

The quantity q_s is not actually measured by the average power meter in this work. It is not negligible, as preliminary tests show that the temperature in the controlled chamber would rise by a fixed amount during the heater effect of the stirrer (from 5 to 7 °C depending on the insulation set-up used for the guarded box when in either the vertical or horizontal orientation). But so long as the Controlled Chamber is operated at a temperature level over and above that caused by the stirrer heating along, the constant amount of energy input q_s would be eliminated as a result of the calculation procedure adopted in this work :-

If $q_1 = q_{h1} + q_s$ for heat-loss estimation and the Controlled Chamber is being maintained at T_c; from Section 5.4 to 5.6, the heat-transfer across the porous plate q_p is calculated from:

$$q_p = q_T - q_1 \qquad (5.3)$$

where: q_T = total heat input from the heater and the fan stirrer to maintain the Controlled Chamber at T_c.

As the heating effect of the stirrer, q_s, is always constant for fixed motor-drive speed, we have:

$$q_T = q_{h2} + q_s \qquad (5.4)$$

where q_{h2} = heat input from the heater.

Substitution from Eq.5.2, we obtain:

$$q_p = q_{h2} + q_s - q_{h1} + q_s$$
$$= q_{h2} - q_{h1} \qquad (5.5)$$

Thus the effect of fan heating is eliminated. It is therefore sufficient just to monitor the heater input in this work and treat the fan stirrer as frictionless. The price to pay is that there is a minimum threshold level at which we can operate the temperature

in the Controlled Chamber in order to obtain accurate measurement of the heat-transfer rate.

The heat input from the heater is measured by the average power meter and is again logged periodically onto the computer.

A range of T_c values would be used to obtain a range of (T_c - T_a) values. A heat loss curve would then be constructed with q_1 plotted against (T_c - T_a).

Typically a run would take about 10 to 20 hours for each T_c value. The long time need is to increase the size of the data field and hence reduce the random error. The heat input and temperature are logged every 1 o r 4 minutes.

N.B. As T_a would vary over the length of the time of the run, its time-averaged value was used in determining T_a.

5.3 MOISTURE LOSS FROM CONTROLLED CHAMBER TO SURROUNDINGS

The same principle as for Section 5.2 is adopted except that the independent variable in this case is the vapour pressure of the air instead of temperature. The fan stirrer has no effect in this case and hygroscopicity of Perspex is treated in the same way as outlined in Section 5.1.2.

$$m_1 = K_1 (P_c - P_a) \qquad (5.6)$$

where: m_1 = moisture loss from controlled chamber,

K_1 = lumped moisture conductance,

and (P_c- P_a) = vapour pressure excess of the controlled chamber over ambient condition.

m_1 is measured by timing the weight loss on the electronic balance and P_c and P_a are measured by the Dew All humidity sensor. The

balance readings are logged by the VAX computer and a run would take about 10 to 20 hours for each P_c value. Values of P_c and P_a are measured intermittently with the Dew All meter.

A moisture loss curve would be constructed with m_1 plotted against (P_c - P_a) values. Time averaged value of P_a is used.

5.4 CHARACTERISTICS OF THE POROUS PLASTIC PLATE

As the resistance to heat and moisture transfer of the porous plastic plate is not negligible compared to the resistance of the air cavity, its thermal conductivity and moisture-diffusion resistance has to be determined accurately.

5.4.1 Thermal Conductivity of Porous Plate.

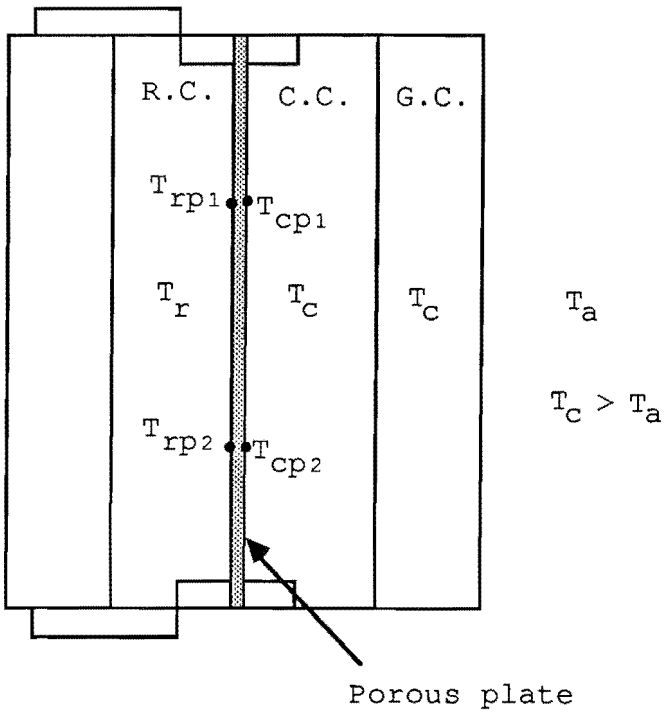

Fig.5.2 Thermal Conductivity of Porous Platic.

A temperature gradient (T_c - T_r) is imposed across the

porous plate, with $T_c > T_r$. Six pairs of differential thermocouples on the each side of the porous plate record the surface conditions across the plate, e.g. $(T_{cp} - T_{rs})$, as well as the temperature variation over each surface, e.g. $(T_{cp1} - T_{cp2})$, etc. The heat transfer across the porous plate is calculated from:

SEE ERRATA SEE ERRATA SEE ERRATA

$$q_p = q_T - q_l \qquad (5.7)$$

where: q_p = heat transfer rate across porous plate,

q_T = heat-input rate from heater,

and q_l = heat-loss rate to surroundings.

Note that q_l can be calculated from the plot of q_l versus temperature excess above ambient $(T_c - T_a)$ (Section 5.2).

A plot of q_p versus ΔT would allow the interpolation of q_p for any ΔT values, ΔT being the spatial average temperature of T_{cp1}, T_{cp2}, etc.

The thermal conductivity may be calculated from Fourier's law:-

$$q_p = k\, A_q \frac{\Delta T}{\Delta X} \qquad (5.8)$$

where: k = thermal conduction of plate,

A_q = surface area of plate = 0.49 m^2 (0.7 m x 0.7 m),

ΔX = distance between the surface thermocouples and is equal to the thickness of the plate if thermocouples are flushed with surface. SEE ERRATA

5.4.2 Moisture Diffusion Resistance of Porous Plastic Plate

The same principle as outlined in Section 5.4.1 is used. A vapour pressure gradient ($P_c - P_r$) is imposed across the porous plastic plate and the resultant total moisture-transfer rate is measured. The moisture-transfer rate across the porous plate m_p is calculated from:

$$m_p = m_T - m_l \qquad (5.9)$$

where: m_T = total moisture loss as recorded by the electronic balance and timing device,

m_l = moisture loss to surroundings (Section 5. 3),

and P_c , P_r = bulk air vapour pressure in the Controlled and Receiving Chamber respectively.

Only the moisture diffusion resistances at two temperature levels are determined , i.e. at 30 °C and 35 °C. Increasing the temperature level increases the vapour pressure of the moist air, but the moisture diffusion resistance is found to be independent of temperature level over the range tested. As no means are available to measure precisely the boundary vapour pressure values on the plate surfaces, an indirect method of estimating the boundary values was given in Appendix 1. This method uses the SEE ERRATA information based on the measurement of the bulk air vapour pressure value (calculated from a dew-point measurement by the Dew All dew-point meter) and the analogy between heat and mass transfer.

A plot of m_p versus values together with the boundary value SEE ERRATA correction, would give the diffusional resistance, r, of the porous plastic:

$$r = \frac{(P_c - P_r)}{m_p} \qquad (5.10)$$

5.4.3 Thermal Emittance of Porous Plastic Plate.

No facility to measure the thermal emittance of the porous plastic was available in the Department of Chemical and Process Engineering, University of Canterbury. A sample was sent to the C.S.I.R.O., Division of Energy Technology, in Victoria , Australia for this measurement to be carried out. The porous plastic was found to be thermally opaque and the emittance is 0.77 for the smooth side and 0.73 for the rough side. The measurements were performed on a Gier Dunkle Infrared Reflectometer Model DF100 at 25 °C and no error limits were available.

5.4.4 Hygroscopicity of Porous Plastic Plate.

Sample strips measuring 200 mm x 50 mm were placed in a desicator and their weights recorded regularly (e.g. once a day) to check for moisture desorption. Alternately the sample strips were placed in a closed jar with distilled water or other salt solution. Their weights were recorded regularly to check for moisture adsorption. Both moisture adsorption or desorption properties are absent for the porous plastic.

5.5 CHARACTERISTIC OF PERSPEX.

5.5.1 Infrared Transmittance of Perspex.

SEE ERRATA

It is of upmost importance that the infrared radiation from the heater in the Guard Chamber does not heat transmit across the Perspex and influence the thermal condition in the Controlled Chamber and vice versa. Otherwise, some form of radiation shield would need to be instored between the Controlled and Guard Chamber. This method would eliminate the advantage of using Perspex because of its transparency. Tests were thus carried out using a Perkin Elmer Infra-red spectrophotometer Model 337 (Instrument No. 349) to

SEE ERRATA

check the infra-red transmission property of the 6-mm thick Perspex sheet. Perspex sheets of other thicknesses (4 mm, 3 mm, 0.37 mm) were also tested to see the variation of transmittance with thickness. All test strips measure 15 mm x 15 mm in the other dimensions. The range of infra-red radiation tested was from wavelength 2.5 to 25 μm. As the emitting source of the spectrophotometer is operated at 1200 K, it is expected that its radiation power is at least stronger than that of the heater which would be operating at 308 to 358 K. The results tested were thus on the conservative side. Appendix 5 gives plots of the radiative power of the spectrophotometer source and the heater on the assumption that each has the characteristic of a gray body. Test results from the infrared spectrophotometer as well as some results from the literature are also given. It is found that 6-mm Perspex sheet is opaque to infrared radiation over the range tested and thus no radiation shield is necessary.

5.5.2 Hygroscopicity of Perspex.

Strips of 6-mm thick Perspex samples of effective surface area 0.022 and 0.019 m^2 were placed in the appropriate humidifying or dehumidifying chamber. Distilled water, various saturated salt solutions and silica gel were used to condition the chambers. The weight loss or gain of the sample strips were recorded over known periods of time, and hence their adsorption or desorption rate can be calculated from the test results (refer to Appendix 5).

5.6 THE MEASUREMENT OF HEAT TRANSFER, MOISTURE TRANSFER AND COMBINED HEAT AND MOISTURE TRANSFER ACROSS THE CAVITY.

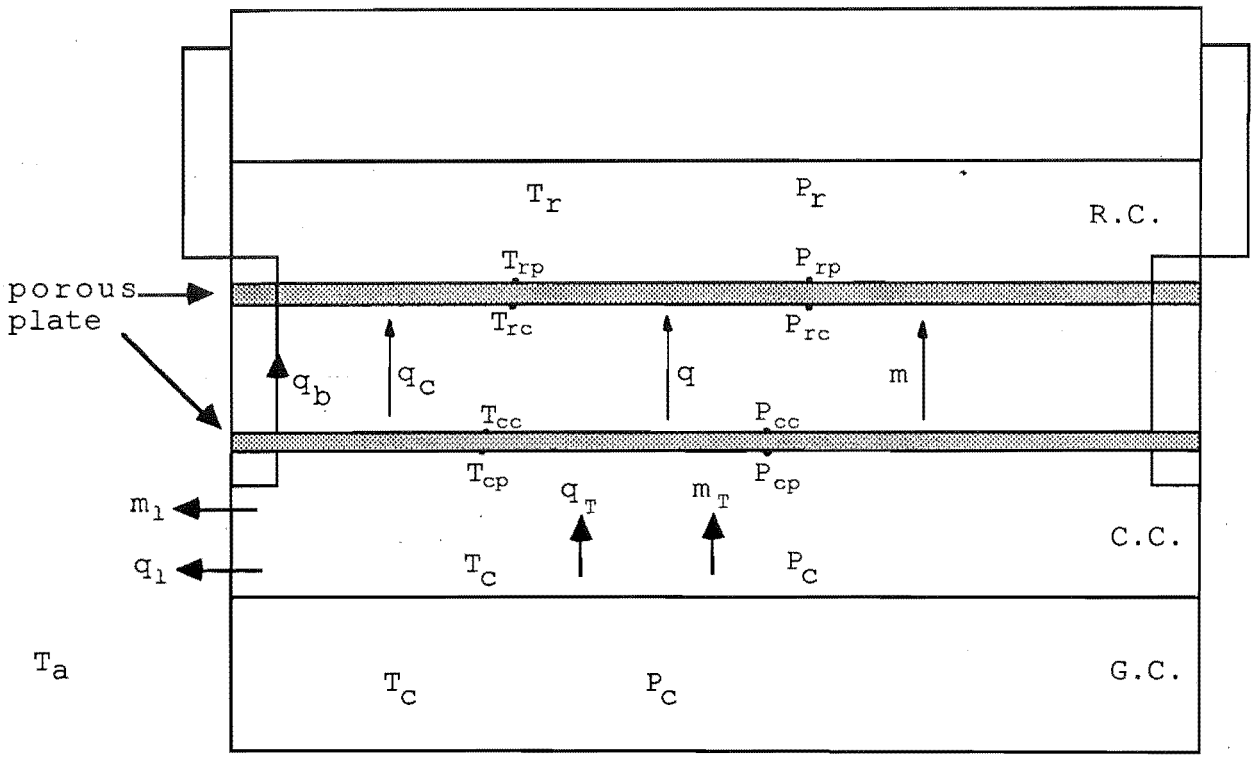

C.C. -Controlled Chamber
G.C. -Guard Chamber
R.C. -Receiving Chamber

The horizontal Test Cavity orientation is illustrated.

For heat transfer alone, the bulk air vapour pressures in CC, GC and RC are equal and hence no vapour pressure gradient exists across the test cavity. The temperature T_c and T_r are controlled to the desired level (with $T_c > T_r$). The plate's surface temperatures T_{cp} and T_{rp} are measured by surface thermocouples which allow the cavity boundary-temperatures T_{cc} and T_{cr} to be calculated as the thermal conductivity of the porous plastic has been found earlier (Section 5.4.1). As a cross-check to these calculated cavity boundary temperature values, six thermocouple points of the

"Version 2" type (Section 4.5) were actually placed on the porous plates surfaces in the test cavity as follows:

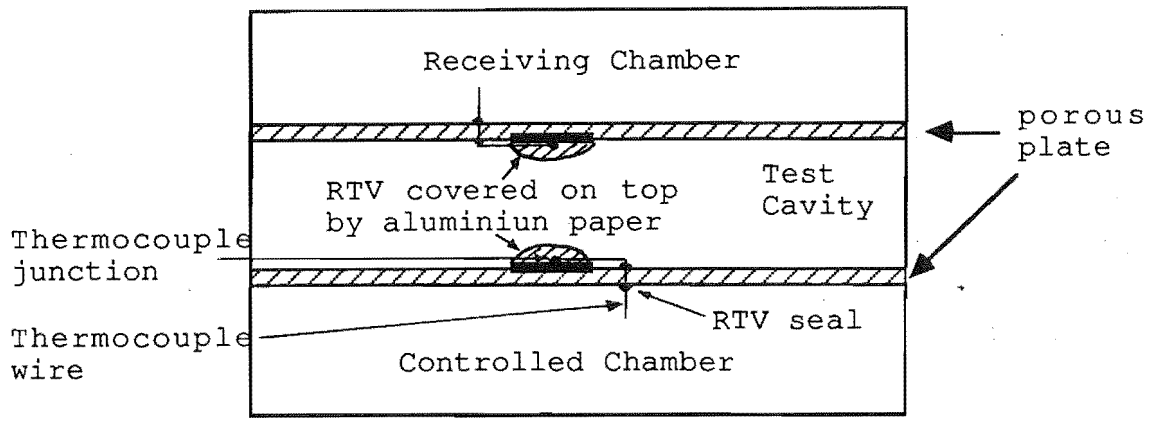

Fig.5.4 "Version 2" Thermocouple in the Test Cavity.

It was found later that these "cavity" thermocouples always gave too high a temperature gradient across the cavity from heat-balance considerations. However, they are still useful for indicating approximate temperature drops across the cavity when these calibrated against the calculated temperatures ($T_{cc} - T_{rc}$) The heat flow across the cavity is given by the relationship:

$$q = q_T - q_l - q_c - q_r - q_m \qquad (4.11)$$

where: q = heat flow across the cavity by conduction and convection,

q_T = total heat input by heater (measured by the average power meter),

q_l = losses from the Controlled Chamber to the surroundings (Section 5.2),

q_c = conduction loss from one chamber to the next along the solid Perspex due to temperature gradient across the cavity (calculated by the usual Fourier's law),

q_c = radiation transfer across the cavity (Appendix 2),

and: q_m = latent heat of vaporisation due to moisture transfer across the cavity and is equal to zero for heat transfer alone only.

Note that as q_1 is only determined for the Controlled Chamber (Section 5.2), this method of calculating the heat balance can only be used to determine accurately the power transfer from the Controlled to the Receiving chamber. Hence, if the downward transfer of heat is desired, the test equipment would need to be turned upside down so that the Controlled Chamber is on top of the Receiving Chamber.

For moisture transfer, both T_c and T_r are controlled to any desired temperature (normally 30, 40 or 50 °C), so that T_{cp} and T_{rp} are made to equal to each other. Under certain experimental conditions, T_c cannot be made to equal to T_r when T_{cp} is made equal to T_{rp} due to the radiative cooling effect of the condenser(which is at very low temperature, e.g. when the bulk air temperature in the Receiving Chamber is at 50 °C and the condenser temperature is at 6 °C). In either case, the temperature level on the porous plates'surface is made equal to each other and no temperature gradient thus exists across the cavity. A moisture gradient is imposed across the cavity (with $P_c > P_r$). The moisture source in CC is a tray containing the humidifying source (either distilled water or saturated salt solution) which is put in compartment G (See Figure 4.1). The tray rest on a recording balance with a data output to log continuously the evaporative loss. The rate of moisture transfer is found as follows:

$$m = m_T - m_1$$

where m = moisture flow across the cavity,

m_T = total evaporative loss recorded by balance and timer,

and m_1 = loss from CC to surroundings (Section 5.3)

The boundary values for the cavity's vapour pressure were calculated from the bulk air vapour pressures in CC and RC, ie. P_c and P_r, together with the moisture-diffusion resistance "r" found in Section 5.4.2 (with correction for the boundary layer degression).

As m_1 is again determined for the Controlled Chamber only, this mass-balance method of determining moisture transfer is only accurate for transfer from the Controlled Chamber to the Receiving Chamber. Reorientation of the cavity geometry would again be needed if downward transfer or horizontal transfer (for vertical cavity) is desired.

Heat and moisture flows received by the Receiving Chamber will not be measured. Both heat and moisture are removed by means of the condenser coil.

Simultaneous heat and moisture transfer in the aiding mode, i.e. when both the heat and moisture gradients are acting in the same direction, can be easily measured by combining the two procedures described above, with heat and moisture transfer occurring from the controlled to the receiving chamber. For heat and moisture transfer in the opposing mode, i.e. when the heat and moisture gradients are acting in the opposite direction; only the moisture transfer rate can be measured accurately with the present set up and the heat-transfer data need to be approximated. This is a direct consequence of the condenser being located in the Receiving Chamber only. It is easy to impose a moisture gradient from the Controlled Chamber to the Receiving Chamber with a reverse temperature gradient present at the same time. This can be done by placing the appropriate moisture source in the Controlled Chamber and operate the cooling water temperature in the Receiving Chamber at some dew point lower than that in CC. The bulk air temperature in RC is then controlled to a higher value than the bulk air temperature in CC, in which its heaters often can be just left off. The reverse temperature gradient across the cavity would need to be estimated from the readings of the thermocouples inside the cavity boundary, since no calculated boundary conditions can be obtained as the precise amount of heat flow from RC to CC is not known (as q_1 for RC is not found). It is not possible to impose a reverse

moisture gradient from RC to CC with heat transfer from CC to RC as there is no means to remove the moisture gain in CC with the present experimental set up. To overcome this problem, another condenser coil would have to be installed in the Controlled Chamber, but this involves extensive modification to the present experimental arrangements.

An easier way to overcome this problem in part would be to find q_1 for the receiving chamber and thus measure accurately the heat ransfer from RC to CC. But again, the lack of a condenser in the Controlled Chamber really restricts the temperature gradient one can impose across the cavity.

CHAPTER 6

RESULTS AND DISCUSSION - ONE POROUS PLATE CASE

The One Porous Plate case refers to the experiments when only one porous plate was present between the Controlled and the Receiving Chambers (designated C.C. and R.C. respectively). The aim of these experiments was to find the characteristic of the porous plastic plate. (Section 5.4)

6.1 HEAT LOSS FROM CONTROLLED CHAMBER TO SURROUNDINGS.

Following the procedure outlined in the Section 5.2, the heat loss from C.C. to surroundings for the case of a single horizontal and vertical Porous Plate case is presented in Fig.6.1. The difference in the heat loss curves for the two cases was a result of the different insulation arrangement for each case. A linear least- squares fit to the data points results in the following equations :-

(i) Vertical case :

$$q_1 = 0.847\ \Delta T_1 - 6.89 \qquad \text{Std dev} = 0.52 \qquad (6.1)$$

(ii) Horizontal case:

$$q_1 = 0.980\ \Delta T_1 - 6.35 \qquad \text{Std dev} = 0.40 \qquad (6.2)$$

where q_1 is in W and ΔT is in degree Celsius.

When the equations in Fig 6.1 are extrapolated back to the y-axis, the temperature difference obtained from the x-axis is thought to represent the rise in temperature in the Controlled Chamber due to the shearing action of the fan stirrer. For the vertical mode, this rise in temperature is 8.1 °C and, for the horizontal mode the rise is 6.5 °C. The difference is a consequence of the different insulation set-up for the two orientations.

Fig. 6.1: HEAT LOSS FROM C.C. WITH NO TEMP GRADIENT ACROSS POROUS PLATE

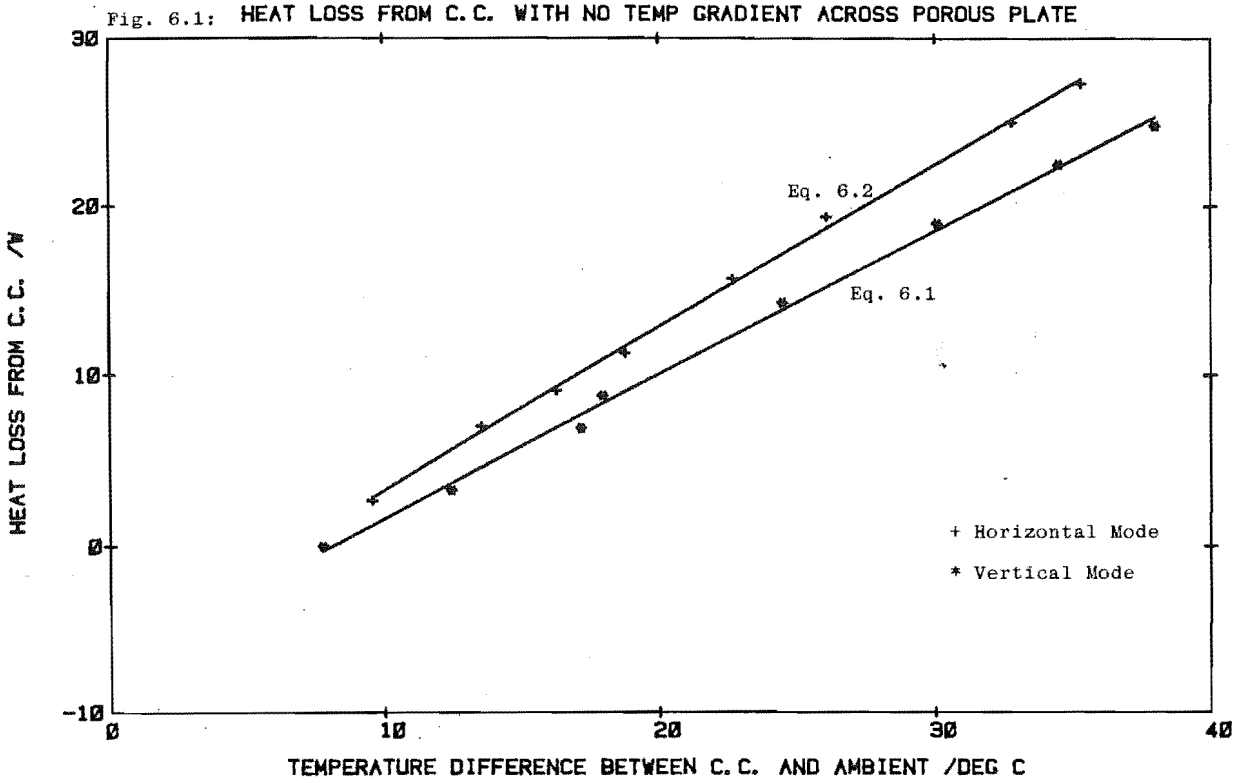

Fig. 6.2: MOISTURE LOSS FROM C.C. TO AMBIENT FOR VARIOUS EXPERIMENTAL CONDITIONS

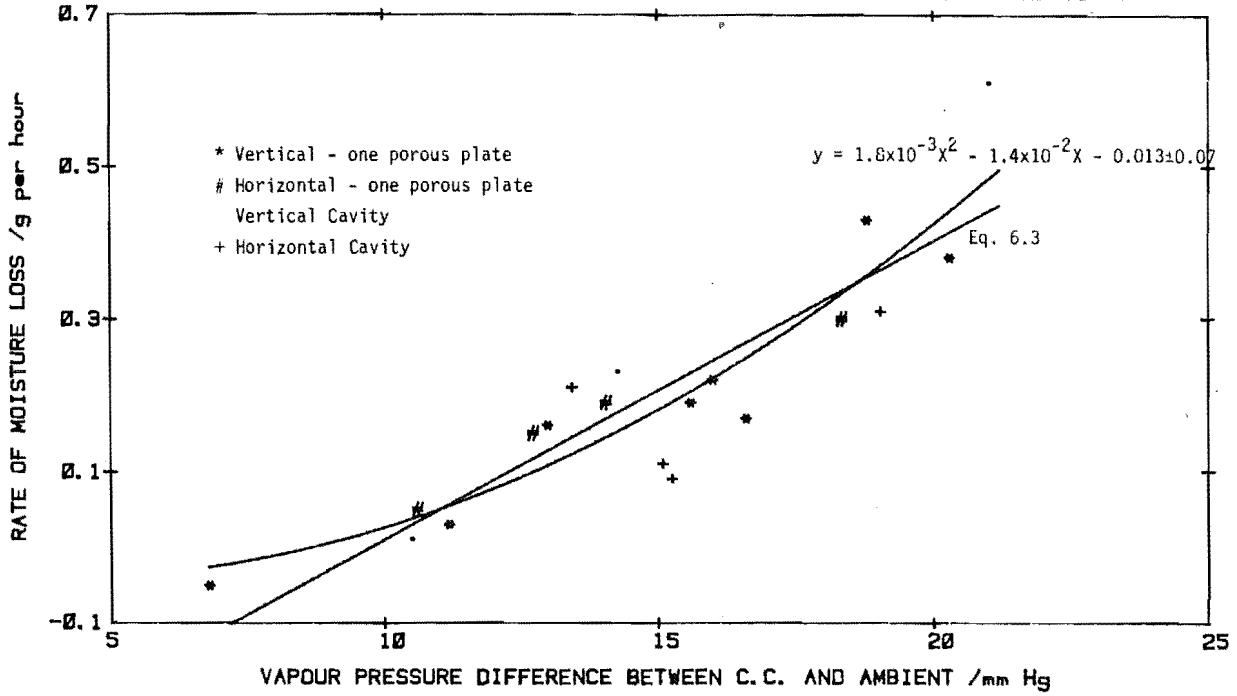

6.2 MOISTURE LOSS FROM CONTROLLED CHAMBER TO SURROUNDINGS.

Fig 6.2 was obtained using the procedure outlined in Section 5.3. It was found that no significant distinction could be made in the moisture-loss rate between the horizontal and vertical configurations for both the One Porous Plate case and the Cavity case. Thus all the data points from the four conditions were plotted together and a common least-squares curve fitted. To illustrate this point, fig. F.3 is the moisture-loss curve for the case of one vertical porous plate only; the moisture loss-rate for ΔP= 15 mm Hg from Fig 6.3 is 0.204 g h^{-1} when calculated using the least-squares line. The corresponding moisture loss-rate calculated using the least-squares curve from Fig 6.2 is 0.206 g h^{-1}. Thus the difference of 0.002 g h^{-1} between the two calculated values is insignificant when compared with the uncertainty of each of the least-squares fit. In Figures 6.2 and 6.3, both first and second-order fits were used. A second-order fit has marginally smaller values of standard deviations, but the increase in accuracy over the first-order fit is insignificant. Thus the equation :

$$m_1 = 0.0392\ \Delta P_1 - 0.382 \quad g\ h^{-1} \qquad \text{Std dev} = 0.06 \qquad (6.3)$$

is used to estimate the rate of moisture loss from the Controlled Chanber to the surroundings for <u>all</u> the experimental conditions. The unit of ΔP in Eq. 6.3 is in mm Hg.

6.3 HEAT TRANSFER ACROSS ONE VERTICAL POROUS PLATE.

The aim here was to find an effective lumped thermal conductivity of the porous plate when it was oriented in the vertical position. The procedure was outlined in Section 5.4.1 and the result was presented in Fig 6.4. Again a linear least-squares fit was used and the best-fit equation is :

Fig. 6.3: MOISTURE LOSS FROM C.C. TO AMBIENT FOR THE CASE OF ONE POROUS VERTICAL PLATE

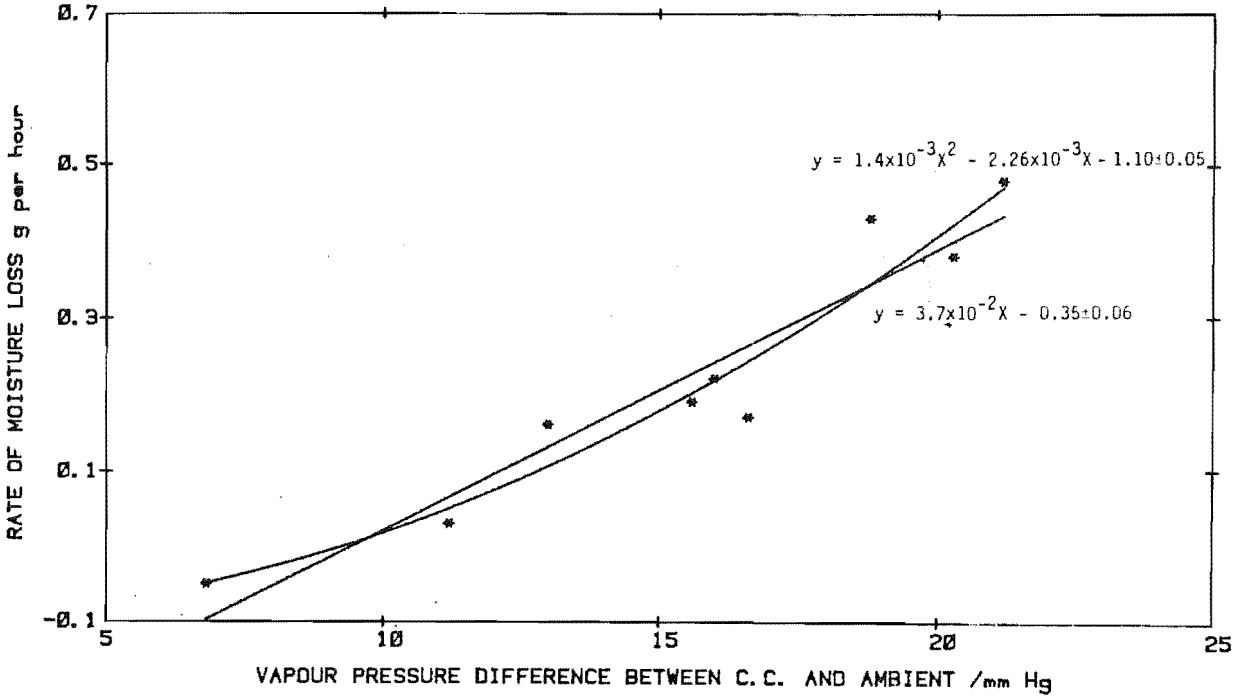

Fig. 6.4: HEAT TRANSFER ACROSS ONE VERTICAL POROUS PLATE

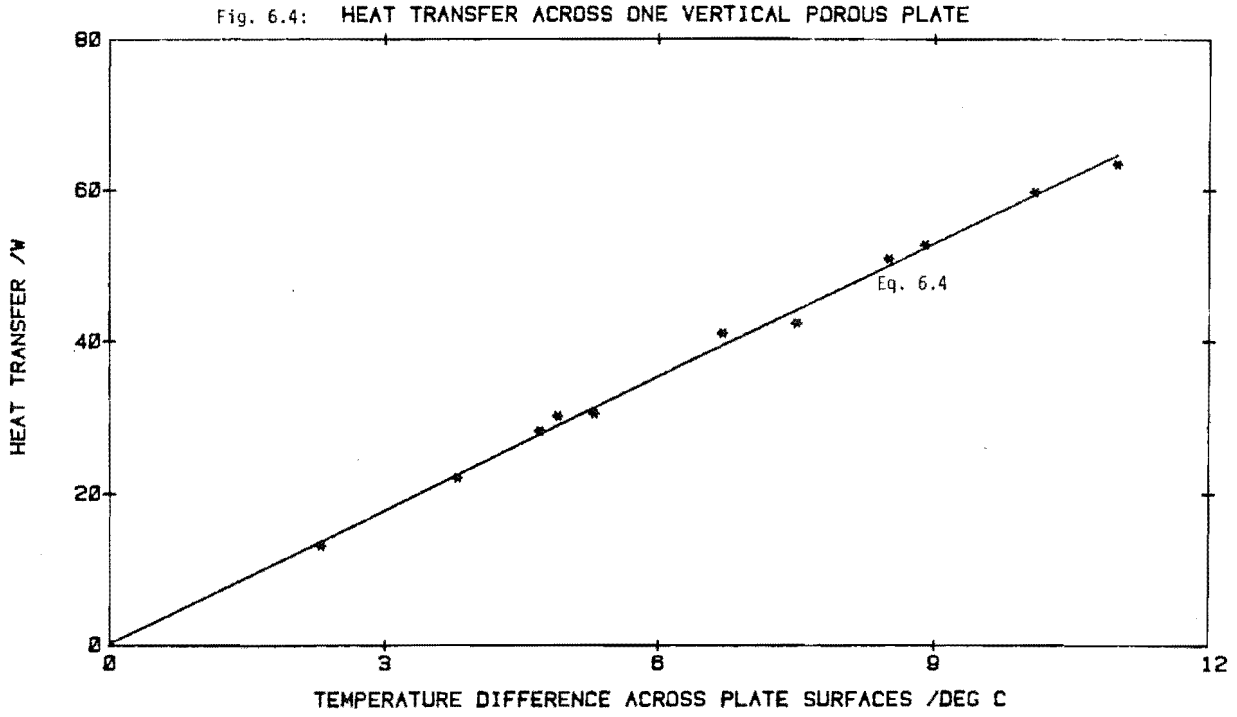

$$q_p = 5.86\ (\Delta T)_p + 0.22 \qquad \text{Std dev} = 1.08 \qquad (6.4)$$

where q_p is in W and ΔT is in degree Celsius respectively.

The lumped thermal conductivity was calculated by the Fourier's law as described by equation (5.8) :

$$k_v = \frac{q_p\ \Delta X}{A\ (\Delta T)_p} \qquad (6.5)$$

Table 6.1 lists the value of k_v with $\Delta X = 4.75 \times 10^{-3}$ m and $A = 0.49 m^2$.

Table 6.1 Lumped Thermal Conductivity of Porous Plastic Plate in the Vertical Mode

$(\Delta T)_p$/ °C	q_p / ± 1.08 W	*k_v/ W $m^{-1}K^{-1}$
2.0	11.53	0.056 ± 9%
4.0	23.15	0.056 ± 4.6%
6.0	34.77	0.056 ± 3.1%
8.0	46.39	0.056 ± 2.3%
10.0	58.01	0.056 ± 1.9%
12.0	69.63	0.056 ± 1.3%

* Note: The percentage error in k_v is derived by assuming that all the error in k_v is due to the error incurred in q_p only. The error in q_p is estimated by the standard deviation of the least-squares curve. The error in $(\Delta T)_p$ is neglected for the moment as it will be included when evaluating the error estimates for the cavity boundary temperature values (see Appendix 4)

6.4 HEAT TRANSFER ACROSS ONE HORIZONTAL POROUS PLATE - UPWARDS TRANSFER.

Similar methodology TO that described in Section 6.3 was employed to obtain a lumped thermal conductivity value for the porous plastic plate when it oriented in a horizontal position. The heat-transfer curve is given in Fig.6.5 and the best fit equation found by the least-squares technique is :-

$$q_p = 5.90(\Delta T)_p + 0.91 \qquad \text{Std dev} = 0.91 \qquad (6.6)$$

where q_p and ΔT are in the units of W and °C respectively.
The lumped thermal conductivity k_H is presented in Table 6.2.

Table 6.2 Lumped Thermal Conductivity of Porous Plastic in Horizontal Mode.

$(\Delta T)_p$/ °C	q_p / ±0.91 W	$^*k_H$/ W $m^{-1}K^{-1}$
2.0	12.82	0.062 ± 7.0%
4.0	24.72	0.060 ± 3.7%
6.0	36.63	0.059 ± 2.4%
8.0	48.53	0.059 ± 1.8%
10.0	60.44	0.059 ± 1.5%
12.0	72.35	0.059 ± 1.3%
14.0	84.25	0.058 ± 1.0%
16.0	96.16	0.058 ± 1.0%

In view of the fact that k_H is consistently greater than k_V, (by 3 to 9 %), Eqs. 6.5 and 6.6 will be used separately for their respective cases. It is not clear if convection had occured in the pores of the porous plate and significantly influenced the lumped thermal conductivity values in either case.

For orientation of the porous plate at any angle other than vertical or horizontal, separate experiments might need to be

Fig. 6.5: HEAT TRANSFER ACROSS ONE HORIZONTAL PLATE

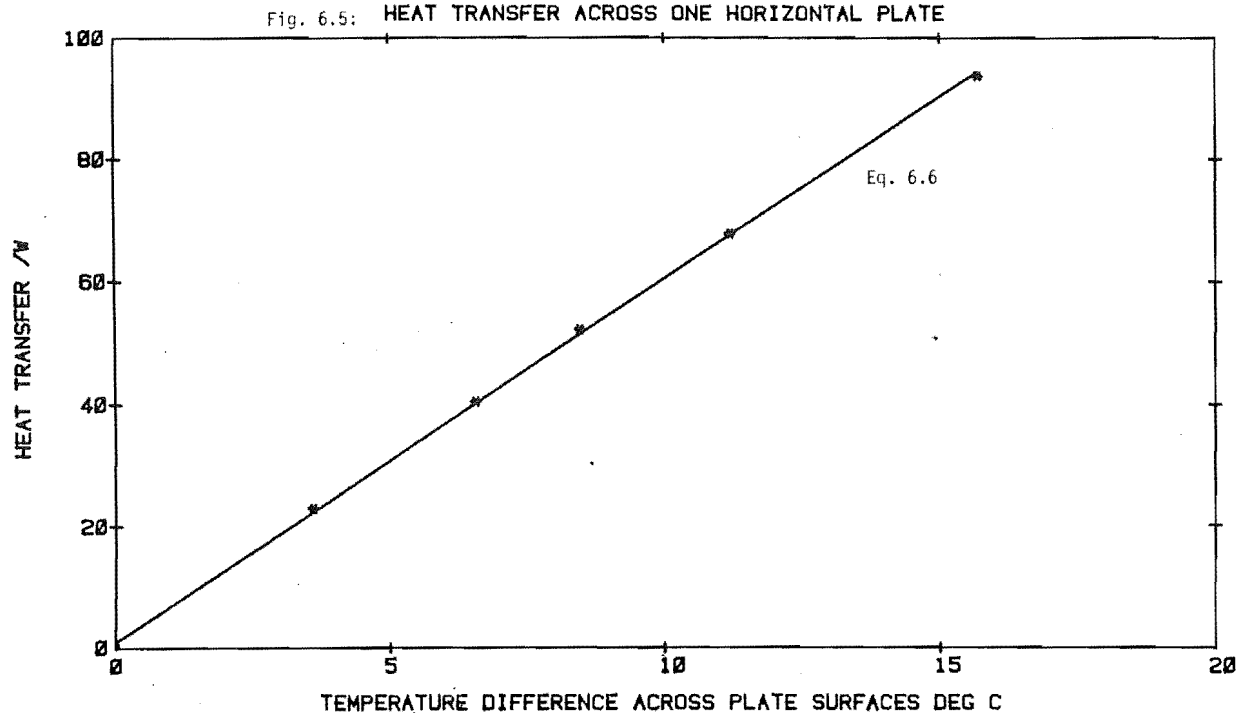

Fig. 6.6: HEAT TRANSFER ACROSS ONE POROUS PLATE

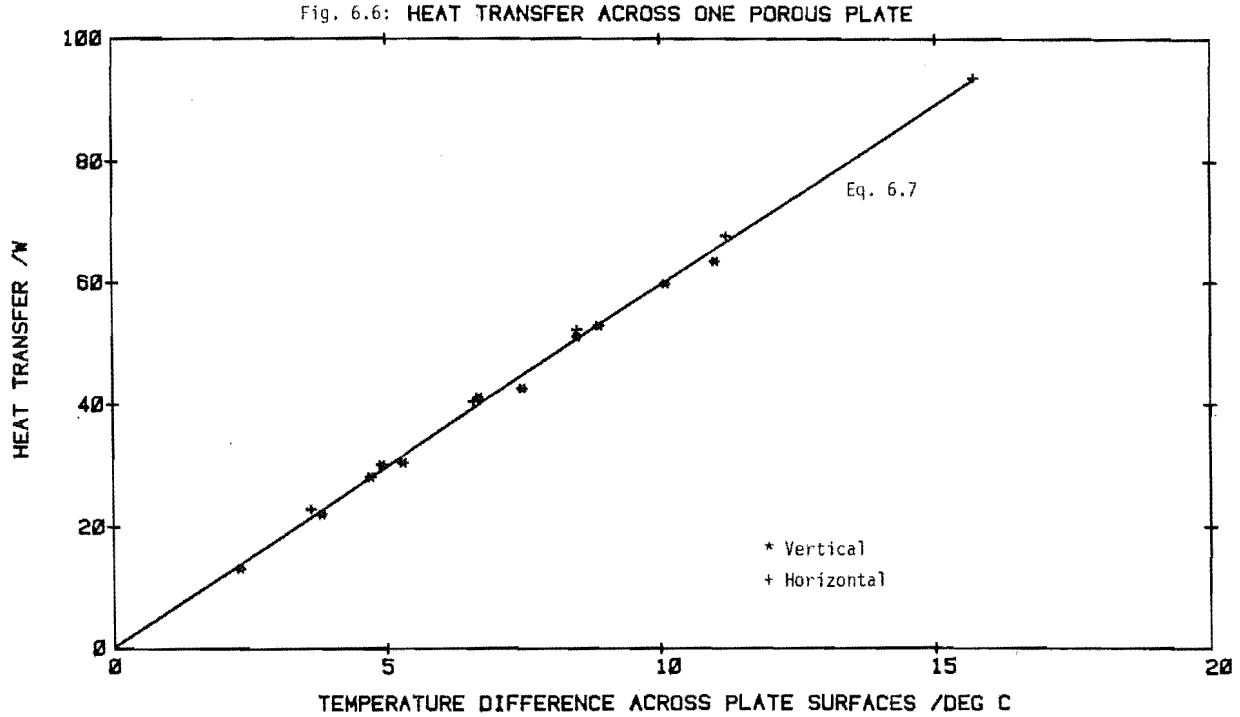

carried out to determine the lumped thermal conductivity value for these cases. If that cannot be conveniently done, then combination of Eqs. 6.5 and 6.6 would provide an "average" lumped thermal conductivity value applicable for all cavity orientation. Fig. 6.6 list all the data points from Figs. 6.4 and 6.5. A best fit equation by the least-squares technique yields :-

$$q_p = 5.94\ \Delta T_p + 0.20 \quad \text{Std Dev} = 1.16 \tag{6.7}$$

where q_p and ΔT are in the units of W and oC respectively.

The lumped thermal conductivity values from Eq.6.7 are listed in Table 6.3.

Table 6.3 "Average" Lumped Thermal Conductivity of Porous Plastic Plate for Any Orientation.

$(\Delta T)_p$/ °C	q_p / ±1.16 W	k/ W $m^{-1}K^{-1}$
2.0	11.96	0.058 ± 8.0%*
4.0	23.85	0.058
6.0	35.75	0.058
8.0	47.64	0.058
10.0	59.53	0.058
12.0	71.42	0.058
14.0	83.29	0.058
16.0	95.21	0.058 ± 1.0%

*The range of the percentage error is similar to that in Table 6.2.

6.5 ISOTHERMAL MOISTURE TRANSFER ACROSS ONE VERTICAL POROUS PLATE.

The procedure for the determination of moisture-diffusion resistance was outlined in Section 5.4.2.. Fig.6.7 illustrates the moisture-transfer rate across one vertical porous plate (m_p) as a

Fig. 6.7: ISOTHERMAL MOISTURE TRANSFER ACROSS ONE VERTICAL PLATE

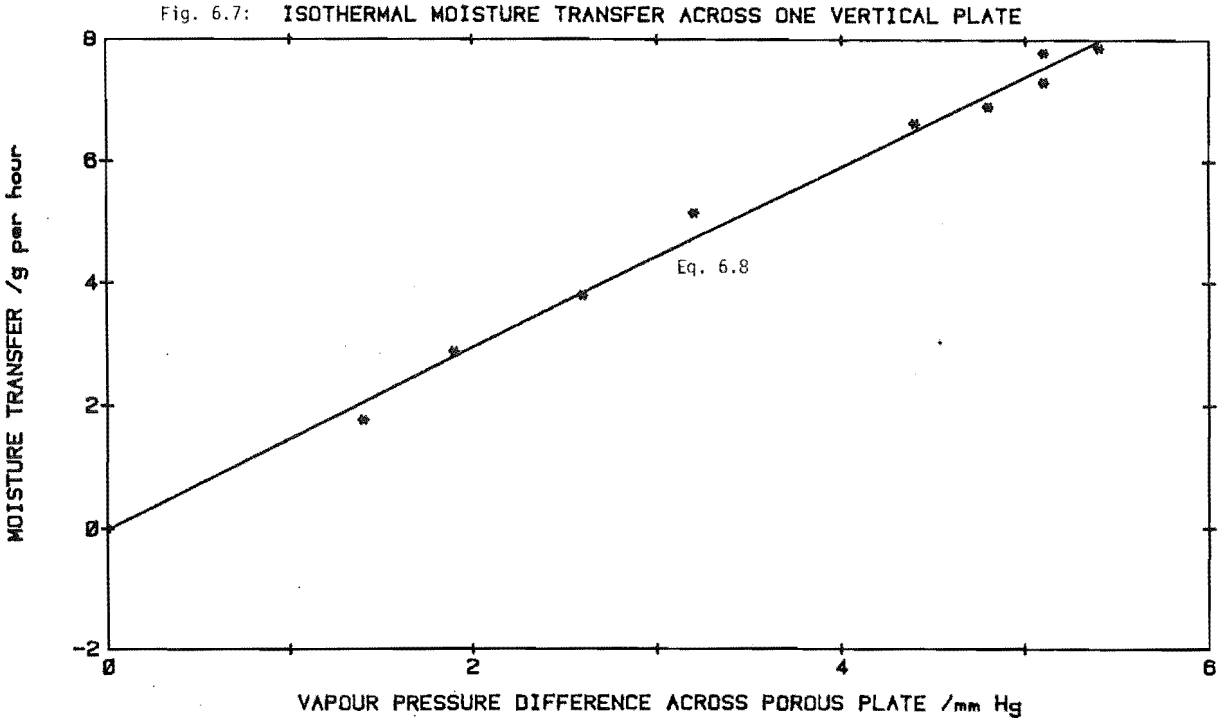

Fig. 6.8: ISOTHERMAL MOISTURE TRANSFER ACROSS ONE VERTICAL POROUS PLATE

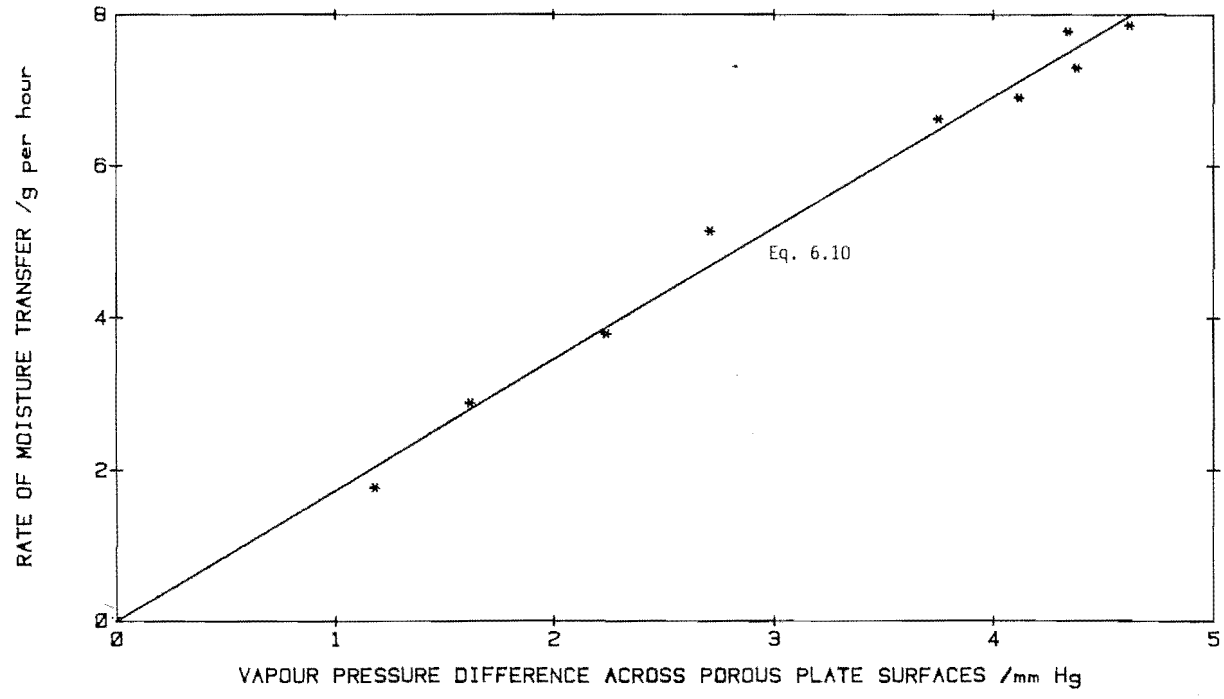

function of the bulk air vapour-pressure difference between the Controlled and Receiving Chamber $(\Delta P)_{bulk}$. A first-order equation derived by the least-squares technique was found to fit the data very well and the equation is :-

$$m_p = 1.48\ (\Delta P)_{bulk} - 0.01 \quad \text{Std dev} = 0.23 \qquad (6.8)$$

where m_p and ΔP are in the units of gh^{-1} and mm Hg respectively.

Using Eq. 6.8, the range of the thermal moisture diffusion resistances was calculated by the formula :-

$$R = \frac{(\Delta P)_{bulk}}{m_p} \qquad (6.9)$$

The values of R are presented in Table 6.4.

Table 6.4 Lumped Moisture-Diffusion Resistance based on Bulk-Air Vapour Pressure Difference for Vertical Porous Plate.

$(\Delta P)_{bulk}$		m_p		R	
mm Hg	Pa	gh^{-1}	$gs^{-1}/x10^{-4}$	$Nsg^{-1}m^{-2}$ $/x10^5$	$Mnsg^{-1}$*
2.0	266.6	2.95	8.19	3.26	0.160
4.0	533.3	5.91	16.42	3.25	0.159
6.0	799.9	8.88	24.67	3.24	0.159

* For surface area of porous plate for moisture transfer =0.49 m^2

The value of "R" from Table 6.4 is the moisture-diffusion resistance of the porous plate based on bulk-air vapour pressure difference. It can be converted into the moisture-diffusion resistance based on the boundary vapour-pressure difference across the porous plate's surfaces by Eq.5.10 and the detailed diagrams and calculations aspect has been presented in Appendix 1. Fig.6.8 presents the moisture-transfer rate across the vertical porous

plate as a function of the surface vapour-pressure difference across the plate following the procedure just mentioned. Again a first-order, best-fit equation derived by the least-squares technique was found to fit the data very well. The equation is :-

$$m_p = 1.727\ (\Delta P)_p \qquad \text{Std dev} = 0.26 \qquad (6.10)$$

where m_p and $(\Delta P)_p$ are in the units of gh^{-1} and mm Hg respectively.

Using Eq.6.10, The lumped moisture-diffusion resistance "r" was calculated and the results are presented in Table 6.5.

Table 6.5 Lumped Moisture-Diffusion Resistance based on Surface Vapour Pressure Difference for Vertical Porous Plate.

$(\Delta P)_{bulk}$		m_p		r	
mm Hg	Pa	gh^{-1}	$gs^{-1}/x10^{-4}$	$Nsg^{-1}m^{-2}/x10^5$	$Mnsg^{-1}$*
2.0	266.6	3.37	9.36	2.85	0.140
4.0	533.3	6.74	18.72	2.85	0.140
6.0**	799.9	10.11	28.08	2.85	0.140

*For surface area of porous plate for moisture transfer =0.49 m^2

** Extrapolated values

Thus the inclusion of the boundary-layer correction in the Controlled and Receiving Chambers has resulted in the moisture-diffusion resistance of the porous plate based on the bulk-air vapour-pressure difference "R" to decrease by about 12 percent. This correction procedure was necessary for the good agreement of experimental and theoretical Sherwood numbers, as will be shown in Chapter 7.

6.6 ISOTHERMAL MOISTURE TRANSFER ACROSS ONE HORIZONTAL POROUS PLATE - UPWARDS TRANSFER.

Following the same principle outlined in Section 6.5, Fig.6.9 shows the moisture-transfer rate as a function of bulk air vapour-pressure difference when the porous plate was oriented in the horizontal position. The least-squares fit equation is :-

$$m_p = 1.44\ (\Delta P)_{bulk} - 0.05 \qquad \text{Std dev=0.10} \qquad (6.11)$$

The moisture-transfer rate as a function of the surface vapour pressure difference ie. with boundary layer correction, is presented in Fig. 6.10. The least square-fit equation for this case is :-

$$m_p = 1.685\ (\Delta P)_{plate} - 0.07 \qquad \text{Std dev=0.12} \qquad (6.12)$$

The units of m_p and $(\Delta P)_{plate}$ in Eqs.6.11 and 6.12 are gh^{-1} and mm Hg respectively.

Tables 6.6 and 6.7 list the moisture-diffusion resistances appropriate to each case.

Table 6.6 Lumped Moisture-Diffusion Resistance based on Bulk-Air Vapour Pressure Difference for Horizontal Porous Plate.

$(\Delta P)_{bulk}$		m_p		R	
mm Hg	Pa	gh^{-1}	$gs^{-1}/x10^{-4}$	$Nsg^{-1}m^{-2}/x10^5$	$Mnsg^{-1}$ *
1.0	133.3	1.39	3.86	3.45	0.169
2.0	266.6	2.83	7.86	3.39	0.166
4.0	533.3	5.73	15.92	3.35	0.164
6.0**	799.9	8.62	23.94	3.34	0.164

*For surface area of porous plate for moisture transfer =0.49 m^2

** Extrapolated values

Fig. 6.9: ISOTHERMAL MOISTURE TRANSFER ACROSS ONE HORIZONTAL POROUS PLATE

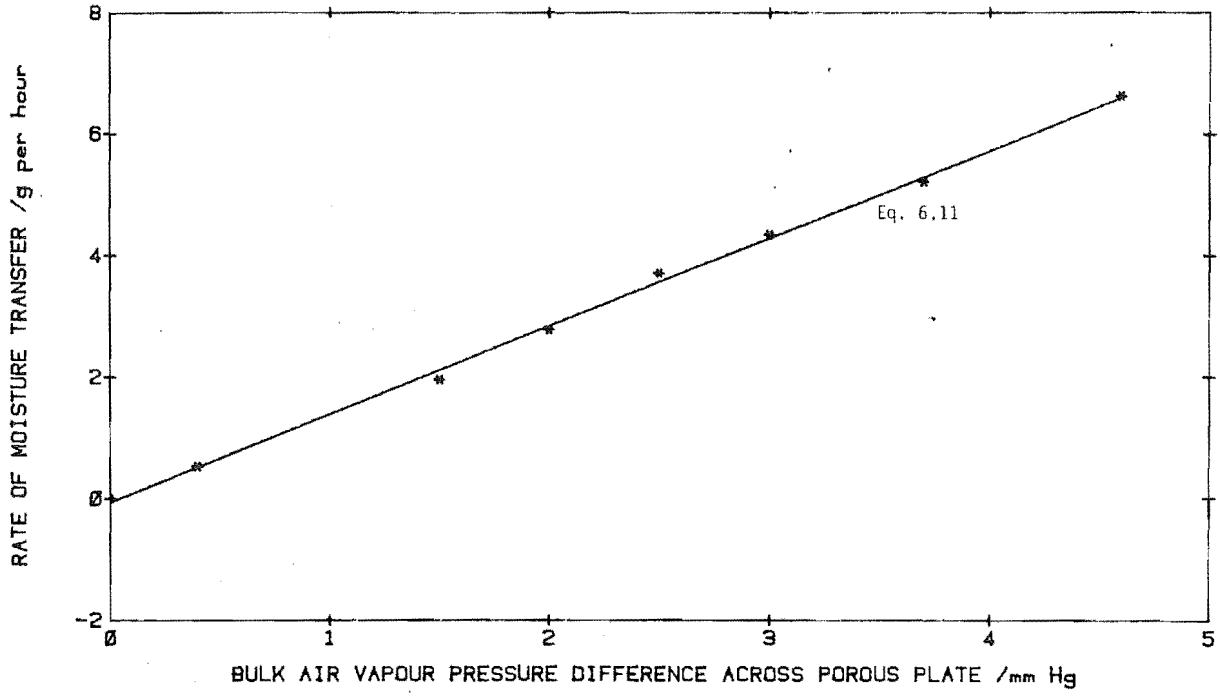

Fig. 6.10: ISOTHERMAL MOISTURE TRANSFER ACROSS ONE HORIZONTAL POROUS PLATE

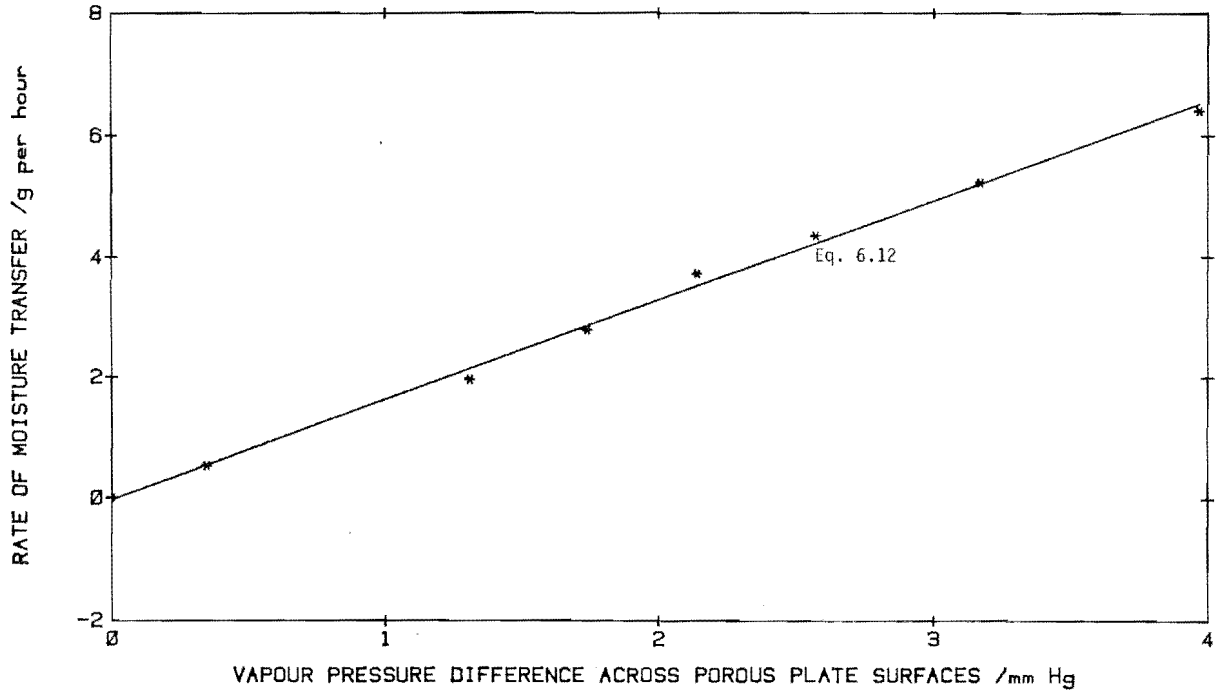

Table 6.7 Lumped Moisture-Diffusion Resistance based on Surface Vapour Pressure Difference for Horizontal Porous Plate.

$(\Delta P)_{bulk}$		m_p		r	
mm Hg	Pa	gh^{-1}	$gs^{-1}/x10^{-4}$	$Nsg^{-1}m^{-2}/x10^5$	$Mnsg^{-1}$ *
1.0	133.3	1.62	4.50	2.96	0.145
2.0	266.6	3.30	9.17	2.91	0.143
4.0	533.3	6.67	18.53	2.88	0.141
6.0**	799.9	10.04	27.89	2.87	0.141

*For surface area of porous plate for moisture transfer =0.49 m^2

** Extrapolated values

As for the vertical porous plate case, "r" is about 12 percent smaller then "R". Typically, the "R" and "r" values for the horizontal porous plate case are about 1 to 3 percent greater than the corresponding "R" and "r" values for the vertical case.

The moisture-diffusion resistances were again determined for the horizontal and vertical porous plate case only. For a porous plate orientation between horizontal and vertical, the moisture-diffusion resistance can be obtained by interpolation between the data for the horizontal and vertical porous plate cases. This has been done in Figs.6.11 and 6.12 where the moisture-transfer rates for both the horizontal and vertical porous plate cases are plotted together against the respective bulk air vapour-pressure difference and the surface vapour-pressure difference respectively. The linear best-fit equations derived by the least-squares technique for Figs. 6.11 and 6.12 are respectively :-

$$m_p = 1.49\ (\Delta P)_{bulk} - 0.07 \qquad \text{Std dev=0.20} \qquad (6.13)$$

$$m_p = 1.73\ (\Delta P)_{plate} - 0.07 \qquad \text{Std dev=0.21} \qquad (6.14)$$

Fig. 6.11: ISOTHERMAL MOISTURE TRANSFER ACROSS ONE POROUS PLATE

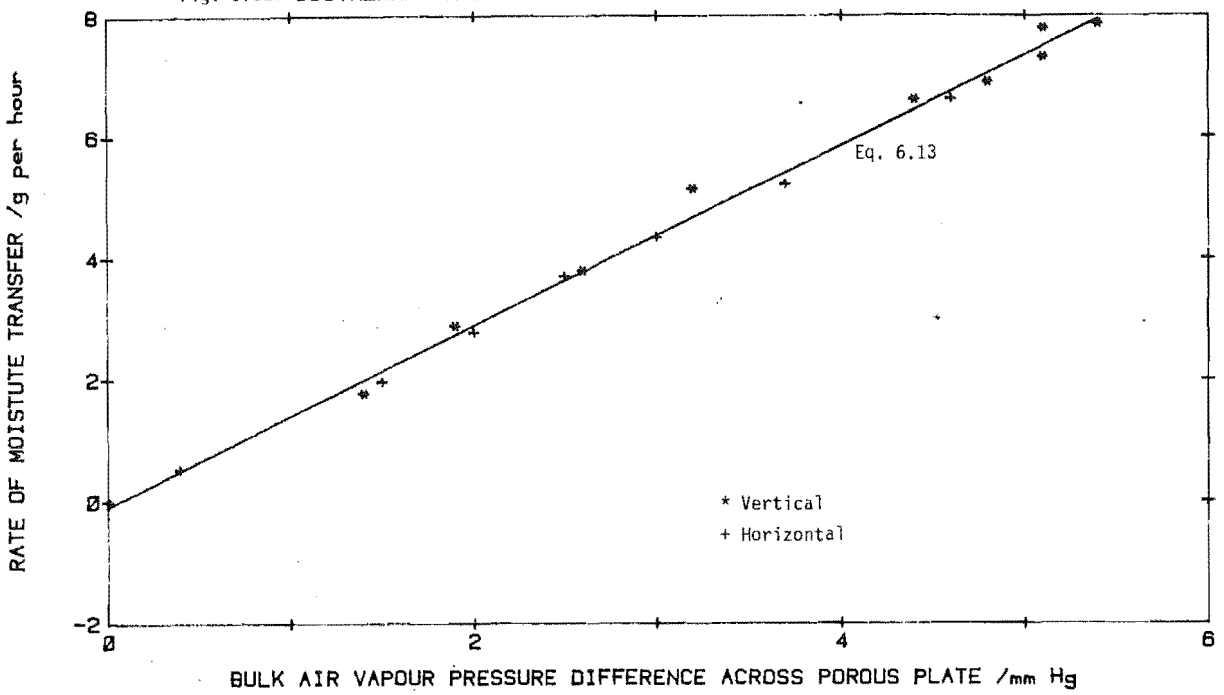

Fig. 6.12: ISOTHERMAL MOISTURE TRANSFER ACROSS ONE POROUS PLATE

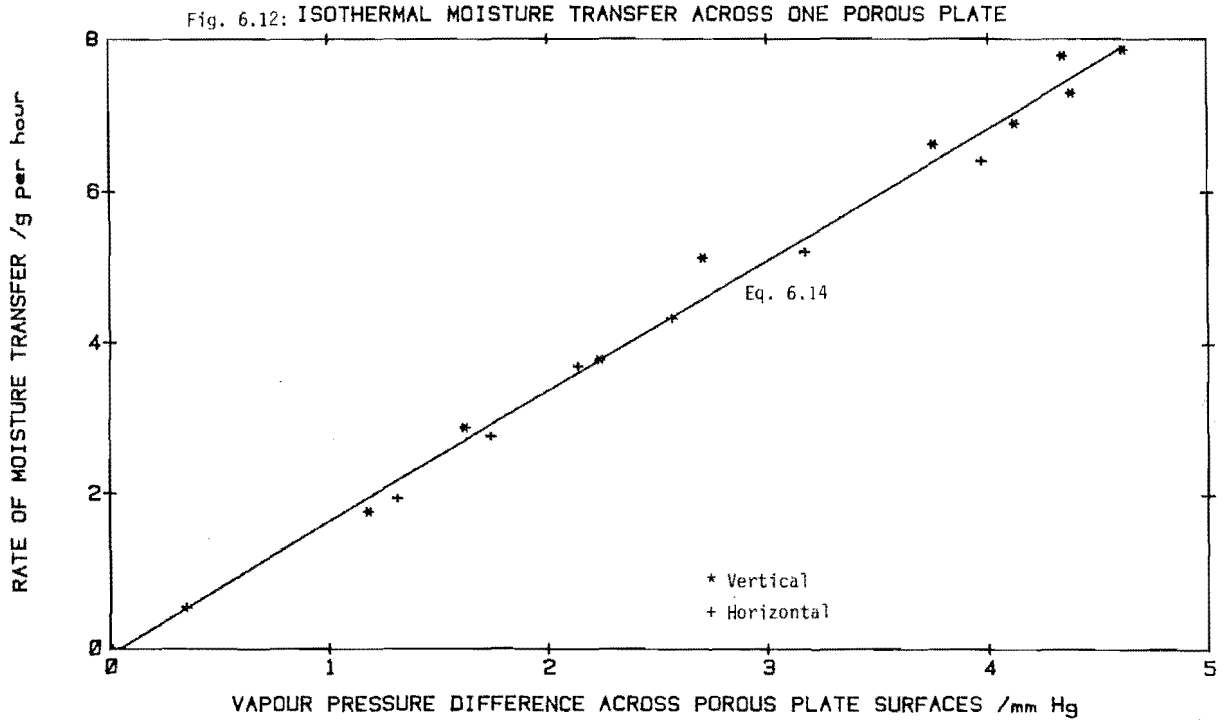

A comparison for the best-fit equations from Figs.6.7, 6.9 and 6.11 is given in Fig. 6.13.

Fig. 6.14 shows that the nominal moisture-loss rate from the Controlled Chamber to the Surroundings was insignificant compared with the nominal moisture transfer across the porous plate. This moisture-loss rate would have included the effect of moisture adsorption by the Perspex side-walls after the "conditioning" period. (see Appendix 5)

In this Chapter we have presented the results of the "preparatory" experiments. These data are needed to obtain the results of the next Chapter, which are the main results sought for by this work. Certain aspects of the results, such as the uniformity of plate's surface temperature and vapour pressure, will be discussed in details in Chapter 7 in relation to the context therein.

Fig. 6.13: ISOTHERMAL MOISTURE TRANSFER ACROSS ONE POROUS PLATE

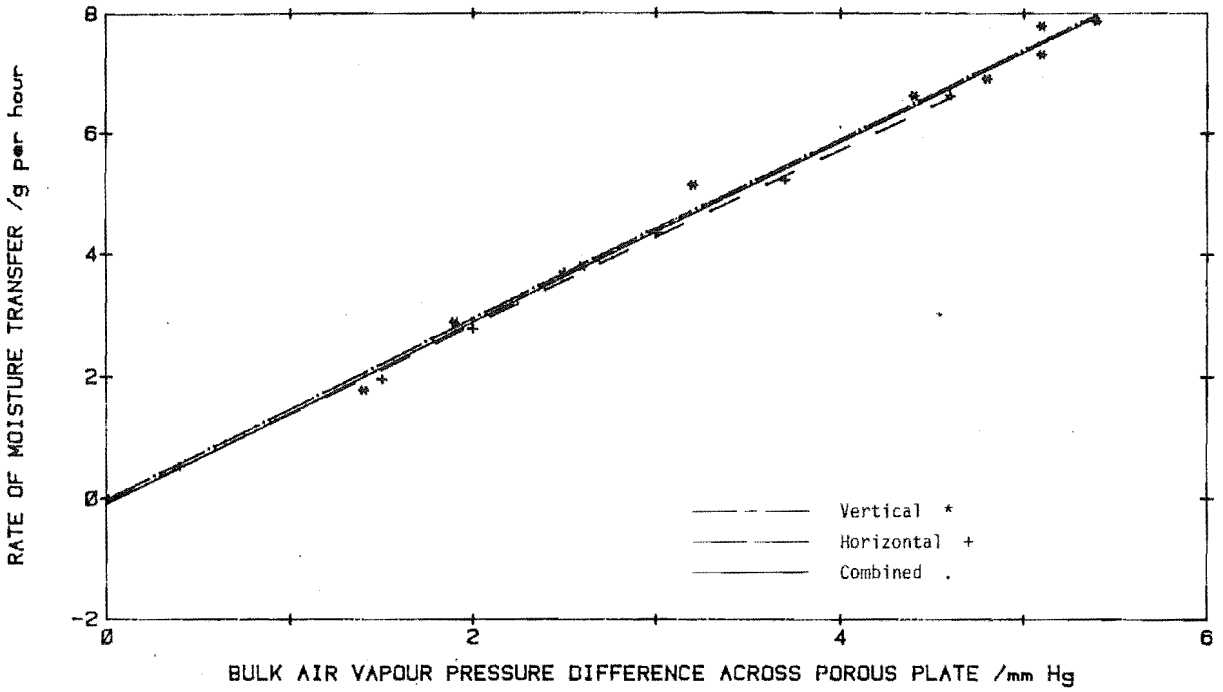

Fig. 6.14: MOISTURE TRANSFER RATE ACROSS POROUS PLATE vs MOISTURE LOSS RATE FROM C.C.

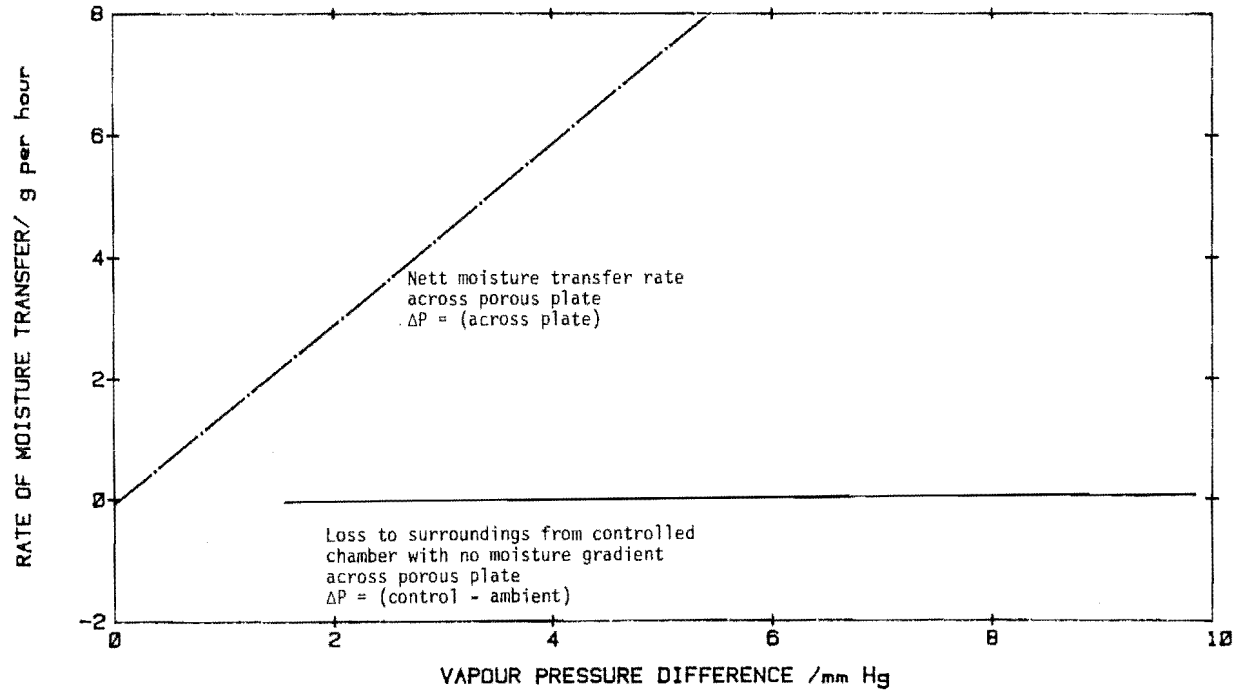

CHAPTER 7 RESULTS AND DISCUSSION

-THE CAVITY CASE

The Cavity case refers to the situation when an air gap was present between the Controlled and the Receiving Chambers. In this Chapter all the experimental results as well as some numerical results on the aspect of heat and moisture transfer rates across the cavity will be presented. The numerical results on the aspects of flow field, temperature field, concentration field and velocity components will be given in Chapter 8.

7.1 HEAT LOSS FROM CONTROLLED CHAMBER TO SURROUNDINGS

Figures 7.1 to 7.3 present the heat loss data from the Controlled Chamber to the surroundings for the case of a vertical cavity, a horizontal cavity with upwards transfer and horizontal cavity with downwards transfer respectively. The procedure for obtaining the data is outlined in Section 5.2 and as for the case of the single porous plate in Section 6.1.1, the difference in the heat loss curves between Figs 7.1 to 7.3 is again assumed to be the result of the different insulation arrangements for each case.

The best-fit equations by the least-squares technique for each case are:

(i) Vertical cavity :

$$q_l = 0.832(\Delta T_l) - 5.85 \quad \text{Std dev=0.21} \qquad (7.1)$$

(ii) Horizontal cavity with upwards transfer :

$$q_l = 0.996(\Delta T_l) - 5.57 \quad \text{Std dev=0.27} \qquad (7.2)$$

(iii) Horizontal cavity with downwards transfer :

$$q_l = 1.054(\Delta T_l) - 6.89 \quad \text{Std dev=0.22} \qquad (7.3)$$

where the units of q_l and ΔT_l are in W and °C respectively

Fig. 7.1: HEAT LOSS FROM C.C. TO AMBIENT -VERTICAL CAVITY

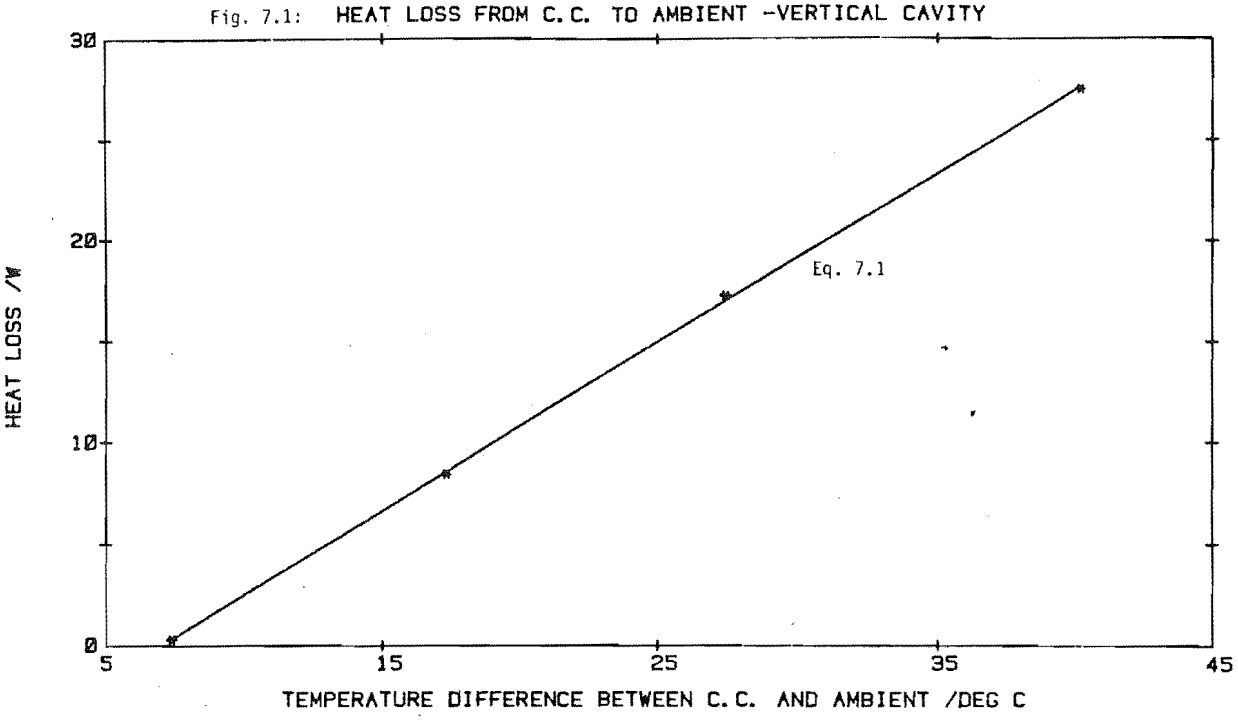

Fig. 7.2: HEAT LOSS FROM C.C. TO AMBIENT -HORIZONTAL CAVITY WITH UPWARDS TRANSFER

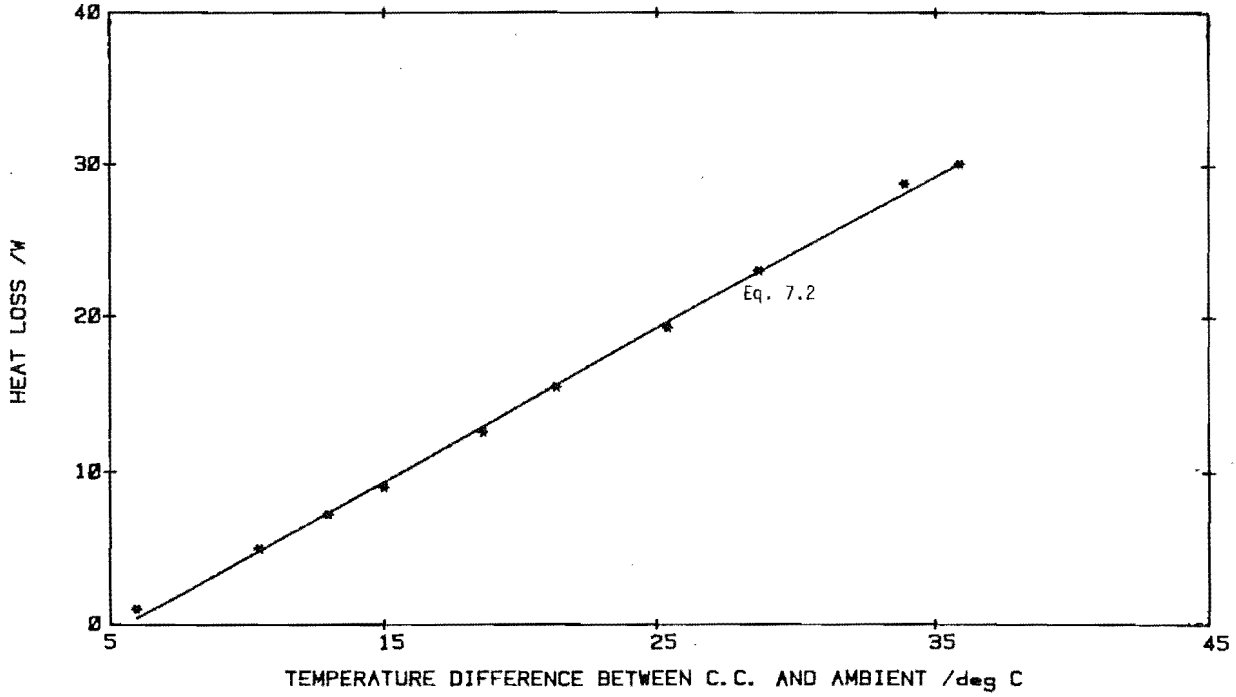

Fig. 7.3: HEAT LOSS FROM C.C. - HORIZONTAL CAVITY WITH DOWNWARDS TRANSFER

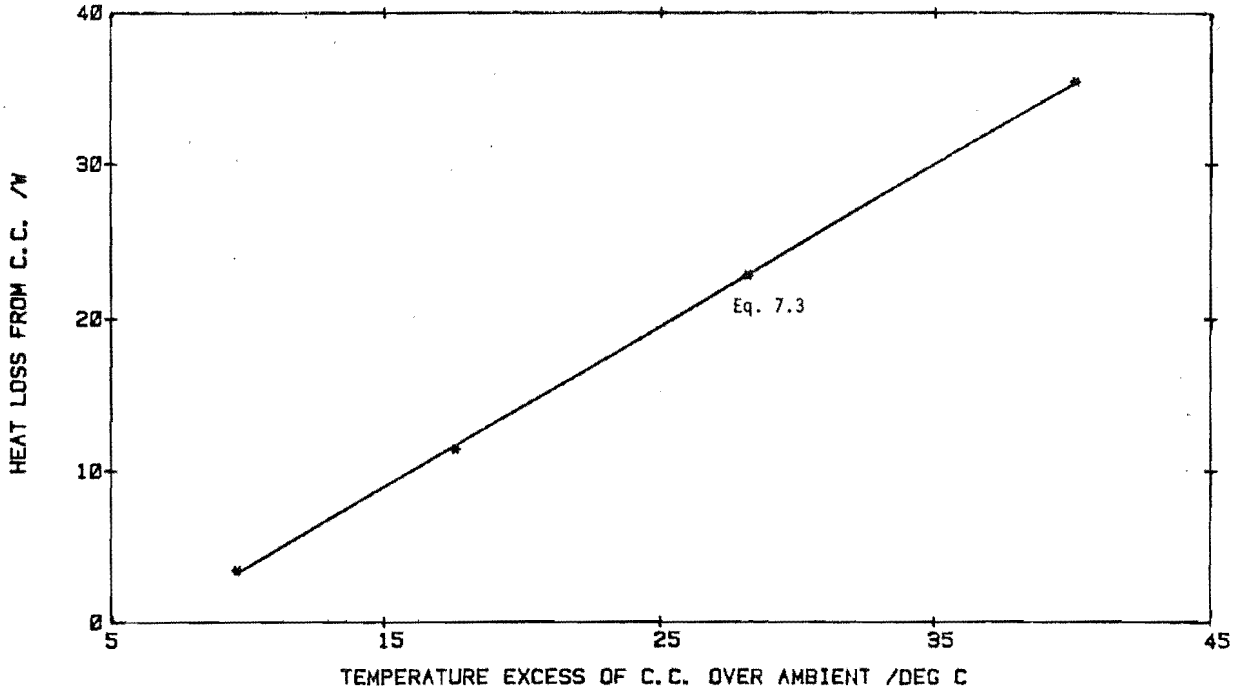

7.2 MOISTURE LOSS FROM CONTROLLED CHAMBER TO SURROUNDINGS

Figure 6.2 and Eq.6.3 are applicable for this case for the reason given in Section 6.1.2.

7.3 HEAT AND MASS TRANSFER IN CAVITY

The heat and mass transfer rates across a cavity for various temperature and/or concentration gradients are expressed in terms of dimensionless parameters as this increases the generality of a solution for a given set of parameters. The use of a suitable dimensionless parameter for heat and mass transfer phenomena also places the driving force for each case on an equal footing, thus allowing the comparison of the relative strength of each convective process.

The dimensionless driving force of the convective process (temperature and/or concentration difference) is expressed in terms of the Rayleigh number (thermal and/or concentration). The heat transfer rate is expressed in terms of the Nusselt number and the mass transfer rate in terms of the Sherwood number (for more details and the definitions of each of the dimensionless number, see Appendix 1.6). The other dimensionless groups relevant to the free convective transfer of heat and mass in a cavity, namely Prandtl number (Pr), Schmidt number (Sc) and the aspect ratio (A) remained a constant in this work as there were no means to vary the aspect ratio. Also the convecting fluid was always air and the diffusing species water vapour (Pr and Sc of course vary slightly with temperature, but this effect is small).

To reiterate Appendix A1.6, one has:

$(Ra)_c = (Gr_c \times Sc)$ Concentration Rayleigh number (7.4)

$(Ra)_T = (Gr_T \times Pr)$ Thermal Rayleigh number (7.5)

$(Ra)_{T,c} = (Ra)_c + (Ra)_T$ Combined Rayleigh number (7.6)

(For more details see Appendix 1.6 equations A1.34 to A1.38)

The concentration Rayleigh number is used when only moisture

gradient is the driving force.

The thermal Rayleigh number is used when only temperature gradient is the driving force.

The combined Rayleigh number is used when both the temperature and concentration gradients are the driving forces.

In using equation 7.6, it is assumed that the buoyancy generating mechanism of the temperature and moisture gradient are indistinguishable from each other, and their relative strength can be represented by the respective Rayleigh number. This is a reasonable assertion as the convective bulk air should not be able to distinguish between the type of buoyancy, but only be affected by the magnitude of the buoyancy force.

7.3.1 Heat and Mass Transfer in Vertical Cavity

Figure 7.4 represent the complete range of experimental Nusselt and Sherwood numbers versus the appropriate Rayleigh numbers for the vertical cavity. The set of experimental conditions consisted of:

(i) heat transfer alone;
(ii) isothermal moisture transfer and
(iii) combined heat and moisture transfer with aiding and opposing gradients.

The experimental apparatus is seen to be more suitable for moisture transfer experiments than for heat transfer experiments because the range of concentration Rayleigh number capable of being generated by the apparatus was about twice of that for the thermal Rayleigh number. This difference is due to the limitation in the boundary conditions that can be generated in the Controlled and Receiving Chambers independently as well as the characteristic of the porous plastic plate. There has been much research being done on the heat transfer aspect of the natural convective flow in a cavity and virtually no work being carried out on the aspect of moisture transfer. This work addresses this deficiency, but is limited in the extent of the heat transfer possible. For temperature differences other than those encountered in the

ERRATA Fig. 7.4: EXPERIMENTAL and THEORETICAL Nu & Sh vs Ra for VERTICAL CAVITY

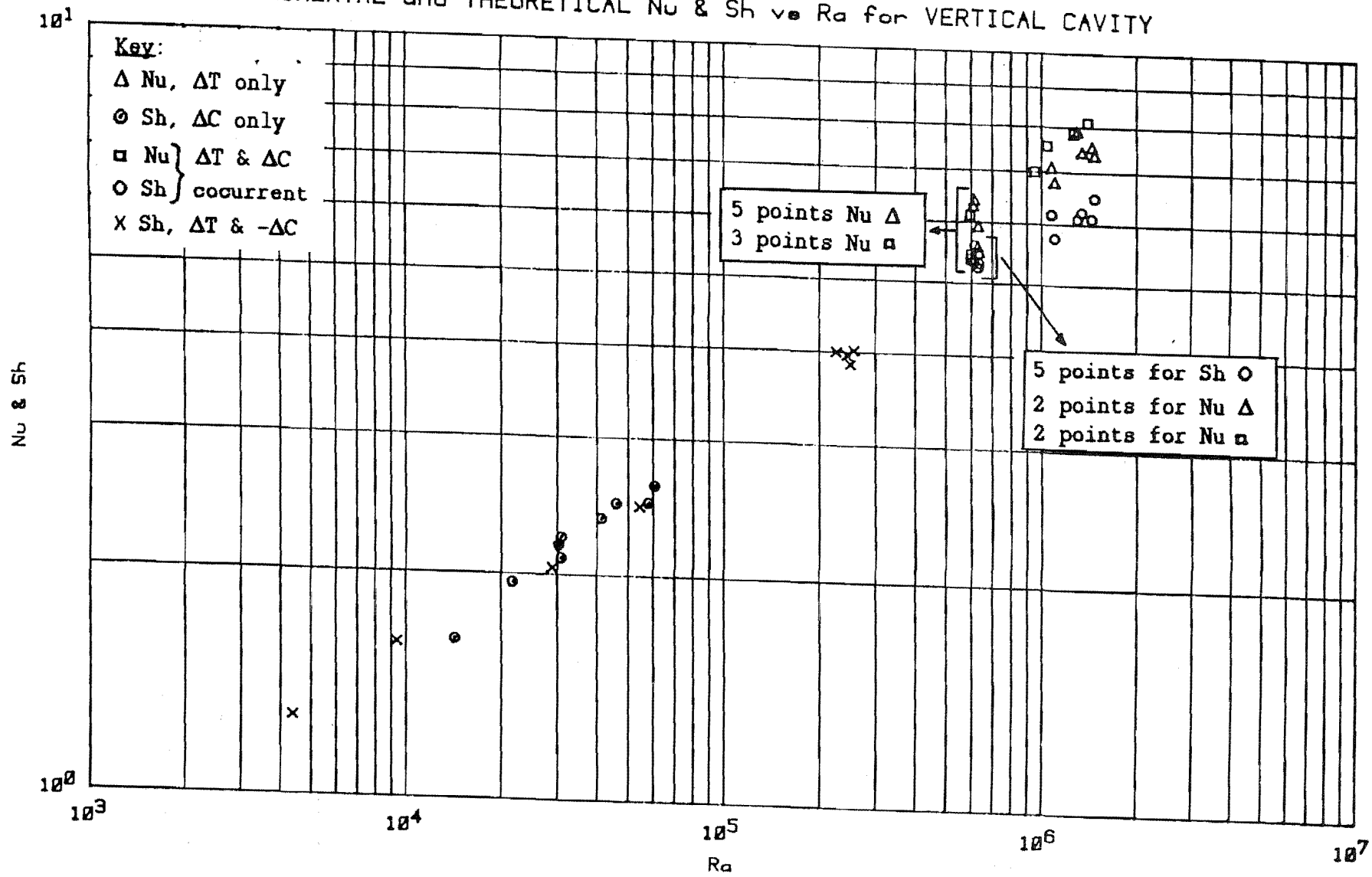

experiments, there are correlations available in the literature from which the rate of heat transfer can be deduced. The heat transfer results from this work can also be compared with the results from the literature to ascertain their validity.

The experimental error limits of Nu for the vertical cavity ranged from ±11 percent for runs at "high" heat transfer rate to ±14 percent for runs at low heat transfer rate. The corresponding error limits for Sherwood number ranged from ±16 percent for a high vapour pressure difference to ± 34 percent for a low vapour pressure difference (for details see Appendix 4). Thus the main source of uncertainty in the heat transfer experiments was the measurement of the heat transfer rates while the main source of uncertainty in the moisture transfer experiments was the evaluation of the cavity vapour pressure or humidity difference. This is a consequence of the inherent inaccuracy of the measuring equipment used, the random factor which affects the quantities being measured and the method of evaluating the cavity boundary conditions adopted in this work.

The range of the temperature difference across the cavity in Figure 7.4 ranged from 6.0 to 16.5 ^{o}C (details can be obtained from Appendix 7). This range represents fairly truthfully the actual temperature difference that may exist in the wall space of a New Zealand house, although under extreme conditions (in summer) the temperature difference in an actual roof space may reached as high as 40 ^{o}C. This extreme condition was not attained in the experiment because to do so would require the Controlled Chamber to operate at rather high temperatures which could damage the guarded box. Alternatively, a new and much more efficient condenser would need to be installed in the Receiving Chamber to reduce the temperature to a much lower level than was possible with the present condenser.

The range of the vapour pressure difference presented in Figure 7.4 ranged from 1.08 mm Hg (144 Pa, 1.44 mbar) to 5.59 mm Hg (747 Pa, 7.47 mbar) which covered the full range of vapour pressure difference one would expect to find in practice (2 to 4 mbar).

Experimental repeatability was better for Sherwood numbers than for Nusselt numbers. Indicated in Figure 7.4 was some repetition of the runs of similar Rayleigh number. The five runs for Sherwood number (HM41, 42, 54, 55 and 65) cluster closer

together in the graph than the corresponding runs for Nusselt number (HM41, 42, 54, 55, 65 and 40, 66, 73). If the slight difference in the Rayleigh numbers between the various runs quoted above was ignored, the Sherwood number had a mean value of 5.3 with a standard deviation of 0.15 or 2.9 percent when the standard deviation was expressed as a percentage of the mean values. The corresponding figure for the group of Nusselts numbers for all the runs quoted above was mean = 5.8 and standard deviation = 0.4 with a percentage of standard deviation of the mean value = 7%. Thus the repeatability of Sherwood numbers is about 2.5 times that of the Nusselt number. This spread of the Nusselt number was however still within the limit of experimental uncertainty due to the measurement inaccuracy of about $\pm$12%. Also it was interesting to note that although the Sherwood number had a proportionately larger experimental uncertainty than that of the Nusselt numbers as reported earlier, their repeatability on the other hand was better than that for the Nusselt numbers.

One disadvantage of using the porous plastic sheet in the heat-transfer experiment is its poor heat conductivity (0.06 $Wm^{-1}K^{-1}$) compared with that of copper or aluminium (400 and 200 $Wm^{-1}K^{-1}$ respectively). Thus uniformity of surface temperature over the porous plate was difficult to achieve in practice and the spread of temperature on the porous plate surface was about 0.3 °C for a temperature difference of 6.0 °C across the cavity; and 0.9 °C for a temperature difference of 20 °C. The deviation of the individual measurement from the mean value was therefore about 5 percent when expressed as a percentage of the mean value. The distribution of the vapour pressure about the porous plate surface was not certain as there was no means for measuring the vapour pressure on either side of the porous plate surface. But on noting that:

(i) the boundary layer thickness would be similar for both the diffusion of temperature and moisture in air and

(ii) the distribution of these quantities on the surface of the porous plate would be governed by the hydrodynamic condition in either the Controlled or the Receiving Chamber (by the action of individual fan stirrer),then it would be expected that the spread of the vapour pressure on the porous plate surface in the

Controlled/Receiving Chamber to be similar to that of the temperature distribution, i.e. 5 % about the mean value. One can only speculate what the spread of the vapour pressure on the surface of the plate in the test cavity itself would be but it was expected to be at least as good as the temperature distribution to judge from the better repeatability of the mass transfer runs as reported earlier.

From Figure 7.4 it can be observed that, on our dimensionless driving force scale (the Rayleigh number), temperature-induced buoyancy is always much stronger (typically 10 times) than the moisture-induced buoyancy for the level of temperature and moisture gradients one would expect to find in an actual building cavity. This point is now illustrated when we compared the results of runs HM43, HM1 and HM58 :-

RUN	ΔP/ Pa	ΔT/°C	$(Ra)_T$	$(Ra)_C$	$(Ra)_{TC}$	Nu	Sh
HM43	533.3	-	-	46000	46000	-	2.47
HM56	-	11.15	1041000	-	1041000	7.56	-
HM58	523.9	11.35	1059000	39000	1100000	6.76	5.76

An additional temperature gradient on top of the moisture gradient significantly affects the total Rayleigh number, the Nusselt number and the Sherwood number, but the reverse is not true.

Irrespective of whether the flow was generated by a pure moisture gradient or combined heat and moisture gradient, the Sherwood numbers in Figure 7.4 can all be characterised by a single correlation found by the least-squares technique:

$$Sh=0.113\ (Ra)^{0.286} \qquad \text{Std dev} = 0.3 \qquad (7.9)$$

This demonstrated the suitability of the Rayleigh number as a measure of the dimensionless driving force. It also supported an earlier claim that the convecting air has no means of distinguishing between the type of buoyancy that is causing the flow, but merely affected by the magnitude of the buoyancy. No other results were available from the literature to be compared with the Sherwood numbers calculated from equation 7.9.

Figure 7.5 presents a comparison between the experimental Sherwood numbers and the theoretical values calculated from the

Fig.7.5: EXPERIMENTAL AND THEORETICAL SHERWOOD NUMBERS FOR VERTICAL CAVITY

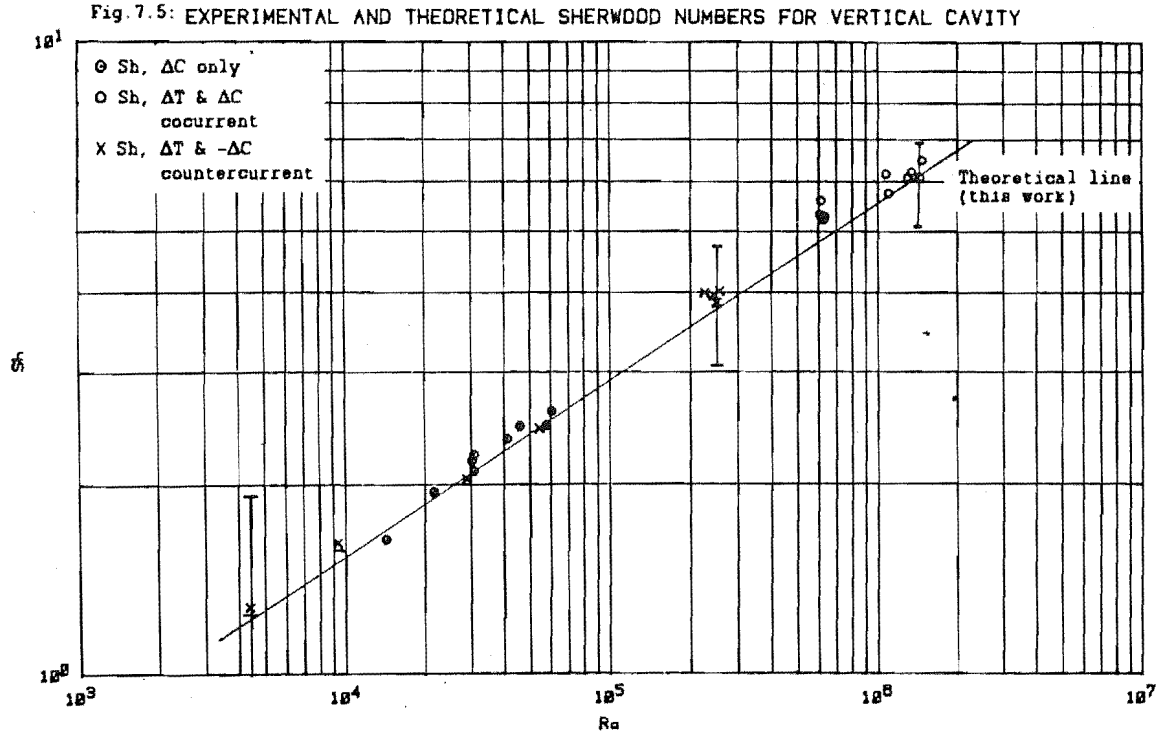

Fig.7.6: EXPERIMENTAL AND THEORETICAL NUSSELT NUMBERS FOR VERTICAL CAVITY

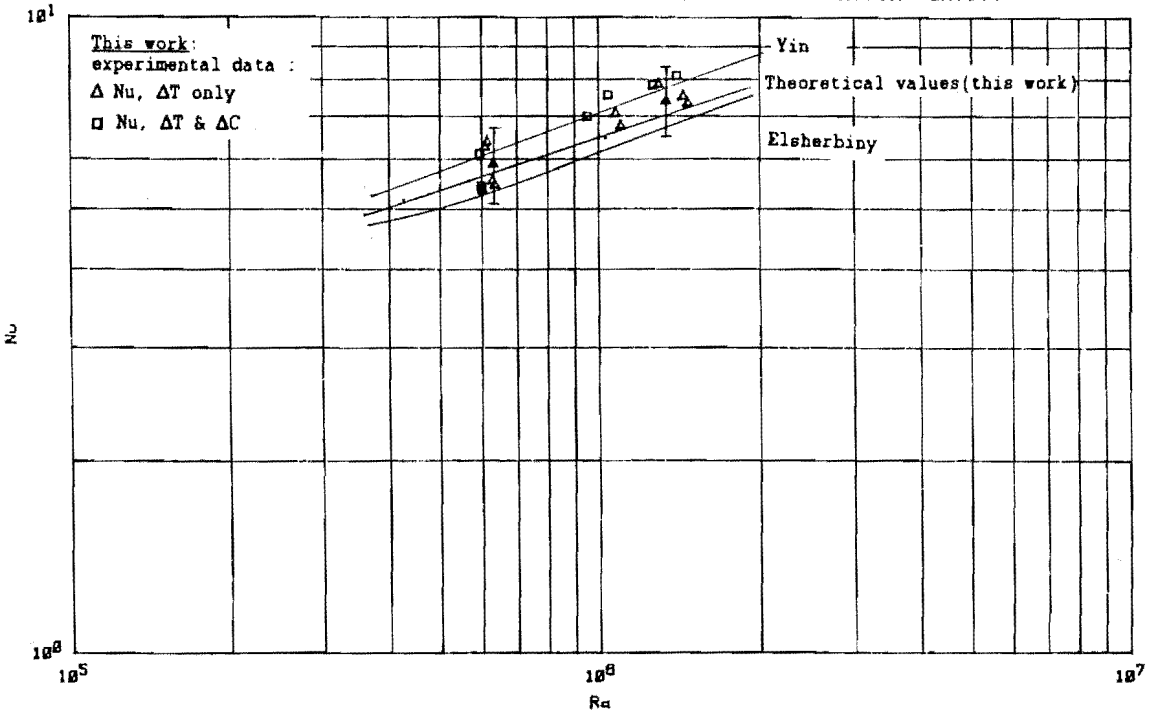

numerical simulation. The agreement is good and well within the experimental uncertainty. More discussion on the aspect of numerical simulation will be given in Chapter 8. The good agreement between experimental and theoretical results suggests that the values presented in Figure 7.5 are reliable and equation 7.9 can be used to predict the moisture transfer in a vertical cavity. Alternatively using the computer model one can confidently predict the Sherwood number at any Rayleigh number between the limits given in Figure 7.5 and more importantly, extend the prediction to other aspect ratios and Rayleigh number ranges where the computer model is expected to hold and where the present apparatus is not capable of producing, for instance at Rayeigh number less that 10^4 and for opposed heat and moisture gradients, without a need for extensive modification to be made to the apparatus.

From Appendix 1, the measurement of the reverse temperature gradients using cavity thermocouples for the case of opposed heat and moisture gradients was only an estimate due to the inherent inaccuracy of the thermocouples. Nonetheless, the Sherwood numbers for these cases in Figure 7.5 (and later Figure 7.8 for the horizontal cavity) agreed well with the theoretical values which suggest that the calibration method adopted for the cavity thermocouples in Appendix 1.6 was reasonable.

The Sherwood numbers for the case of opposing gradients are seen to fall in line with those for the case of aiding gradients in Figure 7.4. The Rayleigh numbers for opposing gradients are expressed as:

$$[Ra]_{T,C} = [Ra]_T - [Ra]_C$$

i.e. the nett dimensionless driving force is the algebraic sum of the two individual opposing driving forces. Thus the Sherwood numbers obtained from the case of opposing gradients would always be smaller than the case of aiding gradients for similar values of $(Ra)_T$ and $(Ra)_C$. But when compared with the isothermal case, the Sherwood numbers for the reverse gradients case can be higher when the temperature gradient is much stronger than the moisture gradient (e. g. for the points at Ra = 2.5 x 10^5 in Figure 7.4). From Appendix 7, it can be seen that the thermal Rayleigh numbers will always be very much (5 to 10 times) stronger than the concentration Rayleigh numbers for the conditions one would expect

to find in an actual building cavity. Thus for the case of reverse gradients in the building cavity, the rate of moisture transfer is not governed by moisture difference but rather by the reverse temperature difference, the transfer being from the side of high moisture concentration to the side of low concentration. It is only in an isothermal cavity that the moisture gradients determine both the rate and the direction of moisture transfer. Also it will be very difficult to stop the flow of either heat or moisture through the cavity by relying on the appropriate reverse gradient in the opposite direction as the condition for this phenomenon to occur does not happen in an actual building cavity. Attempts were made in the experiments to simulate this condition but due to the difficulty in controlling and measuring the precise reverse temperature difference across the cavity needed (less than 0.5 °C typically) and the non-uniformity of surface temperature on each of the plate surfaces, the runs could only be made after a lot of trial and error with large scatter in the data. For instance at Rayleigh number about 5×10^3 the Sherwood numbers obtained from various trials varied from 1.28 (the value plotted) to other values of 1.74, 1. 93 and 2.10 which are not plotted in Figures 7.4 and 7.5. At this limit of operation, the apparatus could not be expected to yield meaningful data consistently and further the experimental technique used was also of a trial and error nature. Hence only the best available points that were in line with the rest of the data had been included in Figures 7.4 and 7.5. In view of this, the two underlined points for Rayleigh number less than 1×10^4 must be treated with some scepticism and prediction of Sherwood number for Ra less than 1×10^4 is best done by the numerical calculation .

Figure 7.6 is a comparison between experiment Nusselt numbers and the correlations of Yin [12] and of Elsherbiny [115] from the literature. The theoretical values results from numerical calculations are also plotted for comparison. The results from this work appeared to agree more closely with the results of Yin than with that of Elsherbiny. But when the experimental uncertainty is taken into account e.g. by observing the length of the error bars about two representative data in Figure 7.6, one cannot really draw a firm conclusion as to which correlations the experimental Nusselt

numbers followed except to say that they agree with literature values within experimental limits. A correlation equation by the least-squares technique when fitted to the data of figure 7.4 produced a standard deviation of about 10% which is comparable with the value of 7.8% quoted by Yin et al [12] and the value of 3.6% quoted by Elsherbiny et al [115] for their experimental data. The correlation equation found by the least-squares technique is:

$$Nu_L = 0.058\ (Ra)^{0.346} \qquad \text{Std dev= } 0.7 \qquad (7.7)$$

which is considerably different from the correlation of Yin [12] :-

$$Nu_L = 0.091\ (Gr)^{0.307}$$

$$= 0.101\ (Ra)^{0.307} \qquad (7.8)$$

for Pr = 0.71, both in terms of the coefficient and the power factor. The correlation presented by Elsherbiny et al [115] was a more complicated form consisted of a three-equation set which took into account the effect of the aspect ratio on top of the effect of Rayleigh number. Thus judging from the limited amount of Nusselt numbers in figure 7.5 and the narrow range of Rayleigh number used, equation 7.7 is not recommended to be used for calculation purposes outside the stated Rayleigh number range. For that range the correlation equation of Yin or Elsherbiny should be used.

Comparison between experimental and theoretical Nusselt numbers for the vertical cavity in Figure 7.6 shows that the experimental Nusselt numbers agree with theoretical values within experimental limits, i.e. the theoretical value would predict all the experimental values with a spread of 12% about the predicted value .

Figure 7.7 compares the theoretical Nusselt numbers over the wider Rayleigh number range of 7×10^3 to 2×10^6 with the experimental correlation values of Yin [12] and of Elsherbiny [115]. The numerical calculations were confined to an aspect ratio of 7. The experimental values of Yin were obtained from cavity of aspect ratio from 4.9 to 78.7 and that of Elsherbiny from 5 to 110. The correlation of Elsherbiny took into account the influence of the aspect ratio on Nusselt number while Yin had grouped all the data under one correlating equation, irrespective of the different aspect ratios. It can be observed that the numerical calculation results agreed more closely with the correlation of Elsherbiny for

Fig.7.7:COMPARISON of THEORETICAL Nu with the CORRELATIONS of (i)Yin & (ii)ElSherbiny

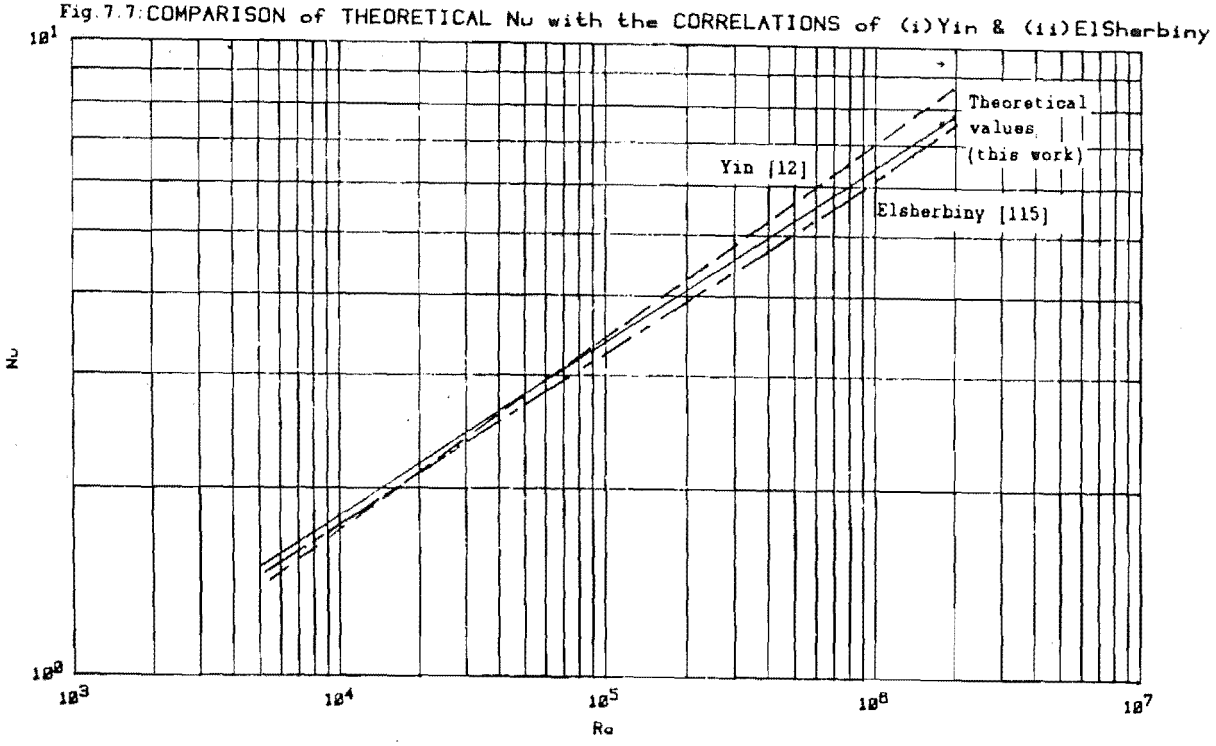

the whole range of Rayleigh number in Figure 7.7, although the theoretical Nu also agreed with the results of Yin within his experimental uncertainty.

As mentioned in Chapter 3, the greatest value of the thermal Grashof number based on air gap thickness which was used to obtain a numerical solution for the natural convection of air in a tall cavity of aspect ratio 5 or greater is 6×10^5 by Probent and Dixon [124]. The numerical results reported in Figure 7.7 thus extends the range of applicability of the numerical method and augment the earlier results of Probert and Dixon [124]. The correlation proposed by Probert and Dixon [124] was:-

$$Nu = 0.256 \ Gr^{0.25} \ (A)^{-0.27}$$

For an aspect ratio of 7.0, Eq. 7.10 is converted into

$$Nu = 0.151 \ Gr^{0.25} \qquad (7.10)$$

The correlation from the numerical calculation of this work was :-

$$Nu = 0.131 \ Gr^{0.276} \qquad (7.11)$$

Equation 7.11 of this work compares more favourably with the experimental correlations of Yin [12] (equation (7.8)) and Elsherbiny [112] for Ralyeigh numbers greater than 2×10^4 than equation 7.10 of Probert and Dixon [124]. Probert and Dixon [124] has taken into account the variation fluid properties with temperature in their calculation since their calculations used temperature differences up 200 °C. The maximum temperature difference for this work is about 20 °C and hence the usual Bousinesq approximation was adopted (see Chapter 3). Even then the results of the calculation from this work is seen to agree closer with the experimental values than that of Probert and Dixon [124]. The discrepancy could have been attributed to the coarser grids (17 x 25) used by Probert and Dixon compared with the denser grids (33 x 71) used in this work.

7.3.2 Heat and Mass Transfer in Horizontal Cavity

Two cases need to be identified with heat and mass transfer in a horizontal cavity. These are :-

(A) Horizontal cavity with upwards transfer of heat and

mass. All Nusselt and Sherwood numbers associated with this case will be designated with the subscript "u";

(B) Horizontal cavity with downwards transfer of heat and mass. All Nusselt and Sherwood numbers associated with this case will be designated with the subscript "d";

Both cases were investigated under the following experimental conditions:-

(i) Heat-transfer alone case; characterised by the subscript "$_T$"

(ii) Isothermal moisture-transfer case; characterised by the subscript "$_c$"

(iii) Combined heat and moisture-transfer case with aiding and opposing flows, characterised by the subscript "$_{T,c}$".

The results for all the runs were plotted in Figure 7.8 in terms of the Nusselt and/or Sherwood numbers against the appropriate Rayleigh number as explained earlier.

From Figure 7.8 it can be concluded that simultaneous heat and moisture-transfer rates in an upwards direction are much greater than in the corresponding cases in a downwards direction, when both driving forces are aiding each other. For the range of $(Ra)_{T,C}$ investigated ($2.0 \times 10^5 < (Ra)_{T,C} < 2.0 \times 10^6$), $(Nu)_u$ and $(Sh)_u$ are about 5 to 9 times that of $(Nu)_d$ and $(Sh)_d$ respectively. The reason for this difference is due to the fact that upwards-transfer gradients generate free convection of air in the cavity while downwards acting gradients suppress such bulk air motion. $(Nu)_u$ ranged from 5.1 to 9.0, while $(Sh)_u$ ranged from 4.7 to 6.8. $(Nu)_d$ and $(Sh)_d$ attained the expected value of about 1.0 and 0.85 respectively within experimental limits.

The range of temperature difference used for the upwards transfer case ranged from 2.5 to 21.0 °C while that for the downwards transfer case ranged from 7.27 to 16.53 °C. Thus both ranges of temperature difference used were of the same order of magnitude. The percentage errors in the Nusselt numbers for the two cases, however, are very different. The small transfer rate for the downwards transfer case resulted in a large percentage error (about

Fig.7.8: EXPERIMENTAL Nu & Sh vs Ra for HORIZONTAL CAVITY

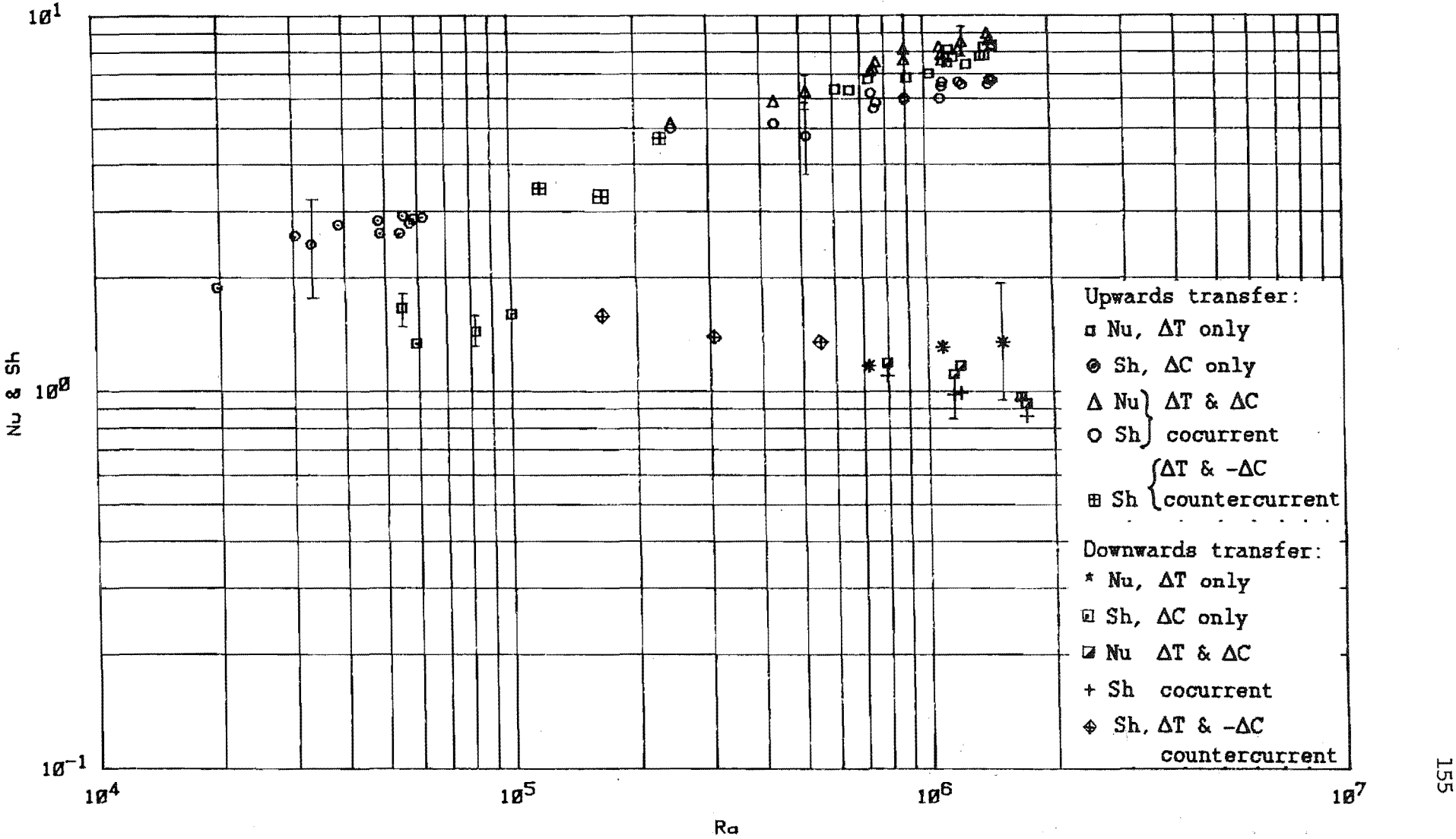

50%) in the Nusselt number. For comparison the corresponding percentage error in the Nusselt numbers for the upwards transfer case ranged from 10 to 15%, which compare favourably with many results reported in the literature. The large percentage error for the downwards transfer case is not desirable, but is unavoidable in this case as the absolute error incurred was in fact only 0.58 W and represents the limit of accuracy of the apparatus.(see run HM24, Appendix 4). To reduce this error would perhaps require a different means of measuring the heat-transfer rate, e.g. by a direct optical method instead of the indirect heat balance adopted for this work. This option is beyond the scope of the present work. In view of the fact that the apparatus worked favourably with the upwards transfer cases, the large percentage error for the downwards transfer cases were tolerated.

The error limits for Sherwood number, on the other hand, is smaller for the downwards transfer case (11%) than the upwards transfer case (19 to 29 %) (see Appendix 4). The small mass-transfer rate for the downwards transfer case did not result in a large percentage error because the method of mass-transfer measurement adopted in this work (Chapter 4) can provide very accurate measurement right up to the smallest mass-transfer rate measured in this work. The main source of error was in the measurement of the humidity difference across the cavity which was determined by the accuracy of the "Dew All" humidity sensor. This uncertainty is ± 0.5 percent in the relative humidity value and when we compare Runs HM2 (upwards transfer) and HM30 (downwards transfer):

RUNS	m /gh^{-1}	ΔP /Pa
HM2	5.68	295
HM30	5.50	1063

The much higher ΔP values for the same mass transfer rate for Run HM30 thus resulted in smaller percentage error for the downwards transfer case.

Typical error bars for Nusselt and Sherwood numbers are plotted in Figures 7.8, 7.9 and 7.11.

Another interesting feature from Figure 7.8 are the results for the opposing gradients case. Six experiments had been

performed, in which one half of the experiments had moisture gradient in a downwards direction and the other half had the moisture gradients in an upwards direction. From Figure 7.8 the points for downwards moisture gradient, but the data for the case of upwards temperature gradient lie almost in line with the points for isothermal transfer as well as simultaneous heat and moisture transfer in the upwards direction. Thus even though the moisture gradient is acting in the downwards direction, the presence of the reverse temperature gradient has increased markedly the rate of moisture transfer compared with the case when no reverse temperature gradient was present. The Rayleigh number for the case of opposing gradients is defined as :-

$$(Ra) = (Ra)_T - (Ra)_C.$$

As $(Ra)_T$ is almost 6 to 7 times greater than $(Ra)_C$ for the three points in question, the free convection current generated would be determined primarily by $(Ra)_T$. Further since the temperature gradient would have been in the upwards direction, this case could be seen as equivalent to the case of upwards moisture transfer with a combined heat and moisture gradient with Rayleigh number equal in magnitude to $\{(Ra)_T - (Ra)_C\}$ for the opposing gradient case.

ie. $\{(Ra)_T + (Ra)_C\}_{upwards} = \{(Ra')_T - (Ra')_C\}_{downwards}$

where the negative sign indicates the downwards direction.

Similarly, for the case of a downwards temperature gradient and a upwards moisture gradient, the corresponding Sherwood number was smaller than the case when no reverse temperature gradient was present. The large effect of the temperature gradient again swamped the effect of the moisture gradient and this is analogous to the case of heat and mass transfer in a downwards direction only:

ie. $\{-(Ra)_T - (Ra)_C\}_{downwards} = \{-(Ra')_T + (Ra')_C\}_{upwards}$

where the negative sign again indicates the downwards direction.

The practical consequence of this is that moisture transfer across an actual building cavity would only be suppressed when the top surface is warmer than the bottom surface. The actual moisture concentration across the cavity does not really govern the rate of moisture transfer unless the cavity has isothermal boundaries (which is rare in practice).

7.3.2.1 Horizontal Cavity with Upwards Transfer. As with the case of the vertical cavity, the dimensionless driving force resulted from temperature difference is about ten times that generated by moisture difference for the level of temperature and moisture gradient one would expect to find in an actual building cavity (temperature differences ranged from 2.5 to 21 °C and moisture vapour pressure differences ranged from 215 Pa to 752 Pa). Thus, while $(Sh)_u$ for the case of isothermal moisture transfer ranged from 1.7 to 2.9, the $(Sh)_u$ for the case of combined transfer ranged from 4.7 to 6.8. The Nusselt number, however, did not show such a large difference. $(Nu)_u$ for case of simultaneous heat and moisture was generally 5% greater than $(Nu)_u$ when the moisture gradient was absent. Since the experimental error in each case was about 12%, the difference cannot be attributed with much significance. The practical implication from this observation is that, while a simultaneous temperature gradient significantly increase the transfer of moisture, the reverse case is not true.

Figure 7.9 is a comparison of the experimental Nusselt number with the experimental correlation of Hollands (118). The theoretical Nusselt number from numerical calculation is also plotted for comparison with the experimental values. The Nusselt numbers from this work are seen to be mostly higher than the correlation of Hollands (by about 8%) but the slope of increase is similar and the two sets of Nusselt numbers generally agree within the experimental uncertainty. The use of Hollands correlation to predict the rate of upwards heat transfer in an horizontal cavity is thus recommended for the range of Rayleigh number outside that of Figure 7.9.

A correlation fitted to the experimental data point in Figure 7.9 by the least square technique yields

$$Nu = 0.157\ Ra^{0.280} \qquad \text{Std dev} = 0.5 \qquad (7.12)$$

Equation 7.12 is a simple power law expression and is specifically for fixed aspect ratio of 7.0 and air being the convecting fluid. The correlation of Hollands (118) is of a much more complicated form which is applicable for multi-Prandtl number cases over the Rayleigh number range of 10^3 to 10^9. Figure 7.9 also presents a comparison between the theoretical Nusselt numbers from numerical

Fig.7.9:EXPERIMENTAL & THEORETICAL Nu for HORIZONTAL CAVITY - UPWARDS TRANSFER

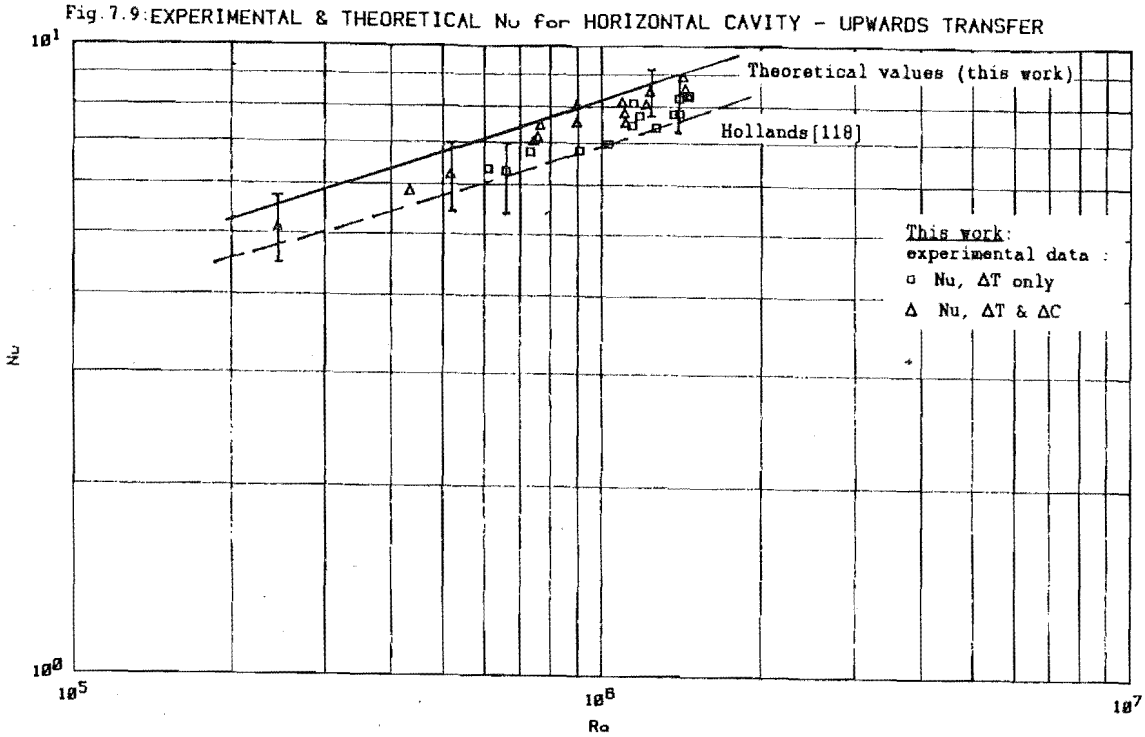

Fig.7.10:COMPARISON of THEORETICAL Nu with the CORRELATION of HOLLANDS

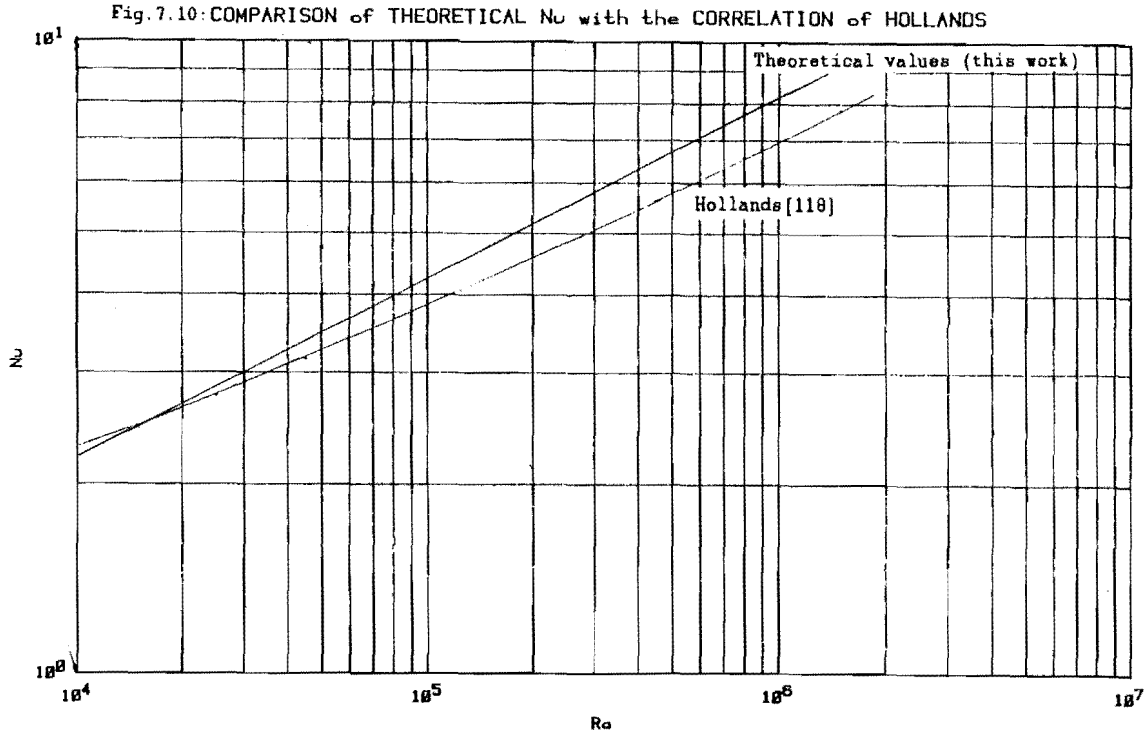

calculation with the various experimental values. More discussion on the aspect of numerical calculation will be given in Chapter 8. The theoretical Nusselt numbers shown are the best available values subjected to some constraints imposed by the computing machine in terms of storage and the speed of computation. The predicted values are generally higher than the experimental value in the correlation of Hollands (18), but are within the experimental uncertainty of most data points.

A least-squares fit on the theoretical data points yield:

$$Nu = 0.165\ (Ra)\ )^{0.282} \qquad (7.13)$$

Comparing equations 7.12 and 7.13 show that the exponents agree closely, but the constant term is higher for equation 7.13 which suggest some systematic error might be present in either the experimental or theoretical values. A More comprehensive comparison between the theoretical values and the experimental correlations of Hollands (118) is presented in Figure 7.10. It is seen that agreement between the two curves in Figure 7.10 is within 10 percent for Rayleigh number up to 10^5, progressively becoming worse as the Rayleigh number is increased (15 % discrepancy at Ra = 1.5 x 10^6). More grid points are needed in the numerical calculations to reduce this discrepancy. The increase in the number of grid points also increases the amount of storage and computing space needed on the computer. A compromise had to be struck between the accuracy of the results and the computing capability available and the data plotted in Figure 7.10 is the result.

As for the case of the vertical cavity, there is no results available from the literature which could be compared with the Sherwood numbers from this work. Thus comparison can only be made between the experimental and theoretical Sherwood numbers from this work and this is presented in Figure 7.11. The experimental Sherwood numbers are seen to agree with the theoretical line within experimental limit. This confirms the validity of the numerical method which can then be used to predict the Sherwood numbers at other aspect ratios and in a Rayleigh number range outside those indicated in Figure 7.11 as long as the model holds (as judged by the stability of the numerical outputs or other criteria available from the literature). The equation of the line plotted in Figure 7.11 calculated by the least-squares technique is :-

Fig.7.11: EXPERIMENTAL and THEORETICAL Sh for HORIZONTAL CAVITY - UPWARDS TRANSFER

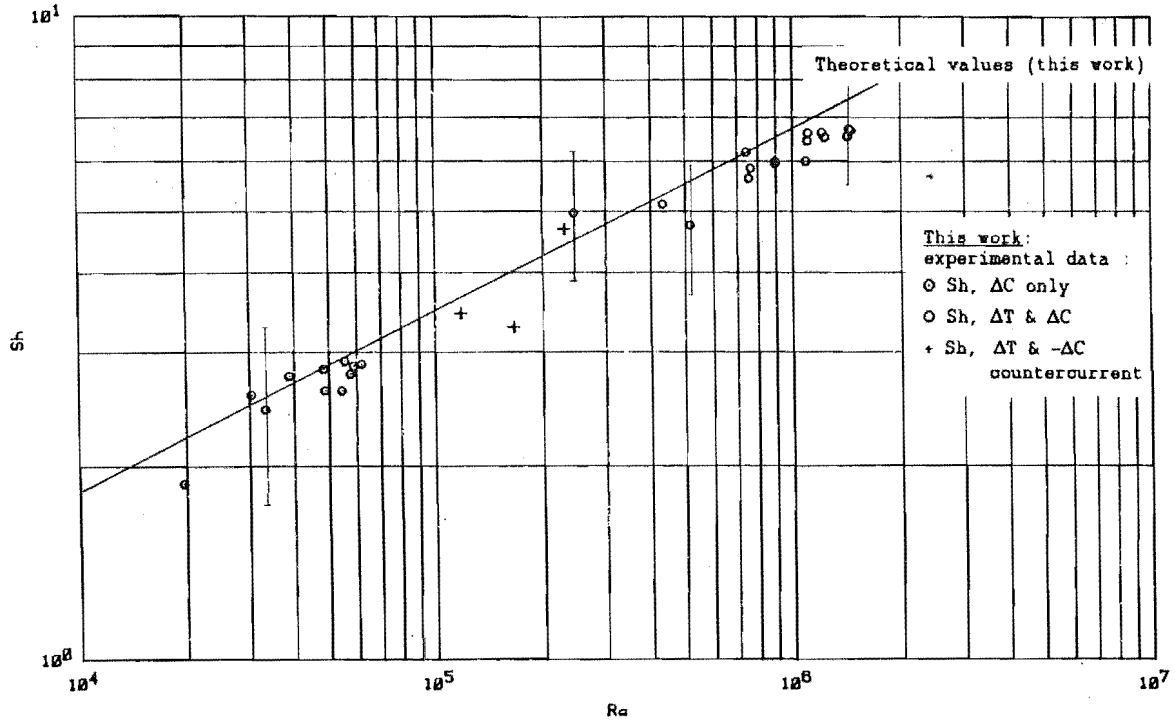

$$Sh = 0.148\ (Ra)^{0.276} \qquad (7.14)$$

Equation 7.14 is calculated for easy comparison with the correlation equation from experimental data. A single correlation fits all the experimental data points in Figure 7.11 very well, irrespective of whether the Sherwood numbers were obtained from the case of moisture gradients only or combined heat and moisture gradients for both aiding and opposing gradients. This again shows that the Rayleigh number is an appropriate way to represent the driving force so that data from different driving force case can be compared on some common ground. The correlation equation for the experimental points found by the least square technique is

$$Sh = 0.144\ (Ra)^{0.272} \qquad \text{Std dev} = 0.5 \qquad (7.15)$$

Equation 7.15 compares very well with equation 7.14 considering the rather large error limits for the experimental points (see error bars for representative points in Figure 7.11).

7.3.2.2 Horizontal Cavity with Downwards Transfer. The Nusselt and Sherwood numbers for the downwards transfer cases are seen to agree with the expected value of 1.0 and 0.85 respectively within experimental limits for the heat transfer and the case for aiding heat and moisture transfer case. The limits for experimental uncertainty have been discussed earlier in section 7.3.2 and are indicated in Figure 7.8. The Sherwood number for the isothermal case does not equal to 0.85 within experimental limits. One possible reason for this discrepancy was the difficulty of maintaining an exact zero temperature gradient across the horizontal cavity. If there were a temperature difference of 0.5 to 0.8 °C of the bottom surface over the top surface the convection current generated by the upwards temperature gradients would have given the Sherwood number indicated in Figure 7.8 (Sh is calculated from equation 7.10 for the upwards transfer case). The experimental uncertainty for the temperature difference for the downwards transfer case is about .36 °C (Appendix 4, Run HM25) and hence the possibility of non-isothermal conditions in the cavity was high indeed. Nevertheless, the results for isothermal moisture transfer in the upwards direction were not affected by this problem, which tends to suggest that another reason was responsible for the rather high Sherwood number. Luikov (25) has indicated that non-uniformity

of vapour concentration over the plate surfaces could have induced a convection current and hence increased the Sherwood number. This deviation of individual measurements from the mean value was shown before to be about 5% of the mean value. This phenomenon is not apparent for the case of simultaneous heat and moisture transfer because of the large stabilising effect of the downwards temperature gradient which suppresses the convective current.

Numerical calculations had indicated that the air in the cavity was stable to any disturbance and no convection resulted. The theoretical Nusselt number is always equal to 1.0 and the Sherwood number equal to 0.85.

CHAPTER 8

NUMERICAL RESULTS AND DISCUSSION.

The Nusselt and Sherwood numbers predicted by the numerical calculation have already been shown to agree well with the experimental values for both the Horizontal and the Vertical Cavity in Chapter 7. In this Chapter, the temperature field, concentration field, stream-function field and the velocity profiles from the numerical calculation will be presented. These fields examine in greater details the transport processes which occur in the cavity and complement the experimental measurements which concerned only the overall rate of heat and mass transfer across the cavity.

8.1 BRIEF COMPARISON BETWEEN THE THREE NUMERICAL METHODS.

The numerical results of the three numerical methods mentioned in Chapter 3 were compared in Appendix 10 to ascertain that :

(i) their computer codes were correct;

(ii) they were suitable to be used as a theoretical model .

We act on the basis that, if a numerical method cannot generate a "correct" solution for a relatively simple case, it will be most unlikely to produce a result for a more complicated case. The "simple" test conditions used to determine the suitability of a numerical method were that of :

(i) a square cavity with the vertical walls at different but uniform temperature corresponding to Rayleigh number of 1.0×10^6 whose solution is well documented in the literature and

(ii) various "easy" conditions for the experimental cavity of aspect ratio seven where a reliable method should work.

The formulation, initial and boundary conditions of the numerical scheme had been given in Chapter 3.

From the results of Appendix 10, the existing methods of

"False-Transient (FT)" (Mallinson and de Vahl Davis [123]) and "Dynamic Alternating Direction Implicit (DADI)" (Doss and Miller [160]) were seen to produce "correct" results for the square cavity at Rayleigh number of $1.0x10^4$ and $1.0x10^6$, but the "hybrid" method proposed by this work in Chapter 3 did not. Both the "hybrid" and the "DADI" methods were about eight times faster in reaching the "steady-state" solutions than the "FT" method (For definition of "steady-state", see Appendix 8). However, for a cavity of aspect ratio of 7.0, the greater speed of convergence of the "DADI" method over the "FT" for the case of the square cavity was not apparent, which is an unfortunate feature.

For a cavity of aspect ratio of 7.0, the "hybrid" method correctly predicted the experimental Nusselt and Sherwood numbers at some Grashof numbers ($4x10^5 > Gr_T > 2x10^5$), but only for the "right" combination of the input parameters. There was, however, no rule as to how to obtain the "right" combination of input parameters and this made the Hybrid method virtually useless. Both "DADI" and "FT" methods correctly predicted the results but were slower in terms of computing time. The "hybrid" method reduced the time to reach "steady-state" solution from about 2 hours of CPU time for either the "FT" or the "DADI" method down to about 12 minutes (Computation being done on a VAX 11-730 minicomputer). But the fact that it nearly always converged to a wrong solution except for some "right" but randomly chosen combinations of the input parameters made it unsuitable to be used as a numerical model. The outputs of the "hybrid" method in Appendix 10 also depended on some parameters, such the false transient factors, the time step of iteration and the boundary vorticity smoothing factors , all of which should not have affected the final value of the steady-state results but only the rate of convergence of the results. Thus it was decided that some (unexplained) errors existed in the "hybrid" method and it was by chance that it appeared to work in the Grashof number range mentioned earlier. No extensive theoretical investigation other than numerical experiments were performed to try to improve the "hybrid" method. The primary aim of this work was the determination of new heat and moisture transfer data by the "novel" experimental method proposed and the production of a numerical code, whether based on new or existing computer method,

was only to test the validity of these experimental data. Thus, if a "better" numerical method than the existing one could be found, it would be used. Otherwise, the existing method would sufficed. In either case, some new results will be reported, as the upper Grashof number range used for this work was the highest the author was awared of for a cavity of aspect ratio equal to 7.0. Also, as no previous simultaneous heat and moisture transfer studies had been reported for a "closed" cavity, the good comparison between experimental and numerical results in this work will also extend the credibility of the existing numerical methods.

The following results were therefore calculated either with the "False Transient (FT)" or the "Dynamic Alternating Direction Implicit (DADI)" methods. Tables 8.1 and 8.2 list the conditions used to obtain the data points in Figs 8.1 and 8.2 respectively for the theorectical Nusselt and Sherwood numbers used in Chapter 7. The following remarks will be useful in explaining some features of Tables 8.1 and 8.2 :-

(1) ADI : The Alternating Direction Implicit method using the "non-conservative" formulation for the convective terms ($U(\partial t/\partial x)$) etc.- See Appendix 8) and the stream function equation was solved by the Successive Over Relaxtion method.

(2) FT-I : The "False Transient" method using the "non - conservative" for the convective terms ($U(\partial t/\partial x)$ etc.) (See Appendix 8).

(3) FT-II: The "False Transient" method using the "conservative" formulation for the convective terms ($U(\partial t/\partial x)$ etc.) (See Appendix 8).

(4) DADI : The "Dynamic Alternating Direction Implicit" method. The "conservative" formulation was used for the convective terms ($U(\partial t/\partial x)$ etc.) (See Appendix 8). The stream function was solved by the "False Transient" method.

(5) M : The number of grid data points in the X-direction.

$\Delta X=7/(M - 1)$ is the step size.

(6) N : The number of grid points in the Y-direction.

$\Delta Y=1/(N-1)$ is the step size.

(7) The time step used for the "ADI" abd the "False Transient" method is typically "0.8 x $(\Delta L)^2$" where ΔL is the smaller of either ΔX or ΔY used. The time step can be increased if the false transient terms were reduced below unity (usually only that for the vorticity equation).

(8) The time step for the "DADI" method was being updated after every iteration, thus no a priori value was needed. The program usually started with $\Delta t = 0.0001$.

(9) The false transient factors used were typically $a_T = 3.0$, $a_C = 3.0$, $a_\varphi = 3.0$ and $a_\zeta = 0.5$ for Grashof number less than $1x10^5$ and $a_T = 1.0$, $a_C = 1.0$, $a_\varphi = 1.0$ and $a_\zeta = 0.2$ or 0.02 or 0.005 or 0.002 for Grashof number greater than $1x10^5$ and more "difficult" conditions.

(10) The temperature and vapour pressure difference given in Tables 8.1 and 8.2* corresponding to the the Rayleigh number listed were calculated for a cavity of gap thickness of 0.1 m.

8.2. THEORETICAL NUSSELT AND SHERWOOD NUMBERS.

From Fig 8.1, the Nusselt and Sherwood numbers calculated from the different methods and formulations all lie in a straight line within the limits of accuracy required by this work ($\pm$ 10% typically). The spread of the data in Fig 8.2 is more considerable but the deviation from the straight line is still within the accuracy for this work.

The number of grid points used in the calculation was the minimum required to obtain a good agreement between experimental and theoretical Nusselt and Sherwood numbers. Two grid points were within the boundary layer at $Gr_T = 1.4\ x10^5$ and one point for $Gr_T = 1x10^6$ for the 71 x 33 grid . It is known that the temperature field and hence the average Nusselt numbers are not sensitive to the number of grid points used [8] and hence they are not a good

*Note :- Tables 8.1 and 8.2 are presented at the end of this Chapter.

Fig.8.1: THEORETICAL Nu & Sh vs. Ra for VERTICAL CAVITY

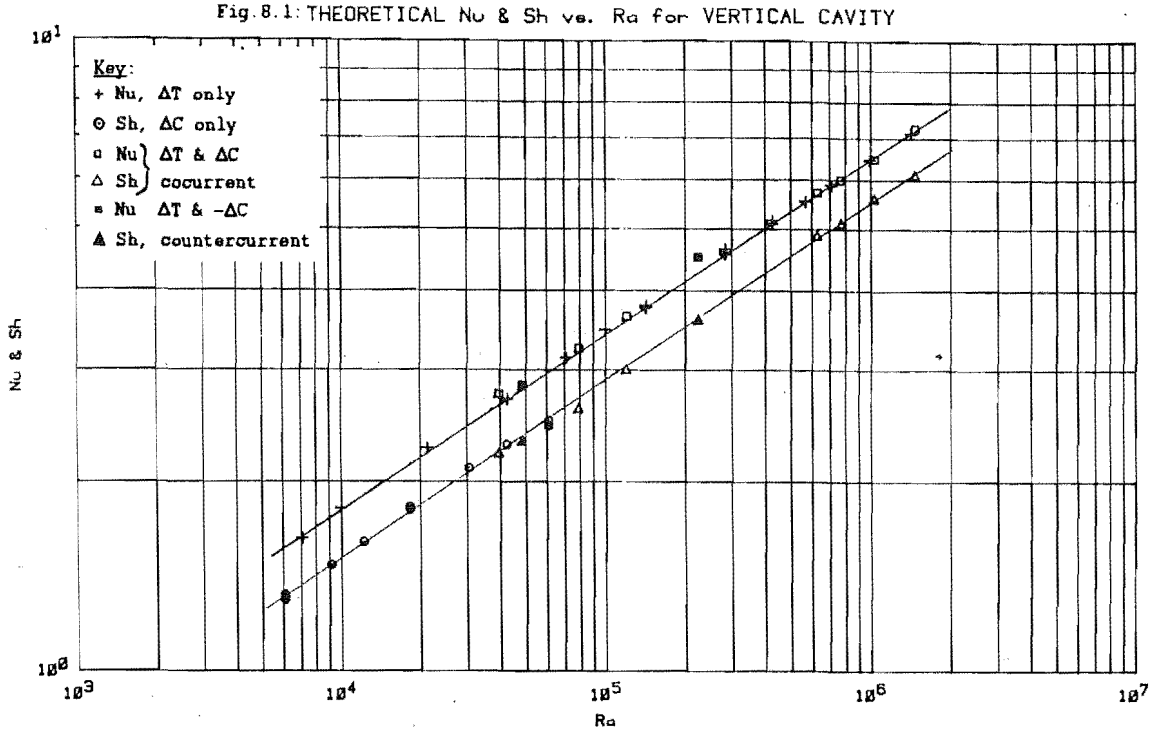

Fig.8.2: THEORETICAL Nu & Sh for HORIZONTAL CAVITY - UPWARDS TRANSFER

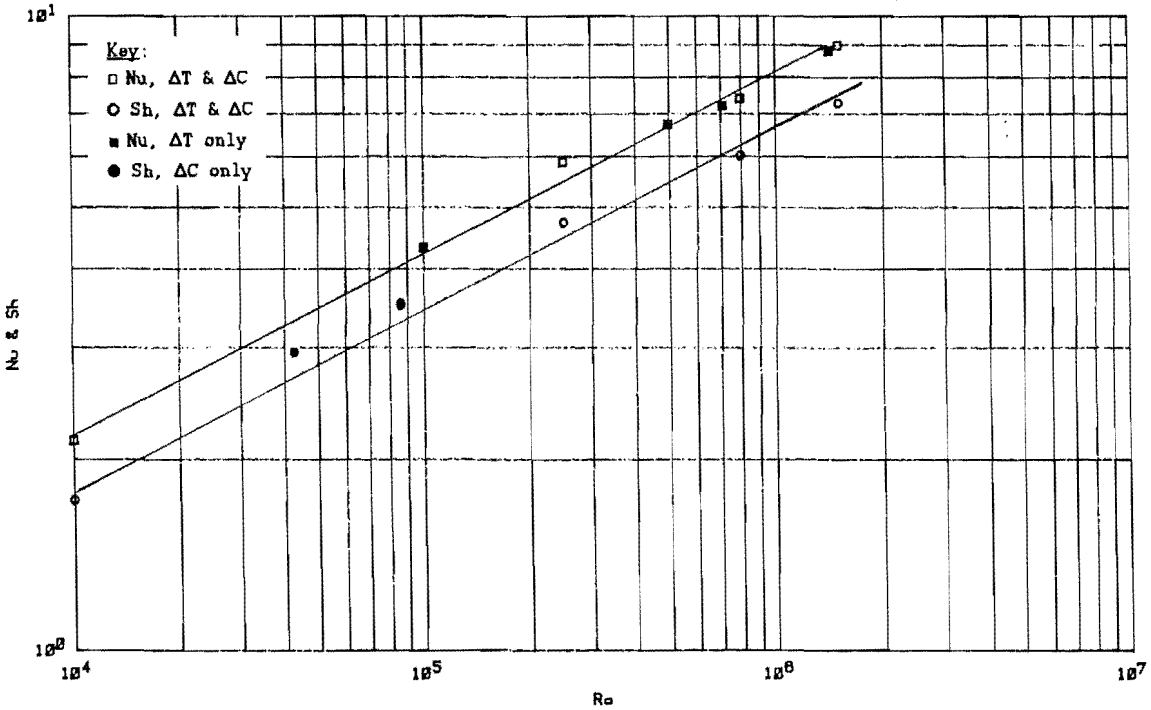

indication of the "accuracy" of the method. In general, the more the grid points, the more accurate is the method but this increase in accuracy has to be balanced by the computing time and the storage capacity available. All computations in this work was carried out on a VAX 11-730 minicomputer. A run using (41 x 21) number of grid points required any time from 30 minutes to 5 hours of CPU time depending on the parameters used for the calculation (False transient factors, convergent criterium etc. - see Appendices 8, 9 and 10). The time needed for the denser grids is proportional to the ratio of the total grid points to that of 41x21 grid for the same parameters used. No extensive investigation is devoted to investigate the "best condition" for convergence, as again this is not the aim of the project.

Comparison between the grid-points distribution in Tables 8.1 and 8.2 revealed that one needs more grid points (especially in the X-direction) for the case of the Horizontal Cavity than the Vertical Cavity to achieve the same level of accuracy. This difference will be explained later in terms of the different flow patterns that exist in the two cavity configuration.

8.3 Temperature and Flow Fields in the Cavity

Tables 8.3 and 8.4* lists the conditions for the representative temperatures (and/or concentration) and stream-function fields which was presented in Figs 8.3 to 8.23. Table 8.3 referred to the Vertical Cavity and Table 8.4 to the Horizontal Cavity. The temperature field plotted is in terms of the dimensionless temperature defined in Chapter 3. For the Vertical Cavity, the right-hand side boundary is the hot wall and characterised by the dimensionless value of 1.0. The left-hand side boundary is the cold wall and has the value of 0.0. For the Horizontal Cavity, the bottom boundary is the hot wall and the top boundary is the cold wall. The equivalent temperature difference, in degrees Celsius, across the cavity for each of the cases plotted is presented in Tables 8.3 and 8.4. The same boundary conditions that have just been defined for the temperature gradient case is also applicable to the concentration gradient case when applicable. The equivalent

* Note :- Tables 8.3 and 8.4 are presented at the end of this Chapter.

moisture concentration difference in kgm^{-3} and vapour pressure difference, in Pascal, are also given in Tables 8.3 and 8.4.

The stream function at a point in the cavity can be regarded as the cumulative volume flow across any line joining that point to the boundary, where the flow is arbitrarily taken as zero. Thus streamlines such as those in Figures 8.4, 8.7 etc. represent the various "contours" of the flow field in the cavity. The streamlines are expressed in terms of their dimensionless values as defined in Chapter 3.

The velocity components at mid-height (X=3.5) and mid-width (Y=0.5) of the cavity are also presented in Figures 8.5, 8.6 etc. Again the dimensionless scale was used and to convert this into the dimensional scale in ms^{-1}, one use the formula :-

$$U(ms^{-1}) = U \text{ (dimensionless)} \times \upsilon/L$$
$$= U \times 1.568\times10^{-4}\ ms^{-1}.$$

where υ = dynamic viscosity = 1.568×10^{-5} m^2s^{-1} for air at 300 K

L = cavity gap width = 0.1 m.

In the following discussion, the Rayleigh (or Grashof) number (thermal,concentration or combined) will be use to characterise the dimensionless driving force across the cavity for the various conditions listed in Tables 8.3 and 8.4.

8.3.1 Vertical Cavity - Isothermal Mass Transfer

Figs 8.3 and 8.4 form two limits which cover the range of Concentration Rayleigh numbers which was used in the experiments for isothermal moisture transfer. The flow fields were seen to consist of a series of longitudinal cells. The magnitude for the cells was three times greater for the case of $Grc=1\times10^5$ than for $Grc=1\times10^4$. No secondary cells were observed for these two cases.

The Concentration field for $Gr_c=1\times10^4$ suggested that most of the moisture transfer across the cavity occurred near the top and the bottom edges by convection with predominantly diffusional transfer occuring in the middle. For $Grc=1\times10^5$, the concentration

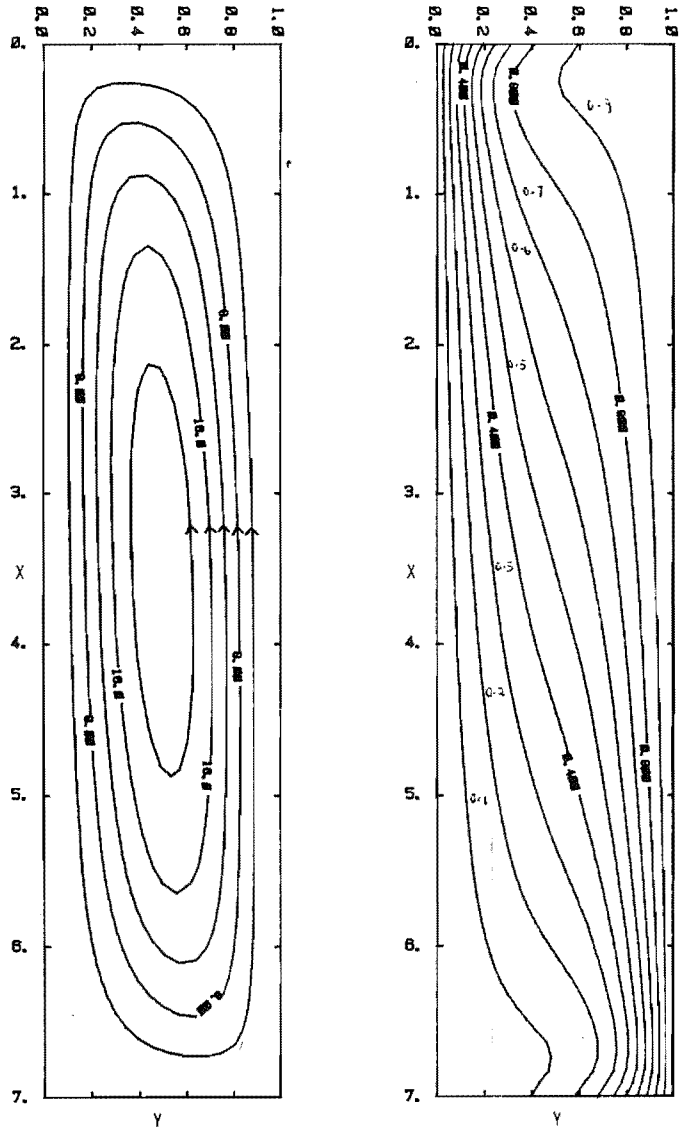

(a) Streamlines (b) Temperature

Fig. 8.3: $Gr_c = 1 \times 10^4$

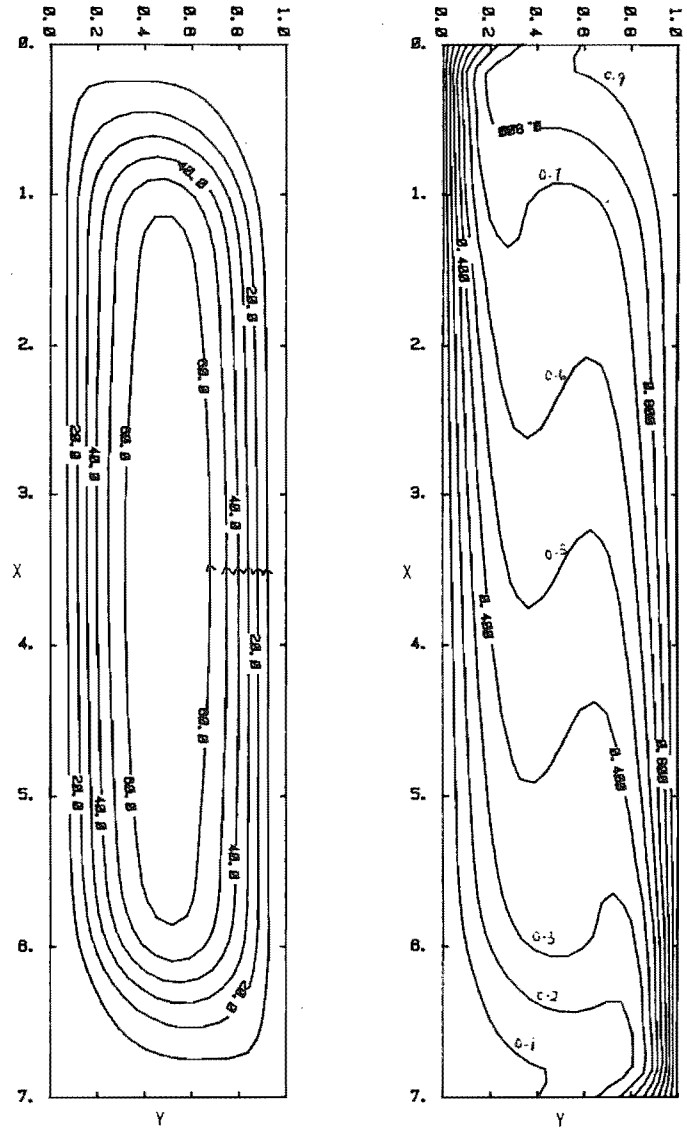

(a) Streamlines (b) Temperature

Fig. 8.4: $Gr_c = 1 \times 10^5$

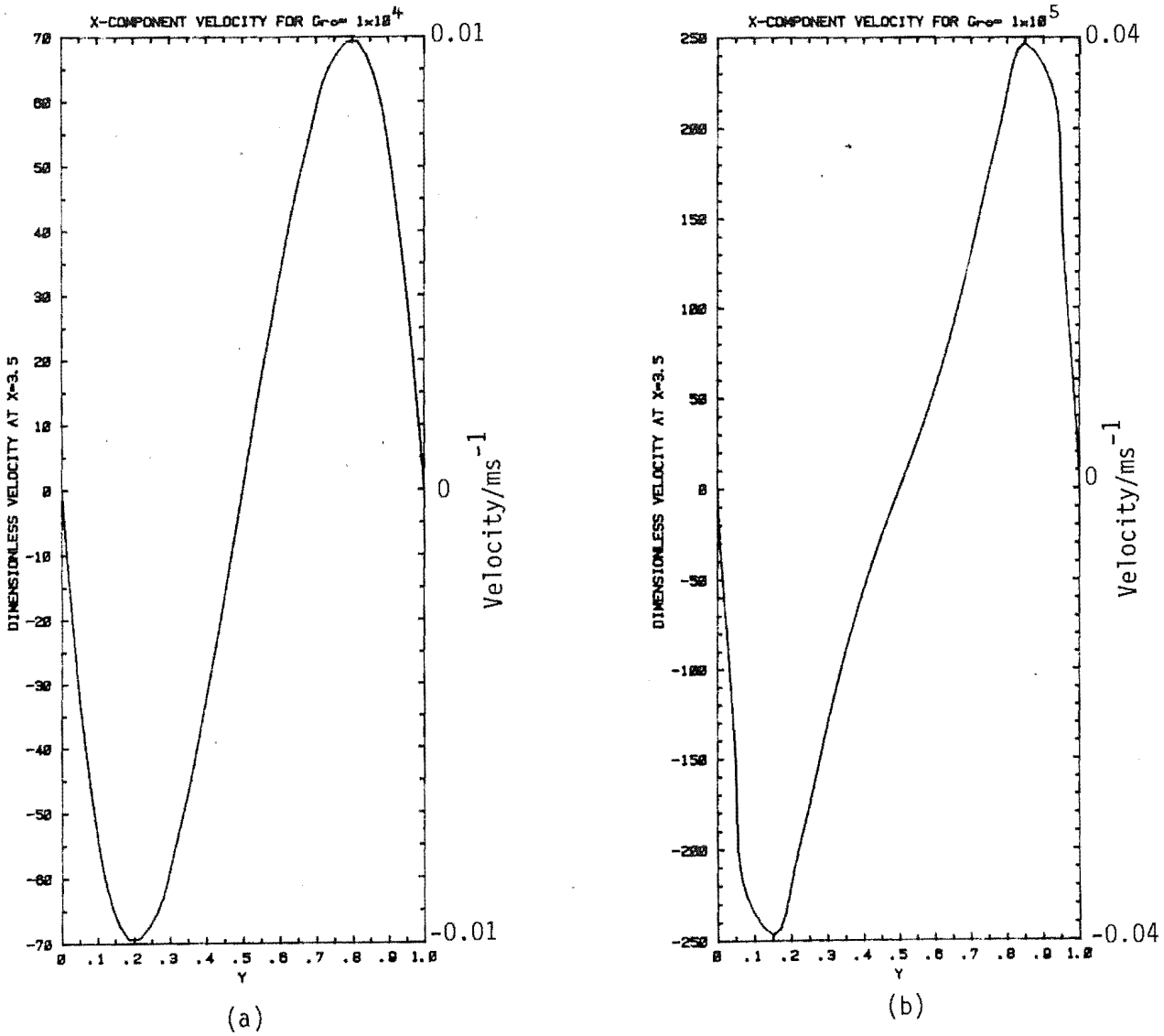
X-COMPONENT VELOCITY FOR Gr=1x10^4
DIMENSIONLESS VELOCITY AT X=3.5
Y
0.01
0
-0.01
Velocity/ms^-1
(a)
X-COMPONENT VELOCITY FOR Gr=1x10^5
DIMENSIONLESS VELOCITY AT X=3.5
Y
0.04
0
-0.04
Velocity/ms^-1
(b)

Fig. 8.5:

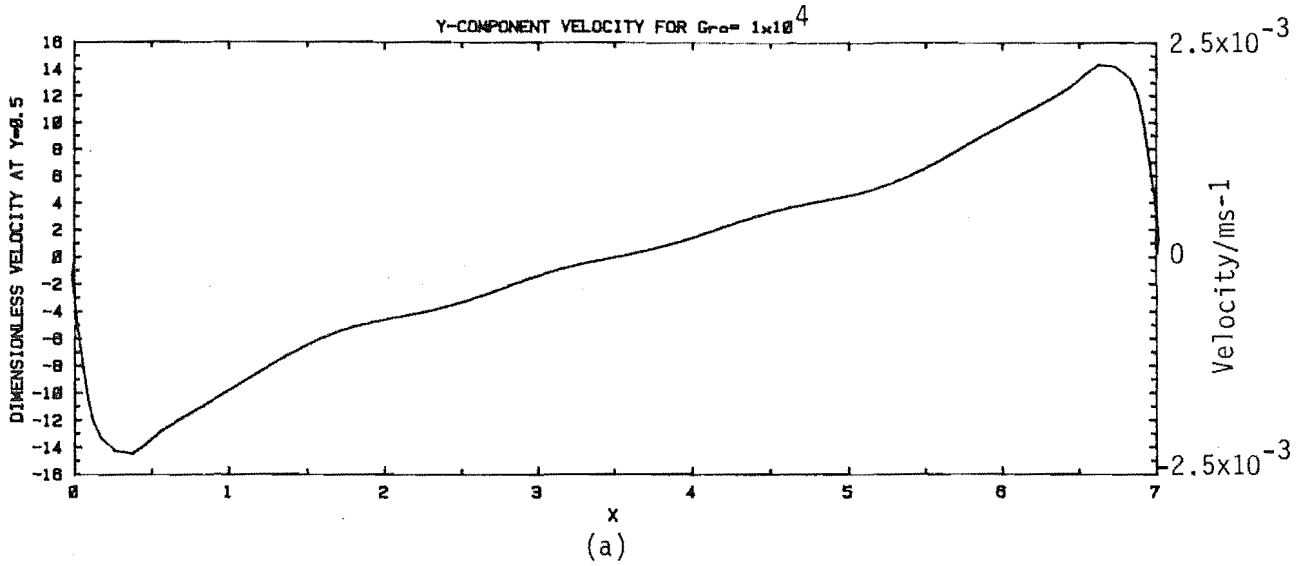
Y-COMPONENT VELOCITY FOR Gro= 1x10^4
DIMENSIONLESS VELOCITY AT Y=0.5
16
14
12
10
8
6
4
2
0
-2
-4
-6
-8
-10
-12
-14
-16
0
1
2
3
4
5
6
7
X
2.5x10^-3
0
-2.5x10^-3
Velocity/ms-1

(a)

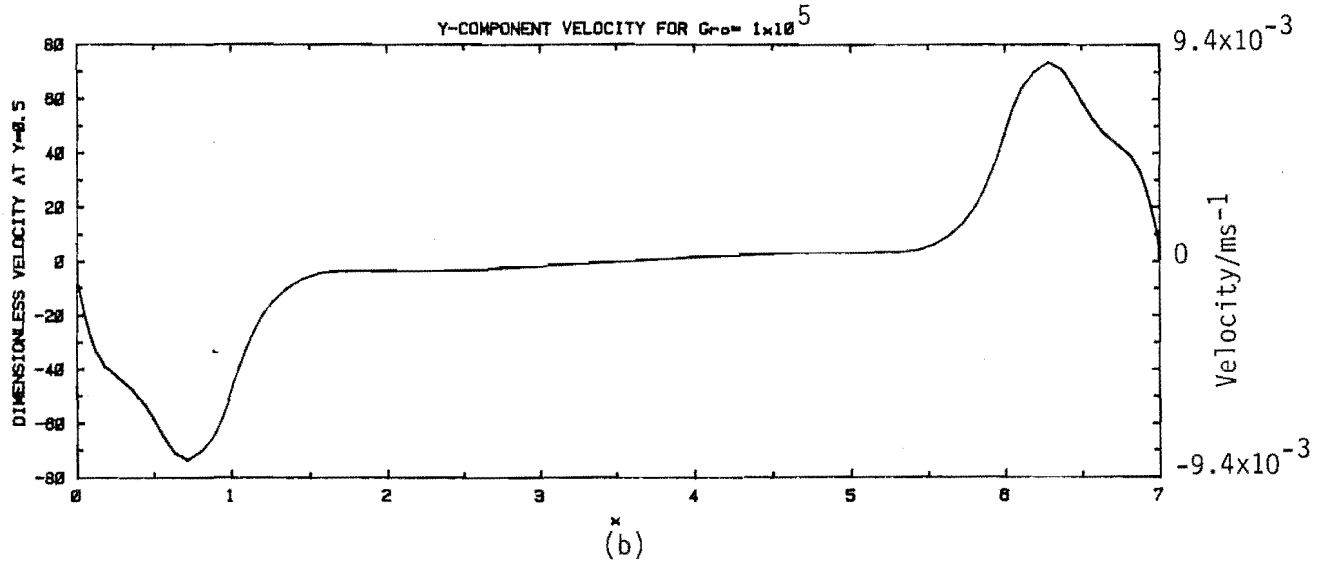
Y-COMPONENT VELOCITY FOR Gro= 1x10^5
DIMENSIONLESS VELOCITY AT Y=0.5
80
60
40
20
0
-20
-40
-60
-80
0
1
2
3
4
5
6
7
X
9.4x10^-3
0
-9.4x10^-3
Velocity/ms-1

(b)

Fig. 8.6:

fields were distorted throughout the whole cavity and a boundary layer behaviour was starting to appear which suggested the convection current and hence the transport of moisture across the cavity was much stronger. The iso-concentration lines were not horizontal in the middle of the cavity but showed a reverse gradient which suggested some local back-diffusion was occurring.

Figs 8.5 and 8.6 present the dimensionless velocity components at mid-height and mid-width of the cavity for the two conditions respectively. The vertical components of the velocity was seen to be much greater than the horizontal components for both cases. Apart from the maxima and minima near to each wall, no additional turning points were obscured in the velocity curves, which suggests the absence of reverse flow.

8.3.2 Vertical Cavity - Heat Transfer alone

Figures 8.7 and 8.8 represent two limits of the stream function and temperature fields within which all experimental heat transfer runs are expected to lie. At $Gr_T = 2 \times 10^5$, secondary cells are seen to appear near the top and the bottom of the cavity. The formation of these secondary cells was by the narrowing of the primary cells at X = 2.0 and then the gradual recession of these divided primary cells. The temperature fields was distorted most at the location of these secondary cells. The presence of the secondary cells was expected to enhance the transfer of heat across the cavity. At $Gr_T = 2 \times 10^6$, the secondary cells are well developed and occupied the top and bottom third of the cavity, some tertiary flows in the middle of the cavity have developed and their flow direction was opposite to that of the main flow.

Figure 8.7 compares favourably with the recent experiment of Linthorst et al [105] for an air-filled cavity of aspect ratio equal to 7.0 with regard to the location and structure of the secondary cells.

At a higher Grashof number, e.g. $Gr_T = 2 \times 10^6$ (Figure 8.8), an erroneous heat source and sink started to appear near the top and bottom of the cavity. This is a consequence of insufficient

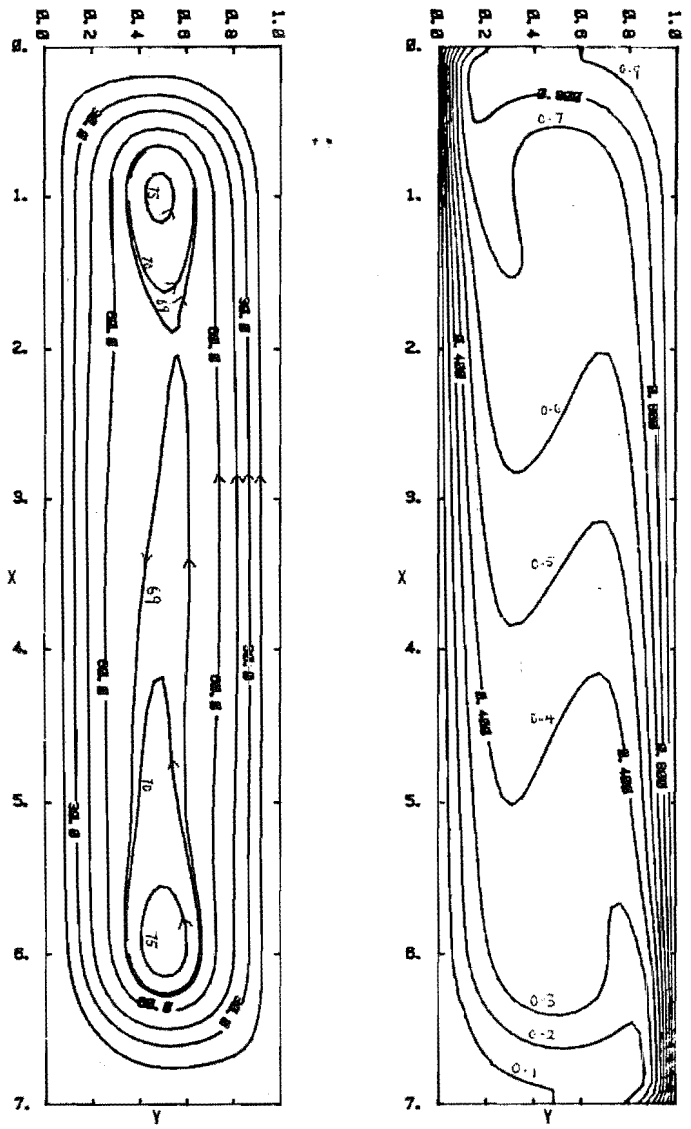

(a) Streamlines (b) Temperature

Fig. 8.7: $Gr_T = 2 \times 10^5$

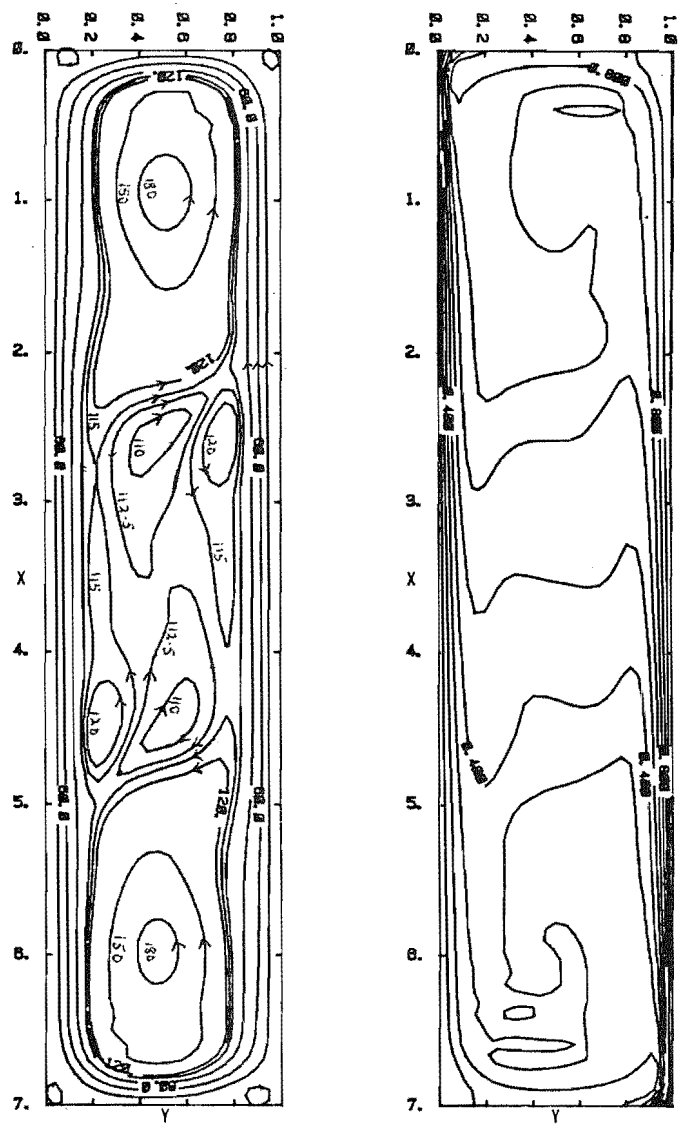

(a) Streamlines (b) Temperature

Fig. 8.8: $Gr_T = 2 \times 10^6$

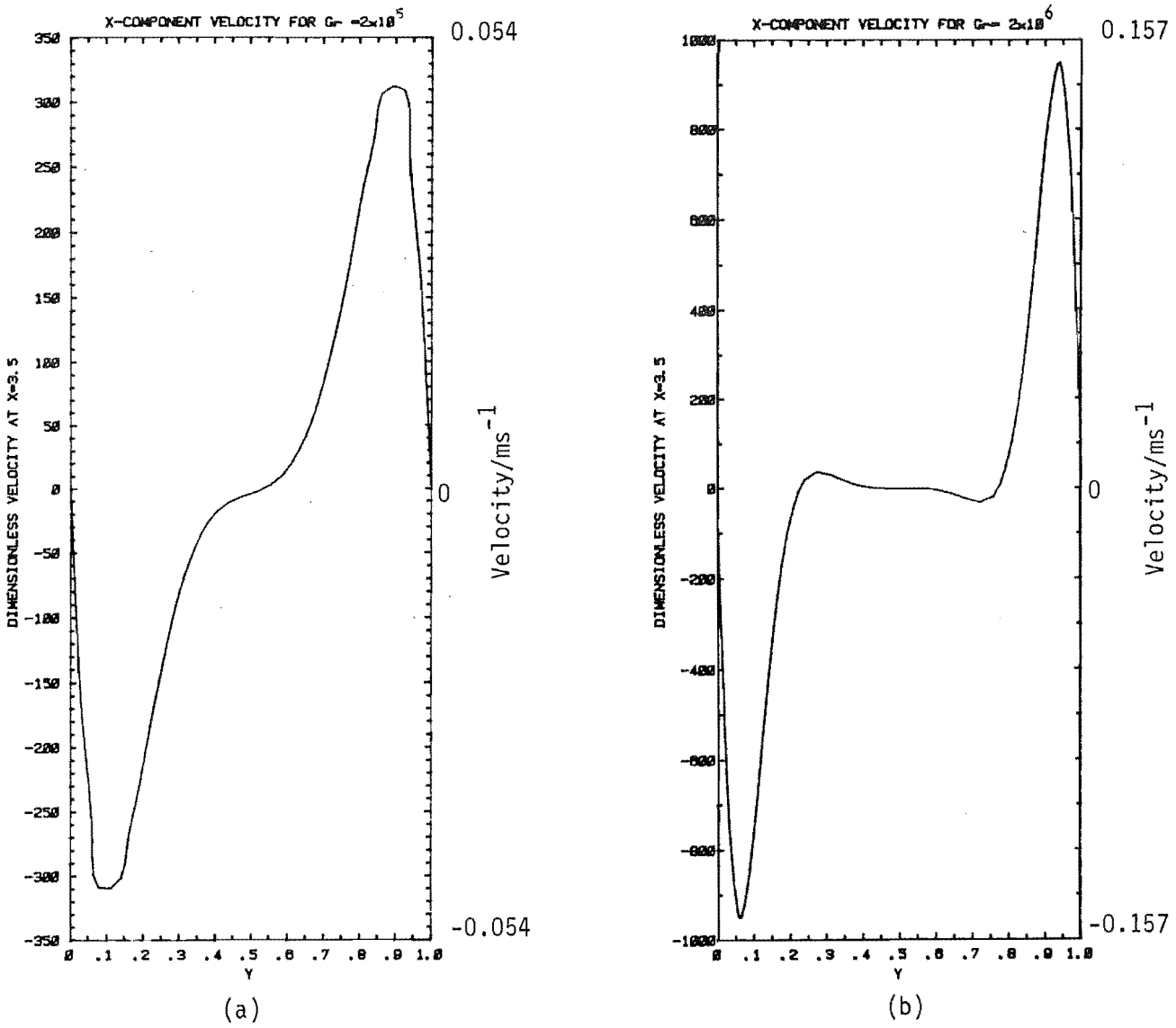
X-COMPONENT VELOCITY FOR Gr =2x10^5
0.054
0
-0.054
Velocity/ms^-1
DIMENSIONLESS VELOCITY AT X=3.5
Y
(a)
X-COMPONENT VELOCITY FOR Gr= 2x10^6
0.157
0
-0.157
Velocity/ms^-1
DIMENSIONLESS VELOCITY AT X=3.5
Y
(b)

Fig. 8.9:

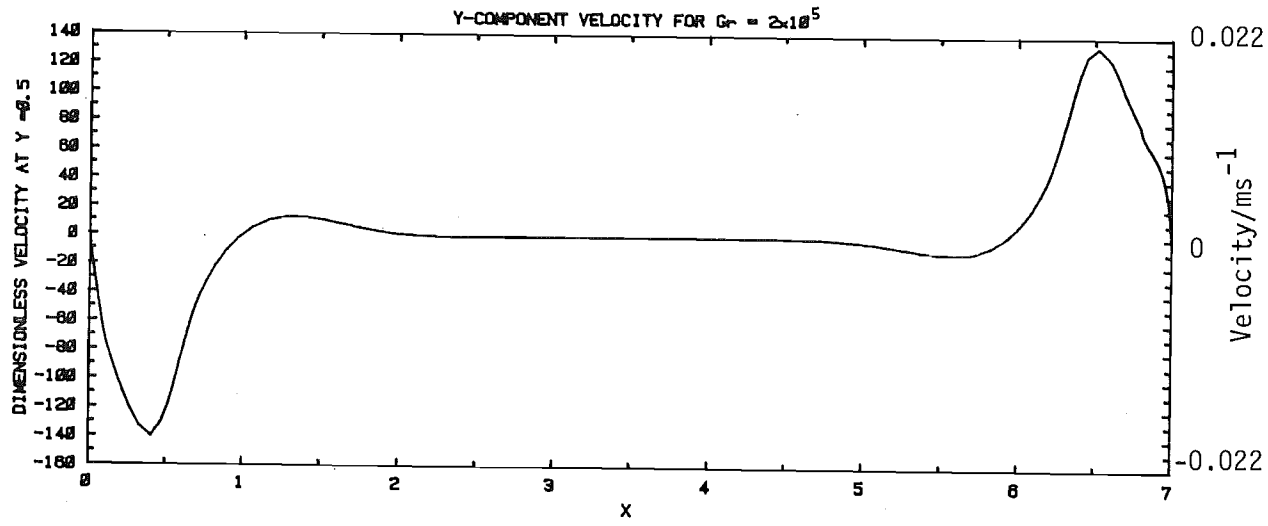
Y-COMPONENT VELOCITY FOR Gr = 2x10^5
DIMENSIONLESS VELOCITY AT Y =0.5
X
Velocity/ms^-1
0.022
0
-0.022

(a)

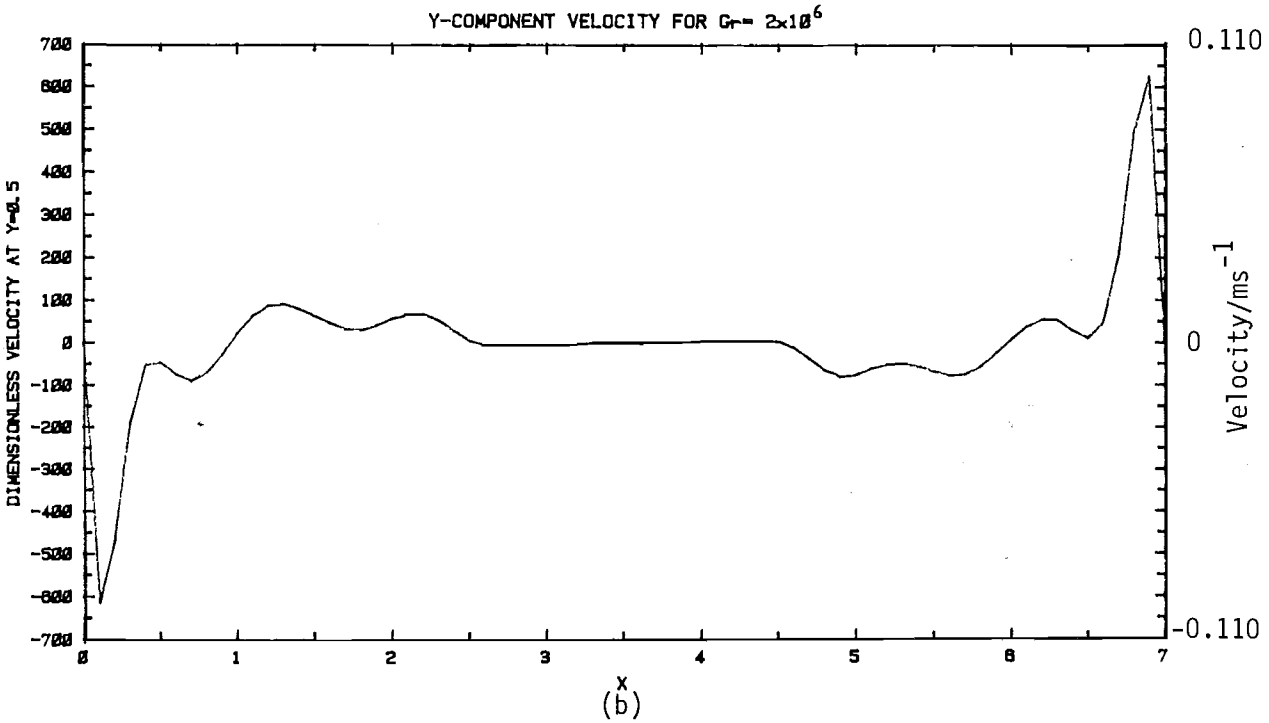
Y-COMPONENT VELOCITY FOR Gr= 2x10^6
DIMENSIONLESS VELOCITY AT Y=0.5
X
Velocity/ms^-1
0.110
0
-0.110

(b)

Fig. 8.10:

grid points being used to resolve the field for the higher Grashof number used. This point will be elaborated on later in relation to Figure 8.13. Since the prediction of Nusselt numbers only utilised the temperature gradients near the hot or the cold wall, the appearance of this fictitious heat source and sink in the middle did not pose a problem in the prediction of the overall rate of heat transfer. It did however cast a doubt on the validity of the flow field which was dependent on the temperature field and vice versa. Effort to eliminate this problem by using more grid points for $Gr_T = 2 \times 10^6$ was not made because of a lack of storage space on the computer and the longer computing time that would have resulted.

The velocity components in Figure 8.9 and 8.10 reflected the compexity of the flow in each case. For $Gr_T = 2 \times 10^5$, the velocity profiles were relatively smooth and indicating mainly the primary flow direction in Figure 8.9 (a) and some effect of a flow reversed due to secondary flow in Figure 8.10(a). For $Gr_T = 2 \times 10^6$, flow reversal can be seen clearly in both Figure 8.9(b) and 8.10(b) due to the effect of both secondary and tertially flow.

8.3.3 Vertical Cavity - Combined Heat and Moisture Transfer

Figure 8.11 was the result of imposing an additional moisture gradient of dimensionless magnitude $Gr_c = 8 \times 10^4$ on the condition used to derive Figures 8.8 to 8.10. There are some changes in the streamlines field at the middle of the cavity with regard to the secondary and the tertiary reverse flow cells, but the form of the primary and secondary flows at each ends was seen to be essentially the same for both sets of figures. The magnitude of the streamlines was slightly larger for Figure 8.11, as expected due to the additional moisture gradient. The temperature fields between Figures 8.8 and 8.11 do not show great discrepancy, except for the isotherms of 0.7 and 0.3, where in both cases the calculation was unable to resolve properly the field near the top and bottom of the cavity due to the strong influence of the recirculating secondary flows. The effect of simultaneous

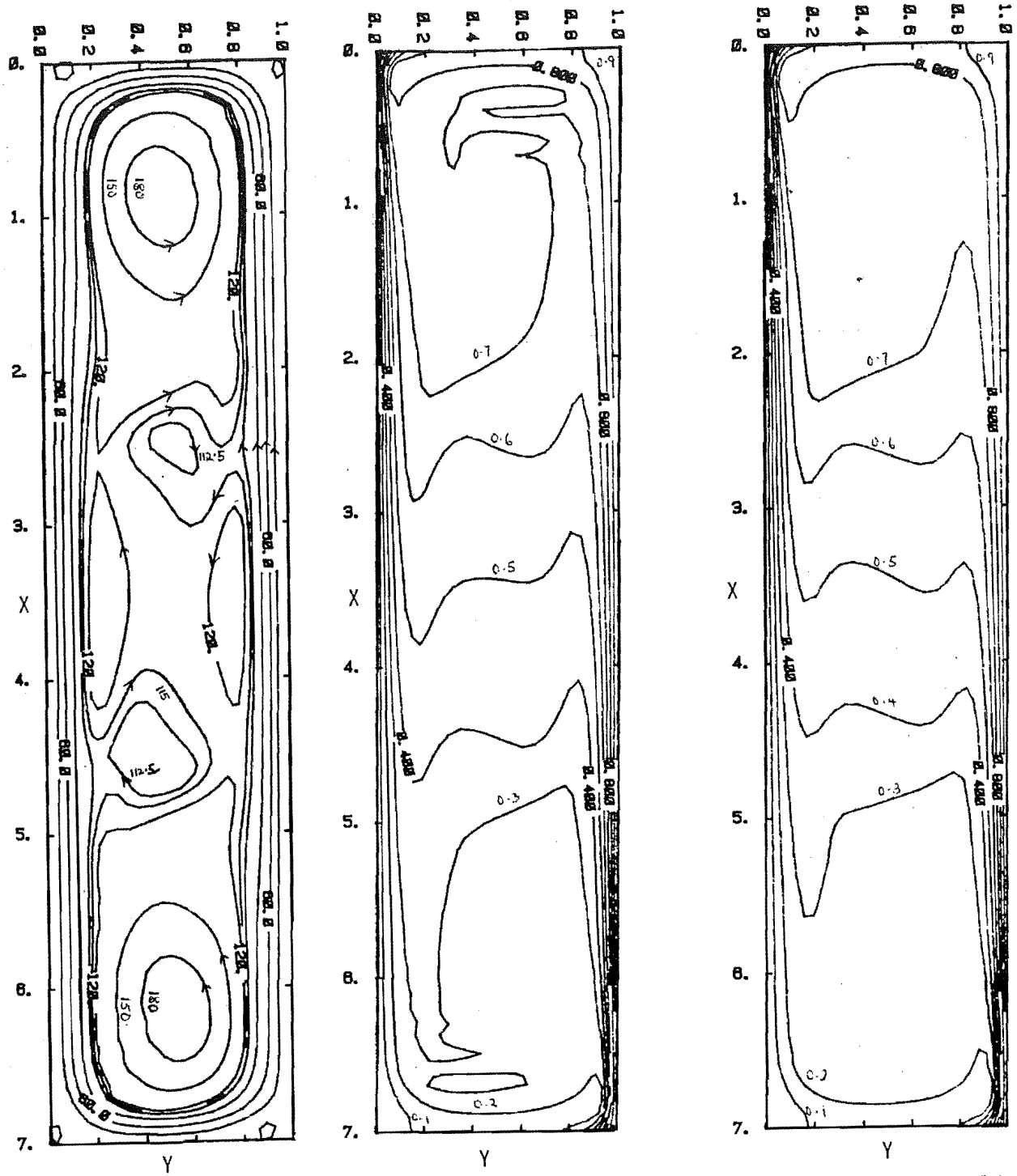

(a) Streamlines Field (b) Temperature Field (c) Concentration Field

Fig. 8.11: $Gr_T = 2 \times 10^6$, $Gr_C = 8 \times 10^4$

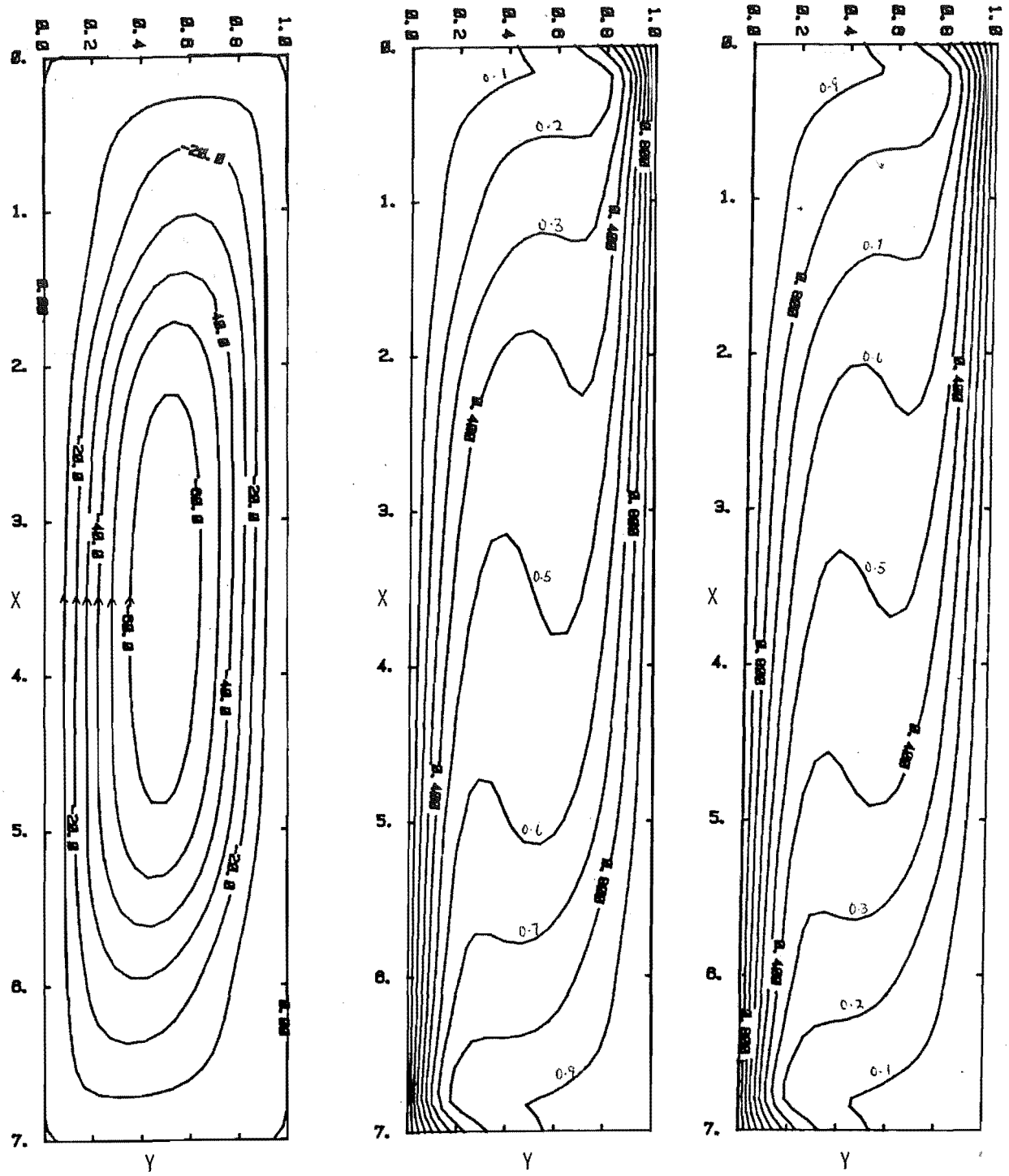

(a) Streamlines (b) Temperature (c) Concentration

Fig. 8.12: $Gr_T = 6 \times 10^4$, $Gr_C = -1.2 \times 10^5$.

temperature gradient on the concentration fields can be observed by comparing Figures 8.11(c) with Figure 8.4 (b). The moisture difference across the cavity for the condition in Figure 8.11 (c) was smaller than that for Figure 8.4 (b), yet the presence of the simultaneous temperature gradient in Figure 8.11 (c) has generated a stronger convective flow in the cavity for that condition than that in Figure 8.4 (b). This is evident from the more pronounced boundary-layer behaviour for the concentration field observed in Figure 8.11 (c) than that in Figure 8.4 (b).

Figure 8.12 is an example of the fields resulted from a reverse gradient case. The concentration gradient was acting from left to right while the temperature gradient was acting from right to left (as indicated by the magnitude of the respective contours). Note that the convective flow cells were rotating in a clockwise direction, i.e. in the direction caused by the predominant moisture gradient. Both the temperature and concentration fields are similar to each other disregard of the direction their respective gradients were acting. If the reverse moisture gradient was absent, the temperature field would be similar to that in Figure 8.4 (b), i.e. a mirror image of that in Figure 8.12 (c). This illustrates fully the interdependance of flow, temperature and concentration fields on each other and the importance of the magnitude and the direction of the dimensionless driving force (the Grashof number).

8.3.4 Vertical Cavity - Comparison of Different Numerical Methods.

Figure 8.13 compares the temperature and stream-function fields obtained from both the "False Transient (FT)" and the "Dynamic Alternating Direction Implicit (DADI)" method for the condition $Gr_T = 1 \times 10^6$. Both stream function plots exhibit similar primary and secondary flows. Both plots also have reverse flow tertially cells at about the same location but the magnitude of the streamlines were smaller for Figure 8.13 (c). The temperature fields are identical except for the two isotherms of 0.7 and 0.3. A greater distortion of these two isotherms seemed to occur for the

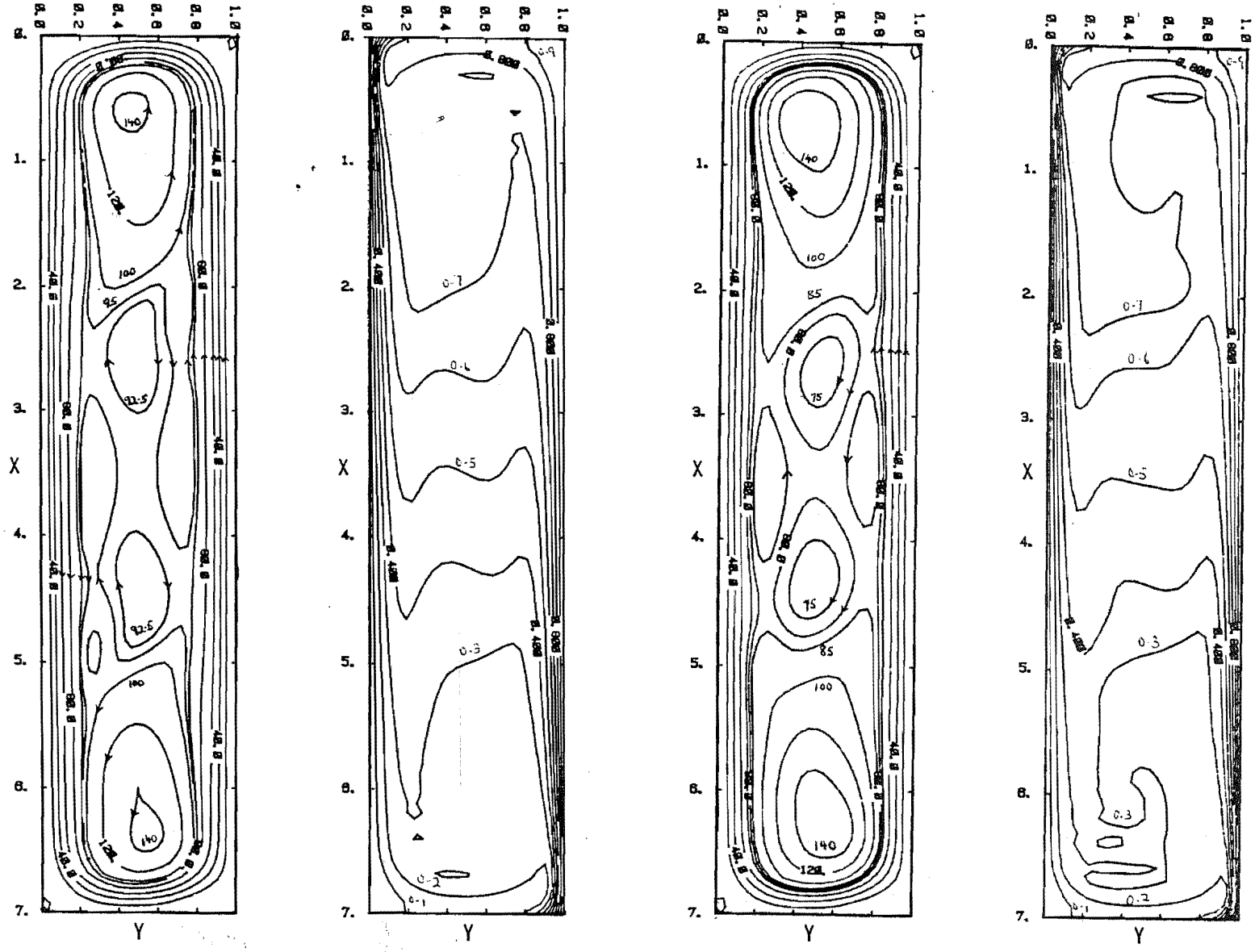

(a) Streamlines (b) Temperature (c) Streamlines (d) Temperature

"False Transient" Method "DADI" Method

Fig. 8.13: $Gr_T = 1 \times 10^6$

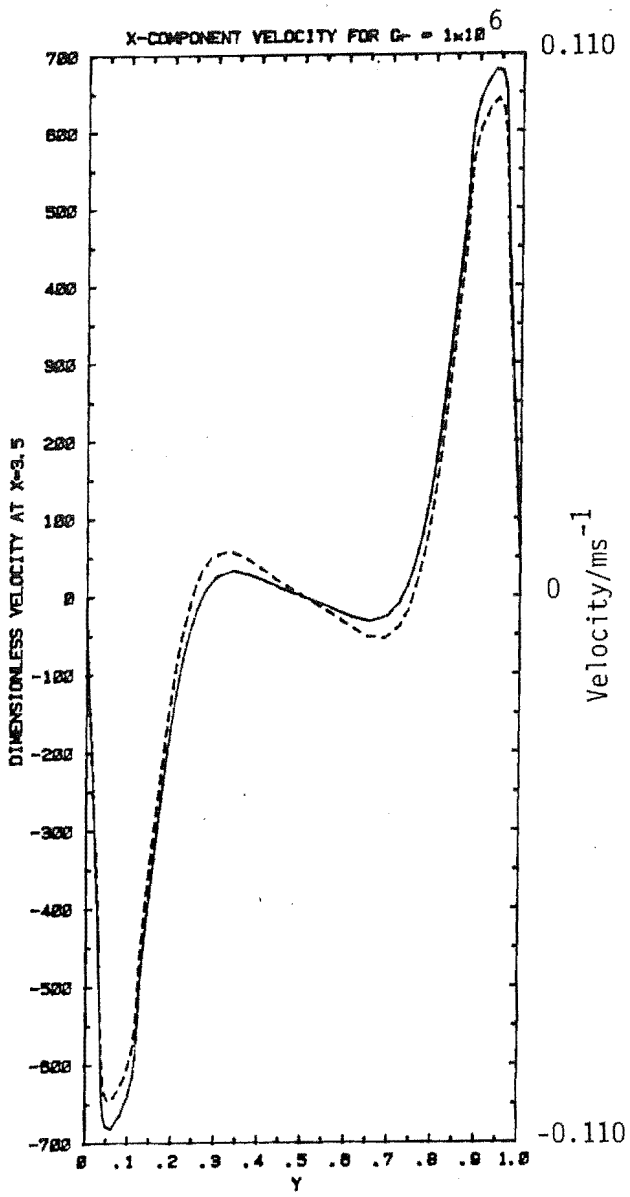
X-COMPONENT VELOCITY FOR G= 1x10^6
DIMENSIONLESS VELOCITY AT X=0.5
Y
0.110
0
-0.110
Velocity/ms^-1
Methods:
"FT"
"DADI"

(a)

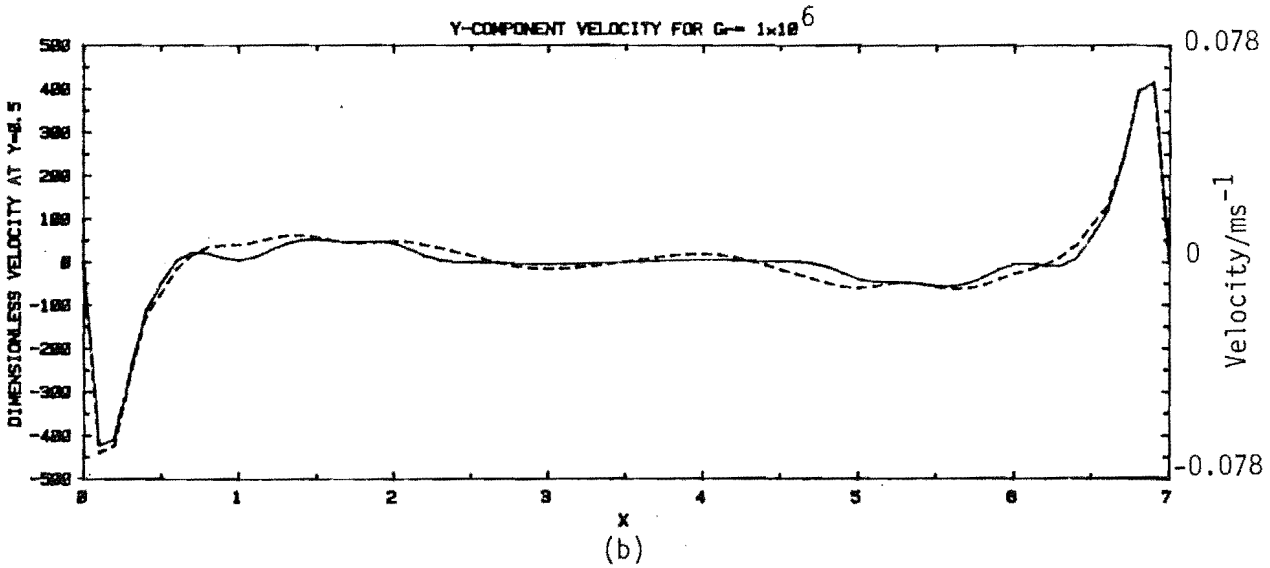
Y-COMPONENT VELOCITY FOR G= 1x10^6
DIMENSIONLESS VELOCITY AT Y=0.5
X
0.078
0
-0.078
Velocity/ms^-1

(b)

Fig. 8.14:

DADI method than for the FT method. Both temperature gradients are however identical next to the walls and hence the Nusselt numbers predicted by both methods would be the same as had indicated in Table 8.1.

Figures 8.14 compares the velocity components for the two methods. The X-component velocities are seen to agree closely except at the turning points; and at the points of maximum velocity, a difference of 7% exist for the two methods. The X-component velocity profiles calculated by both methods reflect the presence of the secondary flow in the middle of the cavity. The Y-component velocity profiles indicated that the strongest flow across the cavity is still near to the top and bottom of the cavity, being mainly convection from the primary cells. The recirculating secondary cells (Fig. 8.13) at the top and bottom third of the cavity does not commence a strong flow. The Y-component velocity clculated by both methods are also seen to agree closely with each other.

8.4 HORIZONTAL CAVITY - UPWARDS TRANSFER.

The flow field in a Horizontal Cavity with upwards transfer consisted of a series of roll cells, each counter-rotating in the opposite direction to its neighbours for all types of boundary conditions. Unlike the vertical cavity, no secondary or tertiary cells were observed on top of the primary cells as the Rayleigh number was increased. However, the large number of primary cells and their orientation in the cavity have meant that the critical length for numerical calculation was that between the adjacent counter-rotating cells in the X-direction (see Figure 3.1, Chapter 3) rather than between the rotating cells and the walls in the Y-direction as for the case of the vertical cavity. This has resulted in an increase in the number of grid points required to produce a solution of comparable accuracy for the horizontal cavity than for the vertical cavity (see Tables 8.1 and 8.2) The CPU time required for a typical run for a (141 x 11) grid would take about 2 hours and a 281 x 21 grid about 12 hours. As stated before,

these time limits are not considered as the fastest available as no detailed investigation on the rate of convergent was carried out. The analysis was calculated with the values of the false transient factors (see Chapter 3) as $a_T = 1.0$, $a_\varphi = 1.0$, $a_C = 1.0$ and a_ζ= 0.2 or 0.05 or 0.005.

Figures 8.15 and 8.16 represent the lower and upper limits of the streamlines and concentration fields expected for the experimental isothermal moisture-transfer case. Both streamline fields consisted of eight counter-rotating cells with the magnitude of the cells in Figure 8.16 (b) being about four times stronger than that in Figure 8.15 (b). The concentration fields, which were parallel horizontal lines when only conduction was the mode of transfer, were distorted by the convective flow field with the contours dipping downwards when the flow is going down and rising upwards when the flow is going up. This distortion was of course greater for Figure 8.16 (a) than for Figure 8.15 (a) because of the greater flow. Moisture was thus first conducted through a thin layer from the bottom boundary into the convecting fluid, being conveyed up the cavity by the convecting cells and then eventually being removed from the top boundary again by conduction from the fluid. Judging from the concentration contours in Fig.8.15(a), a certain amount of moisture diffused horizontally from the locations where the streamlines were moving up to the locations where they are moving down without actually reaching the top boundary. This diffusion process reduced the amount of moisture transfer across the cavity. This diffusion process was expected to continue in Figure 8.16 (a), judging from the fact that the horizontal concentration gradients still exist, although the contours were further spaced in the horizontal direction in this case. The larger up-flow in Figure 8.16 was expected to reduce the significance of this lateral diffusion.

Fig. 8.17 presents the X and Y-velocity components for the case of $Gr_C = 1.41 \times 10^4$ which is the smallest dimensionless driving force case encountered in this work. The velocity profiles resembled laminar flow cases for both Figs 8.17 (a) and (b) which contrasted with Fig. 8.20 for the high dimensionless driving force case ($Gr_T = 2.0 \times 10^6$) where boundary layer behaviour is strongly

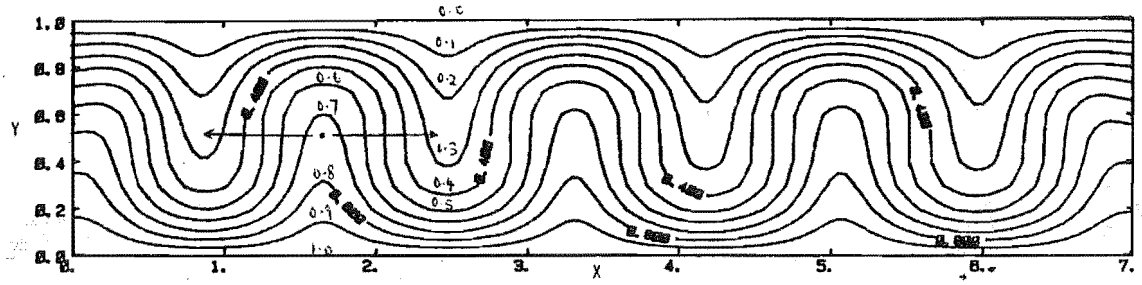

moisture diffusion (a) concentration

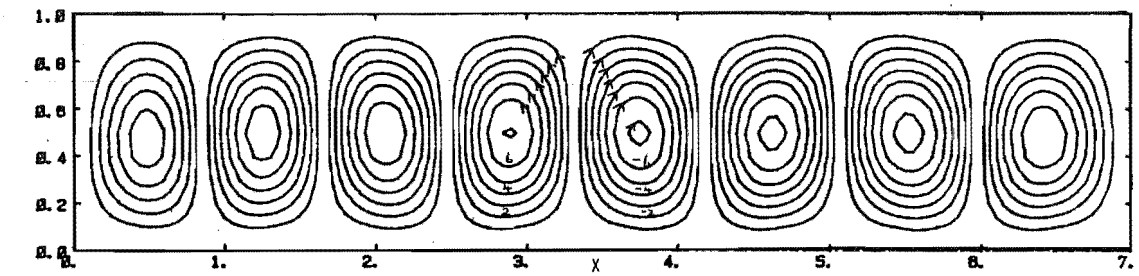

(b) streamlines. Contour level = 1.0

Fig. 8.15: $Gr_c = 1.41 \times 10^4$

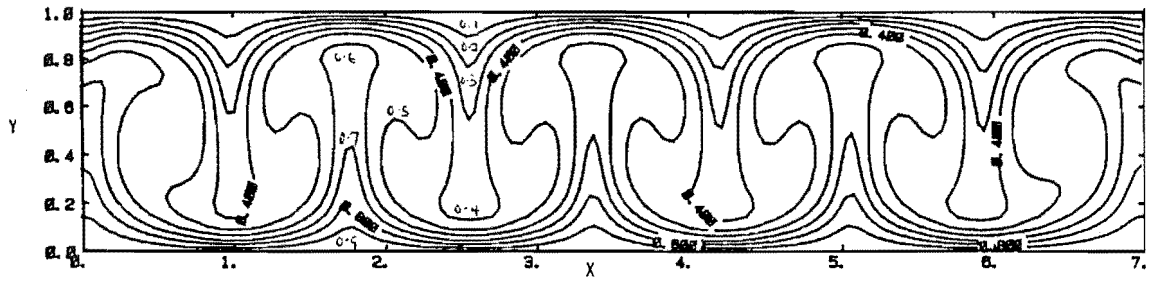

(a) Concentration

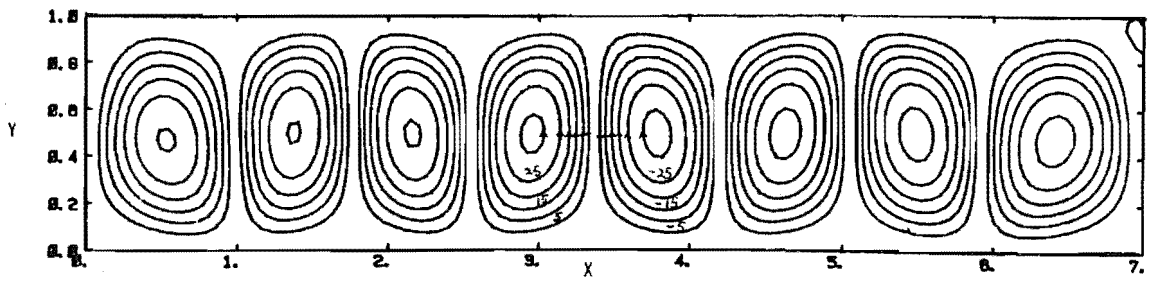

(b) Streamlines, Contour level = 5.0

Fig. 8.16: $Gr_c = 1.41 \times 10^5$

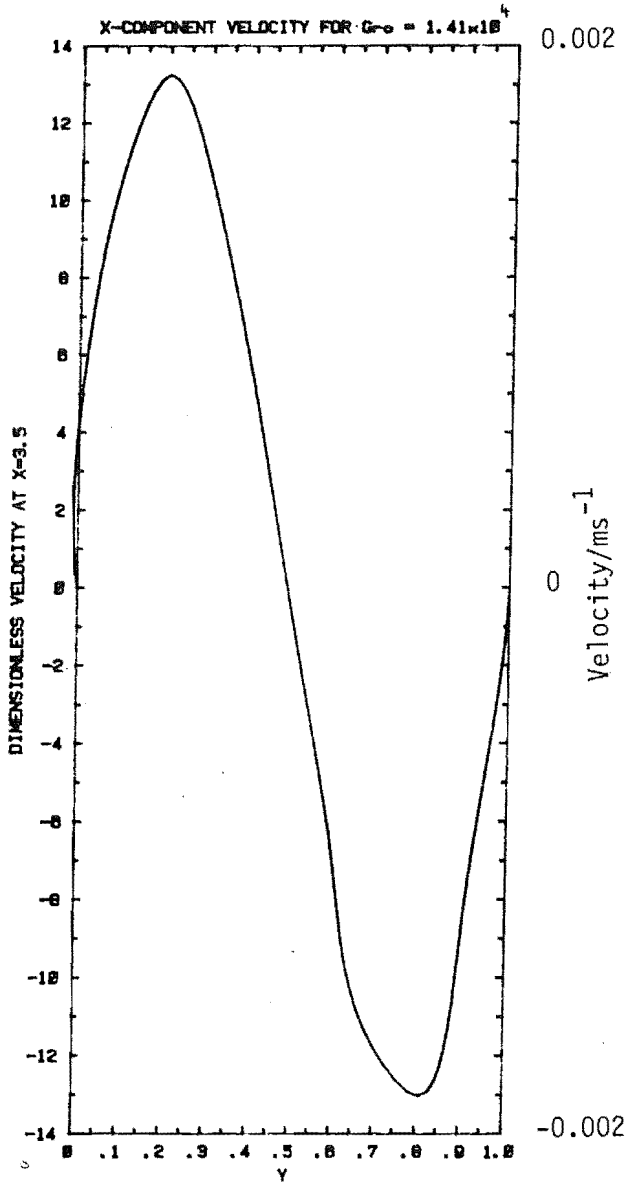
X-COMPONENT VELOCITY FOR Gr= 1.41x10^4
DIMENSIONLESS VELOCITY AT X=3.5
Y
0.002
0
-0.002
Velocity/ms^-1

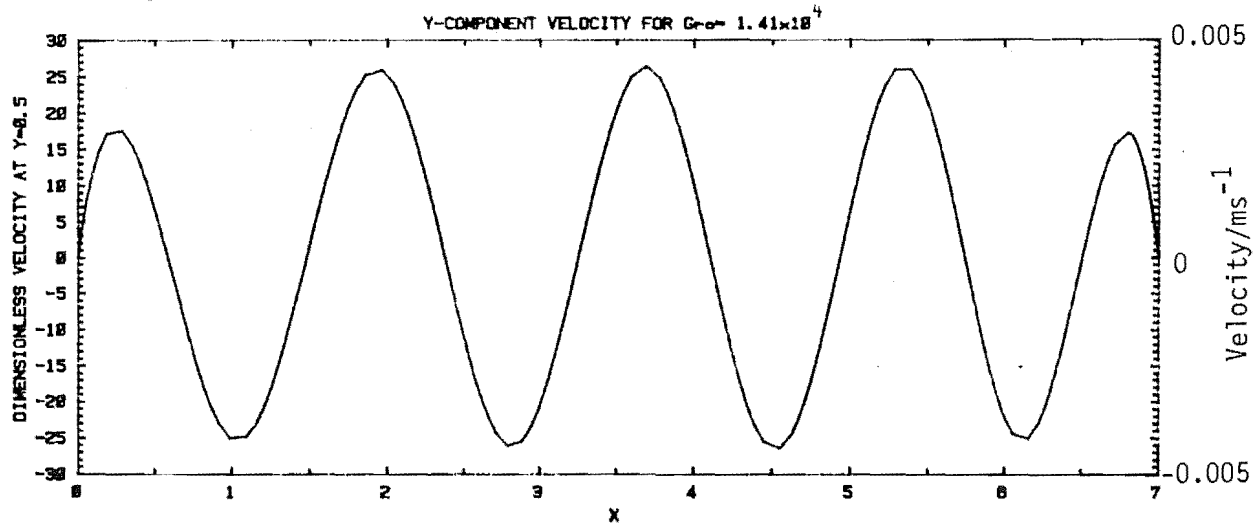
Y-COMPONENT VELOCITY FOR Gr= 1.41x10^4
DIMENSIONLESS VELOCITY AT Y=0.5
X
0.005
0
-0.005
Velocity/ms^-1

Fig. 8.17:

exhibited.

Figures 8.18 and 8.19 presents the corresponding fields for heat transfer case only which represent the lower and upper dimensionless driving force case that can be found in this work. Again counter-rotating cells were observed but the number of cells were reduced to seven in Figure 8.19 (b) compared with eight in Figure 8.18 (b). The two cells immediately adjacent to the walls were also larger than those in the middle. The velocity components at mid-height and at mid-width of the cavity are presented in Figure 8.20. Contrary to the case for the vertical cavity, the Y component velocity was seen to be greater than the X component velocity. Thus the boundary layer was the thinnest at the location between adjacent cells than at locations between the cell and the walls. This explained the need for more grid points in the X-direction than the Y-direction indicated earlier. The temperature fields for $Gr_T = 2 \times 10^6$ (Figure 8.19 (a)) was distorted most at the locations where the streamlines were moving up or down the cavity, but an almost isothermal region existed at the location corresponding to the centre of each rotating cell. From Figure 8.18 and 8.19, heat was conducted through a thin layer from the bottom wall into the cavity, being carried up the cavity by the streamlines moving upwards, and then dissipated into the upper cold wall by conduction. The cold air was then returned to the bottom of the cavity by the downwards moving streamlines. For $Gr_T = 2 \times 10^5$ (Figure 8.18), a certain amount of lateral diffusion as described before was occurring to judge from the form of the concentration contours. The almost isothermal core in Figure 8.19 suggested that conduction through that region was much smaller and most of the heat that was absorbed from the hot wall was effectively dissipated at the cold wall by the strong convection current.

Figures 8.21 and 8.22 had the same temperature difference as Figure 8.19 but with the addition of a simultaneous moisture gradient, equivalent in magnitude to that of Figure 8.16. Figure 8.20 (a) and 8.22 (a) were calculated using the "False Transient" method whereas Figure 8.21 (b) and 8.22(b) were calculated using the "Dynamic Alternating Direction Implicit" method. All the temperature and moisture difference used (see Table 8.2) were

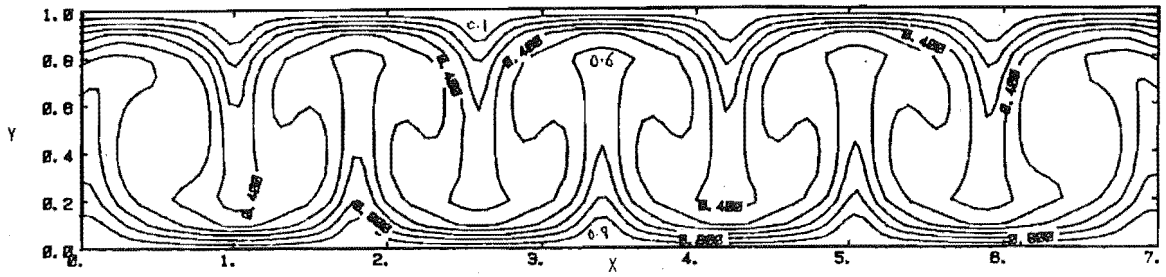

(a) Temperature

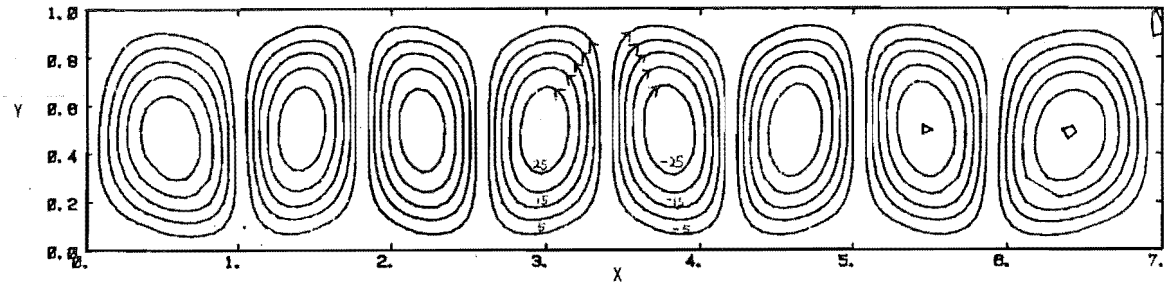

(b) Streamlines. Contour level = 5.0

Fig. 8.18: $Gr_T = 1.41 \times 10^5$

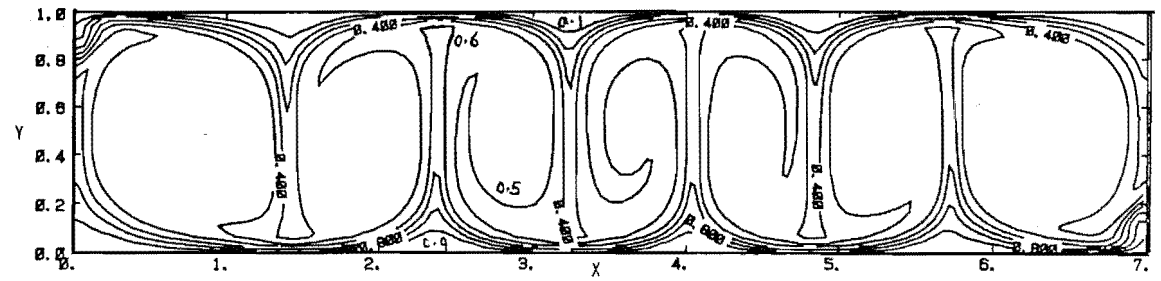

(a) Temperature

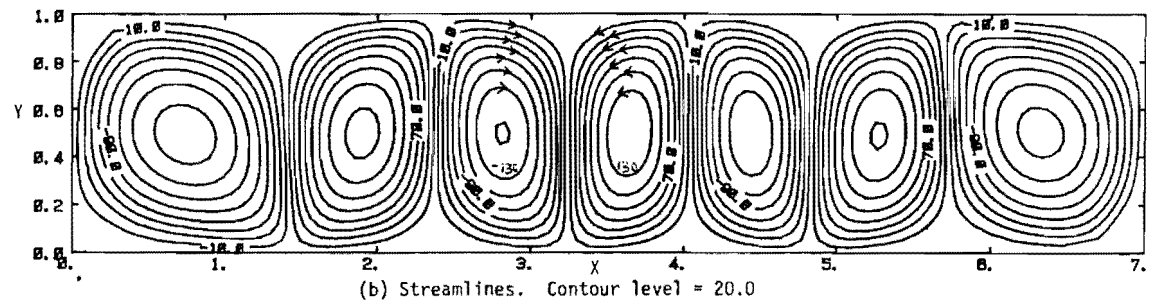

(b) Streamlines. Contour level = 20.0

Fig. 8.19: $Gr_T = 2 \times 10^6$

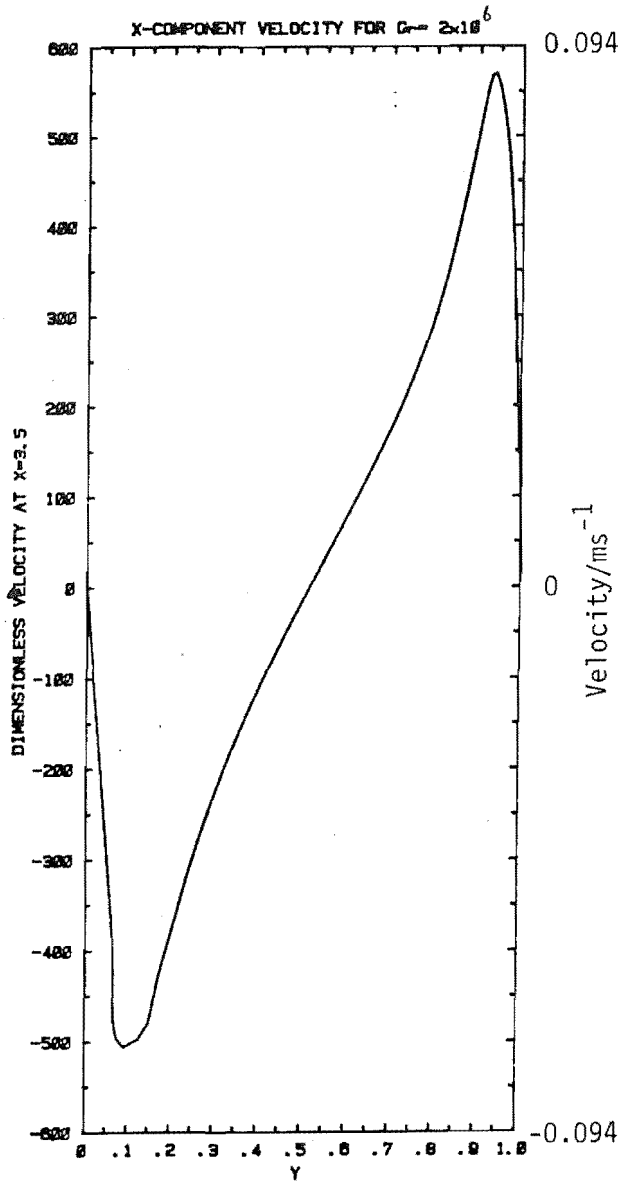
X-COMPONENT VELOCITY FOR Gr= 2x10^6
DIMENSIONLESS VELOCITY AT X=2.5
600
500
400
300
200
100
0
-100
-200
-300
-400
-500
-600
0 .1 .2 .3 .4 .5 .6 .7 .8 .9 1.0
Y
0.094
0
-0.094
Velocity/ms^-1

(a)

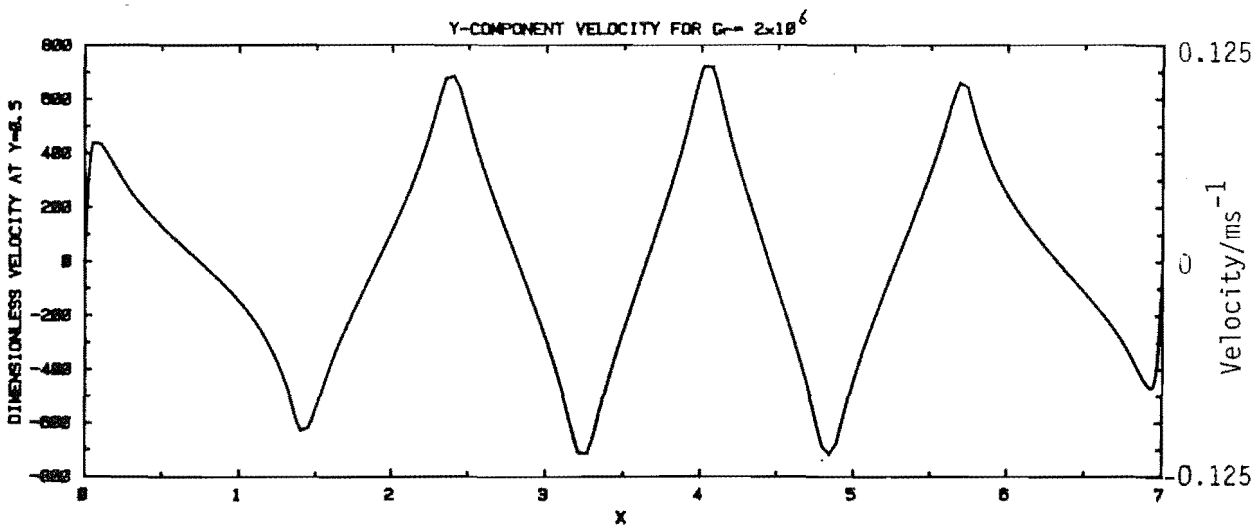
Y-COMPONENT VELOCITY FOR Gr= 2x10^6
DIMENSIONLESS VELOCITY AT Y=4.5
0 1 2 3 4 5 6 7
X
0.125
0
-0.125
Velocity/ms^-1

(b)

Fig. 8.20:

indicative of that found in an actual building cavity. Figures 8.21 and 8.22 were seen to be quite different from Figure 8.16 indicating the strong effect of the simultaneous temperature gradient. Figure 8.21 and 8.22 were quite similar to Figure 8 .19 indicating the weak effect of the simultaneous moisture gradient. The two methods in Figure 8.21 exhibit almost identical streamlines but slight difference exists in the centre of the cavity between the two temperature fields in Figure 8.22. The Nusselt numbers predicted by both the methods were identical as they were calculated from the temperature gradients adjacent to the wall and not affected by the different temperature field in the middle.

Figure 8.23 is an example for the case of reverse moisture gradient. The moisture gradient was acting downwards and if on its own it would sustain a transfer process by diffusion only (thus resulting in a series of parallel horizontal isoconcentration lines in the cavity). However the presence of the upwards and much stronger simultaneous temperature gradient had resulted in a convected flow being generated and the concentration field was modified to look like the temperature field as indicated in Figure 8.23 (a) and (b). Effectively the mode of moisture transfer from the top to the bottom is now equivalent to a case where the moisture gradient is acting from the bottom to the top, while the rate of moisture transfer is of course significantly increased by the convective process in comparison with the diffusion process.

8.5 HORIZONTAL CAVITY - DOWNWARDS TRANSFER.

Finally, no convection was observed for the case when the top boundary had a higher potential than the bottom boundary in a cavity. In all cases tried, the perturbation introduced to an initially stable field (diffusion process dominant) had been unsuccessful in generating any flow and the disturbance disappeared after iteration of the field variables. It as thus concluded that the horizontal cavity with downwards transfer constitutes a stable condition and transfer of heat and moisture is by diffusion only.

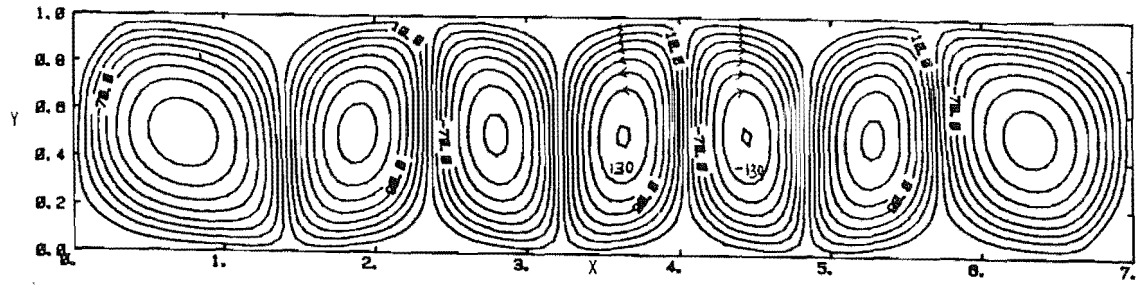

(a) False Transient Method.

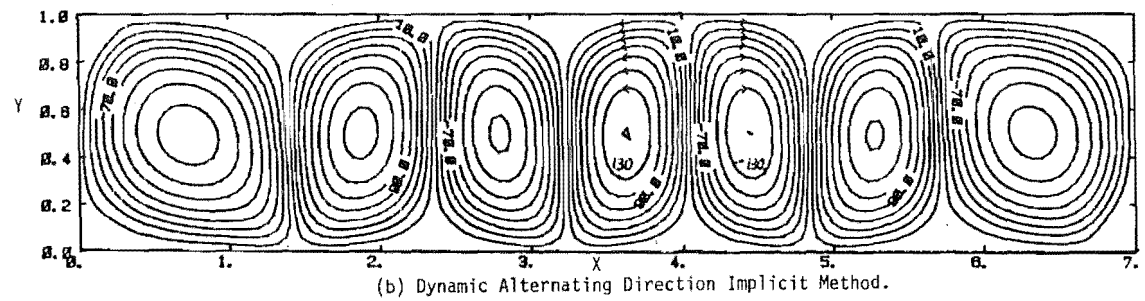

(b) Dynamic Alternating Direction Implicit Method.

Fig. 8.21: $Gr_T = 2 \times 10^6$, $Gr_C = 1.41 \times 10^5$, Streamlines, Contour level = 20.0.

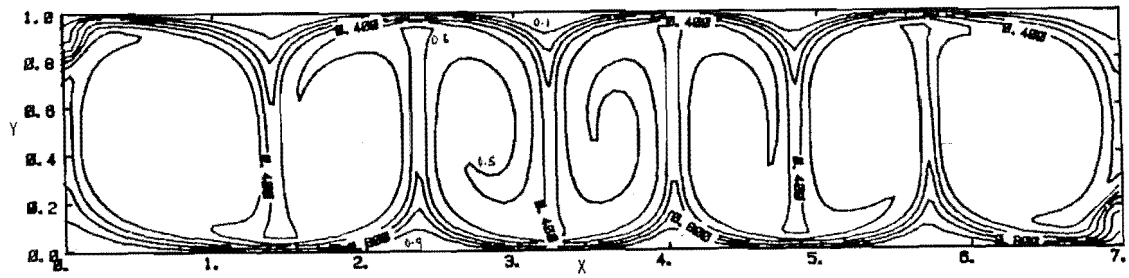

(a) "FT" Method.

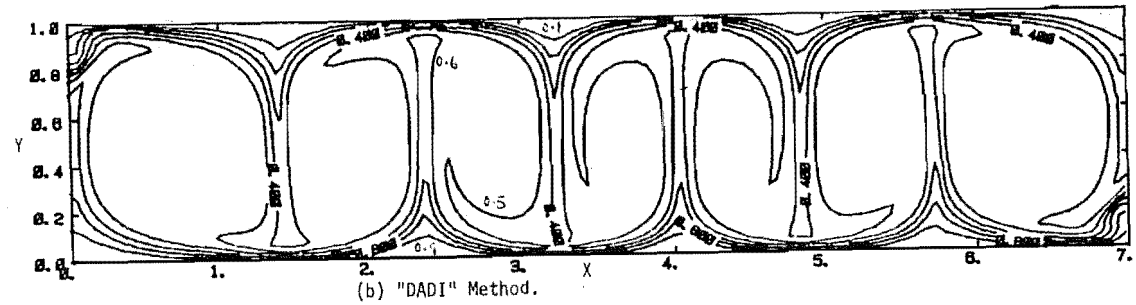

(b) "DADI" Method.

Fig. 8.22: Temperature Fields for $Gr_T = 2 \times 10^6$ and $Gr_C = 1.41 \times 10^5$.

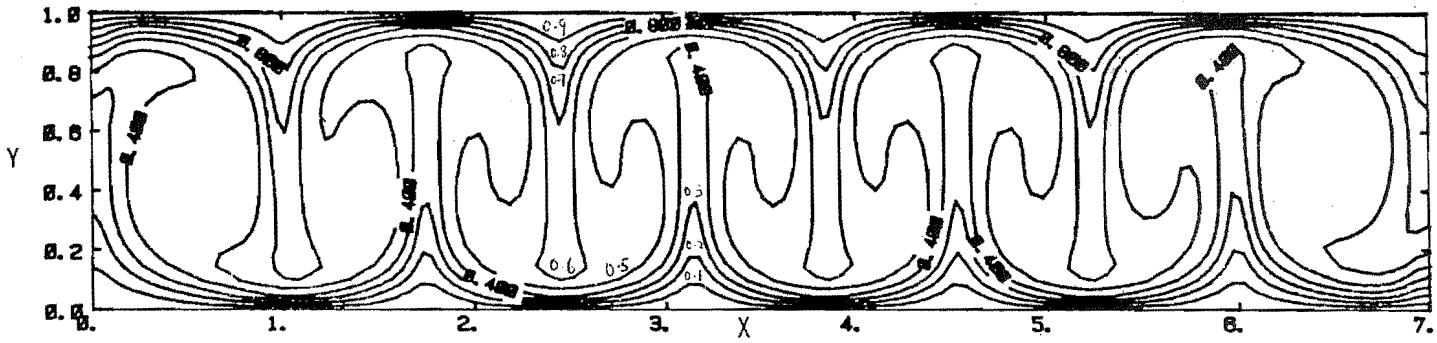

(a) Concentration

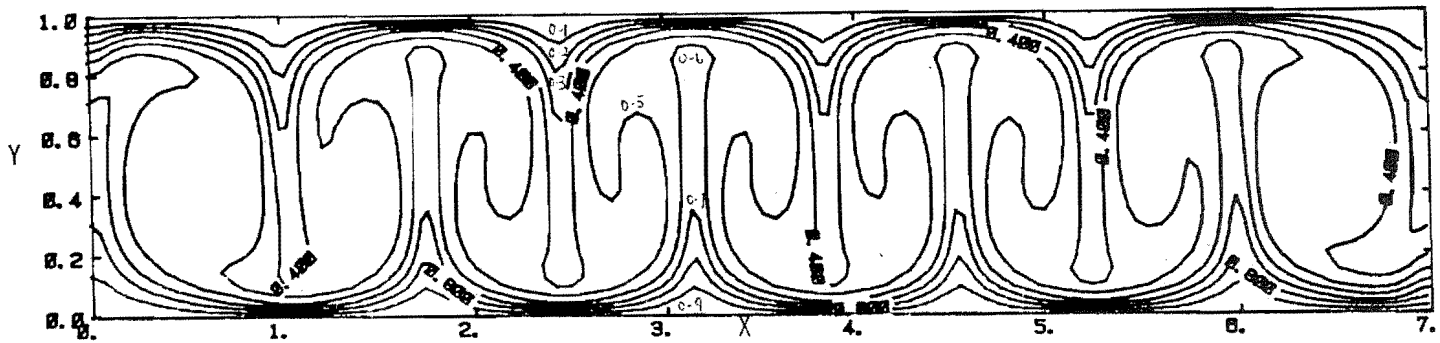

(b) Temperature

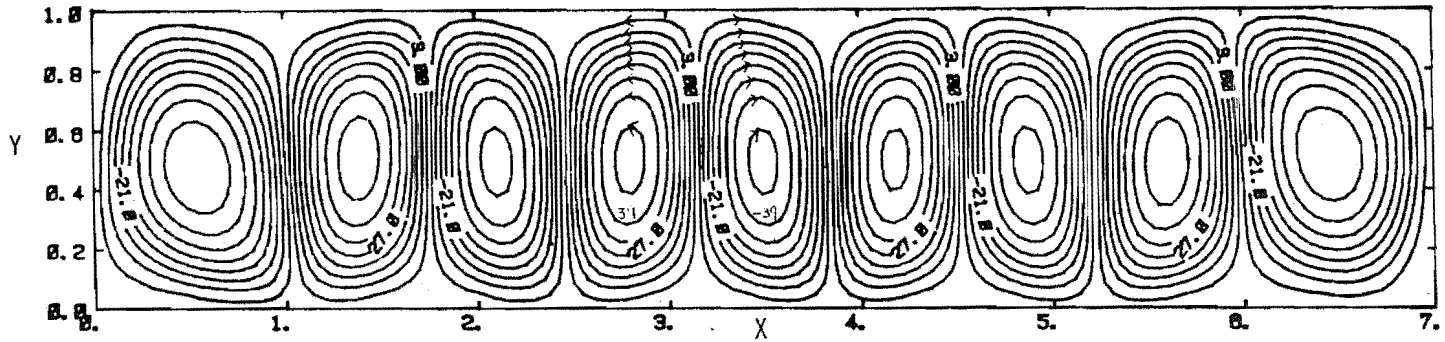

(c) Streamlines, Contour level = 6.0.

Fig. 8.23: $Gr_T = 5.5 \times 10^5$, $Gr_C = -1.4 \times 10^5$

Table 8.1 Numerical Results for Vertical Cavity of Aspect Ratio = 7

Method	Ra	M	N	Nu	Sh	ΔT/°C	ΔP/Pa
ADI	6.10×10^{3}	41	21	-	1.32	-	70.0
ADI	9.15×10^{3}	41	21	-	1.48	-	105.0
ADI	1.22×10^{4}	41	21	-	1.57	-	140.0
ADI	1.83×10^{4}	41	21	-	1.83	-	210.0
ADI	4.27×10^{4}	41	21	-	2.26	-	490.0
DADI	6.10×10^{3}	41	21	-	1.30	-	70.0
DADI	1.83×10^{4}	41	21	-	1.81	-	210.0
DADI	6.10×10^{4}	41	21	-	2.58	-	700.0
FT-II	6.10×10^{3}	41	21	-	1.33	-	70.0
FT-II	3.05×10^{4}	41	21	-	2.13	-	350.0
FT-II	6.10×10^{4}	41	21	-	2.60	-	700.0
ADI	7.10×10^{3}	41	21	1.64	-	0.08	-
ADI	2.13×10^{4}	41	21	2.26	-	0.23	-
ADI	4.26×10^{4}	41	21	2.77	-	0.45	-
ADI	7.10×10^{4}	41	21	3.14	-	0.75	-
FT-I	1.00×10^{4}	41	21	1.82	-	0.11	-
FT-I	1.00×10^{5}	41	21	3.50	-	1.06	-
FT-I	1.42×10^{5}	41	21	3.75	-	1.50	-
FT-I	2.84×10^{5}	41	21	4.60	-	3.00	-
DADI	1.00×10^{4}	41	21	1.79	-	0.11	-
DADI	1.00×10^{5}	41	21	3.45	-	1.06	-
DADI	1.42×10^{5}	41	21	3.70	-	1.50	-
FT-II	2.84×10^{5}	41	21	4.65	-	3.00	-
FT-II	4.26×10^{5}	41	21	5.16	-	4.51	-

Table 8.1 Numerical Results for Vertical Cavity of Aspect Ratio = 7 (CONTD.)

Method	Ra	M	N	Nu	Sh	ΔT/°C	ΔP/Pa
FT-II &DADI	1.42×10^5	71	33	3.79	-	1.50	-
FT-II &DADI	2.84×10^5	71	33	4.57	-	3.00	-
FT-II &DADI	4.26×10^5	71	33	5.08	-	4.51	-
FT-II &DADI	5.68×10^5	71	33	5.52	-	6.01	-
FT-II &DADI	7.10×10^5	71	33	5.83	-	7.52	-
FT-II	9.94×10^5	71	33	6.47	-	10.53	-
FT-II	1.42×10^6	71	33	7.13	-	15.04	-
ADI	3.96×10^4	41	21	2.70	2.21	0.23	300.0
ADI	7.92×10^4	41	21	3.25	2.60	0.45	420.0
ADI	1.20×10^5	41	21	3.65	2.85	0.75	560.0
FT-II	-4.86×10^4 ($Gr_T=6\times10^4$, $Gr_C=-1.2\times10^5$)	41	21	2.84	2.27	0.45	-840.0
FT-II	2.24×10^5 ($Gr_T=4\times10^5$, $Gr_C=-6\times10^4$)	41	21	4.52	3.59	3.00	-420.0

Table 8.1 Numerical Results for Vertical Cavity of Aspect Ratio = 7 (CONTD.)

Method	Ra	M	N	Nu	Sh	$\Delta T/^{\circ}C$	$\Delta P/Pa$
FT-II	6.27×10^5	71	33	5.72	4.87	6.32	350.0
FT-II	1.03×10^6	71	33	6.48	5.58	10.53	420.0
FT-II	7.71×10^5	71	33	6.00	5.10	7.52	700.0
FT=II	1.47×10^6	71	33	7.26	6.10	15.04	600.0

Table 8.2 Numerical Results for Horizontal Cavity of Aspect Ratio = 7 with Upwards Transfer.

Method	Ra	M	N	Nu	Sh	ΔT/°C	ΔP/Pa
FT-II	1.00×10^4	141	11	-	1.73	-	117.0
FT-II	8.60×10^3	141	11	-	1.68	-	100.0
FT-II	4.27×10^4	141	11	-	2.95	-	490.0
FT-II	8.60×10^4	141	11	-	3.53	-	1006.2
FT-II	8.60×10^4	281	21	-	3.50	-	1006.2
FT-II	1.00×10^4	141	11	2.14	-	0.11	-
DADI	1.00×10^4	141	11	2.12	-	0.11	-
FT-II	1.00×10^5	141	11	4.32	-	1.06	-
DADI	1.00×10^5	141	11	4.30	-	1.06	-
FT-II	7.10×10^5	281	21	7.21	-	7.52	-
FT-II	4.97×10^5	281	21	6.73	-	5.26	-
FT-II	1.42×10^6	281	31	8.80	-	15.04	-
FT-II	2.50×10^4 ($Gr_T=5.5\times10^5$, $Gr_C=-1.41\times10^5$)	281	21	5.88	4.73	4.13	-1006.2
FT-II	7.96×10^5 ($Gr_T=1\times10^6$, $Gr_C=1.41\times10^5$)	281	21	7.40	6.02	7.52	1006.2
FT-II	1.51×10^6 ($Gr_T=2\times10^6$, $Gr_C=1.41\times10^5$)	281	31	8.96	7.28	15.04	1006.2

Table 8.3 Lists of Figures and Conditions used for Numerical Calculations for the Vertical Cavity.

Conditions*	Fig	$Gr_T/10^5$	$Gr_C/10^5$	ΔT/°C	ΔC/Kgm^{-3}	ΔP/Pa
Isothermal moisture transfer.[1]	8.3	-	0.10	-	4.820×10^{-4}	70.0
	8.4	-	1.00	-	4.820×10^{-3}	700.0
	8.5					
	8.6					
Heat trasnfer alone.[2]	8.7	2.00	-	1.5	-	-
	8.8	20.0	-	15.0	-	-
	8.9					
	8.10					
Combined heat and moisture transfer.[3]	8.11	20.0	0.80	15.0	3.856×10^{-3}	594.3
Combined heat and moisture transfer.[4]	8.12	0.60	-1.20	0.5	-5.673×10^{-3}	-874.4
Heat trasnfer alone.[5]	8.13	10.0	-	7.5	-	-
	8.14	10.0	-	7.5	-	-

*Note: The following remarks elaborate the conditions listed in Table 8.3. The numbering of these remarks correspond directly to the

indices listed in Table 8.3 :-

1. Figs. 8.3 and 8.4 represent fields which constitute the lower and upper limits for the experimental runs for isothermal moisture transfer case. Figs. 8.5 and 8.6 present the lower and upper limits of the velocity components that can be expected for ths case.

2. Figs. 8.7 and 8.8 represent fields which constitute the lower and upper limits for the experimental runs for heat transfer case only. Figs. 8.9 and 8.10 are the velocity components which represent the lower and upper limits of the velocity that can be expected for this case.

3. Compare Fig. 8.11 with Fig. 8.4 on the effect of additional temperature gradient and Fig. 8.11 with Fig. 8.8 on the effect of additional moisture gradients.

4. Fig. 8.12 is an example of an opposing-gradients run.

5. Figs. 8.13 and 8.14 are comparison of the same function fields obtained from different numerical methods using the same Grashof number and grid-spacings.

Table 8.4 Lists of Figures and Conditions used for Numerical Calculations for the Horizontal Cavity with Upwards Transfer.

Conditions*	Fig	$Gr_T/10^5$	$Gr_C/10^5$	$\Delta T/°C$	$\Delta C/Kgm^{-3}$	$\Delta P/Pa$
Isothermal moisture transfer.[1]	8.15	-	0.14	-	6.796×10^{-4}	100.6
	8.16	-	1.41	-	6.796×10^{-3}	1006.2
	8.17					
Heat trasnfer alone.[2]	8.18	1.41	-	1.1	-	-
	8.19	20.0	-	15.0	-	-
	8.20					
Combined heat and moisture transfer.[3]	8.21	20.0	1.41	15.0	6.796×10^{-3}	1000.6
	8.22	20.0	1.41	15.0	6.796×10^{-3}	1000.6
Combined heat and moisture transfer.[4]	8.23	5.50	-1.41	4.1	-6.796×10^{-3}	-1000.6

*Note : The following remarks elaborate the conditions listed in Table 8.4. The numbering of these remarks correspond directly to the indices listed in Table 8.4 :-

1. Figs. 8.15 and 8.16 represent fields which constitute the lower and upper limits for the experimental runs for isothermal moisture transfer case. Fig. 8.17 presents the lower limit of the velocity components that can be expected for all experimental runs.

2. Figs. 8.18 and 8.19 represent fields which constitute the lower and upper limits for the experimental runs for heat transfer case only. Fig. 8.20 is the velocity components which represent the upper limit of the velocity that can be expected for all experimental runs.

3. Figs. 8.21 and 8.22 are comparison of the same function fields obtained from different numerical methods. Compare Fig. 8.19 with either Figs. 8.21 or 8.22 for the effect of additional moisture gradient. Compare Fig. 8.16 with 8.21 or 8.22 for the effect of additional temperature gradient.

4. Fig. 8.23 is an example of the opposing gradients case.

CHAPTER 9

CONCLUSION

The simultaneous transfer of heat and moisture in a cavity had been investigated experimentally and theoretically. The cavity configurations used were those of a "Vertical Cavity", "Horizontal Cavity with upwards transfer" and "Horizontal Cavity with downwards transfer". Both aiding and opposing-gradients flow were also investigated by a "novel" experimental technique employing a porous platic plate as one cavity wall. This arrangement allowed the imposition of a simultaneous moisture gradient on top of the temperature gradient and vice-versa.The temperature difference used in the experiments ranged from about 4 to 21 °C (corresponding to a Rayleigh number range of $4x10^5$ to $1.47x10^6$). This represented fairly accurately the range of temperature differences found in an actual building cavity, with the exception of extreme conditions expected in summer. The range of the vapour pressure difference used in the experiments varied from 170 Pa to 650 Pa (corresponding to the Rayleigh number range of $2.4x10^4$ to $1.2x10^5$) which covered adequately the range of vapour pressure difference one expect to find in practice.

From the results of the experiments, it was found that the rate of heat and moisture transfer in the Vertical Cavity and the Horizontal Cavity with upwards transfer was five to nine times that of the Horizontal Cavity with downwards transfer. The Nusselt and Sherwood numbers for the Vertical Cavity and the Horizontal Cavity with upwards transfer typically ranged from 5 to 9 and 4.7 to 5.8 respectively, whereas the corresponding Nusselt and Sherwood numbers for the Horizontal Cavity with downwards transfer was found to attain the value of 1.0 and 0.85 respectively within experimental limits. The presence of natural convection in the former two cases was thought to be responsible for the higher transfer rates.

In the case of natural convection resulting from the range of temperature and moisture difference one would expect in practice, the dimensionless driving force corresponding to the temperature

difference (Ra_T) was about ten times that generated by the moisture content difference (Ra_C). Thus while the Sherwood number ranged from 1.7 to 2.9 in the absence of the simultaneous temperature gradient, it increased to 4.7 to 6.8 in the presence of it. The value of the Nusselt numbers, however, did not show any significant increase in the presence of the simultaneous moisture gradient.

The experimental Nusselt and Sherwood numbers reported above were supported by the results from the numerical calculation using a finite-difference technique. From the three numerical methods tried, the False-Transient method [132] and the Dynamic Alternating Direction Implicit [160] were reliable in producing consistent numerical results, but the proposed Hybrid method [Chapter 3] did not. The temperature, concentration, stream-function and velocity components fields obtained from the numerical calculations examined in greater detail the transport processes in the cavity and they complemented the results from the experiments.

RECOMMENDATIONS FOR FUTURE WORK.

During the course of this work, certain shortcomings were encountered which had restricted the scope and accuracy of the results. It is hoped that they will be rectified in the future when continuation of the work in this area is carried out.

(1) The low thermal conductivity of the Porous plastic Plate (0.06 $Wm^{-1}K^{-1}$) had restricted the temperature difference that can be conveniently imposed across the cavity. To reduce this resistance due to the porous medium, other types of porous medium with higher value of thermal conductivity, such as porous stainless or copper plates, might be used in place of the porous plastic plate. The greater rigidity of the porous metallic plate also allows a thinner plate to be used and this has the added effect of further reducing the thermal resistance of the porous medium. The greater conductivity should also ensure better temperature distribution on the surface of the plate and the absolute value of the thermal conductivity be known more accurately because of the relative ease

of experimental determination at a given temperature drop. This feature will allow experiments in the lower temperature difference range (less that 3 °C) to be carried out. The latter is not possible with the present equipment.

(2) The limitation in the (low) temperature level that can be maintained in the Receiving Chamber also restricts the temperature difference that can be imposed across the cavity. Thus improving the condenser circuit, such as providing a greater cooling coil area [Inst P128] and a better refrigerating circuit, will help both in terms of control [Inst 31] and capacity [Inst 599 or 1326]. The coolant circulation pump [Inst 146]should be replaced if possible as the original pump was not designed for continuous operation as demanded and it was a constant source of trouble.

(3) The experimental environment should be controlled if possible. A proportion of the present experimental data during each run had to be discarded when the ambient condition was changing rapidly eg. in the morning when the sun-rays penetrated the room. This caused unwanted disturbance in the experiments and wasted valuable experimental time and efforts.

(4) The numerical calculations had encountered storage and computing time problem on the relatively small VAX 11-730 mini-computer. This has meant that insufficient grid-points had to be used sometimes and this has failed to resolve properly the fine flow structures of the convective process. To obtain the maximum information from a limited computing facility available, some form of grid-transformation technique is advisable for the convective problem of this work. Greater investigation of the feasibilty of the proposed Hybrid method ia also warranted.

(5) Flow visualization experiments can be carried out to test the validity of the flow fields predicted by the numerical methods. The flow visualization technique used will hopefully be one of which quantatitive information such as temperature and concentration gradients can be retrieved at the same time eg.the interferometry technique [36,106,149,168] rather than a purely

qualitative method such the shadowgraph [36,107] or the Schlieren technique [36]. The measurement of the velocity profiles by the laser-doppler anemometer [31,105] can also be used to augment the results of interferometer.The disadvantage of these experiments is of course the expensive equipment required and the difficult experimental technique involved.

(6) To investigate the possibility of using the present experimental set-up with actual building materials as the bounding materials.

NOMENCLATURE

A aspect-ratio, dimensionless,

A_q area for heat and mass transfer, m^2,

ADI Alternating-Direction Implicit method,

C concentration, kg m^{-3} or mole m^{-3} or dimensionless,

ΔC concentration difference, kg m^{-3} or mole m^{-3} or dimensionless,

D molecular diffusivity, m^2s^{-1},

DADI Dynamic Alternating-Direction Implicit method,

E blackbody radiation power, Wm^{-2},

F shape factor for radiation exchange,

FT False-Transient method,

Gr_T thermal Grashof number, dimensionless,

Gr_c concentration Grashof number, dimensionless,

H height of the cavity, m,

J radiosity, Wm^{-2},

K mass-transfer coefficient, $gm^{-2}s^{-1}$,

L cavity gap-width, m,

M,N number of grid-points in the X and Y direction respectively,

Nu Nusselt number,

P_a vapour pressure of ambient condition, mm Hg or Pa,

P_c vapour pressure in the Controlled Chamber, mm Hg or Pa,

P_{cp} vapour pressure at the porous-plate boundary in the Controlled Chamber, mm Hg or Pa,

P_{cc} vapour pressure at the porous-plate boundary in the Test cavity (Controlled Chamber side), mm Hg or Pa,

P_r vapour pressure in the Receiving Chamber, mm Hg orPa,

P_{rp} vapour pressure at the porous-plate boundary in the Receiving Chamber, mm Hg or Pa,

P_{rc} vapour pressure at the porous-plate boundary in the Test cavity (Receiving Chamber side), mm Hg or Pa,

P_T total pressure, mm Hg or Pa,

Pr Prandtl number, dimensionless,

R resistances used in thermal radiation calculation, m^{-2}

Ra_c concentration Rayleigh number, dimensionless,

Ra_T thermal Rayleigh number, dimensionless,

$Ra_{T,C}$ combined Rayleigh number, dimensionless,

S vorticity boundary smoothing parameter,

Sc schmidt number, dimensionless,

Sh Sherwood number, dimensionless,

T temperature, °C or dimensionless,

T_a temperature of ambient condition, °C,

T_c temperature in the Controlled Chamber, °C,

T_{cp} temperature at the porous-plate boundary in the Controlled Chamber, °C,

T_{cc} temperature at the porous-plate boundary in the Test cavity (Controlled Chamber side), °C,

T_r temperature in the Receiving Chamber, °C,

Trp temperature at the porous-plate boundary in the Receiving Chamber, °C,

T_{rc} temperature at the porous-plate boundary in the Test cavity (Receiving Chamber side), °C,

T_D dew-point temperature, °C,

ΔT temperature difference, °C or dimensionless,

U,V dimensionless X and Y-component velocities respectively,

X,Y dimensionless coordinates,

Y humidity, $KgKg^{-1}$

ΔY humidity difference, $KgKg^{-1}$.

a_c false-transient factor for the concentration equation,

a_T false-transient factor for the energy equation,

a_ζ false-transient factor for the vorticity equation,

a_φ false-transient factor for the stream-function equation,

e thermal emittance,

g acceration due to gravity, m^2s^{-1},

h heat-transfer coefficient, $Wm^{-2}K^{-1}$,

k thermal conductivity, $Wm^{-1}K^{-1}$,

m moisture-trasfer rate across the cavity, gh^{-1},

m_T total moisture-trasfer rate recorded by the balance, gh^{-1},

m_l rate of moisture loss from Controlled Chamber to surroundings, gh^{-1},

q rate of heat-transfer across the cavity by bulk-air conduction and convection, W,

q_T total heat input, W,

q_l rate of heat loss from Controlled Chamber to surroundings, W,

q_c rate of heat transfer across the cavity by conduction by the solid joining members at the boundary of the Test Cavity, W,

q_r rate of heat-transfer across the cavity by thermal radiation, W

q_m rate of heat-tranfer across the cavity as a result of the mass-transfer, W,

rh relative humidity, %,

Δt time interval, dimensionless,

u, v dimensional x and y-component velocities, ms^{-1},

x, y dimensional coordinates.

Greek Symbols:

α thermal diffusivity, m^2s^{-1},

β coefficient of volumetric expansion with temperature, K^{-1},

β_T coefficient of volumetric expansion with temperature, K^{-1},

β_c coefficient of volumetric expansion with concentration, m^3kg^{-1},

φ stream-function, m^2s^{-1} or dimensionless,

θ angle on inclination to the vertical, degrees,

ρ density or mass-concentration, kgm^{-3},

υ dynamic viscosity, m^2s^{-1},

ζ vorticity, s^{-1} or dimensionless.

Superscripts :

' denote dimensionless quantity.

Subscripts:

c concentration or moisture-transfer case,
d downwards-transfer case,
i,j grid-point's position at X=i and Y=j,
k intermediate quantity used in the ADI procedure,
n time level n,
n+1 time level n+1,
T temperature or heat-transfer case,
T,c combined temperature and concentration case,
u upwards-transfer case.

REFERENCES.

1. Batchelor G. K. "Heat Transfer By Free Convection Across a Clossed Cavity Between Vertical Boundaries at Different Temperature" Quaterly of Applied Mathematics , vol 12 ,No.3, p 209, 1954.

2. Chung P.M. and Lund C.E. "Downward heat transfer through a joist space " ASHRAE Transactions, Jan. 1959.

3. Eckert E.R.G. and Carlson W.O. "Natural convection in an air layer enclosed between two vertical plates with different temperatures" Int. J. Heat Mass Transfer, vol 2, p.106, 1961.

4. Gill A.E. "The boundary-layer regime for convection in arectangular cativy." J. Fluid Mech. vol 26, part 3 ,p.515, 1966

5. Elder J.W. "Laminar free convection in a vertical slot." J. Fluid Mech. vol 23, part 1, p.77 ,1965.

6. Ostrach S. "Natural convection in enclosures." Advances in Heat Transfer, vol 8, Acadermic Press, N.Y., p.161-227, 1972.

7. Said M.N.A. and Trupp A.C. "Laminar free convection in vertical air-filled cavities with mixed boundary conditions." Chem. Eng. Communication, vol 5, p.93, 1980.

8. Aziz K. and Hellums J.D. "Numerical solution of three-dimensional equation of motion for laminar natural convection." The Physics of Fluids, vol 10, no.2, p.314-324 ,1967.

9. Goldstein R.J. and Chu T.Y. "Thermal convection in a

horizontal later of air." Prog. Heat Mass Transfer ,2, p.55, 1969

10. Luffwendo Lishomwa "Heat transfer through cativy walls." Ph.D Thesis ,Dept Chem. Eng.,U. of Canterbury ,1977

11. Edwards R.M. "Heat transfer through cavity walls." M.Sc. Thesis, University College of Swansea, Glamorgan, 1968.

12. Yin,S.H.; Wung,T.Y. and Chen, K. "Natural convection in an air layer enclosed within rectangular cavities." Int. J. Heat Mass Transfer. vol 21, p.307, 1978.

13. Trethowen, H.A. "Condensation in cavities of building structure." N.Z. Journal of Science, vol 19, p.311, 1976.

14. Trethowen, H.A. "Theory of condensation and mildew." Report C.R.3, Building Research Association of N.Z., 1972.

15. Vos B.H. and Tammes E. "Condensation in structures." (3 articles) Build International (8) 1975 ,p.467

16. Tutt, G.S. "Condensation in attics: Are vapour barrier really the answer ?" Energy and Buildings ,vol 2, p.251, 1979.

17. Burch, D.M.; Contreras,A.G.; Treado, S.J. "Use of low-moisture permeability insulation as an exterior retrofit system- a condensation study." ASHRAE Transaction vol 85, pt 2, p.547 ,1979.

18. Hedden F.H.; Labosky P.; Spray R.A. "Field study of a house destroyed by fungus attack resulting from uncontrolled moisture." A.S.A.E. Pap. 68th Annu. Meet., U. of Calif.,Davis. Jun 22-25 ,1975, pap.75-4007

19. Trethowen H.A. "The need for energy research in buildings." Building Research Association of N.Z. Research report R 31., January, 1980.

20. Dutt, G.S.; Beyea, J.; Sinden, F.W. (1978) "Attic heat loss and conservation policy." ASME Technical paper. no 78-TS-5 (for meet.Nov 5-9,1978).

21. Hollands K.G.T. and Konicek L. "Experimental study of the stability of differentially heated inclined air layers." Int. J Heat Mass Transfer. vol 16, p.1467, 1973.

22. Vest, V.M. and Arpaci V.S. "Stability of natural convection in a vertical slot." J. Fluid Mech. vol.36 p.1, 1969.

23. Unny T.E. "Thermal instability in differentially heated inclined box." Applied Mechanics vol 39(1), 1972.

24. Hart, J. "Stability of the flow in differentially heated inclined box." J. Fluid Mech. vol 35(4),p.775, 1969.

25. Lykov A.V. and Berkotskii B.M. "The onset of convection in cativies with variable wall temperatures" Int. Chemical Engineering vol 9, no.3,p.414, 1969.

26. Quan, C. "High Rayleigh number convection in an enclosure- A numerical study." The Physics of Fluids vol 15 no.1 p.12 1972.

27. Quon C. "Effects of grid distribution on the computation of high Rayleigh number convection in a differentially heated cavity." IN Numerical Properties and Methodologies in Heat Transfer. T.M. Shih editor, Hemisphere Publish. Corp., 1983.

28. Quen, C. "Free convection in an enclosure-Revisited." Trans. ASME J Heat Transfer vol 99, p.340, 1977.

29. Nobuhiro Seki, Shoichiro Fukusako and Hideo Inaba "Visual observation of nataural convection flow in avertical cavity." J. Fluid Mech. vol 84, part 4, p.695, 1978.

30. Bejan, A. "Note on Gill's solution for free convection in

avertical enclosure." J. Fluid Mech., vol 90, no 3, p.561, 1979.

31 Morrison G.L. and Tran V.Q. "Laminar flow structure in a vertical free convective cavities." Int. J Heat Mass Transfer. vol 21, p.203, 1978.

32. G. De Vahl Davis "Laminar natural convection in an enclosed rectangular cavity." Int. J Heat Mass Transfer vol 11,p.1675, 1968.

33. Taylor C. and Ijam A.Z. "A finite element numerical solution of natural convection in enclosed cavities." Computer Method Applied Mech and Eng. v19, p.4209,1979.

34. Wilkes J.O. and Churchill S.W. "The finite difference computation of natural convection in a rectangular enclosure." A.I.Ch.E. Journal vol 12, no 1, p.161, 1966.

35. Kublbeck K., Merker G.P., Straub J. Advanced numerical computation of two dimensional time dependent free convection in cavities." Int. J Heat Mass Transfer vol 23, p.203, 1980.

36. Jaluria Y. "Natural convection Heat and Mass transfer." Pergoman Press 1980

37. Chu,T.Y.; Goldstein R.J. "Turbulent convection in a horizontal layer of air." J. Fluid Mech vol 60, part 1, p.141, 1973.

47. Klushnikov F.V. and Petrazhitskii G.B. "Features of flow and heat transfer in a rectangular with a heated projection in its lower part." High Temp. vol 9, no 1, p.101, 1971.

48. Petrazhitskii G.B., Klyushnikov F.V.,Bekneva E.V. "Numerical study of free convection circulation flows and heat transfer process in cativies of different configuration." Proceedings

ADDENDA TO REFERENCES - PAGE 212

38. Bernad H. Ann. Chim. Phys. vol(7) 23, p.62, 1901.

39. Rayleigh L. Phil. Mag. J. Sci., s6 vol 32, p.529, 1916.

40. Jeffreys H. Phil. Mag., s7 vol 2, p.833, 1926.

41. Jeffreys H. Proc. Roy. Soc., vol A118, p.195, 1928.

42. Malkus W.V.R. "Discrete transitions in turbulent convection." Proc. Roy. Soc., vol A225, p.185, 1954(a).

43. Malkus W.V.R. "The heat transport and spectrum of thermal turbulence." Proc. Roy. Soc., vol A225, p.196, 1954(b).

44. Herring J.R. "Investigation of problems in thermal convection." J. Atmos. Sci., vol 20, p.325-338, 1963.

45. Ozoe H. and Churchill S.W. "Hydrodynamic stability and natural convection in Newtonian and non-Newtonian fluids heated from below." CEP Symposium Series no. 131, Heat Transfer: Fun. Ind. Appl., vol 69, p.126-133, 1973.

46. Herring J.R. "Investigation of problems in thermal convection: Rigid boundaries." J. Atmos. Sci., vol 21, p.277-290, 1964.

of 5th. IHTC, vol III, p.110, Tokyo, 1974.

49. Jokob M. "Free heat convection through enclosed plane gas layers" Trans. ASME, J.Heat Transfer, vol 68, p.189, 1946.

50. Ozoe H.; Sayama H; Churchill S.W. "Natural convection in an inclined square channel" Int. J Heat Mass Transfer vol 17, p.401, 1974.

51. Catton I. "The effect of insulating vertical walls on the onset of motion in a fluid heated from below." Int. J Heat Mass vol 15, p.665, 1972.

52. Heitz W.L , Westwater J.W. "Critical Rayleigh numbers for natural convection of water cofined in square cells with L/D from 0.5 to 8 inches." Trans. ASME J Heat Transfer ,vol 93, p.188, 1971.

53. Dixon M. and Probert S.D. "Heat transfer regimes in vertical, plane-walled,air-filled cavities" Int. J Heat Mass Transfer vol 18, p.709, 1975.

54. Mull W. and Reiher H. "Beih. Z. Gesondheitz-Eng. Reihe 1, 28, (1930) Munich and Berline, Germany.

55. Wilkes J.O. (1963) "The finite-difference computation of natural convection in an enclosed rectangular cativy" Ph.D. Thesis, U. of Michigan, Ann Arbor, Michingan.

56. Pepper D.W. and Harris S.D. "Numerical simulation of natural convection in closed containers by a fully implicit method." J. Fluid Engineering. vol 99, p.649, 1977.

57. Goldstein R.J. "Temperature distribution in a horiontal fluid layer" Chem Eng. Science vol 19, p.997, 1964

58. O'Toole J.L. and Silveston P.L. "Correlation of convection heat transfer in confined horizontal layers." Chem. Eng.

Prog. Symposium 57, No. 32, p.81, 1961.

59. Hollands K.G.T. "Convectional heat transport between rigid horizontal boundaries after instability." Physics of Fluids. vol 8, p.389, 1965.

60. Kraichnan R.H. "Mixing-length analysis of turbulent thermal convection at arbitrary Prandtl number" Physics Fluid. vol. 5, p.1374, 1962.

61. Howard L.W. "Heat transport by turbulent convection" J Fluid Mech. vol 17, p.405, 1963.

62. Fromm J.E. "Numerical solution of the non-linear equations for a heated fluid layer" Physics Fluids. vol. 8, p.1757, 1965.

63. Churchill S.W.; Ozoe H. et al "Three dimensinal numerical analysis of laminar natural convection in a confined fluid heated from below" Trans. ASME, J Heat Transfer, vol 98, p.202, 1976

64. Hollands K.G.T.; Raithby G.D. and Konicek L. "correlation equations for free convection heat transfer in horizontal layers of air and water" Int. J Heat Mass Transfer, vol 18, p.879, 1975.

65. Vahl Davis G.D. and Morrison G.D. "A note on natural convection in a vertical slot" J Fluid Mech. vol 72, p.87, 1975.

66 American Society of Heating, Refrigeration and Air-Conditioning Engineers "ASHRAE Handbook of fundamentals" New York, 1972.

67. Churchill S.W. "Free Convection in Layers and Enclosures" IN Heat Exchanger Design Hanbook Vol 2 - Fluid Mechanics and Heat Transfer. Hemisphere Publishing Corporation. 1983.

68. Trethowen H.A. "The Keiper method for moisture design in

buildings." New Zealand Institute of Engineer Annual Conference, Wellington, Feb. 1979.

69. Powell F. and Robinson H. "The effect of moisture on the heat transfer performance of insulated flat roof construction. "U.S. Department of Commerce. Natural Bureau of Standard Building Science Series, 37, 1971.

70. Sedahmel G.H. and Shemilt A.A. "Free convection mass transfer in vertical annuli" Chem. Eng. Commun. vol 14, p.307, 1982.

71. Ross T.K. and Wragg A.A. "Electrochemical mass transfer studies in annuli" Electrovhim. Acta., 10, p.1093, 1965.

72. Somers E.V. "Theoretical consideration of combined thermal and mass transfer from a vertical flat plate" J. Applied Mech. vol 23, p.295, 1956.

73. Mathers W.G.; Madden A.J.; Piret E.L. "Simultaneous heat and mass transfer in free convection" Ind. Engng. Chem., vol 49, p.961, 1957.

74. Wilcox W.R. "Simutaneous haet and mass transfer in free convection." Chem Engng Sci., 13, p.113, 1961.

75. Lowell R.L. and Adams J.A. "Similarity analysis for multicomponent, free convection." AIAA Jl, vol. 5, p.1360, 1967.

76. Adams J.A. and McFadden P.W. "Simutaneous heat and mass transfer in free convection with opposing body forces" A.I.Ch.E. Jl. vol 12, No.4,p.642, 1966.

77. J.A. Delefuw Denbouter, B. De Munnik and P.M. Heertjse "Simataneous heat and mass transfer in laminar free convection from a vertical plate." Chem. Engng. Sci., vol 23, p.1185, 1968.

78. Gehbart B. and Pera L. "The nature of vertical natural

convection flows resulting from the combined buoyancy effects of thermal and mass transfer." Int. J Heat Mass Transfer vol 14, p.2025, 1971.

79. Pera L. and Gebhart B. "Natural convection flows adjacent to horizontal surfaces resulting from the combined buoyancy effects of thermal and mass diffusion." Int. J. Heat Mass Transfer vol 15, p.269, 1972.

80. Callahan G.D. and Marner W.J. "Transient free convection with mass transfer on an isothermal vertical flat plate" Int. J. Heat Mass Transfer vol. 19,p.165, 1976.

81. Boura A. and Gebhart B. "The stability of a vertical flow which arises from combined buoyancy modes" A.I.Ch.E. Jl., vol 22, no.1, p.94, 1976.

82. Soundalgekar V.M. and Ganesan P. "Finite-difference analysis of transient free convection with mass transfer on an isothermal vertical flat plate." Int. J. Engng. Sci., vol 19, p.757, 1981.

83. Nilson R.H. and Baer M.R. "Double-diffusive counterbuoyant boundary layer in laminar natural convection" Int. J Heat Mass Transfer vol 25, p.285, 1982.

84. Weber J.E. "Convection in porous medium with horizontal and vertical temperarure gradients" Int. J Heat Mass Transfer vol 17, p.241, 1974.

85. Chan B.K.C.; Ivey C.M. and Barry J.M. "Natural convection in enclosed porous media with rectangular boundaries" Trans ASME, J Heat Transfer, vol 92, p.21, 1970.

86. Burns P.J.; Chow L.C.; Tien C.L. "Convection in a vertical slot filled with porous insulation" Int. J Heat Mass Transfer vol 20, p.919, 1977.

87. England W.G. and Emery A.F. "Thermal radiation effects on the

laminar free convection boundary layer of an absorbing gas" Trans ASME, J Heat Transfer, vol 91, p.37, 1969.

88. Noble J.J. "The effect of radiation transfer on natural convection in enclosure: A numerical investigation" Ph.D. Thesis, Massachusetts Institute of Technology, Cambridge, Mass., April, 1968.

89. Allcut E.A. "Analysis of heat transfer through thermal insulating materials-Proceedings general discussion on heat transfer." Inst. Mech. Engrs., LOndon, 1951.

90. Verschoor J.D. and Greebler "Heat transfer by gas conduction and radiation in fibrous insulation." Trans. ASME, J Heat Transfer, vol 74, p.961, 1952.

91. Hurle D.T.J. and Jakeman E. "Significance of the soret effect in the Rayleigh-Jedffreys's problem." Physics of Fluids, vol.12, p.2704, 1969.

92. Chen C.F., Briggs D.G. and Wirtz R.A. "Stability of thermal convection in a salinity gradient due to lateral heating." Int J. Heat Mass Transfer, vol.14, p.57, 1971.

93. Wright J.H. and Loehrke R.I. "The onset of Thermohaline convection in a linearly-stratified horizontal layer." Tran. ASME, J Heat Transfer, p.558, Nov 1976.

94. Suzukawa Y. and Narusawa U. "Structure of growing double-diffusive convection cells." Tran. ASME, J Heat Transfer, vol 104, p.248, 1982.

95. Paliwal R.C. and Chen C.F. "Double-diffusive instability in an inclined fluid layer. Part 1: Experimental investigation." J. Fluid Mech., vol 98, part 4, p.755, 1980.

96. Paliwal R.C. and Chen C.F. "Double-diffusive instability in

an inclined fluid layer. Part 2: Stability analysis." J. Fluid Mech., vol 98, part 4, p.769, 1980.

97. Sarsten J.A. "LNG stratification & roll over." Pipeline and Gas Journal, Sept. 1972, pg. 37.

98. Rabl A. and Nielsen C.E. "Solar ponds for space heating." Soler Energy, vol 17, p.1, 1975.

99. Turner J.S. "Double Diffusive Phenomena." Annual Review of Fluid Mechanics, vol 6, p.37, 1974.

100. Turner J.S. and Stommel H. "A new case of convection in the presence of combined vertical salinity and temperature gradients." Proc. U.S. Natl Acad. Sci., 52, p.49, 1964.

101. Turner J.S. "The behavior of a stable salinity gradient heated from below." J. Fluid Mech., vol 33, p.183, 1968.

102. Takao S. and Narusawa U. "An experimental study of heat and mass transfer across a diffusive interface." Int J Heat Mass Transfer, vol 23, p.1283, 1980.

103. Lee Y. and Korpela S.A. "Multicellular naturel convection in a vertical slot." J. Fluid Mech., vol 126, p.91-121, 1983.

104. Korpela S.A.; Lee Y. and Drummond J.E. "Heat transfer through a double pane window." J. Heat Transfer, Trans. ASME, vol 106, p.824, 1982.

105. Linthorst S.J.M; Schinkel W.M.M. and Hoogendoorn. "Flow structure with natural convection in inclined air-filled enclosures." J Heat Transfer, Trans. ASME, vol 103, p.535-539, 1981.

106. Oertel H. Jr. "Visualization of thermal convection." Proceedings of the 2nd. International Symposium on Flow Visualization, Sept 9-12, Bochum, West Germany,

p.71-76. Edited by Wolfgang Merzkirch.

107. Symons J.G. and Peck M.K. "Natural convection heat transfer through inclined longitudinal slots." J Heat Transfer, Trans ASME, vol106, p.824-829, 1984.

108. Markatos N.C. and Pericleous K.A. "Laminar and Turbulent natural convection in an enclosedcavity." Int J. Heat Mass Transfer, vol 27, p.755-772 1984.

109. Kaviany M. "Effect of a protuberance on thermal convection in a square cavity." J Heat Transfer, Trans ASME, vol 106, p.830-834, 1984.

111. Mallinson G.D. and De Vahl Davis G. "Three-dimensional natural convection in a box: a numerical study." J. Fluid Mech., vol 83, p.1-31, 1977.

112. Phillips T.M. "Natural convection in an enclosed cavity." J. Computational Physics, vol 54, p.365-381, 1984.

113. Akinsete V.A. and Coleman T.A. "Heat transfer by steady laminar free convection in triangular enclosures." Int. J. Heat Mass Transfer, vol 25, p.991-998, 1982.

114. Probert S.D. and Dixon M. "Free convection within a vertical rectangular cavity subjected to large temperature differences." Applied Energy, vol 5, p.233-241, 1979.

115. Elsherbiny S.M.; Raithby G.D. and Hollands K.G.T. "Heat transfer by natural convection across vertical and inclined air layers." J. Heat Transfer, vol 104, p.96-102, 1982.

116. Ozoe H.; Sayama H. and Churchill S.W. "Natural convection patterns in a long inclined rectangular box heated from below:- Part 1 Three directional photography." Int. J. Heat Mass Transfer, vol 20, p.123-129, 1977.

117. Ozoe H.; Yamamoto K.; Sayama H. and Churchill S.W. "Natural

convection patterns in a long inclined rectangular box heated from below:- Part 2 Three-dimensional numerical analysis." Int. J. Heat Mass Transfer, vol 20, p.131-139, 1977.

118. Hollands K.G.T. "Multi-Prandtl number correlation equations for natural convection in layers and enclosures." Int. J. Heat Mass Transfer, vol 27, p.466-468, 1984.

119. Hassan. M. and Mujumdar A.S "Coupled heat and mass transfer in natural convection under flux condition along a vertical cone." Int. Comm. Heat Mass Transfer, vol 11, p. 157-172, 1984.

120. Clifton J.V. and Chapman A.J. "Natural-convection on a finite-size horizontal plate." Int. J. Heat Mass Transfer, vol 12, p.1573-1584, 1969.

121. Hatfield D.W. and Edwards D.K. "Edge and aspect ratio effects on natural convection from the horizontal heated plate facing downdards." Int. J. Heat Mass Transfer, vol 24, p.1019, 1981.

122. Yousef W.W.; Tarasuk J.D. and Mckeen W.J. "Free convection heat transfer from upward-facing isothermal horizontal surfaces." J. Heat Transfer, Trans. ASME, vol 104, p493-500, 1982.

123. Gryzagorridis J. "Natural convection from an isothermal downward facing horizontal plate." Int. Comm. Heat Mass Transfer, vol 11, p183-190, 1984.

124. Aihara T.; Yamada Y and Endo S. "Free convection along the downward-facing surface of a heated horizontal plate." Int. J. Heat Mass Transfer, vol 15, p.2535-2549, 1972.

125. Probert S.D. and Ward J. "Improvements in the thermal resistance of vertical, air-filled, enclosed cavities."

Paper NC3.9, p124-128, Proceedings 5th Int. Heat Trans. Conf., Tokyo, 1974.

126. British Standard Institution, C.P. 3005 "Thermal insulation of pipework and equipment.", 1969.

127. Siad M.N.A. and Trupp A.C. "Laminar free convection in small aspect ratio rectangular with isothermal boundary conditions." J. Heat Transfer, Trans ASME, vol 101, p569-571, 1979.

128. Ozoe H.; Mouri A.; Ohmuro M.;Churchill S.W. and Lior N "Numerical calculation of laminar and turbulent natural convection in water in rectangular channels heated and cooled isothermally on the opposing vertical walls." Int. J. Heat Mass Transfer, vol 28, p.125-138, 1985.

129. Cha C.K. and Jaluria Y. "Recirculating mixed convection flow for energy extraction." Int. J. Heat Mass Transfer, vol 27, p.1801-1812, 1984.

130. Korn, G.R. and Korn, T.M. "Mathematical Handbook for Scientists and Engineers", McGraw-Hill, 1968.

131. Randall K.R.; Mitchell J.W. and El-Wakil M.M. "Natural convection heat transfer characteristic of flat plate enclosures." J. Heat Transfer, Trans ASME, vol 101, p.120-125, 1979.

132. Mallinson G.D. and De Vahl Davis G. "The method of False Transient for the solution of coupled elliptic equations." J. Comp. Physics, vol 12, p.435-461, 1973.

133. Ozoe H.; Yamamoto K.; Sayama H. and Churchill S.W. "Natural circulation in an inclined rectangular channel heated on one side and cooled on the opposite side." Int. J. Heat Mass Transfer, vol 17, p.1209-1217, 1974.

134. Ozoe H.; Sayama H. and Churchill S.W. "Natural convection in

an inclined rectangular channel at various aspect ratios and angles: Experimental measurements" Int. J. Heat Mass Transfer, vol 12, p.1425-1431, 1975.

135. Ozoe H.; Fujii K.; Churchill S.W. and Lior N. "A theoretical based correlation for natural convection in horizontal rectangular enclosures heated from below with arbitrary aspect ratios." Paper NC23, Proceedings 7th Int. Heat Tran. Conf., p.257-262, Sept 1982, Munich, West Germany.

136. Hollands K.G.T.; Unny T.E. and Raithby G.D. "Free convection heat transfer across Inclined air layer." J. Heat Transfer, Trans ASME, vol 98, p.189-193, 1976.

137. Cunnigham M.J.(1983) "A new analytical approach to the long term behaviour of moisture concentrations in building cavities -I. Non-condensing cavity." Bldg Envir., vol 18, p.109-116, 1983.

138. Cunnigham M.J.(1983) "A new analytical approach to the long term behaviour of moisture concentrations in building cavities - II. Condensing cavity." Bldg Envir., vol 18, p.117-124, 1983.

139. Cunnigham M.J.(1984) "Further analytical studies of building cavity moisture concentrations." Bldg Envir., vol 19, p.21-29, 1984.

140. Craig J.R.; Leidenfrost W. "Free convection draft induced by thermal and concentration gradients inside an isothermal, vertical cylinder." Chem Eng. Commun., vol 27, p.129-156, 1984.

141. Farouk B. and Guceri S.I. "Laminar and turbulent natural convection in the annulus between horizontal concentric cylinders." J. Heat Transfer, Trans ASME, vol 104, p.631-636, 1982.

142. Lee Y.; Korpela S.A. and Horne R.N. "Structure of multicellular natural convection in a tall vertical annulus." Paper NC17, Proceedings of 7th Int. Heat Trans. Conf.,p.221-226, Sept 1982, Munich, West Germany.

143. Takata Y.; Iwashige K.; Fukuda K. and Hasegawa S. "Three-dimensional natural convection in an inclined cylindrical annulus." Int. J. Heat Mass Transfer, vol 27, p.747-754, 1984.

144. Hanzawa T. and Kato K. "Heat transfer by natural convection between vertical,enclosed, concentric cylinders with the inner cylinder heated locally." Int. Chem. Engng., vol 24, p.695-701, 1984.

145. Tsui Y.T and Tremblay B. "On transient natural convection heat transfer in the annulus between concentric horizontal cylinders with isothermal surfaces." Int. J. Heat Mass Transfer, vol 27, p.103-110, 1984.

146. Bajorek S.M. and Lloyd J.R. "Experimental investigation of natural convection in partitioned enclosures." J. Heat Transfer, Trans ASME, vol 104, p.527-532, 1982.

147. Nansteel M.W. and Greif R. "Natural convection in undivided and partially divided rectangular enclosures." J. Heat Transfer, Trans ASME, vol 103, p.623-629, 1981.

148. Chang L.C.; Lloyd J.R. and Yang K.T. "A finite difference study of natural convection in complex enclosures." Paper NC11, Proceedings of 7th Int. Heat Trans. Conf., p.183-188, Sept 1982, Munich, West Germany.

149. Gehbart B. and Knowles B. Rev. Sci. Instr., vol 37, p.12, 1966.

150. Kurosaki Y.; Mishina H. and Kashiwagi T. "Heat transfer combined with radiation and natural convection in a

recatangular enclosure." Paper NC16, Proceedings of 7th Int. Heat Trans. Conf., p.215-220, Sept 1982, Munich, West Germany.

151. Alamdari F.; Hammond G.P. and Melo C. "'Approriate' calculation methods for convective heat transfer from building surfaces." 1st U.K. National Conf. on Heat Transfer, The Institute of Chemical Engineers Symposium Series No 86, 1984.

152. Bird R.B.; Steward W.E. and Lightfoot E.N. "Transport Phenomena." John Wiley and Sons, 1960.

153. Roache P.J. "Computational Fluid Dynamics." Hermosa Publishers, 1972.

154. Boussinesq J. "Theorie Analytique de la Chaleur" vol 2, 172, 1903, Ganthier-villars, Paris.

155. Gebhart B. "Buoyancy induced fluid motions characteristic of applications in technology -the 1978 Freeman Scholar Lecture." J. Fluid Engng., vol. 101, p.5-28, 1979.

156. de Vahl Davis G. "Program Frecon for the numerical solution of free convection in a rectangular cavity." Univ. of N.S.W. School of Mech. and Indust. Eng., Report 1976/FMT/1, 1976.

157. Chenoweth D.R. and Paolucci S. "On optimising nonuniform finite-difference grids for boundary regions in transient transport problems." Report SAND81-8204, Sandia Laboratories, 1981.

158. de Vahl Davis G. and Jones I.P. "Natural convection in a square cavity: a comparison exercise." Int. J. for Num. Method in Fluids, vol.3, p227-248, 1983.

159. McDonough J.M. and Catton I. "A mixed finite-difference-

galerkin procedure for two-dimensional convection in a square box." Int. J. Heat Mass Transfer, vol 25, p.1137-1146, 1982.

160. Doss S. and Miller K. "Dynamic ADI method for elliptic equations." SIAM J. Numer. Anal., vol.106, p.837-856, 1979.

161. Touloukian Y.S. and Dewitt D.P.(editors), "Thermal Radiative Properties. Nonmetallic Solids.", The TPRC Data Series, vol. 18, IFI/PLENUM, 1972.

162. Peaceman D.W. and Rachford H.H. Jr. "The numerical solution of parabolic and elliptic differential equations." J. Soc. Indust. Appl. Math., vol. 3, p.28-41, 1955.

163. ASTM C236-80. "Standard Test Method for steady state thermal performance of building assemblies by means of a guarded hot box." Annual Book ofASTM Standards, section 4,vol 04.06, 1984.

164. Cooper P.I. "Heat and mass transfer within a single-effect solar still envelope." Proceedings of 1st Austral. Conf. on Heat and Mass Transfer, Melbourne, 1973.

165. Rheinlander J. "Numerical calculation of heat and mass transfer in solar stills." Solar Energy, vol 28, p.173-179, 1982.

166. I.C.I. Limited "'Perspex' cast acrylic sheet: properties and fabrication techniques." Technical Service Note PX 127, 2nd Ed.,1979.

167. I.C.I. Limited "'Tensol' cements for 'perspex': description, techniques and safety information." Technical Service Note PX 128, 3rd Ed.,1982.

168. Eckert E.R.G. and Goldstein R.J. "Measurements in Heat

Transfer", 2nd Ed., Hemisphere Publishing Corp., 1976.

169. American Society for Testing and Materials "Manual on the use of thermocouples in temperature measurement." ASTM Special Tecnichal Publication 470A, 1974.

170. Nicholas J.V. and White D.R. "Traceable Temperature." DSIR, N.Z., Bulletin 234, 1982.

171. Wong H.Y. "Handbook of Essential Formulae and Data on Heat Transfer for Engineers." Longman, 1977.

172. Seifert, H.S. and Randall H.M. "Transmission and reflection of plastics and metal blacks in the far infrared", Rev Sci Instr., vol 11, p.365-8, 1940.

173. Krischer O.(1962 "Die missenschaftlichen grundlagen der trocknungstechnik", Springer, Berlin/Gottingen/Heidelberg.

174. Personal communication with D. Rodwell of Building Research Establishment, Princess Risborough Laboratory, Aylesbury, Buckinghamshire, HP179PX, England, Oct. 1983.

175. Perry R.H. and Chilton C.H. "Chemical Engineers' Handbook", fifth edition, McGraw-Hill Kogakusha Ltd., 1973.

176. Carnahan B., Luther H.A. and Wilkes J.O. "Applied Numerical Methods." p.571-584, John Wiley & sons, 1969.

177. Chilton, J.H. and Colburn, C.P. "Mass transfer(adsorption) coefficients, Prediction from data on heat transfer and fluid friction", Ind. Eng. Chem., 26, p.183-7, 1934.

178. IN Keey, R.B. "Introduction to Industrial Drying Operations.", p.200, Pergamon Press, 1978.

179. Kays, W.M. and Crawford, M.E. "Convective Heat and Mass Transfer." 2nd. edition, McGraw Hill, 1980.

180. Kasuda T. "Calculation of the temperature of a flat-plate wet surface under adiabatic conditions with respect to the Lewis relation", IN "Humidity and Moisture -Measurement and Control in Science and Industry.", vol 1, Wexler, A (editor), Reinhold, 1965.

181. Keey, R.B. "Introduction to Industrial Drying Operations." Pergamon Press, 1978.

182. Kreith, F. "Principles of Heat Transfer." 3rd. edition, Harper & Row, 1973.

183. Mullin, J.W. "Crystallization." Butterworths, London, 1961.

184. Weast R.C.(editor-in-chief) et.al. "CRC Handbook of Chemistry and Physics", 64th edition, CRC Press Inc., 1983-1984.

185. Davies, O.L. "Statistical Methods in Research and Production", 3rd. edition, Oliver and Boyd, 1967.

APPENDIX 1

DESCRIPTION OF PROGRAMS FOR ANALYSING EXPERIMENTAL DATA AND SAMPLE CALCULATIONS

All the programs described here are written in "Fortran 77" and implemented on the departmental VAX 11/730 computer. The main features used in each program are discussed, but the complete computer listings will not be given as they are easily generated once the principles are known. Sample calculations are given, where applicable, to demonstrate the method and present relevant numerical values.

A1.2 CALCULATION OF MOISTURE TRANSFER BY PROGRAM "RATE-FOR"

The rate of moisture transfer is determined from the mass-time curve of the evaporating source. An example of the mass-time curve is given in Figure A1.1. This curve is obtained from the periodic output of the electronic balance reading the weight of the evaporating source (pan) resting on it. Data are collected every 4 or 12 minutes, depending on the rate of moisture transfer. The curve shown are for data collected every 12 minutes.

The program "RATE.FOR" reads the mass-time data of a run and performs a numerical differentiation on the data to produce a rate of moisture transfer curve as shown in Figure A1.2.

Due to the linearity of the mass-time curve and the lack of significant random fluctuation in the data, the second-order mid-point method was found to be very suitable and was adopted in this work. The 2nd order mid-point formula is:

$$-f'(x_1) = (f_0 - f_2)/2h - \frac{h_2}{6} f'''(e)$$

where the primes refer to differentiation with respect to x.

For other higher order formulae see Perry V (175), p 2-56.

Fig. A1.1: RUN HM1 HEAT AND MASS TRANSFER ACROSS HORIZONTAL CAVITY

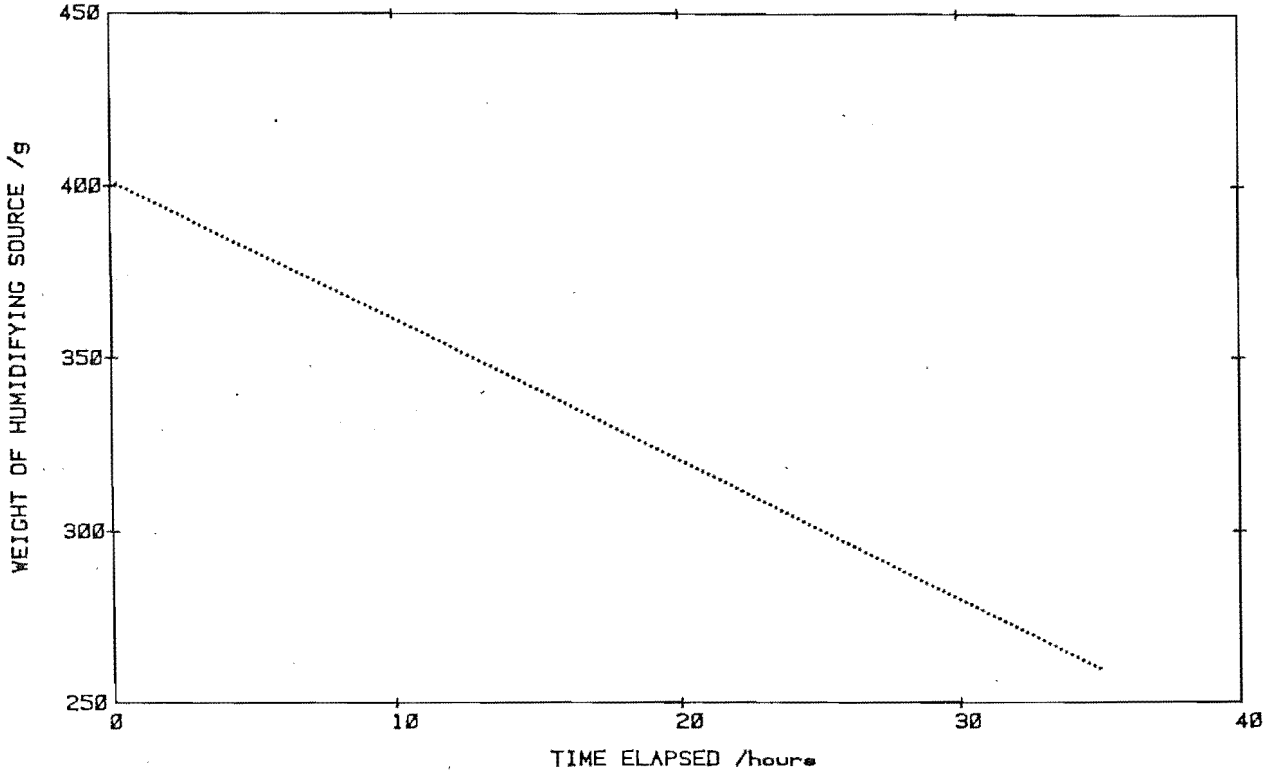

Fig. A1.2: RUN HM1 HEAT AND MASS TRANSFER ACROSS HORIZONTAL CAVITY

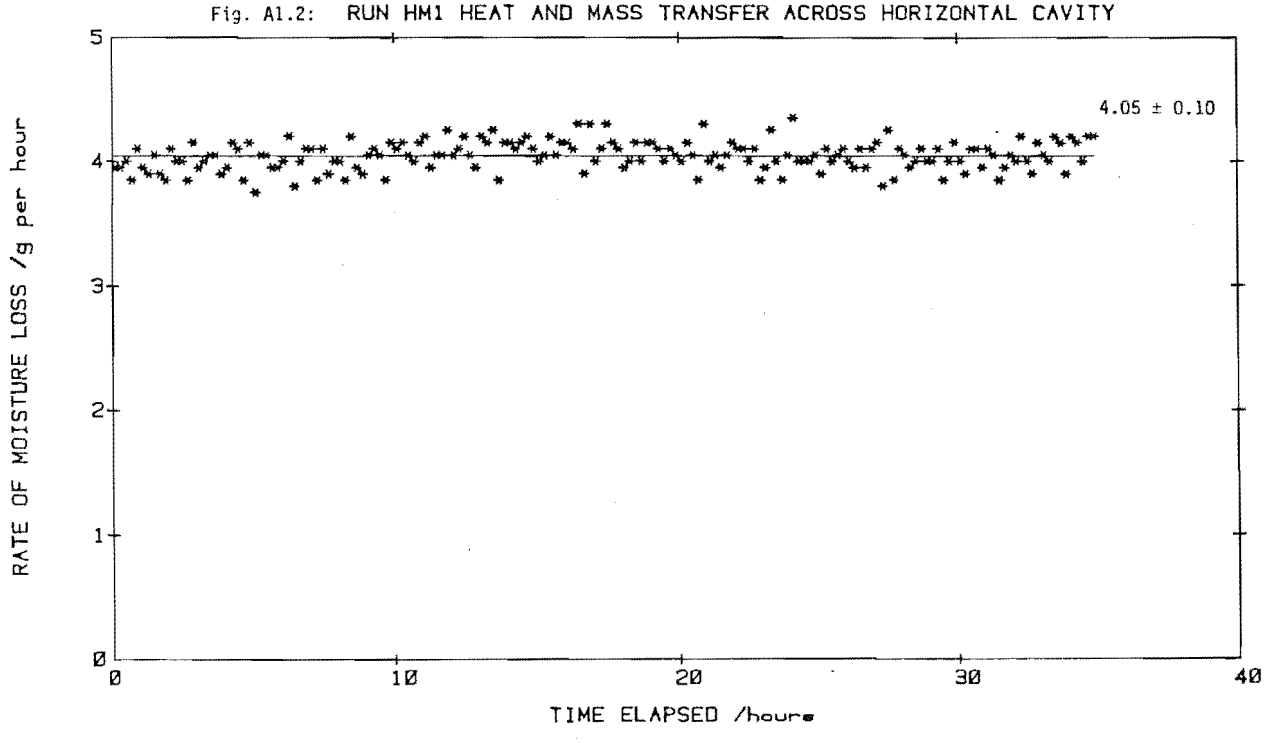

Generally no smoothing was done to the mass-time curve before the numerical differentiation was carried out to produce figure A1.2. An averging process (by program "AVERAGE.FOR") or a least-squares fit of zero order (by program "POLYFIT.FOR") was then performed on the data for the rate of moisture transfer to obtain an average value over the whole time domain of the run. This procedure has the same effect as first fitting a curve to the mass-time data of Figure A1.1 by a least square method and then differentiating the resultant smoothed curve to find the rate of moisture transfer.

The deviation of each data point from the "averaged" line gives an indication of the "error" of the averaging process. This error is estimated from the standard deviation of the least-squares fit. In Figure A1.1, this error is $\pm$ 0.05 gh^{-1} and represents a fairly typical value for all the runs. Thus the percentage error encountered in small mass transfer runs (about 1 gh^{-1}) is 5% and for high mass transfer runs (about 20 gh^{-1}) is 0.25%. This error is probably due to the random fluctuation of the evaporating source due to the disturbance of the fan stirrers as the random fluctuation error was recorded to be of the order of $\pm$ 0.05 g.

A1.3 CALCULATION OF AVERAGE POWER INPUT AND AVERAGE AMBIENT TEMPERATURE BY PROGRAM "AVERAGE.FOR"

Figure A1.3 shows the variation of ambient temperature and fractional power input into the Controlled Chamber over the course of a run. The rise in ambient temperature is invariably due to the penetration of sun rays into the room and its "green house" effect. The fractional power input is seen to decrease when the ambient temperature is increased as a result of less heat loss from the Controlled Chamber to the surroundings. Under such circumstances, not all the result of the whole run will be utilised but only the part where the ambient temperature and the power input remain relatively constant, i.e. from 0 to 15 hours in the case of RUN HM3.

The program "AVERAGE.FOR" is used to determine an arithmetic

Fig. A1.3: Run HM3 Heat and Mass Transfer Across Horizontal Cavity.

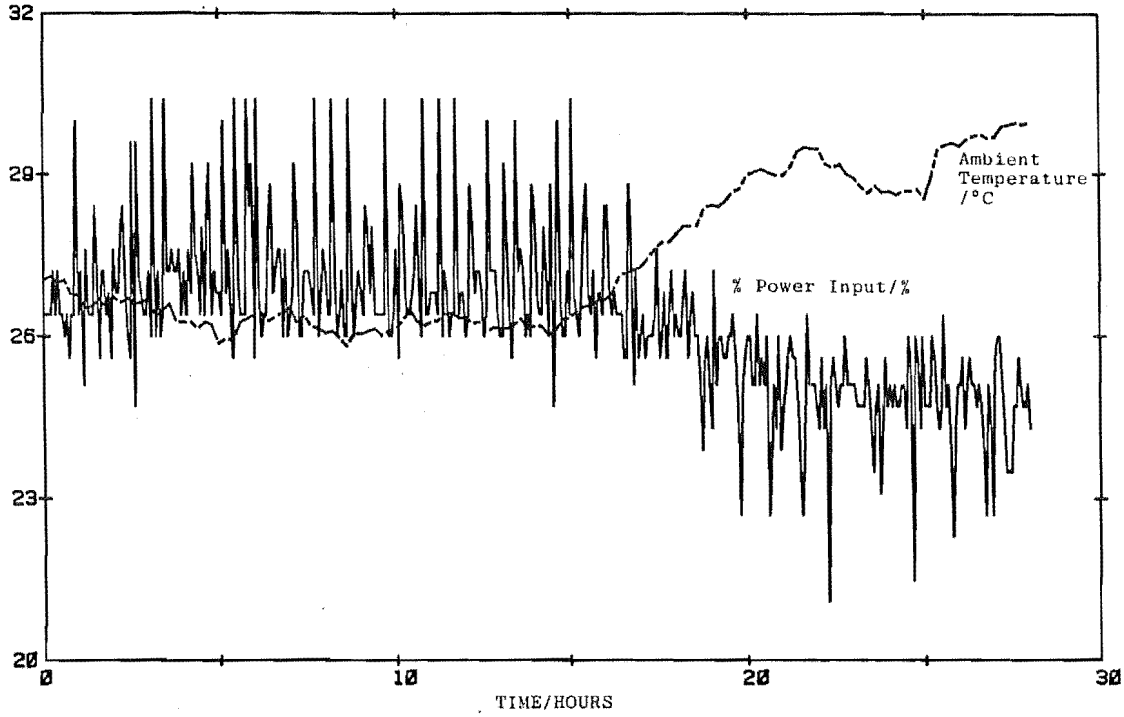

Fig. A1.4: Casella Chart.

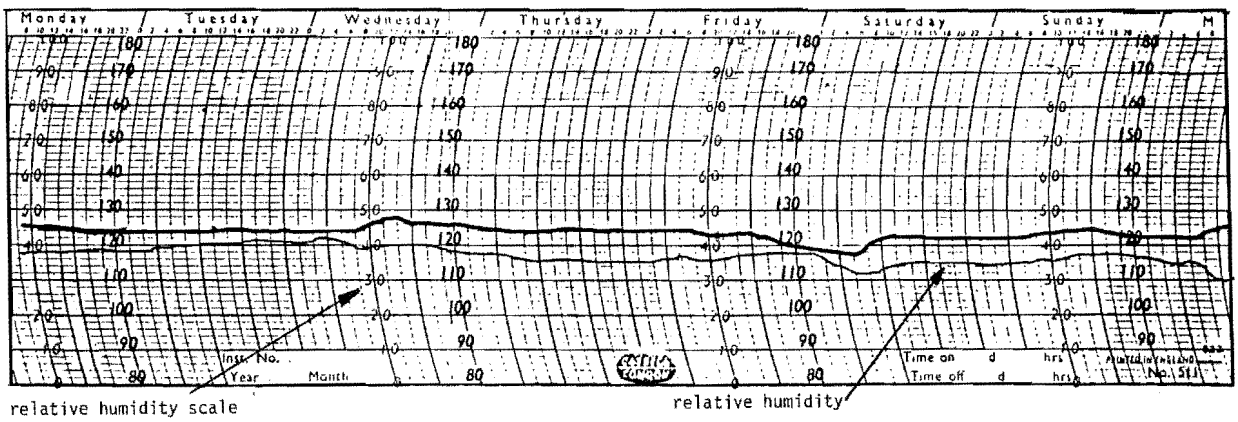

mean of the data points. The average quantities are:

$$\overline{(T_c - T_a)} = \frac{\sum_{i=1}^{n} (T_c)_i - (T_a)_i}{n} \qquad \text{(A1.1)}$$

$$\overline{P} = \frac{\sum_{i=1}^{n} P_i}{n} \qquad \text{(A1.2)}$$

where n is the number of data points over the course of a run,

T_c is the Controlled Chamber temperature,

T_a is the ambient temperature,

P is the power input indicated by the average power meter,

the overbars indicate averaged quantities and the summation is done over n sample points.

As $(T_c)_i$ is kept constant over the course of a run, Eq. A1.1 simplifies to:

$$\overline{(T_c - T_a)} = T_c - \frac{\sum_{i=1}^{n} (T_a)_i}{n} \qquad \text{(A1.3)}$$

as n is finite and the summation terms are convergent (p.4.8-3, reference [130]).

The program first reads the set of data and then the averaging is performed. A standard deviation term is also calculated to indicate the spread of the data (random error).

A1.4 CALCULATION OF AVERAGE AMBIENT RELATIVE HUMIDITY .

Figure A1.4 illustrates the graphical output of the Casella relative humidity recorder. This output is not logged by the VAX computer because there is no link between the two equipments. The averaging of the ambient relative humidity data is thus carried out

by a calculator with standard statistical function.

A1.5 CURVE FITTING OF EXPERIMENTAL DATA BY PROGRAM "POLYFIT".

The procedure of Polynomial Regression is used to fit a functional curve to the data points. First to ninth order regression is available, but the experimental data fall generally into either the zero, first or second-order polynomial function. The principle of the method is as follows:-

Suppose Y_i represents the ith observed dependent variables subjected to random error corresponding to X_i independent variables which are known precisely. We postulated that the variation of Y (the least-squares fit function of Y_i) and X_i can be described by the equation:

$$Y = a + b_1X + b_2X^2 + \ldots + b_nX^n \qquad \text{(A1.4)}$$

The coefficients a, b_1, b_2 ... b_b are obtained by minimising the sum of squares:

$$S = \sum_{i=1}^{m} (Y_i - a - b_1X_i - b_2X_i^2 - \ldots - b_nX_i^n)^2 \qquad \text{(A1.5)}$$

by making

$$\frac{\partial S}{\partial a} , \quad \frac{\partial S}{\partial b_1} , \ldots\ldots\ldots , \quad \frac{\partial S}{\partial b_n} \qquad \text{(A1.5a)}$$

and m is the total number of observations.
This results in n simultaneous equations which are solved by the Gauss-Jordan complete elimination method with maximum pivot strategy. This procedure together with:

$$a = [\sum_{i=1}^{m} (Y_i - b_iX^k)]/m \qquad \text{(A1.5b)}$$

where $X^k = X, X^2, \ldots\ldots, X^n$ as defined in Eq.A1.5; will return the parameters a, b_1, b_2, ... etc are returned together with an estimate of the error in the form of standard deviation "S_{m-2}",

$$\text{eg.} \quad S_{m-2} = \sqrt{\frac{[\sum_{i=1}^{m}(Y_i - a - b_i X^n)]}{m-2}}$$

for a linear least square fit for m data pivot.

In the "POLYFIT" program, the subroutine "REGR" is called to perform the n-th order regression while another subroutine "SIMULI" is called to solve the system of n simultaneous equations. A data-output option is also available to allow the plotting of the least-squares curve fit. A more detailed description on Regression can be found in the book of Carnahan et.al.[176].

A1.6 CALCULATION OF FINAL EXPERIMENTAL RESULTS BY PROGRAM HMTC

The program is summarised by the flow diagram in Figure A1.5. It is the main program which evaluates the final experimental results in the form of Nusselt, Sherwood numbers etc from the values obtained from Section A1.1 - A1.5 and other data measured.

The input data consisted of the following:

(i) Bulk air temperature in C.C. and R.C., T_c and T_r,

(ii) Plate surface temperature in C.C. and R.C., T_{cp} and T_{rp},

(iii) Bulk air humidity in C.C. and R.C., Y_c and Y_r,

(iv) Bulk air vapour pressure in C.C. and R.C., P_c and P_r,

(v) Ambient condition dry-bulb temperature and relative humidity, T_a and $(rh)_a$,

(vi) Gross mass transfer rate, m_T ,

(vii) Gross heat transfer rate, q_T ,

(viii) Heat transfer as a result of moisture transfer, q_m ,

(ix) Thermal emittance of moist air, e_g ,

(x) Cavity surface temperature, T_{cc} and T_{rc}.

Not all the above information is required all the time, and the interactive form of the program allows the easy input of the required data. Other constant values need, such as the universal

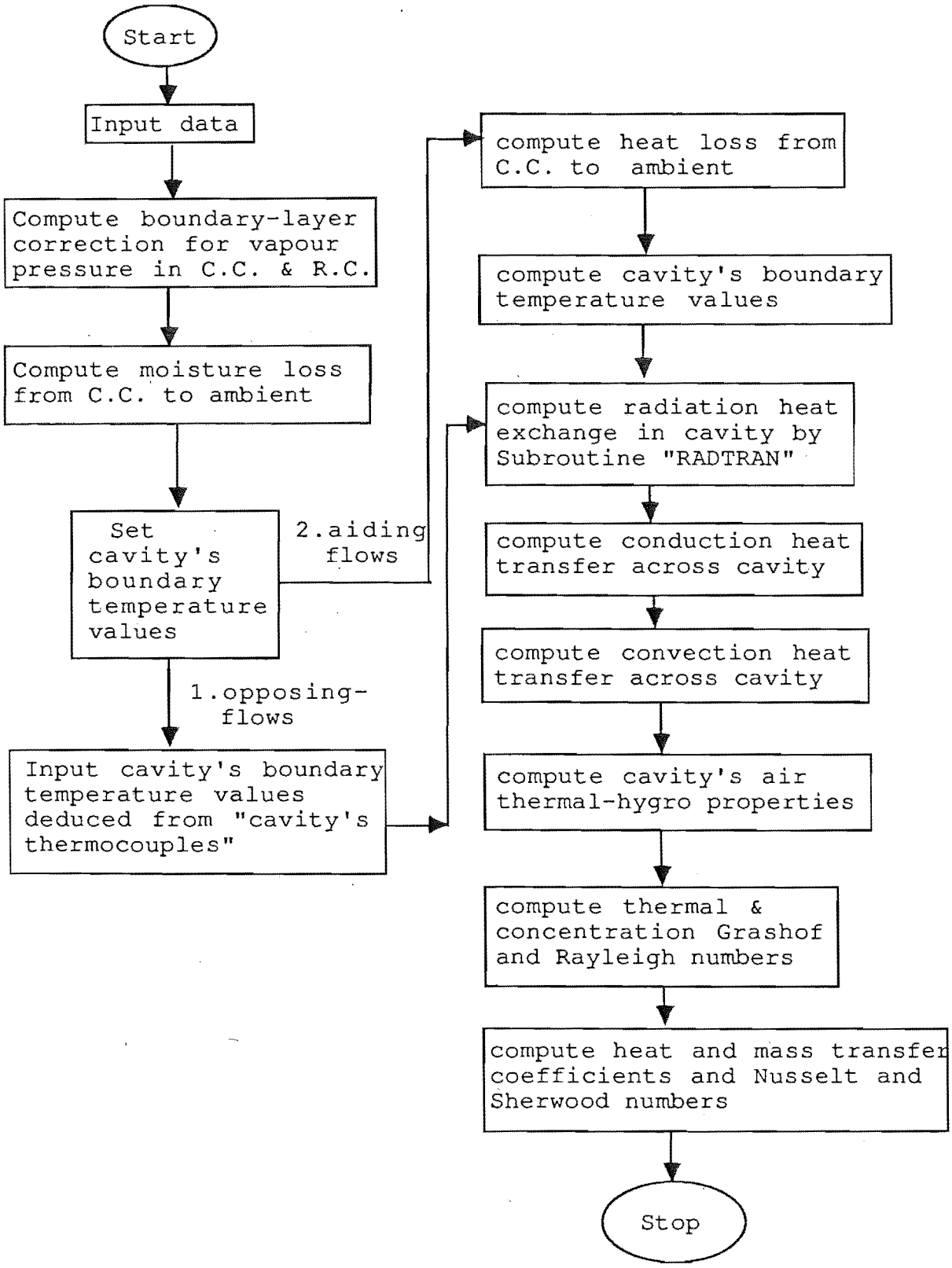

Fig. A1.5 Flow-diagram for the Program "HMTC"

gas constant and total air pressure, are incorporated as part of the program and need not be input.

The first section of the program evaluates the boundary-layer depression due to the concentration boundary layer in the Controlled and Receiving Chamber. This calculation procedure is based on the analogy between turbulent heat and mass transfer suggested by Chilton and Colburn [177] who proposed, in effect, that the heat-transfer coefficient in $Wm^{-2}K^{-1}$ has approximately the same numerical magnitude as the mass-transfer coefficient in units of $gm^{-2}s^{-1}$ for mixtures of air and water vapour.

The heat-transfer coefficient was determined from a "practical" correlation proposed by Treybal[178], which is applicable for heat transfer in dryers with consideration for the air being deflected by baffles and internal heating coils, a condition similar to that found in the Controlled and Receiving Chamber.

The correlation is:

$$Nu_L = 0.055\ (Re_L)^{0.8} \qquad \text{(A1.6)}$$

where Nu_L is the Nusselt number = hL/k

and Re_L is the Reynolds number = uL/υ

The characteristic swept length L used in Equation A1.6 is the length of the porous plastic plate (= 0.7 m). The air velocities in the Controlled and Receiving Chambers are measured to be about 1.2 and 1.5 ms^{-1} respectively.

Other transport properties needed for the evaluation of Nu_L and Re_L are evaluated at the mean temperature level between the bulk air (T_c and T_r) and plate surface temperature (T_{cp} and T_{rp}). The subroutine "SOLVE1" in program "HMTC.FOR" calculated the dynamic viscosity, thermal conductivity and Prandtl number for the appropriate condition. These transport properties are evaluated for dry air only at 101 kPa and the data are obtained from Kay [179]. Kusada [180] has calculated both the dry and completely saturated air transport properties between 10 and 60 °C. The moisture saturated air properties are evaluated by an empirical correlation given by Cheung et.al.. The maximum differences

between these two limits are 0.3%, 0.6% and 2.37% for thermal conductivity, dynamic viscosity and Prandtl number respectively at the temperature of 50 °C. At the temperature of 20 °C, the corresponding differences are only 0.1%, 0.29 and 0.49% respectively. The Prandtl number is used later to correlate the experimental Nusselt number against Rayleigh number for natural convective flow in the cavity and has only a slight effect on Nu ($Nu \propto (Pr)^{0.3}$ approximately); the use of dry air transport properties is thus sufficient. Moreover, the maximum relative humidity level encountered in the experiments was only about 70 percent and accounted for less than 10 percent of the experimental conditions; which suggested that the difference between the moist air and dry air transport properties for 100 percent relative humidity change quoted by Kusada[180] to be an overestimate of the difference that would be expected in actual experimental conditions.

The forced heat-transfer coefficients are found to be about 12.4 $Wm^{-2}s^{-1}$ for the Controlled Chamber and 15.2 $Wm^{-2}s^{-1}$ for the Receiving Chamber. Thus the corresponding mass transfer coefficients are 12.4 $gm^{-2}s^{-1}$ and 15.2 $gm^{-2}s^{-1}$ respectively. The relationship:

$$m = K_c A_q (Y_c - Y_{cp}) \qquad (A1.7)$$

is used to evaluate the bounding humidity Y_{cp},

where m = rate of moisture transfer across porous plate,

K_c = mass transfer coefficient,

Y_c = bulk air humidity ,

Y_{cp} = boundary humidity on the porous plate at the C.C. side,

and A_q = cross sectional area of the porous plate.

The perfect gas assumption is then used to calculate the boundary vapour pressure from the absolute humidity value (e.g. see Keey [181]):

$$P_{cp} = \frac{Y_{cp} P_T}{Y_{cp} + D_m} \qquad (A1.8)$$

where P_{cp} = vapour pressure at the boundary of the porous plastic on the Controlled Chamber side,

P_T = total pressure,

and D_m = molar mass ratio of water vapour and air = 0.622.

Similarly for the receiving chamber:

$$m = K_r A_q (Y_{rp} - Y_r) \qquad \text{(A1.9)}$$

and

$$P_{rp} = \frac{Y_{rp} P_T}{Y_{rp} + D_m} \qquad \text{(A1.10)}$$

The quantities $(P_c - P_{cp})$ and $(P_{rp} - P_r)$ thus constitute the boundary layer depression in C.C. and R.C. respectively.

The next block of the program calculates the moisture loss m_l from the Controlled Chamber to the ambient. The parameters needed here are the difference in vapour pressure between C.C. and ambient, i.e. $(P_c - P_a)$ and the "loss" equation determined from Section 5.3. The difference between the gross moisture transfer rate m_T recorded by the balance and the loss m_l gives the nett rate of moisture transfer through the porous plastic plate.

The next block of program calculates the boundary conditions in the cavity for the vapour pressure values. The relevant information needed is the moisture diffusion resistance of porous plastic plate (from Section 5.4.2) and the boundary layer correction in C.C. and R.C. calculated earlier.

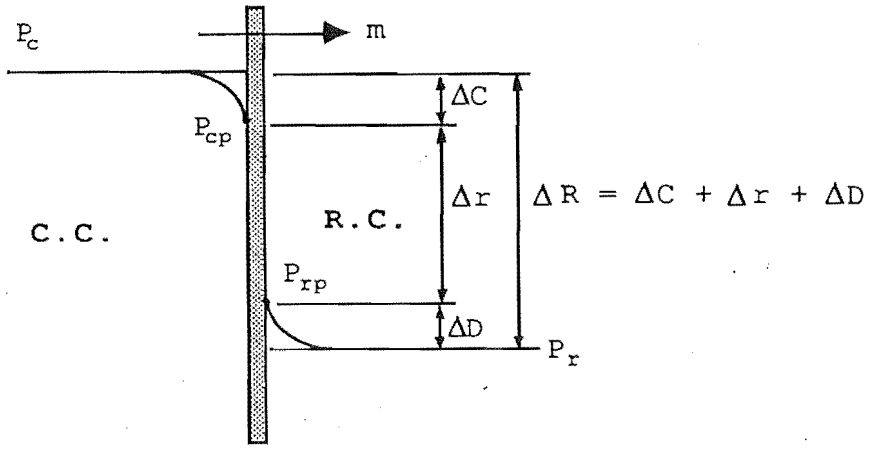

ΔC, Δr, ΔD and ΔR are resistance values.

P_c , P_{cp} , P_{rp} and P_r are vapour pressure values

m is the moisture transfer rate.

Fig A1.6 One Porous Plate Test

From tests on one porous plate:

$$m = \frac{P_c - P_r}{\Delta R} = \frac{P_{cp} - P_{rp}}{\Delta r} \qquad \text{(A1.11)}$$

$$\Delta R = \frac{P_c - P_r}{m} = \frac{(P_c - P_{cp}) + (P_{cp} - P_{rp}) + (P_{rp} - P_r)}{m}$$

$$= \Delta C + \Delta r + \Delta D \qquad \text{(A1.12)}$$

Plots of m versus $(P_c - P_r)$ and m versus $(P_{cp} - P_{rp})$ are given in Chapter 6.

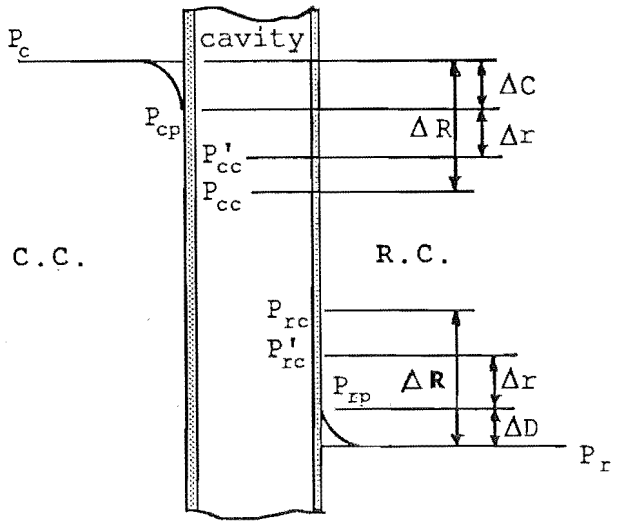

$P'_{cc} = P_{cp} - m\,\Delta r$

$P'_{rc} = P_{rp} + m\,\Delta r$

Δr is obtained from Chapter 6

Total resistance
$=2\,\Delta r + \Delta C + \Delta D$
for transfer from C.C.to R.C.

Fig. A 1.7

Alternatively, and P_{rc} can also be calculated from:

$$P'_{cc} = P_{cp} - m\,\Delta r$$

$$= P_{cp} - m\,(\Delta R - \Delta C - \Delta D)$$

$$= P_c - m\,\Delta R + m\,\Delta D$$

$$= P_{cc} + m\,\Delta D$$

$$= P_{cc} + (P_{rp} - P_r) \qquad \text{(A1.13)}$$

similarly:

$$P'_{rc} = P_{rc} - (P_c - P_{cp}) \qquad \text{(A1.14)}$$

and $$P'_{cc} - P'_{rc} = (P_{cc} - P_{rc}) + (P_c - P_{cp}) + (P_{rp} - P_r) \qquad \text{(A1.15)}$$

where P_{cc} and P_{rc} are calculated from bulk air measurement only, i.e P_c and P_r.

The next step of the program is to calculate the cavity's boundary temperature value. Essentially the same principle as that employed for finding cavity's boundary vapour pressure is used. First the heat loss from C.C. to ambient q_1 is evaluated by the heat loss-equation derived from Section 5.2 and given in Chapter 6. The difference between the total heat input and the heat loss from the Controlled Chamber to the surroundings thus gives the heat transfer through the porous plate(q_p) and hence through the cavity. Knowing the boundary temperature at the porous plate surfaces on

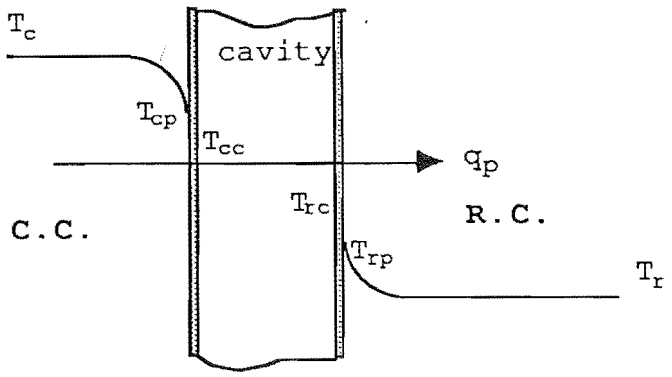

Fig. 1.8 Determination of Cavity Boundary Temperature.

the Controlled and Receiving Chambers sides, the boundary temperature on the porous plate surfaces, on the cavity sides can be calculated as:

$$T_{cc} = T_{cp} - \frac{q_p \, \Delta X}{k \, A_q} \qquad \text{(A1.16)}$$

and

$$T_{rc} = T_{rp} - \frac{q_p \, \Delta X}{k \, A_q} \qquad \text{(A1.16)}$$

where k = thermal conductivity of porous plastic (found from Section 5.4.1. and given in chapter 6),

ΔX = distance between thermocouple points = 4×10^{-3} m*

*Notes: The depths to which the thermocouple junctions are inserted into the porous plastic are different for the case of one porous plate and the case of air cavity as illustrated in Fig.A1.9.

The reason for the change to embedded thermocouples is simply to prevent the thermocouples from falling off from the porous plate as had happened for the case of a single porous plate. The thermal conductivity of the brass rings is 22 $Wm^{-1}K^{-1}$ and can be considered

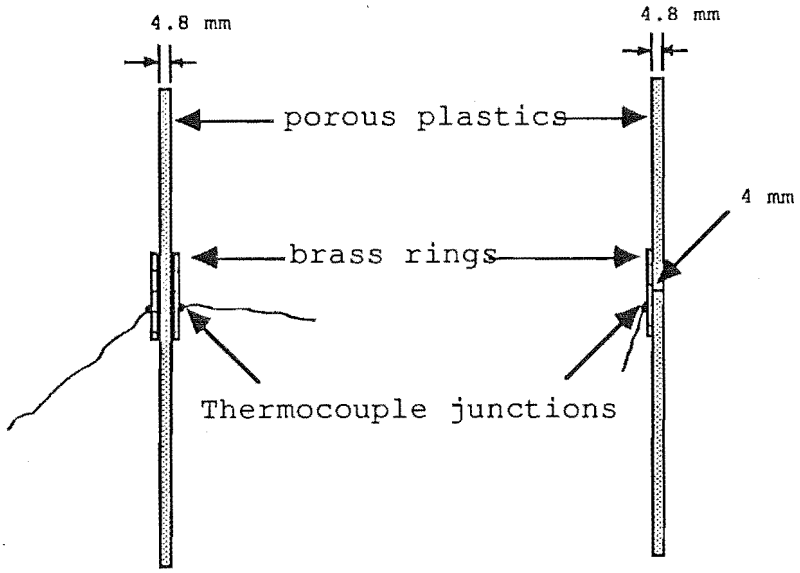

Fig. A1.9

One porous plate case

brass-rings are flushed against surface and ΔX=4.8 mm

Cavity case

brass-rings are embedded 0.75mm into the porous plastic and ΔX=4.0mm.

as an isothermal mass when compared with the thermal conductivity of porous plastic plate = 0.06 $Wm^{-1}K^{-1}$.

As shown on Figure A1.5, the cavity's boundary temperature values can also be specified by using the readings from the "cavity thermocouples" (Section 4.4.5). But as has been explained earlier, "cavity thermocouples" are always less satisfactory in indicating the cavity's boundary temperature values because they always give temperature levels that suggest more heat is transferred across the cavity than the measured value of q_p from heat-balance considerations. The readings are only used for the cases of opposing heat and moisture transfer, when the cavity's boundary temperatures cannot be calculated as stated in Section 5.6. In such cases, Figure A1.10 is used to deduce the reverse cavity temperature gradient.

The next main step of the program is to calculate the heat transfer across the cavity by thermal radiation q_r and by conduction along the solid adjoining member of the cavity q_c so that the portion of heat transfer by natural convection can be isolated (see eg. Section 5.10).

Fig. A1.10: CALIBRATION CURVE FOR 'CAVITY THERMOCOUPLES'

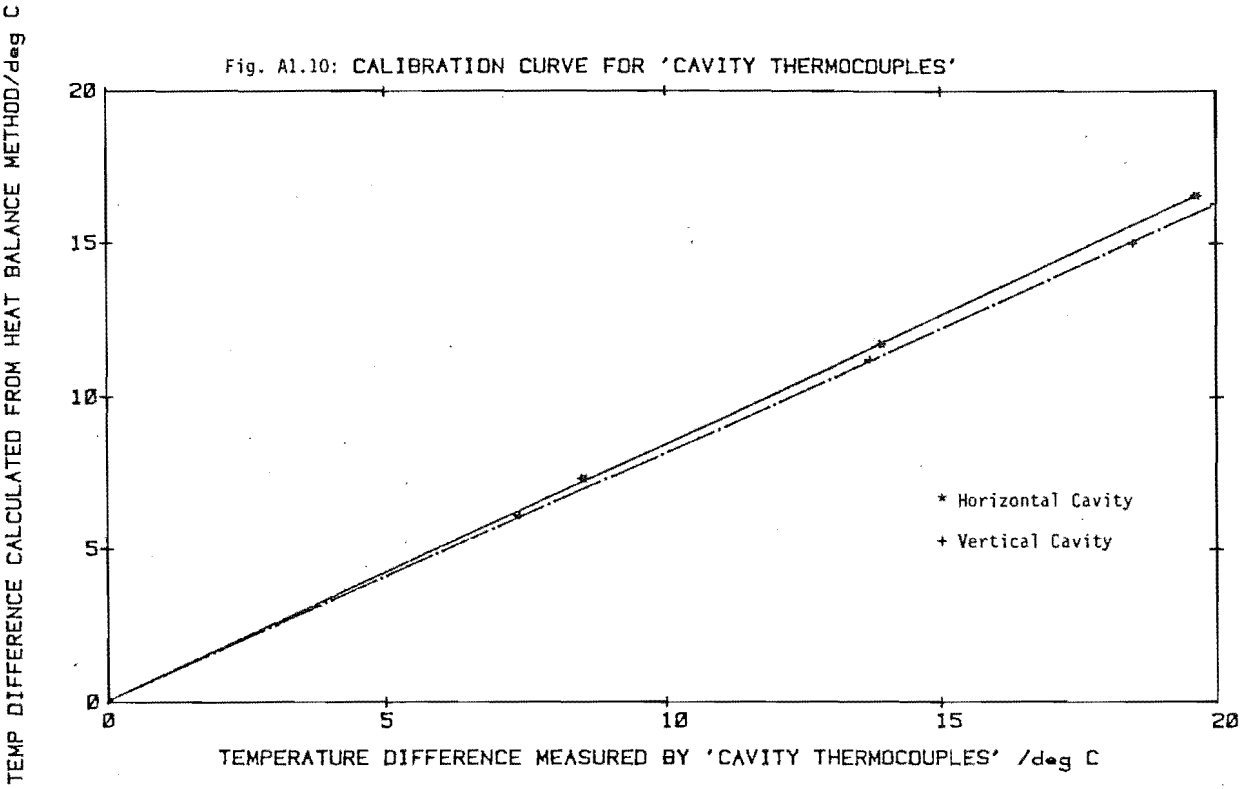

The procedure to calculate the radiation in an absorbing medium is done by subroutine "RADTRAN.FOR". As it is rather elaborate and lengthy, the details of the calculation is given separately in Appendix 2.

The procedure to calculate conduction heat transfer across the cavity by solid joint member is:

$$q_c = k_p A_c \frac{\Delta T}{\Delta X} \qquad \text{(A1.18)}$$

where kp = thermal conductivity of perspex = 0.193 $Wm^{-1}K^{-1}$,

A_c = cross sectional area of perspex = 0.0168 m^2,

ΔX = cavity gap width = 0.1 m,

ΔT = cavity boundary temperature difference.

The hygrothermal properties of the air in the cavity are then evaluated at its mean temperature = $(T_{cc} + T_{rc})/2.0$. As stated earlier in this section, the dynamic viscosity, thermal conductivity and Prandtl number are evaluated for dry air conditions only. Other quantities such as bulk air density and of course moisture concentration are calculated for the moist-air mixture.

To determine total moist air density, we define 1 kg basis of moist air of humidity Y kg water vapour/kg dry air :

$$\text{1 mole of dry air} = 1/M_G \qquad \text{(A1.19)}$$

$$\text{1 mole of water vapour} = Y/M_W \qquad \text{(A1.20)}$$

where M_G and M_W are the molar mass of dry air and water vapour respectively.

$$\text{Total amount of substance } n_T = 1/M_G + Y/M_W \qquad \text{(A1.21)}$$

Assume perfect gas behaviour:

$$P_T V = n_T R T \qquad \text{(A1.22)}$$

where P_T = total gas pressure, Pa,

V = total volume, m^3,

R = universal gas constant = 8314 J/kmol K,

T = temperature, K.

Then,

$$V = n_T \, R \, T / P_T$$

$$= \frac{8314 \cdot (1/M_G + Y/M_W) \cdot T}{101325} \quad m^3 \qquad \text{(A1.23)}$$

for P_T = atmospheric pressure at 101325 Pa.

$$\therefore \quad \rho_T = m_T / V = (1+Y)/V \quad Kgm^{-3} \qquad \text{(A1.24)}$$

where V is given by equation A1.23 and m_T is the total amount of substance in Kg.

Equation A1.24 yields lower bulk air density values ρ_T when the corresponding humidity values Y are higher, ie. moist air is lighter than dry air at the same temperature.

To determine the moisture concentration of water vapour ρ_W (kg water vapour /m^3 moist air) the following calculation procedure is adopted.

$$C_W / C_T = P_W / P_T \qquad \text{(A1.25)}$$

where C_W = moles of moisture in unit volume,

C_T = total moles of moisture and air in unit volume,

P_W = partial vapour pressure of water vapour, Pa,

and P_T = total pressure of moisture and air, Pa.

Now,

$$C_i = W_i / M_i \qquad \text{(A1.26)}$$

where W_i = mass of substance i in volume V,

and M_i = molar mass of substance i in volume V.

$$\therefore \quad \frac{C_W}{C_T} = \frac{P_W}{P_T} = \frac{W_W \, M_T}{W_T \, M_W} \approx \frac{W_W}{W_T \, D_m} \qquad \text{(A1.27)}$$

if we assume that $M_T = M_G$ for the small humidity levels encountered in this work (Y_{max} = 0.028 kg kg^{-1}).

where $D_m = M_W / M_G \approx 0.622$.

$$\therefore \quad W_W = \frac{P_W}{P_T} W_T D_m$$

$$\therefore \quad \rho_W = \frac{W_W}{V} = \frac{P_W W_T}{P_T V} D_m$$

$$= \frac{P_W}{P_T} \rho_T D_m \qquad \text{(A1.28)}$$

For moisture air, volume V is calculated from Eq.A1.23 and ρ_T is calculated from Eq.A1.24). To eliminate P_W and P_T from Eq.A1.28, we use the perfect gas assumption to obtain the expression:

$$\therefore \quad Y = \left(\frac{P_W}{P_T - P_W}\right) D_m \qquad \text{(A1.29)}$$

and $$P_W = \frac{\rho_W}{\rho_T D_m} P_T \quad \text{from Eq A1.28}$$

On substituting Eq.A1.30 into Eq.A1.29, we obtain:

$$\therefore \quad \rho_W = \frac{Y \rho_T}{(1 + Y/D)} \qquad \text{(A1.31)}$$

As each boundary of the cavity is at different temperature and humidity levels from each other, we have:

$$\rho_{WC} = \frac{Y_{CC} \rho_{TCC}}{(1 + Y_{CC}/D)} \quad \text{for Controlled Chamber side} \qquad \text{(A1.32)}$$

and $$\rho_{Wr} = \frac{Y_{rc}\ \rho_{Trc}}{(1 + Y_{rc}/D)} \quad \text{for Receiving Chamber side} \qquad (A1.33)$$

Next the program computer the dimensionless numbers:

$$Gr_T = \frac{g\ \beta\ \Delta T\ L^3}{\upsilon^2} \quad \text{(Thermal Grashof number)} \qquad (A1.34)$$

$$Gr_C = \frac{g\ \beta_C\ \Delta C\ L^3}{\upsilon^2} \quad \text{(Concentration Grashof number)} \qquad (A1.34)$$

where $\Delta T = T_{cc} - T_{rc}$ from Eqs. A1.16 and A1.17,

$\Delta C = \rho_{WC} - \rho_{Wr}$ from Eqs. A1.32 and A1.33,

$\beta = 1/T$; T in degree Kelvin using perfect gas assumtion,

$$\beta_C = \frac{1}{\rho_T}\left(\frac{M_G}{M_W} - 1\right) \quad \text{using perfect gas assumtion,}$$

and L = cavity gap width.

Further,

$$Ra_T = Gr_T\ Pr \quad \text{(Thermal Rayleigh number)} \qquad (A1.36)$$

$$Ra_C = Gr_C\ Sc \quad \text{(Concentration Rayleigh number)} \qquad (A1.37)$$

and for the case of combined heat and moisture transfer, a combined Rayleigh number defined as :

$$(Ra)_{T,C} = Ra_T + Ra_C \qquad (A1.38)$$

is used.

These dimensionless numbers place the respective driving forces due to temperature and concentration difference on an equal footing, thus allowing their relative "strengths" to be compared.

Finally the program computes the overall heat and mass-transfer coefficients across the air cavity and the corresponding Nusselt and Sherwood numbers.

The overall heat transfer coefficient is calculated from:

$$h = \frac{q}{A_q \, (T_{cc} - T_{rc})} \qquad \text{(A1.39)}$$

where q = heat transfer by natural convection + gas conduction

$= q_p - q_c - q_r$

The rest of the symbols have been defined before.

The Nusselt number is calculated from:

$$Nu = \frac{h \, L}{k} \qquad \text{(A1.40)}$$

where k = thermal conductivity of air,

and L = cavity gap width

Nu gives the ratio of convection heat transfer to heat transfer by conduction in the fluid.

The overall mass transfer coefficient is calculated from :

$$K = \frac{m}{A_q \, (Y_{cc} - Y_{rc})} \qquad \text{(A1.41)}$$

where $m = m_T - m_l$

and the rest of the symbols are as defined before.

The Sherwood number is calculated from:

$$Sh = \frac{K \, L}{D \, \rho_T} \qquad \text{(A1.42)}$$

where D = moisture vapour diffusion coefficient,

and ρ_T is evaluated from Eq. A1.24 at temperature

$(T_{cc} + T_{rc})/2.0$.

APPENDIX 2

RADIATION HEAT TRANSFER BETWEEN TWO POROUS PLATE SURFACES IN THE CAVITY.

Thermal radiation has been assumed to occur independently across the cavity and has no effect on the gas conduction and convection which are occuring simultaneously (Sections 1.1.1 and 2.6). However, for better energy balance in the experimental data, the absorptive effect of the water vapour in the air is incorporated in the following calculational procedure. This effect is nearly negligible for the conditions encountered in this work, as can be seen later from the small values of thermal absorbance and emittance obtained. This is a direct consequence of the small humidity level of the air in the cavity. In such cases, the calculational procedure merely reduces back to the case for thermal radiation in a non-absorbing medium.

A 2.1 METHODOLOGY.

The physical situation for thermal radiation in the cavity is depicted in Fig A.2.1, with the following assumptions :-

(i) All the surfaces and the gas exhibit grey body characteristics and the radiation properties are uniform over the entire wavelength range of radiation;

(ii) All surfaces are diffuse;

(iii) Side walls are adiabatic.

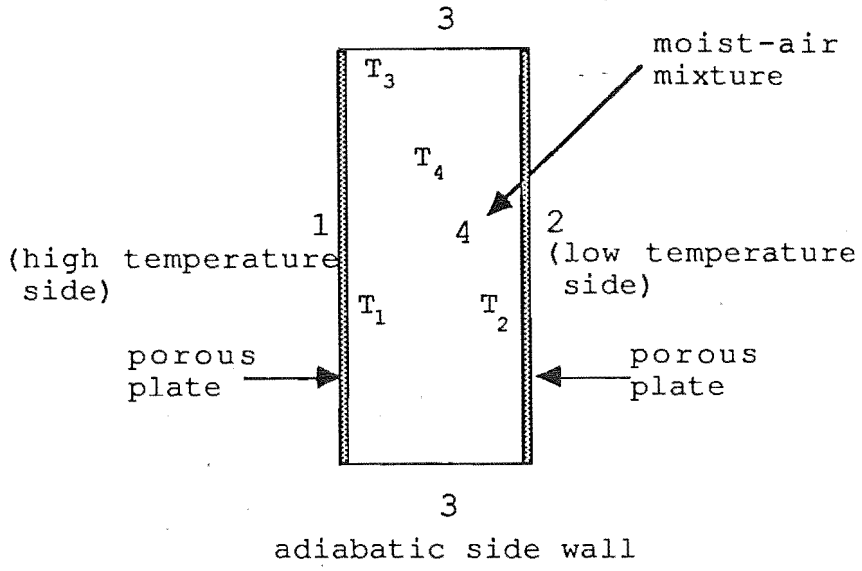

Fig. A 2.1 Radiation Heat Transfer in the Cavity.

Define :

e = thermal emittance,

A_q = area of radiation exchange,

E_b = blackbody radiation power = σT^4,

s = Stefan Boltzman constant= 5.67×10^{-8} $Nm^{-2}K^{-4}$,

F_{ij} = shape factor for radiation from surface i to surface j,

J = radiocity; the rate at which radiation leaves a given surface per unit area, (see Kreith[182])

r = reflectance,

G = Irradiation or radiation per unit time incident on unit surface area,

Subscripts 1, 2, 3 and g refers to surfaces 1, 2, 3 and gas as depicted in Fig A.2.1.

An equivalent network analysis is used and Fig A.2.1 can be represented by the network in Fig A.2.2 (See Kreith [182] Chapter 5 for details).

As no net heat transfer occured at nodes (3) and (4), they act as floating potential whose values (emissive power and temperature) depends only on the relative values of the resistances between the various nodal points i.e. R_1 and R_7 .

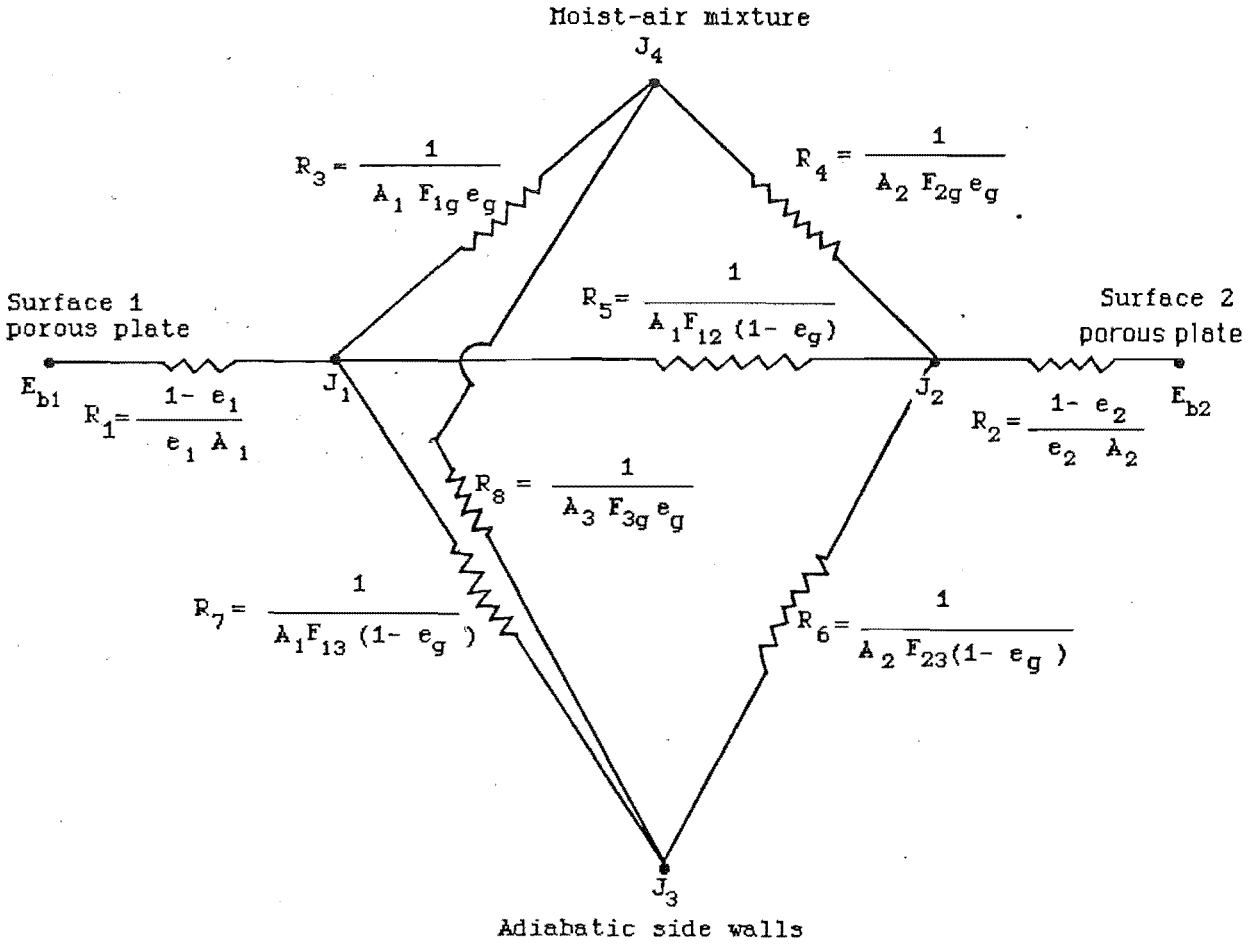

Fig. A2.2 Equivalent Network for Radiation in the Cavity.

$\frac{1 - e_i}{e_i A_i}$ is the surface resistance of surface i

$\frac{1}{A_1 F_{12} (1-e_g)}$ is the resistance to radiation leaving surface 1 and reaching surface 2 in the presence of the gas which has emittance E_g.

$\frac{1}{A_1 F_{1g} e_g}$ is the resistance to radiation leaving surface 1 and absorbed by the gas 3.

The Reciprocity Theorem :

$$A_i F_{ij} = A_j F_{ji}$$

has been employed in deriving the various resistances in Fig A.2.2.

The idea of the network analysis is to solve J_1, J_2, J_3 and J_4 so that the heat transfer by radiation leaving surface 1 (which is equal to the heat received by surface 2) can be calculated. To achieve this we apply Kirchoff's current law at each node and note that the sum of the current entering a given node is zero.
For example for J_1:

$$\frac{E_{b1} - J_1}{R_1} = \frac{J_1 - E_{bg}}{R_3} + \frac{J_1 - J_2}{R_5} + \frac{J_1 - J_3}{R_4}$$

The resultant set of simultaneous equations is :-

$$A_{11}J_1 + A_{12}J_2 + A_{13}J_3 + A_{14}J_4 = B_1 \qquad (A2.1)$$

$$A_{21}J_1 + A_{22}J_2 + A_{23}J_3 + A_{24}J_4 = B_2 \qquad (A2.2)$$

$$A_{31}J_1 + A_{32}J_2 + A_{33}J_3 + A_{34}J_4 = B_3 \qquad (A2.3)$$

$$A_{41}J_1 + A_{42}J_2 + A_{43}J_3 + A_{44}J_4 = B_4 \qquad (A2.4)$$

where :

$$A_{11} = \left(\frac{1}{R_1} + \frac{1}{R_3} + \frac{1}{R_5} + \frac{1}{R_7} \right)$$

$$A_{12} = \frac{-1}{R_7}$$

$$A_{13} = \frac{-1}{R_7}$$

$$A_{14} = \frac{-1}{R_3}$$

$$A_{21} = \frac{-1}{R_5}$$

$$A_{22} = \left(\frac{1}{R_5} + \frac{1}{R_4} + \frac{1}{R_8} + \frac{1}{R_2}\right)$$

$$A_{23} = \frac{-1}{R_8}$$

$$A_{24} = \frac{-1}{R_4}$$

$$A_{31} = \frac{-1}{R_7}$$

$$A_{32} = \frac{-1}{R_8}$$

$$A_{33} = \left(\frac{1}{R_8} + \frac{1}{R_7} + \frac{1}{R_6}\right)$$

$$A_{34} = \frac{-1}{R_6}$$

$$A_{41} = \frac{-1}{R_3}$$

$$A_{42} = \frac{-1}{R_4}$$

$$A_{43} = \frac{-1}{R_6}$$

$$A_{44} = \left(\frac{1}{R_3} + \frac{1}{R_4} + \frac{1}{R_6}\right)$$

$$B_1 = \frac{Eb1}{R1}$$

$$B_2 = \frac{Eb2}{R1}$$

$$B_3 = 0$$

$$B_4 = 0$$

Equations (A2.1) to (A2.4) can be written in terms of matrix notation as :-

$$[A]\ [J] = [B] \qquad \text{(A2.5)}$$

A matrix inversion technique is needed to find the inverse of $[A] = [A]^{-1}$ and the solution for the radiosities is given by :-

$$[J] = [A]^{-1}[C] \qquad \text{(A2.6)}$$

The inverse of matrix [A} is a matrix having the elements :-

$$[A]^{-1} = \begin{bmatrix} C_{11} & C_{12} & C_{13} & C_{14} \\ C_{21} & C_{22} & C_{23} & C_{24} \\ C_{31} & C_{32} & C_{33} & C_{34} \\ C_{41} & C_{42} & C_{43} & C_{44} \end{bmatrix} \qquad \text{(A2.7)}$$

and the solution for the radiosities can be written as :

$$\begin{aligned} J_1 &= C_{11}B_1 + C_{12}B_2 + C_{13}B_3 + C_{14}B_4 \\ J_2 &= C_{21}B_1 + C_{22}B_2 + C_{23}B_3 + C_{24}B_4 \\ J_3 &= C_{31}B_1 + C_{32}B_2 + C_{33}B_3 + C_{34}B_4 \\ J_4 &= C_{41}B_1 + C_{42}B_2 + C_{43}B_3 + C_{44}B_4 \end{aligned} \qquad \text{(A2.8)}$$

A discussion on Matrix Inversion can be found in Carnahan et al [176] pp 271 - 296. The heat transfer across the cavity is then computed as the heat received by surface 2

$$= (J_1 - J_2)\ A_1\ F_{12}\ (1-E_g) + (J_3 - J_2)\ A_3\ F_{32}\ (1-E_g) + (J_4 - J_2)\ A_2\ F_{2g}\ E_g \qquad (A2.9)$$

A.2.2 NUMERICAL VALUES USED IN CALCULATIONS.

Figures from Kreith [182] are reproduced here for easy reference. The numbering of these figures directly corresponds to those used in Kreith.

A2.2.1 Thermal Emittances

(i) Porous plastic plate : smooth side = 0.77 (A2.10)

rough side = 0.73 (A2.11)

(see Section 5.4.3 of this work)

(ii) Moist-air mixture :-

The procedure adopted here is given by Kreith [192] pp. 273 - 283:

(a) Determine the average length of radiant beam, L_r

$Lr = 1.8 \times L$ (Table 5 - 7, no. 3)

$= 0.59$ ft

where L is the cavity gap width = 0.1 m = 0.328 ft.

(b) Determine average cavity temperature:

$$T_{cavity} = (T_{cc} + T_{rc})/2 \qquad (A2.12)$$

(c) Determine average cavity vapour pressure:

$$P_{cavity} = (P_{cc} + P_{rc})/2 \qquad (A2.13)$$

(d) Determine total pressure in cavity:

P_T = 1 atmosphere (101325 Pa) in all cases

NB: The maximum percentage error in P_T = 1 atm when compared with actual measurement of atmospheric pressure in the laboratory over a 20 day period from 20 May to 10 June 1985 is $\pm$ 2.5%, a value much lower than the uncertainty of

reading Fig 5.37 to determine the correction factor C_p.

(e) Determine correction factor C:

Using P_{cavity} and P_T and Fig 5.37, $C_p = 1.0$ (approximately) in all cases.

(f) Determine gas emittance eg:

The gas is absorbing radiation at temperature T_1, T_2 and T_3 and it is emitting radiation at temperature T_g. But as the differences between T_1, T_2 or T_3 and T_g is small (maximum value (T_1, T_2 or T_3) - T_g = 10°C), e_g will be evaluated at the mean temperature in the cavity T_{cavity} determined from Eq. A2.11.

The beam length of radiation $= P_{cavity} \times L_r$

$= P_{cavity} \times 0.59$ ft atm.

Using T_{cavity} and the beam length of radiation and Fig 5.35, e'_g can be found.

(g) Corrected value for gas emittance:

$$e_g = C_p \times e'_g \qquad \text{(A2.14)}$$

A.2.2.2 Area for Radiation Exchange

$$A_1 = A_2 = 0.7 \times 0.7 \text{ m}^2 = 0.49 \text{ m}^2 \qquad \text{(A2.15)}$$

$$A_3 = (0.1 \times 0.7) \times 4 \text{ m}^2 = 0.28 \text{ m}^2 \qquad \text{(A2.16)}$$

where A_1, A_2 = area of porous plastic plate,

A_3 = area of adiabatic side walls;

(for nomenclature, see Fig A2.1)

A2.2.3. Shape Factors

A2.2.3.1 Between surfaces 1 and 2. Two parallel and equal

squares of sides 0.7 m, a distance of 0.1 m apart.

From Fig 5-22, ratio of $\frac{\text{small side}}{\text{distance apart}} = 7.0$;

we obtain, $F_{12} = 0.9$ using curve 6.

As $A_2F_{12} = A_2F_{21}$ and $A_1 = A_2$,

we obtain, $F_{21} = 0.9$. (A2.17)

Similarly from $F_{12} + F_{13} = 1.0$,

we obtain, $F_{13} = 0.1$ and $F_{23} = 0.1$ (A2.18)

Also as $F_{1g} = F_{2g} = F_{3g} = 1.0$ and $A_1F_{13} = A_3F_{31}$ (A2.19)

therefore, $F_{31} = A_1/A_3 \; xF_{13} = 0.175 = F_{32}$ (A2.20)

and $F_{33} = 1 - F_{31} - F_{32} = 0.65$ (A2.21)

To cross check the validity of the above values, Fig 5.21 can also be used to evaluate the shape factor F_{1-3} independently,

$F_{1-3} = 0.025$

which for 4 side walls for a cavity

F_{1-3} (total) = 0.1 as before.

Equations A2.10 to A2.21 are used to determine the various resistances of Fig A2.2 which are in turn used to determine the elements of matrix [A] in Eq. A2.9.

The procedure outlined above is programmed in "RADTRAN.FOR" with a subroutine "MATINV.FOR" to perform the matrix inversion process. "RADTRAN.FOR" is itself a subroutine of program "HMTC.FOR" as described in Appendix 1.

Figures from Kreith [182] :-

Table 5-7. Average lengths of radiant beams in various gas shapes.

Shape	L
1. Sphere	$\frac{2}{3}$ × diameter
2. Infinite cylinder	1 × diameter
3. Space between infinite parallel planes	1.8 × distance between planes
4. Cube	$\frac{2}{3}$ × side
5. Space outside infinite bank of tubes with centers on equilateral triangles; tube diameter equals clearance	2.8 × clearance
6. Same as (5) except tube diameter equals one-half clearance	3.8 × clearance

SOURCE: Ref. 14.

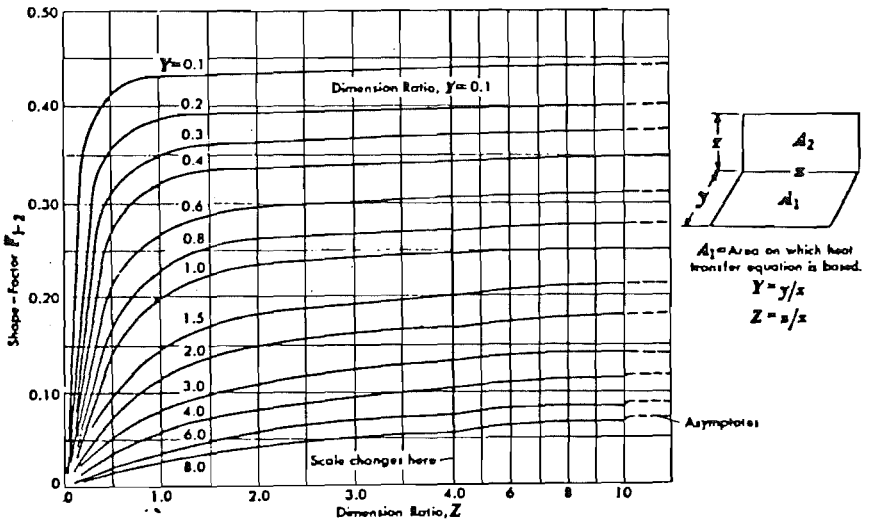

Fig. 5-21. Shape factor for adjacent rectangles in perpendicular planes. (By permission from H. C. Hottel, "Radiant Heat Transmission," *Mechanical Engineering*, Vol. 52, 1930.)

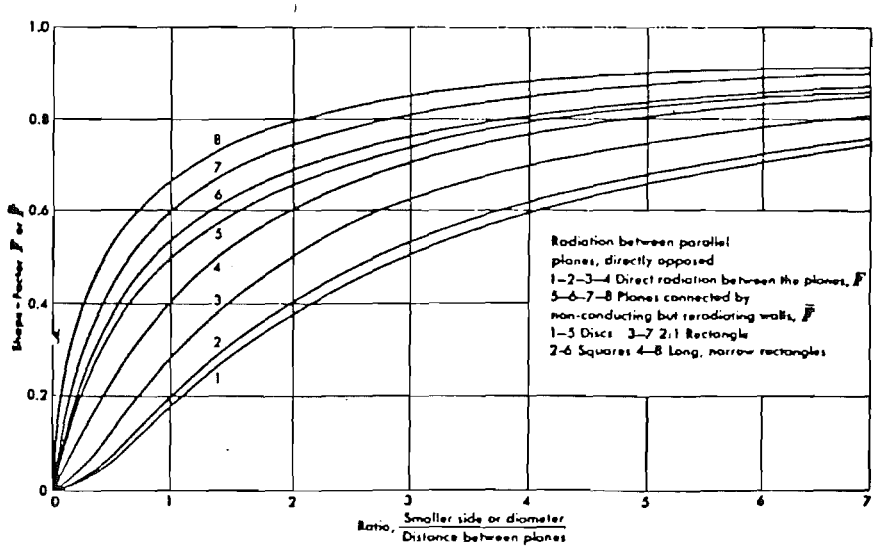

Fig. 5-22. Shape factors for equal and parallel squares, rectangles, and disks. The curves labeled 5,6,7 and 8 allow for continuous variation in the side-wall temperatures from top to bottom. (By permission from H. C. Hottel, "Radiant Heat Transmission," *Mechanical Engineering*, Vol. 52, 1930.)

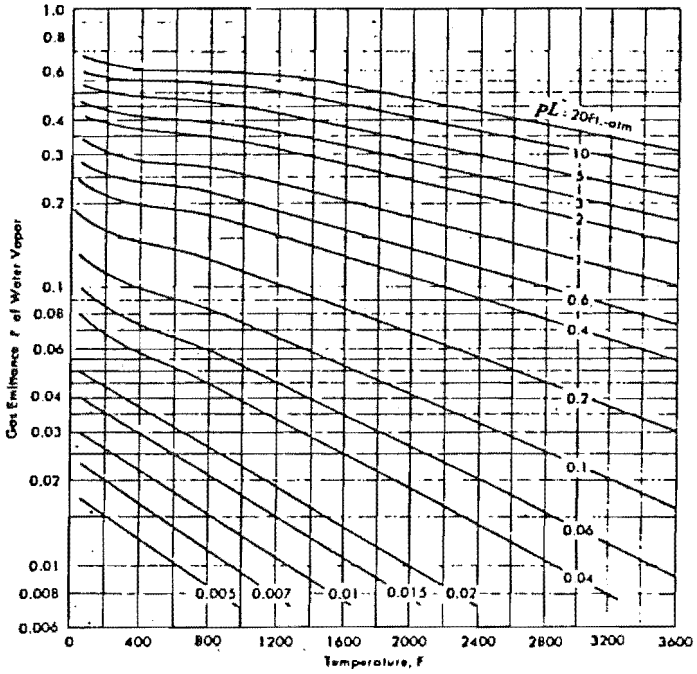

Fig. 5-35. Emittance of water vapor for a hypothetical system at 1 atmosphere total pressure and 0 partial pressure. (By permission from H. C. Hottel and R. S. Egbert, "Radiant Heat Transmission from Water Vapor," *AIChE Trans.*, Vol. 38, 1942)

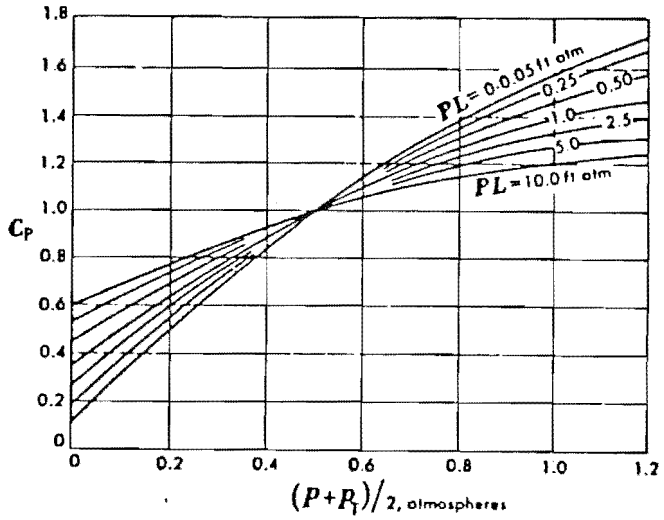

Fig. 5-37. Factor C_p for correcting emittance of water vapor to values of p and p_t other than 0 and 1 atmosphere. (By permission from H. C. Hottel and R. B. Egbert, "Radiant Heat Transmission from Water Vapor," *AIChE Trans.*, Vol. 38, 1942)

APPENDIX 3

HEAT OF CRYSTALLISATION AND THE TRANSFER OF HEAT DUE TO MASS TRANSFER

When a saturated salt solution is used as a humidifying source, the amount of energy required to evaporate m grams of water per second is:

$$q_m = m\ \Delta H_v - (m\ S/M)\ \Delta H_{cryst} \qquad (A3.1)$$

where q_m = heat required, W

ΔH_v = heat of vaporisation, J g^{-1}

ΔH_{cryst} = heat of crystallisation, J mol^{-1} of salt

S = solubility of the salt, g salt/100 g H_2O

M = molecular weight of salt, g mol^{-1}

m = gross mass transfer rate, gs^{-1} (Appendix 1.6)

When distilled water instead of salt solution is used:

$$q_m = m\ \Delta H_v \qquad (A3.2)$$

q_m from either equation (A3.1) or (A3.2) is used as an input parameter for Program "HMTC.FOR" of Appendix 1.6. It is, of course, supplied by the heater in the experiments.

Values of ΔH_{cryst} are scarce in the literature (Mullin [183] p62-64) it is common to derive the values of ΔH_{cryst} from:

$$\Delta H_{cryst} = -\Delta H_{sol}^{\infty} + \Delta H_{dil} \qquad (A3.3)$$

Where $-\Delta H_{sol}^{\infty}$ is the heat of solution at infinite dilution $Wmol^{-1}$

and ΔH_{dil} is heat of dilution Wm^{-1}

In equation (A3.3) ΔH_{cryst} is positive when heat is evolved (exothermic) and negative when heat is absorbed (endothermic). The heat of solution, being the opposite of heat of crystallisation,

therefore has the negative sign. Few values of the heats of dilution ΔH_{dil} are available in the literature, but this quantity is usually only a small fraction of the heats of solutions ΔH_{sol}^{∞} (Mullin [183] p63). Hence we approximate ΔH_{cryst} by:

$$\Delta H_{cryst} = -\Delta H_{sol}^{\infty} \qquad (A3.4)$$

Equation 3.4 is adequate for this work as the heat of crystallisation in turn represents only a very small fraction of the heat of vaporisation ΔH_v in Equation (A3.1), as will be shown below:-

e.g. Run HM5 which has relatively "high" evaporation rate :-
$m = 3.53 \times 10^{-3}$ gs^{-1} of water.

Saturated salt solution used is Potassium Sulphate Solution (K_2SO_4).

Isothermal evaporation at 50 °C.

Solubility of K_2SO_4 in water at 50°C

= 16 g K_2SO_4 /100 g H_2O (Mullin [183] p249)

Rate of K_2SO_4 crystallisation

= (16/100) x 3.52×10^{-3} gs^{-1} of K_2SO_4

= 5.648 x 10-4 gs^{-1} K_2SO_4

Heat of solution of K_2SO_4 ΔH_{sol}^{∞}

= -6.3 Kcal $mole^{-1}$ (Mullin [183] p255)

= -26.37 kJ $mole^{-1}$

$\therefore$ ΔH_{cryst} = 26.37 kJ mol-1 which is exothermic.

Molecular weight of K_2SO_4 = 174.27 $gmol^{-1}$

Rate of energy evolution by K_2SO_4 crystallisation

$$= \frac{5.648 \times 10^{-4}\ gs^{-1}}{174.27\ g\ mol^{-1}} \times 26.37\ 103 \quad J\ mol^{-1}$$

= 0.09 W

ΔH_v at 50 °C = 2382.1 J g^{-1}

m ΔH_v = 3.53 x 10^{-3} x 2382.1 J

= 8.41 W

Therefore ΔH_{cryst} was only 1% of ΔH_v

Furthermore as q_m was only 12.5% of the total heat input q_T, the effect of ΔH_{cryst} is thus not important when K_2SO_4 was the salt solution. They were included in the calculation for q_m in equation (A3.1) nonetheless.

All the salt solutions used in the experiments and some of their relevant properties are summarised in Table A3.1 (data obtained from Mullin [183] and CRC Handbook [184]).

Table A3.1

Salt	Solubility (g salt/100 g H20)				ΔH_{sol}^{∞} (KJ mol^{-1}) at room temp.	M (g mol^{-1}) at 40 °C	ΔH_{cryst} as a % of ΔH_v
	20°C	40°C	60°C	80°C			
Nacl	36.3	36.6	36.6	37.3	-5.02	58.44	1.3
KCl	37.0	40.0	45.5	51.1	-18.42	74.56	4.1
$NaNO_2$	92.9	98.0	-	133	-15.07	69.00	9.0
$Mg(NO)_2$ .6 H2O	125	250	-	v.s.	-15.49	256.41	6.0
K_2CO_3	114	117	127	140	28.88	138.21	10.3
$MgCl_2$ 6 H_2O	167	207	-	367	12.98	203.31	5.5
LiCl	90	90	-	102	-36.42	42.39	32.5
K_2SO_4	13	14.8	18.2	21.4	-26.37	174.27	1.0

From the values of the last column, it can be seem that not all the values of the heat of crystallisation is insignificant when compared with the heat of vapourisation for the transfer of a certain quantity of moisture. If LiCl was to be used as the humidifying source, ΔH_{cryst} clearly needs to be determined accurately.

In this work, only NaCl, KCI, K_2SO_4 and distilled water were used as humidifying sources during an heat and mass transfer run where the value of q_m from equation (A3.1) or (A3.2) need to be determined accurately for heat balance purposes. The rest of the salt solutions were used only to control humidity level in the Receiving Chamber where measurement for heat and mass transfer was not made; or in a run to estimate moisture loss from the Controlled Chamber to ambient. In either cases, the values of q_m is not relevant as no heat balances was carried out. Thus by default the salt solutions with the smaller values of ΔH_{cryst} were used as the humidifying source only. One reason why NaCl. KCI, K_2SO_4 and distilled water were used as humidifying sources was due to their ability to maintain a relatively higher moisture content in the Controlled Chambers compared with the rest of the salt solutions. Another reason was their tendency not to form a "skin" on top of the evaporation pan which slowed down the rate of moisture evaporating from the pan. The smaller rate of salt crystallisation and the crystal structure of NaCl, KCI and K_2SO_4 are thought to be responsible for the nonformation of this "skin". $NaNO_3$, $Mg(NO_3).6H_2O$, K_2CO_3 and $MgCl_2.6H_2O$, however, were particularly prone to this problem. The use of these latter salt solutions was avoided whenever possible.

APPENDIX 4

ERROR LIMITS FOR EXPERIMENTAL NUSSELT AND SHERWOOD NUMBERS

A4.1 NUSSELT NUMBER AND OVERALL HEAT TRANSFER COEFFICIENT

One has,

$$Nu = hL/k \qquad \text{(A1.39)}$$

and $h = q/(A_q(T_{cc}-T_{rc}))$

from Section A1.6. (A1.38)

Define:

$e(A)$ = error of A

$\%e(A)$ = percentage error of A = $(e(A)/A) \times 100\%$

Now,

$$\%e(Nu) = \%e(h) + \%e(L) \qquad \text{(A4.1)}$$

and

$$\%e(h) = \sqrt{(\%e(q))^2 + (\%e(T_{cc}-T_{rc}))^2} \qquad \text{(A4.2)}$$

In equation A4.1, e(L) is a systematic error and is not due to any measurement procedure. If the two porous plates are maintained to a reasonable degree parallel to each other with the right gap width, e(L) can be eliminated. A statistical approach is adopted for (A4.2) because both q and $(T_{cc} - T_{rc})$ are obtained from a large number of measurements.

A.4.1.1 % e(q) :-

From Equation 5.10,

$$q = q_T - q_l - q_c - q_r - q_m \qquad \text{(A4.3)}$$

where q = heat transfer by conduction and free convection across cavity;

q_T = total heat input by heater;

q_l = heat loss from controlled chamber to ambient;

q_c = heat transfer by solid conduction across cavity;

q_r = heat transfer by thermal radiation across cavity;

q_m = heat required to evaporate moisture from the evaporative pan to maintain a steady mass transfer across the cavity.

Errors for q_T, q_l, q_c, q_r and q_m are estimated by the standard deviations S_{n-2} (abbreviated now to S) as each term is the average of a number of measurements.

Thus,

$$e(q) = \sqrt{S^2(q_T) + S^2(q_l) + S^2(q_c) + S^2(q_r) + S^2(q_m)} \qquad (A4.4)$$

$S(q_T)$, $S(q_l)$ and $S(q_m)$ are obtained from Program "POLYFIT" of Appendix 1.5. $S(q_c) \approx 0$ as $qc \approx 0$ and $S(q_r)$ is determined from Section A4.1.3.

A4.1.2 % $e(T_{cc}-T_{rc})$:-

As $(T_{cc} - T_{rc})$ can be found by two methods, $e(T_{cc} - T_{rc})$ correspondingly can be found from:

(i) Readings of Cavity Thermocouples:-

$(T_{cc} - T_{rc})$ is measured directly by six pairs of differential thermocouples and $e(T_{cc} - T_{rc})$ is estimated directly from S_{n-1} calculated from a pocket calculator when calculating the mean of $(T_{cc} - T_{rc})$.

$$\%e(T_{cc}-T_{rc}) = \frac{S(T_{cc}-T_{rc})}{(T_{cc}-T_{rc})} \times 100\% \qquad (A4.5)$$

Thus the spread of the individual measurements about the mean is used as an estimate of the error. This estimate does not include the effect of any long term variation of the mean with time as each individual measurements of $(T_{cc} - T_{rc})$ is not itself an average of

a large number of measurement due to a lack of proper data logging equipment.

(ii) Thermal Conductivity of Porous Plate

In this method T_{cc} and T_{rc} are calculated individually first before $(T_{cc} - T_{rc})$ is calculated (see appendix 1.6)

eg. $T_{cc} = T_{cp} - (\Delta T)_p$

ie. $e(T_{cc}) = \sqrt{S^2(T_{cp}) + S^2(\Delta T)_p}$ (A4.6)

as $e(T_{cp})$ is estimated by $S(T_{cp})$ and $e(\Delta T)$ is estimated by $S(\Delta T)$ (as both T_{cp} and ΔT are themselves calculated from a large sample of data).

$$T_{cp} = \frac{\sum_{i=1}^{n} T_{cpi}}{n} \qquad \text{(A4.7)}$$

where n is the number of measurements to T_{cp}. If we assume that each T_{cpi} is independent of each other due to the fact that their values are governed independently by the thermal and hydrodynamic boundary conditions in the controlled chamber, we obtain (from Davies [185] p.40) :-

$$V(T_{cp}) = (1/n)^2 V(T_{cp1}) + \ldots\ldots\ldots + (1/n)^2 V(T_{cpn}) \qquad \text{(A4.8)}$$

where $V(T_{cpi})$ is the individual variance of measurement T_{cpi}. In the actual experiment, only one thermocouple point out of the total of six has been logged continuously during the course of the experiment due to a lack of data logging equipment. Hence we made the assumption that:

$$V(T_{cp1}) = V(T_{cp2}) = \ldots\ldots\ldots = V(T_{cpn}) \qquad \text{(A4.9)}$$

and equation (A4.8) is then equal to:

$$v(T_{cp}) = \frac{V(T_{cp1})}{n} \qquad \text{(A4.10)}$$

where T_{cp1} is the temperature of the thermocouple junction with continuous data logging and $V(T_{cp1})$ is calculated from a large number of measurements of T_{cp1}.

Similarly for the Receiving Chamber:

$$V(T_{rp}) = \frac{V(T_{rp1})}{n} \qquad \text{(A4.11)}$$

where $V(T_{rp1})$ is again estimated from a large number of measurements for T_{rp1}.

Note that, in this method of calculation the spread of each individual T_{cpi} about its mean T_{cp} is not used as an estimate of error. The latter method is less satisfactory as only six T_{cpi} values can be used and will not give a satisfactory value for the variance of T_{cp}.

Following (A4.6), we have

$$e(T_{rp}) = \sqrt{S^2(T_{rp}) + S^2(\Delta T)} \qquad \text{(A4.12)}$$

and $$e(T_{cc} - T_{rc}) = \sqrt{S^2(T_{cp}) + S^2(T_{cp}) + 2S^2(\Delta T)} \qquad \text{(A4.13)}$$

Whether method (i) or (ii) is used to estimate the error of $(T_{cc} - T_{rc})$ is of course depends on which method is used to determine $(T_{cc} - T_{rc})$.

From equations A4.2, A4.4, and A4.13:

$$\%e(h) = \sqrt{(EQ)^2 + (ET)^2} \qquad \text{(A4.14)}$$

where $$EQ = \frac{\sqrt{S^2(q_T) + S^2(q_1) + S^2(q_c) + S^2(q_r) + S^2(q_m)}}{q}$$

and $$ET = \frac{\sqrt{S^2(T_{cp}) + S^2(T_{cp}) + 2S^2(DT)}}{(T_{cc} - T_{rc})}$$

and %e(Nu) is then calculated from (A4.1).

A4.1.3 Procedure for Determining S(q_r).

From Appendix 2 Equation A2.9, q_r is calculated from :-

$$q_r = (J_1-J_2)\ A_1\ F_{12}(1-e_g) + (J_3-J_{2)}\ A_2\ F_{32}\ (1-e_g) + (J_4-J_2)\ A_2\ F_{2g}\ e_g \qquad (A2.9)$$

To simplify Eq. A2.9, we assume that the thermal radiation in the cavity is analogous to the case of two infinite parallel plates and that the fluid is transparent. This is a reasonable assumption as the first term in (A2.9) accounts for nearly 93% of the magnitude of q_r. Figure A2.2 is then transformed into:

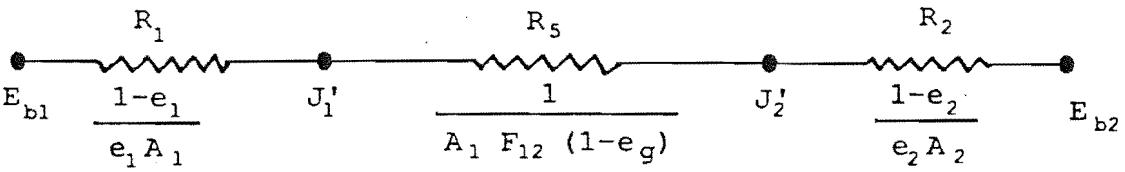

Note that in the Figure , J_1' and J_2' are not equal to J_1 and J_2 in (A2.9) and:

$$q_r = \frac{(J_1' - J_2')}{A_1\ F_{12}\ (1-e_g)} = \frac{\sigma((T_{cc})^4 - (T_{rc})^4)}{R_T} \qquad (A4.15)$$

where $$R_T = \frac{(1-e_1)}{A_1e_1} + \frac{1}{A_1\ F_{12}\ (1-e_g)} + \frac{(1-e_2)}{A_2e_2}$$

and $$ET = \frac{\sqrt{S^2(T_{cp}) + S^2(T_{cp}) + 2S^2(DT)}}{(T_{cc} - T_{rc})}$$

and %e(Nu) is then calculated from (A4.1).

A4.1.3 Procedure for Determining S(q_r).

From Appendix 2 Equation A2.9, q_r is calculated from :-

$$q_r = (J_1-J_2)\ A_1\ F_{12}(1-e_g) + (J_3-J_2)\ A_2\ F_{32}\ (1-e_g) + (J_4-J_2)\ A_2\ F_{2g}\ e_g \qquad (A2.9)$$

To simplify Eq. A2.9, we assume that the thermal radiation in the cavity is analogous to the case of two infinite parallel plates and that the fluid is transparent. This is a reasonable assumption as the first term in (A2.9) accounts for nearly 93% of the magnitude of q_r. Figure A2.2 is then transformed into:

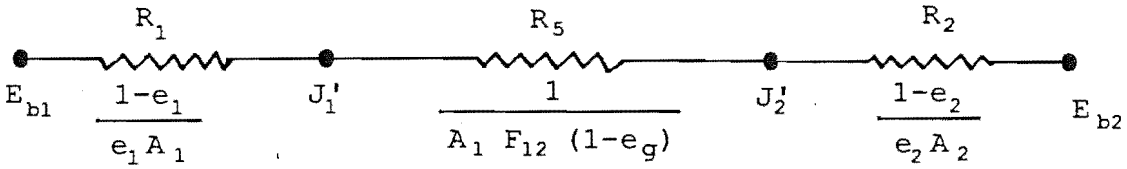

Note that in the Figure, J_1' and J_2' are not equal to J_1 and J_2 in (A2.9) and:

$$q_r = \frac{(J_1' - J_2')}{A_1\ F_{12}\ (1-e_g)} = \frac{\sigma((T_{cc})^4 - (T_{rc})^4)}{R_T} \qquad (A4.15)$$

where $$R_T = \frac{(1-e_1)}{A_1e_1} + \frac{1}{A_1\ F_{12}\ (1-e_g)} + \frac{(1-e_2)}{A_2e_2}$$

The value of q_r from (A4.9) is 18% larger than the value of q_r from Eq. A2.9, but the absolute error should be similar for both cases as it is due to T_{cc} and T_{rc} only.

Rewrite A4.9 as:

$$q_r = B\ ((T_{cc})^4 - (T_{rc})^4) \qquad \text{(A4.16)}$$

where $$B = \frac{\sigma}{R_T}$$

From Davies [185], p41, the variance of q_r can be found from

$$V(q_r) = \left(\frac{\partial q_r}{\partial T_{cc}}\right)^2 V(T_{cc}) + \left(\frac{\partial q_r}{\partial T_{rc}}\right)^2 V(T_{rc})$$

$$+ 2 \left(\frac{dq_r}{dT_{cc}}\right) \left(\frac{dq_r}{dT_{rc}}\right) C(T_{cc}, T_{rc}) \qquad \text{(A4.17)}$$

The use of the variance as an estimate of the error is appropriate here as both T_{cc} and T_{rc} are themselves averages of a number of readings. The covariance term is included as T_{cc} and T_{rc} are not mutually independent of each other and the covariance is calculated from:

$$C(T_{cc}, T_{rc}) = \left(\left(\sum_{k=1}^{N} T_{cck} T_{rck}\right) - N\ T_{cc}\ T_{rc}\right) / (N-1) \qquad \text{(A4.18)}$$

where N is the number of measurements for each T_{cc} and T_{rc} .
In this work T_{cc} and T_{rc} are in turn calculated from T_{cp} and T_{rp} and the covariance term can be estimated from:

$$C(T_{cc}, T_{rc}) \approx C(T_{cp}, T_{rp})$$

$$= \left(\left(\sum_{k=1}^{N} T_{cpk} T_{rpk}\right) - N\ T_{cp}\ T_{rp}\right) / (N-1) \qquad \text{(A4.19)}$$

where T_{cp} and T_{rp} and the mean values of T_{cpk} and T_{rpk} respectively. T_{cpk} and T_{rpk} are the mean values of T_{cpi} and T_{rpi} at time k.

On using the previously made assumption that individual T_{cpi} and T_{rpi} readings are independent of each other, and the fact that only one long term value of T_{cpi} and T_{rpi} is available, designated T_{cp1} and T_{rp1} respectively, equation A4.19 is approximated by:

$$C(T_{cp}, T_{rp}) = \left(\left(\sum_{k=1}^{N} (T_{cp1})_k (T_{rp1})_k - N\, T_{cp1}\, T_{rp1}\right)/(N-1)\right) \qquad (A4.20)$$

Therefore, instead of investigating the covariance of the temperature difference in terms of the mean value of the plate surface temperature, we can only approximate that value with the covariance between two point values on each plate surface due to a lack of sufficient information.

Figure A4.1 and A4.2 illustrate the fluctuation of this surface temperature during the course of a run. Note that the absolute surface temperature level plotted is for the Controlled Chamber only. The corresponding value for the surface temperature in the Receiving Chamber is the difference between the absolute temperature plotted and the temperature difference which is also plotted. Figure A4.1 is a typical case for a low heat transfer run where the temperature difference between T_{cp} and T_{rp} is about 10 °C (corresponding to cavity temperature difference of 6 °C) and Figure A4.2 is a typical case for a high heat transfer run . $(T_{cp} - T_{rp}) = 28$ °C which corresponds to $(T_{cc} - T_{rc}) = 17$ °C.

Using Eqs. A4.16, A4.17 and A4.20:

$$V(q_r) = 16\, B^2\, (T_{cc})^6\, V(T_{cc}) + 16\, B^2\, (T_{rc})^6\, V(T_{rc}) - 32\, B^2\, (T_{cc})^3\, (T_{rc})^3\, C(T_{cc}, T_{rc}) \qquad (A4.21)$$

and $S(q_r) = \sqrt{V(q_r)}$

$S(q_r)$ is the error estimate q_r.

The program "ERROR.FOR" is written to carry out all the foregoing calculations. Typical examples of the error analysis are given below for runs HM1, HM10, HM25, HM40 and HM63. Runs HM1 and

Fig. A4.1: LONG TERM BEHAVIOUR OF SURFACE THERMOCOUPLES IN C.C. AND R.C.

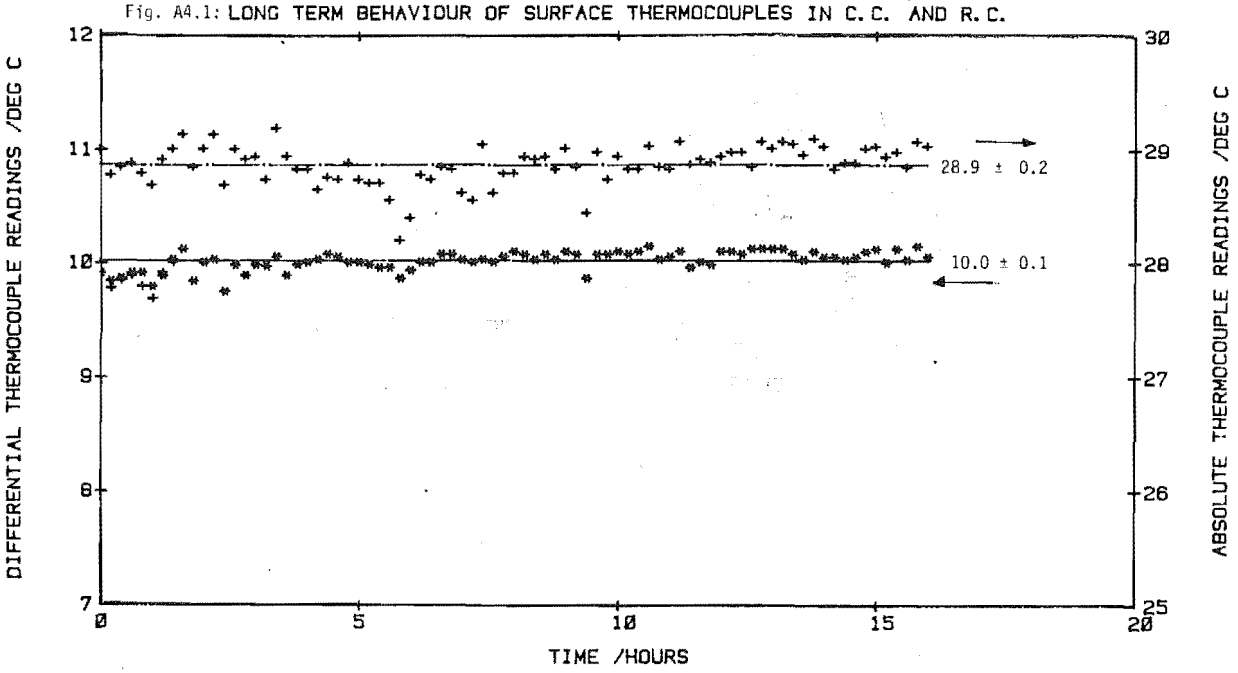

Fig. A4.2: LONG TERM BEHAVIOUR OF SURFACE THERMOCOUPLES IN C.C. AND R.C.

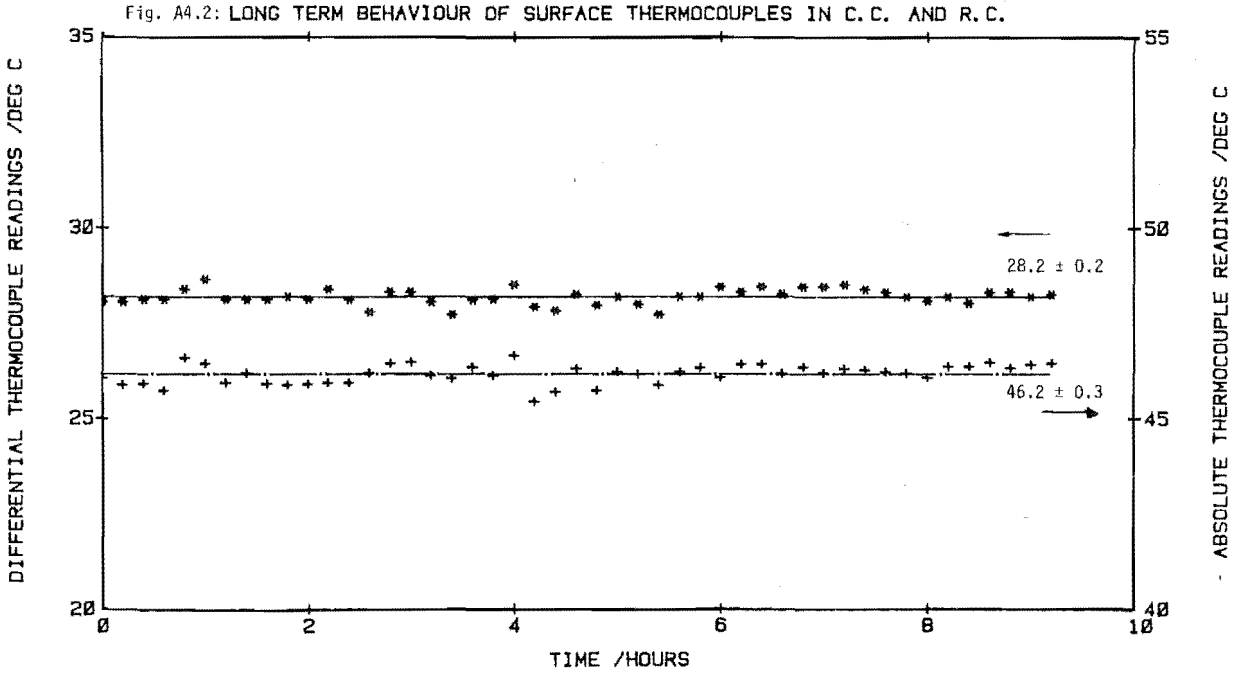

HM10 are representative of the runs for low and high heat-transfer rates respectively for the horizontal cavity with upwards transfer. Run HM25 is for a typical run for downwards heat transfer for the horizontal cavity. Runs HM40 and HM63 are representative of the runs for low and high heat-transfer rates respectively for the vertical cavity. Typical error estimates:

Standard deviation	Runs HM1, HM25, HM40	Runs HM10 and HM63
$S(q_T)$	0.40	1.73
$S(q_l)$	0.22	0.22
$S(q_c)$	0.00	0.00
$S(q_r)$	0.36	0.62
$S(q_m)$	0.05	0.13
$S(T_{cp})$	0.17	0.20
$S(T_{rp})$	0.19	0.32
$S(\Delta T)$	0.16	0.16

Runs	q/W	$(T_{cc}-T_{rc})$/°C	%e(q)/%	%e$(T_{cc}-T_{rc})$/%	%e(h or Nu)/%
HM1	4.12	5.12	14	7	15
HM10	20.02	18.17	9	2	10
HM25	1.11	7.34	52	5	53
HM40	4.70	6.06	12	6	14
HM60	16.97	16.11	11	3	11

A4.2 ERROR LIMITS SHERWOOD NUMBER AND OVERALL MASS TRANSFER.

From Appendix 1.6, we have :

$$Sh = K \cdot L/D\rho \tag{A4.23}$$

and $$K = m/(A_q(\Delta Y)) \tag{A4.24}$$

Now,

$$\%e(Sh) = \%e(K) + \%e(L)$$
$$\approx \%e(K)$$

for reason outlined in A4.1, (A4.25)

and $$\%e(K) = \%e(m) + \%e(\Delta Y) \tag{A4.26}$$

Simple percentage rule is used for Eq.A4.26 because (ΔY) is only measured intermittently and has insufficient data points for a statistical analysis Thus only the determinate error limits for (ΔY) is employed.

A4.2.1 Percentage error in (ΔY)

Using perfect gas assumption:

$$\Delta Y = D_m P_T \frac{\Delta P}{(P_T - P_{cc})(P_T - P_{rc})} \tag{A4.27}$$

where ΔP is the vapour pressure difference across the cavity. For the low humidity level encountered in the experiment, we can assume the total pressure P_T is very much greater than the partial pressures of water vapour P_{cc} and P_{rc} at the cavity boundary, Equation A4.27 can thus be written as :

$$\Delta Y = D_m \frac{\Delta P}{P_T} \tag{A4.28}$$

i.e. $\%\ e(\Delta Y) = \%\ e(\Delta P)$ if D_m and P_T are assumed to have negligible error.

Now:

$$\Delta P = P_{cc} - P_{rc}$$

Arbitrarily we choose the error of ΔP to be:

$$e(\Delta P) = \sqrt{(e(P_{cc}))^2 + (e(P_{rc}))^2} \qquad \text{(A4.29)}$$

and $\%\ e(\Delta Y) = \%\ e(\Delta P)$ as noted before. (A4.30)

Now (with reference to Figure A1.7),

$$P_{cc} = P_{cp} - (\Delta P)_p$$

$$= P_c - (\Delta P)_p + \text{Correction} \qquad \text{(A4.31)}$$

where $(\Delta P)_p$ is the vapour pressure across the porous plate obtained from one porous plate test,

and "Correction" is the boundary layer correction for P_c.

As only determinate errors for vapour pressures P_{cc}, P_{cp} and P_c are available, we estimate $e(P_{cc})$ by:

$$e(P_{cc}) = e(P_c) + e(\Delta P)_p + e(\text{Correction}) \qquad \text{(A4.32)}$$

where $e(P_c) \equiv$ uncertainty in evaluating P_c,

$e(\Delta P)_p \equiv$ uncertainty in evaluating P_{cc} from P_{cp},

and $e(\text{Correction}) \equiv$ uncertainty in evaluating the boundary layer correction.

Now:

$$P_c = (rh) \cdot P^\circ_w$$

where (rh) is the relative humidity,

and P°_w is the saturation vapour pressure.

Therefore,

$$\%e(P_c) = \%e(rh) + \%e(P^\circ_w) \approx \%e(rh) \qquad \text{(A4.33)}$$

ie. $e(P_c) = P_c \times \%e(P_c) = P_c \times (e(rh)/(rh))$

The error, e(rh), is ± 0.5% as claimed by the "Dew-All" humidity sensor manufacturer, with (rh) the average relative humidity in the Controlled Chamber during a run.

From the plots of $(P_c - P_r)$ given in Chapter 6, $e(\Delta P)_p$ in Eq. A4.32 can be obtained.

From Appendix A1.6,

"Correction" = f(h)

where h is the forced heat-transfer coefficient in C.C. or R.C.

As the effect of correction is small, we approximate %e(Correction) = % e(h). The percentage uncertainty in h is about 5% due to the uncertainty in measuring the air velocity used to determine h :

ie. e(Correction) = Correction x 0.05

Thus on substituting equations A4.34 and A4.35 into A4.32, we get,

$$e(P_{cc}) = [P_c \times (e(rh)/(rh))]_{cc} + e(\Delta P)_p + (\text{Correction} \times 0.05) \qquad \text{(A43.6a)}$$

Similarly;

$$e(P_{rc}) = [P_r \times (e(rh)/(rh))]_{Rc} + e(\Delta P)_p + (\text{Correction} \times 0.05) \qquad \text{(A43.6b)}$$

On combining Eqs. A4.36a and b and Eq. A4.30, we find

$$\% \; e(\Delta P) = (1/\Delta P) \sqrt{A^2 + B^2} \qquad \text{(A4.37)}$$

where $A \equiv \{P_c \times [e(rh)/(rh)]_{cc} + e(\Delta P)_p\}$,

$B \equiv \{P_r \times [e(rh)/(rh)]_{RC} + e(\Delta P)_p\}$,

and the error due to the correction term in Eq.A4.36 has been omitted as it accounts for less than 1% of $e(P_{cc})$.

Thus %e(K) is calculated from Eq.A4.26 using the information obtained from Eqs.A4.30 and A4.37. Finally % e(Sh) is calculated using Eq. A4.25.

Note that e(m) in Eq. A4.26 is estimated by the standard deviation term as m is found from a large number of data (see Figure A1.1 and A1.2)

$e(\Delta P)_p$ is obtained from the best fit curve of m versus $(P_c - P_r)$ given in Chapter 6.

The program "ERROR.FOR" is again used to carry out the foregoing calculations and return the error estimates for K and Sh. Typical values for the error limits for RUNS HM1, HM11, HM25, HM40 and HM64 are given below:

Experimental conditions

Runs	P_c/mm Hg	P_r/mm Hg	$(rh)_{cc}$/%	$(rh)_{RC}$/%	m/gh^{-1}	ΔP/mm Hg
HM1	20.33	13.14	62.78	75.47	4.05	1.88
HM10	34.00	7.83	22.76	47.58	18.15	5.64
HM25	21.32	11.38	65.50	74.44	3.03	6.07
HM40	17.65	11.45	54.84	73.54	3.70	1.54
HM60	28.51	6.06	31.75	49.54	14.5	4.91

Error Limits Estimated from Measurements.

Runs	$e(m)$/gh^{-1}	$e((rh)_{cc})$/%	$e((rh)_{RC})$/%	$e(\Delta P)$/mm Hg	$e(\Delta P)$/mmHg
HM1	0.05	0.5	0.5	0.24	0.24
HM10	0.12	0.5	0.5	0.24	0.24
HM25	0.08	0.5	0.5	0.24	0.24
HM40	0.05	0.5	0.5	0.24	0.24
HM60	0.11	0.5	0.5	0.24	0.24

Error Limits Derived from Measurements.

Runs	$e(P_c)$/mm Hg	$e(P_r)$/mm Hg	%(ΔY)/%	%(m)/%	%(K or Sh)/%
HM1	0.16	0.09	28	1	29
HM10	0.75	0.08	18	1	19
HM25	0.16	0.08	8	3	11
HM40	0.16	0.08	33	1	34
HM60	0.45	0.06	15	1	16

Notes:-

(i) Runs HM 1 and 11 represent the low and high moisture transfer rate runs for horizontal cavity with upwards transfer.

(ii) Run Hm25 is a typical case for horizontal cavity with downwards transfer.

(iii) Runs HM41 and 64 represent the low and high moisture transfer rate runs for vertical cavity.

APPENDIX 5

CHARACTERISTIC OF PERSPEX.

5.1 INFRA-RED RADIATION TRANSMITTANCE OF 6MM THICK PERSPEX SHEET.

Fig. 5.1 shows the relative "strength" of radiation power between the emitting source of the Perkin Elmer Infra-Red Spectrophotometer (PEIRS) and the electric resistance heater in the Controlled Chamber as a function of the wavelength of radiation. Each emitting body was assumed to exhibit the characteristic of a grey body. The radiation power is calculated from the formula :-

$$EP = \frac{C_1 E}{\lambda^5 \, (e^{(C_2/\lambda T)} - 1)} \qquad \text{(A5.1)}$$

where EP = monochromatic emissive power of a grey body at temperature T and wavelength λ , W m^{-3}

λ = wavelength of radiation , m

T = absolute temperature of the grey body, deg. K

$C_1 = 374.15 \times 10^{-18}$ Wm^{-18}

C_2 = 14.388 x 10-3 m K

E = thermal emittance of the grey body.

The characteristic temperature of radiation used for the emitting source of the PEIRS was 1470 K which was a value quoted by the manufacturer. The emitting source for the PEIRS is a length of ceramic tubing heated by an internal metallic heater and emits a continuous spectrum of radiation most of which falling within the infra-red region of wavelength from 2.5 to 25 μm. The thermal emittance for ceramics is obtained from Kreith [182] p.237 and is taken to be 0.9.

The electric resistance heater has a finned surface made of brass. The thermal emittance for natural rolled brass is taken to be 0.06 (from Wong [171] p.224). The heater was operating at a

Fig. A5.1: THERMAL RADIATION POWER OF VARIOUS GRAY BODIES

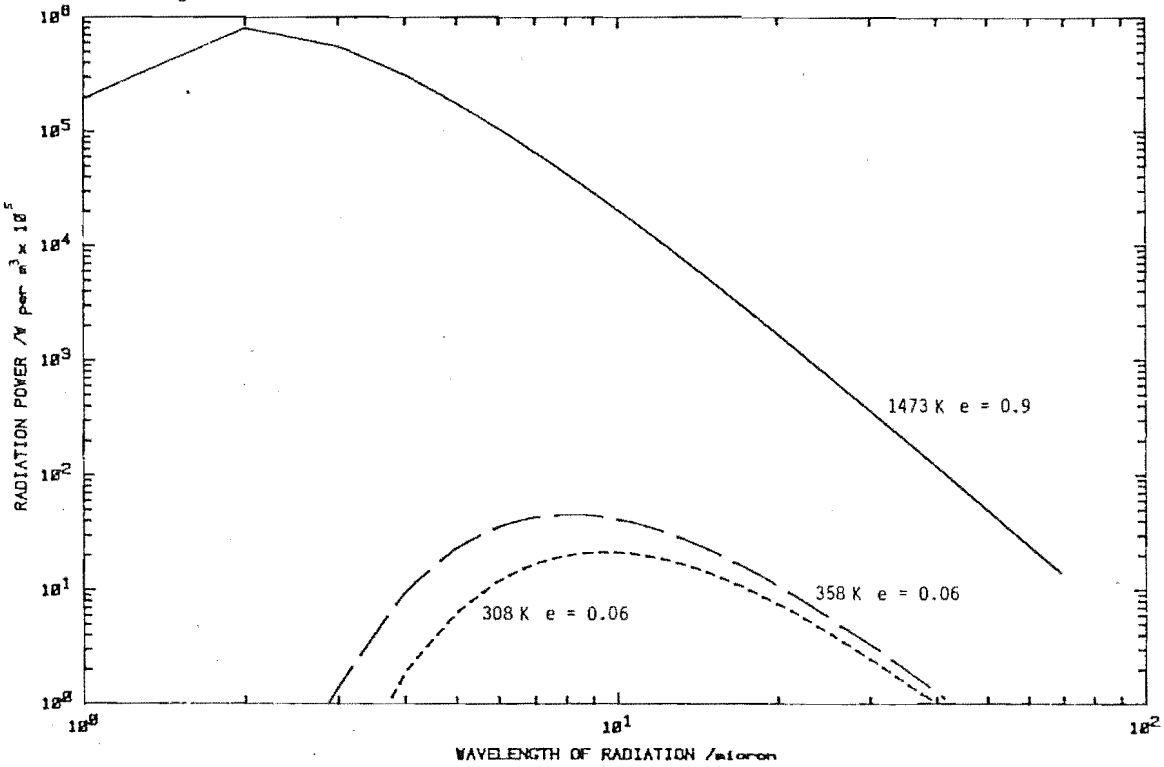

Fig. A5.2: THERMAL RADIATION OF A GRAY BODY AT 308 & 358 K

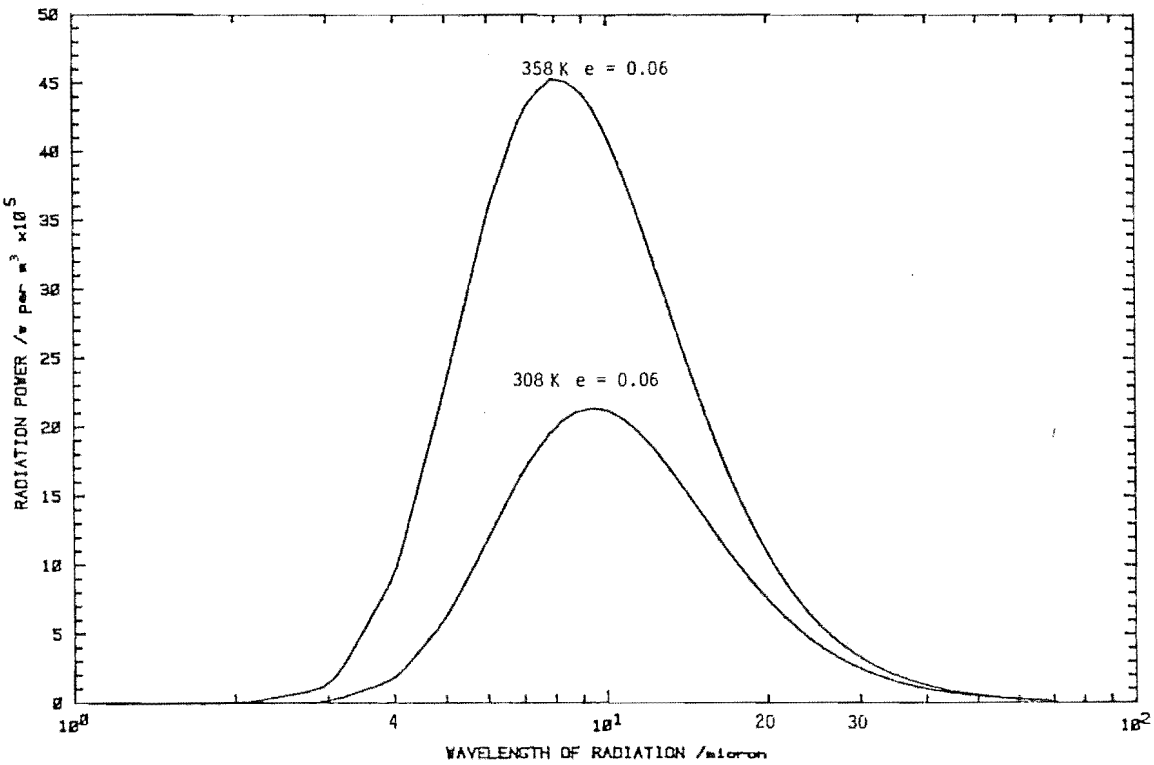

surface temperature between 308 to 358 K (measured experimentally) depending on the temperature in the Controlled Chamber. Hence the emitting power of the heater betweeen these two limits are calculated.(Fig. A5.2)

Using the above values, the radiative power was calculated for the two bodies for the range of wavelength illustrated in Fig. A5.1. From Fig. A5.1, the radiative power from the PEIRS can be seen to be much larger than that from the electric heater. The test carried out on the PEIRS was thus conservative.

Before any tests were carried out on the Perspex sample strips, tests runs were performed on a 0.07mm thick polystyrene film supplied by the PEIRS manufacturer and the resultant spectra compared with the reference spectrum provided. This procedure ensured that the PEIRS was operating properly. Fig. A5.3 illustrates the tests on 6mm thick Perspex sheet. The percentage transmittance of infra-red radiation was observed to be practically nil over the range of wavelength tested except for two small bends (between 4.2 to 4.7 and 6.2 to 6.3 μm), where the percentage transmittance is 1%. This percentage of transmittance would be expected to be much smaller when considering the radiative power of the heater as it is much smaller than that from the PEIRS (Fig. A5.1). The range of wavelengths tested in Fig. A5.3 covers nearly the full range of the expected radiative wavelengths from fig A5.2. For longer wavelengths, Randall [172] has reported the percentage transmission to be 1% at wavelength of 30 μm and 11% at 52 μm for a 0.28-mm thick methyl methacrylate sample. Due to the much thinner sample used by Randall, his result was expected to be an overestimate for the percentage transmittance for the 6mm thick test strip. The effect of sample thickness on the percentage transmittance can be observed by comparing Figs.A5.3 with Fig.A5.4. The much thinner 0.37mm Perspex sheet allowed considerable greater amount of radiation to pass through when all samples are tested on the PEIRS.

Fig. A5.5 is reproduced from ICI Technical note PX127 [166] which again shows the effect of sample thickness on the transmittance of thermal radiation. It also exhibits the good transmittance of Perspex to visible light and the rapid deterioration of this transmittance when entering into the

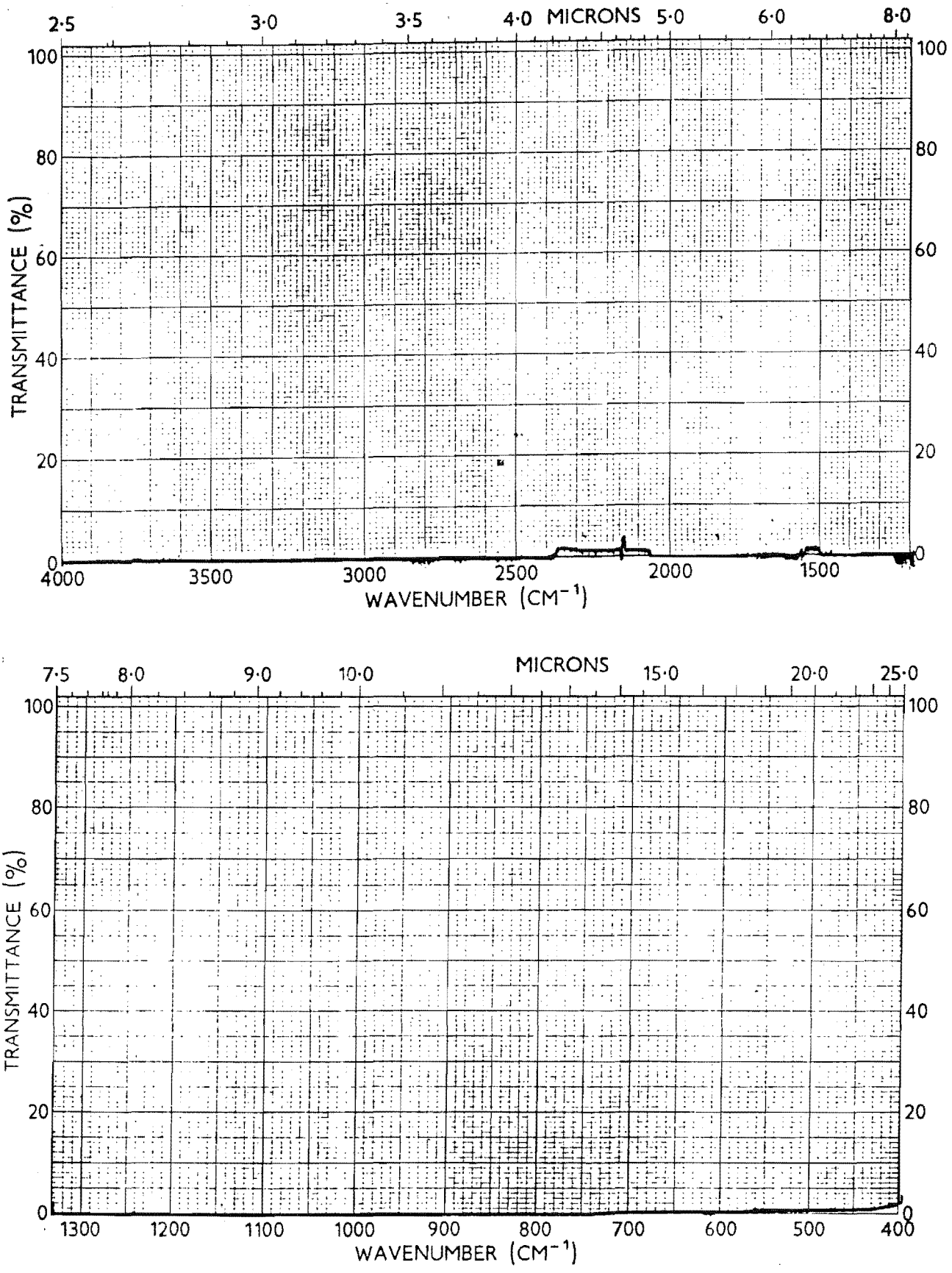

Fig. A5.3: 6 mm thick Perspex sheet tested on the PEIRS.

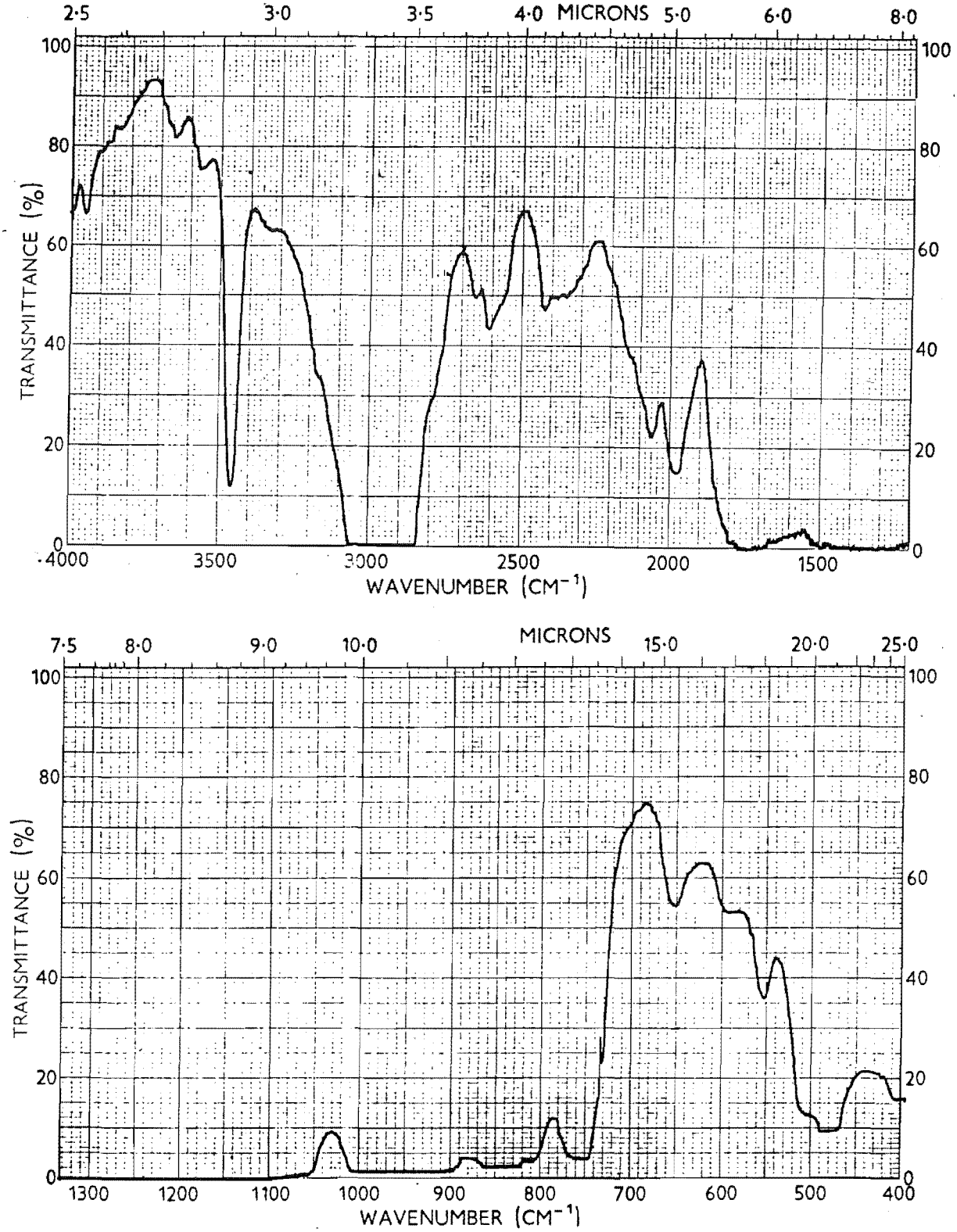

Fig. A5.4: 0.37 mm thick Perspex sheet tested on the PEIRS.

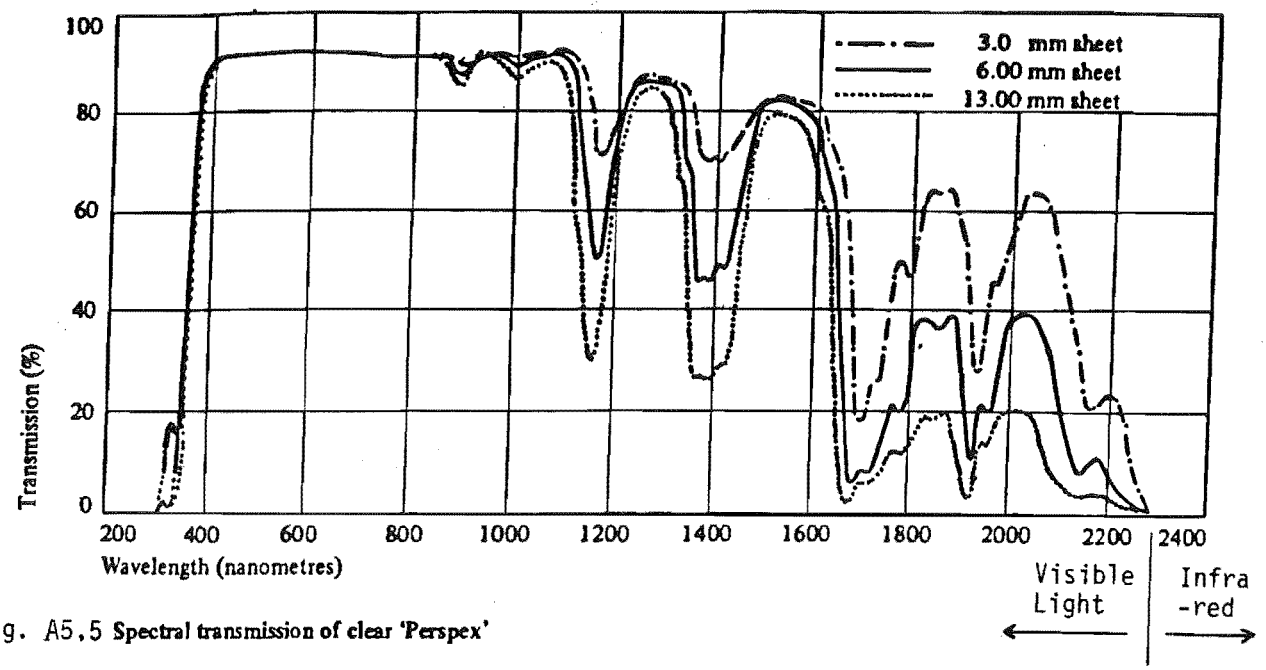

Fig. A5.5 **Spectral transmission of clear 'Perspex'**

Fig. A5.6: THERMOCOUPLES RESPONSE IN C.C. & G.C. WITH G.C. ELECTRIC HEATERS

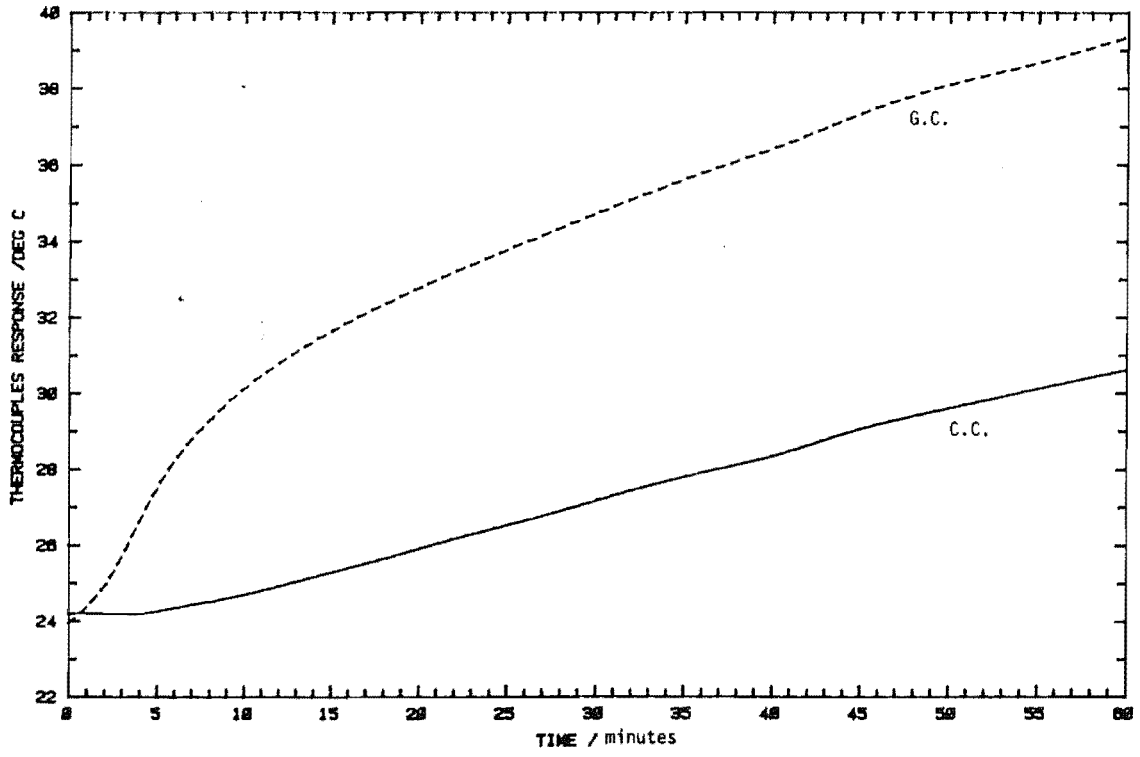

infra-red region.

Finally, Fig. A5.6 is a plot of the thermocouples' outputs measuring bulk air temperature in both the Guard and Controlled Chamber. At time zero, the heater in the Guard Chamber was turned on at maximum power setting and the reponses of all the thermocouples were observed. The thermocouples in the Guard Chamber were observed to react instantaneously, while the thermocouples in the Controlled Chambr did not show any response until after 4 minutes of heating. By 15 minutes of elapsed time, the temperature in the Guard Chamber had risen by 8 degree Celsius while that in the Controlled Chamber had risen by 1 degree Celsius. The eventual increase in the temperature of the Controlled Chamber was due to the secondary heating effect of the Perspex wall which was first heated up by the heater in the Guard Chamber. This rise in temperature was not thought to be as a result of the "leak radiation" from the Guard Chamber as this heating effect would not exhibit a time "lag" as observed.

A5.2 HYGROSCOPICITY OF PERSPEX.

Table A5.1 presents typical results of tests carried out to determine the moisture adsorption and desorption rate of Perspex. The following remarks will be useful in explaining some features of Table A5.1:-

(1) The Perspex samples used had the following dimensions:-

Sample	Surface Area /m^2	Thickness /mm
1	0.022	6
2	0.019	12

(2) Tests 1 to 6 represented extreme conditions and were carried out to check the limits of adsorption or desorption rates for the Perspex samples strips. These conditions were not encountered in the actual experiments.

(3) For comparison with the rate of Perspex adsorption/desorption

presented in Table A5.1, the typical mass-transfer rate across the cavity ranges from 2 $gm^{-2}h^{-1}$ to 20 $gm^{-2}h^{-1}$. An adsorption/ desorption rate is defined as "significant" when the rate is greater than 0.1 $gm^{-2}h^{-1}$, a value which is equivalent to 5 percent of the low mass-trasfer rate and 0.5 percent of the high mass-transfer rate across the cavity.

(4) Thus even for the most severe conditions of Test 1 to 6, the rate is only significant for the first 24 to 48 hours, thereafter the rate falls to below 0.1 $gm^{-2}h^{-1}$ which is of the order of experimental uncertainty in the measurement of mass transfer rate.

(5) The conditions of Test 7 to 11 reflected the range of bulk air relative humidity values that would be encountered in actual experiments. Over this smaller range of relative humidity change,the Perspex adsorption /desorption rate is "significant" (greater than 0.1 gh^{-1}) over the first ten hours or so, after which the rate is again of the order of the experimental uncertainty and thus can be ignored.

Table A5.1 Hygroscopicity of Perspex.

Test no.	Experimental condition	Time elapsed (hrs)	Rate of Adsorption/Desorption sample 1 $gm^{-2}h^{-1}$	sample 2 $gm^{-2}h^{-1}$
1	The samples were placed in a humidifier with environment saturated with distilled water after being in a dehydrated environment (dessicator with silica gel) for 3 months. r.h. = 100%	24.0	0.30	0.29
		48.0	0.17	0.18
		72.0	0.08	0.07
		96.0	0.02	0.04
		120.0	0.02	0.02
		144.0	0.02	0.02
2	Samples had been left in room condition (r.h.= 30 to 50%) for 2 months. They were then put in an humidifier at r.h.= 100%	5.0	0.35	0.41
		24.0	0.17	0.17
		30.0	0.07	0.08
		47.0	0.03	0.04
3	Take samples out of humidifier at the end of Test 2 and exposed to room condition. r.h.= 30 to 50%	24.0	-0.11	-0.18
		48.0	-0.07	-0.05
4	After Test 3, put samples back into humidifier as for Test 1 and 2. r.h.= 100%	24.0	0.15	0.15
		48.0	0.08	0.08
		72.0	0.06	0.07
		96.0	0.03	0.03
		122.0	0.01	0.01
5	After Test 4, take samples out from humidifier and transfer samples to dessicator with silica gel. r.h.= 0 %	7.0	-0.45	-0.47
		25.0	-0.10	-0.09
		55.0	-0.06	-0.07
		86.0	-0.04	-0.03
		99.0	-0.03	-0.03
6	After Test 5, transfer samples from the dessicator into a humidifier with distilled water. r.h.= 100%	10.0	0.36	0.37
		25.0	0.09	0.07
		48.0	0.07	0.07
		79.0	0.04	0.05

Table A5.1 (Contd).

Test no.	Experimental condition	Time elapsed (hrs)	Rate of Adsorption/Desorption sample 1 $gm^{-2}h^{-1}$	sample 2 $gm^{-2}h^{-1}$
7	After Test 6, take samples out of humidifier and left in room condition (rh= 30 to 50 %) for 5 days. The samples were put in humidifier at r.h.= 85%	11.0	0.17	0.19
		26.0	0.04	0.04
		50.0	0.02	0.02
		79.0	0.02	0.02
		91.0	0.02	0.02
		160.0	0.01	0.01
8	The sampls from Test 7 were transfered into a humidifier with r.h.= 55%	5.0	-0.09	-0.08
		20.0	-0.05	-0.08
		60.0	-0.02	-0.02
		150.0	-0.00	-0.00
9	Take out from condition of Test 8 and put in room condition. r.h.= 30 to 50 %	10.0	-0.09	-0.07
		28.0	-0.07	-0.07
		60.0	-0.04	-0.03
		122.0	-0.02	-0.01
10	After Test 9, transfer Perspex samples into a humidifier with r.h.= 55 %	10.0	0.15	0.13
		22.0	0.09	0.10
		47.0	0.04	0.04
		68.0	0.02	0.02
11	Transfer samples from Test 10 into a humidifier with r.h. = 85 %	8.0	0.2	0.22
		20.0	0.1	0.12
		44.0	0.06	0.09

APPENDIX 6

INSTRUMENTS CALIBRATION

A6.1 THERMOCOUPLE CALIBRATION

Both the bulk air and porous plate surface thermocouples were calibrated against a reference temperature source before they were used in the experiment. The aim was to obtain correct temperature values and to eliminate any "bad" thermocouple junction which would give erroneous results. The procedure for calibrating the thermocouples is as follows :-

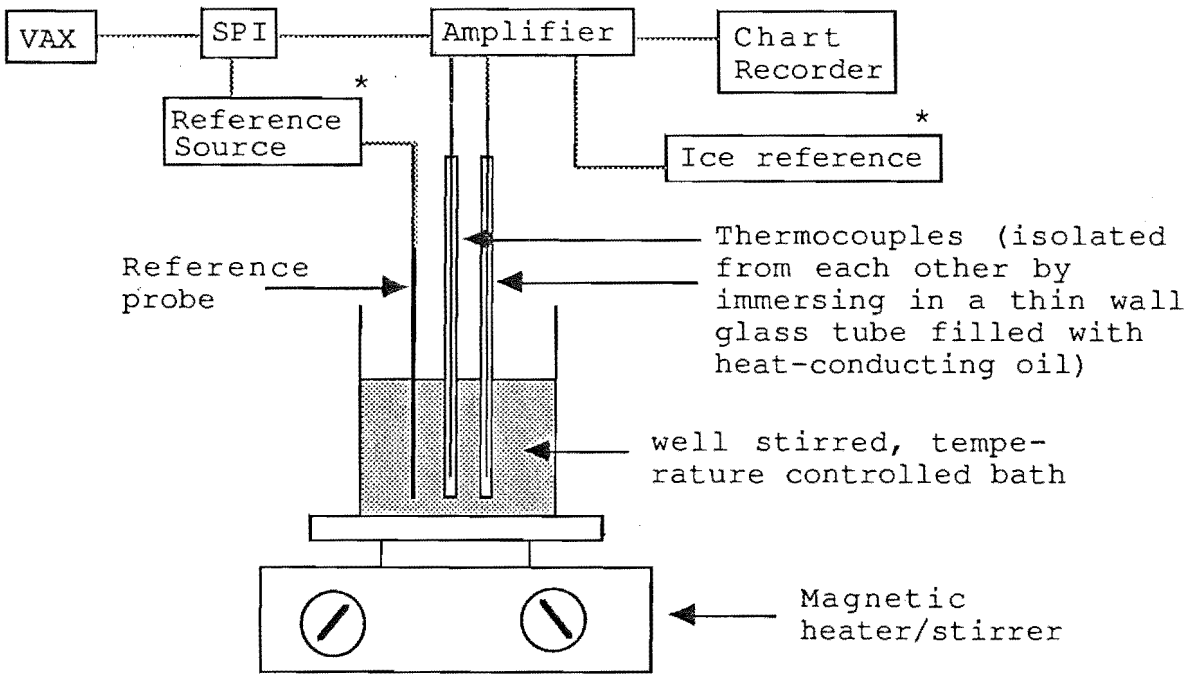

Fig. A6.1 Basic Set-up for Thermocouples Calibration.

* Note :-

(1) There are two reference temperature source being used in the calibration. The first one was the H.P. Quartz Thermometer (Table 4.1) and the second one was the dry-bulb probe of the "Dew-All" Humidity Sensor (Inst 752 Table 4.1). The H.P. Quartz Thermometer was the more accurate of the two and was used to obtain

the calibration depicted in Fig A6.5. Unfortunately the H.P Quartz Thermometer failed to operate subsequently and the "Dew-All" probe was used for all other calibrations.

(2) The ice reference junction was needed for the surface thermocouples only. The bulk air thermocouples amplifier has an in-built function which performed the ice-point compensation.

Fig. A6.2 shows the result of one such calibration. The x-axis is the time elapsed since the turning on of the heater. The y-axis to the left shows the Serial Parallel Interface ("SPI") output and the axis to the right shows the equilavent temperature in degrees Celcius. The calibrating bath was originally filled with a ice/water mixture and the contents were well-stirred throughout the course of the calibration. The heating rate of the heater is adjusted carefully so that no apparent time lag exist between the outputs of the thermocouples junctions being calibrated and the reference source. "Dynamic" calibration (Fig A6.2) was carried out as it produced the maximum number of data points over a given time period.

If there were a negligible time lag between the various thermocouples and reference source outputs in Fig.A6.2, by examining the various curves at the turning points, we could construct from it a calibration curve for the respective thermocouples as illustrated in Fig. A6.3. From the curve, the "SPI" output of the thermocouple readings could be converted into its equilavent value in degree Celsius.

Two types of thermocouple amplifiers were calibrated. The first type was labelled "Chip" in fig A6.2 and A6.3 and this refers to the amplifier with cold junction compensation (Inst P120 Table 4.1). The output of this amplifier to a thermocouple junction input was 10 mV per degree Celsius. In order for the "SPI" to accept the input from this amplifier, a second amplifier circuit was used to convert the output from amplifier P120 into a voltage reading in the range of 0 to 10 V.

The second type of thermocouple amplifier was labelled "Ice" and was just a straight amplifying circuit (Inst 1671 Table 4.1). The ice reference point was needed for the working of this amplifier and the output was again in the range of 0 to 10 V.

"Chip" was used for measuring the bulk air temperature in

Fig. A6.2: THERMOCOUPLES CALIBRATION

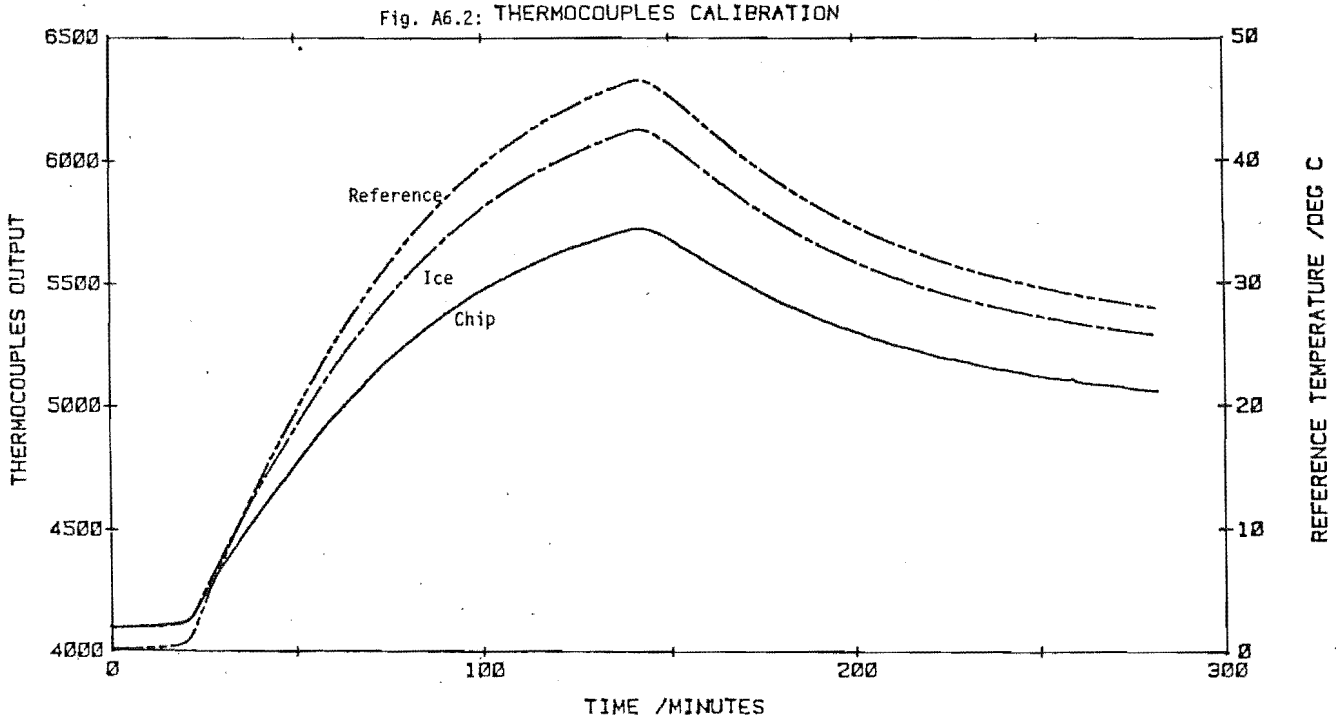

Fig. A6.3: THERMOCOUPLES CALIBRATION

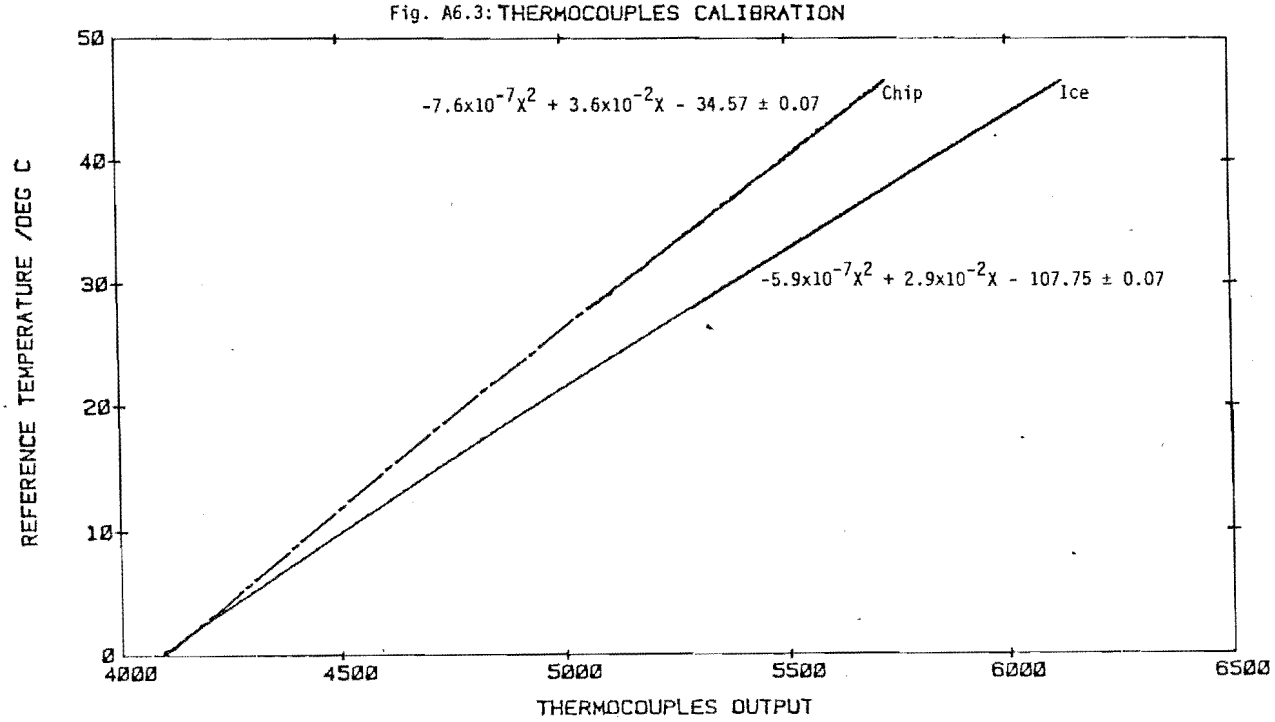

the chambers or the condenser bath temperature; while "Ice" was used for measuring the porous plate surface temperature.

The program "POLYFIT" (Appendix 1.5) was used to fit a curve (normally second-order) to the data points by means of the least-squares criterion, as depicted in fig A6.3. No hysteresis was observed in the calibration curve.

As mentioned earlier, not all the outputs of the thermocouple junctions were logged continuously onto the computer due to a limitation of logging equipment. For those thermocouple junctions whose outputs which were not logged onto the computer, "step-wise" calibration technique was employed. The set-up was essentially the same as that in fig A6.1. The temperature level of the bath was varied from one constant level to the next as shown in the following figure :-

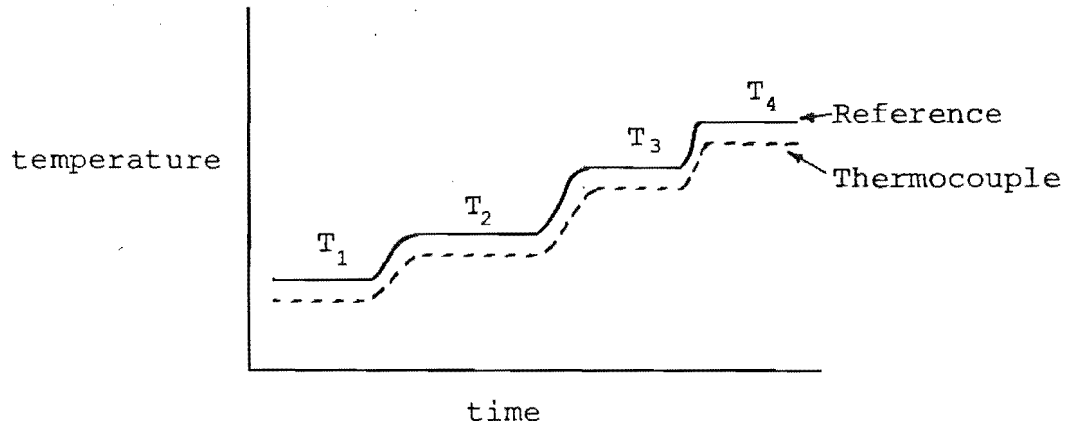

Fig A6.4 Temperature History of a "Step- Wise" Calibration Run.

This allowed ample time at each required temperature level T_1, T_2,.....etc to record manually the outputs of the thermocouple junction.

Fig A6.5 to A6.7 are the calibration curves for the bulk air thermocouples (Inst p120 and P126). Fig A6.5 was the first calibration curve and was used for experiments up to Runs H43. The thermocouple amplifier for this case was left in room condition and it was later found that it was affected slightly by the fluctuation in the room temperature (especially in the summer months when the fluctuation in room temperature was the greatest

Fig. A6.5: CALIBRATION CURVE FOR BULK AIR THERMOCOUPLES - I

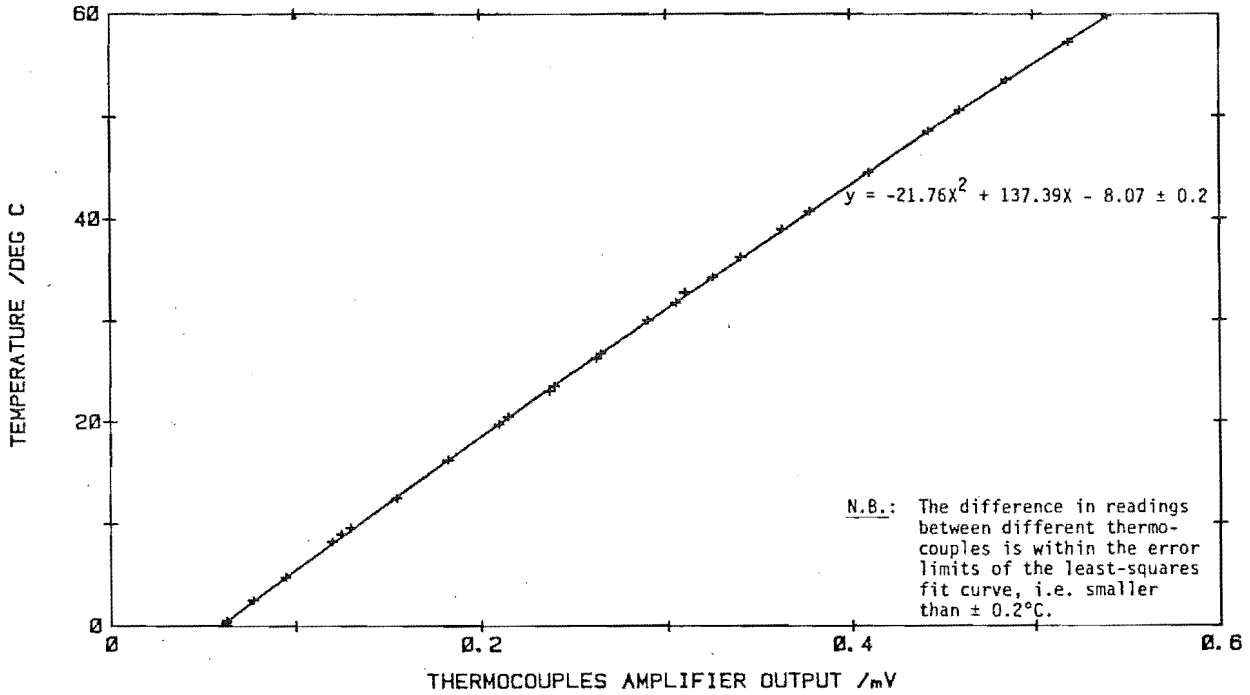

Fig. A6.6: CALIBRATION CURVE FOR BULK AIR THERMOCOUPLES -II

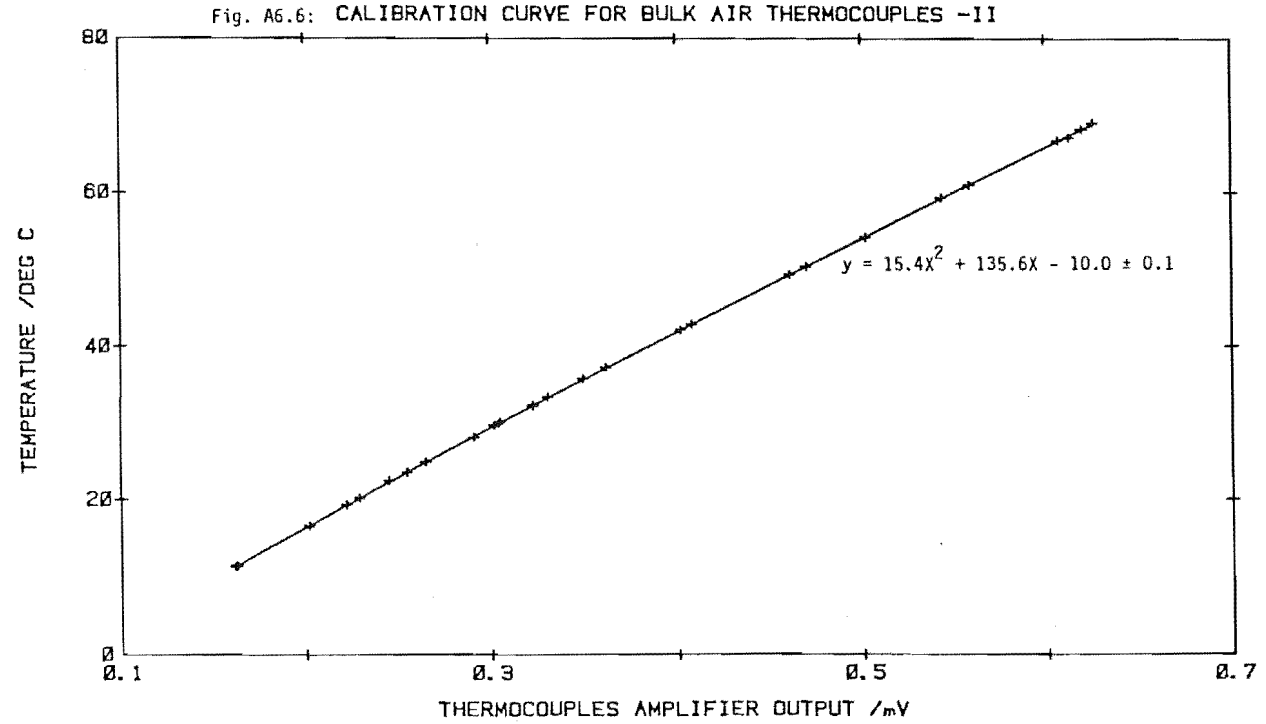

Fig. A6.7: CALIBRATION CURVE FOR BULK AIR THERMOCOUPLES -III

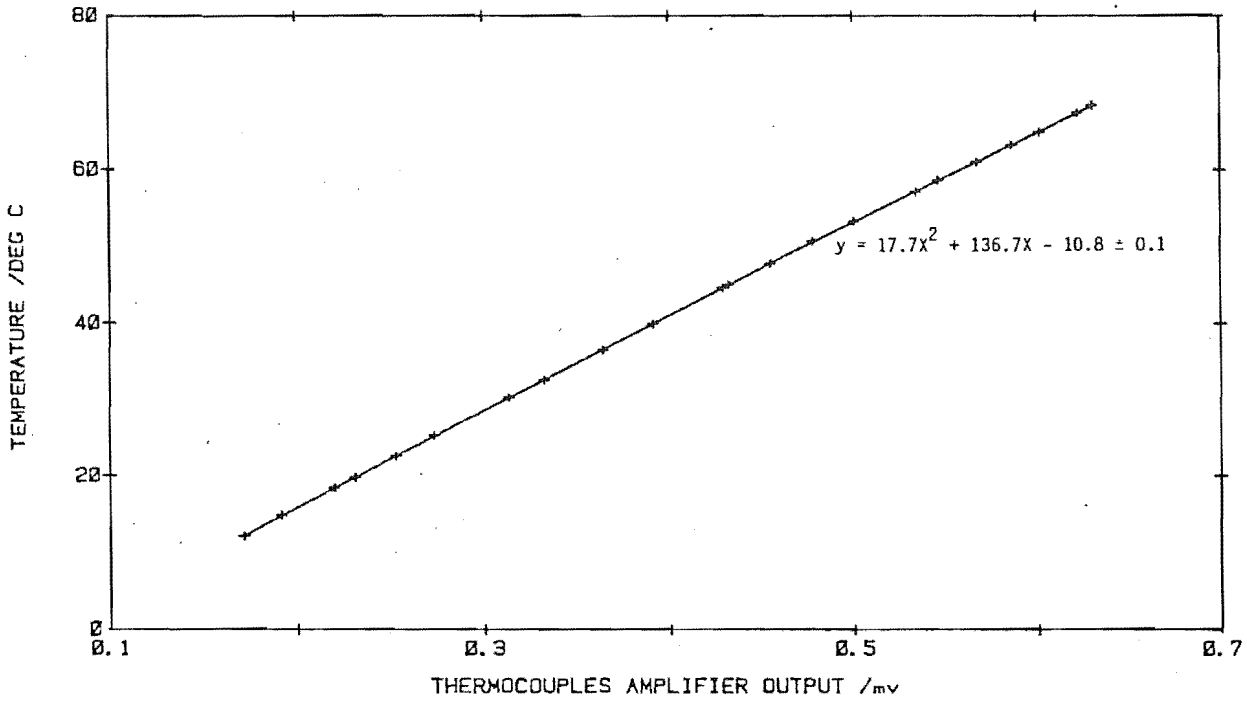

with the maximum penetration of the sun's rays). This fluctuation amounted to ± 0.25 °C which was greater than the uncertainty of the calibration curve. To overcome this problem the thermocouple amplifier (Inst P120) was then placed in a temperature-controlled box set at 30 °C. Fig A6.6 is the calibration curve for this case. During the course of selective runs, the readings of the thermocouples were checked intermittently with the reference source to ascertain that they had not drifted from the calibrated value. Fig A6.6 was applicable for all the experimental runs for the horizontal cavity configuration from Run H43 onwards.

When the Test Cavity was shifted to a vertical cavity configuration, intermittent checking with the reference thermometer revealed that the thermocouple outputs were about 0.5 °C higher than the reference source temperature. No obvious explanation can be given for this drift in the thermocouple readings but one possible cause could be the different state of the thermocouples wires between their positions in the Test Cavity to the amplifier for the two-cavity configuration. For the Horizontal Cavity case, some length of the wires were tied together in a bundle due to the excess length of the wires. No bundle of wires was present for the vertical cavity case. The number of bends and kinks in the wires would therefore be different for the two cases and this could be a factor in the different outputs of the thermocouples circuit. Another, though less likely, reason could be the thermocouple switch had degraded with time. But the fact that the deviation of the thermocouple outputs was sudden when the test cavity configuration was changed and the subsequent non-deviation of the thermocouple output after that tended to favour belief in the former explanation. Nevertheless, another calibration was carried out for the bulk air thermocouple circuits when used for the vertical cavity configuration and this is given in Fig. A6.6.

For the plate surface thermocouples circuit (Inst P127 and 1671), a similar calibration procedure was carried out. As the reference junction in this case was a ice/water mixture, the thermocouple readings were calibrated against a standard reference table for copper-constantine thermocouple. Deviation from the reference table value was found to be ± 0.2 °C over the range of 20 to 60 °C. Thus the values from the the standard reference table

were used to convert the thermocouple output in mV into °C.

A6.2 DEW-POINT METER CALIBRATION

The dew-point readings from the "Dew-All" Humidity Sensor (Inst 752 Table 4.1) were calibrated against reference dew-point temperature obtained from air stream bubbling through saturated salt solution . The calibration set-up and the procedure are described as follows :-

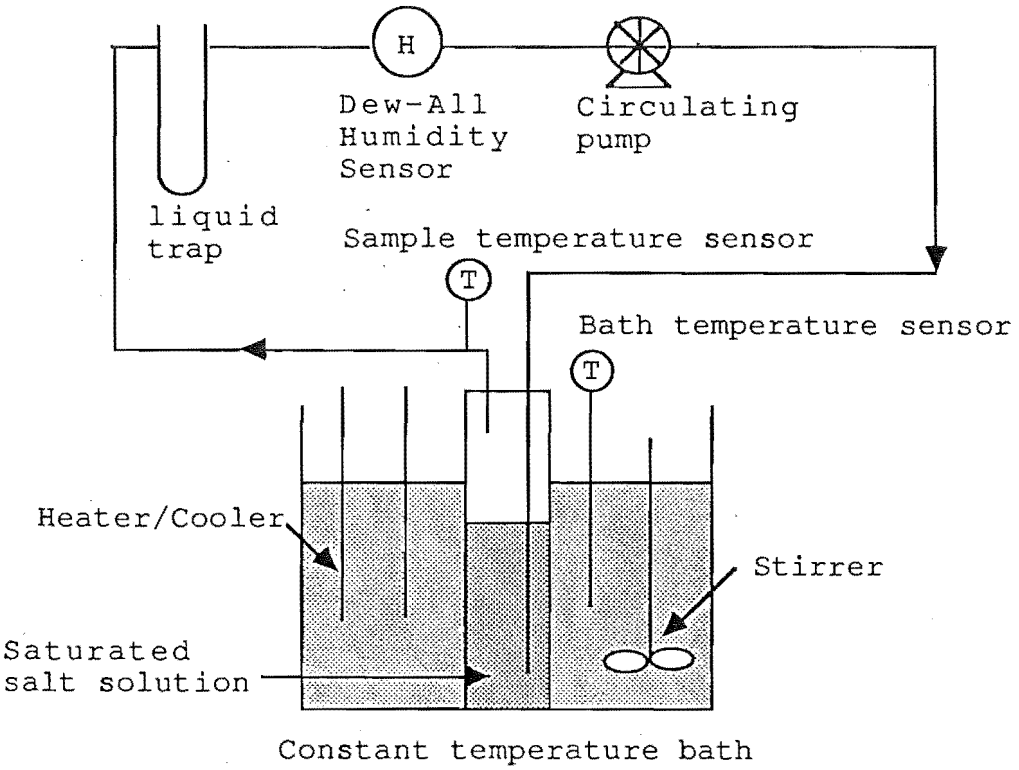

Fig. A 6.8 Calibration Circuit for the Dew-All Humidity Sensor.

Procedure:

(1) The whole system was first flushed with trichloroethylene to remove any traces of oil deposits that may be left by the pump, copper fittings etc. It was then flushed with dry air for about 7 hours.

(2) Teflon tubes and glassware were used to minimise moisture adsorption/desorption by the sampling system.

(3) Saturated salt solutions were allowed to come into thermal

equilibrium with the bath before any measurement. This was achieved by observing the dry-bulb temperature of the gas leaving the wash-bottle agreed with the bath temperature to within ± 0.2°C.

(4) All sample lines were traced heated to prevent moisture condensation. The traced heat temperature would be kept higher (about 10 °C) than the expected dew-point temperature measured.

(5) The temperature of the bath (Inst P129 Table 4.1) was held to within ± 0.05 °C.

(6) A sample was kept circulating for at least 20 minutes before any measurement was taken. The final measurement was obtained when the read-out on the "Dew-All" meter was steady.

(7) The reference relative humidities were obtained from Hickman [149], a copy of which is reproduced here in Fig. A6.9. A range of reference dew-points can be obtained using a combination of distilled water, saturated sodium chloride and potassium carbonate solutions and a range of dry-bulb temperature from 18 to 30 °C.

The result of the calibration is presented in Fig. A6.9. The range of the dew-points calibrated was from 6.9 °C to 27.3°C. A best-fit equation for the data by the least-squares technique yielded a standard deviation of 0.13 °C; which was within the accuracy limit (± 0.3°C) of the dew-point readings of the "Dew All" Sensor. Table A6.1 lists the range of calibration conditions.

Fig. 6.9: CALIBRATION CURVE FOR 'DEW-ALL' DEW POINT SENSOR

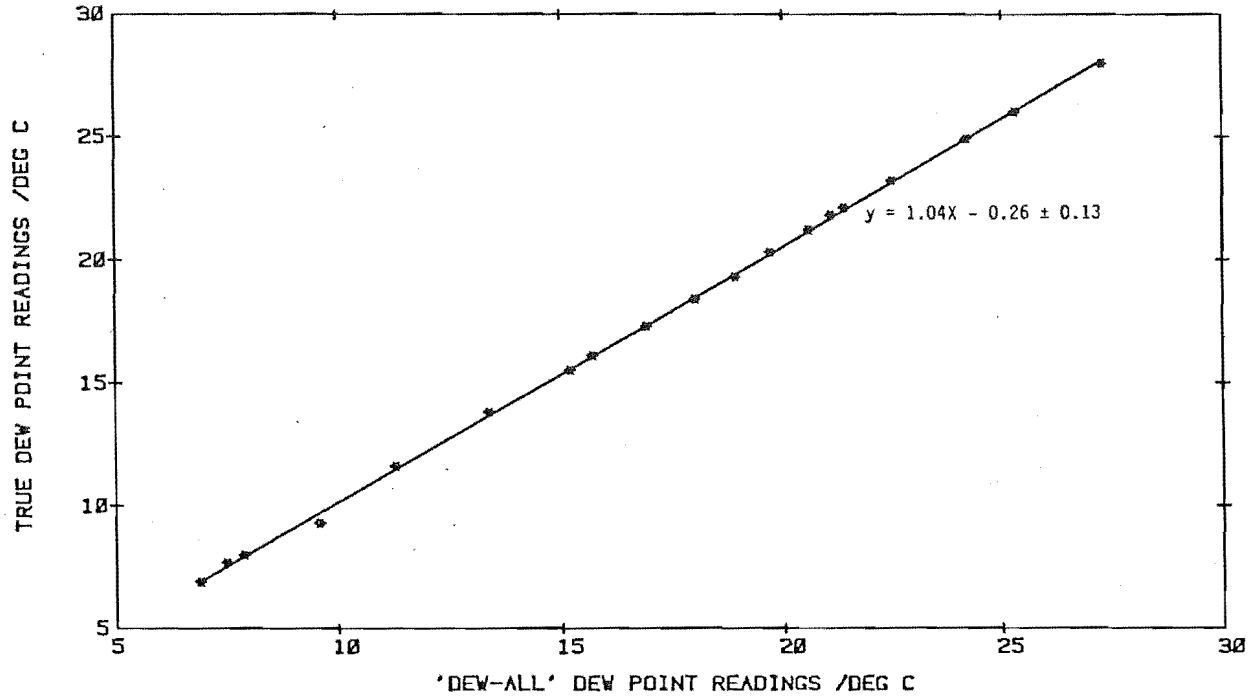

Table A6.1 "Dew-All" Humidity Sensor Calibration Conditions.

Run	Salt solutions	Dry bulb temp /°C	Reference r.h./%	Expected dew-point /°C	Measured dew-point /°C	Measured r.h./%
1	DW*	22.1	100.0	22.1	21.4	96.4
2	DW	18.4	100.0	18.4	18.0	97.5
3	NaCl*	33.0	75.0	28.0	27.3	72.2
4	NaCl	31.0	75.0	26.0	25.3	71.8
5	NaCl	28.1	75.0	23.2	22.5	71.7
6	NaCl	29.8	75.0	24.9	24.2	72.0
7	NaCl	26.6	75.0	21.8	21.1	71.8
8	NaCl	26.0	75.0	21.2	20.6	72.2
9	NaCl	24.0	75.0	19.3	18.9	73.2
10	NaCl	25.0	75.0	20.3	19.7	72.5
11	NaCl	21.7	76.0	17.3	16.9	74.1
12	NaCl	19.7	76.0	15.5	15.2	75.0
13	K_2CO_3*	19.5	44.0	6.9	6.9	44.0
14	K_2CO_3	20.4	44.0	7.7	7.5	43.3
15	K_2CO_3	20.8	43.8	8.0	7.9	43.3
16	K_2CO_3	22.6	43.5	9.6	9.3	42.7
17	K_2CO_3	25.0	43.0	11.6	11.3	42.2
18	K_2CO_3	27.5	43.0	13.8	13.4	41.9
19	K_2CO_3	30.1	43.0	16.1	15.7	41.8

* Note: (i) DW = Distilled Water
(ii) NaCl = Saturated Sodium Chloride Solution
(iii) K_2CO_3 = Saturated Potassium Carbonate Solution.

APPENDIX 7

TABLES OF COMPLETE EXPERIMENTAL DATA.

A7.1 PROGRAM FOR ACCEPTING DATA INPUTS FROM THE SERIAL PARALLEL INTERFACE (SPI).

The raw experimental data is logged onto the VAX computer via the Serial Parallel Interface (SPI). The procedure for data acceptance is controlled by software written in the high-level Basic language. The program was also responsible for the generation of data files from all the measuring instruments. The first step was to open all the data files needed and assign data filenames to each file. A command "#R" then wakes the SPI up i.e telling the SPI to send data from the measuring elements (eg. thermocouples, average power meter etc) to the computer to be computed and then written onto each file. Once the data at a specific time had been computed and written, the program would "hibernate" the SPI until the timing device in the program "wakes" the SPI again to accept new data. The data transferred from the SPI to the computer is in the RS232C ASCII format. The data was interpreted by the program as a number between 4095 and 8190 which corresponded to 0 to 10V analog output from the measuring elements . The program then computed the required quantity (eg. temperature,power input etc) from this number. The timing device in the program was controlled by the keyword "SLEEP".

A7.2 PRESENTATION OF EXPERIMENTAL DATA.

All the experimental data used to produce the graphs in Chapter 6 and 7 are presented in this Appendix. It is in a form which had been evaluated from the raw data. No raw experimental data is presented in this Appendix as to do so would greatly increase the bulk of this thesis. The data had all been stored in floppy disks and are available upon request from the project supervisor.

A7.3 Tables of Experimental Data :-

Table A7.1 Heat Loss From Controlled Chamber (C.C.) to Surroundings - One Vertical Porous Plate Case.(Fig.6.1)

Run no	Temp C.C. °C ± 0.1	Temp Ambient °C ± 0.3	ΔT_1 °C	Heat loss W
H9	40.0	22.0	18.0	8.8
H21	34.2	21.7	12.5	3.3
H25	39.8	23.3	17.2	6.9
H27	49.8	19.7	30.1	19.0
H28	60.0	22.0	38.0	24.0
H29	30.0	22.2	7.8	0.0
H30	47.0	22.5	24.5	14.3
H30a	56.5	22.0	34.5	22.5

Table A7.2 Heat Loss From Controlled Chamber (C.C.) to Surroundings - One Horizontal Porous Plate Case.(Fig.6.2)

Run no	Temp C.C. °C ± 0.1	Temp Ambient °C ± 0.3	ΔT_1 °C	Heat loss W
H31	40.5	26.9	13.6	7.0
H32	45.5	26.7	18.8	11.3
H33	50.8	28.1	22.7	15.7
H34	63.0	27.7	35.3	27.3
H35	55.3	29.4	38.0	19.4
H36	61.0	28.2	32.8	25.0
H37	43.8	27.5	16.3	9.1
H38	36.2	26.6	9.6	2.7

Table A7.3 Moisture Loss From Controlled Chamber (C.C.) to Surroundings- Various Experimental Conditions.(Fig.6.3)

Run no	Condition*	P_c/mm Hg	P_a/mm Hg	ΔP_1/mm Hg	m/gh^{-1}
M3	V-PP	27.1	8.3	18.8	0.43
M7	V-PP	28.0	6.8	21.2	0.48
M9	V-PP	22.1	9.1	13.0	0.16
M10	V-PP	15.0	8.2	6.8	-0.05
M11	V-PP	18.5	7.3	11.2	0.03
M12a	V-PP	24.9	8.9	16.0	0.22
M13	V-PP	24.8	9.2	15.6	0.19
M14	V-PP	27.5	7.2	20.3	0.38
M22a	H-PP	27.1	8.8	18.3	0.30
M22b	H-PP	24.9	10.8	14.1	0.19
M22c	H-PP	22.0	9.3	12.7	0.15
M22d	H-PP	18.3	7.7	10.6	0.05
M29	H-C	28.0	9.0	19.0	0.31
M30	H-C	25.1	11.6	13.4	0.21
M31	H-C	24.4	9.3	15.1	0.11
M32	H-C	23.7	9.4	15.3	0.09
HM39a	V-C	28.7	7.7	21.0	0.61
HM39b	V-C	18.5	8.0	10.5	0.01
HM39c	V-C	24.9	10.6	14.3	0.23

*Notes :- V-PP : One Vertical Porous Plate
H-PP : One Horizontal Porous Plate
H-C : Horizontal Cavity
V-C : Vertical Cavity

Table A7.4 Heat Transfer Across One Vertical Porous Plate (Fig.6.4)

Run	T_c °C	T_{cp} °C	T_{rp} °C	T_r °C	T_a °C	ΔT_p °C	q_T W	q_a W	q_p W
H10	40.1	37.4	32.1	30.0	23.0	5.3	38.1	7.6	30.5
H11	40.0	37.2	29.7	25.6	23.0	7.5	49.9	7.4	42.5
H12	31.3	28.9	24.2	21.5	22.5	4.7	28.7	0.5	28.2
H13	40.0	36.7	28.2	23.2	23.5	8.5	58.1	7.1	51.0
H14	39.7	36.3	27.4	22.1	22.5	8.9	60.5	7.7	52.8
H16	34.6	31.7	25.0	21.0	22.5	6.7	44.40	3.3	41.1
H17	28.8	26.7	22.9	21.0	22.0	3.8	22.1	0.0	22.1
H18	26.0	24.4	22.1	21.0	22.1	2.3	13.20	0.0	13.2
H19	45.3	40.6	29.6	24.4	23.0	11.0	75.4	11.9	63.5
H20	31.3	28.7	23.8	21.0	22.8	4.9	30.5	0.3	30.2
H22	40.3	36.9	26.8	20.9	22.7	10.1	67.8	8.0	59.8

Table A7.5 Heat Transfer Across One Horizontal Porous Plate(Fig6.5)

Run	T_c °C	T_{cp} °C	T_{rp} °C	T_r °C	T_a °C	ΔT_p °C	q_T W	q_a W	q_p W
H39	30.0	26.5	22.9	21.4	23.3	3.6	23.1	0.2	22.9
H40	35.6	31.4	24.8	22.7	27.4	6.6	42.1	1.7	40.4
H41	40.3	35.7	27.3	24.0	27.1	8.5	58.5	6.6	52.2
H42	47.3	42.0	30.7	27.0	28.4	11.2	79.8	12.1	67.7
H43	57.7	51.4	35.7	30.9	26.5	15.7	117.9	24.2	93.7

Table A7.6 Isothermal Moisture Transfer Across One Vertical Porous Plate Based on Bulk Air Vapour Pressure Difference (Fig.6.6)

Run	T_c °C	$(rh)_c$ %	P_c mmHg	T_r °C	$(rh)_c$ %	P_r mmHg	ΔP_p mmHg	m_T gh^{-1}	m_l gh^{-1}	m_p gh^{-1}
M4	30.0	58.0	18.5	30.0	43.0	13.7	4.8	6.88	-0.02	6.90
M5	30.0	54.0	17.2	30.0	38.0	12.1	5.1	7.81	0.03	7.78
M6	30.0	53.0	16.9	30.0	36.0	11.5	5.4	7.83	-0.03	7.86
M16	30.1	75.0	24.0	30.1	69.0	22.1	1.9	3.10	0.22	2.88
M17	30.0	70.0	22.3	30.0	62.0	19.7	2.6	3.96	0.17	3.79
M18	30.0	62.0	19.7	30.0	52.0	16.5	3.2	5.22	0.08	5.14
M19	30.0	57.0	18.1	30.0	43.0	13.7	4.4	6.68	0.06	6.62
M20	30.0	54.0	17.2	30.0	38.0	12.1	5.1	7.30	0.00	7.30
M21	32.0	80.0	28.5	32.0	76.0	27.1	1.4	2.1	0.33	1.77

Table A7.7 Isothermal Moisture Transfer Across One Horizontal Porous Plate Based on Bulk Air Vapour Pressure Difference (Fig.6.6)

Run	T_c °C	$(rh)_c$ %	P_c mmHg	T_r °C	$(rh)_c$ %	P_r mmHg	ΔP_p mmHg	m_T gh^{-1}	m_l gh^{-1}	m_p gh^{-1}
M23	30.3	79.8	25.8	30.3	78.3	25.4	0.4	0.83	0.30	0.53
M24	30.2	71.7	23.1	30.2	67.1	21.6	1.5	2.13	0.18	1.95
M25	31.0	64.5	21.7	31.0	58.5	19.7	2.0	2.87	0.11	2.77
M26	30.0	60.0	19.1	30.0	52.1	16.6	2.5	3.72	0.02	3.70
M27	30.0	52.8	16.8	30.0	43.6	13.8	3.0	4.28	-0.06	4.34
M28	30.0	46.6	14.8	30.0	34.8	11.1	3.7	5.15	-0.07	5.22
M28b	30.0	57.5	18.3	30.0	43.0	13.7	4.6	6.64	0.02	6.62

Table A7.8 Heat Loss From Controlled Chamber (C.C.) to Surroundings - Vertical Cavity Case.(Fig.7.1 Chapter 7)

Run no	Temp C.C. °C ± 0.1	Temp Ambient °C ± 0.2	ΔT_1 °C	Heat loss W
H70	30.0	22.6	7.4	0.30
H71	38.9	21.6	17.3	8.43
H72*	49.1	21.6	27.5	17.54
H73*	61.6	21.4	40.2	27.83
H74*	61.5	21.3	40.2	27.17
H75*	49.2	21.8	27.4	16.96

* Notes :-

(i) Runs H73 and H74 were avaraged to give q_1 = 27.50 W

(ii) Runs H72 and H75 were averaged to give ΔT_1 = 27.45 °C and q_1= 17.25 W.

Table A7.9 Heat Loss From Controlled Chamber (C.C.) to Surroundings - Horizontal Cavity Case with Upwards Transfer. (Fig.7.2)

Run no	Temp C.C. °C ± 0.1	Temp Ambient °C ± 0.2	ΔT_1 °C	Heat loss W
H45	38.2	25.2	13.0	7.25
H46	45.6	27.0	18.6	12.60
H47	56.7	28.0	28.7	23.05
H48a	61.8	27.9	33.9	28.83
H48b	62.7	26.8	35.9	30.13
H49	52.8	27.4	25.4	19.32
H50	49.1	27.8	21.3	15.50
H51	42.4	27.4	15.0	9.02
H52	36.8	26.3	10.5	5.00
H53	31.0	25.0	6.0	1.00

Table A7.10 Heat Loss From Controlled Chamber(C.C.) to Surroundings - Horizontal Cavity Case With Downdards Transfer. (Fig.7.3)

Run no	Temp C.C. °C ± 0.1	Temp Ambient °C ± 0.2	ΔT_1 °C	Heat loss W
H66	29.9	20.3	9.6	3.41
H67	39.2	21.6	17.6	11.43
H68	49.9	21.7	28.2	22.79
H69	62.0	21.9	40.1	35.46

Table A7.11 Heat and Mass Transfer Across a Vertical Cavity -

Experimental Conditions and Results.

Run	T_c °C	T_{cp} °C	T_D °C	P_c mmHg	P_{cp} mmHg	T_r °C	T_{rp} °C	T_D °C	P_r mmHg	P_{rp} mmHg	T_{cc} °C	T_{rc} °C	P_{cc} mmHg	P_{rc} mmHg	T_a °C	P_a mmHg	q_T W	q_l W	q_c W	q_r W	q_m W	m_T gh^{-1}	m_l gh^{-1}	Ra x10^5	Nu	Sh
HM40	30.1	29.1	7.4	7.73	7.71	18.0	18.3	7.4	7.73	7.71	26.98	20.92	7.52	7.52	23.0	6.53	15.18	0.06	0.20	10.22	-	3.70	0.00	5.96	6.11	-
HM41	30.2	29.1	20.1	17.65	17.45	18.0	18.8	13.3	11.45	11.62	26.97	20.93	15.13	13.77	22.9	8.01	17.87	0.22	0.20	10.16	2.47	3.70	0.00	6.10	6.27	5.32
HM42	30.0	29.1	23.0	21.08	20.77	17.9	18.7	13.5	11.61	11.86	27.01	20.79	17.49	15.14	23.2	7.89	18.67	-0.19	0.20	10.43	3.92	5.80	0.14	6.36	5.46	6.30
HM43	30.0	29.8	23.0	22.53	22.27	30.5	29.7	15.0	12.79	13.00	29.40	19.64	19.64	15.64	23.0	7.58	-	-	-	-	-	4.78	0.20	0.46	-	2.47
HM44	30.0	29.9	20.8	18.43	18.28	30.5	29.8	14.3	12.23	12.35	29.85	29.85	16.66	13.97	23.0	6.74	-	-	-	-	-	2.85	0.08	0.31	-	2.23
HM45	32.0	32.5	21.7	19.48	19.28	39.4	36.7	15.0	12.79	12.97	33.45	36.45	17.11	15.14	23.0	6.52	-	-	-	-	-	3.88	0.13	-2.27	-	4.05
HM46	31.2	31.6	24.3	22.79	22.51	39.2	36.4	15.4	13.13	13.37	32.65	36.05	19.41	16.47	22.0	6.14	-	-	-	-	-	5.61	0.27	-2.51	-	3.85
HM47	31.4	31.9	23.1	21.19	20.85	39.7	36.3	10.4	9.46	9.76	32.75	36.15	17.07	13.55	21.6	6.77	-	-	-	-	-	6.72	0.18	-2.45	-	3.96
HM48	31.3	31.8	19.8	17.32	17.08	39.7	36.5	10.1	9.27	9.48	32.75	36.15	14.48	12.08	21.4	5.93	-	-	-	-	-	4.56	0.06	-2.57	-	4.02
HM49	30.4	30.0	19.9	17.43	17.22	31.7	29.8	9.5	8.90	9.09	30.10	30.10	14.96	11.35	21.6	6.19	-	-	-	-	-	3.98	0.06	0.41	-	2.36
HM50	30.6	30.2	23.2	21.32	21.02	32.0	30.0	9.5	8.91	9.18	30.10	30.10	17.64	12.56	21.6	6.77	-	-	-	-	-	6.02	0.19	0.58	-	2.48
HM54	30.0	29.0	18.7	16.19	15.92	17.9	18.7	8.2	8.16	8.38	26.87	20.83	13.11	11.18	22.6	7.20	18.76	0.31	0.20	10.14	3.23	4.83	-0.03	0.61	6.38	5.60
HM55	30.0	29.0	21.9	19.72	19.35	17.9	18.7	8.4	8.27	8.58	26.90	20.80	15.41	12.52	23.3	7.72	19.40	-0.27	0.20	10.24	4.67	6.92	0.09	6.32	5.90	5.23
HM56	39.2	37.1	7.4	7.73	7.71	15.5	17.3	7.0	7.50	7.53	32.78	21.62	7.51	7.73	21.5	6.92	39.49	8.88	0.36	19.43	-	-	-	10.42	7.56	-
HM57	39.1	37.1	22.7	20.69	20.27	15.6	17.4	8.0	8.05	8.40	32.86	21.64	15.73	12.95	22.4	6.70	43.38	8.05	0.36	19.47	5.31	8.02	0.17	10.74	7.07	6.17
HM58	39.1	37.1	26.0	25.20	24.66	15.5	17.3	8.3	8.22	8.68	32.88	21.52	18.63	14.70	23.2	8.10	44.35	7.30	0.37	19.69	7.15	10.68	0.29	11.00	6.76	5.75
HM59	49.6	46.8	30.9	33.50	32.68	17.2	19.5	8.7	8.44	9.15	40.72	25.58	23.58	18.24	22.6	5.76	70.41	16.61	0.49	27.82	10.87	16.43	0.71	13.41	7.40	6.22
HM60	49.6	46.8	28.4	29.02	28.34	17.3	19.9	8.6	8.38	8.96	40.74	25.96	20.90	16.40	22.5	6.54	68.29	16.70	0.48	27.21	8.76	13.38	0.50	12.97	7.86	6.09
HM61	49.6	46.8	8.4	29.02	28.34	17.3	19.9	8.6	8.38	8.96	40.74	25.96	8.19	8.19	22.0	5.95	59.97	16.95	0.48	27.39	-	-	-	12.66	7.84	-
HM62	49.5	46.5	30.1	31.99	31.13	14.5	17.2	3.9	6.05	6.80	40.02	23.68	21.65	16.27	22.1	5.98	73.99	16.95	0.53	29.67	11.28	17.04	0.64	14.71	7.33	6.49
HM63	49.4	46.5	3.3	5.81	5.80	14.4	17.1	3.0	5.68	5.70	39.85	23.75	5.65	5.94	22.3	5.65	63.62	16.70	0.52	29.43	-	-	-	14.03	8.11	-
HM64	49.4	46.6	28.1	28.51	27.77	14.3	17.6	3.9	6.06	6.69	40.15	24.05	19.68	14.77	22.2	5.82	71.92	16.78	0.52	29.27	9.60	14.50	0.51	14.41	7.52	6.10
HM65	30.0	29.1	22.9	20.96	20.64	17.9	18.8	13.2	11.38	11.64	27.02	20.88	17.34	14.94	22.8	6.66	18.97	0.14	0.20	10.31	3.99	5.90	0.18	6.29	5.55	5.24
HM66	30.0	29.0	12.5	10.88	10.86	18.0	18.8	12.3	10.73	10.74	26.95	20.85	10.74	10.87	22.3	6.46	15.22	0.56	0.20	10.25	-	-	-	6.00	5.44	-
HM67	30.0	29.8	23.2	21.34	21.28	30.5	29.7	21.2	18.88	18.93	29.10	29.70	20.73	19.48	22.8	7.90	-	-	-	-	-	1.10	0.14	0.14	-	1.64
HM68	30.0	29.8	26.2	25.53	25.38	30.5	29.7	21.7	19.47	19.60	29.70	29.70	23.81	21.16	22.8	8.74	-	-	-	-	-	2.99	0.28	0.30	-	2.18
HM69	32.6	32.5	24.4	22.92	22.59	34.5	32.4	9.8	9.09	9.39	32.15	32.15	18.82	13.15	22.8	8.33	-	-	-	-	-	6.68	0.19	0.63	-	2.45
HM69a	32.6	32.5	24.4	22.92	22.59	34.5	32.4	9.8	9.09	9.35	32.15	32.25	18.82	13.15	22.8	8.33	-	-	-	-	-	6.68	0.19	0.54	-	2.45
HM70	32.3	32.5	24.5	23.07	22.74	34.6	33.0	9.3	8.79	9.08	33.01	33.51	19.15	12.66	21.3	6.63	-	-	-	-	-	6.47	0.26	0.29	-	2.04
HM71	30.5	30.4	23.6	21.85	21.80	31.6	30.6	20.8	18.42	18.48	30.62	30.82	21.11	19.17	24.2	6.34	-	-	-	-	-	1.39	0.23	0.04	-	1.28
HM72	30.4	30.4	23.6	21.85	21.80	31.5	30.7	21.2	18.88	18.94	30.62	30.82	21.12	19.62	24.0	7.83	-	-	-	-	-	1.31	0.17	-0.09	-	1.62

Table A7 11 Contd.

Run	T_c °C	T_{cp} °C	T_b °C	P_c mmHg	P_{cp} mmHg	T_r °C	T_{rp} °C	T_D °C	P_r mmHg	P_{rp} mmHg	T_{cc} °C	T_{rc} °C	P_{cc} mmHg	P_{rc} mmHg	T_a °C	P_a mmHg	q_T W	q_l W	q_c W	q_r W	q_m W	m_T gh^{-1}	m_l gh^{-1}	Ra $x10^5$	Nu	Sh
HM73	30.4	29.3	12.3	10.14	10.70	18.2	19.1	12.3	10.14	10.70	27.26	21.12	10.72	10.72	23.9	-	14.33	-0.44	0.20	10.38	-	-	-	6.02	5.37	-
HM74	39.2	37.1	9.1	8.67	8.65	17.5	19.0	9.1	8.67	8.69	33.20	22.88	8.75	8.75	25.6	-	33.23	5.47	0.33	18.13	-	-	-	9.52	7.00	-
HM75	32.6	32.4	24.4	22.92	22.58	34.4	32.4	9.8	9.09	9.40	32.35	32.35	13.26	22.8	8.33	-	-	-	-	-	-	6.85	0.19	0.61	-	2.61
HM76	30.0	29.8	24.7	23.36	23.25	30.5	29.7	21.5	19.25	19.32	30.05	30.05	22.24	20.33	23.0	8.33	-	-	-	-	-	1.95	0.21	0.22	-	1.95

Table A7.12 Heat and Mass Transfer Across a Horizontal Cavity with downwards transfer - Experimental Conditions and Results.

Run	T_c °C	T_{cp} °C	T_b °C	P_c mmHg	P_{cp} mmHg	T_r °C	T_{rp} °C	T_D °C	P_r mmHg	P_{rp} mmHg	T_{cc} °C	T_{rc} °C	P_{cc} mmHg	P_{rc} mmHg	T_a °C	P_a mmHg	q_T W	q_l W	q_c W	q_r W	q_m W	m_T gh^{-1}	m_l gh^{-1}	Ra $x10^5$	Nu	Sh
HM124	30.4	29.2	14.3	12.23	12.23	17.80	18.2	14.3	12.23	12.23	27.33	20.07	-	-	21.9	-	15.59	2.07	0.24	12.20	-	-	-	7.17	1.17	-
HM125	30.4	29.2	23.2	21.32	21.17	17.8	18.1	13.2	11.38	11.52	27.32	19.98	19.38	13.31	23.2	8.5	16.44	0.70	0.24	12.27	2.13	3.45	0.12	7.95	1.19	1.10
HM126	30.3	29.7	23.2	21.33	21.16	30.3	29.8	14.2	12.15	12.30	-	-	19.30	14.16	23.6	8.3	-	-	-	-	-	3.31	0.13	0.59	-	1.34
HM127	32.6	32.7	23.1	21.19	20.20	38.9	36.4	15.0	12.79	13.01	33.20	35.60	18.15	15.05	23.5	-	-	-	-	-	-	4.91	0.12	-1.66	-	3.28
HM128	39.3	37.5	28.3	28.85	28.59	18.9	19.5	13.0	11.22	11.46	34.37	22.63	25.59	14.46	25.4	8.6	34.25	7.76	0.38	20.61	3.72	5.54	0.39	11.96	1.17	0.99
HM129	39.6	37.8	14.3	12.23	12.21	18.3	19.5	14.3	12.23	12.24	34.56	22.70	-	-	23.6	-	33.27	9.97	0.38	20.91	-	-	-	10.84	1.31	-
HM130	39.3	38.7	27.6	27.70	27.41	39.3	38.7	15.0	12.79	13.05	-	-	24.22	16.24	23.4	6.9	-	-	-	-	-	5.91	0.41	0.82	-	1.44
HM131	39.3	36.7	24.5	23.07	22.84	39.3	37.8	14.7	12.55	12.74	-	-	20.42	15.16	23.8	5.8	-	-	-	-	-	4.44	0.28	0.55	-	1.66
HM132	39.3	37.6	25.0	23.75	23.56	19.0	19.6	12.9	11.16	11.32	34.42	22.77	21.43	13.45	24.0	7.2	34.38	9.24	0.38	20.51	2.60	3.88	0.26	11.51	1.11	0.98
HM133	43.0	40.5	26.2	25.52	25.23	13.7	15.1	4.9	6.49	6.78	36.10	19.52	22.15	9.86	23.9	6.7	48.62	13.24	0.54	28.95	3.82	5.73	0.34	16.68	0.97	0.95
HM134	42.9	40.3	4.9	6.49	6.52	13.5	15.1	4.9	6.49	6.56	35.87	19.52	-	-	23.5	-	45.59	13.56	0.53	28.67	-	-	-	15.17	1.35	-
HM135	42.9	40.4	29.8	31.45	31.11	13.5	15.1	4.9	6.49	6.79	36.03	19.50	27.26	10.64	22.5	6.3	50.72	14.61	0.54	28.81	4.78	7.18	0.56	17.14	0.93	0.86
HM136	42.3	41.3	27.6	27.72	27.29	42.3	41.3	8.1	8.10	8.49	-	-	22.98	12.98	25.3	7.7	-	-	-	-	-	8.07	0.38	1.00	-	1.60
HM137	42.3	42.3	25.5	24.48	24.0	50.9	46.7	9.1	8.67	9.12	43.55	47.35	18.60	14.50	25.0	9.0	-	-	-	-	-	9.57	0.22	-2.30	-6.58	4.69
HM138	44.3	44.3	25.9	25.02	24.3	50.9	46.7	9.1	8.67	9.12	44.95	47.35	19.45	14.01	24.7	12.5	-	-	-	-	-	8.98	0.11	-1.18	-	3.45

Table A7.13 Heat and Mass Transfer Across a Horizontal Cavity with Upwards Transfer- Experimental Conditions and Results

Run	T_c °C	T_{cp} °C	T_D °C	P_c mmHg	P_{cp} mmHg	T_r °C	T_{rp} °C	T_D °C	P_r mmHg	P_{rp} mmHg	T_{cc} °C	T_{rc} °C	P_{cc} mmHg	P_{rc} mmHg	T_a °C	P_a mmHg	q_T W	q_l W	q_c W	q_r W	q_m W	m_T gh^{-1}	m_l gh^{-1}	Ra x10^5	Nu	Sh
HM1	30.2	29.2	22.4	20.33	20.11	20.0	20.7	15.4	13.14	13.30	27.53	22.38	17.64	15.77	24.3	10.8	16.00	0.28	0.17	8.73	2.76	4.07	-0.01	5.17	6.20	4.76
HM2	33.0	31.6	22.2	20.13	19.78	17.6	18.6	12.1	10.59	10.87	28.92	21.32	16.43	14.22	25.6	10.9	25.68	1.80	0.25	12.91	3.81	5.66	-0.02	7.55	7.13	5.64
HM3	36.7	35.1	23.6	21.83	21.44	17.4	18.7	10.6	9.58	9.92	31.53	22.27	17.02	14.34	27.2	12.0	34.66	3.89	0.30	16.02	4.92	7.37	0.0	8.95	8.03	5.99
HM4A	43.7	41.4	25.8	24.89	24.36	18.0	19.8	9.4	8.84	9.28	36.66	24.56	18.46	15.18	27.0	7.5	52.11	11.06	0.39	21.70	6.76	10.14	0.30	11.03	7.78	6.45
HM5	49.6	46.9	28.2	9.25	-	19.2	21.6	9.6	9.25	-	41.22	27.17	20.72	16.83	27.2	6.3	66.37	16.74	0.45	26.08	8.41	12.71	0.50	12.12	8.03	6.64
HM6	49.5	46.8	10.1	9.25	-	19.2	21.6	10.1	9.25	-	41.22	27.17	-	-	27.1	7.0	57.71	16.74	0.43	25.14	-	-	-	11.47	8.10	-
HM7	49.5	46.9	28.6	29.33	28.66	18.7	20.9	9.6	8.97	9.54	40.98	26.77	21.13	17.06	26.7	8.0	68.15	17.14	0.46	26.30	8.62	13.02	0.45	12.35	8.42	6.35
HM9	33.2	31.7	21.2	18.88	18.52	15.1	16.4	7.2	7.62	7.92	28.43	19.57	14.14	11.98	26.0	8.4	29.73	1.50	0.29	14.90	4.56	6.77	0.03	8.96	7.53	6.00
HM10A	60.0	56.1	32.6	36.85	35.89	19.2	22.4	7.6	7.83	8.65	48.32	30.13	25.06	19.48	27.5	8.7	94.62	26.89	0.59	35.41	11.89	18.83	0.70	14.63	8.27	6.70
HM10B	60.0	56.1	-	-	-	19.5	22.9	-	-	-	48.48	30.46	-	-	-	-	83.32	27.80	0.58	35.35	-	-	-	14.02	8.24	-
HM11	60.0	56.3	31.2	34.16	33.28	19.5	22.7	7.6	7.83	8.58	48.50	30.48	23.46	18.40	24.8	7.5	96.70	29.49	0.58	35.24	11.02	17.10	0.53	14.40	8.52	6.73
HM14	60.0	56.2	28.0	28.38	27.68	19.4	22.5	7.7	7.94	8.52	48.28	30.34	20.12	16.08	25.4	7.9	93.95	28.89	0.58	35.01	8.34	13.10	0.42	14.28	8.89	6.55
HM15	59.7	56.9	33.2	38.17	37.27	29.10	30.0	12.7	11.02	11.79	50.71	36.17	27.13	21.93	24.0	6.8	85.67	29.99	0.47	29.43	11.16	17.81	0.85	11.07	7.51	6.63
HM16	59.7	57.7	34.0	39.93	39.16	38.7	38.0	18.4	15.89	16.55	53.09	42.55	30.35	25.35	25.2	6.8	71.48	28.59	0.34	22.20	9.73	15.60	0.92	7.64	7.43	5.85
HM17	59.7	57.7	32.0	35.65	35.0	39.2	38.5	18.4	15.89	16.44	53.30	42.91	27.69	23.73	25.7	6.7	68.23	28.31	0.32	21.63	8.66	13.02	0.72	7.43	7.03	6.20
HM18	59.7	57.0	31.3	34.48	33.71	29.1	30.0	13.3	11.45	12.10	50.71	36.33	25.32	20.49	25.6	7.5	83.05	28.39	0.44	29.17	9.32	14.84	0.62	10.82	8.16	6.00
HM19	30.8	31.4	25.2	24.04	23.90	39.6	36.4	18.7	16.18	16.31	32.35	34.75	22.09	18.12	24.2	10.0	-	-	-	-	-	3.12	0.17	-1.59	-	1.57
HM20	34.7	35.0	29.0	30.03	29.92	48.50	49.80	24.8	23.48	23.59	37.50	42.28	28.46	25.05	-	11.4	-	-	-	-	-	2.72	0.35	-3.08	-	1.40
HM21	35.7	36.2	30.2	34.08	34.00	56.70	51.70	28.7	29.30	29.61	41.15	46.75	33.17	30.45	-	9.3	-	-	-	-	-	2.30	0.59	-5.30	-	1.35
HM22	30.1	29.4	21.5	19.25	19.04	21.6	22.5	14.7	12.46	12.65	28.08	23.73	16.68	15.01	23.5	7.86	14.67	1.16	0.14	7.47	2.65	4.00	0.07	4.33	5.83	5.14
HM23	30.1	29.6	21.9	19.72	19.51	25.6	26.0	15.8	13.29	13.46	29.05	26.59	17.29	15.68	22.9	6.43	10.08	1.61	0.08	4.29	2.49	3.83	0.14	2.45	5.10	4.98
H54	31.3	30.1	-	-	-	17.8	18.7	-	-	-	27.79	21.01	-	-	25.5	-	17.33	0.21	0.22	11.47	-	-	-	6.59	6.31	-
H55	33.7	32.3	-	-	-	18.1	19.2	-	-	-	29.60	21.90	-	-	26.8	-	21.40	1.30	0.25	13.20	-	-	-	7.36	6.77	-
H56	38.0	36.2	-	-	-	18.1	19.4	-	-	-	32.71	22.89	-	-	27.0	-	31.12	5.39	0.32	16.99	-	-	-	9.08	6.81	-
H57	43.0	40.9	-	-	-	18.6	20.7	-	-	-	36.62	24.98	-	-	25.6	-	43.17	11.76	0.38	20.75	-	-	-	10.28	6.98	-
H58	49.2	46.6	-	-	-	20.1	22.3	-	-	-	41.23	27.61	-	-	25.6	-	56.54	17.94	0.44	25.40	-	-	-	11.40	7.46	-
H59	54.0	51.2	-	-	-	22.1	24.5	-	-	-	45.24	30.46	-	-	28.7	-	62.95	19.63	0.48	28.51	-	-	-	11.78	7.73	-
H60	57.7	54.7	-	-	-	23.0	25.2	-	-	-	48.15	31.75	-	-	27.6	-	71.42	24.41	0.53	31.25	-	-	-	12.68	7.40	-
H61	64.3	60.8	-	-	-	24.6	26.8	-	-	-	53.17	34.43	-	-	26.5	-	86.64	32.08	0.61	36.74	-	-	-	13.71	7.48	-
H62	70.0	66.1	-	-	-	24.6	28.5	-	-	-	57.39	37.21	-	-	25.0	-	102.05	39.25	0.65	42.45	-	-	-	14.45	7.80	-

Table A7.13 Contd.

Run	T_c °C	T_{cp} °C	T_D °C	P_c mmHg	P_{cp} mmHg	T_r °C	T_{rp} °C	T_D °C	P_r mmHg	P_{rp} mmHg	T_{cc} °C	T_{rc} °C	P_{cc} mmHg	P_{rc} mmHg	T_a °C	P_a mmHg	q_T W	q_l W	q_c W	q_r W	q_m W	m_T gh^{-1}	m_l gh^{-1}	Ra $x10^5$	Nu	Sh
M65	70.8	67.21	-	-	-	24.6	27.1	-	-	-	57.67	36.66	-	-	25.2	-	108.72	29.85	0.68	44.35	-	-	-	14.65	8.35	-
M33	30.2	30.0	22.3	20.81	20.71	30.7	30.0	18.3	16.33	16.40	30.0	30.0	19.45	17.67	23.5	10.4	-	-	-	-		2.04	0.03	0.34	-	2.43
M34	30.2	29.9	23.6	22.11	21.96	30.7	29.9	19.1	16.61	16.73	30.0	30.0	20.39	18.31	22.5	10.5	-	-	-	-	-	2.68	0.07	0.39	-	2.69
M35	30.2	30.1	21.7	19.48	19.26	30.7	30.1	13.0	11.28	11.44	30.0	30.0	16.82	13.88	21.9	10.5	-	-	-	-	-	3.38	-0.03	0.56	-	2.94
M36	30.2	30.0	21.7	19.47	19.25	30.7	30.0	12.6	10.97	11.13	30.0	30.0	16.75	13.63	22.1	9.2	-	-	-	-	-	4.14	0.02	0.59	-	2.86
M37	30.2	30.0	22.9	20.95	20.76	30.7	30.0	16.0	13.59	13.72	30.0	30.0	18.67	15.80	22.4	8.3	-	-	-	-	-	3.53	0.12	0.54	-	2.55
M38	30.2	30.2	25.1	23.88	23.78	30.7	30.2	21.8	19.63	19.70	30.2	30.2	22.55	20.95	22.9	9.9	-	-	-	-	-	2.14	0.17	0.31	-	2.60
M39	30.2	30.2	25.7	24.77	24.72	30.7	30.2	24.1	22.53	22.56	30.2	30.2	24.19	23.10	22.7	7.7	-	-	-	-	-	1.08	0.29	0.20	-	1.66
M40	35.0	34.7	26.1	25.24	25.09	35.3	34.7	20.2	17.75	17.88	34.7	34.7	22.87	20.10	22.7	7.9	-	-	-	-	-	3.86	0.30	0.49	-	2.70
M41	35.3	35.1	24.6	23.20	22.96	35.7	35.1	15.6	13.49	13.56	35.1	35.1	19.98	16.54	21.2	8.5	-	-	-	-	-	4.90	0.20	0.61	-	2.89
M42	35.3	35.0	25.2	24.05	23.83	35.7	35.0	17.7	15.25	15.45	35.0	35.0	21.27	18.00	20.9	9.3	-	-	-	-	-	4.64	0.20	0.58	-	2.74
M43	30.2	30.0	22.7	20.67	20.49	30.7	30.0	15.9	13.56	13.72	30.0	30.0	18.40	15.80	21.8	10.7	-	-	-	-	-	3.46	0.01	0.49	-	2.86

APPENDIX 8

FINITE DIFFERENCE EQUATIONS.

The principle of the "Alternating Direction Implicit" (ADI) method was demonstrated in Section 3.8 when the differential equation for the stream function (Eq.3.3, Chapter 3) was transformed into its finite-difference equation. In this Appendix, the same procedure is used to transform the rest of the governing differential equations (Eqs. 3.31 to 3.36, Chapter 3) into their finite-difference forms.

As for the case in section 3.8, we define the following quantity (for instance, Concentration) which will be used in the finite difference equations as :-

$C_{i,j,n}$

where i, j = grid-points at (i,j)

and n = time level n.

If only the quantity "C" is written, it is understood that the default grid point values are "i" and "j" and the default time level to be "n".

eg. $C_{i+1} = C_{i+1,j,n}$

$C_{j-1,n+1} = C_{i,j-1,n+1}$ etc.

A 8.1 THE EQUATION OF SPECIES CONCENTRATION.

The equation of species concentration (Eq.3.32, Chapter 3) and the equation of energy (Eq. 3.31) are identical in form and hence their corresponding finite-difference approximations will also be identical. Hence the equation of species concentration will be used as an example for both set of equations. We now make two changes to the equation based on the experience gained by other

workers in the field, so that the resultant finite difference equation has the most favourable characteristics when used in the numerical calculation. The first change was proposed by de Vahl Davis [156] who rewrote Eq. 3.32 in the form of :-

$$\frac{1}{a_c}\frac{\partial C}{\partial t} + Sc\left(U\frac{\partial C}{\partial X} + V\frac{\partial C}{\partial Y}\right) = \nabla^2 C \qquad \text{(A9.1)}$$

As a_c is only an arbitrarily-chosen factor, it does not matter if the factor Sc has been omitted in the first term. This change made the solution times become more or less independent of Sc [156]. The second change was recommended by Roache [153] and it changes the convective term in Eq. A9.1 from

$$\left(U\frac{\partial C}{\partial X} + V\frac{\partial C}{\partial Y}\right) \qquad \text{(A9.2)}$$

to

$$\left(\frac{\partial (CU)}{\partial X} + \frac{\partial (CV)}{\partial Y}\right) \qquad \text{(A9.3)}$$

with the help of the continuity equation (Eq.3.1). Eqs. A9.2 and A9.3 are mathematically equivalent but the latter lead to numerical conservation of the concentration by the finite-difference approximation. (Roache[153] pg. 11 & 28). Eq. A9.2 is commonly refered to as the "non-conservative" form and Eq. A9.3 the "conservative form" of the convective term.

Using the two changes above, we rewrite Eq. A9.1 as :-

$$\frac{1}{a_c}\frac{\partial C}{\partial t} + Sc\left(\frac{\partial (CU)}{\partial X} + \frac{\partial (CV)}{\partial Y}\right) = \nabla^2 C \qquad \text{(A9.4)}$$

We apply the finite difference approximation to Eq. A9.4 using the "Alternating Direction Implicit" (ADI) procedure of Peachman and Rachford [162] (which had been described in section 3.8).

First half time step

$$\frac{1}{a_c}\left(\frac{C_k - C}{\Delta t/2}\right) + Sc\left[\frac{U_{i+1}C_{i+1,k} - U_{i-1}C_{i-1,k}}{2\,\Delta X}\right]$$

$$+ Sc\left[\frac{V_{j+1}C_{j+1} - V_{j-1}C_{i-1}}{2\,\Delta Y}\right]$$

$$= \frac{C_{i+1,k} + C_{i-1,k} - 2C_k}{(\Delta X)^2} + \frac{C_{j+1} + C_{j-1} - 2C}{(\Delta Y)^2}$$

Rearranging,

$$-\left[\frac{Sc\,a_c\,U_{i-1}}{2\,\Delta X} + \frac{a_c}{(\Delta X)^2}\right] C_{i-1,k} + \left(\frac{2}{\Delta t} + \frac{2\,a_c}{(\Delta X)^2}\right) C_k$$

$$+\left[\frac{Sc\,a_c\,U_{i+1}}{2\,\Delta X} - \frac{a_c}{(\Delta X)^2}\right] C_{i+1,k} = -\frac{a_c\,Sc}{2\,\Delta Y}(V_{j+1}C_{j+1} - V_{j-1}C_{i-1})$$

$$+ \frac{2}{\Delta t} C + \frac{a_c}{(\Delta Y)^2}(C_{j+1} + C_{j-1} - 2C)$$

This completes the first half sweep of the method.

Second half time step:

$$\frac{1}{a_c}\left(\frac{C_{n+1} - C}{\Delta t/2}\right) + Sc\left[\frac{U_{i+1}C_{i+1,k} - U_{i-1}C_{i-1,k}}{2\,\Delta X}\right]$$

$$+ Sc\left[\frac{V_{j+1}C_{j+1,n+1} - V_{j-1}C_{i-1,n+1}}{2\,\Delta Y}\right]$$

$$= \frac{C_{i+1,k} + C_{i-1,k} - 2C_k}{(\Delta X)^2} + \frac{C_{j+1,n+1} + C_{j-1,n+1} - 2C_{n+1}}{(\Delta Y)^2}$$

Rearranging,

$$-\left[\frac{Sc\ a_c\ V_{i-1}}{2\ \Delta Y} + \frac{a_c}{(\Delta Y)^2}\right] C_{j-1,n+1} + \left(\frac{2}{\Delta t} + \frac{2\ a_c}{(\Delta Y)^2}\right) C_{n+1}$$

$$+\left[\frac{Sc\ a_c\ V_{j+1}}{2\ \Delta Y} - \frac{a_c}{(\Delta Y)^2}\right] C_{i+1,n+1} = -\frac{a_c\ Sc}{2\ \Delta X}(U_{i+1}C_{j+1,k} - U_{i-1}C_{i-1,k})$$

$$+\frac{2}{\Delta t} C_k + \frac{a_c}{(\Delta X)^2}\left(C_{j+1,k} + C_{j-1,k} - 2C_k\right) \qquad \text{(A9.6)}$$

This completes the full sweep of the method.

A 8.2 THE EQUATION OF ENERGY.

As has been stated before, the finite-difference approximation of the energy equation is identical in form to the concentration equation. Thus Eqs. A9.5 and A9.6 are also applicable for the energy equation with the following modifications :-

(i) "C" is replaced by "T" ;
(ii) "Sc" is replaced by "Pr" and
(iii) "a_c" is replaced by "a_T" .

A8.3 THE EQUATION OF VORTICITY.

The "ADI" procedure with the "conservative" form of formulatioon for the convective terms is again employed :-

First half time-step :

$$-\left[\frac{a_\zeta U_{i-1}}{2\,\Delta X} + \frac{a_\zeta}{(\Delta X)^2}\right]\zeta_{i-1,k} + \left(\frac{2}{\Delta t} + \frac{2\,a_\zeta}{(\Delta X)^2}\right)\zeta_k$$

$$+\left[\frac{a_\zeta U_{i+1}}{2\,\Delta X} - \frac{a_\zeta}{(\Delta X)^2}\right]\zeta_{i+1,k} = -\frac{a_\zeta}{2\,\Delta Y}\left(V_{j+1}\zeta_{j+1} - V_{j-1}\zeta_{i-1}\right)$$

$$+\frac{2}{\Delta t}\zeta + \frac{a_\zeta}{(\Delta Y)^2}\left(\zeta_{j+1} + \zeta_{j-1} - 2\,\zeta\right) + \frac{a_\zeta\, Gr_T \cos\theta}{2\,\Delta Y}$$

$$\left(T_{j+1,n+1} - T_{j-1,n+1}\right) - \frac{a_\zeta\, Gr_T \sin\theta}{2\,\Delta X}\left(T_{i+1,n+1} - T_{i-1,n+1}\right) + \frac{a_\zeta\, Gr_C \cos\theta}{2\,\Delta Y}$$

$$\left(C_{j+1,n+1} - C_{j-1,n+1}\right) - \frac{a_\zeta\, Gr_C \sin\theta}{2\,\Delta X}\left(C_{i+1,n+1} - C_{i-1,n+1}\right) \qquad \text{(A9.7)}$$

This completes the first half sweep of the method.

Second half time step:

$$-\left[\frac{a_\zeta V_{i-1}}{2\,\Delta Y} + \frac{a_\zeta}{(\Delta Y)^2}\right]\zeta_{j-1,n+1} + \left(\frac{2}{\Delta t} + \frac{2\,a_\zeta}{(\Delta Y)^2}\right)\zeta_{n+1}$$

$$+\left[\frac{a_\zeta V_{j+1}}{2\,\Delta Y} - \frac{a_\zeta}{(\Delta Y)^2}\right]\zeta_{j+1,n+1} = -\frac{a_\zeta}{2\,\Delta X}\left(U_{i+1}\zeta_{i+1,k} - U_{i-1}\zeta_{i-1,k}\right)$$

$$+\frac{2}{\Delta t}\zeta_k + \frac{a_\zeta}{(\Delta X)^2}\left(\zeta_{i+1,k} + \zeta_{i-1,k} - 2\,\zeta_k\right) + \frac{a_\zeta\, Gr_T \cos\theta}{2\,\Delta Y}$$

$$\left(T_{j+1,n+1} - T_{j-1,n+1}\right) - \frac{a_\zeta\, Gr_T \sin\theta}{2\,\Delta X}\left(T_{i+1,n+1} - T_{i-1,n+1}\right) + \frac{a_\zeta\, Gr_C \cos\theta}{2\,\Delta Y}$$

$$(C_{j+1,n+1} - C_{j-1,n+1}) - \frac{a_\zeta \, Gr_c \, \sin\theta}{2\,\Delta X} (C_{i+1,n+1} - C_{i-1,n+1}) \qquad \text{(A9.8)}$$

This completes the full sweep of the method.

A8.4 BOUNDARY CONDITIONS AND FINITE-DIFFERENCE EQUATIONS AT THE BOUNDARIES.

The equations given previously (Eqs. A9.5 to A9.8) are applicable at the interior points of the solution region from i=2 to M-1 and j=2 to N-1 only (refer to Fig.3.1). They must be solved in conjunction with the appropriate boundary conditions which are either defined in section 3.4.2, Chapter 3, or calculated from the interior field variables during each round of the iteration process.

A8.4.1 Boundary Equation For The Concentration Equation.

The concentration field at the bOundaries Y=1 and Y=N are constant values defined explicitly and need not be calculated. The concentration field at the boundaries X=1 and X=M is not constant with a value defined explicitly and the field needs to be calculated at every sweep of the iteration.

It is recalled from Section 3.4.2 that, at X=1 and X=M :-

(i) the velocities U and V are zero on the boundaries ;

(ii) $\partial C/\partial X = 0$ ie. adiabatic walls and

(iii) The finite difference approximation to the second derivatives on the boundaries can be obtained from a Taylor's series expansion :-

eg. for the boundary X=1,

$$C_{2,j} = C_{1,j} + \Delta X \left(\frac{\partial C}{\partial X}\right)_{1,j} + \frac{(\Delta X)^2}{2} \left(\frac{\partial^2 C}{\partial X^2}\right)_{1,j} + \ldots\ldots\ldots$$

which implies,

$$\left(\frac{\partial^2 C}{\partial X^2}\right)_{1,j} = \frac{2}{(\Delta X)^2}\,(C_{2,j} - C_{1,j}) \qquad \text{(A9.9)}$$

as $\left(\frac{\partial C}{\partial X}\right)_{1,j} = 0$

Similarly on the boundary X=M,

$$\left(\frac{\partial^2 C}{\partial X^2}\right)_{M,j} = \frac{2}{(\Delta X)^2}\,(C_{M-1,j} - C_{M,j}) \qquad \text{(A9.10)}$$

Noting the above, the governing equation for species concentration (Eq.A9.1) at the boundaries X=1 and X=M is simplified into :

$$\frac{1}{a_c}\,\frac{\partial C}{\partial t} = \nabla^2 C \qquad \text{(A9.11)}$$

Applying the finite-difference approximation by the ADI technique to Eq.A9.11 yields,

First half time step :

$$\frac{1}{a_c}\left(\frac{C_{1,j,k} - C_{1,j}}{\Delta t/2}\right) = \frac{2(C_{2,j,k} + C_{1,j,k})}{(\Delta X)^2} + \frac{C_{1,j+1} + C_{1,j-1} - 2C_{1,j}}{(\Delta Y)^2}$$

rearranging, (for i= 1 and j= 2 to N-1)

$$\left(\frac{2}{\Delta t} + \frac{2\,a_c}{(\Delta X)^2}\right) C_{1,j,k} - \frac{2\,a_c}{(\Delta X)^2}\,C_{2,j,k} = \frac{2}{\Delta t}\,C_{1,j} + \frac{a_c}{(\Delta Y)^2}\,(C_{1,j+1} + C_{1,j-1} - 2C_{1,j}) \qquad \text{(A9.12)}$$

Similarly for i=M and j= 2 to N-1,

$$-\frac{2a_c}{(\Delta X)^2} C_{M-1,j,k} + \left(\frac{2}{\Delta t} + \frac{2a_c}{(\Delta X)^2}\right) C_{M,j,k}$$

$$= \frac{2}{\Delta t} C_{M,j} + \frac{a_c}{(\Delta Y)^2} \left(C_{M,j+1} + C_{M,j-1} - 2C_{M,j}\right) \qquad \text{(A9.13)}$$

Second half time-step :

for i =1 and j =2 to N-1,

$$-\frac{a_c}{(\Delta Y)^2} C_{1,j-1,n+1} + \left(\frac{2}{\Delta t} + \frac{2a_c}{(\Delta Y)^2}\right) C_{1,j,n+1} - \frac{a_c}{(\Delta Y)^2} C_{1,j+1,k}$$

$$= \frac{2}{\Delta t} C_{1,j,k} + \frac{2a_c}{(\Delta X)^2} \left(C_{2,j} - 2C_{1,j,k}\right) \qquad \text{(A9.14)}$$

Similarly for i=M and j= 2 to N-1,

$$-\frac{a_c}{(\Delta Y)^2} C_{M,j-1,n+1} + \left(\frac{2}{\Delta t} + \frac{2a_c}{(\Delta Y)^2}\right) C_{M,j,n+1} - \frac{a_c}{(\Delta Y)^2} C_{M,j+1,k}$$

$$= \frac{2}{\Delta t} C_{M,j,k} + \frac{2a_c}{(\Delta X)^2} \left(C_{M-1,j} - 2C_{M,j,k}\right) \qquad \text{(A9.15)}$$

A8.4.2 Boundary Equation For The Energy Equation.

The finite-difference approximation for the energy boundary equation is identical in form to the concentration boundary equation. Thus Eqs.A9.11 and A9.15 are also applicable for the Energy boundary equation with the following modifications :- (as for the interior points)

(i) "C" is replaced by "T" ;

(ii) "Sc" is replaced by "Pr" and

(iii) "a_c" is replaced by "a_T".

Attention is also needed when using Eqs. A9.6, A9.14 and 9.15 (second half time-step equations) at the points j=2 and j=N-1for i=1 to M (see Fig. A9.1) :-

eg. for Eq. 9.6 : $C_{i,j-1,n+1}$ at j=2 = $C_{i,1,n+1} = 0.0$

and $C_{i,j+1,n+1}$ at j=N-1 = $C_{i,N,n+1} = 1.0$

from definition of boundary conditions in Section 3.4.2. On noting this fact and the boundary equations(Eqs. A9.12 to A9.15) defined above, the finite-difference equations A9.5, A9.6 and A9.12 to A9.15 represent a tridiagonal systems of equations and can be easily solved by the Thomas Algorithm [156,176].

A8.4.3 Boundary Equation For The Vorticity Equation.

Unlike the temperature, concentration or the stream function equations, no explicit boundary conditions can be specified for the vorticity function. It has to be calculated at every step of the iteration process using appropriate relationship linking the boundary vorticity with the relevant variables. Several of these relationships have been presented in the literature (8, 34, 88, 113,156) and the one chosen for this work is the Wood's two-point formula suggested by Noble [88 pg 140] :

(i) for the boundaries i=1 and i=M; and j=2 to N-1

$$\zeta_{i=1} = -\frac{\zeta_{i=2}}{2} - 3\frac{\varphi_{i=2}}{\Delta X^2} \qquad \text{(A9.16)}$$

$$\zeta_{i=M} = -\frac{\zeta_{i=M-1}}{2} - 3\frac{\varphi_{i=M-1}}{\Delta X^2} \qquad \text{(A9.17)}$$

(ii) for the boundaries j=1 and j=N; and i=2,M-1,

$$\zeta_{j=1} = -\frac{\zeta_{j=2}}{2} - 3\frac{\varphi_{j=2}}{\Delta Y^2} \qquad \text{(A9.18)}$$

$$\zeta_{j=N} = -\frac{\zeta_{j=N-1}}{2} - 3\frac{\varphi_{j=N-1}}{\Delta Y^2} \qquad \text{(A9.19)}$$

In the actual calculation sequence (Fig.3.3, Chapter 3), the interior vorticity values are calculated first using Eqs A9.7 and 9.8 with the (known) boundary vorticity values from the previous time step as the boundary condition. In this way Eqs A9.7 and A9.8 are transformed into tridiagonal system of equations and can be solved by the Thomas Algorithm. The stream function is then evaluated by the procedure outlined in section 3.8, Chapter 3 before the boundary vorticity values at the latest time step are calculated with Eqs. A9.16 to A9.19. Thus the boundary vorticity values always lags the interior vorticity values in the calculation procedure and this often leads to instability of the numerical method. A more detailed discussion on this aspect of the numerical methods can be found in the literature [8,55,88] .

One way to improve the stability of the method is by the use of a "boundary smoothing parameter "S" as proposed by Noble [88]:-

$$\zeta_{n+1} = s\,\zeta_{n+1} + (1-s)\,\zeta_n$$

in which ζ_{n+1} is the boundary vorticity at the new time level n+1; and ζ_n is the boundary vorticity at the old time level n;

The parameter "S" has a value of between 0 and 1 and it effectively relaxes the value of the boundary vorticity at each iteration cycle. For this work, it was found that if the false transient-factors (Chapter 3) were chosen properly, the use of "S" became redundant.

A8.5 VELOCITY COMPONENTS.

The velocity components are evaluated using Eq.3.35, Chapter 3 :

$$U = \frac{\partial \varphi}{\partial Y} \quad \text{and} \quad V = -\frac{\partial \varphi}{\partial X} \tag{3.35}$$

at all the interior points only as the velocities at the boundaries have been defined as equal to zero. A simple, two-point, centre-difference formula is used to approximate Eq. 3.35 :-

$$U = \frac{\varphi_{j+1} - \varphi_{j-1}}{2\,\Delta Y} \tag{A9.20}$$

and

$$V = -\frac{\varphi_{i+1} - \varphi_{i-1}}{2\,\Delta X} \tag{A9.21}$$

for i= 2 to M-1 anf j=2 to N-1.

This ends one complete cycle of the iteration as depicted in Fig. 3.3. The next stage is to check for the convergence of the computed fields by the following criterium :-

$$EO = \frac{\sum_{i=a}^{b} \sum_{j=c}^{d} |Z_{n+1} - Z_n|}{a \cdot b \cdot Z_{max}} \tag{A9.22}$$

where EO is the convergence criterion,

Z_{n+1} is the latest field variables computed at time level n+1,

Z_n is the previous field variables computed at time level n,

and Z_{max} is the largest absolute value of the latest field variables computed at time level n+1.

The iteration process is said to have "converged" and the solutions attained "steady-state" values when EO is less than some predetermined value (typically $1x10^{-4}$ or $1x10^{-5}$). The summation in

Eq. 9.22 is for :

	Function Fields Z	Summation Variables a	b	c	d
1.	Vorticity	1	M	1	N
2.	Stream-function	2	M-1	2	N-1
3.	Temperature	1	M	2	N-1
4.	Concentration	1	M	2	N-1

The mean Nusselt number is obtained from the formula :

$$Nu_o = -\frac{1}{H}\int_0^H \left.\frac{\partial T}{\partial Y}\right|_{y=0 \text{ or } 1} dX \qquad \text{(A9.23)}$$

A second-order finite-difference approximation is used to represent $\partial T/\partial Y$:-

$$\frac{\partial T}{\partial Y} = \pm \frac{(-3T_1 + 4T_2 - T_3)}{2\,\Delta Y} \qquad \text{(A9.24)}$$

and the numerical integration used is the Simpson rule.

Similarly the mean Sherwood number is obtained from the formula :

$$Sh_o = -\frac{1}{\rho H}\int_0^H \left.\frac{\partial C}{\partial Y}\right|_{y=0 \text{ or } 1} dX \qquad \text{(A9.25)}$$

and

$$\frac{\partial C}{\partial Y} = \pm \frac{(-3C_1 + 4C_2 - C_3)}{2\,\Delta Y} \qquad \text{(A9.26)}$$

The positive sign in Eqs. A9.24 and A9.26 is applicable for conditions at the wall at Y=1 and the negative sign for the wall at Y=N. At the wall Y=N, the folowing equivalents for the subscripts apply: 1 ≡ N-1, 2 ≡ N-2, and so on.

APPENDIX 9

PROGRAM LISTINGS OF NUMERICAL METHODS AND THEIR ESSENTIAL FEATURES.

All the numerical calculations were carried out on the Departmental VAX 11-730 mini-computer and the programming language used was Fortran 77. The complete program listing for the Dynamic Alternating Direction Implicit method ("DADI") is presented in this Appendix. The computer programs for the False-Transient ("FT") and the Hybrid methods can be easily derived from the given program as will shown later in this Appendix.

The program for the "DADI" method (and indeed the other two methods) consists of one main program and fourteen subprograms. The main program is titled "DADI" and it essentially performs the following tasks:-

(i) accepts input data;
(ii) calculates constants;
(iii) sets initial and boundary conditions;
(iv) calls subroutines which carried out the numerical calculations;
(v) tests for convergence of iterated solutions;
(vi) updates new time step of iteration if necessary;
(vii) calculates Nusselt and Sherwood numbers;
(viii) stops iteration if CPU time limit is exceeded;
(ix) calls subroutine to output data.

(see also Chapter 3 Figs. 3.2 and 3.3 for more information).

Comments given in the computer programs will help to elaborate these features at the respective places where these functions are carried out. The appropriate symbols used in the program are also defined at the beginning of the computer program. The main program goes from line 0001 to 0916 of the computer listing.

The subprograms consisted of the following :-
SOLVE1A, SOLVE2A, SOLVE3A, SOLVE4A, SOLVE5A, SOLVE6A, STEST7A, STEST7B, STEST8A, SOLCN1A, SOLCN2A, SOLCN3A,

SOLCN4A, WTEST1A.

The function of each of these subprograms is defined at the beginning of the respective program.

The computer program for the subprogram "WTEST1A" is only partly listed but all its essential features are included. This is the subroutine used to output the numerical calculation data and the user can choose to output the data in any format he wishes. It will serve no purpose to list the complete program here, except to give examples of the format of the output data used in this work.

The simulation program as presented is a batch-wise version. In view of the long computer time required for a typical run, the job is always run as a batch job. For very simple test cases, it is nevertheless useful to run the program in a terminal interactive mode, which may be obtained from the program listed.

The data input to the main program is by way of a separate block data file "TEST" (Listing A9.1). Thus the main program need not be recompiled if only the input data is to be changed. All the input parameters listed in data file "TEST" are either defined in the data file itself or in the beginning of the main program "DADI".

All the programs also have two "INCLUDE" statements. The first "INCLUDE" statement obtains the values of "M" and "N" which define the dimensions of the matrices used in the calculations from the subprogram "DIMEN" (Listing A9.2). The second "INCLUDE" statement obtains the common blocks values from the subprogram "COMMON" (Listing A9.3).

To convert the computer program of the "DADI" method into that for the "FT" method, lines 0494 to 0714 are removed from the program listing. The extra matrices for the "DADI" method (TEMP2, TEMP3 etc.) can be removed if desired to reduce the storage requirement of the program but this step is not necessary. The name of matrices which are passed to the subroutine "WTEST1A" for outputting of course need to be that of TEMP1 etc. instead of TEMP2 etc.. The rest of the subprograms remain unchanged. (see also Chapter 3 Figs. 3.2 and 3.3)

To convert the computer program into that for the Hybrid method, lines 0698 to 0714 should be replaced by the section of the program given in Listing A9.4. The rest of the main and

sub-programs remain unchanged.

For all the programs for the three different methods, the initial condition can either be fields of zero values or the steady -state values of some previous calculations. The programs also handle the simultaneous gradients case with either aiding or opposing flows for both the horizontal and vertical cavity configuration. The proper calculation condition is selected by giving the appropriate values to the respective control parameters in data file "TEST" without a need to change the main computer program. The "right" values of these control parameters to be used are defined in the data file "TEST".

To start the calculation for a horizontal cavity with initial condition consisting of a conduction or diffusion field, perturbation of the initial field is necessary. This is done by increasing or decreasing the values of the temperature or the concentration fields at two (or more) randomly selected (often symetrical) points by 0.1 or 0.2.

To produce the stream function and temperature fields plots as those presented in Chapter 8, the stream function and temperature fields were first stored in matrices which were output by the subprogram "WTEST1A". These matrices were then fed into a graphics utilities program developded by The National Centre for Atmospheric Research (NCAR), U.S.A.. The graphics utilities are a collection of high-level subroutines for graphical display of data and the family chosen for this work to produce the plots is the "contour plotting family". It produces contour plots of two-dimensional data, with choice of labelling, smoothing and removal of crowded lines as those presented in Chapter 8.

```
DATA FOR PROGRAM DADI.FOR
L=0: ZERO STARTING VALUES      L=1: START WITH PREVIOUS VALUES
L1=0: HEAT TRANSFER ONLY       L1=1: HEAT AND MASS TRANSFER
L1=2: MASS TRANSFER ONLY
CON10=0.0:PRINT ALL FIELDS     CON10 =1.0:PRINTT HNU & SH ONLY
NCO=0: COCURRENT FLOW          NCO=1: COUNTERCURRENT FLOW
 S      = 1.00                 DELT   = 1.0E-04
 EO     = 1.0E-04              EI     = 1.0E+01
 DELX   = 0.05                 DELY   = 0.05
 GR     = 1.410E+04            PR     = 0.71
 M      = 21                   N      = 21
 L      = 0                    L1     = 0
 GRC    = 0.000E+05            SC     = 0.61
 ALFAT  = 0.10                 ALFAC  = 1.000
 ALFAV  = 10.0                 ALFAS  = 10.0
 CON10  = 0.0                  BETA   = 0.0
 NCPU   = 6480000              NCO    = 0
```

Listing 1: Data File "TEST.DAT".

```
      PARAMETER MD=21
      PARAMETER ND=21
```

Listing 2: Program "DIMEN.FOR".

```
      COMMON /BLK2/STRFI(MD,ND),X(MD),Y(ND),VORBG(MD,ND)
      COMMON /BLK4/A(MD),B(MD),C(MD),D(MD),ALPHA(MD),SEE(MD),HNU(5)
      COMMON /BLK5/TEMPO(MD,ND),VORT(MD,ND),SH(5)
      COMMON /BLK6/CONO(MD,ND),GRDT(MD,2),GRDC(MD,2)
      COMMON /BLK7/S,GR,EO,EI,DELX,DELY,DELT,M,N,PR,NT
      COMMON /BLK8/NOIT,NOITI,NOITT,ALFAT,ALFAC,ALFAV,ALFAS
      COMMON /BLK9/CON2,CON3,CON4,CON5,CON6,CON7,CON8,CON9,CON10
      COMMON /BLK10/L,L1,GRC,SC,CON11,CON12,CON13,BETA
```

Listing 3: Program "COMMON.FOR".

```
      IF(L1.EQ.2) GOTO 232
      TTP=TSUM/ATSUM
  232 IF(L1.EQ.0) GOTO 234
      CTP=CSUM/ACSUM
  234 STP=SSUM/ASSUM
      VTP=VSUM/AVSUM
      PRINT 3123,TTP,STP,VTP,CTP
 3123 FORMAT(1X,'TTP=',F10.4,2X,'STP=',F10.4,2X,'VTP='
     1 F10.4,2X,'CTP='
     1 F10.4)
C     TEST FOR TPs TO DETERMINE NEW TIME STEP
      NW=0
      IF(L1.EQ.2) GOTO 513
      IF(TTP.GT.0.6) TDELT=1.0/16.0*TDELT
      TCON1=2.0/TDELT
      IF(TTP.GT.0.6) NW=NW+1
  513 IF(L1.EQ.0) GOTO 523
      IF(CTP.GT.0.6) CDELT=1.0/16.0*CDELT
      CCON1=2.0/CDELT
      IF(CTP.GT.0.6) NW=NW+1
  523 IF(STP.GT.0.6) SDELT=1.0/16.0*SDELT
      SCON1=2.0/SDELT
      IF(STP.GT.0.6) NW=NW+1
      IF(VTP.GT.0.6) VDELT=1.0/16.0*VDELT
      IF(VTP.GT.0.6) NW=NW+1
      VCON1=2.0/VDELT
      IF(L1.EQ.1) GOTO 533
      IF(NW.EQ.3) GOTO 100
      GOTO 543
  533 IF(NW.EQ.4) GOTO 100
  543 IF(L1.EQ.2) GOTO 212
      IF(TTP.LE.0.6. AND .TTP.GT.0.4) TDELT=(1.0/4.0)*TDELT
      IF(TTP.LE.0.4. AND .TTP.GT.0.3) TDELT=(1.0/2.0)*TDELT
      IF(TTP.LE.0.3. AND .TTP.GT.0.1) TDELT=SQRT(3.0)*TDELT
      IF(TTP.LE.0.1. AND .TTP.GT.0.05) TDELT=2.0*TDELT
      IF(TTP.LE.0.05. AND .TTP.GE.0.0) TDELT=4.0*TDELT
      IF(TDELT.LT.1.0E-4) TDELT=1.0E-4
      TCON1=2.0/TDELT
  212 IF(L1.EQ.0) GOTO 214
      IF(CTP.LE.0.6. AND .CTP.GT.0.4) CDELT=(1.0/4.0)*CDELT
      IF(CTP.LE.0.4. AND .CTP.GT.0.3) CDELT=(1.0/2.0)*CDELT
      IF(CTP.LE.0.3. AND .CTP.GT.0.1) CDELT=SQRT(3.0)*CDELT
      IF(CTP.LE.0.1. AND .CTP.GT.0.05) CDELT=2.0*CDELT
      IF(CTP.LE.0.05. AND .CTP.GE.0.0) CDELT=4.0*CDELT
      IF(CDELT.LT.1.0E-4) CDELT=1.0E-4
      CCON1=2.0/CDELT
  214 IF(STP.LE.0.6. AND .STP.GT.0.4) SDELT=(1.0/4.0)*SDELT
      IF(STP.LE.0.4. AND .STP.GT.0.3) SDELT=(1.0/2.0)*SDELT
      IF(STP.LE.0.3. AND .STP.GT.0.1) SDELT=SQRT(3.0)*SDELT
      IF(STP.LE.0.1. AND .STP.GT.0.05) SDELT=2.0*SDELT
      IF(STP.LE.0.05. AND .STP.GE.0.0) SDELT=4.0*SDELT
      IF(SDELT.LT.1.0E-4) SDELT=1.0E-4
      SCON1=2.0/SDELT
      IF(VTP.LE.0.6. AND .VTP.GT.0.4) VDELT=(1.0/4.0)*VDELT
      IF(VTP.LE.0.4. AND .VTP.GT.0.3) VDELT=(1.0/2.0)*VDELT
      IF(VTP.LE.0.3. AND .VTP.GT.0.1) VDELT=SQRT(3.0)*VDELT
      IF(VTP.LE.0.1. AND .VTP.GT.0.05) VDELT=2.0*VDELT
      IF(VTP.LE.0.05. AND .VTP.GE.0.0) VDELT=4.0*VDELT
      IF(VDELT.LT.1.0E-4) VDELT=1.0E-4
      VCON1=2.0/VDELT
      PRINT 3106,TDELT,SDELT,VDELT,CDELT
      PRINT 99,TCON1,SCON1,VCON1,CCON1
 3106 FORMAT(1X,'TDELT=',F8.4,2X,'SDELT=',F8.4,2X,'VDELT='
     1 F8.4,2X,'CDELT=',F8.4)
   99 FORMAT(1X,'TCON1=',F9.2,3X,'SCON1=',F9.2,3X,'VCON1='
     1 F9.2,2X,'CCON1=',F9.2)
```

Listing 4: Insert for "Hybrid" Method.

```
0001    C       PROGRAM DADI.FOR
0002    C
0003    C
0004    C       NUMERICAL SOLUTION OF NATURAL CONVECTIVE HEAT &
0005    C       MASS TRANSFER IN A CAVITY WITH OPPOSITE WALLS AT
0006    C       DIFFERENT CONCENTRATION & TEMPERATURE AND ADIBATIC
0007    C       SIDE WALLS USING THE DYNAMIC ALTERNATING DIRECTION
0008    C       IMPLICIT METHOD.
0009    C
0010    C       NOMENCLATURE:-
0011    C       *************
0012    C       ALFAC = FALSE TRANSIENT TERM FOR CONCEN FIELD
0013    C       ALFAS = FALSE TRANSIENT TERM FOR STRF FIELD
0014    C       ALFAT = FALSE TRANSIENT TERM FOR TEMP FIELD
0015    C       ALFAV = FALSE TRANSIENT TERM FOR VORTY FIELD
0016    C       BETA = ANGLE OF INCLINATION TO THE VERTICAL :
0017    C              BETA = 0 DEG VERTICAL CAVITY
0018    C              BETA = 90 DEG HORIZONTAL CAVTY
0019    C       CONCEN = CONCENTRATION FIELD
0020    C       CONO = INTERMEDIATE COCENN FIELD FOR ADI METHOD
0021    C       DELX = GRID SPACING IN THE X-DIRECTION
0022    C       DELY = GRID SPACING IN THE Y-DIRECTION
0023    C       DELT = TIME INCREMENT
0024    C       EO = OUTER CONVERGENCE CRITERION
0025    C       EI = INNER CONVERGENCE CRITERION
0026    C       GR = GRASHOF NUMBER BASED OF CAVITY WIDTH
0027    C       GRC = CONCENTRATION GRASHOF NUMBER
0028    C       HNU = NUSSELT NUMBERS
0029    C       M = NUMBER OF GRID POINTS IN THE X-DIRECTION
0030    C       N = NUMBER OF GRID POINTS IN THE Y-DIRECTION
0031    C       NCU = CPU TIME LIMIT COUNTER
0032    C       PR = PRANDTL NUMBER
0033    C       S = BOUNDARY SMOOTHING PARAMETER
0034    C       SC = SCHMIDT NUMBER
0035    C       SH = SHERWOOD NUMBERS
0036    C       STRF = STREAM FUNCTION FIELD
0037    C       STRFI = INTERMEDIATE STRF FIELD FOR ADI METHOD
0038    C       TEMP = TEMPERATURE FIELD
0039    C       TEMPO = INTERMEDIATE TEMP FIELD FOR ADI METHOD
0040    C       UELTY = X-COMPONENT OF THE VELOTY
0041    C       UELM = UELTY COMPONENT AT X=3.5
0042    C       VELTY = Y-COMPONENT OF THE VELOTY
0043    C       VELM = VELTY COMPONENT AT Y=0.5
0044    C       VORTY = VORTICITY FIELD
0045    C       VORT = INTERMEDIATE VORTY FIELD FOR ADI METHOD
0046    C       X = COORDINATES IN THE DIRECTION PARALLEL TO THE
0047    C           PLATES
0048    C       Y = COORDINATES IN THE DIRECTION NORMAL TO THE
0049    C           PLATES
0050    C
0051    C       DIMENSION STATEMENTS ARE READ FROM FILE 'DIMEN.FOR'
0052    C       COMMON STATEMENTS ARE READ FROM FILE COMMA.FOR
0053            IMPLICIT REAL*8 (A-H,O-Z)
0054            INCLUDE 'DIMEN.FOR'
0057            DIMENSION VORTY(MD,ND),VORTY1(MD,ND),VORTY2(MD,ND)
0058            DIMENSION VORTY3(MD,ND)
0059            DIMENSION STRF(MD,ND),STRF1(MD,ND),STRF2(MD,ND)
0060            DIMENSION STRF3(MD,ND)
0061            DIMENSION TEMP(MD,ND),TEMP1(MD,ND),TEMP2(MD,ND)
0062            DIMENSION TEMP3(MD,ND)
0063            DIMENSION UELTY(MD,ND),UELTY1(MD,ND),UELTY2(MD,ND)
0064            DIMENSION UELTY3(MD,ND)
0065            DIMENSION VELTY(MD,ND),VELTY1(MD,ND),VELTY2(MD,ND)
0066            DIMENSION VELTY3(MD,ND)
0067            DIMENSION CONCEN(MD,ND),CONCEN1(MD,ND),CONCEN2(MD,ND)
0068            DIMENSION CONCEN3(MD,ND)
0069            INCLUDE 'COMMON.FOR'
0078    C
0079    C       INPUT PARAMETERS -READ FROM TEST.DAT
0080            OPEN(UNIT=5,FILE='TEST.DAT',STATUS='OLD')
0081            READ(5,305)
0082            READ(5,305)
0083            READ(5,305)
0084            READ(5,305)
0085            READ(5,305)
0086            READ(5,305)
0087            READ(5,310)S,DELT
0088            READ(5,310)EO,EI
0089            READ(5,310)DELX,DELY
0090            READ(5,310)GR,PR
0091            READ(5,320)M,N
0092            READ(5,330)L,L1
0093            READ(5,310)GRC,SC
0094            READ(5,310)ALFAT,ALFAC
0095            READ(5,310)ALFAV,ALFAS
0096            READ(5,310)CON10,BETA
0097            READ(5,340)NCPU,NCO
0098            CLOSE(UNIT=5,STATUS='SAVE')
0099     305    FORMAT(70X)
0100     310    FORMAT(10X,G20.8,10X,G20.8)
0101     320    FORMAT(10X,I4,26X,I4)
0102     330    FORMAT(10X,I5,25X,I4)
0103     340    FORMAT(10X,I8,22X,I3)
0104    C
0105            PRINT 400,S,DELT,EO,EI
0106            PRINT 350,DELX,DELY,GR,PR
0107            PRINT 355,M,N,SC,GRC,BETA
0108            PRINT 352,ALFAT,ALFAC,ALFAV,ALFAS
0109            PRINT 357,L,L1,CON10,NCO
0110    C
0111     400    FORMAT(2X,'S='F4.2,4X,'DELT='F6.4,4X,
0112         1  'EO='F8.6,4X,'EI='F7.2)
0113     350    FORMAT(2X,'DELX='F5.3,3X,'DELY='F8.6,3X,
0114         I  'GR='F9.1,3X,'PR='F7.3)
0115     355    FORMAT(2X,'M='I3,3X,'N='I2,3X,'SC='F7.3,3X,
0116         1  'GRC='F9.1,3X,'BETA='F5.1)
0117     357    FORMAT(2X,'L='I2,6X,'L1='I2,6X,'CON10='F3.1,3X,
0118         1  'NCO='I2)
0119     352    FORMAT(2X,'ALFAT='F7.4,4X,'ALFAC='F7.4,4X,
0120         1  'ALFAV='F7.4,4X,'ALFAS='F7.4)
0121    C
0122    C       IF L=1, PREVIOUS RESULTS ARE USED AS INITIAL-
0123    C       CONDITION
0124            IF(L.EQ.0) GOTO 382
0125            OPEN(UNIT=30,FILE='TEMP.DAT',STATUS='OLD')
0126            DO I=1,5
0127            READ(30,370)
0128            END DO
0129     370    FORMAT(70X)
0130     372    FORMAT(:,11(1X,6(E20.13)/))
0131            DO I=1,M
0132            READ(30,372)(TEMP(I,J),J=1,N)
0133            END DO
0134            CLOSE(UNIT=30,STATUS='SAVE')
0135    C
0136            OPEN(UNIT=32,FILE='STRF.DAT',STATUS='OLD')
0137            DO I=1,5
0138            READ(32,370)
0139            END DO
0140            DO I=1,M
```

```
      READ(32,372)(STRF(I,J),J=1,N)
      END DO
      CLOSE(UNIT=32,STATUS='SAVE')
C
      OPEN(UNIT=34,FILE='UELTY.DAT',STATUS='OLD')
      DO I=1,5
      READ(34,370)
      END DO
      DO I=1,M
      READ(34,372)(UELTY(I,J),J=1,N)
      END DO
      CLOSE(UNIT=34,STATUS='SAVE')
C
      OPEN(UNIT=36,FILE='VELTY.DAT',STATUS='OLD')
      DO I=1,5
      READ(36,370)
      END DO
      DO I=1,M
      READ(36,372)(VELTY(I,J),J=1,N)
      END DO
      CLOSE(UNIT=36,STATUS='SAVE')
C
      OPEN(UNIT=38,FILE='VORTY.DAT',STATUS='OLD')
      DO I=1,5
      READ(38,370)
      END DO
      DO I=1,M
      READ(38,372)(VORTY(I,J),J=1,N)
      END DO
      CLOSE(UNIT=38,STATUS='SAVE')
C
      OPEN(UNIT=40,FILE='CONCEN.DAT',STATUS='OLD')
      DO I=1,5
      READ(40,370)
      END DO
      DO I=1,M
      READ(40,372)(CONCEN(I,J),J=1,N)
      END DO
      CLOSE(UNIT=40,STATUS='SAVE')
C
C     COMPUTE CONSTANTS
382   CON1=(2.0/DELT)
      CON2=DELX*DELX
      CON3=DELY*DELY
      CON4=2.0/(DELX*DELX)
      CON5=1.0/(2.0*DELX)
      CON6=1.0/(2.0*DELY)
      CON7=2.0/(DELY*DELY)
      CON8=((M-1)*DELX)/((N-1)*DELY)
      CON9=0.0
      CON11=0.0
      CON12=0.0
      CON13=0.0
C     CON9 TO CON13 ARE NOT USED FOR THE MOMENT
C
C     FOR PREVIOUS VALUES AS INITIAL CONDITIONS, GOTO 362
      IF(L.EQ.1) GOTO 362
C
C     FOR ZERO INITIAL CONDITIONS:-
C     SET INITIAL CONDITIONS FOR ALL THE FIELDS
      DO I=1,M
      DO J=1,N
      VORTY(I,J)=0
      VORT(I,J)=0
      TEMP(I,J)=0
      TEMPO(I,J)=0
      STRF(I,J)=0
      STRFI(I,J)=0
      UELTY(I,J)=0
      VELTY(I,J)=0
      VORBG(I,J)=0
      CONCEN(I,J)=0
      CONO(I,J)=0
      END DO
      END DO
C
C     FOR ZERO INITIAL CONDITIONS:-
C     SET BOUNDARY CONDITIONS FOR THE FOLLOWING
C     FIELDS :-
C
      DO I=1,M,M-1
      DO J=1,N
      VORTY1(I,J)=0.0
      VORT(I,J)=0.0
      STRF1(I,J)=0.0
      STRF2(I,J)=0.0
      STRF3(I,J)=0.0
      STRFI(I,J)=0.0
      UELTY1(I,J)=0.0
      UELTY2(I,J)=0.0
      UELTY3(I,J)=0.0
      VELTY1(I,J)=0.0
      VELTY2(I,J)=0.0
      VELTY3(I,J)=0.0
      END DO
      END DO
      DO J=1,N,N-1
      DO I=2,M-1
      VORTY1(I,J)=0.0
      VORT(I,J)=0.0
      STRF1(I,J)=0.0
      STRF2(I,J)=0.0
      STRF3(I,J)=0.0
      STRFI(I,J)=0.0
      UELTY1(I,J)=0.0
      UELTY2(I,J)=0.0
      UELTY3(I,J)=0.0
      VELTY1(I,J)=0.0
      VELTY2(I,J)=0.0
      VELTY3(I,J)=0.0
      END DO
      END DO
      DO I=1,M
      TEMP(I,1)=0.0
      TEMP1(I,1)=0.0
      TEMP2(I,1)=0.0
      TEMP3(I,1)=0.0
      TEMP(I,N)=1.0
      TEMP1(I,N)=1.0
      TEMP2(I,N)=1.0
      TEMP3(I,N)=1.0
      TEMPO(I,1)=0.0
      TEMPO(I,N)=1.0
      END DO
C     IF NCO=1 :COUNTERCURRENT FLOW
      IF(NCO.EQ.1) GOTO 3110
      DO I=1,M
      CONCEN(I,1)=0.0
      CONCEN1(I,1)=0.0
      CONCEN2(I,1)=0.0
      CONCEN3(I,1)=0.0
      CONCEN(I,N)=1.0
```

```
0273            CONCEN1(I,N)=1.0
0274            CONCEN2(I,N)=1.0
0275            CONCEN3(I,N)=1.0
0276            CONO(I,1)=0.0
0277            CONO(I,N)=1.0
0278            END DO
0279            GOTO 364
0280     3110   DO I=1,M
0281            CONCEN(I,1)=0.0
0282            CONCEN1(I,1)=0.0
0283            CONCEN2(I,1)=0.0
0284            CONCEN3(I,1)=0.0
0285            CONCEN(I,N)=1.0
0286            CONCEN1(I,N)=1.0
0287            CONCEN2(I,N)=1.0
0288            CONCEN3(I,N)=1.0
0289            CONO(I,1)=0.0
0290            CONO(I,N)=1.0
0291            END DO
0292            GOTO 364
0293    C
0294    C       SET BOUNDARY CONDITIONS FOR CASE USING PREVIOUS
0295    C       VALUES AS INITIAL CONDITIONS:-
0296    C
0297     362    DO I=1,M,M-1
0298            DO J=1,N
0299            VORTY1(I,J)=VORTY(I,J)
0300            VORT(I,J)=VORTY1(I,J)
0301            STRF1(I,J)=0
0302            STRF2(I,J)=0
0303            STRF3(I,J)=0
0304            STRFI(I,J)=0
0305            UELTY1(I,J)=0
0306            UELTY2(I,J)=0
0307            UELTY3(I,J)=0
0308            VELTY1(I,J)=0
0309            VELTY2(I,J)=0
0310            VELTY3(I,J)=0
0311            END DO
0312            END DO
0313            DO J=1,N,N-1
0314            DO I=2,M-1
0315            VORTY1(I,J)=VORTY(I,J)
0316            VORT(I,J)=VORTY1(I,J)
0317            STRF1(I,J)=0
0318            STRF2(I,J)=0
0319            STRF2(I,J)=0
0320            STRFI(I,J)=0
0321            UELTY1(I,J)=0
0322            UELTY2(I,J)=0
0323            UELTY3(I,J)=0
0324            VELTY1(I,J)=0
0325            VELTY2(I,J)=0
0326            VELTY3(I,J)=0
0327            END DO
0328            END DO
0329            DO I=1,M
0330            TEMP(I,1)=0
0331            TEMP1(I,1)=0
0332            TEMP2(I,1)=0
0333            TEMP3(I,1)=0
0334            TEMP(I,N)=1.0
0335            TEMP1(I,N)=1.0
0336            TEMP2(I,N)=1.0
0337            TEMP3(I,N)=1.0
0338            TEMPO(I,1)=0
0339            TEMPO(I,N)=1.0
0340            END DO
0341            IF(NCO.EQ.1) GOTO 3114
0342            DO I=1,M
0343            CONCEN(I,1)=0.0
0344            CONCEN1(I,1)=0.0
0345            CONCEN2(I,1)=0.0
0346            CONCEN3(I,1)=0.0
0347            CONCEN(I,N)=1.0
0348            CONCEN1(I,N)=1.0
0349            CONCEN2(I,N)=1.0
0350            CONCEN3(I,N)=1.0
0351            CONO(I,1)=0.0
0352            CONO(I,N)=1.0
0353            END DO
0354            GOTO 364
0355     3114   DO I=1,M
0356            CONCEN(I,1)=0.0
0357            CONCEN1(I,1)=0.0
0358            CONCEN2(I,1)=0.0
0359            CONCEN3(I,1)=0.0
0360            CONCEN(I,N)=1.0
0361            CONCEN1(I,N)=1.0
0362            CONCEN2(I,N)=1.0
0363            CONCEN3(I,N)=1.0
0364            CONO(I,1)=0.0
0365            CONO(I,N)=1.0
0366            END DO
0367    C
0368    C
0369    C       SET ITERATION COUNTER NOIT
0370     364    NOIT=0
0371            NTEST=10
0372    C       NTEST IS A COUNTER CONTROLLING THE OUTPUT OF
0373    C       INTERMEDIATE RESULTS IF DESIRED
0374    C
0375    C       ITERATION STARTS HERE :-
0376      100   NOIT=NOIT+1
0377    C
0378    C       SET BOUNDARY CONDITIONS FOR VORTY FIELDS AT
0379    C       N+1 LEVEL
0380            DO I=1,M,M-1
0381            DO J=1,N
0382            VORTY1(I,J)=VORTY(I,J)
0383            VORT(I,J)=VORTY1(I,J)
0384            END DO
0385            END DO
0386            DO J=1,N,N-1
0387            DO I=2,M-1
0388            VORTY1(I,J)=VORTY(I,J)
0389            VORT(I,J)=VORTY1(I,J)
0390            END DO
0391            END DO
0392    C
0393            IF(L1.EQ.2) GOTO 145
0394    C       ADVANCED TEMPERATURE FIELD BY ADI METHOD
0395    C     IF L1=0 OR 1
0396            CALL SOLVE1A(CON1,UELTY,VELTY,TEMP)
0397    C       SOLVE1 SOLVES FOR ALL TEMP(I,J,k) FOR I=1,M &
0398    C     J=2,N-1
0399    C
0400            CALL SOLVE2A(CON1,TEMP1)
0401    C       SOLVE2 CALCULATES ALL TEMP1(I,J) FOR I=1 &
0402    C     J=2,N-1
0403    C
0404            CALL SOLVE3A(CON1,UELTY,VELTY,TEMP1)
```

```
C       SOLVE3 CALCULATES ALL TEMP1(I,J) FOR I=2,M-1 &
C     J=2,N-1
C
        CALL SOLVE4A(CON1,TEMP1)
C       SOLVE4 CALCULATES ALL TEMP1(I,J) FOR I=M &
C     J=2,N-1
C
C       NOTE THAT IN SOLVE2, 3 & 4; TEMP(I,J,k) IS
C     REPRESENTED BY TEMP0(I,J)
C
C       NEXT CALCULATE CONCENTRATION FIELD BY ADI
C     METHOD IF L1 = 1 OR 2
C
 145    IF (L1.EQ.0) GOTO 150
C
        CALL SOLCN1A(CON1,UELTY,VELTY,CONCEN)
C       SOLCN1A CALCULATES ALL CONCEN(I,J,K) FOR I=1,M
C      AND J=2,N-1
C
        CALL SOLCN2A(CON1,CONCEN1)
C       SOLCN2 CALCULATES ALL CONCEN1(I,J) FOR I=1 &
C      J=2,N-1
C
        CALL SOLCN3A(CON1,UELTY,VELTY,CONCEN1)
C       SOLCN3 CALCULATES ALL CONCEN1(I,J) FOR I=2,M-1 &
C      J=2,N-1
C
        CALL SOLCN4A(CON1,CONCEN1)
C       SOLCN4 CALCULATES ALL CONCEN1(I,J) FOR I=M &
C      J=2,N-1
C
C       NOTE THAT IN SOLCN 2,3 & 4 CONCEN(I,J,K) IS
C      REPRESENTED BY CONO(I,J)
C
C       NEXT CALCULATES VORTY1(I,J) BY ADI METHOD
C
 150    CALL SOLVE5A(CON1,UELTY,VELTY,TEMP1,VORTY,VORTY1,
     1  CONCEN1)
C       SOLVE5 CALCULATES VORTY(I,J,k) FOR I=2,M-1 & J=2,N-1
C
C       NOTE THAT IN SOLVE5 VORTY(I,J,k) IS REPRESENTED BY
C       VORT(I,J)
C
        CALL SOLVE6A(CON1,UELTY,VELTY,TEMP1,VORTY1,CONCEN1)
C       SOLVE6 CALCULATES VORTY1(I,J) FOR I=2,M-1 & J=2,N-1
C       NOTE THAT IN SOLVE6 VORTY(I,J,k) IS REPRESENTED BY
C       VORT(I,J)
C
C       NEXT CALCULATES STRF1(I,J) AT THE SAME TIME LEVEL
        CALL STEST7A(CON1,STRF,VORTY1)
C       STRF1(I,J) IS CALCULATED FOR I=2,M-1 & J=2,N-1
C
        CALL STEST7B(CON1,STRF1,VORTY1)
C
C       NEXT CALCULATES X & Y VELOCITIES COMPONENT AT EACH
C       INTERIOR GRID POINTS ONLY :-
        CALL STEST8A(STRF1,UELTY1,VELTY1)
C
C
C       NEXT UPDATE THE BOUNDARY VORTICITY VALUES
C       ALONG THE VERTICAL WALLS :-
        DO I=2,M-1
        VORTY1(I,1)=-3.0*STRF1(I,2)/CON3-VORTY1(I,2)/2.0
        VORTY1(I,N)=-3.0*STRF1(I,N-1)/CON3-VORTY1(I,N-1)/
     1  2.0
        END DO
C       ALONG THE HORIZONTAL WALLS :-
        DO J=2,N-1
        VORTY1(1,J)=(-3.0*STRF1(2,J)/CON2)-(VORTY1(2,J)/2.0)
        VORTY1(M,J)=(-3.0*STRF1(M-1,J)/CON2)-(VORTY1(M-1,J)/
     1  2.0)
        END DO
C
C       ASSIGN VALUES TO CORNER VORTICITIES
        VORTY1(1,1)=(VORTY1(1,2)+VORTY1(2,1))/2.0
        VORTY1(1,N)=(VORTY1(1,N-1)+VORTY1(2,N))/2.0
        VORTY1(M,1)=(VORTY1(M-1,1)+VORTY1(M,2))/2.0
        VORTY1(M,N)=(VORTY1(M,N-1)+VORTY1(M-1,N))/2.0
C
C       BOUNDARY VORTICITY SMOOTHING -IF S=1.0 NO SMOOTHING
        DO I=1,M
        VORTY1(I,1)=S*VORTY1(I,1)+(1.0-S)*VORTY(I,1)
        VORTY1(I,N)=S*VORTY1(I,N)+(1.0-S)*VORTY(I,N)
        END DO
        DO J=2,N-1
        VORTY1(1,J)=S*VORTY1(1,J)+(1.0-S)*VORTY(1,J)
        VORTY1(M,J)=S*VORTY1(M,J)+(1.0-S)*VORTY(M,J)
        END DO
C
C       CALCULATE FROM N+1 LEVEL TO N+2 LEVEL
C
C       ASSIGN BOUNDARY VALUES TO VORTY2
        DO I= 1,M,M-1
        DO J=1,N
        VORTY2(I,J)=VORTY1(I,J)
        VORT(I,J)=VORTY2(I,J)
        END DO
        END DO
        DO J=1,N,N-1
        DO I=2,M-1
        VORTY2(I,J)=VORTY1(I,J)
        VORT(I,J)=VORTY2(I,J)
        END DO
        END DO
        IF(L2.EQ.2) GOTO 178
        CALL SOLVE1A(CON1,UELTY1,VELTY1,TEMP1)
        CALL SOLVE2A(CON1,TEMP2)
        CALL SOLVE3A(CON1,UELTY1,VELTY1,TEMP2)
        CALL SOLVE4A(CON1,TEMP2)
 178    IF(L1.EQ.0) GOTO 182
        CALL SOLCN1A(CON1,UELTY1,VELTY1,CONCEN1)
        CALL SOLCN2A(CON1,CONCEN2)
        CALL SOLCN3A(CON1,UELTY1,VELTY1,CONCEN2)
        CALL SOLCN4A(CON1,CONCEN2)
 182    CALL SOLVE5A(CON1,UELTY1,VELTY1,TEMP2,VORTY1,
     1  VORTY2,CONCEN2)
        CALL SOLVE6A(CON1,UELTY1,VELTY1,TEMP2,VORTY2,
     1  CONCEN2)
        CALL STEST7A(CON1,STRF1,VORTY2)
        CALL STEST7B(CON1,STRF2,VORTY2)
        CALL STEST8A(STRF2,UELTY2,VELTY2)
C       NEXT UPDATE THE BOUNDARY VORTICITY VALUES
C       ALONG THE VERTICAL WALLS :-
        DO I=2,M-1
        VORTY2(I,1)=-3.0*STRF2(I,2)/CON3-VORTY2(I,2)
     1  /2.0
        VORTY2(I,N)=-3.0*STRF2(I,N-1)/CON3-
     1  VORTY2(I,N-1)/2.0
        END DO
C       ALONG THE HORIZONTAL WALLS :-
        DO J=2,N-1
        VORTY2(1,J)=(-3.0*STRF2(2,J)/CON2)-(VORTY2(2,J)
```

```
     1  /2.0)
        VORTY2(M,J)=(-3.0*STRF2(M-1,J)/CON2)-
     1  (VORTY2(M-1,J)/2.0)
        END DO
C
C       ASSIGN VALUES TO CORNER VORTICITIES
        VORTY2(1,1)=(VORTY2(1,2)+VORTY2(2,1))/2.0
        VORTY2(1,N)=(VORTY2(1,N-1)+VORTY2(2,N))/2.0
        VORTY2(M,1)=(VORTY2(M-1,1)+VORTY2(M,2))/2.0
        VORTY2(M,N)=(VORTY2(M,N-1)+VORTY2(M-1,N))/2.0
C
C       BOUNDARY VORTICITY SMOOTHING
        DO I=1,M
        VORTY2(I,1)=S*VORTY2(I,1)+(1.0-S)*VORTY1(I,1)
        VORTY2(I,N)=S*VORTY2(I,N)+(1.0-S)*VORTY1(I,N)
        END DO
        DO J=2,N-1
        VORTY2(1,J)=S*VORTY2(1,J)+(1.0-S)*VORTY1(1,J)
        VORTY2(M,J)=S*VORTY2(M,J)+(1.0-S)*VORTY1(M,J)
        END DO
C
C       N+2 LEVEL SOLUTION COMPLETED
C
C       CALCULATE N+2 LEVEL SOLUTION WITH 2*TIME STEP
C
        DELT=2.0*DELT
        CON1=2.0/DELT
C       SET BOUNDARY CONDITIONS FOR VORTY3
        DO I= 1,M,M-1
        DO J=1,N
        VORTY3(I,J)=VORTY(I,J)
        VORT(I,J)=VORTY3(I,J)
        END DO
        END DO
        DO J=1,N,N-1
        DO I=2,M-1
        VORTY3(I,J)=VORTY(I,J)
        VORT(I,J)=VORTY3(I,J)
        END DO
        END DO
C       CALCULATE NEW FIELDS
        IF(L1.EQ.2) GOTO 188
        CALL SOLVE1A(CON1,UELTY,VELTY,TEMP)
        CALL SOLVE2A(CON1,TEMP3)
        CALL SOLVE3A(CON1,UELTY,VELTY,TEMP3)
        CALL SOLVE4A(CON1,TEMP3)
 188    IF(L1.EQ.0) GOTO 192
        CALL SOLCN1A(CON1,UELTY,VELTY,CONCEN)
        CALL SOLCN2A(CON1,CONCEN3)
        CALL SOLCN3A(CON1,UELTY,VELTY,CONCEN3)
        CALL SOLCN4A(CON1,CONCEN3)
 192    CALL SOLVE5A(CON1,UELTY,VELTY,TEMP3,VORTY,
     1  VORTY3,CONCEN3)
        CALL SOLVE6A(CON1,UELTY,VELTY,TEMP3,VORTY3,
     1  CONCEN3)
        CALL STEST7A(CON1,STRF,VORTY3)
        CALL STEST7B(CON1,STRF3,VORTY3)
        CALL STEST8A(STRF3,UELTY3,VELTY3)
C       NEXT UPDATE THE BOUNDARY VORTICITY VALUES
C       ALONG THE VERTICAL WALLS :-
        DO I=2,M-1
        VORTY3(I,1)=-3.0*STRF3(I,2)/CON3-VORTY3(I,2)
     1  /2.0
        VORTY3(I,N)=-3.0*STRF3(I,N-1)/CON3-
     1  VORTY3(I,N-1)/2.0
        END DO
C       ALONG THE HORIZONTAL WALLS :-
        DO J=2,N-1
        VORTY3(1,J)=(-3.0*STRF3(2,J)/CON2)-
     1  (VORTY3(2,J)/2.0)
        VORTY3(M,J)=(-3.0*STRF3(M-1,J)/CON2)-
     1  (VORTY3(M-1,J)/2.0)
        END DO
C
C       ASSIGN VALUES TO CORNER VORTICITIES
        VORTY3(1,1)=(VORTY3(1,2)+VORTY3(2,1))/2.0
        VORTY3(1,N)=(VORTY3(1,N-1)+VORTY3(2,N))/2.0
        VORTY3(M,1)=(VORTY3(M-1,1)+VORTY3(M,2))/2.0
        VORTY3(M,N)=(VORTY3(M,N-1)+VORTY3(M-1,N))/2.0
C       BOUNDARY VORTICITY SMOOTHING
        DO I=1,M
        VORTY3(I,1)=S*VORTY3(I,1)+(1.0-S)*VORTY(I,1)
        VORTY3(I,N)=S*VORTY3(I,N)+(1.0-S)*VORTY(I,N)
        END DO
        DO J=2,N-1
        VORTY3(1,J)=S*VORTY3(1,J)+(1.0-S)*VORTY(1,J)
        VORTY3(M,J)=S*VORTY3(M,J)+(1.0-S)*VORTY(M,J)
        END DO
C
C       CALCULATION FOR N+2 FIELDS FROM N FIELDS COMPLETED
C       CALCULATE TEST CRITERION TP OF DOSS & MILLER :-
        DELT=0.5*DELT
        CON1=2.0/DELT
        TSUM=0.0
        SSUM=0.0
        VSUM=0.0
        CSUM=0.0
        IF(L1.EQ.2) GOTO 184
        DO I=1,M
        DO J=1,N
        G=ABS(TEMP2(I,J)-TEMP3(I,J))
        G=G*G
        TSUM=TSUM+G
        END DO
        END DO
 184    IF(L1.EQ.0) GOTO 186
        DO I=1,M
        DO J=1,N
        G3=ABS(CONCEN2(I,J)-CONCEN3(I,J))
        G3=G3*G3
        CSUM=CSUM+G3
        END DO
        END DO
 186    DO I=1,M
        DO J=1,N
        G1=ABS(STRF2(I,J)-STRF3(I,J))
        G1=G1*G1
        SSUM=SSUM+G1
        G2=ABS(VORTY2(I,J)-VORTY3(I,J))
        G2=G2*G2
        VSUM=VSUM+G2
        END DO
        END DO
        TSUM=SQRT(TSUM)
        SSUM=SQRT(SSUM)
        VSUM=SQRT(VSUM)
        CSUM=SQRT(CSUM)
        ATSUM=0.0
        ASSUM=0.0
        AVSUM=0.0
        ACSUM=0.0
        IF(L1.EQ.2) GOTO 198
```

```
0669            DO I=1,M
0670            DO J=1,N
0671            G4=ABS(TEMP2(I,J)-TEMP(I,J))
0672            G4=G4*G4
0673            ATSUM=ATSUM+G4
0674            END DO
0675            END DO
0676     198    IF(L1.EQ.0) GOTO 202
0677            DO I=1,M
0678            DO J=1,N
0679            G7=ABS(CONCEN2(I,J)-CONCEN(I,J))
0680            G7=G7*G7
0681            ACSUM=ACSUM+G7
0682            END DO
0683            END DO
0684     202    DO I=1,M
0685            DO J=1,N
0686            G5=ABS(STRF2(I,J)-STRF(I,J))
0687            G5=G5*G5
0688            ASSUM=ASSUM+G5
0689            G6=ABS(VORTY2(I,J)-VORTY(I,J))
0690            G6=G6*G6
0691            AVSUM=AVSUM+G6
0692            END DO
0693            END DO
0694            ATSUM=SQRT(ATSUM)
0695            ASSUM=SQRT(ASSUM)
0696            AVSUM=SQRT(AVSUM)
0697            ACSUM=SQRT(ACSUM)
0698            SUM=TSUM+SSUM+VSUM+CSUM
0699            ASUM=ATSUM+ASSUM+AVSUM+ACSUM
0700            TP=SUM/ASUM
0701    C
0702    C       TEST FOR TP TO DETERMINE NEW TIME STEP
0703            IF(TP.LT.0.6) GOTO 3111
0704            DELT=(1.0/16)*DELT
0705            CON1=2.0/DELT
0706            GOTO 100
0707     3111   IF(TP.LE.0.6. AND .TP.GT.0.4) DELT=(1.0/4.0)*DELT
0708            IF(TP.LE.0.4. AND .TP.GT.0.3) DELT=(1.0/2.0)*DELT
0709            IF(TP.LE.0.3. AND .TP.GT.0.1) DELT=SQRT(3.0)*DELT
0710            IF(TP.LE.0.1. AND .TP.GT.0.05) DELT=2.0*DELT
0711            IF(TP.LE.0.05. AND .TP.GE.0.0) DELT=4.0*DELT
0712            CON1=2.0/DELT
0713            PRINT 99,CON1,DELT
0714      99    FORMAT(1X,'CON1='G10.3,3X,'DELT='G10.3)
0715            IF(L1.EQ.2) GOTO 91
0716    C
0717    C       CALCULATE CONVERGENT FACTOR FOR EACH FIELD :-
0718    C       TEMPERATURE FIELD :-
0719            TESTT=0.0
0720            TMAX=0.0
0721            DO I=1,M
0722            DO J=2,N-1
0723            TESTT=TESTT+ABS(TEMP2(I,J)-TEMP1(I,J))
0724            IF(ABS(TEMP2(I,J)).GT.TMAX) TMAX=ABS(TEMP2(I,J))
0725            TEMP(I,J)=TEMP2(I,J)
0726            END DO
0727            END DO
0728            IF(TMAX.LT.0.001) GOTO 91
0729            TESTT=TESTT/(TMAX*M*(N-1))
0730    C
0731      91    IF (L1.EQ.0) GOTO 90
0732    C
0733    C
0734    C       CONCENTRATION FIELD :-
0735            TESTC=0.0
0736            CMAX=0.0
0737            DO I=1,M
0738            DO J=2,N-1
0739            TESTC=TESTC+ABS(CONCEN2(I,J)-CONCEN1(I,J))
0740            IF(ABS(CONCEN2(I,J)).GT.CMAX) CMAX=
0741          1 ABS(CONCEN2(I,J))
0742            CONCEN(I,J)=CONCEN2(I,J)
0743            END DO
0744            END DO
0745            IF(CMAX.LT.0.001) GOTO 90
0746            TESTC=TESTC/(CMAX*M*(N-1))
0747    C
0748    C
0749    C       VORTICITY FIELD:-
0750      90    TESTV=0.0
0751            VMAX=0.0
0752            DO I=1,M
0753            DO J=1,N
0754            TESTV=TESTV+ABS(VORTY2(I,J)-VORTY1(I,J))
0755            IF(ABS(VORTY2(I,J)).GT.VMAX) VMAX=
0756          1 ABS(VORTY2(I,J))
0757            VORTY(I,J)=VORTY2(I,J)
0758            END DO
0759            END DO
0760            IF(VMAX.LT.0.001) GOTO 92
0761            TESTV=TESTV/(VMAX*M*N)
0762    C
0763    C
0764    C       STREAM FUNCTION FIELD:-
0765      92    TESTS=0.0
0766            SMAX=0.0
0767            DO I=2,M-1
0768            DO J=2,N-1
0769            TESTS=TESTS+ABS(STRF2(I,J)-STRF1(I,J))
0770            IF(ABS(STRF2(I,J)).GT.SMAX) SMAX=
0771          1 ABS(STRF2(I,J))
0772            STRF(I,J)=STRF2(I,J)
0773            UELTY(I,J)=UELTY2(I,J)
0774            VELTY(I,J)=VELTY2(I,J)
0775            END DO
0776            END DO
0777            IF(SMAX.LT.0.001) GOTO 97
0778            TESTS=TESTS/(SMAX*(M-1)*(N-1))
0779    C
0780    C       IF NOIT=NTEST PRINT INTERMEDIATE VALUES
0781     97     IF(NOIT.NE.NTEST) GOTO 3170
0782            PRINT 106,NOIT,NTEST
0783      106   FORMAT(1X,'NOIT=',I4,3X,'NTEST=',I4)
0784            PRINT 3123,SUM,ASUM,TP
0785    C       PRINT 3121,ATSUM,ASSUM,AVSUM,ACSUM
0786    C       PRINT 3131,TSUM,SSUM,VSUM,CSUM
0787            PRINT 83,TESTT,TESTV,TESTS,TESTC
0788            PRINT 305
0789    C 3121  FORMAT(1X,'ATSUM='G10.3,2X,'ASSUM='G10.3,2X,
0790    C     1 'AVSUM='G10.3,2X,'ACSUM='G10.3)
0791     3123   FORMAT(1X,'SUM='G10.3,2X,'ASUM='G10.3,2X,
0792          1 'TP='G10.3)
0793    C3131   FORMAT(1X,'TSUM='G10.3,2X,'SSUM='G10.3,2X,
0794    C     1 'VSUM='G10.3,2X,'CSUM='G10.3)
0795     83     FORMAT(1X,'TESTT='F7.5,3X,'TESTV='F7.5,
0796          1 3X,'TESTS='F7.5,2X,'TESTC='F7.5)
0797    C
0798    C       CALCULATE INTERMEDIATE NUSSELT NUMBERS
0799    C     (OR SHERWOOD NO)
0800    C       GRDT = TEMPERATURE GRADIENT AT THE WALL
```

```
      DO I=1,M
      GRDT(I,1)=(-3.0*TEMP1(I,1)+4.0*TEMP1(I,2)-
     1 TEMP1(I,3))/(2.0*DELY)
      GRDT(I,2)=(3.0*TEMP1(I,N)-4.0*TEMP1(I,N-1)+
     1 TEMP1(I,N-2))/(2.0*DELY)
      END DO
      XX=0
      AA=0
      DO I=2,M-1,2
      YY=XX+GRDT(I,1)
      XX=YY
      BB=AA+GRDT(I,2)
      AA=BB
      END DO
      XX1=0
      XX2=0
      DO I=3,M-2,2
      XX3=XX1+GRDT(I,1)
      XX4=XX2+GRDT(I,2)
      XX1=XX3
      XX2=XX4
      END DO
C     AVERAGE HNU IS CALCULATED FROM SIMPSON RULE
      HNU(1)=((DELX/3.0)*(GRDT(1,1)+4.0*XX+2.0*XX1+
     1 GRDT(M,1)))/((M-1)*DELX)/((N-1)*DELY)
      HNU(2)=((DELX/3.0)*(GRDT(1,2)+4.0*AA+2.0*XX2+
     1 GRDT(M,2)))/((M-1)*DELX)/((N-1)*DELY)
      PRINT 3172,HNU(1),HNU(2)
 3172 FORMAT(1X,'HNU(1)='F7.2,3X,'HNU(2)='F7.2)
      NTEST=NTEST+10
C
C     SET CPU TIME LIMIT
 3170 CALL LIB$STAT_TIMER(%REF(2),ICPU)
C     IF ICPU IS GREATER THAN NCPU, STOP AND PRINT
C    RESULTS
      IF(ICPU.GT.NCPU) GOTO 9110
      IF(BETA.EQ.90.0) GOTO 216
      IF(NOIT.LT.10) GOTO 100
  216 IF(L1.EQ.2) GOTO 218
      IF(TESTT.GT.EO)GOTO 100
  218 IF(L1.EQ.0) GOTO 204
      IF(TESTC.GT.EO)GOTO 100
  204 IF(TESTV.GT.EO)GOTO 100
      IF(TESTS.GT.EO)GOTO 100
      PRINT 83,TESTT,TESTV,TESTS,TESTC
C
C     CALCULATE STEADY STATE NUSSELT AND SHERWOOD
C    NUMBERS
 9110 DO I=1,M
      GRDT(I,1)=(-3.0*TEMP1(I,1)+4.0*TEMP1(I,2)-
     1 TEMP1(I,3))/(2.0*DELY)
      GRDT(I,2)=(3.0*TEMP1(I,N)-4.0*TEMP1(I,N-1)+
     1 TEMP1(I,N-2))/(2.0*DELY)
      END DO
      XX=0
      AA=0
      DO I=2,M-1,2
      YY=XX+GRDT(I,1)
      XX=YY
      BB=AA+GRDT(I,2)
      AA=BB
      END DO
      XX1=0
      XX2=0
      DO I=3,M-2,2
      XX3=XX1+GRDT(I,1)
      XX4=XX2+GRDT(I,2)
      XX1=XX3
      XX2=XX4
      END DO
      HNU(1)=((DELX/3.0)*(GRDT(1,1)+4.0*XX+2.0*XX1+
     1 GRDT(M,1)))/((M-1)*DELX)/((N-1)*DELY)
      HNU(2)=((DELX/3.0)*(GRDT(1,2)+4.0*AA+2.0*XX2+
     1 GRDT(M,2)))/((M-1)*DELX)/((N-1)*DELY)
C
C     ON 26/12/85 THE CORRECT SHERWOOD NUMBER FORMULATION
C   IS GIVEN WITH THE INCLUSION OF THE DRY AIR DENSITY
C   TERM TO THE DENOMINATOR OF THE EQUATION FOR CALCULATING
C   SH. THUS ALL PREVIOUS SHERWOOD NUMBERS OBTAINED FROM
C   THE CALCULATION NEED TO BE DIVIDED BY THE DENSITY OF
C   AIR TO OBTAIN THE CORRECT VALUES.
C
      DO I=1,M
      GRDC(I,1)=(-3.0*CONCEN2(I,1)+4.0*CONCEN2(I,2)-
     1 CONCEN2(I,3))/(2.0*DELY)
      GRDC(I,2)=(3.0*CONCEN2(I,N)-4.0*CONCEN2(I,N-1)+
     1 CONCEN2(I,N-2))/(2.0*DELY)
      END DO
      XX=0
      AA=0
      DO I=2,M-1,2
      YY=XX+GRDC(I,1)
      XX=YY
      BB=AA+GRDC(I,2)
      AA=BB
      END DO
      XX1=0
      XX2=0
      DO I=3,M-2,2
      XX3=XX1+GRDC(I,1)
      XX4=XX2+GRDC(I,2)
      XX1=XX3
      XX2=XX4
      END DO
      SH(1)=(((DELX/3.0)*(GRDC(1,1)+4.0*XX+2.0*XX1+
     1 GRDC(M,1)))/((M-1)*DELX)/((N-1)*DELY))/1.177
C     1.177 IS THE DENSITY OF DRY AIR AT 300 DEG K
      SH(2)=(((DELX/3.0)*(GRDC(1,2)+4.0*AA+2.0*XX2+
     1 GRDC(M,2)))/((M-1)*DELX)/((N-1)*DELY))/1.177
C
C
C     WRITE STEADY STATE OUTPUT
      CALL WTEST1A(TEMP2,STRF2,VORTY2,UELTY2,VELTY2,
     1 CONCEN2)
      STOP
      END
```

```
      SUBROUTINE SOLVE1A(CON1,UELTY,VELTY,TEMP)
C     THIS SUBROUTINE CALCULATES TEMP(I,J,k) FOR
C     I=1,M & J=2,N-1
C     TEMP(I,J,k) IS REPRESENTED BY TEMP0(I,J)
      IMPLICIT REAL*8 (A-H,O-Z)
C     DIMENSION STATEMENTS ARE READ FROM 'DIMEN.FOR'
      INCLUDE 'DIMEN.FOR'
      DIMENSION UELTY(MD,ND),VELTY(MD,ND),TEMP(MD,ND)
C     COMMON STATEMENTS ARE READ FROM 'COMMON.FOR'
      INCLUDE 'COMMON.FOR'
C     SPECIFY COEFFICIENT MATRIX
      DO I=1,M
      B(I)=(CON1+ALFAT*CON4)
      END DO
      C(1)=CON4*ALFAT
      A(M)=CON4*ALFAT
      DO 32 J=2,N-1
      DO I=2,M-1
      A(I)=(PR*ALFAT*UELTY(I-1,J)*CON5)+(ALFAT/CON2)
      END DO
      DO I=2,M-1
      C(I)=(ALFAT/CON2)-(PR*ALFAT*UELTY(I+1,J)*CON5)
      END DO
      DO I=2,M-1
      D(I)=(CON1*TEMP(I,J))-(PR*ALFAT*CON6*(VELTY(I,J+1)*
     1  TEMP(I,J+1)-VELTY(I,J-1)*TEMP(I,J-1)))+(ALFAT*
     2  (TEMP(I,J+1)+TEMP(I,J-1)-(2.0*TEMP(I,J)))/CON3)
      END DO
      D(1)=CON1*TEMP(1,J)+ALFAT*(TEMP(1,J+1)+TEMP(1,J-1)
     1  -2.0*TEMP(1,J))/CON3
      D(M)=CON1*TEMP(M,J)+ALFAT*(TEMP(M,J+1)+
     1  TEMP(M,J-1)-2.0*TEMP(M,J))/CON3
C
C     MATRIX IS SPECIFIED
C     NEXT SOLVE FOR TEMP0(I,J) BY THOMAS ALGORITHM
      ALPHA(1)=B(1)
      DO I=2,M
      ALPHA(I)=B(I)-(A(I)*C(I-1))/ALPHA(I-1)
      END DO
      SEE(1)=D(1)
      DO I=2,M
      SEE(I)=D(I)+(A(I)*SEE(I-1))/ALPHA(I-1)
      END DO
      TEMP0(M,J)=SEE(M)/ALPHA(M)
      DO I=M-1,1,-1
      TEMP0(I,J)=(SEE(I)+C(I)*TEMP0(I+1,J))/ALPHA(I)
      END DO
   32 CONTINUE
      RETURN
      END
```

```
      SUBROUTINE SOLVE2A(CON1,TEMP1)
C     THIS SUBROUTINE CALCULATES TEMP(I,J,NT+1)
C     FOR I=1 & J=2,N-1
C     TEMP(I,J,k) IS REPRESENTED BY TEMP0(I,J)
      IMPLICIT REAL*8 (A-H,O-Z)
      INCLUDE 'DIMEN.FOR'
      DIMENSION TEMP1(MD,ND)
      INCLUDE 'COMMON.FOR'
      I=1
      DO J=2,N-1
      B(J)=CON1+(2.0*ALFAT)/CON3
      END DO
      DO J=2,N-2
      C(J)=ALFAT/CON3
      END DO
      DO J=3,N-1
      A(J)=ALFAT/CON3
      END DO
      D(2)=CON1*TEMP0(1,2)+2.0*ALFAT*(TEMP0(2,2)-
     1  TEMP0(1,2))/CON2+ALFAT/CON3*TEMP0(1,1)
      D(N-1)=CON1*TEMP0(1,N-1)+2.0*ALFAT*(TEMP0(2,N-1)-
     1  TEMP0(1,N-1))/CON2+ALFAT*TEMP0(1,N)/CON3
      DO J=3,N-2
      D(J)=CON1*TEMP0(1,J)+2.0*ALFAT*(TEMP0(2,J)-
     1  TEMP0(1,J))/CON2
      END DO
C
C     MATRIX IS SPECIFIED
C     SOLVE TEMP1(1,J) BY THOMAS ALGORITHM :-
      ALPHA(2)=B(2)
      DO J=3,N-1
      ALPHA(J)=B(J)-(A(J)*C(J-1))/ALPHA(J-1)
      END DO
      SEE(2)=D(2)
      DO J=3,N-1
      SEE(J)=D(J)+(A(J)*SEE(J-1))/ALPHA(J-1)
      END DO
      TEMP1(1,N-1)=SEE(N-1)/ALPHA(N-1)
      DO J=N-2,2,-1
      TEMP1(1,J)=(SEE(J)+C(J)*TEMP1(1,J+1))/ALPHA(J)
      END DO
      RETURN
      END
```

```
      SUBROUTINE SOLVE3A(CON1,UELTY,VELTY,TEMP1)
C     THIS SUBROUTINE CALCULATES TEMP(I,J,NT+1)
C     FOR I=2,M-1 & J=2,N-1
C     TEMP(I,J,k) IS REPRESENTED BY TEMP0(I,J)
      IMPLICIT REAL*8 (A-H,0-Z)
      INCLUDE 'DIMEN.FOR'
      DIMENSION UELTY(MD,ND),VELTY(MD,ND),TEMP1(MD,ND)
      INCLUDE 'COMMON.FOR'
      DO J=2,N-1
      B(J)=CON1+2.0*ALFAT/CON3
      END DO
      DO 52 I=2,M-1
      DO J=3,N-1
      A(J)=(VELTY(I,J-1)*ALFAT*PR*CON6)+ALFAT/CON3
      END DO
      DO J=2,N-2
      C(J)=ALFAT/CON3-(VELTY(I,J+1)*ALFAT*PR)*CON6
      END DO
      D(2)=CON1*TEMP0(I,2)+((PR*VELTY(I,1)*ALFAT)*CON6+
     1 ALFAT/CON3)*TEMP0(I,1)-(ALFAT*PR*CON5)*(UELTY(I+1,2)*
     2 TEMP0(I+1,2)-UELTY(I-1,2)*TEMP0(I-1,2))+ALFAT*
     3 (TEMP0(I+1,2)-2.0*TEMP0(I,2)+TEMP0(I-1,2))/CON2
      D(N-1)=CON1*TEMP0(I,N-1)+(ALFAT/CON3-PR*VELTY(I,N)*
     1 ALFAT*CON6)*TEMP0(I,N)-ALFAT*PR*CON5*(UELTY(I+1,N-1)*
     2 TEMP0(I+1,N-1)-UELTY(I-1,N-1)*TEMP0(I-1,N-1))+ALFAT/
     3 CON2*(TEMP0(I+1,N-1)-2.0*TEMP0(I,N-1)+TEMP0(I-1,N-1))
      DO J=3,N-2
      D(J)=CON1*TEMP0(I,J)-(PR*ALFAT*CON5*(UELTY(I+1,J)*
     1 TEMP0(I+1,J)-UELTY(I-1,J)*
     2 TEMP0(I-1,J)))+ALFAT/CON2*(TEMP0(I+1,J)-2.0*
     3 TEMP0(I,J)+TEMP0(I-1,J))
      END DO
C
C     MATRIX IS SPECIFIED
C     SOLVE FOR TEMP1(I,J) BY THOMAS ALGORITHM
      ALPHA(2)=B(2)
      DO J=3,N-1
      ALPHA(J)=B(J)-(A(J)*C(J-1))/ALPHA(J-1)
      END DO
      SEE(2)=D(2)
      DO J=3,N-1
      SEE(J)=D(J)+(A(J)*SEE(J-1))/ALPHA(J-1)
      END DO
      TEMP1(I,N-1)=SEE(N-1)/ALPHA(N-1)
      DO J=N-2,2,-1
      TEMP1(I,J)=(SEE(J)+C(J)*TEMP1(I,J+1))/ALPHA(J)
      END DO
 52   CONTINUE
      RETURN
      END
```

```
      SUBROUTINE SOLVE4A(CON1,TEMP1)
C     THIS SUBROUTINE SOLVES FOR TEMP(I,J,NT+1)
C     FOR I=M &J=2,N-1
C     TEMP(I,J,k) IS REPRESENTED BY TEMP0(I,J)
      IMPLICIT REAL*8 (A-H,0-Z)
      INCLUDE 'DIMEN.FOR'
      DIMENSION TEMP1(MD,ND)
      INCLUDE 'COMMON.FOR'
      DO J=2,N-1
      B(J)=CON1+(2.0*ALFAT)/CON3
      END DO
      DO J=2,N-2
      C(J)=ALFAT/CON3
      END DO
      DO J=3,N-1
      A(J)=ALFAT/CON3
      END DO
      D(2)=CON1*TEMP0(M,2)+(2.0*ALFAT/CON2*(TEMP0(M-1,2)-
     1 TEMP0(M,2)))+ALFAT/CON3*TEMP0(M,1)
      D(N-1)=CON1*TEMP0(M,N-1)+2.0*ALFAT/CON2*
     1 (TEMP0(M-1,N-1)-TEMP0(M,N-1))+ALFAT/CON3*TEMP0(M,N)
      DO J=3,N-2
      D(J)=CON1*TEMP0(M,J)+2.0*ALFAT/CON2*(TEMP0(M-1,J)-
     1 TEMP0(M,J))
      END DO
C     MATRIX IS SPECIFIED
C     SOLVE FOR TEMP1(I,J) BY THOMAS ALGORITHM :-
      ALPHA(2)=B(2)
      DO J=3,N-1
      ALPHA(J)=B(J)-(A(J)*C(J-1))/ALPHA(J-1)
      END DO
      SEE(2)=D(2)
      DO J=3,N-1
      SEE(J)=D(J)+(A(J)*SEE(J-1))/ALPHA(J-1)
      END DO
      TEMP1(M,N-1)=SEE(N-1)/ALPHA(N-1)
      DO J=N-2,2,-1
      TEMP1(M,J)=(SEE(J)+C(J)*TEMP1(M,J+1))/ALPHA(J)
      END DO
      RETURN
      END
```

```
      SUBROUTINE SOLCN1A(CON1,UELTY,VELTY,CONCEN)
C     THIS SUBROUTINE CALCULATES CONCEN(I,J,k)
C     FOR I=1,M & J=2,N-1
C     CONCEN(I,J,k) IS REPRESENTED BY CONO(I,J)
      IMPLICIT REAL*8 (A-H,O-Z)
      INCLUDE 'DIMEN.FOR'
      DIMENSION UELTY(MD,ND),VELTY(MD,ND),CONCEN(MD,ND)
      INCLUDE 'COMMON.FOR'
      DO I=1,M
      B(I)=(CON1+ALFAC*CON4)
      END DO
      C(1)=CON4*ALFAC
      A(M)=CON4*ALFAC
      DO 132 J=2,N-1
      DO 136 I=2,M-1
      A(I)=(SC*ALFAC*UELTY(I-1,J)*CON5)+(ALFAC/CON2)
      C(I)=(ALFAC/CON2)-(SC*ALFAC*UELTY(I+1,J)*CON5)
      D(I)=(CON1*CONCEN(I,J))-(SC*ALFAC*CON6*(VELTY(I,J+1)*
     1 CONCEN(I,J+1)-VELTY(I,J-1)*CONCEN(I,J-1)))+(ALFAC*
     2 (CONCEN(I,J+1)+CONCEN(I,J-1)-(2.0*CONCEN(I,J)))/CON3)
  136 CONTINUE
      D(1)=CON1*CONCEN(1,J)+ALFAC*(CONCEN(1,J+1)+
     1 CONCEN(1,J-1)-2.0*CONCEN(1,J))/CON3
      D(M)=CON1*CONCEN(M,J)+ALFAC*(CONCEN(M,J+1)+CONCEN
     1 (M,J-1)-2.0*CONCEN(M,J))/CON3
C     MATRIX IS SPECIFIED
C
C     SOLVE CONO(I,J) BY THOMAS ALGORITHM
      ALPHA(1)=B(1)
      DO I=2,M
      ALPHA(I)=B(I)-(A(I)*C(I-1))/ALPHA(I-1)
      END DO
      SEE(1)=D(1)
      DO I=2,M
      SEE(I)=D(I)+(A(I)*SEE(I-1))/ALPHA(I-1)
      END DO
      CONO(M,J)=SEE(M)/ALPHA(M)
      DO I=M-1,1,-1
      CONO(I,J)=(SEE(I)+C(I)*CONO(I+1,J))/ALPHA(I)
      END DO
  132 CONTINUE
      RETURN
      END
```

```
      SUBROUTINE SOLCN2A(CON1,CONCEN1)
C     THIS SUBROUTINE CALCULATES CONCEN(I,J,NT+1)
C     FOR I=1 & J=2,N-1
C     CONCEN(I,J,k) IS REPRESENTED BY CONO(I,J)
      IMPLICIT REAL*8 (A-H,O-Z)
      INCLUDE 'DIMEN.FOR'
      DIMENSION CONCEN1(MD,ND)
      INCLUDE 'COMMON.FOR'
      I=1
      DO J=2,N-1
      B(J)=CON1+(2.0*ALFAC)/CON3
      END DO
      DO J=2,N-2
      C(J)=ALFAC/CON3
      END DO
      DO J=3,N-1
      A(J)=ALFAC/CON3
      END DO
      D(2)=CON1*CONO(1,2)+2.0*ALFAC*(CONO(2,2)-CONO(1,2))/
     1 CON2+ALFAC/CON3*CONO(1,1)
      D(N-1)=CON1*CONO(1,N-1)+2.0*ALFAC*(CONO(2,N-1)-
     1 CONO(1,N-1))/CON2+ALFAC*CONO(1,N)/CON3
      DO J=3,N-2
      D(J)=CON1*CONO(1,J)+2.0*ALFAC*(CONO(2,J)-CONO(1,J))/
     1 CON2
      END DO
C
C     MATRIX IS SPECIFIED
      ALPHA(2)=B(2)
      DO J=3,N-1
      ALPHA(J)=B(J)-(A(J)*C(J-1))/ALPHA(J-1)
      END DO
      SEE(2)=D(2)
      DO J=3,N-1
      SEE(J)=D(J)+(A(J)*SEE(J-1))/ALPHA(J-1)
      END DO
      CONCEN1(1,N-1)=SEE(N-1)/ALPHA(N-1)
      DO J=N-2,2,-1
      CONCEN1(1,J)=(SEE(J)+C(J)*CONCEN1(1,J+1))/ALPHA(J)
      END DO
      RETURN
      END
```

```
      SUBROUTINE SOLCN3A(CON1,UELTY,VELTY,CONCEN1)
C     THIS SUBROUTINE CALCULATES CONCEN(I,J,NT+1)
C     FOR I=2,M-1 & J=2,N-1
C     CONCEN(I,J,k) IS REPRESENTED BY CONO(I,J)
      IMPLICIT REAL*8 (A-H,O-Z)
      INCLUDE 'DIMEN.FOR'
      DIMENSION UELTY(MD,ND),VELTY(MD,ND),CONCEN1(MD,ND)
      INCLUDE 'COMMON.FOR'
      DO J=2,N-1
      B(J)=CON1+2.0*ALFAC/CON3
      END DO
      DO 152 I=2,M-1
      DO J=3,N-1
      A(J)=(VELTY(I,J-1)*ALFAC*SC*CON6)+ALFAC/CON3
      END DO
      DO J=2,N-2
      C(J)=ALFAC/CON3-(VELTY(I,J+1)*ALFAC*SC)*CON6
      END DO
      D(2)=CON1*CONO(I,2)+((SC*VELTY(I,1)*ALFAC)*CON6+
     1 ALFAC/CON3)*CONO(1,1)-(ALFAC*SC*CON5)*(UELTY(I+1,2)
     2 *CONO(I+1,2)-UELTY(I-1,2)*CONO(I-1,2))+ALFAC*
     3 (CONO(I+1,2)-2.0*CONO(I,2)+CONO(I-1,2))/CON2
C
      D(N-1)=CON1*CONO(I,N-1)+(ALFAC/CON3-SC*VELTY(I,N)*
     1 ALFAC*CON6)*CONO(I,N)-ALFAC*SC*CON5*(UELTY(I+1,N-1)*
     2 CONO(I+1,N-1)-UELTY(I-1,N-1)*CONO(I-1,N-1))+ALFAC/
     3 CON2*(CONO(I+1,N-1)-2.0*CONO(I,N-1)+CONO(I-1,N-1))
C
      DO J=3,N-2
      D(J)=CON1*CONO(I,J)-(SC*ALFAC*CON5*(UELTY(I+1,J)*
     1 CONO(I+1,J)-UELTY(I-1,J)*
     2 CONO(I-1,J)))+ALFAC/CON2*(CONO(I+1,J)-2.0*CONO(I,J)+
     3 CONO(I-1,J))
      END DO
C     MATRIX IS SPECIFIED
C
      ALPHA(2)=B(2)
      DO J=3,N-1
      ALPHA(J)=B(J)-(A(J)*C(J-1))/ALPHA(J-1)
      END DO
      SEE(2)=D(2)
      DO J=3,N-1
      SEE(J)=D(J)+(A(J)*SEE(J-1))/ALPHA(J-1)
      END DO
      CONCEN1(I,N-1)=SEE(N-1)/ALPHA(N-1)
      DO J=N-2,2,-1
      CONCEN1(I,J)=(SEE(J)+C(J)*CONCEN1(I,J+1))/ALPHA(J)
      END DO
152   CONTINUE
      RETURN
      END
```

```
      SUBROUTINE SOLCN4A(CON1,CONCEN1)
C     THIS SUBROUTINE SOLVES FOR CONCEN(I,J,NT+1)
C     FOR I=M & J=2,N-1
C     CONCEN(I,J,k) IS REPRESENTED BY CONO(I,J)
      IMPLICIT REAL*8 (A-H,O-Z)
      INCLUDE 'DIMEN.FOR'
      DIMENSION CONCEN1(MD,ND)
      INCLUDE 'COMMON.FOR'
      DO J=2,N-1
      B(J)=CON1+(2.0*ALFAC)/CON3
      END DO
      DO J=2,N-2
      C(J)=ALFAC/CON3
      END DO
      DO J=3,N-1
      A(J)=ALFAC/CON3
      END DO
      D(2)=CON1*CONO(M,2)+(2.0*ALFAC/CON2*(CONO(M-1,2)-
     1 CONO(M,2)))+ALFAC/CON3*CONO(M,1)
      D(N-1)=CON1*CONO(M,N-1)+2.0*ALFAC/CON2*
     1 (CONO(M-1,N-1)-CONO(M,N-1))+ALFAC/CON3*CONO(M,N)
      DO J=3,N-2
      D(J)=CON1*CONO(M,J)+2.0*ALFAC/CON2*(CONO(M-1,J)-
     1 CONO(M,J))
      END DO
C     MATRIX IS SPECIFIED
C
      ALPHA(2)=B(2)
      DO J=3,N-1
      ALPHA(J)=B(J)-(A(J)*C(J-1))/ALPHA(J-1)
      END DO
      SEE(2)=D(2)
      DO J=3,N-1
      SEE(J)=D(J)+(A(J)*SEE(J-1))/ALPHA(J-1)
      END DO
      CONCEN1(M,N-1)=SEE(N-1)/ALPHA(N-1)
      DO J=N-2,2,-1
      CONCEN1(M,J)=(SEE(J)+C(J)*CONCEN1(M,J+1))/ALPHA(J)
      END DO
      RETURN
      END
```

```
      SUBROUTINE SOLVE5A(CON1,UELTY,VELTY,TEMP1,VORTY,
     1  VORTY1,CONCEN1)
C     THIS SUBROUTINE SOLVES FOR VORTY(I,J,k)
C     FOR I=2,M-1 & J=2,N-1
C     VORTY(I,J,k) IS REPRESENTED BY VORT(I,J)
      IMPLICIT REAL*8 (A-H,O-Z)
      INCLUDE 'DIMEN.FOR'
      DIMENSION UELTY(MD,ND),VELTY(MD,ND),TEMP1(MD,ND)
      DIMENSION VORTY(MD,ND),VORTY1(MD,ND),CONCEN1(MD,ND)
      INCLUDE 'COMMON.FOR'
      DO I=2,M-1
      B(I)=CON1+2.0*ALFAV/CON2
      END DO
      DO 60 J=2,N-1
      DO I=3,M-1
      A(I)=(UELTY(I-1,J)*ALFAV*CON5)+(ALFAV/CON2)
      END DO
      DO I=2,M-2
      C(I)=ALFAV/CON2-UELTY(I+1,J)*ALFAV*CON5
      END DO
      D(2)=CON1*VORTY(2,J)+ALFAV*GR*CON6*COSD(BETA)*
     1(TEMP1(2,J+1)-TEMP1(2,J-1))-GR*ALFAV*CON6*SIND(BETA)*
     2(TEMP1(3,J)-TEMP1(1,J))+(ALFAV/CON3)*(VORTY(2,J+1)
     3+VORTY(2,J-1)-2.0*VORTY(2,J))-(ALFAV*CON6)*(
     4VELTY(2,J+1)*VORTY(2,J+1)-VELTY(2,J-1)*VORTY(2,J-1))
     5+(UELTY(1,J)*ALFAV*CON5+ALFAV/CON2)*VORTY1(1,J)+ALFAV
     6*GRC*CON6*COSD(BETA)*(CONCEN1(2,J+1)-CONCEN1(2,J-1))
     7-ALFAV*GRC*CON6*SIND(BETA)*(CONCEN1(3,J)-CONCEN1(1,J))
C
      D(M-1)=CON1*VORTY(M-1,J)+ALFAV*GR*CON6*COSD(BETA)*
     1(TEMP1(M-1,J+1)-TEMP1(M-1,J-1))-GR*ALFAV*CON6*
     2SIND(BETA)*(TEMP1(M,J)-TEMP1(M-2,J))+ALFAV/CON3*
     3(VORTY(M-1,J+1)+VORTY(M-1,J-1)-2.0*VORTY(M-1,J))
     4-(ALFAV*CON6)*(VELTY(M-1,J+1)*VORTY(M-1,J+1)-
     5VELTY(M-1,J-1)*VORTY(M-1,J-1))+(ALFAV/CON2-UELTY(M,J)
     6*ALFAV*CON5)*VORTY1(M,J)+ALFAV*GRC*CON6*COSD(BETA)*
     7(CONCEN1(M-1,J+1)-CONCEN1(M-1,J-1))-ALFAV*GRC*CON6*
     8SIND(BETA)*(CONCEN1(M,J)-CONCEN1(M-2,J))
C
      DO 1=3,M-2
      D(I)=CON1*VORTY(I,J)+GR*CON6*ALFAV*COSD(BETA)*
     1(TEMP1(I,J+1)-TEMP1(I,J-1))-GR*CON6*ALFAV*SIND(BETA)*
     2(TEMP1(I+1,J)-TEMP1(I-1,J))+ALFAV/CON3*(VORTY(I,J+1)
     3+VORTY(I,J-1)-2.0*VORTY(I,J))-ALFAV*CON6*(VELTY(I,J+1)
     4*VORTY(I,J+1)-VELTY(I,J-1)*VORTY(I,J-1))+ALFAV*
     5COSD(BETA)*GRC*CON6*(CONCEN1(I,J+1)-CONCEN1(I,J-1))-
     6GRC*ALFAV*CON6*SIND(BETA)*(CONCEN1(I+1,J)-
     7CONCEN1(I-1,J))
      END DO
C     MATRIX IS SPECIFIED
C
C     SOLVE FOR VORT(I,J) BY THOMAS ALGORITHM
      ALPHA(2)=B(2)
      DO I=3,M-1
      ALPHA(I)=B(I)-(A(I)*C(I-1))/ALPHA(I-1)
      END DO
      SEE(2)=D(2)
      DO I=3,M-1
      SEE(I)=D(I)+(A(I)*SEE(I-1))/ALPHA(I-1)
      END DO
      VORT(M-1,J)=SEE(M-1)/ALPHA(M-1)
      DO I=M-2,2,-1
      VORT(I,J)=(SEE(I)+C(I)*VORT(I+1,J))/ALPHA(I)
      END DO
   60 CONTINUE
      RETURN
      END
```

```
      SUBROUTINE SOLVE6A(CON1,UELTY,VELTY,TEMP1,VORTY1,
     1  CONCEN1)
C     THIS SUBROURINE SOLVES FOR VORTY(I,J,NT+1)
C     FOR I=2,M-1 & J=2,N-1
C     VORTY(I,J,k) IS REPRESENTED BY VORT(I,J)
      IMPLICIT REAL*8 (A-H,O-Z)
      INCLUDE 'DIMEN.FOR'
      DIMENSION UELTY(MD,ND),VELTY(MD,ND),TEMP1(MD,ND)
      DIMENSION VORTY1(MD,ND),CONCEN1(MD,ND)
      INCLUDE 'COMMON.FOR'
      DO J=2,N-1
      B(J)=CON1+2.0*ALFAV/CON3
      END DO
      DO 64 I=2,M-1
      DO J=3,N-1
      A(J)=(VELTY(I,J-1)*ALFAV*CON6)+ALFAV/CON3
      END DO
      DO J=2,N-2
      C(J)=ALFAV/CON3-(VELTY(I,J+1)*ALFAV*CON6)
      END DO
      D(2)=CON1*VORT(I,2)+GR*CON6*ALFAV*COSD(BETA)*(
     1TEMP1(I,3)-TEMP1(I,1))-GR*CON6*ALFAV*SIND(BETA)*
     2(TEMP1(I+1,2)-TEMP1(I-1,2))+ALFAV/CON2*(VORT(I+1,2)
     3+VORT(I-1,2)-2.0*VORT(I,2))-ALFAV*CON5*(UELTY(I+1,2)
     4*VORT(I+1,2)-UELTY(I-1,2)*VORT(I-1,2))+(VELTY(I,1)*
     5ALFAV*CON6+ALFAV/CON3)*VORTY1(I,1)+ALFAV*GRC*CON6*
     6COSD(BETA)*(CONCEN1(I,3)-CONCEN1(I,1))-GRC*ALFAV*
     7CON6*SIND(BETA)*(CONCEN1(I+1,2)-CONCEN1(I-1,2))
C
      D(N-1)=CON1*VORT(I,N-1)+ALFAV*GR*CON6*COSD(BETA)*
     1(TEMP1(I,N)-TEMP1(I,N-2))-GR*ALFAV*CON6*SIND(BETA)*
     2(TEMP1(I+1,N-1)-TEMP1(I-1,N-1))+ALFAV/CON2*
     3(VORT(I+1,N-1)+VORT(I-1,N-1)-2.0*VORT(I,N-1))-ALFAV
     4*CON5*(UELTY(I+1,N-1)*VORT(I+1,N-1)-UELTY(I-1,N-1)*
     5VORT(I-1,N-1))+(ALFAV/CON3-VELTY(I,N)*CON6*ALFAV)*
     6VORTY1(I,N)+GRC*CON6*ALFAV*COSD(BETA)*(CONCEN1(1,N)-
     7CONCEN1(I,N-2))-GRC*CON6*ALFAV*SIND(BETA)*
     8(CONCEN1(I+1,N-1)-CONCEN1(I-1,N-1))
C
      DO J=3,N-2
      D(J)=CON1*VORT(I,J)+GR*ALFAV*CON6*COSD(BETA)*
     1(TEMP1(I,J+1)-TEMP1(I,J-1))-GR*CON6*ALFAV*SIND(BETA)
     2*(TEMP1(I+1,J)-TEMP1(I-1,J))+ALFAV/CON2*(VORT(I+1,J)
     3+VORT(I-1,J)-2.0*VORT(I,J))-ALFAV*CON5*(UELTY(I+1,J)
     4*VORT(I+1,J)-UELTY(I-1,J)*VORT(I-1,J))+GRC*ALFAV*
     5CON6*COSD(BETA)*(CONCEN1(I,J+1)-CONCEN1(I,J-1))-
     6GRC*ALFAV*CON6*SIND(BETA)*(CONCEN1(I+1,J)-
     7CONCEN1(I-1,J))
      END DO
C     MATRIX IS SPECIFIED
C
C     SOLVE FOR VORTY1(I,J) BY THOMAS ALGORITHM :-
      ALPHA(2)=B(2)
      DO J=3,N-1
      ALPHA(J)=B(J)-(A(J)*C(J-1))/ALPHA(J-1)
      END DO
      SEE(2)=D(2)
      DO J=3,N-1
      SEE(J)=D(J)+(A(J)*SEE(J-1))/ALPHA(J-1)
      END DO
      VORTY1(I,N-1)=SEE(N-1)/ALPHA(N-1)
      DO J=N-2,2,-1
      VORTY1(I,J)=(SEE(J)+C(J)*VORTY1(I,J+1))/ALPHA(J)
      END DO
   64 CONTINUE
      RETURN
      END
```

```
      SUBROUTINE STEST7A(CON1,STRF,VORTY1)
C     THIS SUBROUTINE CALCULATES STRFI(I,J)
C     FOR I=2,M-1 & J=2,N-1
      IMPLICIT REAL*8 (A-H,O-Z)
      INCLUDE 'DIMEN.FOR'
      DIMENSION STRF(MD,ND),VORTY1(MD,ND)
      INCLUDE 'COMMON.FOR'
      DO I=2,M-1
      B(I)=CON1+(2.0*ALFAS)/CON2
      END DO
      DO I=3,M-1
      A(I)=ALFAS/CON2
      END DO
      DO I=2,M-2
      C(I)=ALFAS/CON2
      END DO
      DO 70 J=2,N-1
      DO I=2,M-1
      D(I)=(STRF(I,J)*CON1)+((ALFAS/CON3)*(STRF(I,J+1)+
     1 STRF(I,J-1)-2.0*STRF(I,J)))+(ALFAS*VORTY1(I,J))
      END DO
C
C     MATRIX IS SPECIFIED
      ALPHA(2)=B(2)
      DO I=3,M-1
      ALPHA(I)=B(I)-(A(I)*C(I-1))/ALPHA(I-1)
      END DO
      SEE(2)=D(2)
      DO I=3,M-1
      SEE(I)=D(I)+(A(I)*SEE(I-1))/ALPHA(I-1)
      END DO
      STRFI(M-1,J)=SEE(M-1)/ALPHA(M-1)
      DO I=M-2,2,-1
      STRFI(I,J)=(SEE(I)+C(I)*STRFI(I+1,J))/ALPHA(I)
      END DO
 70   CONTINUE
      RETURN
      END
```

```
      SUBROUTINE STEST7B(CON1,STRF1,VORTY1)
C     THIS SUBROUTINE SOLVES FOR STRF(I,J) FOR
C     I=2,M-1 & J=2,N-1
      IMPLICIT REAL*8 (A-H,O-Z)
      INCLUDE 'DIMEN.FOR'
      DIMENSION STRF1(MD,ND),VORTY1(MD,ND)
      INCLUDE 'COMMON.FOR'
      DO J=2,N-1
      B(J)=CON1+(2.0*ALFAS)/CON3
      END DO
      DO J=3,N-1
      A(J)=ALFAS/CON3
      END DO
      DO J=2,N-2
      C(J)=ALFAS/CON3
      END DO
      DO 72 I=2,M-1
      DO J=2,N-1
      D(J)=(CON1*STRFI(I,J))+((ALFAS/CON2)*(STRFI(I+1,J)
     1 +STRFI(I-1,J)-2.0*STRFI(I,J)))+(ALFAS*VORTY1(I,J))
      END DO
C     MATRIX IS SPECIFIED
C
C     NEXT SOLVE STRF(I,J) BY THOMAS ALGORITHM
      ALPHA(2)=B(2)
      DO J=3,N-1
      ALPHA(J)=B(J)-(A(J)*C(J-1))/ALPHA(J-1)
      END DO
      SEE(2)=D(2)
      DO J=3,N-1
      SEE(J)=D(J)+(A(J)*SEE(J-1))/ALPHA(J-1)
      END DO
      STRF1(I,N-1)=SEE(N-1)/ALPHA(N-1)
      DO J=N-2,2,-1
      STRF1(I,J)=(SEE(J)+C(J)*STRF1(I,J+1))/ALPHA(J)
      END DO
 72   CONTINUE
      RETURN
      END
```

```
      SUBROUTINE STEST8A(STRF1,UELTY1,VELTY1)
C     THIS SUBROUTINE CALCULATES UELTY(I,J) & VELTY(I,J)
C     FOR I=2,M-1 & J=2,N-1
      IMPLICIT REAL*8 (A-H,O-Z)
      INCLUDE 'DIMEN.FOR'
      DIMENSION STRF1(MD,ND),UELTY1(MD,ND),VELTY1(MD,ND)
      INCLUDE 'COMMON.FOR'
C
C     UELTY =(X-COMPONENT VELOCITY)
      DO 80 I=2,M-1
      DO 82 J=2,N-1
      UELTY1(I,J)=(STRF1(I,J+1)-STRF1(I,J-1))*CON6
   82 CONTINUE
   80 CONTINUE
C
C     VELTY =(Y-DIRECTION)
      DO 84 J=2,N-1
      DO 86 I=2,M-1
      VELTY1(I,J)=(STRF1(I-1,J)-STRF1(I+1,J))*CON5
   86 CONTINUE
   84 CONTINUE
      RETURN
      END
```

```
      SUBROUTINE WTEST1A(TEMP2,STRF2,VORTY2,UELTY2,VELTY2,
     1  CONCEN2)
C
C     SUBPROGRAM TO OUTPUT THE RESULTS OF NUMERICAL
C     CALCULATION
C
C     DIMENSION STATEMENTS ARE READ FROM FILE 'DIMEN.FOR'
      IMPLICIT REAL*8 (A-H,O-Z)
      INCLUDE 'DIMEN.FOR'
      DIMENSION TEMP2(MD,ND),STRF2(MD,ND),VORTY2(MD,ND)
      DIMENSION UELTY2(MD,ND),VELTY2(MD,ND)
      DIMENSION CONCEN2(MD,ND)
C     COMMON STATEMENTS ARE READ FROM FILE 'COMMON.FOR'
      INCLUDE 'COMMON.FOR'
      TIME=NOIT*DELT
      DO I=1,M
      X(I)=I*DELX-DELX
      END DO
      DO J=1,N
      Y(J)=J*DELY-DELY
      END DO
      LE=(M+1)/2
      LEE=(N+1)/2
C
C
      IF (CON10.EQ.1.0) GOTO 3005
C
C  AN EXAMPLE OF PRINTING THE TEMPERATURE FIELD :-
C
      OPEN(UNIT=4,FILE='TEMP.DAT',STATUS='NEW')
      WRITE(4,400)S,DELT,EO,EI
      WRITE(4,350)DELX,DELY,GR,PR
      WRITE(4,355)M,N,SC,GRC,BETA
      WRITE(4,352)ALFAT,ALFAC,ALFAV,ALFAS
      WRITE(4,1530) NOIT,NOITT,NOITI,TIME
      DO I=1,M
      WRITE(4,1550)(TEMP2(I,J),J=1,N)
      END DO
      CLOSE(UNIT=4,STATUS='SAVE')
C
      .
      .
      .
  PRINT OTHER FIELD VARIABLES IF DESIRED
      .
      .
      .
      .
      .
C
C  AN EXAMPLE OF PRINTING THE X-COMPONENT VELOCITY :-
C
      OPEN(UNIT=2,FILE='UELM.DAT',STATUS='NEW')
      WRITE(2,400)S,DELT,EO,EI
      WRITE(2,350)DELX,DELY,GR,PR
      WRITE(2,355)M,N,SC,GRC,BETA
      WRITE(2,352)ALFAT,ALFAC,ALFAV,ALFAS
      WRITE(2,1530) NOIT,NOITT,NOITI,TIME
      DO J=1,N
      WRITE(2,1560)Y(J),UELTY2(LE,J)
      END DO
      CLOSE(UNIT=2,STATUS='SAVE')
C
```

```
C
C     PRINTING SHERWOOD & NUSSELT NUMBERS :-
C
 3005    OPEN(UNIT=24,FILE='SHWOD.DAT',STATUS='NEW')
         WRITE(24,400)S,DELT,EO,EI
         WRITE(24,350)DELX,DELY,GR,PR
         WRITE(24,355)M,N,SC,GRC,BETA
         WRITE(24,352)ALFAT,ALFAC,ALFAV,ALFAS
         WRITE(24,1530) NOIT,NOITT,NOITI,TIME
         DO I=1,M
         WRITE(24,1560)X(I),GRDC(I,1),GRDC(I,2)
         END DO
         WRITE(24,1670)SH(1)
         WRITE(24,1672)SH(2)
         CLOSE(UNIT=24,STATUS='SAVE')
C
         OPEN(UNIT=22,FILE='NUSET.DAT',STATUS='NEW')
         WRITE(22,400)S,DELT,EO,EI
         WRITE(22,350)DELX,DELY,GR,PR
         WRITE(22,355)M,N,SC,GRC,BETA
         WRITE(22,352)ALFAT,ALFAC,ALFAV,ALFAS
         WRITE(22,1530) NOIT,NOITT,NOITI,TIME
         DO I=1,M
         WRITE(22,1560)X(I),GRDT(I,1),GRDT(I,2)
         END DO
         WRITE(22,1660)HNU(1)
         WRITE(22,1662)HNU(2)
         CLOSE(UNIT=22,STATUS='SAVE')
C
C
400      FORMAT(2X,'S='F4.2,4X,'DELT='F6.4,4X,'EO='F8.6,4X,
     1   'EI='F7.2)
 352     FORMAT(1X,'ALFAT='F7.4,5X,'ALFAC='F7.4,5X,'ALFAV='
     1   F7.4,5X,'ALFAS='F7.4)
 350     FORMAT(2X,'DELX='F8.5,4X,'DELY='F8.5.5X,'GR='F9.1,
     1   4X,'PR='F7.3)
 355     FORMAT(2X,'M='I3,4X,'N='I3,4X,'SC='F7.3,4X,'GRC='
     1   F9.1,4X,'BETA='F5.1)

 305     FORMAT(70X)
 310     FORMAT(10X,G20.8,10X,G20.8)
 320     FORMAT(10X,I4,26X,I4)
 330     FORMAT(10X,I5,25X,I4)
C
C
 1530    FORMAT(10X,'NOIT='I4,5X,'NOITT='I4,5X,'NOITI='I4,
     1   5X,'TIME='F6.3)
 1540    FORMAT(10X,'NOIT='I4,5X,'NOITT='I4,5X,'NOITI='I4,
     1   5X,'TIME='F6.3)
 1550    FORMAT(:,11(1X,6(E20.13)/))
 1660    FORMAT(5X,'THE AVERAGE NUSSELT NUMBER ALONG COLD
     1   WALL='.F5.2)
 1662    FORMAT(5X,'THE AVERAGE NUSSELT NUMBER ALONG HOT
     1   WALL='.F5.2)
 1670    FORMAT(5X,'THE AVERAGE SHERWOOD NUMBER ALONG COLD
     1   WALL='.F5.2)
 1672    FORMAT(5X,'THE AVERAGE SHERWOOD NUMBER ALONG HOT
     1   WALL='.F5.2)
 1560    FORMAT(F12.6,F12.6,F12.6)
 1667    RETURN
         END
```

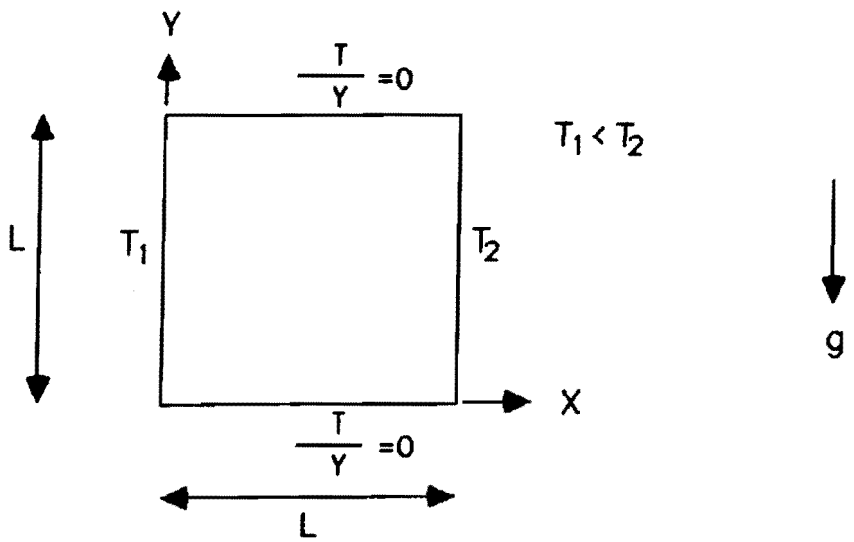

Fig. A10.1 Nomenclature for The Square Cavity Test Case.

APPENDIX 10

VALIDIFICATION OF THE NUMERICAL METHODS.

The results of the numerical calculations for a cavity of aspect ratio of 7.0 had already been shown in Chapter 7 to agree well with the experimental values from the literature and from this work. In this Appendix, the validity of the computer codes used to generate those solutions is justified by comparing their outputs with known numerical results documented in the literature. In addition a comparison between the various numerical methods proposed in Chapter 3 will also be presented to test the usefulness of the proposed "Hybrid" method.

A10.1 COMPARISON OF NUMERICAL RESULTS FROM THIS WORK WITH THE "BENCHMARK" SOLUTION OF DE VAHL DAVIS [158].

The test conditions used were those of a square cavity with its opposite vertical walls at different but uniform temperature. The horizontal walls were adiabatic and all four walls were non-slip and impermeable to the bulk flow. The fluid in the cavity had a Prandtl number of 0.7, and two-dimensionional analysis with the usual Boussinesq approximation was adopted. The coordinates system and other relevant features for these test conditions are presented in Fig. A10.1. This cavity configuration was recently being used as a test case for a comparative exercise whereby many authors submitted their computational results which were then compared in a paper by de Vahl Davis and Jones [158]. Thus the "reference" solution is well documented and can be confidently regarded as "correct".

The parameters used in the calculations were for Rayleigh numbers of $1x10^4$ and $1x10^6$. The condition of Ra = $1x10^4$ constituted an "easy" condition whereby a reliable method should give a correct result and comparison with the reference solution should be good. The condition of Ra = $1x10^6$ constituted a "difficult" condition to

compute because of the considerable resultant flow in the cavity and this was also the highest Rayleigh number used in the comparative exercise proposed by de Vahl Davis and Jones[158] mentioned earlier. As noted by them, it was the condition with the greatest potential for errors to occur. Thus if comparison was good for the condition of Ra= $1x10^6$, it will be expected to be good for the lower Rayleigh range. The number of grid points used for the computations in Tables A10.1 and A10.2 were 41 x 41 points.

Tables A10.1 and A10.2 list the results of the comparison. The nomenclature used are defined as follows :-

$|\varphi|_{mid}$ = stream function at the middle of the cavity.

U_{max} = the maximum vertical velocity on the horizontal
Y mid-plane and its location at Y.

V_{max} = the maximum horizontal velocity on the vertical
X mid-plane and its location at X.

Nu_o = average Nusselt number on the hot wall

Nu_{max} = the maximum local Nusselt number on the hot wall
X and its location at X.

Nu_{min} = the minimum local Nusselt number on the hot wall
X and its location at X.

FT = False-Transient Method.

DADI = Dynamic Alternating Direction Implicit Method.

S = Boundary vorticity smoothing factor

For the definition of other symbols, see the nomenclature.

From Table A10.1, the "gentle" condition of Ra= $1x10^4$ results in good agreement between the numerical results from either the "FT" or "DADI" methods and the reference solution with discprepancy generally within 3 percent. The agreement for the Hybrid method is good for all the quantities for the condition S= 1.0 but for S=0.3, the agreement is only good for the Nusselt numbers, but poor for the velocity components and the stream function. The value of "S" did not affect the results of either the "FT" ot the "DADI" methods.

Table A10.1 Comparison Between the Numerical Results from This Work for Ra= 1×10^4 and the "Benchmark" Solution of de Vahl Davis and Jones[158] (a_T=3.0, a_φ=3.0, a_ζ=0.5, M=41, N=21 for all columns).

Quantity	de Vahl Davis	FT	DADI	Hybrid	Hybrid
S	1.0	1.0	1.0	0.3	1.0
$\lvert\varphi\rvert_{mid}$*	5.071	5.10	5.07	6.70	4.78
V_{max}*	16.18	16.5	16.1	20.5	16.0
X	0.823	0.82	0.82	0.88	0.87
U_{max}*	19.62	18.8	18.4	24.0	18.0
Y	0.119	0.12	0.14	0.11	0.12
Nu_o	2.238	2.24	2.24	2.55	2.20
Nu_{max}	3.528	3.58	3.57	4.18	3.56
X	0.143	0.15	0.15	0.15	0.276
Nu_{min}	0.586	0.61	0.61	0.61	0.61
X	1.0	1.0	1.0	1.0	1.0

*Note:

As the scaling factor for the stream function and velocity used by de Vahl Davis and Jones[158] was different from that of this work , a comparison can only be made if the results from this work were to multiply by the correction factor υ/α where α =thermal diffusivity and υ = kinematic viscosity. The parameter "α" was used by de Vahl Davis and Jones[158] used the scaling factor while "υ" was used in this work. The values of α and υ at 300 K for dry air was used and the correction factor is 0.7076. This correction procedure was done before the results from this work were presented in Tables A10.1 and A10.2.

Table A10.2 Comparison Between the Numerical Results from This Work for Ra= $1x10^6$ and the "Benchmark" Solution of de Vahl Davis and Jones[158] (a_T = 1.0, a_φ = 1.0, a_ζ = 0.005 Or 0.002).

Quantity	de Vahl Davis	FT	DADI	Hybrid	Hybrid
M	61 or 81	41	41	41	61
N	61 or 81	41	41	41	61
$\lvert\varphi\rvert_{mid}$*	16.32	19.35	17.07	73.96	27.84
V_{max}*	64.63	76.35	65.04	258.8	115.9
X	0.850	0.88	0.86	0.925	0.10
U_{max}*	219.36	216.5	203.8	335.0	283.0
Y	0.038	0.04	0.04	0.05	0.97
Nu_o	8.817	9.24	9.27	9.70	8.29
Nu_{max}	17.925	17.3	18.1	19.0	16.0
X	0.0378	0.06	0.06	0.10	0.03
Nu_{min}	0.989	1.05	1.00	1.00	1.41
X	1.0	0.99	0.99	0.98	1.0
CPU	-	7:59:41	1:51:32	1:57:45	4:13:49

* see footnote of Table A10.1

From Table A10.2, the results from the "FT" and "DADI" methods can be said to agree reasonably well with the "benchmark" solution considering the fact that the "benchmark" solution was calculated with much denser grids of 61x61 and 81x81 points whereas the results from this work were calculated from 41x41 grid. Between the "FT" and "DADI" methods, the greatest discrepancy Of 18

percent occured for the horizontal velocity component for the "FT" method but agreement for the Nusselt numbers for both methods was good and discrepancy was less that 5 percent. The Hybrid method is shown to produce erroneous results especially with regard to the stream function and the velocity components where a discrepancy as high as 300 percent for V_{max} exists for the M=41 and N=41 case. Increasing the grid-points to 61x61 did reduce the discrepancy but the results are still further away from the benchmark solution then either the "FT" or the "DADI" methods calculated with only 41x41 points. Note that the deviation from the benchmark solution is the greatest for the stream function and the velocity components values and comparatively less for the Nusselt numbers. Both the "DADI" and the "Hybrid" methods are about four times faster than the "FT" method in reaching the steady-state solution.

For both set of test conditions, the results from the Hybrid method were seen to deviate considerably from the benchmark solution except for certain condition where the right combination of the input parameters did produce a "correct" solution. However there was no rule as to how to obtain the "correct combination" of the input parameters consistently and almost invariably the "incorrect" results listed in Tables A10.1 and A10.2 were typical of the results produced by the Hybrid methods for other range of test conditions. It would be too cumbersome to list all the test values but an indication of this fact can be gained by comparing only the average Nusselt numbers obtained from some of the tests presented in Table A10.3. As the average Nusselt number is a poor indication of the "accuracy" of a method as seen from the results of Tables A10.1 and A10.2, a poor agreement for this quantity means that agreement for the other quantities are going to be worse.

Table A10.3 Comparison of Average Nusselt Number for a square cavity at Ra= $1x10^4$ using the Hybrid method.

Benchmark Solution	Hybrid Method	S	a_T	a_ζ	a_φ
2.24	2.56	0.3	3.0	0.5	3.0
2.24	2.82	0.3	0.5	0.5	0.5
2.24	2.11	0.3	10	0.1	10
2.24	2.28	0.3	8.0	0.125	8.0
2.24	2.20	1.0	3.0	0.5	3.0
2.24	3.07	1.0	0.5	0.5	0.5
2.24	1.40	1.0	10	0.1	10
2.24	1.91	1.0	8.0	0.125	8.0
2.24	1.88	1.0	5.0	0.20	5.0

The values of the Nusselt number in Table A10.3 compare poorly with the benchmark values except for the two underlined values. The Nusselt numbers are also seen to vary with the "false-transient" factors "a" (Chapter 3) which is an unfavourable feature as the false-transient factors were only intended to speed up the rate of convergence to the steady state values and not supposed to affect the uniqueness of the steady state solutions (which is known to exist in this case). The value of the boundary vorticity smoothing parameter "S" is also seen to affect the steady-state solutions.

Figs A10.2 and A10.3 compare the stream function and temperature fields calculated from the "DADI" and the "Hybrid" methods respectively for the 41x41 grid-points condition. The stream function and temperature fields obtained from the "FT" method was similar to that of Fig. A10.2 and would not be repeated here. Fig. A10.2 is thought to be correct as it compares favourably with the results in the literature [26,112] whereas Fig. A10.3 showed erroneous results for both the fields. Fig. A10.4 is the fields for the 61x61 grid-points condition calculated by the

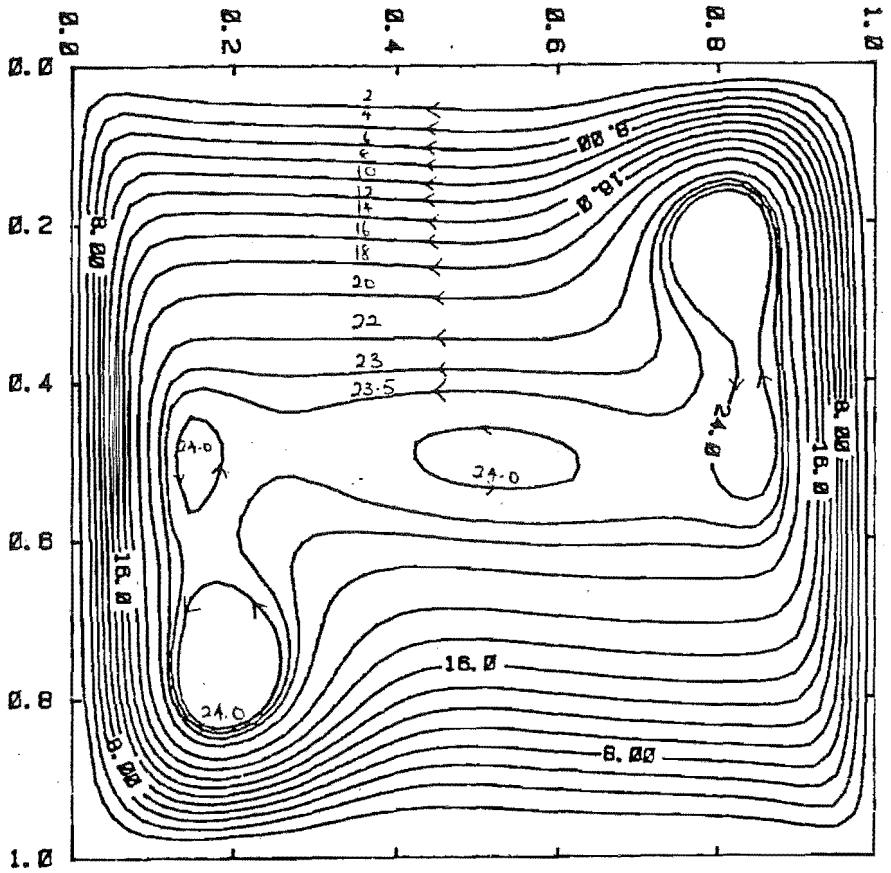

(a) Streamlines

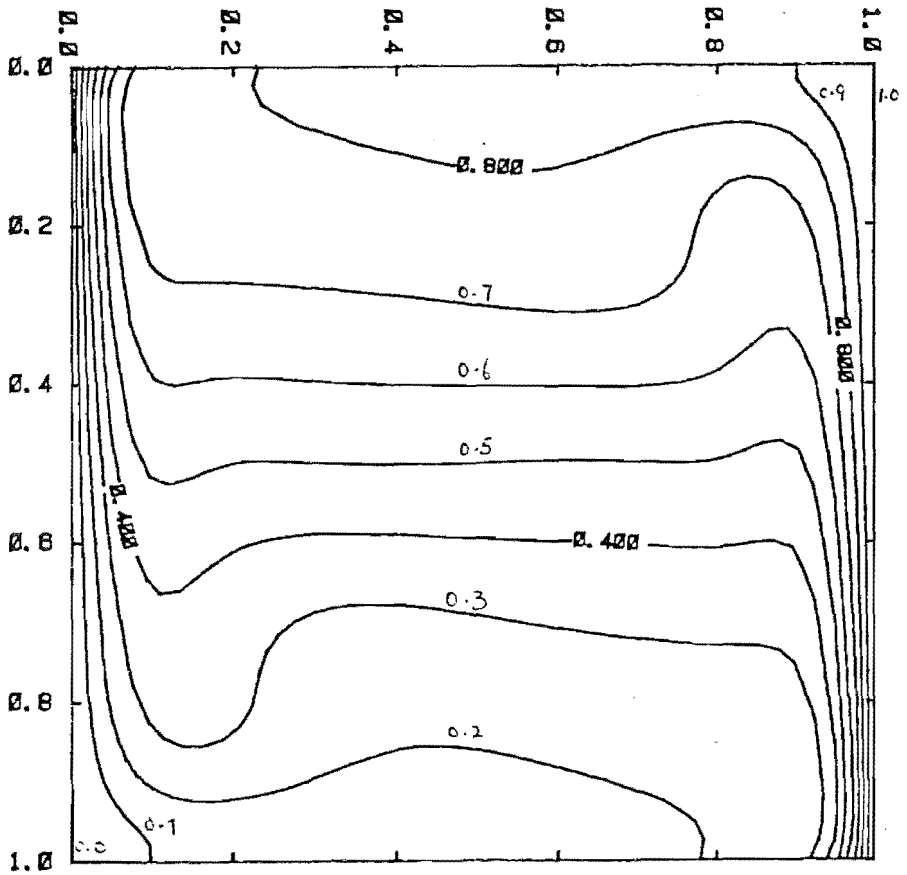

(b) Temperature

Fig. A10.2: DADI $Ra_T = 1 \times 10^6$, M = 41, N = 41.

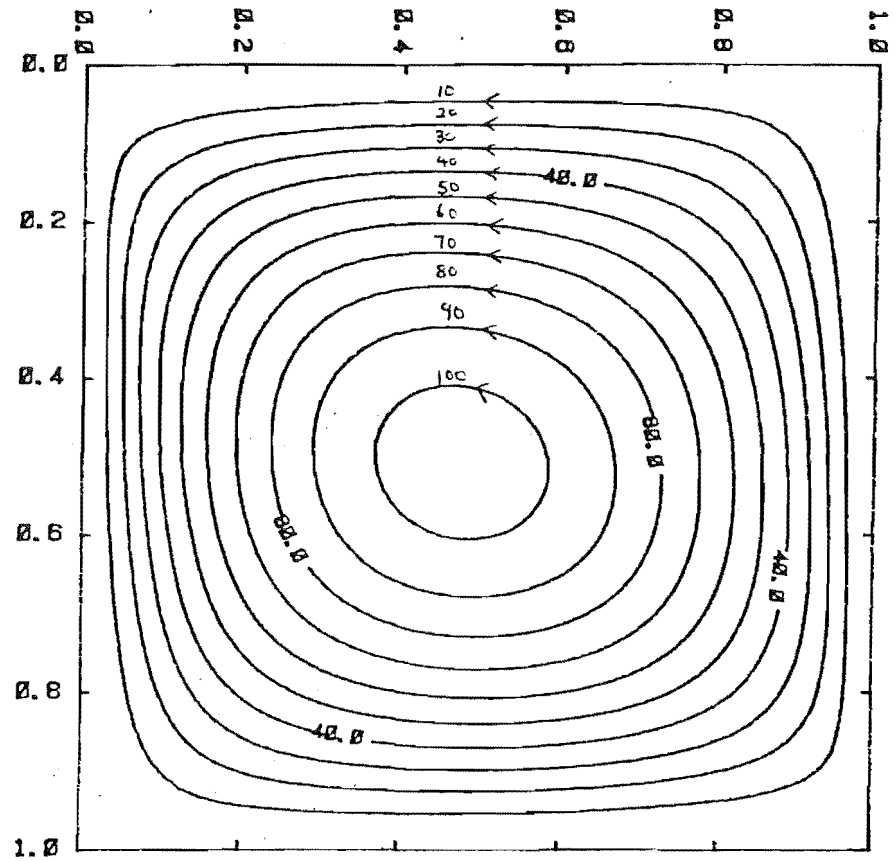

(a) Streamlines

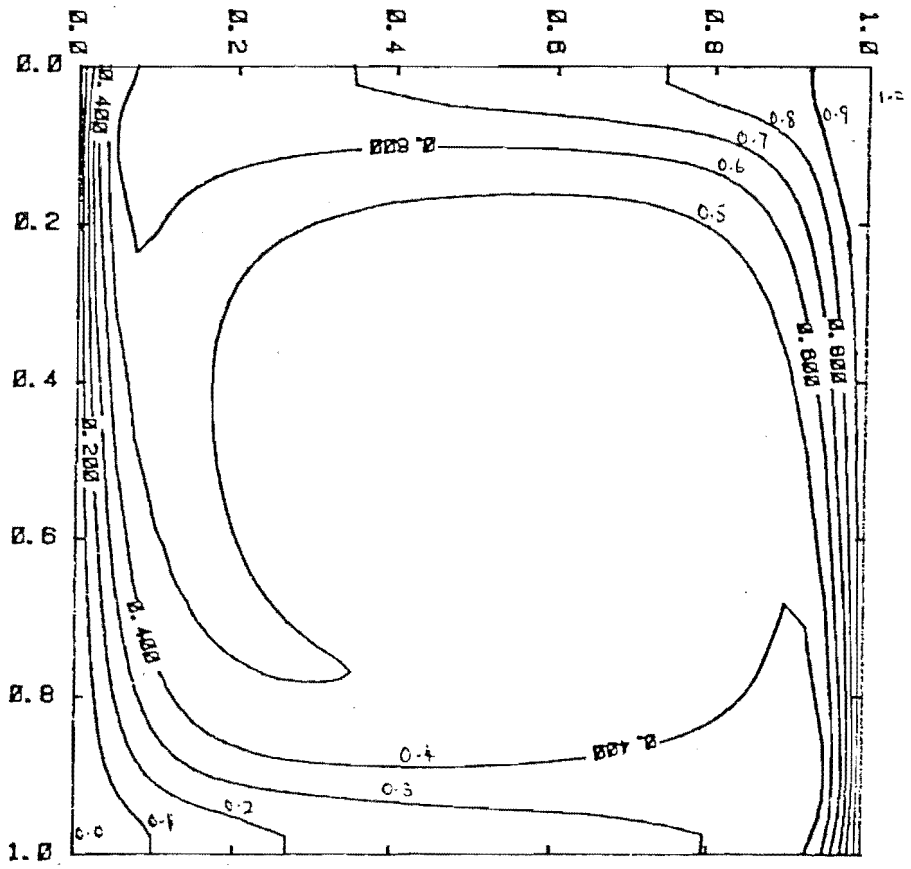

(b) Temperature

Fig. A10.3: Hybrid method $Ra_T = 1 \times 10^6$, M = 41, N = 41.

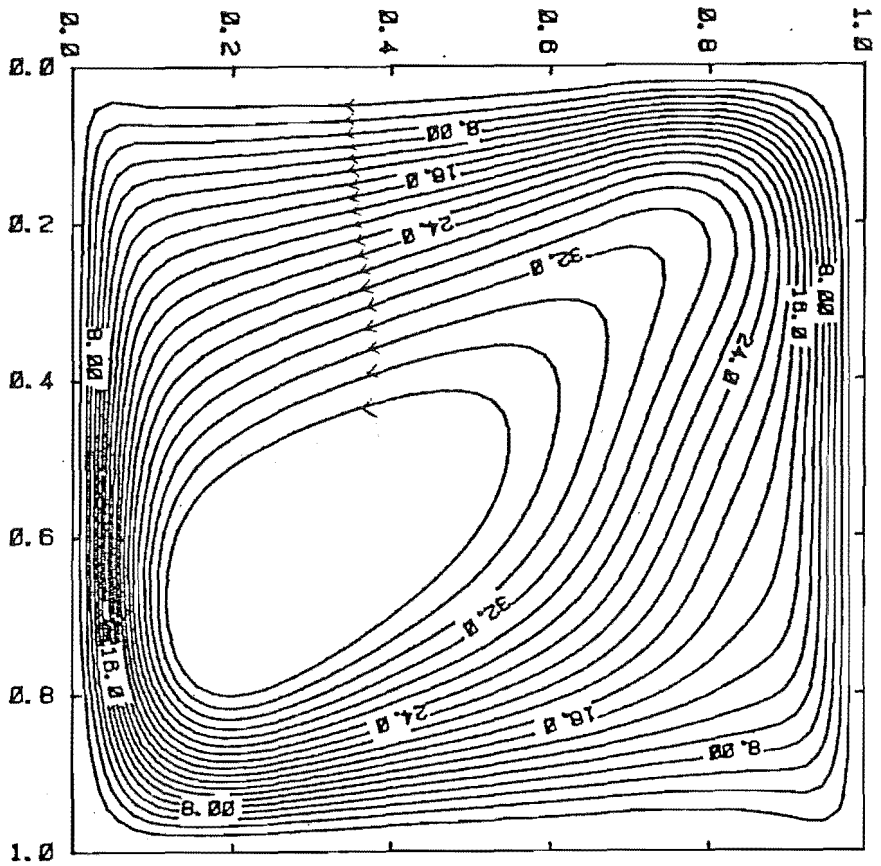

(a) Streamlines

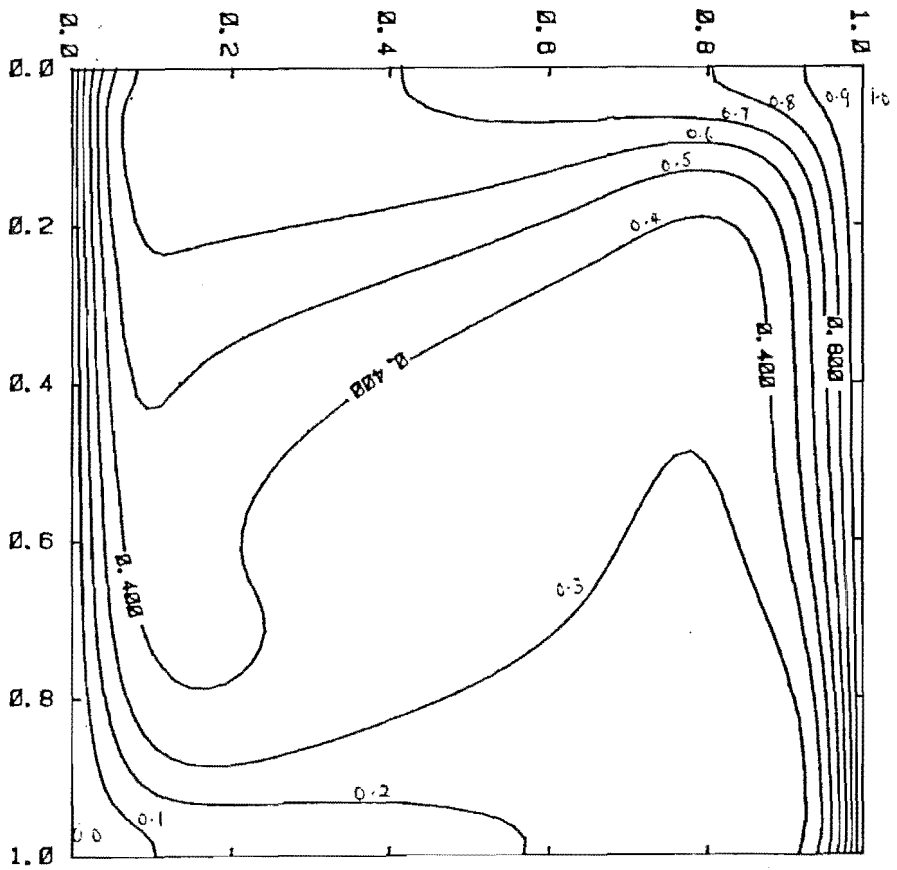

(b) Temperature

Fig. A10.4: Hybrid method, $Ra_T = 1 \times 10^6$, M = 61, N = 61.

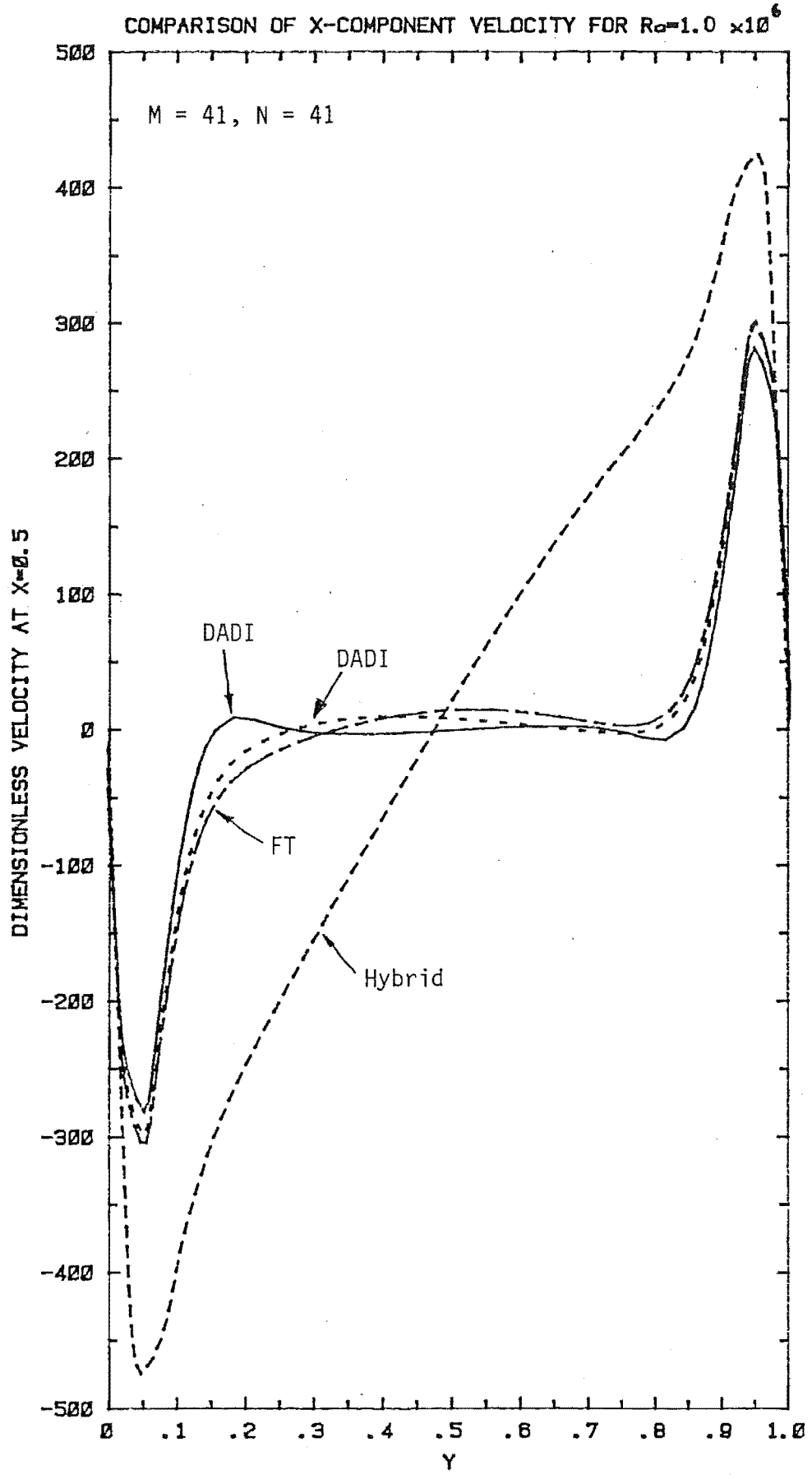
COMPARISON OF X-COMPONENT VELOCITY FOR Re=1.0 x10^6
M = 41, N = 41
DIMENSIONLESS VELOCITY AT X=0.5
Y
500
400
300
200
100
0
-100
-200
-300
-400
-500
0
.1
.2
.3
.4
.5
.6
.7
.8
.9
1.0
DADI
DADI
FT
Hybrid

Fig. A10.5

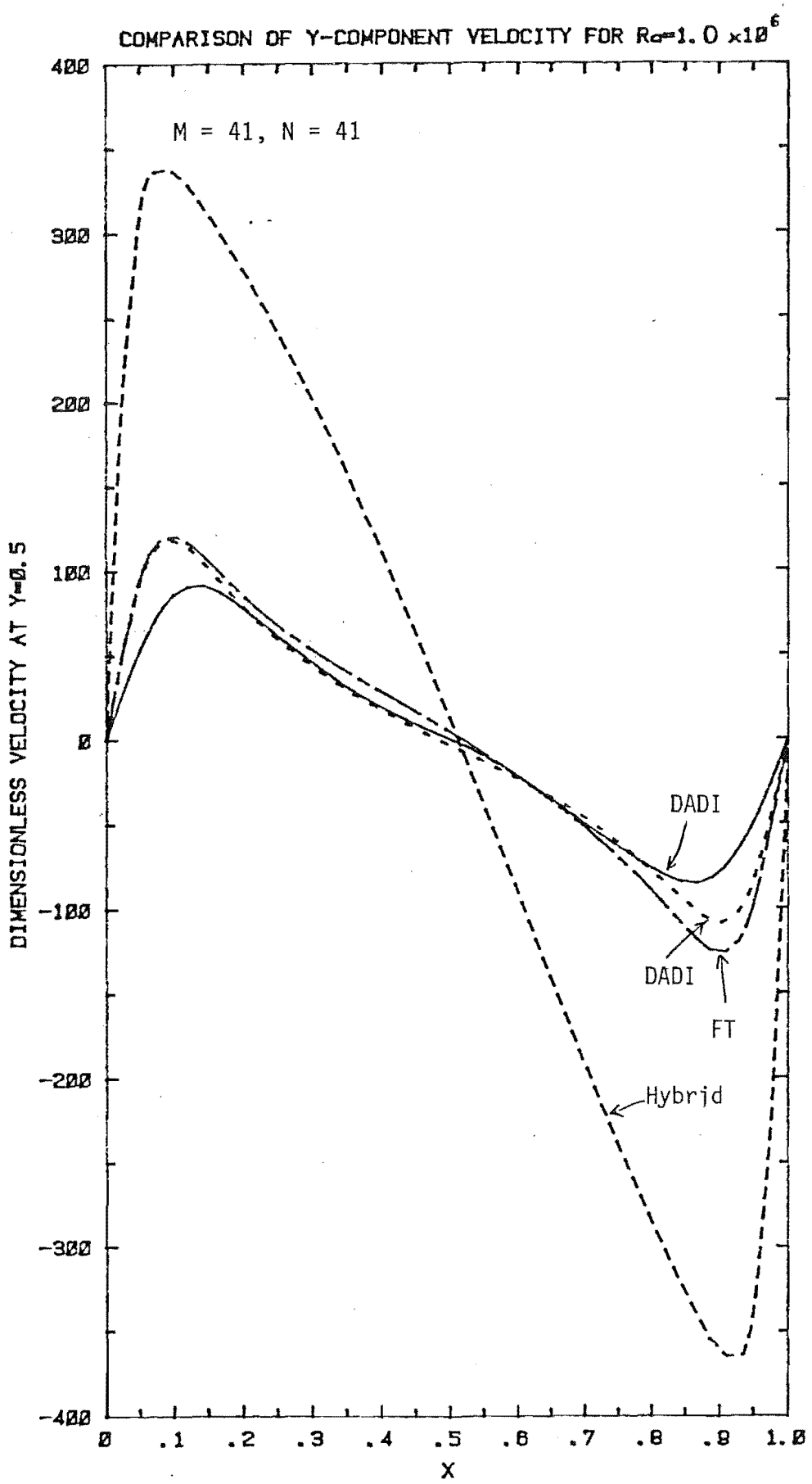
COMPARISON OF Y-COMPONENT VELOCITY FOR Re=1.0 x10^6
M = 41, N = 41
DIMENSIONLESS VELOCITY AT Y=0.5
X
400
300
200
100
0
-100
-200
-300
-400
0
.1
.2
.3
.4
.5
.6
.7
.8
.9
1.0
DADI
DADI
FT
Hybrid

Fig. A10.6

Hybrid method. The stream function and the temperature fields is still very much different from the benchmark solution in Fig. A10.2. Thus increasing the grid-points for the Hybrid method did not appear to increase the accuracy of its solution.

Figs. A10.5 and A10.6 compare the vertical and horizontal velocity components respectively. Again the results from the hybrid method is shown to be very different from that of the "FT" or the "DADI" methods. Also shown in Figs. A10.5 and A10.6 are the results of another calculation run using the "DADI" method for the same Ra but different false-transient factors values. The velocity components ,which had been shown before in Tables A10.1 and A10.2 to be a very sensitive measure as to the "accuracy" of a numerical method, are seen to agree closely for the two "DADI" runs. This shows that the false-transient factors do not have to affect the final steady state value as for the case of the Hybrid method.

A10.2 COMPARISON BETWEEN THE THREE NUMERICAL METHODS FOR A CAVITY OF ASPECT RATIO 7.0.

Table A10.4 presents the results of the various numerical calculations that had been carried out to further test the validity of the "Hybrid" method. The calculations had all been carried out for a cavity of aspect ratio 7.0 and Prandtl number of 0.7 with heat transfer across the cavity. Only the average Nusselt number from each calculation was presented and has been noted before; if the degree of accuracy for the Nusselt numbers is poor, then the degree of accuracy for the rest of the quantities is going to be worse. The symbols used in Table A10.4 had been defined in nomenclature.

For comparison with the values of Table A10.4, the Nusselt numbers calculated from the methods of "FT" or "DADI" and the experimental correlation of Elsherbiny [115] are listed in Table A10.5.

Table 10.4 Comparison Between the Average Nusselt Numbers from the Hybrid Method Using Various Parametric Values for a Cavity of Aspect Ratio 7.0.

Ra	M	N	Δt	S	a_T	a_φ	a_ζ	Nu
$1x10^4$	41	21	0.002	1.0	5.0	5.0	0.2	1.40
$1x10^4$	41	21	0.002	1.0	3.0	3.0	0.5	1.73
$1x10^4$	41	21	0.002	1.0	8.0	8.0	0.125	1.27
$1x10^4$	41	21	0.002	0.3	3.0	3.0	0.5	1.22
$1x10^4$	41	21	0.008	1.0	3.0	3.0	0.5	1.08
$1x10^4$	41	21	0.0002	0.3	8.0	8.0	0.125	1.49
$1x10^4$	36	11	0.008	1.0	3.0	3.0	0.5	2.33
$1x10^4$	57	17	0.003	0.3	1.0	1.0	1.0	1.46
$1x10^4$	71	21	0.002	0.3	8.0	8.0	0.125	1.25
$1x10^4$	71	11	0.008	0.3	1.0	1.0	1.0	1.96
$1x10^4$	101	21	0.002	1.0	8.0	8.0	0.125	1.27
$1x10^4$	101	21	0.004	1.0	8.0	8.0	0.125	1.40
$1x10^4$	113	17	0.0001	0.3	2.0	2.0	0.5	2.94
$2x10^5$	41	21	0.001	0.3	3.0	3.0	0.50	3.9
$2x10^5$	113	33	0.0001	0.3	2.0	2.0	0.50	6.00
$4x10^5$	41	21	0.001	0.3	3.0	3.0	0.50	4.60
$6x10^5$	41	21	0.001	0.3	2.0	2.0	0.50	4.90
$6x10^5$	81	21	0.001	0.3	2.0	2.0	0.50	5.76
$6x10^5$	81	41	0.001	0.3	2.0	2.0	0.50	4.80

Table A10.5 Numerical Results from "DADI" or "FT" Methods and the Experimental Correlation of ElSherbiny [115].

Ra	DADI or FT*	ElSherbiny [115]
$1x10^4$	1.79	1.75
$2x10^5$	3.80	3.94
$4x10^5$	4.56	4.76
$6x10^5$	5.15	5.32

*Notes :- Disregard the values of M, N, a_T, a_φ, and a_ζ; the Nusselt numbers calculated by the DADI or the FT methods were always the same as long as M and N were sufficiently large to resolve the fields.

From Table 10.5, the results from either the "DADI" or the "FT" methods are observed to agree closely with the experimental correlation of ElSherbiny [115]. As for the square cavity case, the results from the Hybrid method vary with the number of grid-points used (as expected), the boundary vorticity smoothing parameter, and the false transient factors. The last two factors should not have affected the steady-state solutions. Only at certain combination of the input parameters, the Nusselt numbers (underlined) are seen to agree with the correlation values of ElSherbiny [115].

From the results presented in this Appendix, it was decided that the proposed Hybrid method has some unexplained errors in the method and it was consequently judged unsuitable to be used as a model. All numerical predictions in this work were therefore done by either the "FT" or the "DADI" methods.

ERRATA

1. In Table of Contents, "REFENRENCES" should be "REFERENCES".
2. Page 4, paragraph 1, line 1. "Quantiitative.." should be "Quantitative..".
3. Page 5, under the section of "Definition:" :-
   line 2. "..edges AD and BC.." should read "..edges AB and CD.."
   line 3. "..edges AB and DC.." should read "..edges AC and BD.."
   line 5. "..$\partial T/\partial z = 0$ and $\partial P/\partial z = 0$ at z=0 and z=H.." should read "..$\partial T/\partial y = 0$ and $\partial P/\partial y = 0$ at x=0 and x=H.."
   line 7. "z=0 and z=H" should read "x=0 and x=H".
4. Page 6, under the section of "Definition:", line 2. "..edges DA and CD.." should read "..edges AB and CD..".
5. Page 7, under subsection (iii), all the "AD" should be replaced by "AB".
6. Page 9, Section 2.1.1 should read "2.1.1 Flow Patterns in Vertical Cavities".
7. Page 10, paragraph 2, line 1. "..finte.." should be "..finite..".
8. Page 11, line 3. "..obtained critical Grashof.." should read "..obtained a critical Grashof..".
9. Page 11, paragraph 2, line 3. "Fig.3.3" should be "Fig.2.3".
10. Page 12, paragraph 1, line 7. "..cells.." should be "..cell..".
11. Page 13, paragraph 1, line 4. "..form.." should be "..forms..".
12. Page 13, paragraph 3, line 5. "..both side of.." should read "..both sides of..".
13. Page 14, line 3. "..conditiion.." should be "..condition..".
14. Page 14, paragraph 3, line 3. "..compulations.." should be "..computations..".
15. Page 14, paragraph 4, line 4. "..affect.." should be "..affected..".
16. Page 15, paragraph 3, line 1. "..numerical solution of.." should read "..the numerical solutions of..".
17. Page 15, paragraph 3, line 2. "..multicellar.." should be "..multicellular..".
18. Page 15, paragraph 3, line 5. "..depended.." should be "..dependent..".
19. Page 16, Section 2.1.2. should read "2.1.2. Flow Patterns in Horizontal Cavities".
20. Page 16, last line. "..The convective air is being able to escape.." should read "..The convective air is able to escape..".
21. Page 17, Section 2.1.2.2.1, line 2. "..layers.." should be "..layer..".
22. Page 18, line 16. "..occurance.." should be "..occurrence..".
23. Page 18, Section 2.1.2.3, paragraph 2, line 3. "..prefered.." should be "..preferred..".

Wee, H K. Heat and mass transfer in confined spaces (Thesis)?.
-Errata.

24. Page 21, paragraph 2, line 10. "..perpendicular to channel.." should read "..perpendicular to the channel..".
25. Page 22, line 3 and line 10, "degree" should be "degrees".
26. Page 22, line 6. "..pattern.." should be "..patterns..".
27. Page 23, Section 2.2.1.1, line 9 . "..resulted from.." should read "..that resulted from..".
28. Page 24, paragraph 1, line 3. "Fig.8" should be "Fig. 2.8".
29. Page 24, paragraph 2, line 2. "..these.." should be "..the..".
30. Page 24, paragraph 2, line 5. "..Much stronger flows in than the.." should read "..Much stronger flows than in the..".
31. Page 24, Fig. 2.8. The vertical-axis label should read "Temperature difference" and not "Dimensionless Temperature" as indicated. Also delete the letter "I" from Fig. 2.8(b).
32. Page 25, paragraph 2, line 1. "First elaborate experiments.." should read "The first elaborate experiments..".
33. Page 26, paragraph 3, line 2. ".. a air-filled cavity.." should be "..an air-filled cavity..".
34. Page 26, paragraph 3, line 14. "..correction.." should be "..convection ..".
35. Page 27, paragraph 2, line 4. "Aspect ratio.." should read "The aspect ratio..".
36. Page 27, paragraph 3, line 8. "..temperature.." should be "..temperatures..".
37. Page 27, paragraph 3, line 10. "..difference.." should be "..differences..".
38. Page 28, 7th line from the bottom. ".. eperimental.." should be "..experimental..".
39. Page 30, paragraph 1, line 5. "..near lower(hotter) surface.." should read "..near the lower(hotter) surface..".
40. Page 30, paragraph 3, line 4. "..inverse-disrance.." should be "..inverse-distance..".
41. Page 31, paragraph 5, line 3. "..publication.." should be "..publications..".
42. Page 34, "2.3 Mass Transfer in Cavity" should read "2.3 Mass Transfer in Cavities".
43. Page 34, paragraph 1, line 4. "..occurance.." should be ".. occurrence..".
44. Page 34, paragraph 1, line 8. "..processess.." should be "..processes..".

45. Page 34, paragraph 1, line 9. "..such method.." should read "..such a method..".
46. Page 35, paragraph 1, line 1. "..Trethowin.." should be "..Trethowen..".
47. Page 35, paragraph 1, line 12. "..on the cavity.." should read "..in the cavity..".
48. Page 35, paragraph 1, line 16. "..through wall.." should read "..through the wall..".
49. Page 36, Section 2.4, paragraph 2, line 3. "..un-saturated.." should be "..unsaturated..".
50. Page 37, paragraph 2, the first sentence should read "Using a Mach-Zehnder interferometer, Adams and McFaddin(76) performed an experimental study on heat and mass transfer of p-dichlorobenzene sublimating from a heated vertical surface into air.".
51. Page 37, paragraph 2, line 7. "..omited.." should be "..omitted..".
52. Page 37, paragraph 2, line 13. "..were good.." should be ".. was good..".
53. Page 38, sixth line from the bottom, "chemical" means "mass".
54. Page 39, second line from the bottom, "..resulrs were summarised .." should read "..results are summarised..".

54a. Page 46, para. 2, line 6. "..did not being.." should read "..was not.."

55. Page 47, paragraph 1, line 8. "..are mainly concerned.." should read "..is mainly concerned..".
56. Page 47, paragraph 2, line 2. "..a air-water mixture.." should read "..an air-water mixture..".
57. Page 48, line 5. "..had been.." should read "..has been..".
58. Page 48, line 6. "..has also been.." should read "..have also been..".
59. Page 48, Section 2.6, line 4. "..ondensation.." should be "..condensation..".
60. Page 48, Section 2.6, line 9. "..transfer heat and moisture.." should read "transfer of heat and moisture..".
61. Page 48, second line from bottom. "This sentiment were shared.." should read "This sentiment was shared..".
62. Page 49, paragraph 1, line 2. "..on confined spaces.." should read "in confined spaces..".
63. Page 49, fourth line from the top, "..reactor.." should be "..reactors..".
64. Page 50, line 4. "losses from building.." should read "..losses from a building..".
65. Page 50, line 6. "..environmint.." should be "..environment..".

Wee, H.K. Heat and mass transfer in confined spaces (Thesis)[4].

Errata

66. Page 51, paragraph 1, line 23. "..interpolation of results.." should read "..extrapolation of results..".
67. Page 51, paragraph 1, line 24. "..to carried out.." should read "..to carry out..".
68. Page 53, paragraph 1, line 9. "..will be given.." should read "..are given..".
69. Page 54 β instead of "B_T" is the coefficient of expansion with temperature.
70. In Page 55 and Page 63, "BSL(152).." denotes "Bird,Steward and Lightfoots(152)..".
71. Page 56, Equation (3.6) should read "$\partial^2/\partial x^2 + \partial^2/\partial y^2$"
72. Page 56, fourth line from the bottom. "..unknown.." should be "..unknowns..".
73. Page 57, line 8, delete the index "(3.9)".
74. Page 58, Section 3.4.1, line 9. "..upmost.." should be "..utmost..".
75. Page 58, last line. "..in the expanse of.." should read ".. at the expense of..".
76. Page 59, the second equation number "(3.12a)" should be "(3.12b)".
77. Page 59, the second equation number "(3.13a)" should be "(3.13b)".
78. Page 60, Section 3.5, line 2, replace "the foregoing dimensional equations " with "the set of governing dimensional equations..".
79. Page 60, Section 3.5, line 5. ".. dimensionless group.." should be "..dimensionless groups..".
80. Pg 60, Section 3.5, line 6. "..made.." should be "..makes..".
81. Page 60, Section 3.5, line 10. "..introduced.." should be "..introduce..".
82. Page 62. The second equation index "(3.22)" should be "(3.23)".
83. Page 63. The equation index "(3.18)" should be "(3.24)".
84. Page 63, paragraph 1, line 10. "..spare coordinate.." should read "..space coordinate..".
85. Page 64, paragraph 1, line 4. The sentence "The method basically make..." should read "The method basically makes a change of the independent variables so that the domain is mapped into a new coordinate system where the variation of the intermediate values of the solution is not so rapid."
86. Page 64, paragraph 1, line 8. "..has.." should be "..have..".
87. Page 81, paragraph 1, line 7. "..of air gap.." should read "..of the air gap..".
88. Page 85, paragraph 3, line 9. "..instored.." should be "..installed..".

Wee, H.K. Heat and mass transfer in confined spaces (Thesis) 5.
- Errata

89. Page 85, paragraph 3, line 10. "..were used.." should read "..was used..".
90. Page 85, paragraph 3, line 11. "..at both sides.." should read "..on both sides..".
91. Page 98, paragraph 1, line 3. "..constantine.." should read "..constantan..".
92. Page 99, line 2. "..was adopted.." should read "..were adopted..".
93. Page 101, delete "being" from the last line.
94. Page 107, paragraph 1, line 4. "..lower than the ambient.." should read " ..lower than the ambient temperature..".
95. Page 107, paragraph 1, line 6. "..monitored by the four thermocouple positions.." should read "..monitored by the four thermocouples..".
96. Page 107, delete "to be" from the last line.
97. Page 110, the equation "$q_p = q_{h2} + q_s - q_{h1} + q_s$" should read "$q_p = q_{h2} + q_s - (q_{h1} + q_s)$".
98. Page 112, Fig. 5.2. "..Porous Platic.." should read "Porous Plastic..".
99. Page 113, line 2. "..on the each side.." should read "..on each side.."
100. Page 113, line 3, "..$T_{cp} - T_{rs}$.." should be "..$T_{cp1} - T_{rp1}$..".
101. Page 113, last line. "..flushed.." should be "flush..".
102. Page 114, paragraph 2, line 8. "..was given in.." should read ".. is given in ..".
103. Page 114, paragraph 3, line 1. "..m_p versus values.." should read "..m_p versus ($P_c - P_r$) values..".
104. Page 115 Section 5.5.1, line 1. "..upmost.." should be "..utmost..".
105. Page 115 Section 5.5.1, line 5. "..instored.." should be "..installed..".
106. Page 124, paragraph 1, line 7. "..fig. F.3.." should be "..fig.6.3.."
107. Page 127, paragraph 1, line 1. "..TO that.." should be "..to that..".
108. Page 144, the Title of the graph should be "Fig. 7.4: Experimental Nu & Sh.." and not "Fig. 7.4: Experimental and Theoretical Nu & Sh..".
109. Page 150, line 4. "..the transfer being from the side of.." should read "..but the direction of the transfer is still from the side of high..".
110. Page 153, paragraph 1, line 18. "..the variation fluid properties.." should read "..the variation of fluid properties..".
111. Page 153, paragraph 1, line 20. "..up 200 ^{o}C.." should read "..up to 200 ^{o}C..".
112. Page 153, "Heat and Mass Transfer in Horizontal Cavity" should read "Heat and Mass Transfer in a Horizontal Cavity."

Errata

113. Page 154, paragraph 2, line 1. "..were plotted.." should read "..
..are plotted..".
114. Page 158, line 3. "..resulted.." should be "..resulting..".
115. Page 158, line 11. "..$(Nu)_u$ for case of.." should read "..$(Nu)_u$
for the case of..".
116. Page 158, paragraph 1, last line. "..increase.." should be
"..increases..".
117. Page 160, paragraph 2, line 3. Delete the word "systematic".
118. Page 160, paragraph 3, line 1. "..there is no results" should
read "..there are no results".
119. Page 162, sixth line from the bottom. "..36 ^{o}C.." should be ".."
0.36 ^{o}C..".
120. Page 164, Section 8.1, line 2. "..Chapter 3 were compared.."
should read "..Chapter 3 are compared..".
121. Page 164, second last line. "..had been.." should read "..have
been..".
122. Page 165, paragraph 1, line 12 from the bottom. "..such the .."
should read "..such as the..".
123. Page 166, line 3. "..sufficed.." should be "..suffice..".
124. Page 166, line 6. "..awared.." should be "..aware..".
125. Page 168, Figs. 8.1 and 8.2, the top line in each of the figures
denotes Nu and the lower line denotes Sh.
126. Page 170, paragraph 2, line 4. "..one use.." should be "..one uses
..".
127. Page 170a, Figs 8.3(b) and 8.4(b), the caption for each of the
figures should read "Concentration" and not "Temperature".
128. Page 173, paragraph 1, line 6. "..obscured.." should be ".."
observed..".
129. Page 173, paragraph 2, line 2. "..temperature fields.." should read
"..temperature field..".
130. Page 177, line 9. "Effort.." should be "Efforts..".
131. Page 177, paragraph 1, line 1. "..reflected.." should be "..reflect
..".
132. Page 177, paragraph 1, line 5. "..reversed.." should be "..reversal
..".
133 Page 177, paragraph 1, last line. "..tertially flow.." should read
"..tertiary flow..".
134. Page 177, last line. "The effect of simultaneous.." should read
"..The effect of a simultaneous..".
135. Page 180, paragraph 1, line 1. "..resulted.." should be
"..resulting..".

136. Page 180, paragraph 2, line 6. "..tertially.." should read "..tertiary..".
137. Page 183, line 3. "..as had indicated.." should read ".. as indicated..".
138. Page 183, paragraph 1, second last line. "..clculated.." should be "..calculated..".
139. Page 184, line 2. "..convergent.." should be "..convergence..".
140. Page 187, line 2. "..for heat transfer case.." should read "..for the heat transfer case..".
141. Page 187, paragraph 1, line 5. "..were.." should be "..was..".
142. Page190, line 7. "..but slight difference.." should read "..but a slight difference..".
143. Page 190, line 13. "..and if on its own.." should read "..and on its own..".
144. Page 190, Section 8.5, line 6. "It as thus.." should read "It was thus..".
145. Page 201, paragraph 1, second last line. "..expect.." should be "..expects..".
146. Page 202, eighth line from the bottom. "..porous stainless.." should read "..porous stainless steel..".
147. Page 203, paragraph 3, last line. "..ia.." should be "..is..".
148. Page 204, line 1. "..such the Shadowgraph.." should read "..such as the Shadowgraph..".
149. Page 307 to 310: estimates of the experimental errors are presented in Appendix 4, page 273 & 277.
150. Page 316, Section A8.4.1, index (ii), "ie. adiabatic walls" should read "ie. no mass transfer at the walls".